IMAGE INTENSIFIER SYMPOSIUM

24-26 October 1961
Fort Belvoir, Va.

Sponsored by:

· The National Aeronautics and Space Administration · The U.S. Army Engineer Research and Development Laboratories ·

Office of Scientific and Technical Information

National Aeronautics and Space Administration

PROCEEDINGS

of the

IMAGE INTENSIFIER SYMPOSIUM

October 24–26, 1961

Fort Belvoir, Virginia

PREFACE

This volume presents the results of the Image Intensifier Symposium held on October 24-26, 1961, at Fort Belvoir, Va., and jointly sponsored by the National Aeronautics and Space Administration and the U.S. Army Engineer Research and Development Laboratories.

Very significant advances in the science, technology, and application of image tubes have been made since October 1958 when the USAERDL sponsored the first Image Intensifier Symposium. This second symposium was held to provide an opportunity for those interested in image tubes to meet and compare notes on these advances.

It is our hope that symposia such as this may be held in the future as warranted by progress in this field.

CONTENTS

COMPONENTS OF IMAGE INTENSIFIER TUBES

Chairman, Peter Wargo

APPLICATIONS OF IMAGE INTENSIFIER TUBES

Chairman, Gerard F. Mulders

APPLICATIONS OF IMAGE INTENSIFIER TUBES

Chairman, Bernard Linden

1. SUMMARY OF BRITISH IMAGE TUBE SYMPOSIUM

Ray V. Hembree, *Research Projects Division, George C. Marshall Space Flight Center, NASA*

The Second Symposium on Photoelectric Imaging Devices as Aids to Scientific Observation was held at the Imperial College, London, on September 5–8, 1961. Since the proceedings of the London meeting are to be published by Academic Press by June 1962, this summary will be quite brief.

Approximately 200 persons attended the meeting, and during the 4 days, some 60 papers were presented. The growing interest in the photoelectric imaging field is evidenced by the increase in the number of papers by a factor of 2 over the first symposium of 1958.

A. Lallemand, Paris Observatory, opened the first session with a short talk on the Lallemand electronic camera. Some of the problems encountered with its use and the prospects for future use in astronomy were discussed. It is significant to note that in 1958 it was reported to have been in use at two observatories, whereas it is presently being utilized at five observatories including Lick Observatory, Mount Hamilton, Calif.

Eight additional papers followed regarding the Lallemand camera. G. Wlerick, Paris Observatory, reported on some laboratory experiments designed to study the properties of photocathodes such as drying, cooling, ionic pumping, and other factors that influence the pressure and sensitivity of photocathodes used in the electronic camera. Dr. Wlerick also discussed the use of the Lallemand camera in photographing the planets, Uranus, Jupiter, and Saturn at Pic-du-Midi Observatory. Using the same equipment, J. Rosch described the photography of double stars. M. Duchesne, Paris Observatory, described a magnifying electronic camera under development that is to be used in conjunction with a scintillation chamber for nuclear physics. G. E. Kron discussed the modified Lallemand image tube that is used experimentally at Lick Observatory, and M. F. Walker discussed some recent observations obtained with it. Dr. Kron also

suggested that a xerographic process of some kind be substituted for the photographic emulsion so that it can be baked clean. This would insure longer life and the use of the Lallemand tube would be simplified.

W. A. Hiltner, Yerkes Observatory, described an electrostatically focused electronographic image tube of new design, incorporating a barrier-membrane of aluminum oxide to separate the electron-sensitive emulsion from the photocathode section of the tube. When the tube is used at the focus of the 40-inch refractor, the sky background is 160 times greater than the tube background. Eight- to ten-hour exposures are possible before the background density exceeds 0.1. Sensitivity is 30 A L and 40 line-pairs/mm resolution has been achieved. Only 5 minutes are required to change plates.

Two additional papers on electronography were presented describing work at the Imperial College. Image tubes have been constructed using thin mica end windows. One such tube with a 6.3-micron window can withstand 3 atmospheres of pressure and resolves 55 to 60 line-pairs/mm. However, an operating potential of 50 kv is required for some 80 percent of the electrons to penetrate the mica window.

Closed-circuit television certainly held an important place among the topics of the London meeting. Over one-third of the papers were concerned directly with television pickup tubes or with their use as a vital part of an image intensifying system.

S. Miyashiro of Japan described several methods of minimizing the black-border effect produced by image orthicon tubes. The most successful method was accomplished by adding another collector mesh electrode in the image section of a standard image orthicon tube and controlling the voltage independently to that of the other electrodes. In addition to collecting the undesirable secondary electrons, it has the advantage of focusing them. In the examples shown, the

1

black-border effect was definitely minimized, but the image seemed slightly softer. The same speaker presented results of experiments conducted to produce changes in magnification with an image orthicon tube. The maximum zooming ratio achieved to date is 1.7 to 1.8. Larger ratios are expected in the future.

Characteristics of magnesium oxide targets versus those of conventional glass targets for image orthicons were discussed by R. B. Burtt of England. Magnesium oxide targets developed within his laboratory show a gain in sensitivity approximately an order of magnitude over glass targets. He also described an image orthicon with an aluminum oxide target capable of storing a star image for 3 days with no apparent image depreciation.

J. A. Hynek discussed the potentialities and limitations of image-scanning techniques in astronomy. Two programs were described: one at the Dearborn Observatory where an image orthicon system is attached to an 18-inch refractor, and the other at Organ Pass Station in New Mexico, where a 12-inch reflector, coupled with an image orthicon system, is used. At Dearborn, such problems as enhancement of contrast determination, the detection of faint objects, and the study of slow-scan techniques are being investigated. At Organ Pass, the investigations include the resolution of spectral class differences in objective prism spectroscopy, and the determination of positional resolution of astroids and other slow-moving astronomical objects. Dr. Hynek proposed a monochromatic scanning beam for improving the image orthicon tube for astronomical uses.

J. H. DeWitt, Jr., reported on an image orthicon system using slow readout that is in use at the Dyer Observatory. The equipment was recently evaluated at the Lowell Observatory on the 24-inch telescope and gains of 100-plus over fast photographic plates were achieved. Limitations of the system are evident in the resolution and the dynamic light range. Also described was a method for electronic widening of spectra.

W. C. Livingston described an image-orthicon camera chain that is in use at Kitt Peak for stellar photometry. Some of the electronic features include direct coupled blanking and scanning circuits to obtain time independent operation. By sequential scanning, "crosstalk" between the reading and image sections of the orthicon is eliminated. The Kinescope image

diameter was found to be a linear function of stellar magnitude over a range of six magnitudes.

E. W. Dennison, Sacramento Peak Observatory, discussed the application of an image-orthicon intensifier system in solar photometry. He proposes to take advantage of the rapid photometric readout of the image orthicon to record motion pictures of solar corona where rapidly changing phenomena takes place.

It might be appropriate at this point to mention some work done by W. A. Baum while at the Imperial College. Dr. McGee presented the paper in Dr. Baum's absence. An instrument was designed and constructed for making quantitative "astronomical" tests in the laboratory. A small test image is projected with a controlled amount of light onto the photocathode of a tube being evaluated. The test image consists of a resolution pattern, three calibrated sequences of simulated spectrum lines, a calibrated sequence of simulated star images against a "sky" background, an intensity step wedge, a sequence of double stars, a contrast-dilution test, and a scheme for measuring magnification and distortion. Except for the last item, the performance of the tube can be quantitatively specified by simple inspection of the image recorded by the tube. This device was proposed as a laboratory standard for measurement and testing of photoelectric imaging tubes and the attendees indicated considerable interest in it.

Five papers were presented on the subject of X-ray image intensification employing closed-circuit television coupled with image intensifier tubes. G. W. Goetze, Westinghouse, discussed results of an experimental system that incorporates a transmission secondary emission multiplier section directly into the X-ray image intensifier, thereby avoiding losses due to optical coupling. W. Herstel, Leiden University Hospital, showed motion pictures taken with his system, and C. A. Greatorex, Institute of Cancer Research, England, described image storage techniques applied to diagnostic X-ray image intensification.

Several papers were concerned with vidicon-type tubes. Included were: a lead-oxide vidicon by E. F. de Haan, Phillips Research Laboratories, Netherlands; an infrared-sensitive vidicon equipped television demonstrated by W. Heimann, Germany; a UV-sensitive vidicon discussed by J. Wardley, EMI, England; the Ebicon described by R. J. Schneeberger, Westinghouse; and the Tenicon (a high resolution information storage

2

tube) by B. W. Manley, Mullard. Research Laboratories, England.

Some 10 papers were presented on the use of image intensifiers in nuclear track recording. O. Gildermeister, Bonn University, described an image intensifier system designed for particle track recording that incorporates a four-stage image-converter tube. D. A. Hill, MIT, described a three-stage cascaded image intensifier tube combined with an image orthicon in a Bendix Lumicon system to record particle tracks in a sodium chloride crystal chamber 15 cm$\times$15 cm$\times$10 cm. Approximately 400 $\times$ photon gain is achieved with this system. G. T. Reynolds discussed filament scintillation chamber experiments conducted at Princeton University. J. A. Newth, Imperial College, described a system utilizing two 5-stage image intensifier tubes used to photograph cosmic ray tracks in a sodium iodide crystal. R. F. Doolittle, STL, suggested the application of scintillation chambers for space research to measure gamma ray flux, very high cosmic radiation, and radiation belts.

Other topics presented include progress reports on solid-state image amplifiers and the channeled image intensifier; image intensification for direct observation and for high-speed photographic recording.

The London meeting was a success in that it provided an opportunity not only for formal presentations but also for personal discussions with research workers interested in advancing the state of the art and with those who use the various devices and techniques as practical tools.

The many progress- and improvement-type papers indicate that a considerable amount of work is being done. The increasing use of photo-electric imaging devices is quite evident.

It is obvious that each new advancement is the product of much intense effort. Some expressed the belief that the state of the art is advancing slower than was anticipated a few years ago; however, the general feeling was one of optimism. Most of the speakers spoke enthusiastically about their future plans for research and development in their respective areas. It is apparent that this is certainly a business for serious professionals who have chosen a difficult field.

Discussion

A. B. Doty, Jr.: How can proceedings be obtained? Were any I.O. tube developments indicated whose performance, i.e., size, SNR, electron optics, surpass U.S. developments, typified by the RCA 4½-inch I.O.?

R. V. Hembree: The proceedings of the London meeting are scheduled to be published by Academic Press by June 1962. No; I do not remember any reported image orthicon tube developments that particularly surpass U.S. development.

A. B. Doty, Jr.: What industrial activities made contributions in Europe on image tubes? Can good tubes be purchased there now?

R. V. Hembree: Several industrial firms demonstrated image tubes at the meeting and indicated that they were commercially available.

2. ASTRONOMICAL REQUIREMENTS FOR IMAGE TUBES

Nancy G. Roman, *Chief, Astronomy and Solar Physics Programs, NASA*

Since with the almost singular exception of the sun, astronomical sources are exceedingly faint by terrestrial standards, the use of image tubes, particularly with electronic intensification, presents exciting possibilities for astronomy. Already the use of image tubes has given us excellent photographs of the planets, the sun, and the spectra of rapidly varying stars too faint to be observed in detail by conventional photographic techniques. The type of image tubes required for astronomical and space uses can probably best be described by outlining the many problems to be attacked with these tubes.

Perhaps the area in which image tubes have proved most fruitful in astronomy to date has been in obtaining high-resolution photographs of the planets. Turbulence in the terrestrial atmosphere continually distorts portions of the image received at the surface of the earth. On nights of good seeing, the whole image of the planet will move together, but rarely will the image stay in one position for more than a small fraction of a second of time. Most studies of the planets have been made visually, since the eye can catch the short intervals in which the image is good and ignore the rest of the signal. However, visual observations suffer both from subjective interpretations and the lack of a permanent record.

Image intensifiers, by shortening the exposures needed to obtain useful pictures of the planets by factors of 10 to 100, have permitted astronomers to make use of these small intervals of time to obtain excellent photographs. At maximum, planets have a diameter of approximately 1 minute of arc. Thus, even the best of seeing normally will restrict resolution to something of the order of 200 lines per image—not a difficult achievement for present-day image tubes. The details on planets are of very low contrast. Hence the possibility of increasing the contrast in a small portion of the dynamic range of the tube is potentially valuable. Small changes in

the low-contrast features are of great interest. Therefore, to make maximum use of the image tubes for these purposes, it is important that the tube be sufficiently constant in its intensity response to be used for photometric studies. Dimensional stability is also important if the images are to be measured for mapping, or compared for small changes in detail.

Image tubes have also been used for studying the infrared spectra of the sun in wavelengths in which photographic plates are quite insensitive. For the sun, sensitivity often is no problem, and for studies of a few major lines, excessively high resolution is not needed. However, for studies of spectral details over a moderate wavelength range, both high sensitivity and high resolution may be required.

Turning to objects other than the sun and the nearest planets, intensity becomes a crucial factor. Image tubes have permitted spectroscopic observations of faint stars and high-dispersion spectra of moderately bright stars which without the use of image intensifiers would require prohibitively long exposure times. For this use, it is important to have a moderate dynamic range with fine gradations which can be depended upon to reproduce themselves time and time again so that the resulting observations can be used for photometric reductions. For such observations, resolution also becomes important, although spectroscopic observations are simplified by the fact that the image tube may be essentially one dimensional. It is desirable to observe regions of the spectrum 200–300 Å in length at one time, with a resolution of the fraction of an angstrom, if possible. We would thus like to go to image tubes with as many as a thousand lines per frame, or even higher for some applications. Presently we are using photographic plates up to 10–20 inches in length with a resolution of 30–40 microns, or resolutions of the order of 10^4 lines per frame, so image tubes have a long way to go before competing with photographic plates in resolution

even for such one-dimensional sources as stellar spectra.

The possibility of expanding contrasts at low light levels is an intriguing one in the use of image tubes for faint astronomical sources. We must battle the signal-to-noise ratio which the brightness of the sky background always imposes, but the use of really high resolution, plus appreciable image intensification at low light levels, may ultimately permit us to resolve the centers of globular clusters and extragalactic nebulae on a somewhat routine basis.

For the space program, image tubes become even more important than they do for ground-based astronomy. At the present time, few satellites and a comparatively small fraction of our rockets provide the possibility of recovery. At best, recovery adds to the cost and complexity of the instrumentation. Thus, most data which we obtain from space must be sent back over telemetry links. The electronic readout image tube is a natural substitute for photographic plates in space applications. In addition to all of the uses which I have just outlined for ground-based astronomy, space astronomy extends the requirements for such tubes to higher resolution, since the atmosphere no longer limits the resolving power of most instruments, and to a very much broader wavelength range. We are now interested in using image tubes throughout the region of the spectrum in which focusing optics can be obtained; that is, from a few hundred angstroms in the ultraviolet down to tens of microns in the infrared. Ultimately, we should hope to use the image tubes to obtain measurements of close double stars, measurements of stellar parallaxes which involve the accurate measurement of shifts of star images of a thousandth of a second of arc relative to images within tens of minutes of arc, and other astrometric problems. For these, the linearity as well as the resolution of the tube becomes crucial and well beyond the present state of the art. For space astronomy as for ground-based astronomy, sensitivity, resolution, linearity and constancy of dynamic range, good gray scale resolution, and ultimately, linearity and calibratable linear range are important.

Turning to fields other than astronomy, in the conventional sense, we find image tubes being used for the exploration of the lunar and planetary surfaces. For these, vidicons within the present state of the art are satisfactory, but weight,

power consumption, and reliability will always be important considerations in the design and selection of such tubes, as well as the ruggedization required for all space applications. Moreover, ultimately we will want to extend the use of these tubes beyond the visual region of the spectrum to both the far infrared and the ultraviolet.

Tiros has shown the usefulness of television techniques for meteorology. An important need in the meteorological program is sufficient sensitivity to provide pictures of cloud cover at night in the absence of moonlight and sufficient dynamic range to provide not only day and night pictures with the same tube, but pictures of the cloud cover of the earth at times when part of the picture is sunlit and part in total darkness. For meteorology it is also important to use the near infrared, since in this region we can obtain greater contrast between the clouds and the ground, particularly at night. For nighttime use it is important for these tubes to discriminate against night sky emission. Thus, we must have tubes with sufficient sensitivity to permit the use of filters, or with a built-in narrow wavelength sensitivity.

Image tubes are also being used to study particle paths in scintillators, thus eliminating the need to recover large emulsion packs as is currently done using balloons and more recently the NERV probe. Needless to say, television will play many roles in monitoring equipment and increasing visibility in both manned and unmanned space flight.

There is an anticipated need for the use of image intensifiers in automatic control of space vehicles. Dimensional stability and freedom from need for maintenance are the prime requirements for this application. Also amplification, resolution, and dynamic range are important.

Image tubes also have a currently minor, but potentially important, role in the tracking of satellites. For this use it must be possible to combine the detector system with an automatic technique for determining the satellite position and feeding the necessary information into the computer. It is possible to do this with current tubes, but linearity and good dimensional stability would make the task appreciably easier. For tracking the satellites we are now launching, it is important to have tubes which are capable of tracking 10th to 12th magnitude objects at night and 4th magnitude objects by day, with an

6

accuracy of 5 seconds of arc or better. In a few years, as lunar shots become increasingly important, optical tracking must have the capability of tracking 16th to 18th magnitude objects by day, and 8th to 9th magnitude objects by night with an accuracy of 2 seconds of arc. Only if optical tracking meets these conditions will it be useful in that stage of the development of the space program.

For later periods in the program we are already beginning to consider the use of masers not only for tracking beacons but also for telemetry. To accomplish this we must have an image tube with a fast response time which can see 20th magnitude at night and 10th to 11th magnitude during the day, and can track with an accuracy of better than 1 second. Eventually, we may even wish to put tracking stations on the moon. This will permit us to extend our wavelength range considerably but, in common with all space applications, will require serious consideration of problems such as the weight and complexity of the tracking station, and its ability to operate in the hostile environment.

I trust that this brief review of currently foreseeable uses for image tubes has presented enough problems to provide each of you a challenge.

Discussion

R. W. DECKER: Could you give me explicit specifications for an IR image tube (beam readout), using a spectral range of approximately 1 to 22 that would be useful and desirable for one of the applications you described?

N. G. ROMAN: This is a good question. I am tempted to say, "Glad you asked it," and sit down. However, I shall try to be a bit more helpful by giving some figures for two examples:

(a) *Star mapping in the IR.* A GO star, similar to the sun, of apparent visual magnitude zero (very bright) has an intensity between 1 and 2 microns of 5.4×10^{-2} ergs/cm²/sec. To map an appreciable number of stars, one would want to go to perhaps 10th-magnitude stars; i.e., 10,000 times fainter. Thus, with a 10-inch telescope each star would have an image brightness of 2.7×10^{-3} ergs in the spectral band. Provided it were not too bad, linear resolution would not be critical. About 200 lines per frame would be useful. Observing stars cooler than GO would increase their brightness appreciably in this spectral range, but the stars become rapidly fainter toward longer wavelengths so this may be a typical figure for this project.

(b) *Infrared map of Mars.* The thermal radiation received from Mars at opposition is 2.1×10^{-4} ergs/cm²/sec. Most of this emission is in the 1- to 22-micron region, so for the present purposes we might assume that all of it is. To obtain $0''.5$ resolution on the planet, we would need 200 lines per frame or 40,000 picture elements. Thus, for a 10-inch telescope, we would need a sensitivity of $2.6/10^{-6}$ ergs/sec/picture element. Integration to build up the image is quite possible for either application provided resolution is not degraded thereby.

R. C. HULER: How much improvement do you experience in use of image orthicon tubes over conventional photography for stars?

N. C. ROMAN: This ranges from 10 to 100 times, depending on the brightness of the star. Photographic plates are increasingly poor at lower intensities because of reciprocity failure.

A. D. COPE: Does the term "dynamic range" apply to range in a single frame or the operating range for successive frames?

N. C. ROMAN: We would like the large dynamic range in a single frame in many cases. However, we would be willing to compromise on obtaining it with a few successive frames with the same instrument.

3. SOLID STATE IMAGE INTENSIFIERS

F. H. NICOLL *RCA Laboratories, Radio Corp. of America*

Introduction

The combination of electroluminescent layers with photoconductive layers to form imaging panels is now several years old. During this time single element devices of many kinds have also been made which will perform various functions. For the present discussion only those which have been made in panel form and which use radiant input will be covered. The continuing interest in image-intensifying panels is shown by the fact that many research laboratories in the United States and others in Holland, England, Germany, and Russia have made such panels, although the results have not been published in all cases. A good bibliography of published papers on the subject has been prepared by Ivey[12] and several review papers on image intensifiers have also been written.[345]

Two types of panel have been described in the literature: one combines the properties of light sensitivity and light emission in one physical layer,[6] and the other separates the two by using discrete electroluminescent and photoconductive layers. It now appears from published results that this latter approach may be more desirable because the special properties of a highly sensitive photoconductor and an efficient electroluminescent material can be optimized in the two separate layers. In addition, the use of two layers allows great flexibility in design and, as will be pointed out later, makes it possible to construct panels suitable for different radiant inputs, or having different input-output characteristics. Color imaging panels and light-triggered storage panels can also be made. Many of the variations in characteristics are achievable because of the possibility of choosing independently the desired photoconductive and electroluminescent materials for the layers. Freedom in controlling impedance match and feedback between the layers is also of great importance.

Operating Principles of Solid-State Image Intensifiers

A simple elemental intensifier unit is a series combination of a photoconductive cell and an electroluminescent panel with an a.c. voltage across it. To be representative of a panel device, these two elements should be the same size, since in general the image intensifier panel will have equal input and output area. The simplest form of the device also requires an opaque shield to prevent output electroluminescent light from feeding back to the photoconductor at the input. Operation as an intensifier involves a decrease in impedance of the photoconductor when light falls on it. This in turn causes an increase in current flow resulting in light emission from the electroluminescent layer. In practice, only the change of resistance of the photoconductor needs to be considered, since change of capacity with light can be neglected. However, under zero illumination, it is necessary that the capacity of the photoconductor should be considerably less than that of the electroluminescent layer. Since dielectric constants of the two materials are similar, this means the photoconductive layer must be, in effect, several times thicker than the electroluminescent layer. This condition greatly affects the design of image intensifier panels.

It is clear that the mode of operation of a panel is also greatly affected by the presence or absence of light feedback from output to input. The presence of an opaque barrier between input and output means that the photoconductor operation is independent of the electroluminescent output. A simple photoconductor will merely decrease in resistance as light falls on it, with the result that output light will increase with increasing input light. If the photoconductor alone shows bistable operation, then image storage can be obtained in a panel without optical feedback.

9

Optical feedback when properly controlled can be used to alter the input-output characteristics considerably. Full optical feedback gives bistable action and image storage is possible. Partial feedback alters the rise and decay characteristics of the panel. In the presence of optical feedback it is always necessary to maintain some form of elemental compartmentalization in order to prevent lateral light spreading and consequent degradation or loss of the image.

Large-area panels of various types became possible with the development of sensitive photoconductive material in suitable form. Up to the present the only such materials of high sensitivity (amperes/lumen) are cadmium sulfide and cadmium selenide in the form of powders and sintered layers. These materials, however, have made possible the construction of a number of panel devices. Most of these have been realized with photoconductive powders embedded in plastic, controlling electroluminescent layers of phosphor powders embedded in plastic. Since present electroluminescent layers require a.c. in order to operate, so also do the intensifying panels.

It is of interest to point out how the use of powders has helped to make possible the rather high-quality images which have been obtained. Finely divided powders are excellent means of averaging nonuniformities in individual particle properties and in effect trade some loss in overall sensitivity for increased uniformity and picture quality.

Solid Layer Panels

The simplest form of image intensifier panel is merely two contiguous layers of photoconductor and electroluminescent material, with an opaque insulating layer between them to prevent optical feedback. This type is shown in figure 3-1. As pointed out earlier, the photoconductor layer should be several times thicker than the electroluminescent layer so that light emission from the electroluminescent layer will not occur with the photoconductor in the dark. This immediately poses a problem. Since commonly used electroluminescent layers are about 1 mil thick, the photoconductive layer must be 5 to 10 mils thick. A 10-mil-thick layer is however very opaque to light, and thus under illumination only the top portion becomes conducting. This simple type of panel nevertheless has a use in X-ray image intensification because X-rays can penetrate the photoconductive layer quite well. Figure 3-2 shows the transfer characteristic for X-ray input. In addition, the output characteristic of a commonly used fluoroscope screen is shown. It is clear that a gain of about 100 × in image brightness is obtained for a given X-ray input. This type of panel intensifier has already found some application in industrial radiography[7][8] and in medical fluoroscopy.[9] It is capable of good halftone rendition, and image quality is comparable with a fluoroscope screen. Difficulty still exists in some applications because of the slow response of the photoconductor, which at low input intensity may amount to many seconds.

INCIDENT X-RAY IMAGE
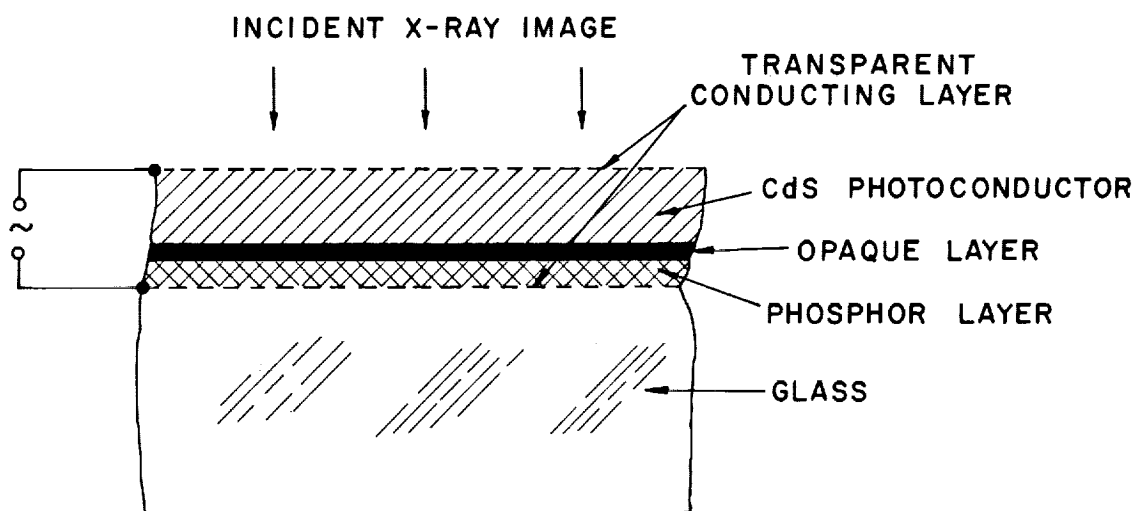
FIGURE 3-1.—X-ray image intensifier.
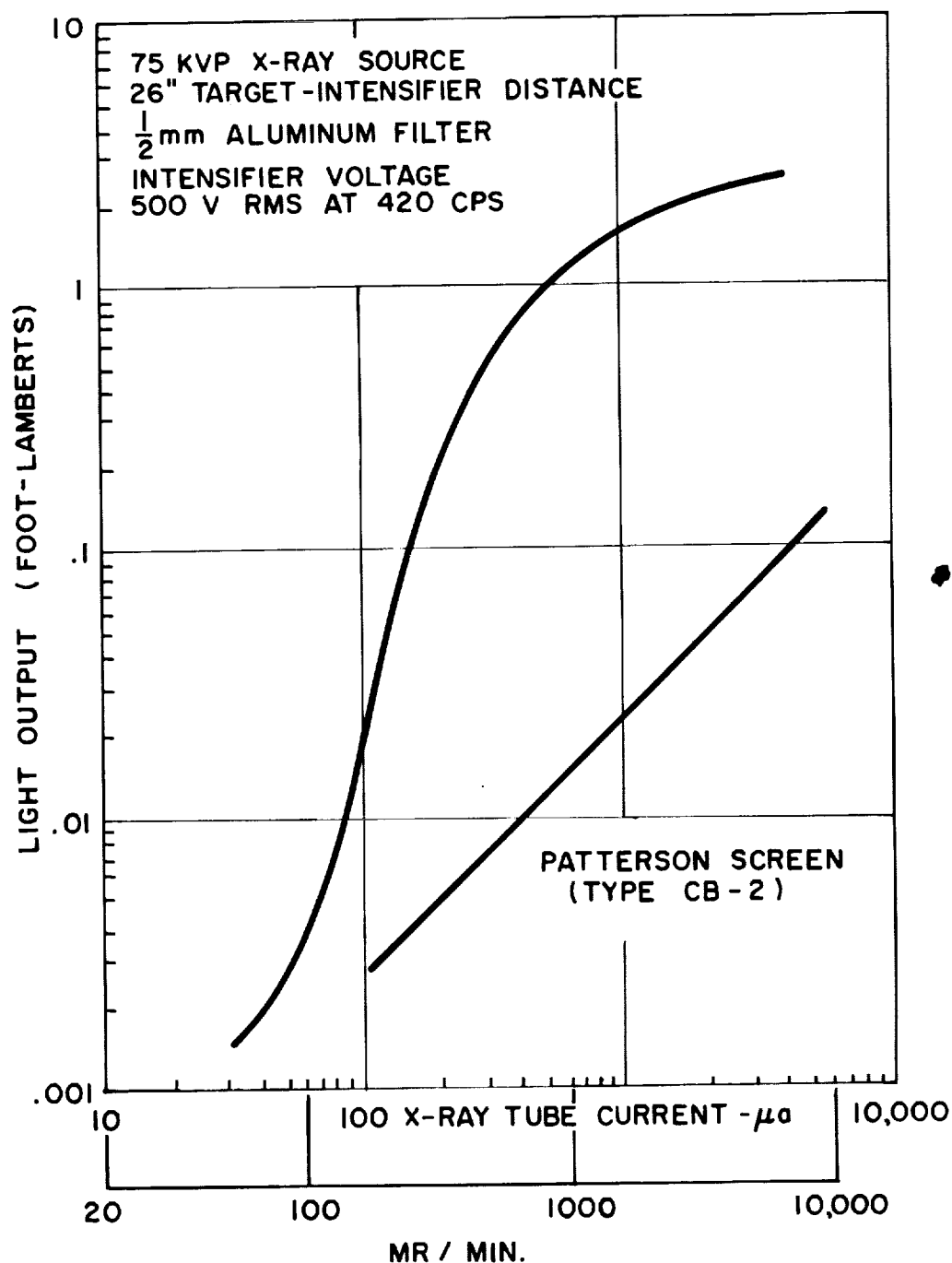
FIGURE 3-2.—Input-output characteristic of fluoroscopic screen and X-ray image intensifier.

Grooved Photoconductor Panels

The use of grooving in the photoconductor layer is one straightforward technique which has been used as a means of obtaining complete light excitation of the photoconductor from the top electrode to the electroluminescent layer. This can be seen in figure 3-3 which shows how the sides of the photoconductive ridges are completely exposed to light. Photocurrent flowing down the sides of the grooves must be spread out again to fill the same projected area on the electroluminescent layer. This is done with the current diffusing layer. Panels of this type have been made with an input-output gain of 800

11

INCIDENT LIGHT IMAGE

CONDUCTING STRIPS

CdS
PHOTOCONDUCTOR

CURRENT DIFFUSING
LAYER

OPAQUE LAYER

PHOSPHOR

TRANSPARENT
CONDUCTING
LAYER

GLASS
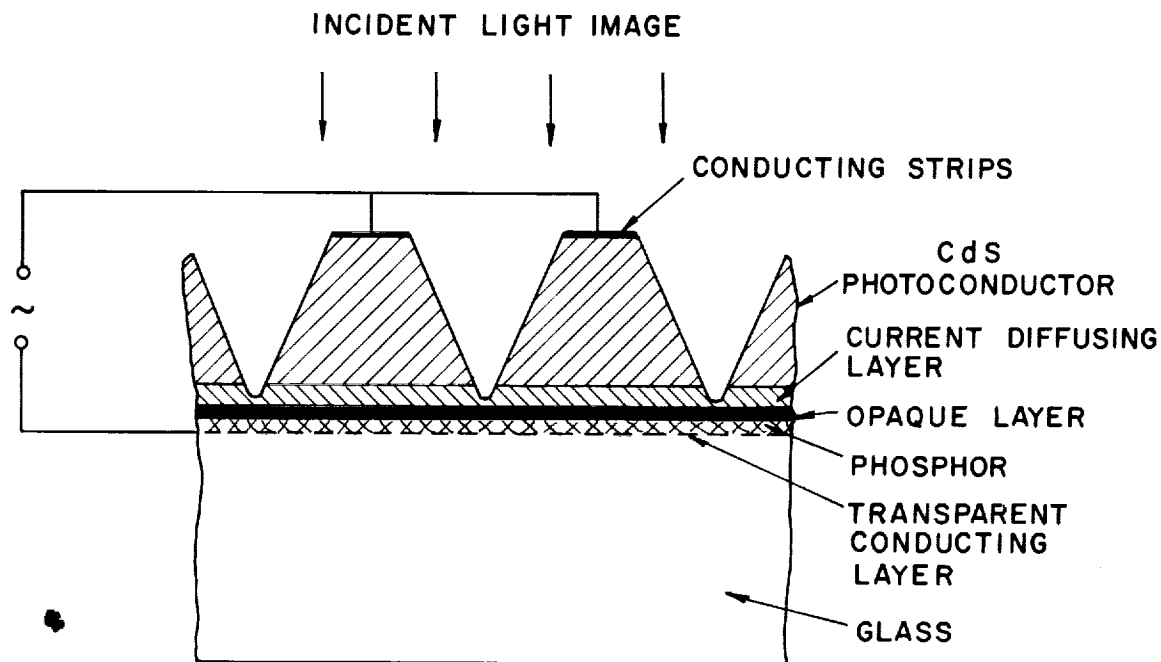
FIGURE 3–3.—Light-sensitive image intensifier.

INCIDENT COLOR IMAGE

CdS
PHOTOCONDUCTOR

CONDUCTING STRIPS

CdSe
PHOTOCONDUCTOR

CURRENT
DIFFUSING LAYER

OPAQUE LAYER

YELLOW
PHOSPHOR

TRANSPARENT
CONDUCTING
LAYER

BLUE
PHOSPHOR

GLASS
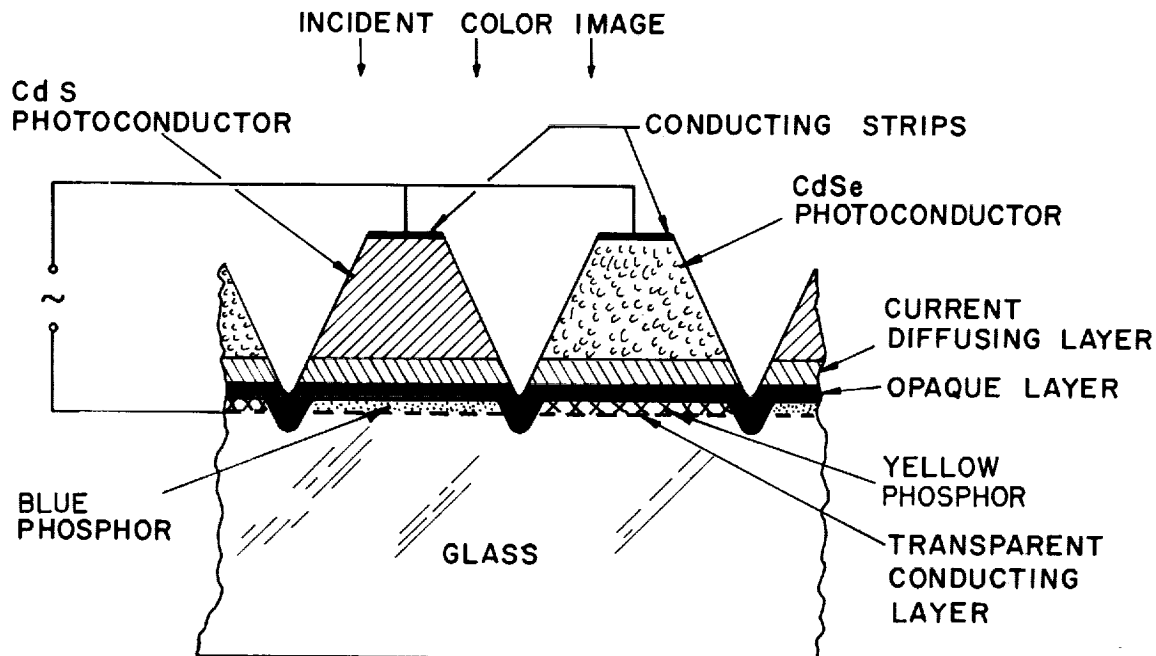
FIGURE 3–4.—Two-color input, two-color output image intensifier.

times, an input threshold of 3×10^{-3} foot-candles and a resolution of 500 lines on a 12-inch panel.[10]

Two-Color Panels

The two photoconductive powders suitable for image intensifier use are cadmium sulfide and cadmium selenide. The peak sensitivities of these materials occur at 6,000 and 8,000 Å, respectively. Although the response curves overlap somewhat, the two materials can be used to make a special type of two-color input intensifier having a two-color output. The two-color panel is a modified grooved photoconductor type (fig. 3–4) in which one set of photoconductive ridges is

12

made of cadmium sulfide powder controlling a strip of blue-emitting electroluminescent phosphor. Another interdigitated set of photoconductive ridges is made of cadmium selenide powder and controls a yellow-emitting electroluminescent phosphor. It can be seen then that a visible light source (with no infrared) striking the entire input side of the panel excites only the cadmium sulfide ridges and produces a blue picture on the output. An infrared picture on the input, however, excites only the cadmium selenide which produces a yellow output picture. These panels have been made in 6-inch size with 40 ridges/inch. The panel serves mainly to demonstrate the two-color technique, since its usefulness is limited to specially filtered input sources.[11]

Sintered Layer Panels

Slow response is a problem with the powder-type image intensifiers. Cadmium selenide powder has a faster response than cadmium sulfide powder, but it is not fast enough for use with moving images of low intensity. Cadmium selenide sintered layers, however, are considerably faster, although retaining the property of high sensitivity to light. In an effort to discover the possibilities of sintered cadmium selenide in an image intensifier, measurements have been made on a single element composed of a photoconductive cell controlling an electroluminescent cell.[12] The range of performance is indicated in table 3–I where two extremes of operation are given.

TABLE 3–I.—*Sintered CdSe Image Intensifier*

Operating frequency (cps)	Input (foot-candles)	Output (foot-lamberts)	Rise time (sec)	Decay time (sec)	Maximum energy gain
10,000	0.1	50	0.15	0.02	100
420	.002	12	2.0	.3	1,200

At 10 kc it can be seen that rise and decay are rapid and output intensity is high, but gain is low. This can be contrasted with the performance at 420 cps where speed of response is low and output intensity is low but the gain is very high. These results point up a characteristic of image intensifiers in general; viz, that operating parameters allow one to increase speed of response at the expense of overall gain.

Six-inch intensifier panels have been made using sintered cadmium selenide in a special construction as illustrated in figure 3–5. In this construction the photoconductive layer and the electroluminescent layer are built up separately on two glass plates which are later cemented together with a thermosetting current-diffusing layer having a nonlinear current-voltage characteristic. The electroluminescent layer is made as usual by a spraying technique. The photoconductive layer is, however, applied by spraying followed by high-temperature firing on a grooved glass plate having conducting lines at the groove bottoms. This structure has some design advantages since the whole photoconductive layer is excited by light. Also the absence of photoconductive material

filling the grooves reduces the layer capacitance.

Although these panels have fast response, high output and high gain, good image quality was difficult to obtain because of nonuniformity of gain. This was directly due to photoconductor nonuniformity. Sintered photoconductor sensitivity is a function of the firing temperature and ambient atmosphere during firing. It is therefore difficult to make a uniform layer. This difficulty points up again the advantage of using powder photoconductors which, although nonuniform from grain to grain, are highly uniform on the average in a layer composed of many particles.

Optical-Feedback Type Image-Storage Panels

Since the first panel-type image intensifiers were made, it has been realized that optical feedback could be used to provide bistable operation and various proposals have been made and some panels constructed.[13][14][15] The differences in the various types are mainly in the method of preventing feedback light from spreading. The simplest type [13] and one which has been made in a 6-inch size is that shown in figure 3–6. The two

13

CONDUCTING LINES

GLASS

SINTERED CdSe PHOTOCONDUCTIVE LAYER

CURRENT DIFFUSING LAYER

OPAQUE LAYER

PHOSPHOR LAYER

TRANSPARENT CONDUCTING COATING

GLASS
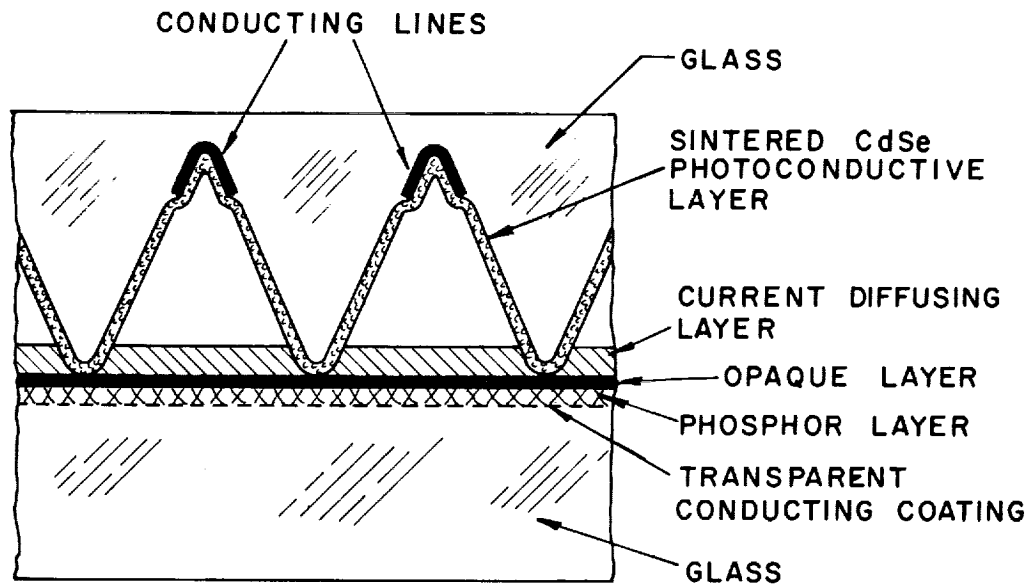
FIGURE 3-5.—Sintered CdSe image intensifier.

CdS PHOTOCONDUCTOR

CONDUCTING LINES

ELECTROLUMINESCENT PARTICLES

OPAQUE LAYER

TRANSPARENT CONDUCTING COATING

ELECTROLUMINESCENT LAYER

GLASS
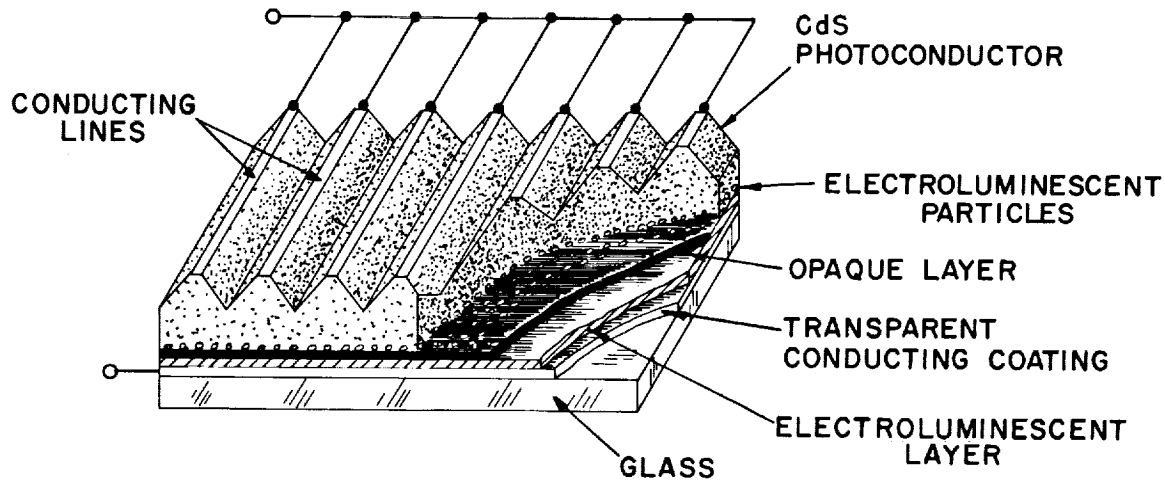
FIGURE 3-6.—Storage image intensifier with optical feedback.

main design features are first, the separation of the feedback electroluminescence dots from the viewing electroluminescent layer.[14] This prevents room light or halation of the emitted light from feeding back to the photoconductor. Second, the feedback electroluminescent layer is broken up very simply into small areas, thus preventing sideways light spreading and triggering of adjacent elements.

These storage panels have the same resolution as other grooved panels, about 40 lines/inch, and provide good long-time storage. Removal and reapplication of the voltage erases one image and

resets the panel for another image. More rapid erasure is possible with special circuit techniques. The input light required to trigger on a stored image is about 1 foot-candle-second with an input threshold of about 0.02 foot-candle.

Bistable Photoconductor-Type Image Storage Panel

A new effect discovered in cadmium selenide photoconductors [16] makes possible the construction of image storage panels without feedback. Certain problems are involved in obtaining proper impedance match between the photoconductive

14
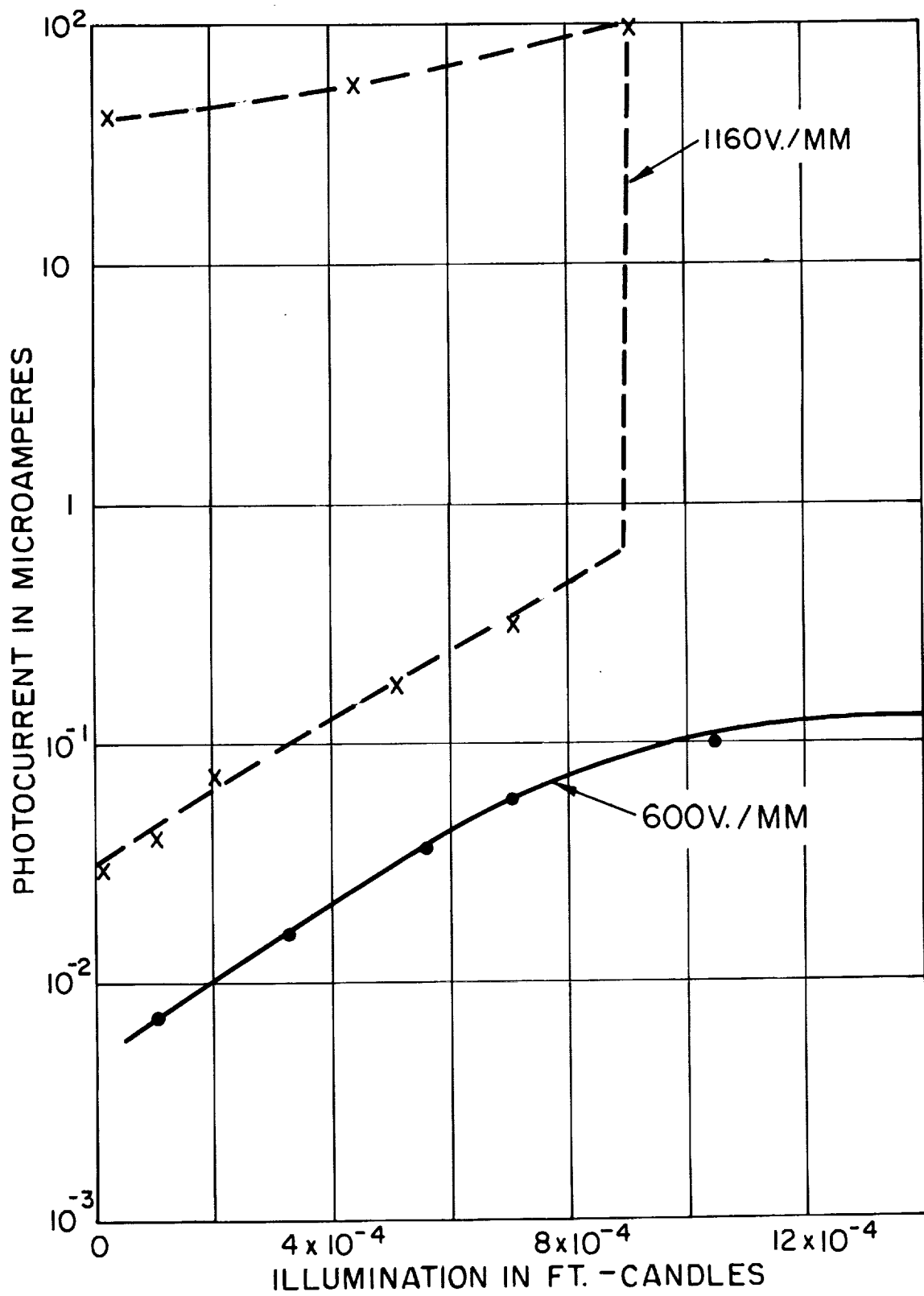
FIGURE 3–7.—Bistable behavior of CdSe powder.

layer and the electroluminescent layer, but the panel structure is that of the conventional grooved photoconductor image intensifier.

The bistable characteristics of the cadmium selenide photoconductor alone are shown in figure 3-7, where photocurrent is plotted as a function of illumination for two different voltages applied to the photoconductor. For fields of 600-v/mm, photocurrent increases gradually with illumination. At higher fields of 1,160 v/mm, the photocurrent increases gradually with illumination at first, but at a critical level photocurrent suddenly rises by over 100×.

Output remains at this high level even if the illumination is reduced or dropped to zero. Removal and reapplication of the voltage after about one-tenth second restores the photoconductor to its original condition ready for light triggering again. The photoconductor alone, with careful adjustment, will trigger with as little as 10^{-4}-foot-candle illumination, using an exposure of 10^{-3} foot-candle-seconds.

Three-inch and six-inch storage panels using CdSe powder without feedback have been made which can be triggered with 10^{-2} foot-candle-second and have a threshold value of about 5×10^{-4} foot-candles. Because of the particular nature of the powder, some halftones are obtained in the picture due to different triggering levels of individual particle chains.

Comparison of Performance Characteristics of Panels

Several types of image intensifiers and image storage panels have been described which use different photoconductors in several different designs. It is of interest to compare the important operating characteristics of the more basic types of simple image intensifiers and image storage panels. An accurate comparison is not easy to make, especially since the photoconductors have infrared response outside the visible spectrum. In table 3-II, comparing the various panels, input light levels are given as equivalent foot-candles.

TABLE 3-II—*Comparison of Grooved Image Intensifier Panels*

| Panel type	Photoconductor material	Threshold input equivalent (foot-candle)	Exposure for maximum gain equivalent (foot-candle-second)	Gain	Recovery time between images (sec)
Amplifier	CdS (powder)	0.003	0.3	800	15–60
Amplifier	CdSe (sintered)	.001	.01	1,200	1
Storage (with feedback)	CdS (powder)	.02	1.0	200	5
Storage (with feedback)	CdS (sintered)	.02	1.0	[1] 200	15
Storage (without feedback)	CdSe (powder)	[1] .0005	.01	2,000	.1

[1] Probably.

An equivalent foot-candle is considered as an intensity approximately equivalent to a foot-candle, but matching the photoconductor in spectral characteristics. The use of these units makes possible a significant comparison of the devices using different photoconductors. Gain is taken from experimental results and is the maximum ratio of output luminance to input illuminance.

Table 3-II compares five different panel types. CdS powder and CdSe sintered layers are compared in panel amplifiers, but CdSe powder layers are not included. This is because CdSe powder, when operated at high fields, exhibits bistable operation and the device becomes an image storage panel which is included in the table. CdSe

powder at low fields is rather insensitive and gives small gain.

Two types of image storage panel using optical feedback are tabulated, one using CdS powder and one using CdS sintered material. In addition, an image storage panel using the bistable property of CdSe powder is included. CdSe powder devices with optical feedback have not been made because of the spectral mismatch between the photoconductor and the electroluminescent material. On the other hand, CdSe sintered layers can be used to make sensitive feedback and nonfeedback devices. Thus far no actual panels have been made, so these devices are not included in the table.

16

Table 3-II shows the marked superiority of both CdSe powder and sintered layers over CdS layers of both powder and sintered types. The highest gain, most rapid recovery time, and the lowest input-light threshold is obtained with the CdSe powder used in an image storage panel without optical feedback. However, a CdSe sintered layer used in an image amplifier is a close second in performance.

Further improvement in device characteristics can be expected if CdSe sintered layers are used either with optical-feedback storage or with bistable operation of the photoconductor. Improvement in the present type of image panel using the CdSe and conventional electroluminescent layers depends to a large extent on technique advances in making large uniform photoconductive layers. Improved panel designs will also be needed to realize the full potentialities of the sintered CdSe.

Conclusion

The properties of presently available photoconductors in combin.tion with the well-known a.c.-operated electroluminescent layers have not yet been fully exploited in image intensifiers or storage panels. Furt .er improvements in the design of these rather conventional panels may still be expected. On the other hand, there is no doubt that further improvements can also be expected as materials research progresses. Improved photoconductors *alone* would increase performance of the panels, but it has also been clear for some time that an improvement in efficiency of the conventional electroluminescent layer *alone* would immediately provide improved performance. Still greater improvement would be realized if the electroluminescent layer were d.c. operated. This is because the sensitive photoconductors operate better on d.c.

In the more immediate future is the possibility of making much thinner electroluminescent layers. These would allow the use of thin photoconductive layers which hopefully would be thin enough to transmit light. Panels could then be constructed with the sandwich design which is simple and can provide high resolution.

One other possibility for the rather remote future is the use of some solid-state amplifying layer between the photoconductor and electroluminescent layer. Various schemes of this sort have been proposed in literature, including the use of transistors, dielectric amplifiers, and also magnetic devices. While many of these can be demonstrated as very effective in single-element intensifiers, the problems are manifold in designing and making large, high-resolution image intensifier panels.

Altogether there is every reason to believe that solid-state image intensifiers will improve considerably as the research on light sensitive and light emissive materials continues. As the panels improve they should become competitive with photoelectric image intensifiers in more than the very few special applications where this is now the case.

Discussion

Martin Dachs: What is spectral response of CdSe powder? What is "quantum efficiency" (i.e. watts of incident input versus photocurrent output)?

F. H. Nicoll: The peak response of CdSe powder is at 800μ. At 700μ it has about one tenth the peak response, and at 1μ the response is approximately 25 percent. Quantum efficiency is a little hard to define for the powder photoconductor since photocurrent varies as a high power of the applied field. At very high fields the ratio of photocurrent to dark current is low, so one must operate around 1,000 volts/mm. A gap structure 5 mm $\times$ 0.5 mm illuminated with tungsten light 0.05 foot-candle will give approximately 300μ amps with the field applied across the short dimension.

W. F. Niklas: How do the noise levels compare for photoconductors and photoemitters?

F. H. Nicoll: Noise level in a good single crystal of CdS should be due to photons alone and be comparable with photoemission. However, in most practical cases, contacts contribute noise, and in the case of powder photoconductors, contacts between particles contribute more noise.

A. E. Anderson: What is the lowest input light level at which the full resolution capability of CdSe image intensifier screen is obtained?

F. H. Nicoll: The lowest input light level which would give an image with CdSe sintered material is approximately 102^{-3} foot-candles.

E. Levinthal: What is the cause of threshold behavior?

F. H. Nicoll: Threshold behavior is related to the nonlinearity of both photoconductor and

electroluminescent layer. There are, no doubt, other causes for the behavior, but no investigation of them has been carried out.

R. H. HARDIE: Why are the grooves cut in the photoconductor layer?

F. H. NICOLL: The grooves are cut in the photoconductor layer so that light will illuminate the photoconductor surface from the top electrode to the electroluminescent layer. A solid layer absorbs light so strongly that only the top portion becomes conducting, leaving the remainder as a high-impedance capacitor.

G. SUITS: What is the cause for the increased photoconductive response of CdS and CdSe for d.c. operation compared to a.c. operation?

F. H. NICOLL: The increased sensitivity with d.c. operation is characteristic of powders particularly, and is related to the fact that current varies as the fourth power of the voltage. With a.c., the useful portion of the cycle is rather small.

I. LEVIN: Do you think that the sintered CdS and CdSe layers are more sensitive to incident radiation because more impurity centers are produced by sintering? Is not the greater d.c. sensitivity due to the semiconducting behavior? Have only the Cd compounds been used for the semiconducting layer?

F. H. NICOLL: I doubt whether the increased sensitivity of sintered layers is due to increase of impurity centers, since the powders are also fired, but not as a layer. The elimination of barriers in the sintered layers is part of the story and associated with this is a linear voltage-current relationship. Cd compounds are the only compounds with sufficient sensitivity for solid-state image intensifier use at the present time.

R. L. ZASTROW: What is the resolution attainable (in line pairs/mm)?

F. H. NICOLL: The thickness of the photoconductor, which is approximately 0.4 mm, limits the resolution to near this value.

J. F. ROESLER: What kind of binder do you use for keeping the CdS together? Which kind of epoxy? What sort of material is the opaque layer made of?

F. H. NICOLL: The binder used with the CdS powder is Ciba CN502 diluted one part CN502 to five parts diocetone alcohol. The alcohol finally evaporates, leaving the particles bonded together.

References

1. IVEY, H. F.: *Bibliography on Electroluminescence and Related Topics.* Part I, IRE Trans. of the Professional Group on Electron Devices, vol. ED-6, No. 2, 1959, pp. 203-215.
2. IVEY, H. F.: *Bibliography on Electroluminescence and Related Topics.* Part II, Jour. Electrochem. Soc., vol. 108, No. 6, 1961, pp. 590-599.
3. KAZAN, B., and NICOLL, F. H.: *Solid-State Light Amplifiers.* J. Opt. Soc. Amer., vol. 47, 1957, p. 887.
4. LOEBNER, E. E.: *Recent Developments in Solid-State Image Transducers.* Solid-State Physics in Electronics and Telecommunications, vol. 4, pt. II, 1958, pp. 762-775.
5. GARLICK, G. F. J.: *Solid-State Image Amplifiers.* Jour. of Scientific Instru., vol. 34, 1957, p. 473.
6. CUSANO, D. A.: *Single-Layer Image Intensifying Screens With High Resolution.* Image Intensifier Symposium, October 1958, pp. 185-199.
7. HADLEY, C. P., and CHRISTENSEN, R. W.: *Solid-State X-ray Image Intensifiers.* Non-Destructive Testing, vol. 19, No. 5, 1961, pp. 321-322.
8. WILBURN, D. K.: *A Solid-State Electroluminescent X-ray Intensifier.* Non-Destructive Testing, vol. 19, No. 5, 1961, pp. 323-326.
9. KAZAN, B., and GODFREY, E. W.: *Experimental Results With the Panel X-ray Amplifier.* Radiology, vol. 72, No. 6, 1959, p. 858.
10. KAZAN, B.: *An Improved High-Gain Panel Light Amplifier.* Proc. IRE, vol. 45, 1957, p. 1358.
11. NICOLL, F. H., and SUSSMAN, A.: *Two-Color Input–Two-Color Output Image Intensifier Panel.* Proc. IRE, vol. 48, 1960, p. 1842.
12. NICOLL, F. H.: *Properties of a Single-Element Light Amplifier Using Sintered CdSe Photoconductive Material.* RCA Rev., vol. 20, 1959, p. 658.
13. HOOK, H. O., and GIAMO, E. C.: *Research on Opto-Electronic Computer Components.* Contract No. AF19(604)-4959, November 30, 1960.
14. KAZAN, B.: *A Feedback Light-Amplifier Panel for Picture Storage.* Proc. IRE, vol. 47, 1959, p. 12.
15. BILLUPS, R. R., ROTSTEIN, J., and GARDNER, W. L., JR.: *Solid-State Display Panels With Photoconductive Control.* Lincoln Lab. Tech. Rep., No. 223, 1961.
16. NICOLL, F. H.: *A Hysteresis Effect in Photoconductive Cadmium Selenide and Its Use in a Solid-State Image Storage Device.* RCA Rev., vol. 19, 1958, p. 77.

18

4. OBJECTIVE METHODS IN IMAGE INTENSIFIER EVALUATION

John Johnson, *Warfare Vision Branch, USAERDL*

Introduction

The purpose of this paper is to present a brief review of objective image tube evaluation methods and techniques. We shall specifically restrict ourselves to the problem of evaluating the content and structure of images since this is the central consideration involved.

The Problem

The basic problem with which we are concerned is schematically indicated in figure 4-1. In
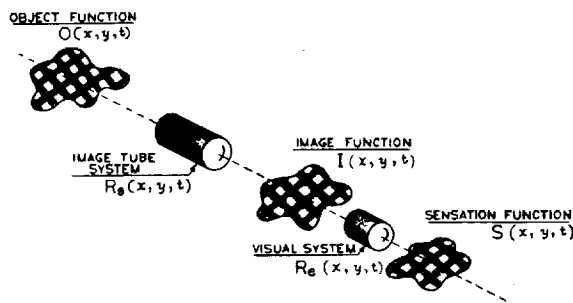
FIGURE 4-1.—Schematic diagram of basic image evaluation problem.

general, we start with an object function or message which may be described in the space-time domain by a two-dimensional intensity distribution $O(x, y)$ which varies in time. This object intensity distribution is modified and usually degraded by the image tube into an image intensity function $I(x, y, t)$. Subsequently the physical image intensity distribution is processed and transduced by the human visual channel into a sensation distribution $S(x, y, t)$ which in turn generates, somewhere in the brain, an image recognition decision. What we would like to be able to do is to calculate the particular effects which the image tube response function $Rs(x, y, t)$ has on the visual decision making processes for

real, meaningful objects. This is not possible at the present time for two reasons.

(1) Because of their high information content, real objects are very difficult to define and manipulate mathematically.

(2) We do not yet understand the basic mechanisms underlying the processes of vision and image recognition in the brain.

Since we cannot solve the general imagery problem, we must content ourselves with a more modest goal. That is, with the examination of methods of objective image analysis which will allow the evaluation of physical images in terms of their subjective impressions of sharpness, graininess, and tone.

The Threshold Resolution Method

At the present time the most widely used and most widely criticized test for visual sharpness is the method of threshold resolution. This test is schematically indicated in figure 4-2. The object message for this test is a series of black and white lines. The line width is progressively decreased until the visual observer is no longer able to discern line structure in the image. The reciprocal of the width of a black-and-white pair indicates the threshold line frequency in line pairs/unit. The test is relatively simple and if
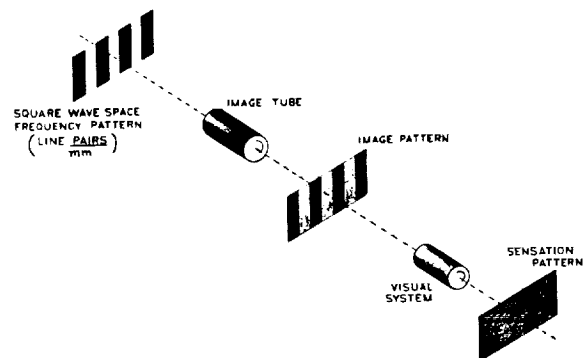
FIGURE 4-2.—Method of visual image evaluation.

19

FIGURE 4-3.—Objective image evaluation based on square wave analysis.

degradation contributions of a number of image forming elements in cascade.

Square Wave and Sine Wave Response Methods

In the late forties and early fifties, Schade, Coltman, and others developed objective image evaluation techniques based on the methods of square wave and sine wave analysis. The essence of the square wave response method is indicated schematically in figure 4-3. The experimental setup is the same as for the threshold resolution test, except that the visual observer has been replaced by a photomultiplier-slit assembly. The sampling slit measures the intensity distribution of the image of the optical bar pattern as the line frequency is progressively increased. As might be expected, the a.c. modulation continuously decreases as a function of line frequency which indicates that the image tube acts as a low pass space filter. The square wave amplitude response method has been used at USAERDL since 1953 for the evaluation of lenses and image tube systems.

In figure 4-4, we indicate some of the qualitative properties of square wave response measurements. The effect of the filtering response of the image

carefully carried out gives good reproducible results. There are however several disadvantages to this method.

(1) It is not an objective method but a visual one.

(2) It assesses the system at only a particular line frequency and gives no indication of what is happening at lower frequencies.

(3) It does not allow assessment of the

DETAIL PROPERTIES OF SCANNED FREQUENCY PATTERNS

$$\text{AMPLITUDE RESPONSE} = \frac{\psi'_N}{\psi_0} \qquad \text{FLUX RESPONSE} = \frac{\psi_N}{\psi_0}$$
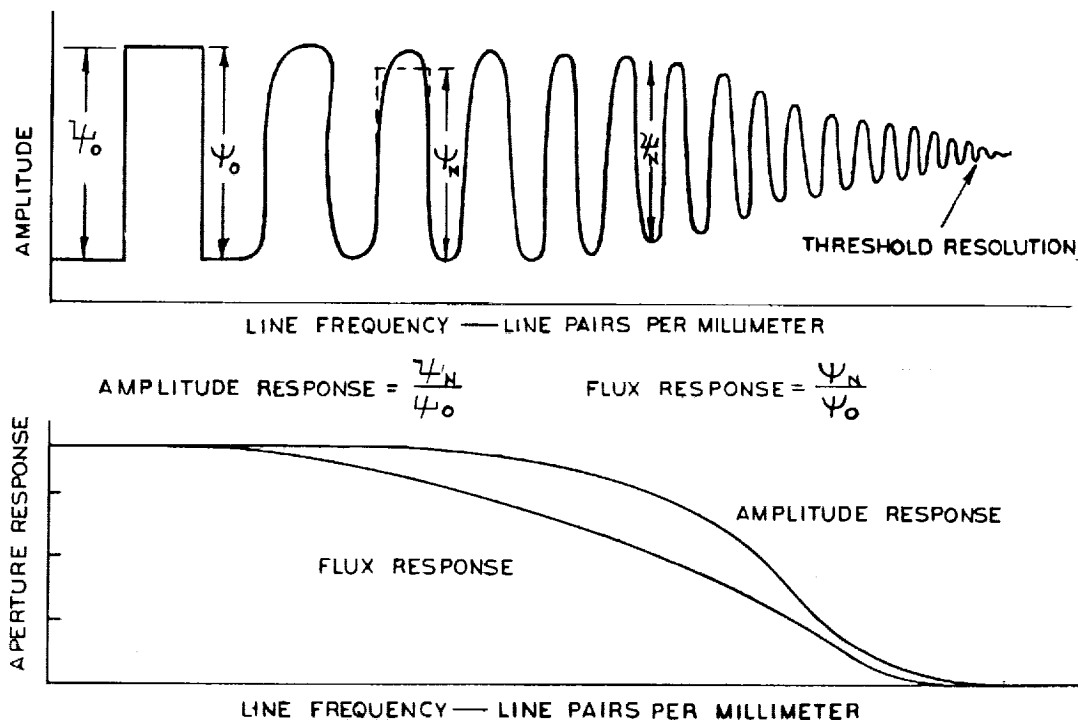
FIGURE 4-4.—Definitions of square wave amplitude and flux response factors

20

tube is to first degrade the square wave nature of the object pattern and then at higher frequencies to reduce the pattern amplitude. The square wave amplitude response at a frequency N is defined as—

$$r_a = \frac{\text{a.c. amplitude] at } N}{\text{a.c. amplitude] at frequency} \rightarrow 0} \qquad (1)$$

Both response factors are plotted against line frequency in the lower half of figure 4-4. It is obvious that the square wave flux response factor is the more sensitive measure of image quality. The important consideration is that the square wave response factors permit objective assessment of image quality over the whole range of available line number frequencies.

A rather elegant way to eliminate the necessity for measuring mean flux values is to replace the square wave pattern with a sine-wave-type optical pattern. This eliminates the effect of wave shape distortion encountered at low line numbers and results in a single measure of image

However, this response factor does not measure the filtering action of the image tube which results in the wave edge distortion at low line number. A somewhat better image sharpness measure is the square wave flux response. This is defined at a frequency N by

$$r_f = \frac{\text{[Mean value of flux over a half wave] at } N}{\text{[Mean value of flux over a half wave] at frequency} \rightarrow 0} \qquad (2)$$

quality, the sine wave response factor. This is defined at a line number N by

$$r = \frac{\text{[a.c. amplitude] at } N}{\text{[a.c. amplitude] at frequency} \rightarrow 0} \qquad (3)$$

The sine wave response is shown as a function of frequency in figure 4-5. The overall function is a completely objective measure of image quality. The function is independent of object contrast and easily allows determination of the effects of a number of imaging elements in cascade. The only problem with sine wave image analysis is the nonavailability of sine wave optical patterns. As a single valued number for image
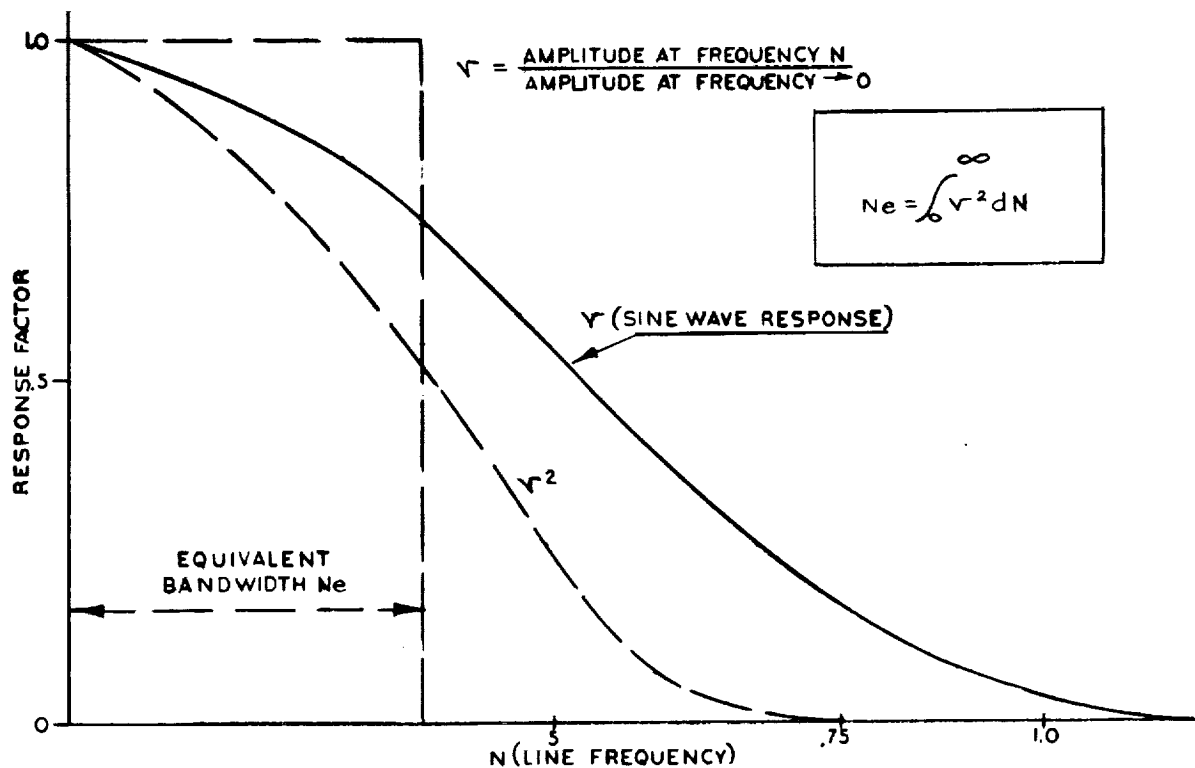
Figure 4-5.—Sine wave image analysis and definition of equivalent bandwidth Ne.

21
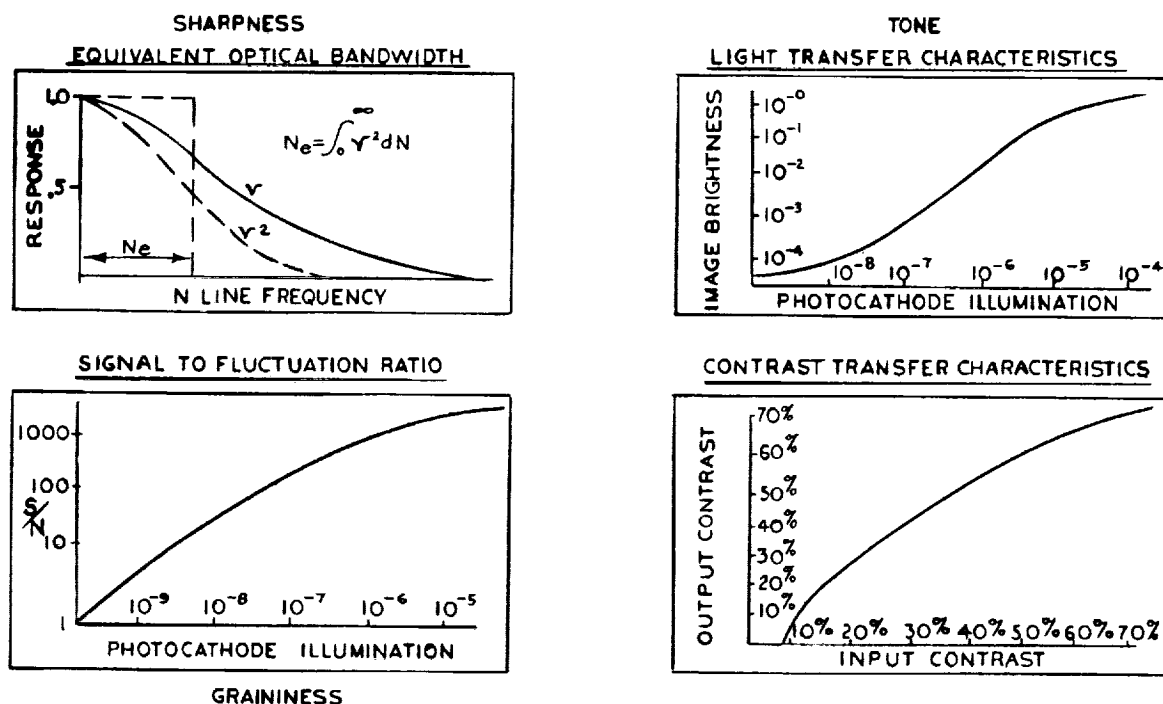
FIGURE 4-6.—The image structure factors which define image quality.

quality, Schade has proposed the equivalent band-width Ne. It is well known from optical communication theory that the energy or power under the sine wave response function may be calculated by integrating the square of the sine wave response function. The equivalent bandwidth Ne defines the equivalent energy in rectangular form such that at the bandwidth frequency Ne the sine wave energy falls suddenly to zero. The Ne figure of merit represents, however, a compromise measure in which the low frequency responses are considerably favored over the high frequency responses. It is to be expected that this will give misleading results in images in which the act of recognition depends strongly on the perception of small detail, sharp edges, or equivalently the high frequency image content.

Image Fidelity Factors

The sine wave response function measures the ability of an image system to reproduce faithfully sinusoidal variations in space intensity over a wide frequency range. It is, however, not a complete measure of image quality in itself since

it does not include the d.c. image levels nor the variations in image structure with time. In figure 4-6, we indicate the factors which objectively determine overall image quality. These are:

    sine wave response function.
    signal to fluctuation ratio.
    d.c. transfer function.

The signal-to-fluctuation ratio is a measure of point-by-point time variations in image structure. It is normally measured objectively by sampling the image through a known aperture and measuring the r.m.s. noise level in a known electrical bandwidth. The signal to r.m.s. noise ratio is an adequate measure of image structures which vary in time if the power spectrum of the noise is flat. If it is not, then it is necessary to measure the power density spectrum of the noise. The d.c. transfer functions express the relationship between input and output image powers. It includes the effects of d.c. noise, linearity, gamma, and large-scale image scatter. The objective methods of measurement of d.c. transfer factors are well known and will not be considered further here.

22

Sine Wave Contrast Response

The question naturally arises as to whether it is possible to combine the individual image factors into a single objective image quality measure. One way in which this can be accomplished is to generalize the sine wave response function to include the d.c. and r.m.s. noise levels. Figure 4-7 illustrates the concept of sine wave contrast response. This image measure is based on a frequency by frequency comparison of the image sine wave modulation to the object sine wave modulation. The sine wave contrast response at a frequency N is defined as:

$$C_r = \frac{\text{output sine wave modulation}}{\text{input sine wave modulation}} \bigg] \text{ at frequency } N \tag{4}$$

$$\text{Sine wave modulation} = -\frac{E_{max.} - E_{min.}}{E_{min.} + \text{r.m.s. noise}}$$

The sine wave contrast response function has a basic advantage over the sine wave amplitude response. The comparison wave in the former is the input wave form, while in the latter it is the wave modulation in the output wave at a fre-quency approaching zero. For logical reasons, it certainly seems preferable to use as the basic wave form the input wave form and to compare it, frequency by frequency, to the output wave form.

The sine wave contrast response function is a completely objective measure of image quality which should correlate with the subjective impressions of image sharpness, graininess, and tone. It should be noted that the sine wave contrast response is independent of the contrast in the object. The performance of an image intensifier is completely specified by the sine wave contrast response functions measured at various levels of photocathode illumination. It should be noted the sine wave contrast responses should be measured both statically and dynamically. That is, for still and moving patterns at various speeds referred to the photocathode.

Comparison of Various Image Quality Factors

In order to compare qualitatively the various image quality measures, pictures were taken of the imagery generated by a thin film image orthicon at 1.8×10^{-5} ft.-c. and 2.7×10^{-6} ft.-c
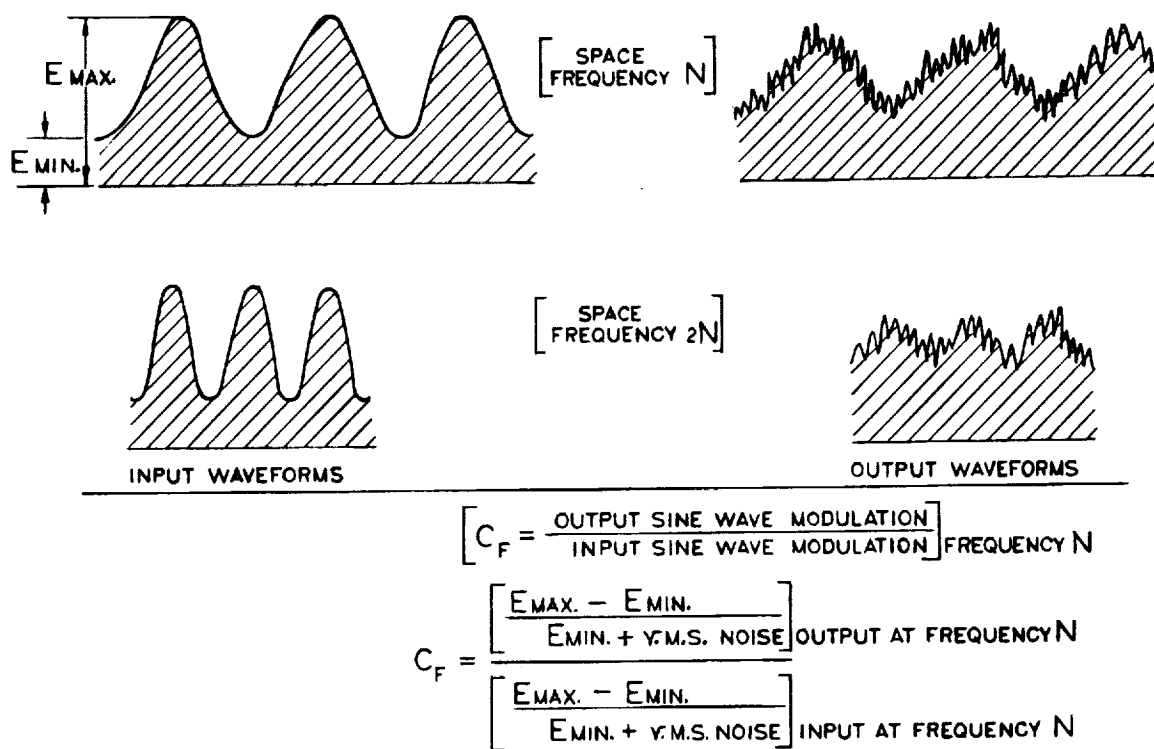
FIGURE 4-7.—Definition of sine wave contrast response.

23

illumination on the photocathode. These are shown in figure 4–8. There is evidently a considerable difference in image quality between the two pictures. Table 4–I indicates the threshold resolution and equivalent bandwidths Ne measured with square waves for the two pictures.

TABLE 4–I

Photocathode illumination (foot-candles)	Threshold resolution, TV lines	Ne, TV lines
1.8×10⁻⁵ ft.-c.................	425	95
2.7×10⁻⁶ ft.-c.................	300	85

On the basis of these two measures, we would expect that the differences in image quality between the two pictures are less than 25 percent. The square wave contrast response functions plotted beneath each picture indicate much greater differences, especially in the lower line number frequencies. At these low frequencies the differences in contrast response is almost an order of magnitude. Overall, the square wave

contrast response functions objectively show the large differences in picture quality which are evident in visual observation. Square wave patterns were used in these tests because of the nonavailability of sine wave optical patterns.

Objective Image Evaluation Instrumentation

The basic instrumentation required for objective evaluation of image tubes is shown in figure 4–9. This setup could be used to evaluate the static and dynamic sine wave contrast response as a function of photocathode illumination and image movement. It provides for direct measurement through playback from magnetic tape recording into d.c., r.m.s., and wave analyzer meters. In addition, the instrumentation would provide for objective measurements of optical image distortion by allowing conversion of the linear dimensions of photocathode images into countable pulses. It is expected that this type of image evaluation facility will be assembled at USAERDL during the next few months.

PHOTOCATHODE ILLUMINATION 2.7 × 10⁻⁵ F.C.

THRESHOLD RESOLUTION 425 T.V. LINES
$N_e = 95$

PHOTOCATHODE ILLUMINATION 1.8 × 10⁻⁶ F.C.

THRESHOLD RESOLUTION 300 T.V. LINES
$N_e = 85$
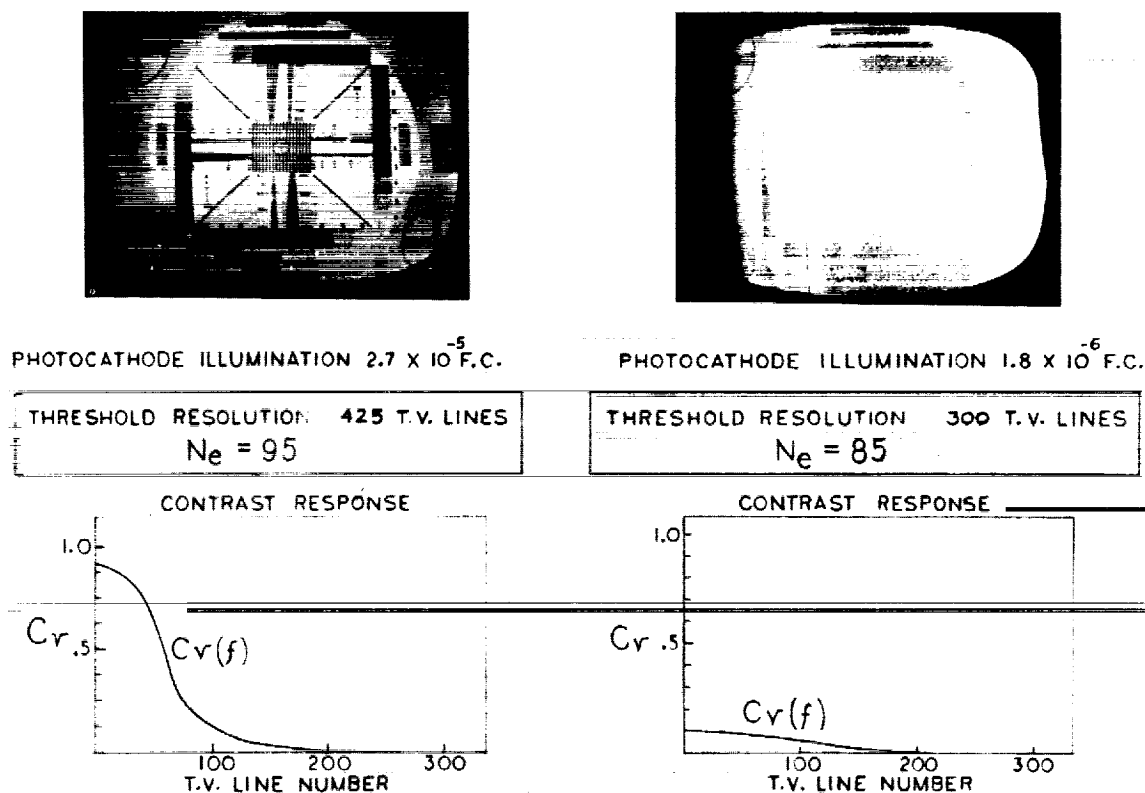
FIGURE 4–8.—Pictorial comparison of various image quality measures.
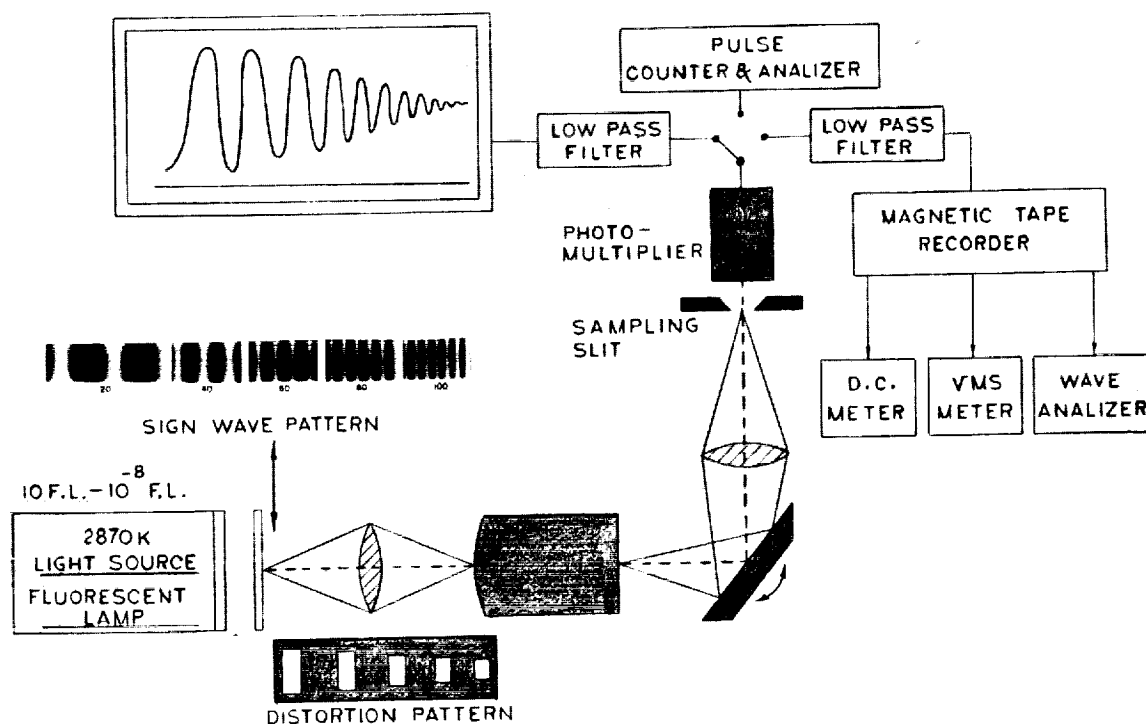
FIGURE 4-9.—Objective image evaluation instrumentation.

Summary

In summary then, the sine wave contrast response function seems to be the best overall objective measure of image quality. It is to be noted that the measure oversimplifies the effect of fluctuation noise on image quality. Certainly, extensive tests are required to fully demonstrate the advantages and limitations of this image evaluation concept for various types of imagery.

Discussion

G. A. MORTON: How do you take into account the arbitrary background level setting in determining the "sine wave contrast response" of an intensifier orthicon?

J. JOHNSON: I agree that scantype electron beam pickup tubes do present a problem in image evaluation since they permit a limited degree of contrast enhancement. However, even for this type of pickup tube, a maximizing of the optical signal to background ratio (contrast) over a band of optical frequencies would seem to be the best overall figure of merit.

W. F. NIKLAS: Has the concept of contrast detail reproducibility, as known in radiology, been considered for image converters?

J. JOHNSON: The problem with the contrast detail reproducibility concept is that it does not allow synthesis of the performance of a number of imaging stages in cascade from the properties of the individual stages. This requires sine wave analysis techniques.

N. S. KAPANY: It is very refreshing to see the concept of "spatial frequency response" come in the evaluation of image intensifiers. However, it would seem to me that the problem is extremely complex.

Before we can assess the information transfer characteristics of a multistage image intensifier, the interaction of the following complex variables must be evaluated:

a. Electron optical aberrations.

b. Phosphor point spread function.

c. Coupling element performance—when a multistage unit is being considered.

d. Spectral and angular distribution of input and output energy.

e. The film characteristics.

f. Properties of lens systems employed.

g. Psychophysiological effects—scotopic and photopic vision, state of adaptation, etc.

5. ELECTRON BOMBARDMENT INDUCED CONDUCTIVITY INCLUDING ITS APPLICATION TO ULTRAVIOLET IMAGING IN THE SCHUMAN REGION

R. J. SCHNEEBERGER, G. SKORINKO, D. D. DOUGHTY, and W. A. FIEBELMAN, *Research Laboratories, Westinghouse Electric Corp.*

Phenomenon of Bombardment Induced Conductivity

Bombardment-induced conductivity effects have been observed and measured by a number of investigators.[1-4] Work at our laboratories in this field was started in 1952 and consisted of measurements on a variety of dielectric materials, each of which was fabricated into a target consisting of the material under study sandwiched between two electrodes. The targets were placed in a demountable vacuum system where they could be bombarded through the thin aluminum electrode by a controlled source of electrons of voltage V_0 from a flooding gun. In the absence of bombarding electrons, the current I through the dielectric due to the polarizing voltage V is negligible. When bombarding electrons of current I_0 penetrate the material, an appreciable fraction of the large number of low energy carriers produced throughout the bulk of the material move under the influence of the applied field and result in a current I which, in some materials, can be orders of magnitude greater than I_0. The ratio I/I_0 is defined as the gain of the target and is a measure of the bombardment induced conductivity.

Applications to Image Intensification

In the well-known vidicon, conductivity in the dielectric (photoconductor) is produced by the interaction of photons with the material. Redington[5] and Rose[6] have shown that quantum yields (conduction electrons per photon) for materials suitable for photoconductive camera tubes with space charge limited dark currents cannot exceed unity with present television standards and acceptable response times. While quantum yields approaching unity have been attained in vidicons, the yields generally obtained in practice are about 0.2. Since the ultimate sensitivity of this tube already has been approached, there is little incentive for further work in this direction. Induced conductivity effects in dielectrics, produced by bombarding electrons (Ebicon principle) rather than by photons (vidicon principle), suggest schemes whereby the practical sensitivity can be increased by several orders of magnitude.

Haine et al.[7] have described an image intensifier for the electron microscope which uses the principle of electron bombardment induced conductivity in a thin film of selenium. Decker and Schneeberger[8][9] have reported on a television pickup tube based on this same principle which has a sensitivity approaching that of the image orthicon. This pickup tube, known as the Ebicon, is simple and rugged and requires a minimum amount of associated circuitry for its operation. It consists of an electron imaging section coupled to a vidicon-like scanning section by an Ebic target which, in addition to permitting integration and storage between scans, provides an essentially noiseless preamplification of the signal before it is fed to the video amplifier. Amplification occurs from the fact that bombarding electrons from the photoemissive cathode of the electron imaging section induce conductivity in the target material.

Figure 5–1 is a schematic of an Ebicon. The target consists of a dielectric layer deposited on a thin film of aluminum on aluminum oxide which serves the purpose of a support and a signal electrode. In operation, the scanning gun electrons, landing at energies below the first crossover of the dielectric, charge the surface to cathode or ground potential. The positive potential applied to the signal electrode provides the polarizing voltage. After the scanning beam charges each element of the insulator surface, no current flows from the signal electrode. When a light image is

Aluminum Film   Insulating Layer

Target

Lithium Fluride Window

Photo Surface

To Video Amplifier

IMAGE SECTION

SCANNING SECTION
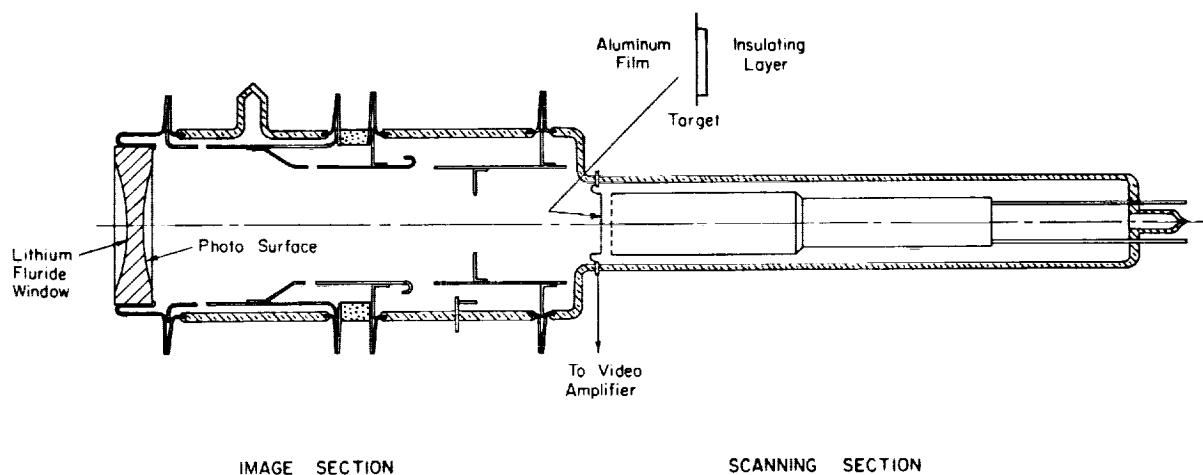
UVICON

FIGURE 5-1.—Schematic of Ebicon-Uvicon tube.

focused onto the photoemissive cathode, the emitted electrons are accelerated and focused onto the target by the electrostatic image section. Here they induce conductivity in the dielectric which causes each element of the scanned surface to act as a leaky capacitor and change from ground potential to some positive potential during one frame time. This change in potential is a function of the intensity of bombardment and thus of the intensity of light falling on the photocathode. Each element will be charged back to cathode potential when touched by the beam. This charging current, which is equal to the bombarding current multiplied by the gain of the target, flows through a resistor from which the video signal is derived.

Experimental tubes have been built with useful target gains of more than 500. If one compares an Ebicon with a vidicon on the assumption that the quantum yield of the photosensitive surfaces are equal in both tubes, the Ebicon will be the more sensitive by the gain factor of its target. A higher signal-to-noise ratio will exist in the low lights than with a return-beam amplification tube like the image orthicon where beam noise increases with a decrease in signal. By not requiring a return beam multiplier, the Ebicon is relatively simple in structure, requires less circuitry than tubes with multipliers, and lends itself very well to an electrostatically deflected and focused scanning section. Theile [10] has shown that under optimum scanning rates and with a

properly designed peaked amplifier, the signal-to-noise ratio obtained with the multiplier type of signal derivation is approached by the simpler method without multiplier for total target charges of the order of some 10^{-7} coulombs. Charges of this magnitude are characteristic of Ebicon targets.

Ultraviolet Imaging in the Schuman Region

A group of ultraviolet sensitive Ebicons (referred to in this section as Uvicons) has been developed for use in rocket and satellite experiments to map the sky with broad-band television photometers in 3 spectral regions between 1,050 and 3,000 Å, and with a slitless spectroscope sensitive between 1,050 and 2,000 Å.[11] This work is known as Project Celescope and has been organized under the Smithsonian Institution Astrophysical Observatory to initiate, design, and operate the Observatory's program of observational astrophysics from space. It is presently operating as part of the National Aeronautics and Space Administration's Orbiting Astronomical Observatories (OAO) program.

Three basic spectral types of Uvicons are being developed with long wavelength cutoffs at 1,500, 2,000, and 3,000 Å. The photoelectric thresholds of BaF_2, CsI, and Cs_2Te photosurfaces (fig. 5-2) are used to achieve these characteristics. A LiF window with a short wavelength cutoff at 1,050 Å is used on all types. All types are identical both electrically and mechanically. Short wave-

28
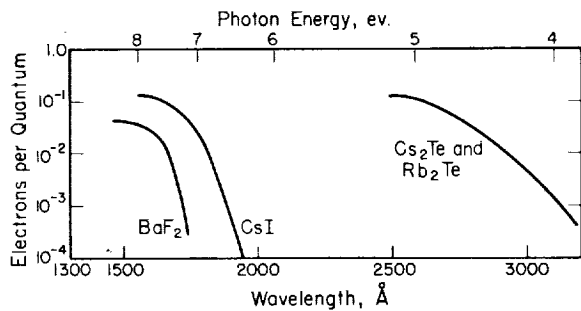
FIGURE 5–2.—Photoelectric threshold of a variety of ultraviolet photosurfaces.

length cutoffs above 1,050 Å can be obtained by the use of suitable optical filters placed in front of the tubes. Transmission properties of various optical materials in the wavelength region of interest are shown in figure 5–3.
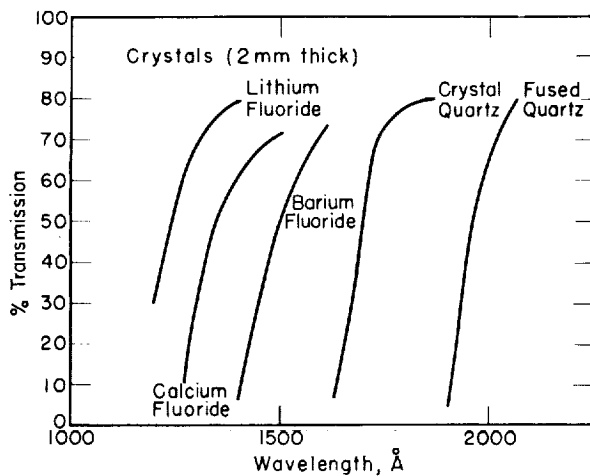
FIGURE 5–3.—Transmission properties of ultraviolet filter materials.

Prototypes have been ruggedized to survive a rocket launch environment. Operable tubes have been built with electrostatically focused and deflected scanning sections employing targets which can be slow scanned. The schematic shown in figure 5–1 is the prototype Uvicon design. The LiF window is ground so that the back surface has the curvature necessary for the object plane of the electron imaging section. The front surface has a curvature such that a sharp UV image is formed on the curved back surface of this LiF lens by an optical system consisting of a concave mirror and this lens. Figure 5–4 is a photograph of one of the Uvicons built to date.
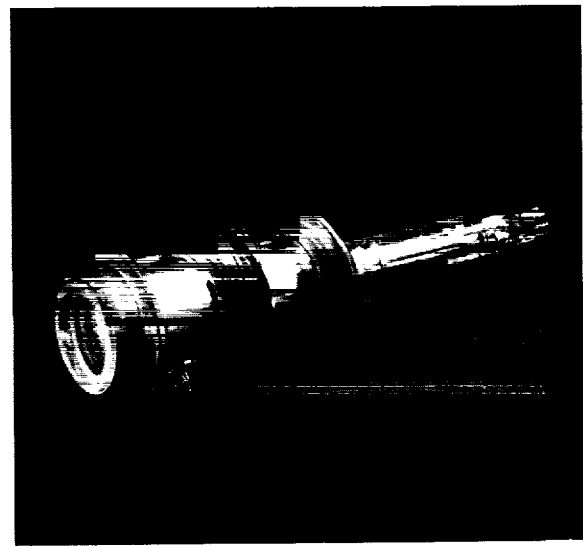
FIGURE 5–4.—Photograph of Uvicon tube.

Photosurfaces

Ultraviolet-sensitive photosurfaces using the previously mentioned materials and reported on in the literature [12] [13] have been of the type where the photoelectrons emerge from the same side that the radiation is incident. Since these photoelectric materials are highly insulating, the transmission-type photosurfaces required for Uvicon tubes posed the problem of obtaining a substrate which is both ultraviolet transmitting and electrically conducting. A 100 Å thick film of either palladium,[14] or nickel, evaporated on the back surface of the LiF window, was chosen because of their ultraviolet transmission properties (fig. 5–5) and its resistance to attack from the AgCl[15] used to seal the window. This layer maintains the fixed potential of the photoemitting surface necessary for imaging the emitted electrons
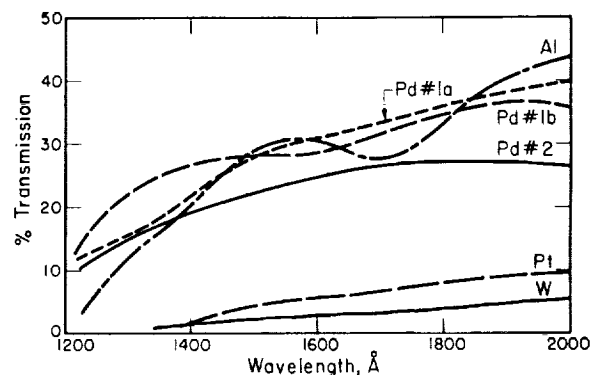
FIGURE 5–5.—Ultraviolet transmission properties of some thin metal films.

29

The semitransparent metallic layers are prepared by evaporating all of a measured amount of either nickel or palladium from a 0.040-inch tungsten-stranded filament. A LiF test blank fastened on the underside of the plate which supports the LiF window is used to check the electrical conductivity of the deposited layer. A film having a resistance of approximately 1,100 ohms between two probes, placed 1 centimeter apart, is suitable for use in the Uvicon tube. The thickness of these films was measured with an interferometer of the type described by Tolansky.[16] Our experience has shown that films of this thickness are necessary to maintain electrical continuity of the film through a 12-hour 350°C bakeout of the tube. Palladium is somewhat more transparent to the short-wavelength ultraviolet radiation than is nickel; however, palladium reacts with the tellurium used in the preparation of a Cs_2Te photosurface, hence it cannot be used as a subsurface for the Cs_2Te photosurface.

The Cs_2Te photosurface cannot be exposed to air and must therefore be prepared after the tube has been evacuated. The nickel substrate is evaporated on the window prior to assembly of the tube. Retractable filaments for the evaporation of a tellurium layer and the subsequent introduction of cesium vapor are manipulated into position through the tube pumpout stem by a small magnet. While the cesium and tellurium are reacting, the photosurface is continuously irradiated with energy from a mercury lamp and the photocurrent is measured. A series of filters transmissive in the UV are inserted between the lamp and the photosurface. By this procedure the formation of the photosurface is continuously monitored, and cesiation is stopped at the proper time. Our experience has been consistent with that of Taft in that overcesiation increased the long-wavelength response of the tube.

The CsI and BaF_2 photosurfaces are obtained by completely evaporating a measured amount of either material from a molybdenum boat. These surfaces may be exposed to air after their formation. Photosurfaces approximately 400 Å thick provide the maximum yield in the spectral region of interest. The thickness of these layers was again measured by the Tolansky interferometer technique.

Targets

The dielectric material used for the target is As_2S_3. The properties of this material, particu-

larly the time constant, depend upon its purity and the conditions of evaporation. Before installation in sealed-off tubes, each target is pretested in a demountable vacuum system. The scanning section consists of a standard magnetic-type vidicon gun. Instead of a photosurface for the source of electrons in the imaging section, a flooding electron gun with a tungsten filament is used. A series of parallel bars in the path of the flooding electrons cast a bar shadow pattern on the target. By deflecting the flooding electrons with a magnet, the apparent source of electrons can be moved, and thus it is possible to move the shadow pattern across the target. The moving pattern offers a convenient qualitative method of observing time constant effects

A quantitative determination of the time constant of an As_2S_3 target has been obtained by feeding the video signal to an A-scope. The trace obtained is shown in figure 5–6. The time for the signal to rise to $(1-1/e)$ of its final value varies from 0.1 sec to 0.2 sec, depending upon the target and its operating conditions. The time for the signal to decay $1/e^{th}$ of its initial value varies from 0.2 to 0.03 sec.
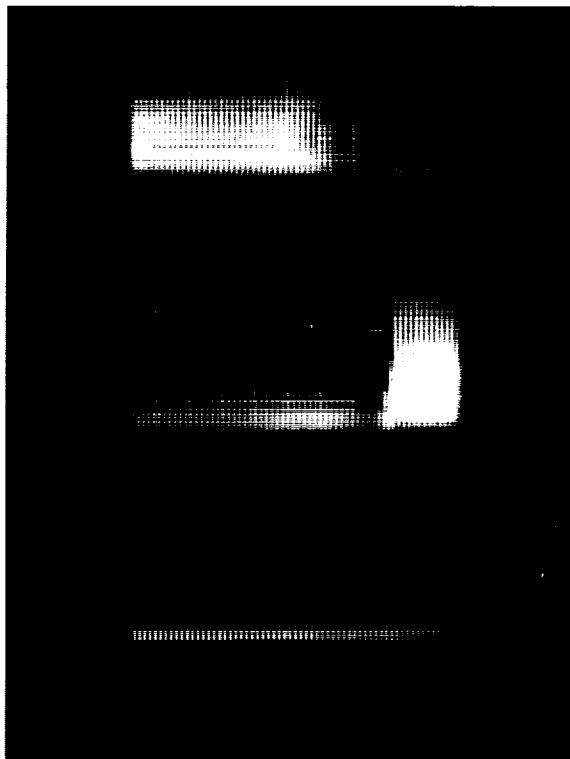
FIGURE 5–6.—Time constant of typical As_2S_3 target—each large reticule division on the horizontal scale is 0.1 second—each vertical trace is a $\frac{1}{60}$-second field.

General Characteristics of the Uvicon

A resolution of 500 television lines has been measured across the useful diameter of a Uvicon tube. This corresponds to 8.3 line pairs/mm at the photocathode surface. Figure 5-7 is a photograph taken from a monitor of a test pattern televised by a Uvicon.
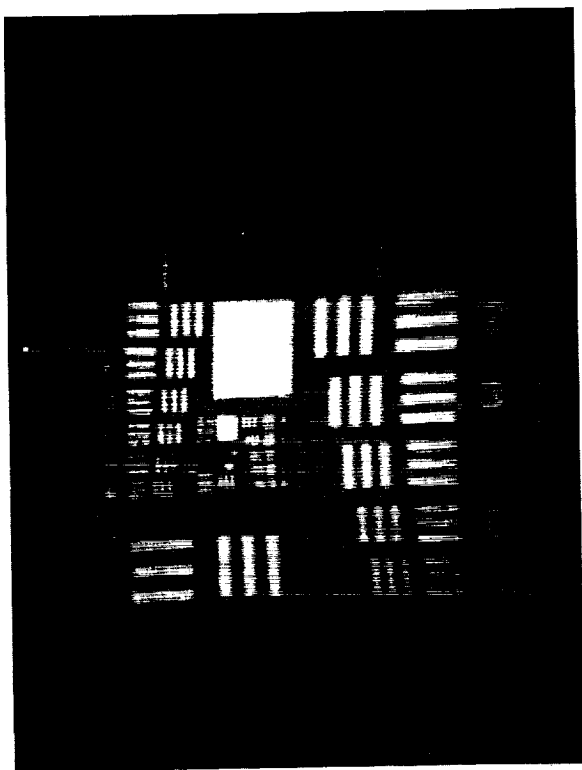
FIGURE 5-7.—Test pattern televised by a Uvicon tube.

Shown in figure 5-8 are target gain measurements obtained from a typical tube while it was transmitting an image. Since the higher gains are associated with the lower bombarding densities, gammas of less than unity are characteristic of this particular material as shown in figure 5-9.

A photocurrent (independent of the energy of the exciting photons) of 4×10^{-13} amps/cm^2 from the photocathode generates a signal equal to the noise when a 5 mc/sec bandwidth, 60 interlaced frames/sec industrial-type vidicon camera is used to operate the scanning section. For photons of $\lambda = 1,600$ Å, using our determination of 5 percent

quantum yield, this is a threshold signal of about 10^{-10} watts/cm^2.

We have made an estimate of the quantum yield of the tube at the peak of its response curve. A thermopile has been calibrated against a tungsten lamp. The thermopile was then used to measure the Zn 2140 Å, Cd 2289 Å, and Hg 2537 Å lines. These sources were then used to calibrate a photomultiplier equipped with a uranium-salt-impregnated window. This photomultiplier was then used to measure the output at the three points stated above of a Seya-Namioka-type monochrometer equipped with a hydrogen discharge lamp. The relative output of the monochrometer (fig. 5-10) was determined by use of a photomultiplier sensitized to the extreme ultraviolet by a coating of sodium
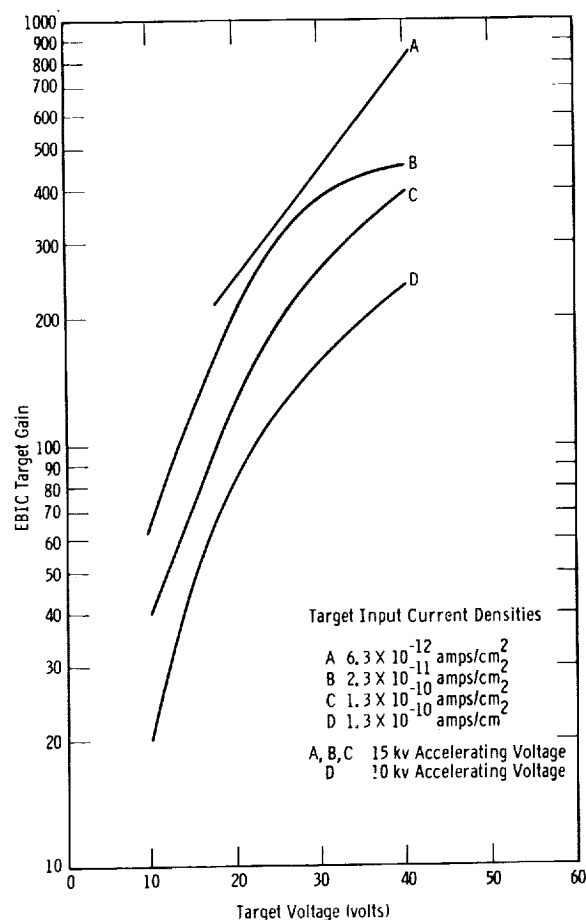
FIGURE 5-8.—Ebic target gain measurements obtained from a typical Uvicon with As$_2$Se$_3$ target.

31
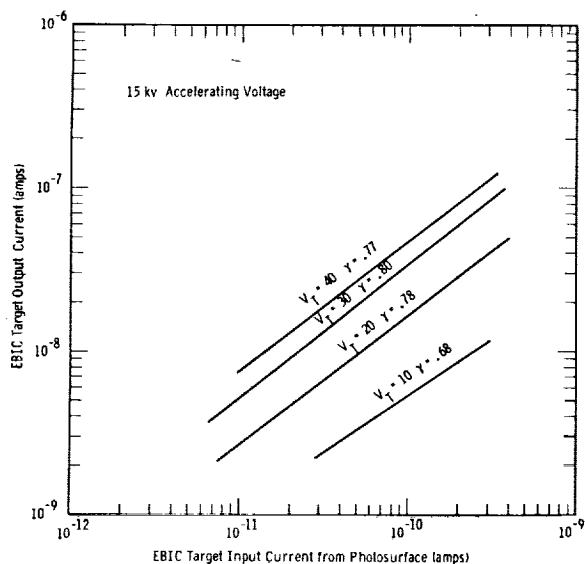
FIGURE 5-9.—Transfer characteristics measured on a typical Uvicon with As_2S_3 target.

FIGURE 5-11.—Trace of the hydrogen spectrum obtained with a Cs_2Te photosurface.

FIGURE 5-10.—Trace of the hydrogen spectrum obtained with a photomultiplier tube coated with sodium salicylate. The spectrometer lead an 1,100 line/cm grating and a LiF window on the exit part.
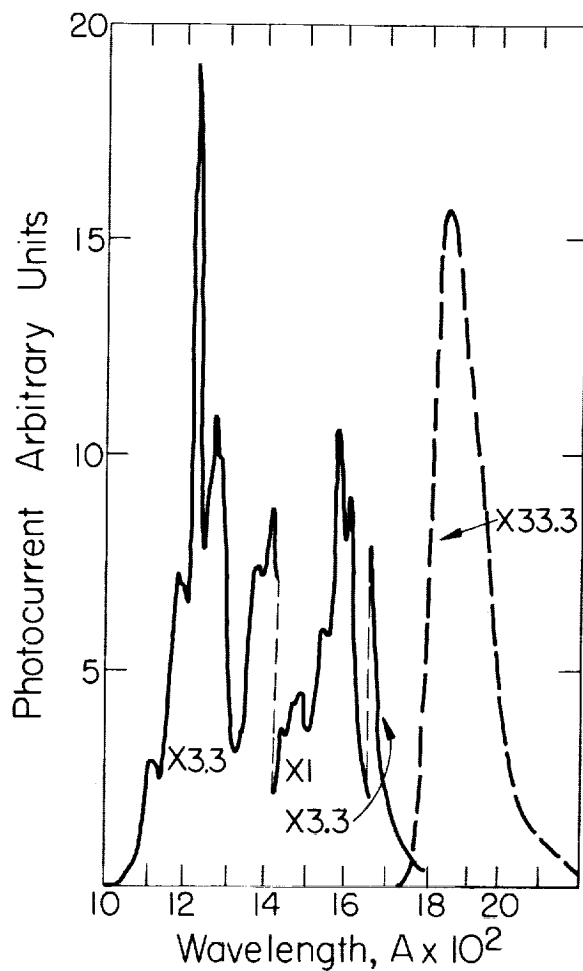
FIGURE 5-12.—Trace of the hydrogen spectrum obtained with a CsI photosurface. The dotted curve was obtained with an air path of 1 inch in order to remove second-order energy.

32
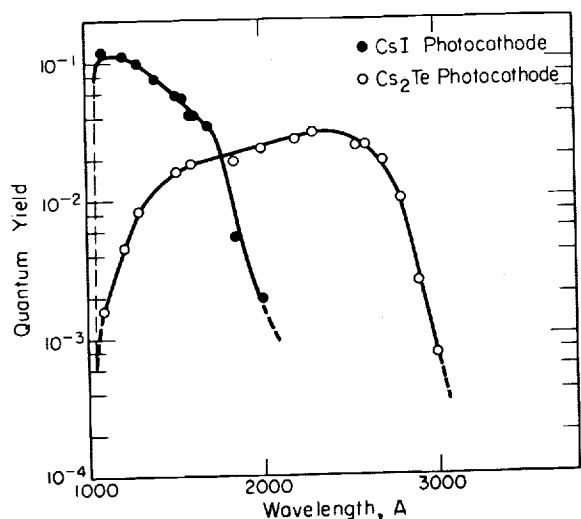
FIGURE 5–13.—Spectral response curves of the CsI and Cs₂Te photosurfaces derived from the data exhibited in figures 10, 11, and 12.

salicylate. Johnson et al.[17] have reported that this fluorescent material has a quantum efficiency approximately independent of wavelength over the range 900 to 2,300 Å. We believe that 5 percent of the photons incident on the LiF window of the tube are effective in providing a signal at 1,600 Å in a CsI-type tube.

The spectral response of the tube has been determined with the aid of a Jarell-Ash, Seya-Namioka vacuum scanning monochrometer equipped with a windowless hydrogen discharge lamp.[18] The photocurrent measured when the Uvicon with CsTe (fig. 5–11) or CsI (fig. 5–12) photosurface was irradiated with the ultraviolet energy obtained from the monochrometer was compared with the current measured with the sensitized photomultiplier as a detector. The spectral response of the CsI and CsTe is shown in figure 5–13.

Discussion

A. B. DOTY: Does the Ebicon have resolution and SNK comparable to vidicon when used in typical television application? Have you any knowledge of planned availability of these tubes?

G. SKORINKO: Resolution will be very slightly degraded especially at the edges due to the electron imaging section.

B. R. LINDEN: Was there a reaction between the target and photocathode? Can the tube be baked at a high temperature? Was there any ion feedback problem in the image section?

G. SKORINKO: None yet observable; however, there is a shield between the target and photocathode for those photosurfaces prepared in the tube. The target limits the bakeout temperature to 100° C. We use a prebake procedure. Ion feedback is not a problem.

W. F. NIKLAS: What limits the resolution in the Ebicon—the imaging section, the target, or the electron beam?

G. SKORINKO: Probably the imaging section.

N. S. KAPANY: You showed us the image of a resolution chart, but did not give the figures. Could you tell us what the resolution of the tube is?

G. SKORINKO: At least 16 lines/mm at the center.

R. AIKENS: What possibility is there of obtaining Ebicon with a S–20 or S–10 photosurface? Where are they available?

G. SKORINKO: Ebicon tubes with these photosurfaces should be available in the first or second quarter of 1962. Contact R. E. Rees at the Westinghouse Electronic Tube Division, Elmira, N.Y.

I. LEVIN: Can you say that those dielectrics which are suitable for your tubes are good secondary-electron emitters?

G. SKORINKO: We have not investigated the secondary emission properties of these dielectrics.

D. A. CUSANO: How does the life of this EBIC, As₂S₃ target, since the target here is under volume bombardment, compare to the life of an image orthicon target? Could you give a value?
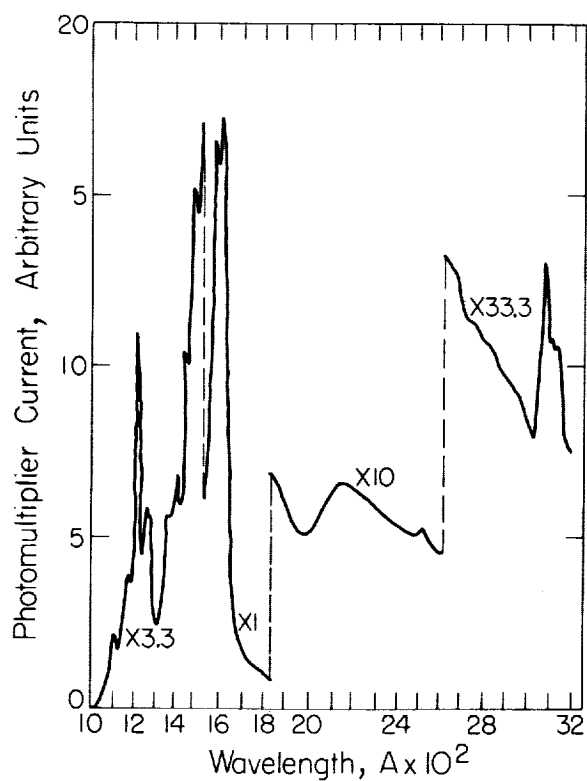
G. SKORINKO: No; only that we have had tubes with As₂S₃ targets for approximately 1 year with intermittent usage, with no observable deterioration.

J. ROESLER: Did you have any other conductive layers beneath the photosurface such as oxides for example?

G. SKORINKO: No.

E. LEVINTHAL: What was UV transmission of nickel substrate?

33

G. Skorinko: Approximately 30 percent at 1,600 Å.

G. G. Barton, Jr.: What is the integration capabilities of this tube and is integration linear?

G. Skorinko: Integration has been observed to be linear; we have achieved very good integration up to 30 sec.

References

1. Pensak, L.: Phys. Rev., vol. 75, 1949, p. 472.
2. Ansbacher, F., and Ehrenberg: *Electron-Bombardment Conductivity of Dielectric Films*. Proc. of Physical Soc. of London, vol. 64, sec. A, April 1951, pp. 362–379.
3. Spear, W. E.: *Electron Bombardment Effects in Thin Dielectric Layers*. Proc. of Physical Soc. of London, vol. 68, sec. B, 1955, pp. 991–1000.
4. Lempert, J., and Klotzbaugh, G.: WADD Tec. Note, 60–307, 1961.
5. Redington, R. W.: J. Appl. Phys, vol. 29, 1958, p. 189.
6. Rose, A.: Helv. Phys. Acta, vol. 30, 1957, p. 242.
7. Haine, M. E., Ennos, A. E., and Einstein, P. A.: *An Image Intensifier for the Electron Microscope*. Advances in Electronics and Electron Physics, vol. XII, 1960, pp. 317–325.
8. Schneeberger, R. J., ad Decker, R. W.: *A Bombardment Image Tube*. Proc. of Conf. on Opt. Pulse Ranging, January 1956.
9. Decker, R. W., and Schneeberger, R. J.: *Image Tube Utilizing Bombardment Induced Conductivity*. IRE Natl. Cov. Record, pt. 3, 1957.
10. Theile, R.: *On the Signal-to-Noise Ratio in Television Storage Tubes*. Adv. in Electronics and Electron Phys., vol. XII, 1960, pp. 277–289.
11. Whipple, F. L., and Davis, R. J.: Astron, J., vol. 65, 1960, p. 285.
12. Phillipp, H. R., and Taft, E. A.: J. Phys. Chem. Solids, vol. 1, 1956, p. 159.
13. Taft, E., and Apker, L.: *Photoemission from Cesium and Rubidium Tellurides*. J. Opt. Soc. Amer., vol. 43, No. 2, February 1953, pp. 81–83.
14. Feibelman, W. A.: Westinghouse Research Memo 71F189–M14–X, 1955.
15. Vogl, T. P., McIntosh, R. O., and Garbury, M.: U.S. Patent 2,966,592.
16. Tolansky, S.: *Multiple Beam Interferometry*. Clarendon Press, Oxford, 1948.
17. Johnson, F. S., Watancebe, K., and Tonsey, R.: JOSA, vol. 41, 1951, p. 702.
18. Hartman, P. L.: JOSA, vol. 51, 1961, p. 113.

6. RCA DEVELOPMENTAL CASCADE IMAGE CONVERTER TUBES*

R. G. STOUDENHEIMER, *Electron Tube Division, Radio Corp. of America*

Introduction

Cascaded image converter tubes are one of the simplest forms of image intensifiers In these tubes, photons having a few electron-volts of energy transfer their energy to photoelectrons which are then accelerated by an electric field to attain an energy of 10,000 or more electron-volts. The electron energy is transferred to a phosphor screen, and then into light, with a net gain of 30 to 100 in radiant energy. Any number of stages may be cascaded by means of proper optical coupling to provide an intensified image.

The wide variety of experimental and scientific applications has made necessary the development of numerous types of cascaded image tubes differing in size and method of electron focusing. Electrostatically focused cascaded image tubes have been reported previously. Three-stage tubes have been made with radiant flux gains as high as 10^5. Recently magnetically focused cascaded image tubes have also been made in an effort to improve edge resolution, reduce distortion, and also reduce the physical size.

General Description of Cascaded Image Tubes

All RCA developmental cascaded image tubes are constructed with modular stages which can be welded together to make one, two, three or four stages, as desired. The outside diameter of electrostatic types is 4 inches; of magnetic types, 3¼ inches or 7 inches. All cascaded image tubes have essentially unity magnification so that the size of the output image is nearly the same as the size of the input image. However, on special request cascaded tubes have been made with a magnification of less than 1.

The electrostatic cascaded image tubes made by RCA are shown in figure 6-1. The largest tube at the top is a three-stage tube, the middle tube is a two-stage tube, and the bottom tube is a smaller two-stage tube approximately 2 inches in diameter. The smaller two-stage tube is an early experimental version and is now obsolete.

The magnetically focused tubes are shown in figure 6-2. The tube at the left is a two-stage tube using a 3¼-inch cathode; the middle tube is a three-stage tube using a 1½-inch cathode. A two-stage version of this smaller tube is also being made for special experimental uses. At the right is shown a three-stage tube using a 3½ inch cathode.

The magnetically focused tubes must be operated within a uniform axial magnetic field. This field can be provided by a solenoid or a permanent magnet. A permanent magnet was designed for the small three-stage tube. This magnet, shown in figure 6-3, is made of Alnico V
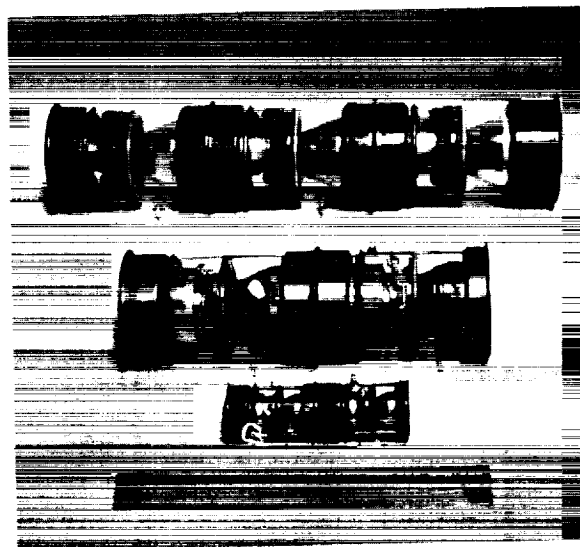
FIGURE 6-1.—Electrostatically focused cascaded image tubes developed by RCA.

FIGURE 6-2.—Magnetically focused cascaded image tubes developed by RCA.

FIGURE 6-3.—Permanent magnet and associated three-stage cascaded image tube.

and is designed to provide the required magnetic field with a minimum size and weight of magnetic material. The axial magnetic field provided by this magnet is shown in figure 6-4.

In some of the magnetically focused tubes, it was found desirable to pot a voltage-divider network around the tube. The voltage divider at the tube reduces greatly the number of leads which must be brought outside the magnet. A tube placed inside a close-fitting permanent magnet requires insulation and shock mounting
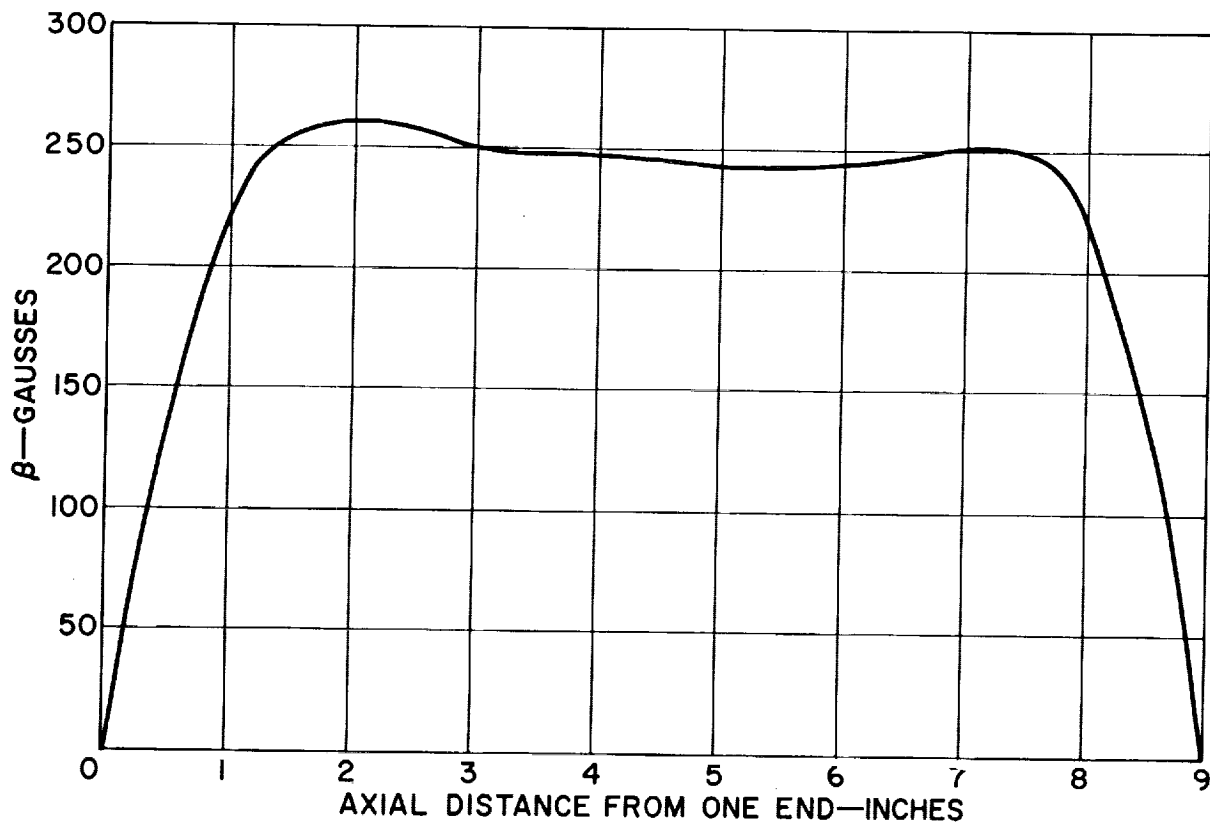
FIGURE 6-4.—Axial magnetic field of focusing magnet.
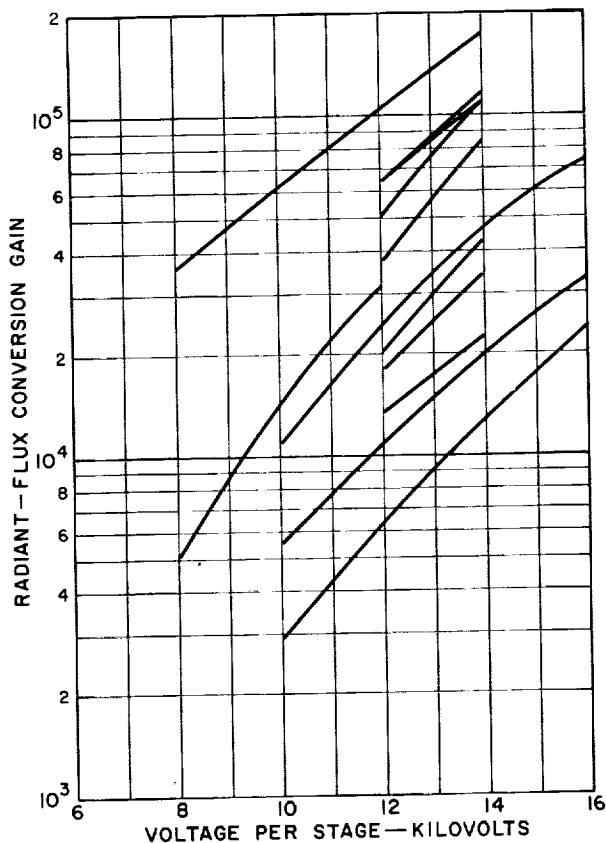
FIGURE 6-5.—Conversion gain characteristics of a number of three-stage electrostatically focused image tubes.

which is ideally supplied by a resilient plastic such as Silastic.

Performance of Cascaded Image Tubes

The performance of cascaded image tubes can be illustrated by reference to the three-stage electrostatically focused tube. The relatively large number of manufactured tubes has permitted the compilation of statistical data illustrating the spread in conversion gain of three-stage tubes (see figure 6-5).

Gain in this tube is nearly independent of the illumination level except at very low light levels, where the photocurrent density becomes very small (about 3×10^{-11} amp/cm^2). At a current density of less than 3×10^{-13} amp/cm^2, the gain of a first stage using P11 or P20 phosphor is again independent of illumination level, but is only about one-half the gain at high current densities. At the very low illumination levels where minimum conversion gain is observed, the current density is so low that the scintillations of individual electrons are observed. The lower gain is probably associated with decreased screen efficiency as the screen excitation changes from a steady state to pulsed (individual-electron) excitation of elemental screen areas. The gain of the second and third stages is also reduced at low current densities, but in some cases not as much as the gain of the first stage.

The screen background at voltages below 10 kilovolts per stage is usually due only to amplified thermionic emission from the first photocathode. The background can be increased ten to a hundred times by a trace of field emission, or by secondary emission from the cathode resulting from positive ion bombardment. As the voltage across the first stage of a low-background tube is increased, the screen background changes from only the individual thermionic electron scintillations to additional brighter random scintillations caused by bundles of electrons released simultaneously from a point on the cathode. At higher voltages, these bright scintillations increase in number and their density pulsates. At still higher voltages, a pulsating discharge appears in which individual scintillations cannot be observed. Some three-stage tubes have operated effectively in certain applications at voltages as high as 20 kilovolts per stage. However, in all tubes operated at this voltage, multiple electron scintillations are numerous; the majority of tubes have such a high background that individual electron scintillations are difficult or impossible to recognize.

Visual resolution of the electrostatically focused cascaded image tube is about 17 to 20 line-pairs per millimeter at the center of the photocathode, and about 8 to 10 line-pairs per millimeter at the edge. Resolution at the center of the electrostatic tube and all magnetic tubes is limited by the screen and the separator between cathode and screen. At the edge, resolution is limited at least partially by the electron optical resolution.

Pincushion distortion is usually present in electrostatically focused tubes, and becomes especially severe when tubes are cascaded. To minimize the magnitude of the pincushion distortion, a 4-inch envelope diameter is used, but only a 1-inch central area of the cathode and screen is used for imaging purposes.

Although the large three-stage electrostatically focused image intensifier has been very useful to demonstrate the feasibility of cascaded image tubes as image intensifiers, its large size and small cathode diameter make it undesirable for many

37
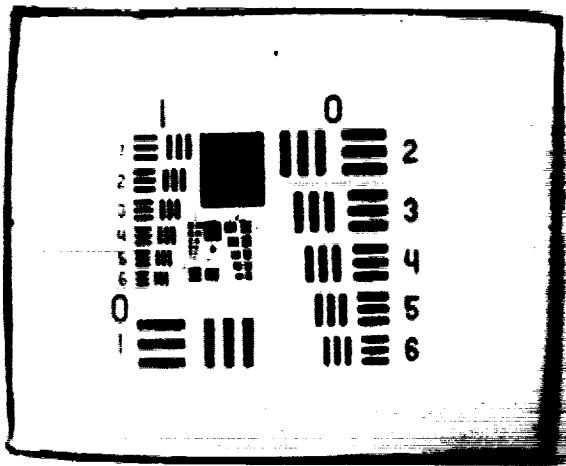
FIGURE 6–6.—Image quality of three-stage magnetically focused image tube.

FIGURE 6–7.—Electron scintillations in three-stage electrostatically focused image tube.

applications. Magnetically focused tubes were developed to increase the useful area of the image and to reduce overall length. Large magnetically focused tubes operating at 20 kilovolts per stage have provided conversion gains as high as 75 per stage. Smaller magnetically focused tubes operating at about 14 kilovolts per stage provide gains of 30 to 40 per stage.

The resolution of magnetically focused tubes is about the same as the center resolution of electrostatically focused tubes, and has the advantage of being much more uniform over the entire cathode. Resolution of two-stage tubes has been measured as high as 25 line-pairs per millimeter.

Magnetically focused tubes are generally afflicted with a type of distortion known as "S" or spiral distortion. Although the distortion can hardly be detected in a single-stage tube, it is observable in three-stage tubes, especially if long straight lines exist in the image (see fig. 6–6).

To reduce axial spiral distortion to a minimum, it is necessary that both the magnetic and electrical fields be axial and have the lowest possible radial components. A uniform magnetic field can be disturbed by magnetic tube parts. The uniform electric field should be formed by either essentially parallel closely spaced cathode and screen, or by a multiple number of accelerating annular electrodes. RCA tubes use a multiple number of ring electrodes for the following reasons:

> 1. The wider spacing of cathode and screen permits higher tube operating voltages and higher conversion gain.

2. Along the bulb wall, conductive electrodes are necessary to shield the electrons from disturbing bulb-wall charges. The voltage difference between adjacent electrodes can be lower with many electrodes than with only two. As a result, field emission is easier to eliminate with many accelerating electrodes.

Electron scintillations can be seen in any of the three-stage tubes. However, two 3-stage tubes must be coupled with a lens in order to photograph the electron scintillations. Figure 6–7 shows the electron scintillations photographed when a faint illumination pattern in the form of an A was projected on the first cathode.

Other Developments

All applications of image intensifiers are not satisfied by the tube developments just described. In particular, image intensifiers for nuclear track imaging require a first stage with a large photocathode for direct coupling to a large fiber scintillation chamber. A special two-stage image intensifier is in development for this application. The intensifier consists of a demagnifying electrostatically focused first stage having a cathode diameter of 8 inches and a P15 phosphor for microsecond image storage. The second stage is an electrostatically focused shutter tube with unity magnification. The first stage has already been developed and the second stage is in the early stages of development.

The first stage is shown in figure 6–8. The cathode faceplate has a thickness of only 1 milli-

FIGURE 6-8.—First stage of a large-window cascaded image tube for nuclear track imaging.

meter to permit coupling to the fiber scintillation chamber by direct contact. With a P15 phosphor, the first stage operating at a voltage of 20 kilovolts has a gain of 15 to 30. Resolution is about 3 line-pairs per millimeter over the entire 8-inch cathode, and pincushion distortion is about 6 percent. Several of these first-stage tubes have been made as a single unit and are now in use by at least two workers using the luminescent chamber to study high-energy nuclear particles.

The large size of the first stage makes it especially sensitive to stray magnetic fields. The earth's magnetic field is strong enough to introduce observable astigmatism.

In nuclear track imaging a delay of about 10^{-6} to 10^{-7} second is needed after the occurrence of a nuclear track, to identify the type of track and to gate the following stage to permit the track to be intensified and recorded. This delay has been accomplished so far by storing the track on a phosphor with a persistence of a few microseconds. Although the phosphor storage is needed, it also has the objectionable characteristics of storing and releasing some energy for periods of time longer than a few microseconds. The long-delayed emission of light reduces time resolution and causes tracks to persist as undesired noise.

This noise could be greatly reduced if the required delay necessary for track identification and gating could be obtained by using a long electron transit time. Transit time was calculated for the nuclear track intensifier by plotting reciprocal velocity as a function of axial distance and making a graphical integration of the area under the curve (see fig. 6-9). The transit time

T is calculated from the equation $T = \frac{1}{v} dx$, where v is electron velocity and x is axial distance from cathode. By graphical integration, $T = 2.3 \times 10^{-8}$ second. This transit time must be increased by at least five times before it can be used for image storage in a nuclear track imaging system. However, studies are in progress on a means of obtaining a longer transit time.

Other workers desirous of photographing faint phenomena are interested in using fiber optics to couple the output stage to the photographic film. Experiments are progressing with the use of fiber optics ranging in diameter from 1 inch to 3½ inches. Initial tests with fiber optics having a numerical aperture of 0.8 to 0.9 have shown a need for an opaque cladding around the low index jacket to absorb scattered light which is not piped. The effect of the opaque cladding is illustrated in figure 6-10 which contains two photographs exposed by contact of the film against the fiber optics output window of an image tube. The fiber optics in each case had a numerical aperture of about 0.85. However, the fiber optics
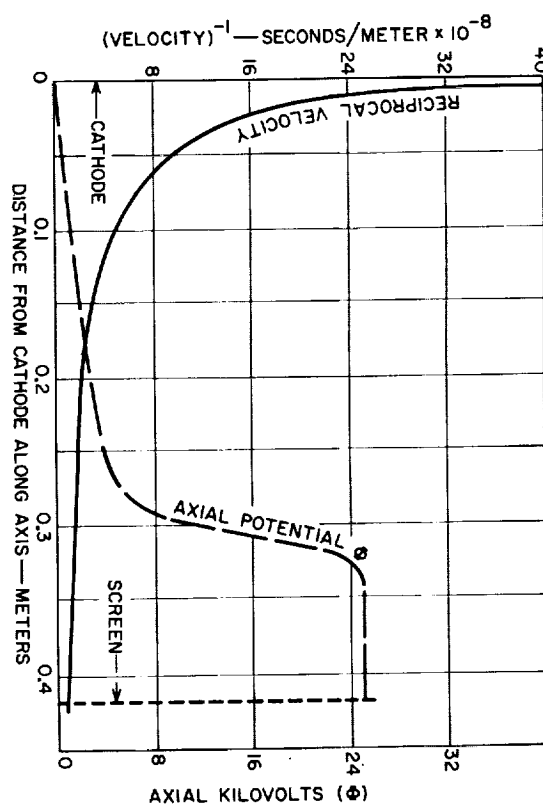
FIGURE 6-9.—Axial potential and reciprocal velocity of large-window image tube.

39
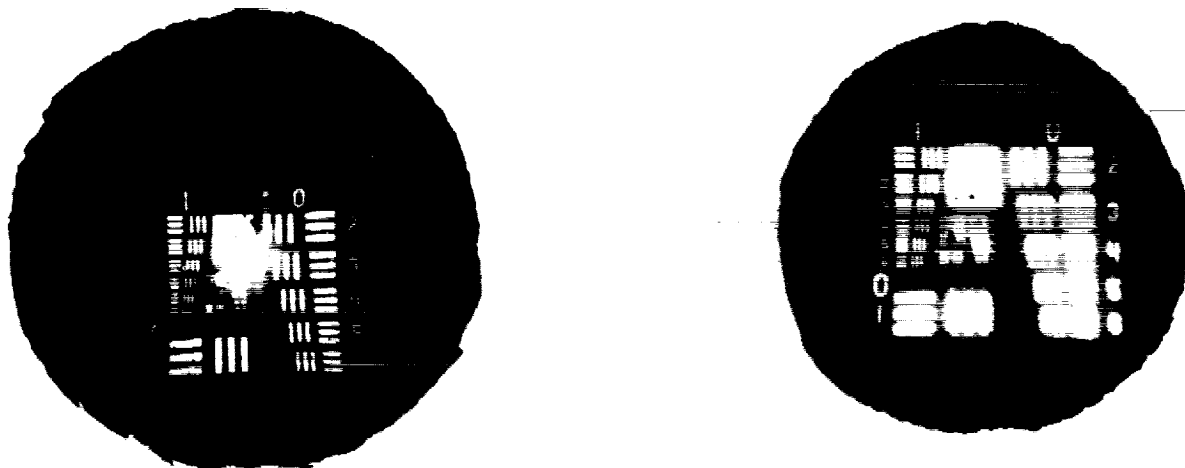
FIGURE 6-10.—Contact picture from fiber optics image tube.

in (a) had an outer opaque jacket, while in (b) the opaque cladding was omitted.

Acknowledgment

The developments described in this paper represent the work of many people. The electrostatically focused image tubes were made under the supervision of Mr. J. C. Moor. Mr. G. N. Butterwick is largely responsible for the design of the magnetically focused image tube. Mr. A. L. Morehead designed the permanent magnets used for focusing the magnetic image tubes. The large nuclear track intensifier tubes were made under the supervision of Mr. R. D DesRochers. Mr. G. W. Francis supervised the work on the fiber-optics image tubes. The work would have been impossible without support from the U.S. Army Engineer Research and Development Laboratories, the Atomic Energy Commission, the Air Force Aeronautical Systems Laboratory, and the Carnegie Institution of Washington. Appreciation is also expressed for the support and encouragement given by Dr. Ralph W. Engstrom and Dr. David W. Epstein in this work.

Discussion

A. B. DOTY: Has any thought been given to using a low gain stage with a vidicon, say RCA 1½ inch?

R. G. STOUDENHEIMER: Yes, the camera tube development group has made both image orthicons and vidicons with fiber optic input windows. These tubes have been coupled to an image tube intensifier stage with a fiber optic output window. Improvements were seen necessary in some of the early-tubes to realize a useful system. These improvements are now being pursued.

F. REPLOGLE, Jr.: When you speak of ultimate image resolution, to what contrast do you refer?

R. G. STOUDENHEIMER: The resolution of image converter tubes is usually stated in terms of the limiting resolution where the contrast is 3 percent or 4 percent.

J. F. ROESLER: Did I understand correctly that you used 1-mil-thick glass to withstand 1 atmosphere? If so, was it reinforced? Was there any special handling of structural design? How did you know exactly when 1 mil of glass was left?

R. G. STOUDENHEIMER: The thickness of the glass in the image tube with the 8-inch cathode is 0.030 to 0.040 inch. Strength to withstand atmospheric pressure is obtained from its radius of curvature (11 inches), combined with a thick rim of glass (0.090 inch) at the edge. The center thin section is obtained by etching from the original 0.090-inch thickness, and thickness is controlled by measuring the ultraviolet transmission at about 3,100 Å.

J. LEMPERT: Please comment on relative resolution of electrostatic versus magnetic image sections.

R. G. STOUDENHEIMER: At present the same center resolution appears to be present in both magnetic

and electrostatic stages. This common resolution limit must certainly be the resolution capability of the phosphor screen which is identical in both types. Ordinarily, resolution of the screen is about 50 to 60 line-pairs per millimeter, but may be more or less in special cases. Evaporated screens of willemite have provided a resolution of over 100 line-pairs per millimeter in small electrostatic stages. The electron image of magnetic types has not yet been studied with such high resolution screens. However, theory predicts approximately equal resolution for the two types under conditions of unity magnification and equal electric field at the cathode. Voltage ripple or magnetic field variations are factors which can degrade resolution in magnetic stages, but are not resolution degrading factors in electrostatic tubes. High edge resolution is easy to attain in magnetic stages, but very difficulty to attain in electrostatic stages.

G. T. REYNOLDS: How were the spots on the A-pattern picture identified as single electrons?

R. G. STOUDENHEIMER: The spots were identified visually by defocusing the first stage. In some tubes, both bright and faint scintillations could be observed in the screen background. The bright scintillations were demonstrated to arise from bundles of electrons released at the first photocathode when they were defocused by adjusting the first grid voltage away from the value of optimum focus. As the scintillations were defocused, the defocused spot broke up into a number of electrons in the original bright scintillation. In the A-pattern illustrated, all scintillations were of the faint type and the appearance of the scintillations was essentially unchanged by defocusing the first stage. Although single electrons could be observed visually from a three-stage tube, only the bright or multiple electron scintillation were bright enough to be photographed. The A-pattern was photographed by intensifying the image further with a second three-stage tube, coupled to the first, with a high-speed lens. The relatively large size of the electron scintillations is due to the poor quality of the coupling lens.

J. A. HALL: Why was halo on the slide showing fiber optics patterns apparently less in the upper left corner? (fig. 6–10(b)).

R. G. STOUDENHEIMER: In the slide the halo in the upper left corner was much less than is seen in paper prints of the same negative. The reason is partly because the slide was made on a high-contrast emulsion which made an area of low brightness appear black. However, halo is also greater around large bright areas than around small bright areas. The area of both the numbers and the lines is greater in the lower left corner than in the upper right corner, making halo somewhat brighter in the lower left portion.

H. SHABANOWITZ: For both the electrostatic and electromagnetic focused tubes, the ratio of overall tube diameter to photocathode diameter was in the order of 2. What is the variation in resolution from center to edge of the tube? Is variation less for the electromagnetic as compared to electrostatic tube?

R. G. STOUDENHEIMER: All the tubes are experimental and changes are continually being made to improve the edge resolution. The three-stage electrostatic tube, made primarily for nuclear track imaging, is 4 inches in diameter and uses a 1-inch photocathode. In this tube, center resolution is about 18 line-pairs per millimeter and edge resolution (never optimized) is about 9 line-pairs per millimeter. The best uniformity which can be reported for a 2-inch electrostatic stage with a 1-inch cathode is a resolution of 64 line-pairs per millimeter at the center of the screen and 44 line-pairs per millimeter at the edge. In the three-stage magnetic tube, with a 1½-inch cathode, center resolution is about 18 line-pairs per millimeter and edge resolution is about 16 line-pairs per millimeter.

7. THE ISOCON: A LOW NOISE, WIDE SIGNAL RANGE CAMERA TUBE*

A. D. COPE, *Astro-Electronics Division, Radio Corp. of America*

Introduction

Since the development of the image orthicon by A. Rose, P. K. Weimer, and H. B. Law,[1] a variety of improvements and modifications affecting the image section have been applied for increasing the amplitude of the potential generated at the target by a particular photon flux.

The problem of concern in the present discussion is the limited fraction of the incident scanning beam which is energetically able to reach a target element whose potential is less than 1 or 2 volts positive with respect to the cathode reference potential. When the output is derived from the return beam, the signal modulation represents only a fraction of the total current. There is also the awkward property that the current maximum occurs when the signal is zero.

An attack upon these scanning limitations by P. K. Weimer resulted in the image isocon.[2] More recently the electron optics of this type tube was examined further under the WADD contracts reported in WADD TN60-123 and TR60-843.

Isocon scan offers an alternative to orthicon return beam scan. The advantages are high signal modulation, high signal-to-noise ratio, the capability to handle an exceptionally wide dynamic range in a single scene, and a signal polarity which gives a minimum output signal for minimum photon input. The cost of these characteristics is increased electron optical complexity. The study being reported here evaluates the performance of image isocon tubes which may be considered as modified image orthicons.

Means for Obtaining Isocon Scan

A camera tube scanning beam is collimated to reduce as much as possible those electrons with energy components at right angles to the tube axis. This beam is accelerated parallel to a uniform magnetic field. The individual electrons follow helical paths with a diameter which is related to the component of kinetic energy at right angles to the electric field.

The orbit time for electrons with a common axial kinetic energy is constant so that periodically along the direction of the magnetic field, all electrons which originated from one point are brought to focus.

The specular reflection of these electrons by a retarding field in the target region does not disturb this restricted energy distribution. However, a sizable fraction of the electrons which strike the target may be elastically scattered. Since the scattering is nonspecular, most of the scattered electron energies will lie outside the restricted energy range of the reflected electrons.

The fundamental problem in the design and operation of isocon optics is to achieve efficient collection of the scattered electrons while discriminating against the specularly reflected electrons of the return beam. This process is complicated by a number of disturbing effects, each of which must be separately and adequately controlled for the achievement of good performance. To the extent that these effects are not removed, they may be overcome by increasing the transverse energy of the reading beam. However, this causes a broadened axial velocity distribution which reduces the ability of the beam to discharge the target, and can impair the modulation and the resolution.

Figure 7-1(a) shows the spatial distribution permitted when the primary beam has barely sufficient energy to land. The scattered electrons will lie within the circular area of diameter $2(d_1 + d_2)$ while the specularly reflected electrons are within the smaller circle of diameter $2d_1$.

Figure 7–1(b) shows the distribution when the primary beam lands with finite axial energy. In this case some of the axial energy may be converted to transverse energy and the perimeter of the scattered electron distribution is correspondingly larger.

It should be emphasized that the distribution of scattered electrons within the indicated boundaries of figure 7–1 is not known. The boundaries are simply limits imposed by conservation of momentum and energy in the scattering process, assuming all the energy and momentum is in the transverse plane after scattering. In actual fact, the distribution may have important structure and much useful information remains unexplored concerning the scattering properties of surfaces.

Figure 7–2 is a schematic diagram of an isocon employing a circular axially centered separation aperture. A tube of this design is operable with orthicon scan when an axially alined scanning beam is used. The separation aperture is sufficiently large for both the scanning and the return beam to pass unhindered.

The tube is designed to operate with the beam having a specific number of helical loops and focus nodes between the exit aperture of the gun and the target. The separation aperture is located midway between two nodal points where electrons of a common point of origin are most widely dispersed according to their transverse energies.

Isocon operation is achieved by perturbing the magnetic field with the alinement coil to produce a fixed transverse velocity component in the beam. Steering fields are provided to make the return beam straddle the edge of the separation aperture at a point where the bulk of the scattered electrons are closer to the tube axis than the reflected electrons. The flexibility to choose the point along the aperture edge at which the separation is to take place allows one to seek the optimum operating condition.

The fringe of the magnetic deflection field must not appreciably overlap the space between gun and separation aperture. Also the steering and deflection regions should not overlap extensively. If these non-time-varying magnetic deflection fields extend into the time-varying magnetic deflection fields, the beam will pass through different portions of the steering field as it scans the target. As the steering field cannot easily

(a) PRIMARY BEAM HAS JUST SUFFICIENT ENERGY TO LAND

(b) PRIMARY BEAM HAS MORE THAN SUFFICIENT ENERGY TO LAND.
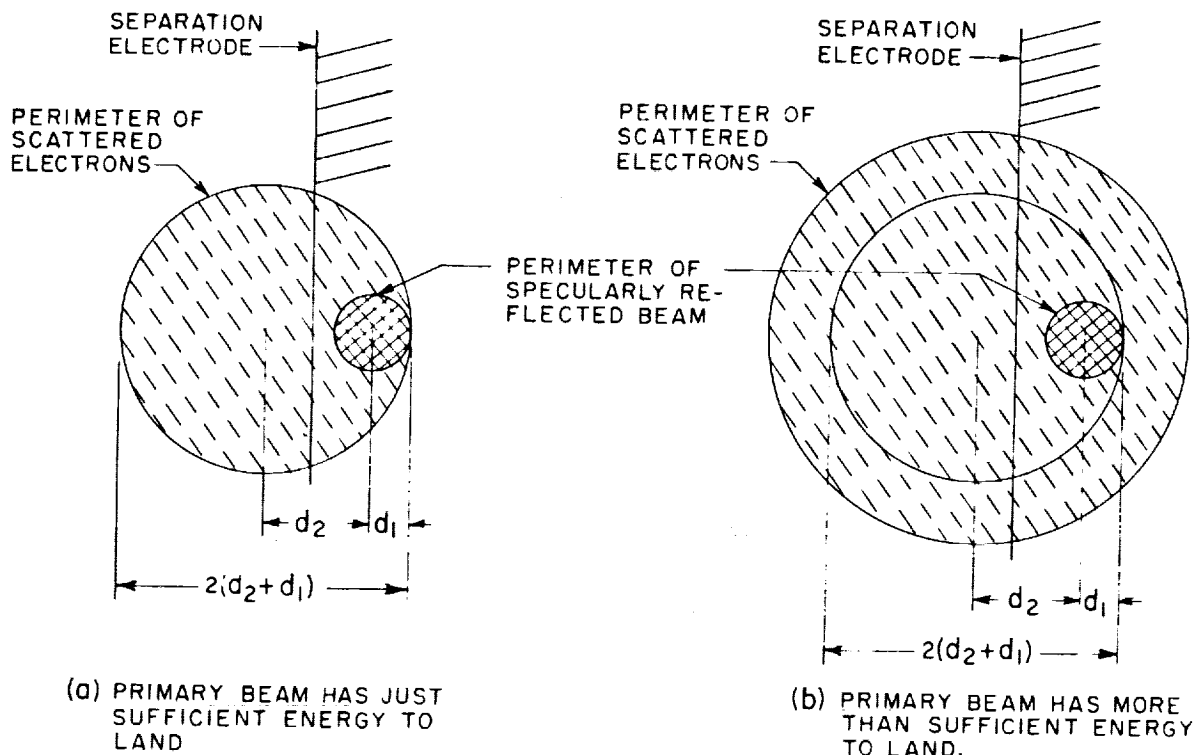
FIGURE 7–1.—Separation of specularly reflected beam from scattered electrons.
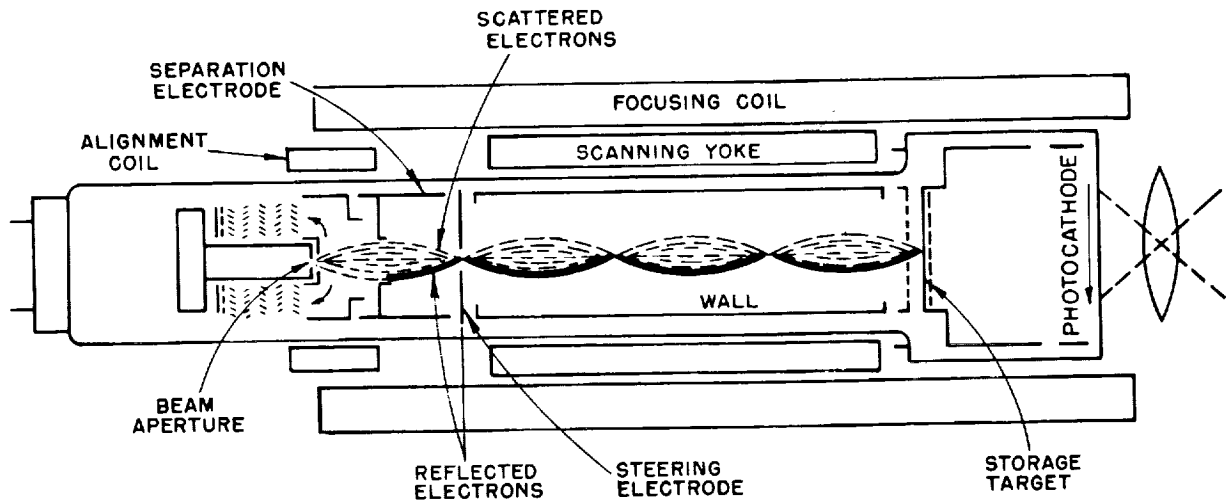
FIGURE 7-2.—Dual operating mode isocon with steering in the plane of a node in beam focus.

be made uniform over a large cross section of the tube, it has proved advantageous to apply steering at a nodal point where the deflection is small.

Orthicon adjustment for this tube is no more complex than for the regular image orthicon. The transition from orthicon to isocon operation takes place without interrupting the output signal, making the setup of this type of isocon simpler than for other designs. The large opening to the electron multiplier is potentially a drawback in that spurious currents can find easy access to the output electrode. However, by minimizing such undesired currents, it has been possible to obtain highlight modulation equivalent to any reported in isocon operation.

Performance With Isocon Scan

To obtain a coordinated set of results for all aspects of the tube operation, measurements were made with several dual operation isocon tubes under various illumination conditions. Measured simultaneously were the photocathode current, stored target signal, target gain, beam modulation, signal-to-noise ratio, and dynamic range. Similar data were taken with standard image orthicon tubes.

Signal-to-Noise Ratio

Shown in figure 7-3 is the signal-to-noise ratio as a function of incident photocathode illumination for orthicon and isocon scan using a dual mode tube with a low target capacitance (0.030-inch spacing between target and collector mesh). The

beam current was retained at the level required for the highlight condition. In addition the value of the signal modulation

$$\left(\frac{\text{Signal current}}{\text{Total output current}} \right)$$

is given as a function of illumination for each scanning mode. Shown in figure 7-4, as a function of illumination, is the secondary emission ratio of the target and the steady-state output current for each mode of operation. Note that appreciable gain from the target is not realized until the output signal has dropped by an order of magnitude from the value at full charge.
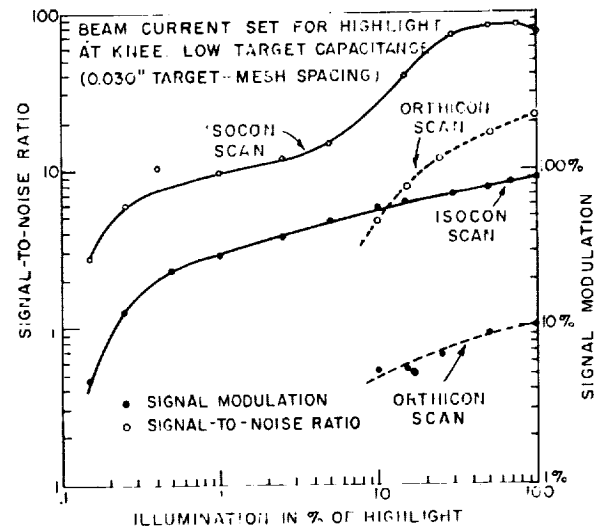
FIGURE 7-3.—Signal-to-noise ratio and signal modulation as a function of illumination for a dual mode isocon tube.

45
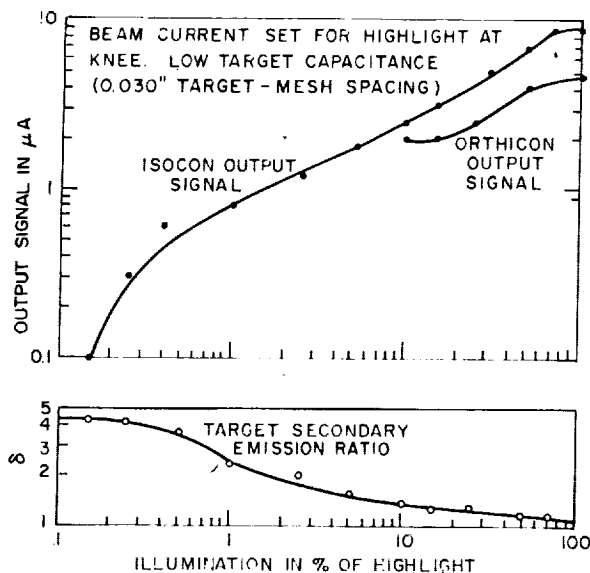
FIGURE 7-4.—Output signal and target secondary emission ratio as a function of illumination for a dual mode isocon tube.

Within this range the gamma of the tube is not unity, but about 0.5. These two bits of information concur in indicating that the stored signal is being distorted by secondary electrons from bright areas falling back on the darker areas of the target.

It is interesting, at a particular illumination, to note the relative magnitude of the signal read at the target and the output signal for each operating mode. The target signal is smaller
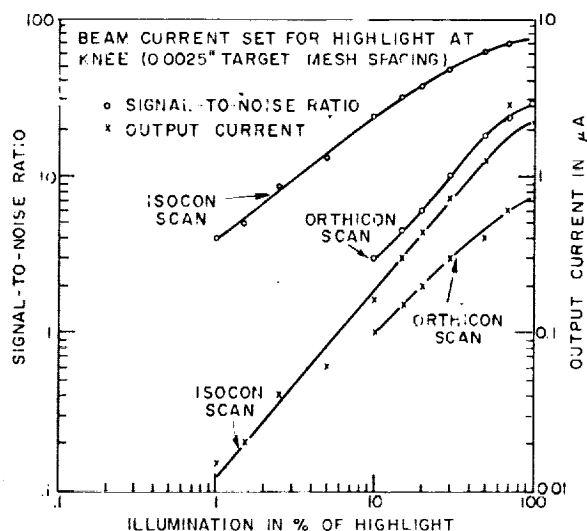
FIGURE 7-5.—Signal-to-noise ratio and output current as a function of illumination for a dual mode isocon.
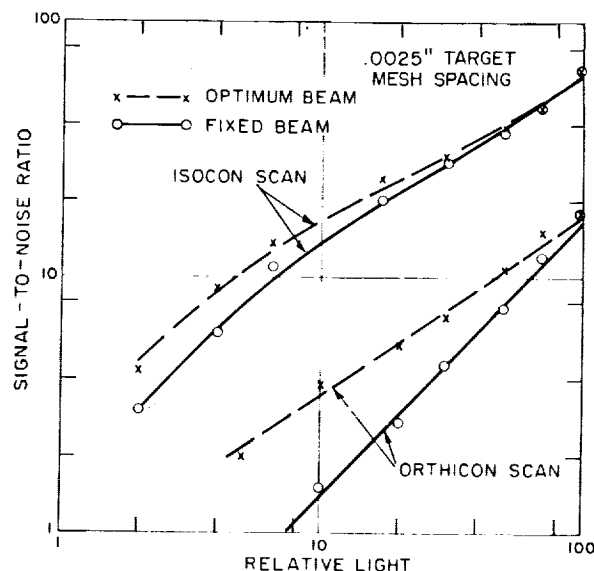
FIGURE 7-6.—Experimental signal-to-noise performance.

in the case of isocon scan because the oblique beam is not driving the potential as far negative as the orthogonal beam. An increased collector mesh potential would help to overcome this. Despite this signal loss at the target, the isocon output signal is larger. This results from the gain achieved in the scattering process, since on the average three incident electrons are scattered for each electron which is retained at the target to neutralize one stored charge.

In tubes with 5820 target-mesh spacing (0.0025 inch), the target secondary emission remains high almost to the point where the target is at full charge. As shown in figure 7-5, output signal as a function of illumination gives a unity gamma. Shown also is the signal-to-noise ratio as a function of illumination for each type of scan in a dual mode tube.

When the beam current is adjusted for its optimum value at each illumination level, the signal-to-noise ratio as a function of illumination in a dual mode isocon performs as shown in figure 7-6. It is seen that the curves for orthicon and isocon scan are essentially parallel. This results from the modulation remaining almost constant when the beam current is optimum, as shown in figure 7-7. At some low value of illumination the modulation drops and decreases rapidly, with further reduction in illumination. The signal-to-noise ratio decreases rapidly in this illumination range and the threshold of operation is at hand. This occurs at a higher
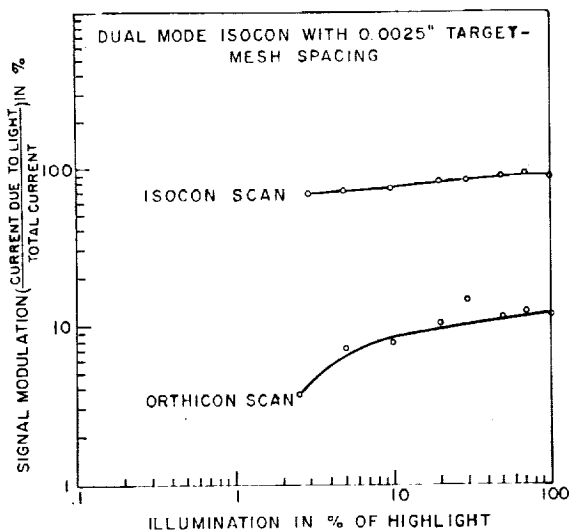
FIGURE 7-7.—Signal modulation as a function of illumination when beam current is optimum at each point.

FIGURE 7-8.—Sine-wave aperature response.

illumination level for orthicon than for isocon scan. The signal-to-noise ratio for isocon scan of a particular target charge has consistently been at least three times greater than for orthicon scan in dual mode tubes.

The S/N performance of a standard image orthicon tube lies between that of the two modes of operation for laboratory-constructed dual mode tubes. At full target charge, the differences are minimum. Signal-to-noise ratios were determined experimentally as the peak-to-peak signal divided by one-sixth the peak-to-peak noise.

Dynamic Range

Curves of signal-to-noise ratio as a function of illumination, under the condition that the beam current required to discharge the highlight signal is employed at all light levels, are given in figures 7-3, 7-5 and 7-6. The dynamic range of the tube is the range of variation in light level which lies between the full target charge highlight and that low light associated with the minimum signal-to-noise ratio which is considered tolerable. For isocon scan there is an order of magnitude improvement over orthicon scan.

Aperture Response

The aperture response for isocon scan with no beam deflection effects is somewhat inferior to that for orthicon scan. When beam deflection at the target is permitted to give a differentiated signal along a given direction (in this case along a horizontal line), the isocon response can be enhanced (fig. 7-8).
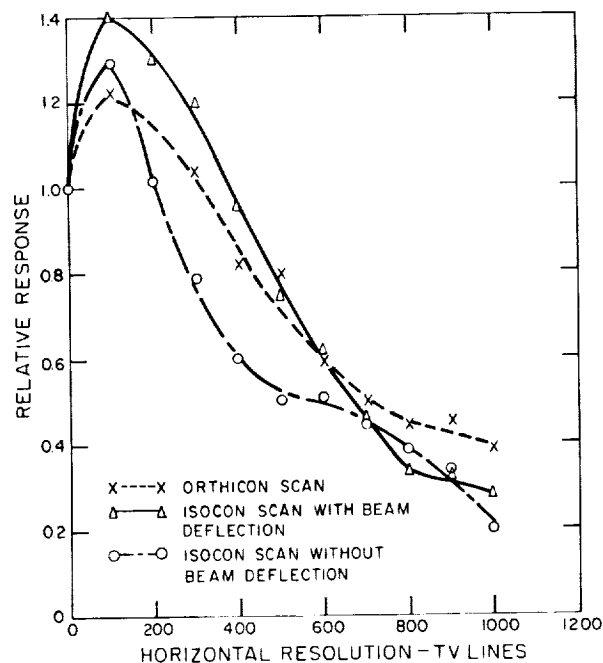
Sine-wave response for orthicon scan of a dual mode tube employing the full target area was measured to be equivalent to a standard image orthicon type 5820. Operating in a 20-Mc video channel, a typical Ne value is 250 lines. In operation near threshold illumination, a difference of 50 to 100 TV lines in favor of isocon scan can be expected.

Special Detection Problems

The effectiveness of the isocon scanning beam in discharging a signal was evaluated by illuminating with a flash exposure and noting the signal amplitude for the first, second, third, etc., scan after removal of the light. The oscilloscope traces of a selected horizontal scanning line in successive frames is shown in figure 7-9. There is seen to be little residual signal remaining after the first scan either for isocon or orthicon scan over a considerable range of light levels.

The isocon scanning limitations for pulse illumination as experienced in scintillation amplifiers may thus be expected to be similar to those encountered with orthicon scan.

Another application with demands which differ from normal scenes is that of astronomical observation. Here the signal consists of bright

47
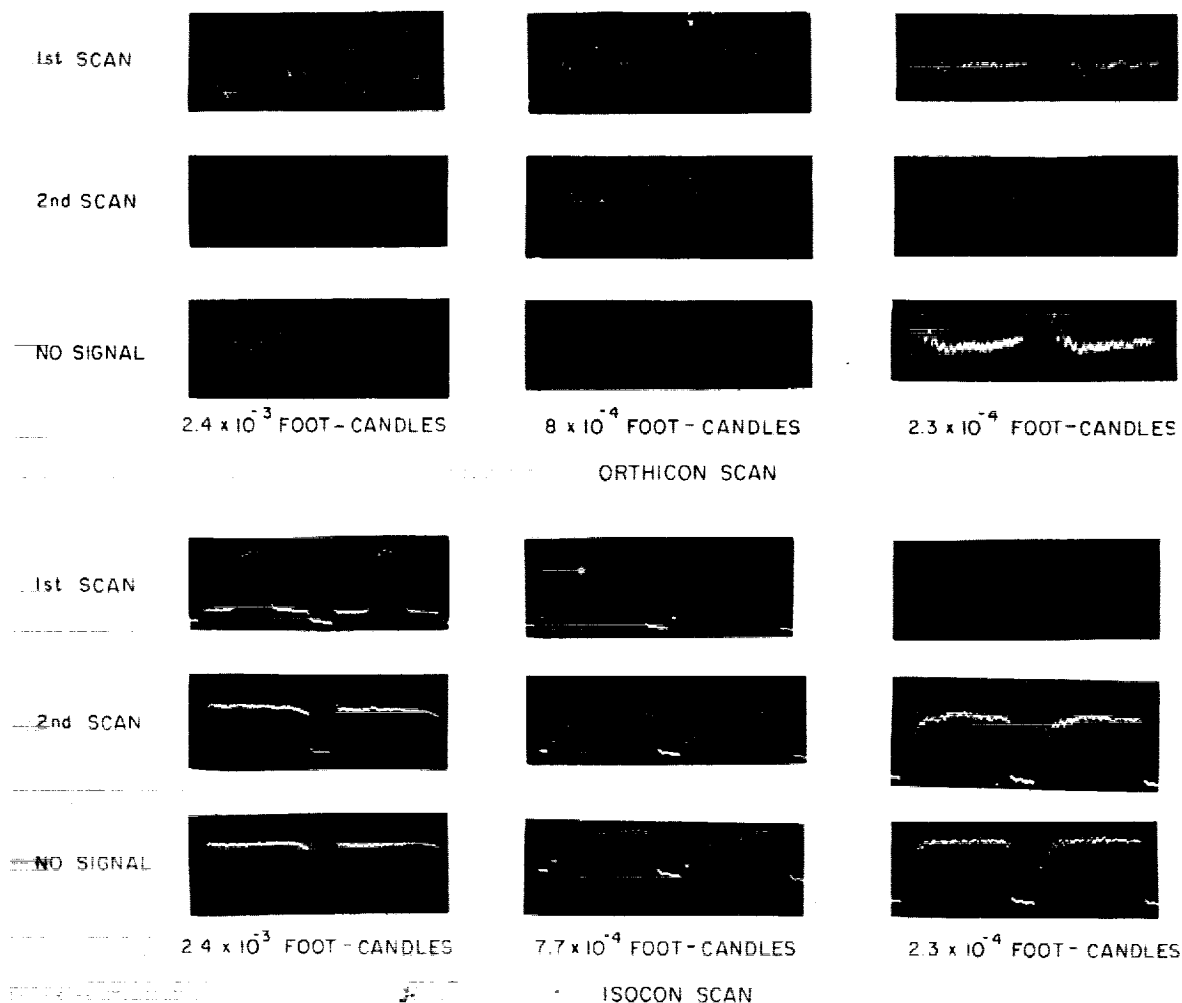
FIGURE 7-9.—Signal erasure of 8.4-millisecond illumination pulse.

points in a dark field. Spreading of point charge concentrations will destroy the ability to detect faint signals in the surrounding region. The low noise attendant with the beam level required to discharge bright point images is an advantage of isocon scan. The familiar dark field background of the image orthicon is absent with isocon scan.

Still another type of readout can be accomplished with isocon scan which is not possible with orthicon scan. Beam bending effects on a low velocity scanning beam can be used to advantage. The beam is totally reflected at the target and only the beam bending occurring at potential steps in the stored signal provides displacement modulation for separating displaced electrons from reflected electrons. A nondestruc-

tive scanning of a signal in the form of a differentiated display is the result.

Displacement modulation has also been achieved by scanning along the recorded track on a magnetic tape. Beam deflection caused by the varying magnetic field present with normal recording levels proved adequate to give a resolvable signal from a wavelength on the tape of the order of 1 mil, a dimension which is comparable with the beam diameter.

Summary

The result of this investigation into the merits of the isocon scanning principle are encouraging. Selective collection of the scattered electrons to form the video signal can be achieved with high

48

efficiency, using the tube designs developed during this study. Indications from the analytical examination of the electron optical problem are that further improvements in the quality of performance should be achievable with careful matching of tube and deflection yoke geometries.

The complexity of adjustment for optimum operation with isocon scan has been reduced and excellent stability of adjustment has been observed.

In comparison with orthicon scan of stored signals of the same magnitude, isocon scan has shown—

1. A factor of 2–3 improvement in signal-to-noise ratio over a wide range of light levels below the full target charge region.

2. At least an order of magnitude reduction in the low-light level threshold.

3. An order of magnitude greater dynamic range in a single scene.

4. Comparable highlight resolution and superior low-light resolution.

Discussion

R. L. ZASTROW: What is the predominant source of noise which limits sensitivity of the image isocon?

A. D. COPE: The dominant noise of the isocon for threshold signals comes from the shot noise of the dark current. As the target potentials, representing the input information, decreases to values smaller than 0.1 volt, the ratio of signal current to total output current drops from 0.9 to 0.01 or less. This limitation occurs at an order of magnitude lower illumination than it would with orthicon scan. The dark current is entirely spurious and represents the departure of the practical from the ideal device. In the absence of dark current, the limiting noise would be the amplified photoelectron noise carried by the scattered electrons.

S. READ, Jr.: What are some of the disadvantages of image orthicon?

A. D. COPE: The major disadvantage of the isocon is its electron optical complexity which makes initial adjustment of this tube more difficult than other camera tubes. The optimum setup is arrived at by qualitative evaluation of the output image. It has been our experience that once the potentials for operation have been established, the performance is quite stable.

H. J. HANNAM: Were the results described for glass target tubes, and was the target processing "normal"?

A. D. COPE: The tube results described were obtained with conventional glass targets and normal tube processings. The single exception is that there was no processing of the scanned face of the target to reduce scattering. For this reason the orthicon performance of dual mode tubes is somewhat less than optimum. Dual mode tubes give, on the average, a factor of 3 greater signal-to-noise ratio for isocon operation than is obtained with orthicon operation. This improvement drops to a value closer to 2 when compared with standard image orthicon tubes.

A. B. DOTY: Would it be possible to trade some of the dynamic range and good S/N ratio for far more lines?

A. D. COPE: Isocon scan is not different from orthicon scan in that the number of lines or the total number of resolved elements in the raster is dependent on the effective beam spot diameter. More elements per raster means less signal per element and increased noise resulting from the increased frequency band. To preserve the minimum beam spot diameter which gives the best possible signal from a small elemental area, one would sacrifice some dynamic range.

References

1. ROSE, A., WEIMER, P. K., and LAW, H. B.: *The Image Orthicon.* Proc. IRE, vol. 34, July 1946, pp. 424–432.
2. WEIMER, P. K.: *The Image Isocon.* RCA Rev., vol. 10, September 1949, pp. 366–386.

8. IMAGE INTENSIFIER ORTHICON TUBES

F. David Marschka, *Electron Tube Division, Radio Corp. of America*

Introduction

The development of the image intensifier orthi-con represents one of the more fruitful approaches to the problem of extending the limit of human vision to extremely low-light levels. It is the purpose of this paper to describe the development of the image intensifier orthicon within the Radio Corp. of America.

An image intensifier orthicon is a television camera tube which utilizes elements of the image converter and the image orthicon. The primary purpose of this combination is to shift or, better yet, expand the operating range to lower light levels with the least possible degradation in performance.

Historically, the idea of image intensification, as it is used in the intensifier orthicon, was evolved in the 1930's. However, it was not until the mid-1940's that electron tube technology had progressed to the point where practical image intensifiers could be made. During the 1940's with the advent of the cesium-antimonide photo-cathode, development work was done on multi-stage image intensifiers at the RCA Laboratories with both ERDL and Bureau of Ships support. In 1951, research in the area of the image intensi-fier orthicon was done at the laboratories under a Navy contract. During the period from 1954 through 1960, the laboratories continued intensi-fier orthicon research under Air Force contracts. Out of this effort, considerable improved one- and two-stage intensifier orthicons were built. By the end of this period, the techniques of intensifier orthicon construction were developed to the point where primary photocathode sensitivity was averaging 150 microamperes per lumen and the intensifier gains of one- and two-stage tubes were as high as 80 and 800, respectively.

In the latter part of 1957, work commenced in the Electron Tube Division at Lancaster, Pa., toward the development of a one-stage image intensifier orthicon. From that time to the present, the major portion of intensifier orthicon development in the tube division has been supported by ERDL. The following describes the Electron Tube Division development programs in this field.

The RCA C73477, C74036, and C74093

Late in 1957, work was initiated on the develop-ment of the C73477 image intensifier orthicon under contract DA44-009-ENG-3254. Figure 8-1 is an outline drawing of the C73477. The tube design was made up of an electrostatically focused tetrode intensifier section; the intensifier element, which was comprised of an aluminized P-11 phosphor (silver-activated zinc sulfide), a thin glass substrate, and an S-11 (cesium anti-monide) photocathode; and the image orthicon section. The storage target of the image orthicon section was a special glass having a resistivity of the order of 10^{12} ohm-centimeters. The primary photocathode was of the S-20 (multialkali) type.

Calculations predicted that a properly processed C73477 would be capable of an intensifier current gain of up to 90, with a maximum limiting resolu-tion of 150 TV lines and a signal-to-noise ratio of 3 (2-megacycle passband) at 10^{-7} foot-candles first photocathode illumination. This perform-ance was based on the use of a 30-frame 525-line TV system. Actual C73477 measured perform-ance indicated gains on the order of 20 to 30, with a limiting resolution of 75 to 100 TV lines, and a signal-to-noise ratio of less than unity at 10^{-7} foot-candles first photocathode illumination. With continued effort under contract DA44-009-ENG-3501, processing improvements augmented tube performance whereby intensifier gains up to 40 and 100 TV lines at 5×10^{-8} foot-candles photo-cathode illumination were realized.

With the independent development of the high-gain storage target, it was possible to carry forward the development of the C74036 intensifier orthicon. This tube is interchangeable with the C73477, but considerably improved in per-formance, due to the addition of a high-gain
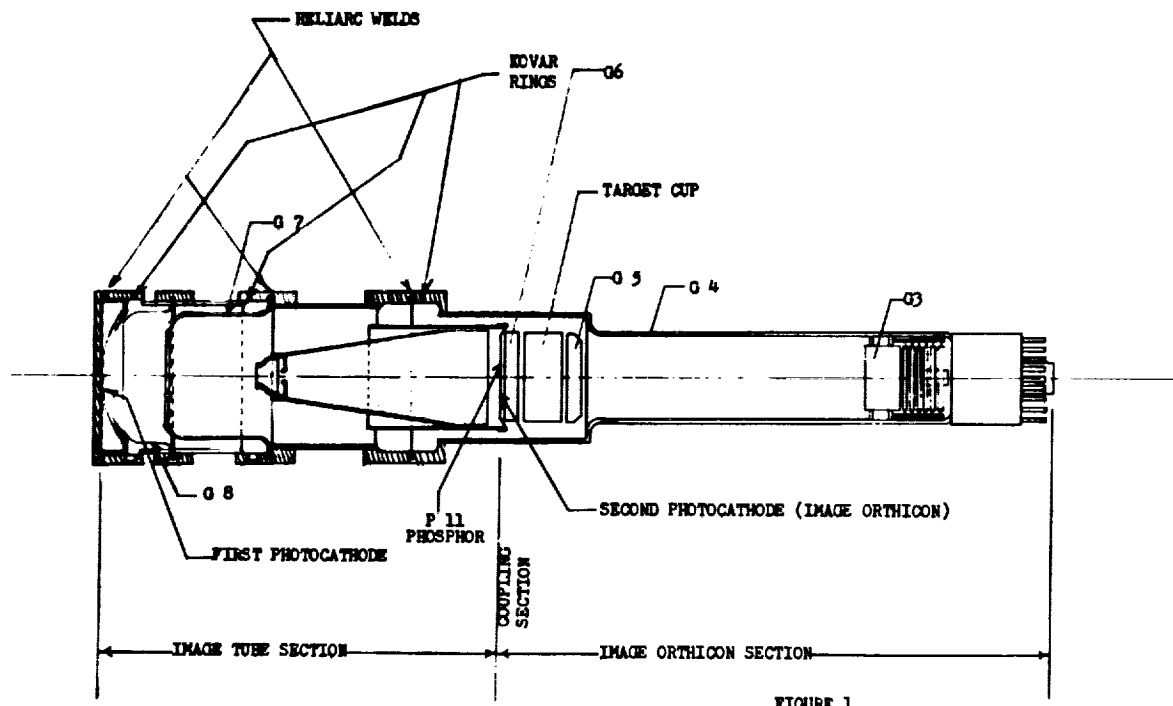
51

FIGURE 8-1.—Cross sectional drawing of C 73477 tube

oxide target and an S-20 second photocathode. Figures 8-2, 8-3, and 8-4 show characteristic performance of the C74036 with respect to resolution, signal output, and signal-to-noise ratio as a function of photocathode illumination. Intensifier current gains up to 90 have been measured on tubes of this type.

Using a rather simplified treatment of signal to noise in the C74036, it is interesting to note that one should very nearly expect photoelectron limited operation. If we assume M photoelectrons per picture element per scan from the first

FIGURE 8-2.—Resolution versus light level of C74036. Light source: 2870°K. Test pattern: High contrast square wave (black lighted). Lens: Kodak television Ektanon 135 mm., f 3.8. Standard TV rates.

FIGURE 8-3.—Signal output versus illumination of C74036. Light source: 2870°K with Wratten neutral density filters. Standard TV rates.

52

photocathode and assign a modest intensifier gain of 50 and a target gain of 10, the signal is $500M$. The noise at the target is $500\sqrt{M}$. Using a beam modulation of 5 percent, the noise due to the scanning beam is $\sqrt{500 \times 20M}$ or $100\sqrt{M}$. The signal-to-noise ratio then is

$$S/N = \frac{500M}{\sqrt{10^4M + 25 \times 10^4M}} = 0.98\sqrt{M}.$$

It has been shown that the signal-to-noise ratio due to the photoelectron emission from the primary photocathode is just $\sqrt{M}$; hence, in the first analysis, it is evident that the C74036 is capable of photoelectron noise limited operation.

Recognizing the need for improved highlight resolution, the C74093 was developed. Figure 8–5 shows a comparison of this tube with the C74036. The C74093 uses a triode image converter section rather than the tetrode design of the C74036. It was expected that the approximate factor of two improvement in resolution of the triode section would carry through in the C74093 with some gain in highlight resolution. Several tubes of this type have been made with comparable low light performance to that of the C74036, but more tubes will have to be made to show any significant gain in highlight resolution. Parallel with the development of the C74036, work was being carried on to develop the C74081

FIGURE 8–5.—Photograph of C74093 and C74036.
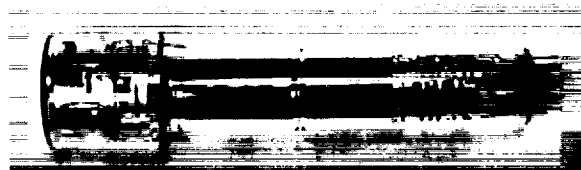
FIGURE 8–6.—Photograph of C74081 2-inch image orthicon.

2-inch image orthicon under contract DA44–009–Eng–4575. Figure 8–6 is a photograph of the C74081.

The RCA C74060

The C74060 is an image intensifier isocon designed around the C74036 and using the dual mode isocon structure described by Cope in (WADD TN60–123 and TR60–843). A feasibility study is being carried on with Air Force support (AF33(616)–7696) utilizing the C74060. The objective is to determine whether the gains in signal-to-noise and dynamic range due to the isocon 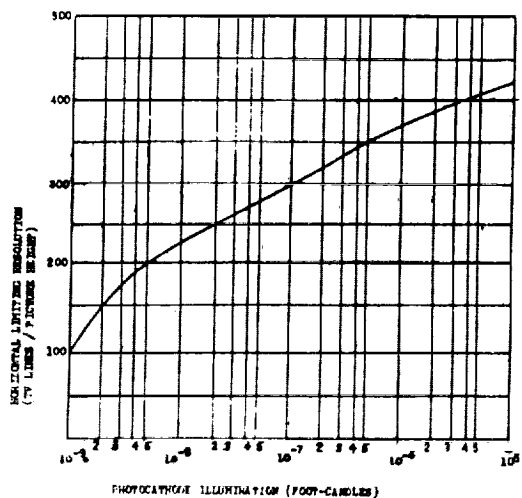mode of operation will lead to a significant improvement in an intensifier isocon design. Tests to determine the scatter gain of various storage targets are being carried out on the same project.

Experience to date indicates that the isocon mode of operation can be achieved with very little change from conventional orthicon operating procedure. At the same time, the expected signal-to-noise improvement and wider dynamic range has been realized in a number of the tubes. Quantitative data pertaining to the scatter gain coefficient of various target materials is not yet available; however, magnesium oxide targets, due to their improved secondary emission gain and storage properties, seem to show the greatest promise.
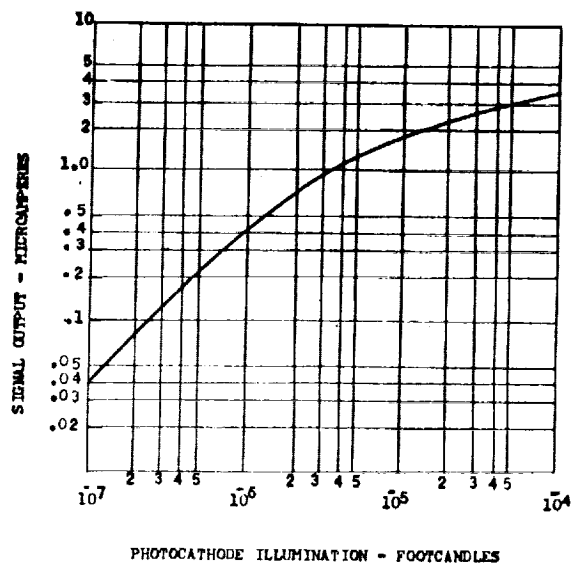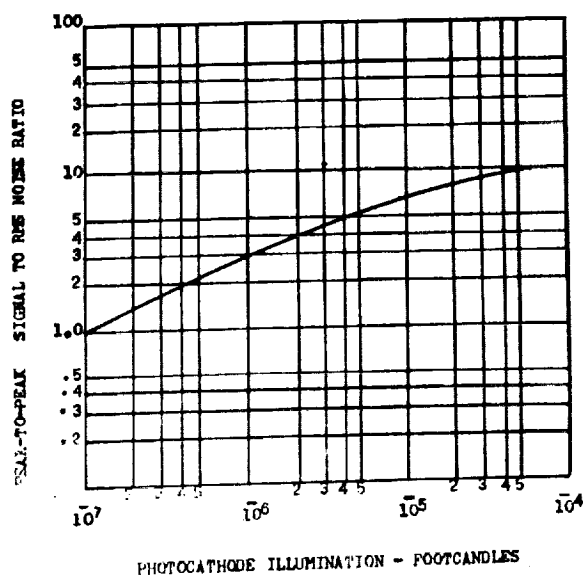

PHOTOCATHODE ILLUMINATION - FOOTCANDLES

FIGURE 8–4.—S/N versus illumination of C74036. Light source: 2870°K with Wratten neutral density filters. Standard TV rates. Bandwidth: 8 MC.
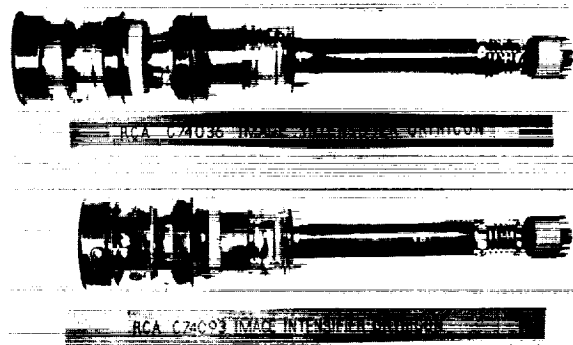
53

Conclusions

The programs just discussed have been very encouraging to date. The electrostatic intensifier orthicons, C74036 and C74093, are pilot production items whose low light capabilities are equal to or better than any known practical design. These tubes very closely approach photoelectron noise limited operation in the range of 10^{-9} to 10^{-7} foot-candles highlight illumination on the photocathode.

The image intensifier orthicon at present can be improved in at least four areas; namely, highlight resolution, distortion and edge resolution, tube size, and processing technology. Certainly highlight resolution could be improved upon by further work on the intensifier element. Work in the field of thin evaporated phosphors should prove highly rewarding in this area. Independent effort on storage targets and electron guns promise improved performance. Problems of cold emission, scintillation noise, and photocathode uniformity (to name a few) are capable of solution with advances in processing technology.

Discussion

J. R. WATERS: Is it possible to modify the C74036 to use a flat glass front window (rather than a convex one) to facilitate lens coupling?

F. D. MARSCHKA: It is certainly possible to use a flat front window in the C74036; however, this would comprise tube performance by causing extreme "pincushion" distortion and loss of resolution toward the edges of the picture area. The convex window is used to partially compensate for these distortions which are caused by the curvature of the electrostatic image field.

F. INAMI: Has anyone used these to look at 0.1-microsecond light flashes? Can deflection plates be placed in the intensifier section to get time versus distance information?

F. D. MARSCHKA: To the best of my knowledge, no one has used an image intensifier orthicon to look at 0.1-microsecond light flashes. Dr. Reynold's work at Princeton is probably the most informative in this respect. Deflection plates can be placed in the intensifier section. They could be used as an additional tool in a number of ways to study short time duration phenomena.

54

9. WESTINGHOUSE WX-4826 ASTRACON: A TRANSMISSION SECONDARY EMISSION IMAGE INTENSIFIER

H. RICHARD GROO III, *Electronic Tube Division, Westinghouse Electric Corp.*

Introduction

The following paper describes the Westinghouse WX-4826, a high gain image intensifier now being produced at the Westinghouse Electronic Tube Division in Elmira, N.Y. The WX-4826 is an image intensifier using transmission secondary electron multiplication (TSEM) to achieve high electron gain. The TSEM method of obtaining electron gain is in contrast to the cascaded phosphor-photosurface multiplying elements now in use in other image intensifiers. A prototype of the present TSEM image intensifier was described at the Image Intensifier Symposium held at Fort Belvoir, Va., in October 1958.[1] This work was described by Art Anderson and Milton Wachtel of the Westinghouse Research Laboratories. The WX-4826 is a continued development of that work by the Westinghouse Research Laboratory and the Westinghouse Electronic Tube Division. The later work was supported in large part by the Engineers Research and Development Laboratory at Fort Belvoir, Va.[2]

TSEM Principle

Before describing the tube, a brief history of the TSE principle would be in order. It was proposed at one time that electrons could be accelerated into a thin foil at high energy and, under the proper conditions of energy and film thickness, secondary electrons could be collected from the opposite or transmission side. Orvin,[3] Lubszynski,[4] and McGee[5] in the 1930's suggested that this principle could be used as a device to give electron multiplication. This idea was not pursued actively because films that were thin enough to allow use of relatively low accelerating voltages, and films that had reasonable secondary yield could not be obtained. Twenty years later in 1953, Ernest J. Sternglass of the Westinghouse Research Laboratories proposed a new direct-view image intensifier tube using a strong thin TSEM dynode structure which gave high yields at low accelerating voltages and overcame all of these early difficulties.[6][7][8] This dynode structure has led to the development of a practical TSEM image intensifier. The early development of the TSEM image intensifiers was accomplished with mesh-supported dynodes, but all current tubes employ edge-supported dynodes which are free of the extraneous mesh pattern.

General Description of the WX-4826

The WX-4826 shown in figure 9-1 is comprised of a compact rugged metal ceramic and glass tube envelope about 5½ inches long and 3 inches in

FIGURE 9-1.—Photograph of Westinghouse WX-4826 transmission secondary emission image intensifier.

55
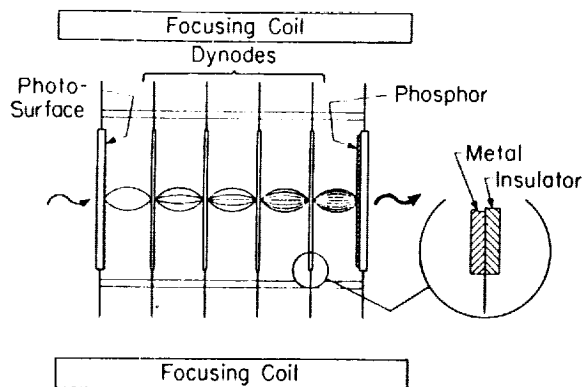
FIGURE 9-2.—Schematic of transmission secondary emission intensifier.

diameter. It contains a photoemissive photosurface, 5 TSEM edge-supported dynodes, and a phosphor. A schematic diagram of the tube outlining its action is shown in figure 9-2.

The input light is focused on the photosurface where it is converted to photoelectrons. These photoelectrons are accelerated to the first TSEM dynode where, on the average, 6 secondary electrons are generated for each primary electron. These secondary electrons are emitted from the transmission side of the dynode and are accelerated to the next dynode where they are again multiplied. After the last dynode, the electrons are accelerated to the phosphor where they are converted back to light for direct viewing or for

photography. Focusing of the electrons between stages in the tube is accomplished by an axial magnetic field provided by a solenoid or cylindrical permanent magnet surrounding the tube.

The photocathode in the present tube is an antimony-cesium (Cs_3Sb) type photosurface processed to give good sensitivity and low dark current. This photosurface is recessed within the tube and is a flipover type. The purpose for this design is to keep alkali vapor, generated during processing of the photosurface, from diffusing throughout the tube. If the alkali vapor is allowed into the TSEM part of the tube, it leads to undesirable background and instability. In addition to this special photocathode processing, the compartmentalized design of the multiplying stages further reduces background by preventing ion and light feedback from stage to stage, while the plane parallel construction allows the image to be intensified with little or no geometrical distortion and relatively little loss in resolution from center to edge. (See fig. 9-3.)

The TSEM dynodes in the WX-4826, one of which is shown in figure 9-4, consist of a very thin supporting film of aluminum oxide, Al_2O_3, on which a conductive layer of aluminum and a transmission secondary emitting material, in this case potassium chloride, KCl, have been deposited. Typical gain characteristics for these TSE films before tube processing are shown in figure 9-5. The maximum electron gain is between 6 and 7

FIGURE 9-3.—Photograph of output image TSE image intensifier Westinghouse type WX-4826 USAF 1951 Resolution Test Chart.

FIGURE 9-4.—Photograph of TSE dynode edge-supported type.

56

DESCRIPTION OF DYNODE:
Support Layer Al_2O_3
Conductor   Al
Secondary Emitter   KCl

DATA MEASURED IN DEMOUNTABLE SYSTEM PRIOR TO NORMAL
EXHAUST PROCESSING.

GAIN

ELECTRON GAIN

PRIMARY ENERGY - KILOVOLTS D.C.

FIGURE 9-5.—Edge-supported TSEM dynode character-
istics.

at 4,000 to 5,000 volts primary energy. In the WX–4826, there are five TSE dynodes. The total gain in completed tubes is shown in figure 9–6. In the WX–4826 electron, gains of 10,000 are readily obtained. The resultant brightness gain and photon gain characteristics of the tube with this electron gain are 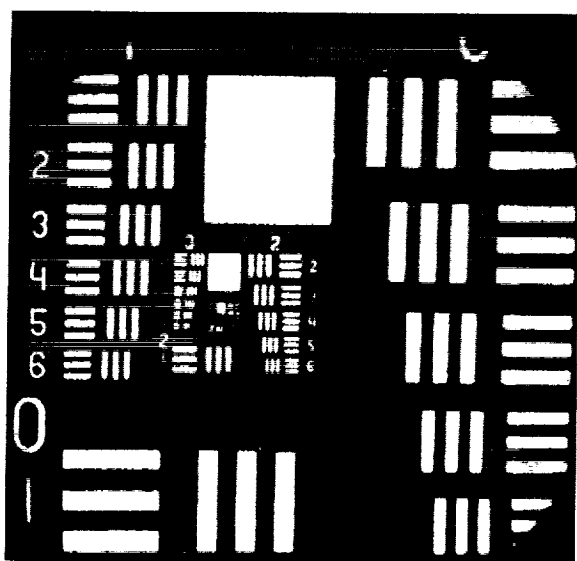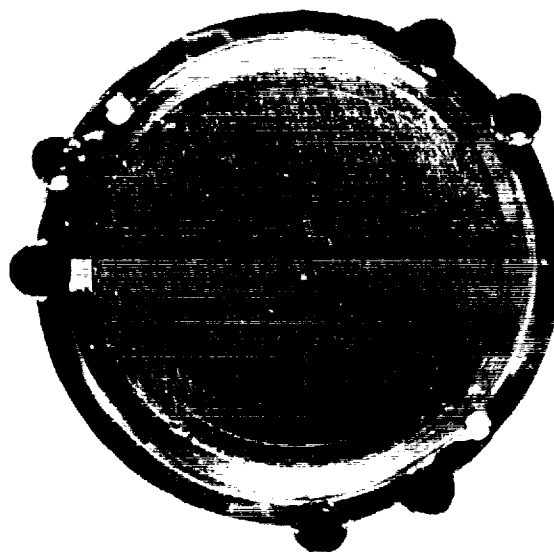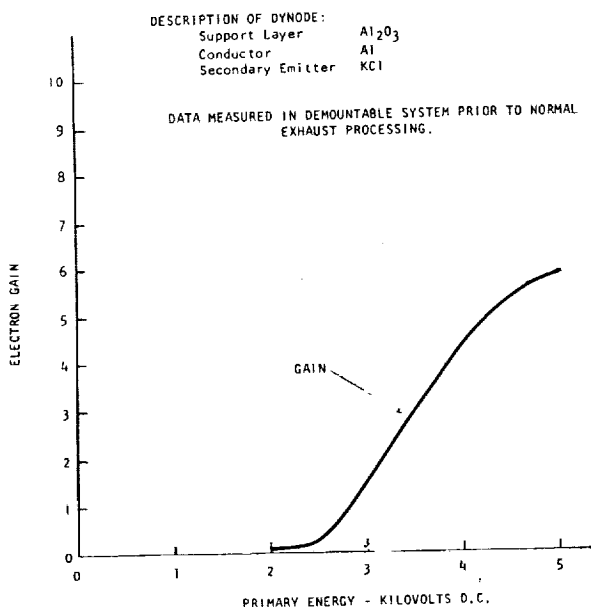shown in figure 9–7. These results were obtained with a type P11 (blue) phosphor. Use of a P20 (yellow-green) output phosphor, which is also available, further increases the brightness gain. With these high gains it is possible to record on film scintillations caused by single photoelectrons. Thus, the tube has the "ultimate" theoretical gain. Photoelectron noise limited images thus obtained appear as shown in figure 9–8.

It is interesting to note that even though the image has passed through 5 TSEM stages and a phosphor stage, it is still possible to obtain image resolution greater than 30 line-pairs/millimeter. At this point, we have been limited by the resolution of our output phosphor. This indicates the resolution capability of single TSEM films is greater than 100 line-pairs/millimeter.

Advantages of the TSEM Image Intensifier

One of the most important advantages of the TSEM approach is that the TSEM film characteristics can be measured prior to use in a final tube. With preinspected dynodes and phosphor,

it is then necessary to make only *one* good photo-surface instead of two, three, or even four, in the same envelope. As image tube engineers know, this can be a blessing in complex tubes. Another advantage is the inherently high-resolution capability of the TSEM films which is now being confirmed by actual observation.

Life

One of the goals of the development work supported by ERDL was to improve the life characteristics of the TSEM image intensifier. Early work gave widely scattered data on life. Recent data in WX–4826 indicate less than 10 percent decrease in electron gain after 10 millicoulombs/cm^2 have been extracted from the last dynode. This is equivalent to an output current of 5×10^{-9} amperes/centimeter^2 for approximately 500 hours.[9] During this same time interval, we have observed an approximate 35 to 40 percent falloff of photo-response in the flipover cathode type tubes. This has been confirmed by other investigators.[10] This falloff may be due to dissociation under dynamic conditions such as will be discussed by Dr. Linden [11] or to attack by products from the dissociation of the TSEM dynodes during operation. This falloff is observed primarily during operation and not during shelf life. To solve this problem we now have developmental tubes in which the photosurface is on the input window and the first dynode acts as a vapor barrier between the photocathode and the TSEM part of the tube. Indications are that this will substantially decrease the rate of photoresponse decay.

Applications

Westinghouse TSEM image intensifiers have been applied to the field of nuclear physics, astronomy, X-ray, and gamma ray studies, high-speed photography, and low light level viewing.

A nuclear scintillation track camera,[12] as shown in figure 9–9, using two Astracons was operated by Dr. Gerhard Goetze and Dr. Helmut Kanter of the Westinghouse Research Laboratories. With this scintillation track camera, Drs. Goetze and Kanter were able to obtain pictures of particle tracks in a NaI crystal. For this application one of the Astracons was gated with 1-millisecond pulses, but gating times less than 1 microsecond are believed possible with suitable pulse circuitry.

In astronomy, Astracons with permanent magnet focusing were tested on the telescope at
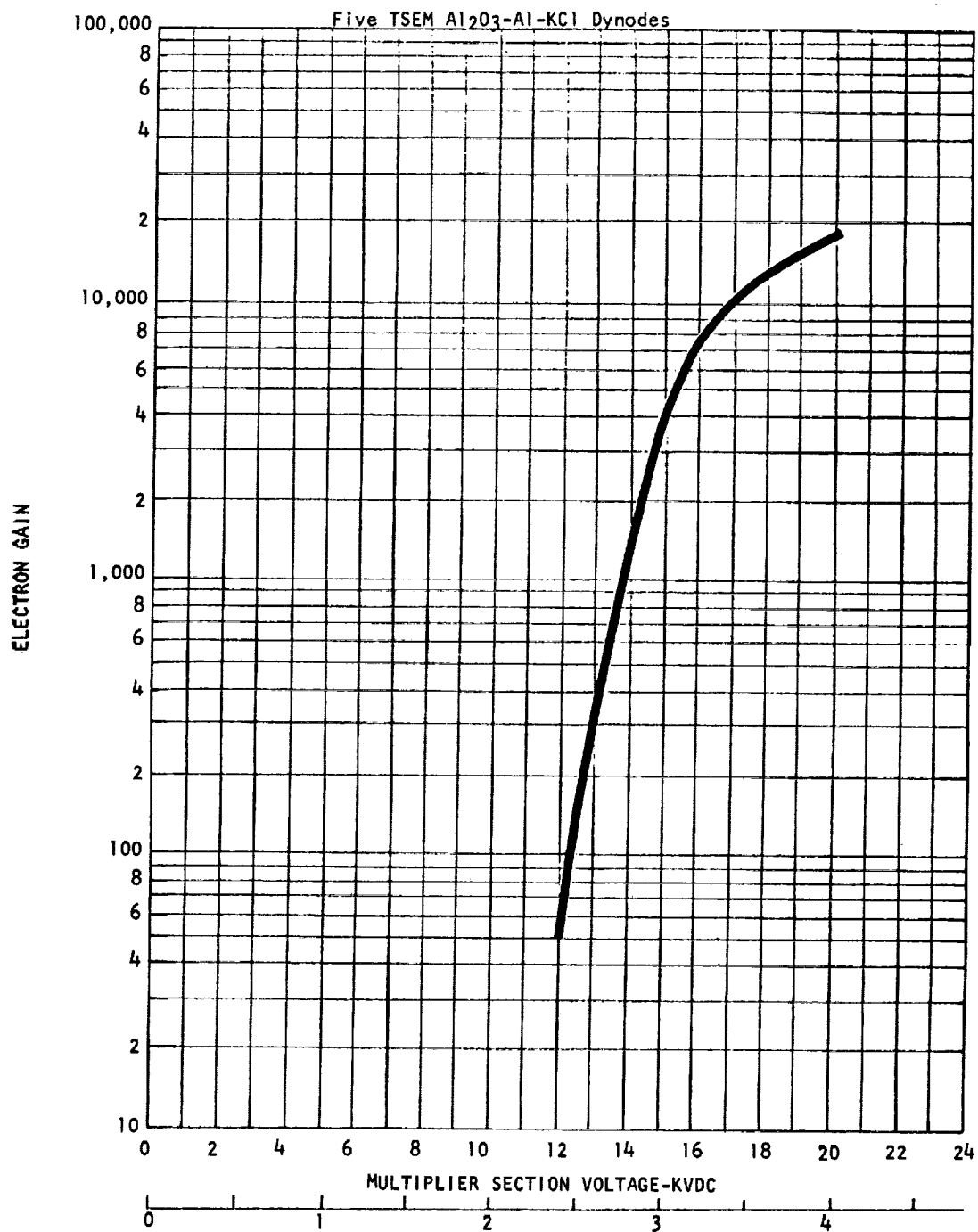
FIGURE 9–6.—Total electron gain characteristics Astracon type WX–4826.
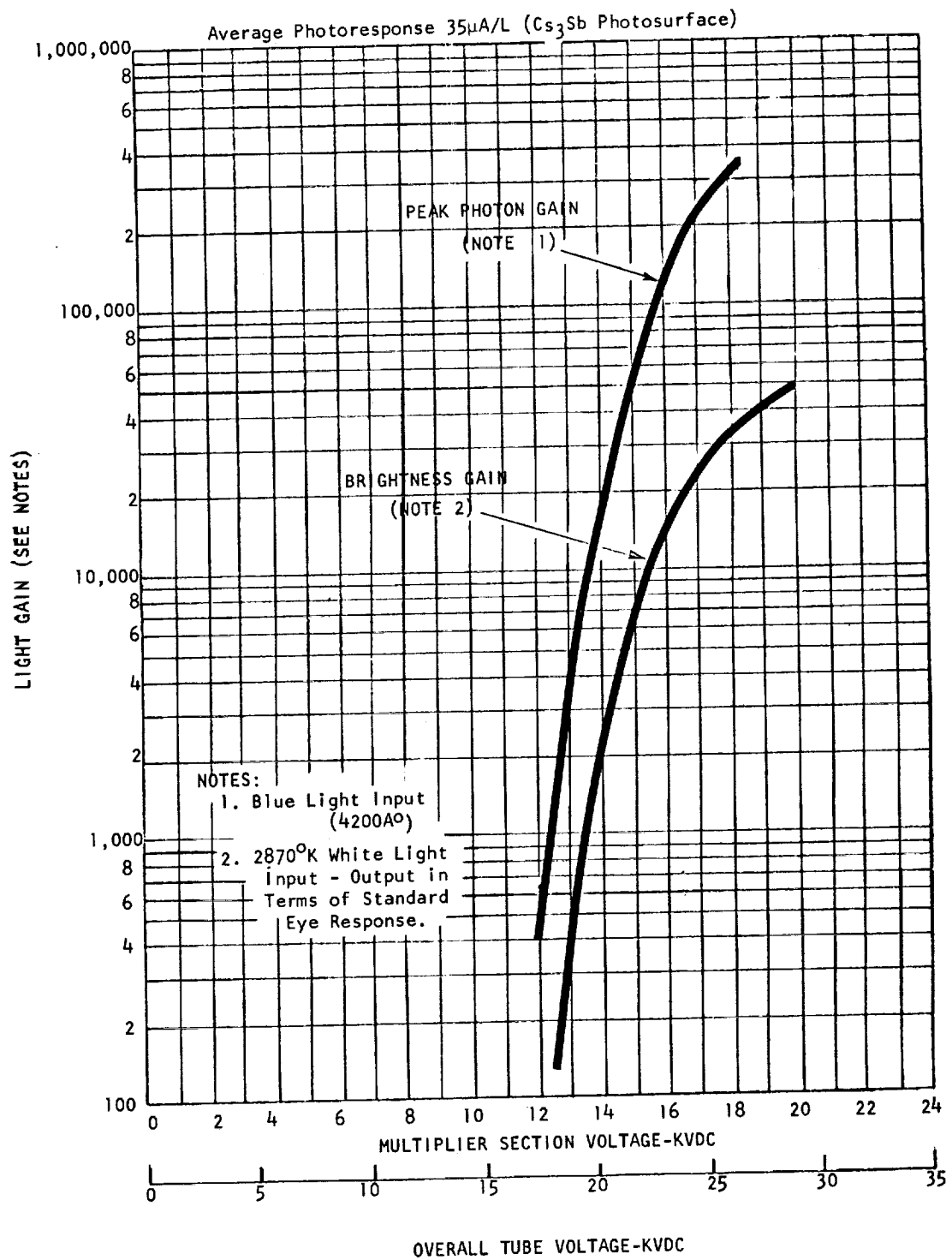
FIGURE 9–7.—Light gain characteristics Astracon type WX–4826.
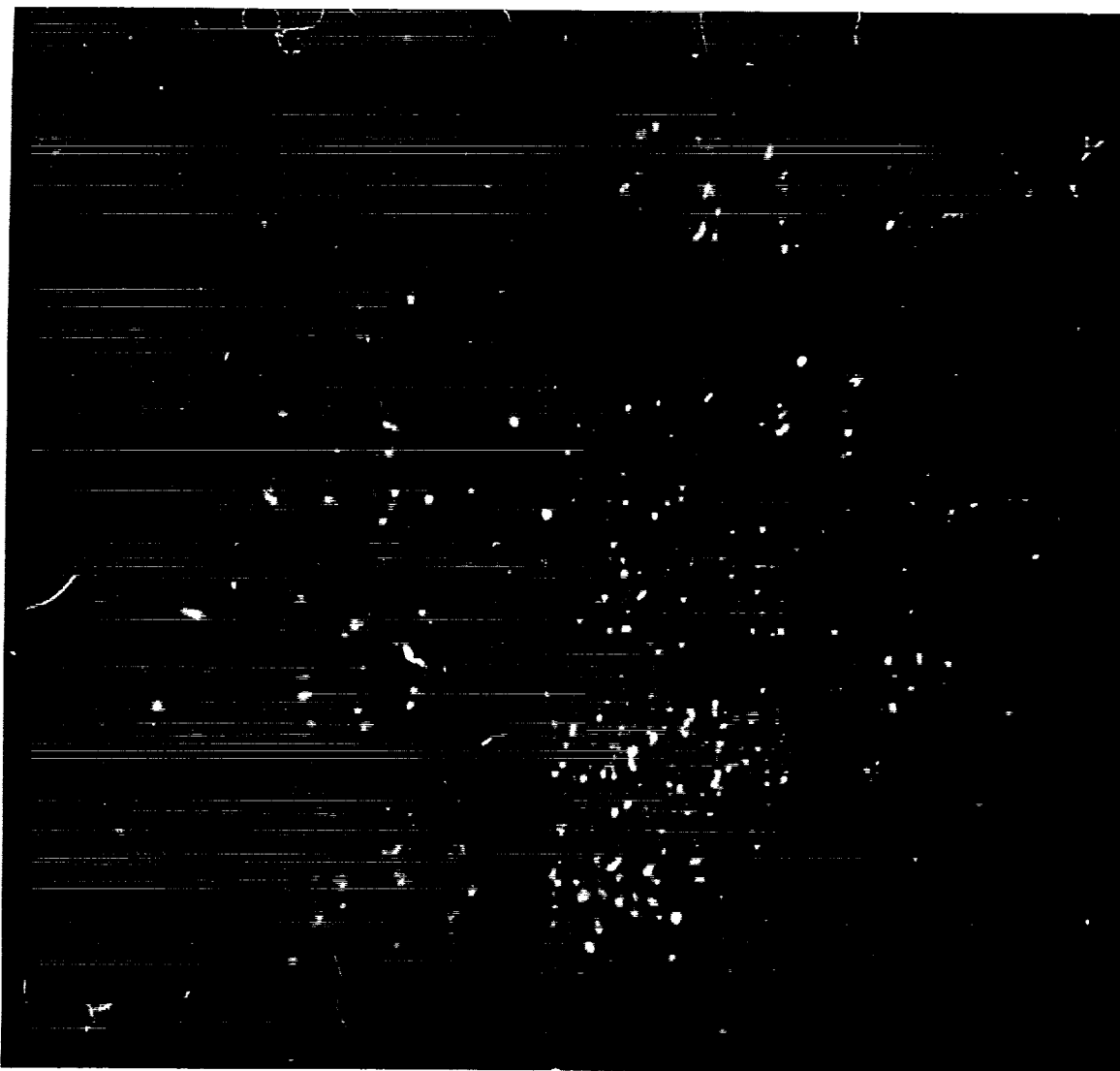
FIGURE 9-8.—Photograph of output image (USAF 1951 Resolution Test Chart). TSE image intensifier Westinghouse type WX-4826—Photoelectron noise limited image at very low light level.

Lowell Observatory in Flagstaff, Ariz.,[13] by Goetze of Westinghouse and Kent Ford of Carnegie Institution. These tests showed a gain in exposure time of 150 times and a total information gain of 3 times over conventional photography.

In the fields of physics, recent Astracons have been used to intensify the image of phosphor screens to allow direct observations of Laue patterns [14] for X-ray diffraction studies, and to show feasibility of pinhole camera techniques for studying the gamma ray radiation pattern of large areas without scanning.[15] The Astracon

has also been used for low light level viewing, but the results are incomplete.

There is one application as yet not pursued for the TSEM section of this tube. This is in the field of photosurface or emission studies. The TSEM part of the tube can be used to give sufficient gain and spatial resolution to allow fundamental studies of such phenomena as thermionic emission from photosurfaces.

Other developments include the addition of fiber-optic input and output windows for improved coupling to other devices, and the use of different photosurfaces for reduced background and in-
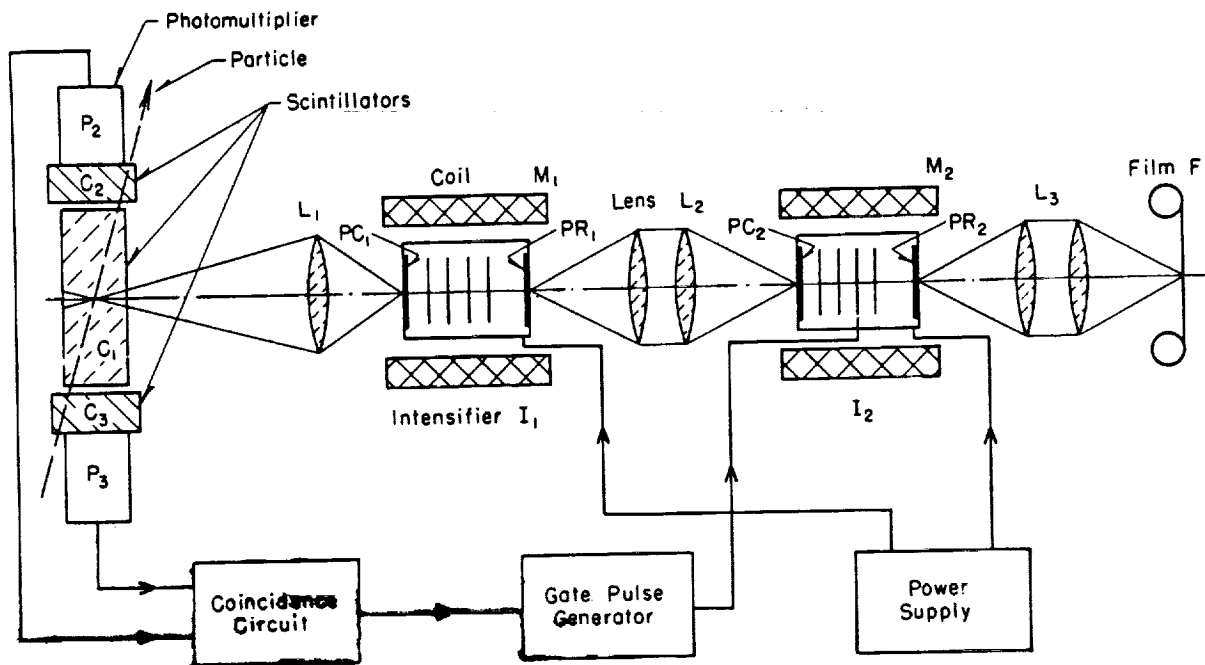
FIGURE 9-9.—Nuclear track camera.

creased sensitivity over the presently used Cs_3Sb photosurface. Larger and/or smaller size designs to accommodate a wide range of applications also appear feasible now.

One of the major new developments in the TSEM image intensifiers, is in the TSEM film itself and will be discussed in a paper by Dr. G. W. Goetze [16] of the Westinghouse Research Laboratories.

Acknowledgments

Discussion

S. READ, Jr.: What performance disadvantages are encountered with TSE tubes?

H. R. GROO: This depends entirely on the application. Since the device is electromagnetically focused, it is necessary to provide a magnetic field either with a permanent magnet, which adds weight to the equipment, or with an electromagnet, which requires additional power and in some cases cooling. The condition of electromagnetic focusing also increases the degree of ripple and regulation required in the high voltage power supply to obtain and maintain optimum focus.

M. ROME: What is the loss in contrast due to the 30-percent high-energy transmission electrons? Why isn't the scattering film to reduce high-energy primary electrons any longer used if the percentage is so high for transmitted primaries?

H. R. GROO: The loss in contrast depends on the type of scene viewed and the light level involved. The factor to consider is not the number of primary electrons which penetrate, but instead the ratio of secondary electrons emitted to the number of incident primaries which penetrate the film. This ratio for typical operating conditions is 20 to 1 or higher, so you can see that the contribution of penetrating primaries is quite small. Furthermore, since the magnetic focusing field is so large (500-600 gauss), the penetrating primaries are well constrained. The scattering layer is not used because it did not improve the performance of the dynode appreciably.

W. F. NIKLAS: What are the maximum contrast, maximum life, maximum cathode loading? Is electrostatic focus possible?

61

H. R. GROO: *Maximum contrast*—Depending on the input scene, the light level, and the exposure time, it is possible to achieve nearly 100 percent contrast in the output image.

Maximum life—The maximum life depends, of course, upon the definition of "life." The present tube life is limited by the decrease in photocathode sensitivity during operation. Some data on this subject are reported in the Final Report, USAERDL Contract DA–44–009–ENG–4531. Life is of the order of hundreds of hours at moderately low light levels. New designs in which the photosurface is isolated from the dynodes are expected to have much longer life.

Maximum cathode loading—This has not been determined.

Electrostatic focusing—This is possible, but would result in much loss of resolution except on axis. Proximity focusing is being investigated now. The high-gain dynodes discussed later by Dr. Goetze of the Westinghouse Research Laboratories may be the answer to conventional electrostatic focusing with TSE dynodes.

W. T. POWERS: Will cooling extend the tube life?

H. R. GROO: No data are available. The life should be quite adequate for most astronomical applications now.

G. T. REYNOLDS: Have you made any quantitative measurements of the fraction of single electrons leaving the photocathode that can be recorded at the output?

H. R. GROO: We do not have such data yet. I would like to discuss the problem with you later. Because of statistics at the first dynode, some photoelectrons will not be multiplied at all. How large this number is, we do not now know.

A. B. DOTY: Has the possibility of using these intensifier tubes with a vidicon been considered? (The application of interest is such that illumination typical of TV studios can be supplied but not enough to obtain acceptable lag.)

H. R. GROO: Yes; this has been considered and tried. I have no data available at the moment, but will be glad to discuss the matter later.

References

1. WACHTEL, M. M., DOUGHTY, D. D., and ANDERSON, A. E.: *The Transmission Secondary Emission Image Intensifier.* Proc. of Image Intensifier Symp., Oct. 1961.
2. USAERDL Contract No. DA–44–009–ENG–4531, Proj. No. 8–23–10–500.
3. ORVIN: Brit. Pat. No. 445156, 1934.
4. LUBSZNSKI, H. G.: Brit. Pat. No. 457493, 1935.
5. McGEE, J. D.: Brit. Pat. No. 504927, 1937.
6. STERNGLASS, E. J.: U.S. Pat. No. 2,905,804.
7. STERNGLASS, E. J., et al.: U.S. Pat. No. 2,898,499.
8. STERNGLASS, E. J.: *Transmission Secondary Electron Multiplication for High Resolution Counting and Imaging.* Phys. Rev., vol. 100, 1955, p. 1238.
9. Final Report, USAERDL Contract No. DA–44–009–ENG–4531, Proj. No. 8–23–10–500, October 1961.
10. Private Communication with Dr. D. L. Emberson.
11. LINDEN, B. R.: *Survey of Work at CBS Laboratories on Photoelectronic Image Devices.* Proc. of Image Intensifier Symp., October 1961.
12. GOETZE, G., and KANTER, H.: *A High Gain Intensifier System With Fast Shutter Action for Applications in High Energy Physics.* Nuc. Instru. and Methods, vol. 8, 1961, pp. 224–228.
13. BAUM, W. A., HALL, J., MARTON, L. L., and TUVE, M. A.: Astronomical Yearbook 1959–1960. Carnegie Institute of Washington, pp. 298–299.
14. TAYLOR, A., and GOETZE, G. W.: *The Direct Viewing and Rapid Photographic Recording of X-ray Diffraction Patterns.* (To be published in J. of Applied Physics.)
15. KELLER, E., and GOETZE, G. W.: *A High Sensitivity Gamma Ray Pinhole Imaging Device.* (To be published in Rev. of Scientific Instruments).
16. GOETZE, G. W.: *Transmission Secondary Emission From Low Density Deposits of Insulators.* Proc. of Image Intensifier Symp., October 1961.

10. NOISE PROBLEMS IN CONTINUOUS CHANNEL ELECTRON MULTIPLIERS

John M. Grant, *Advanced Development Laboratory, ITT Federal Laboratories*
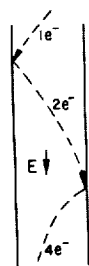
The continuous channel multiplier is, in theory, a very simple amplifying device; it consists only of a high-resistance hollow pipe, or a bunch of such pipes, with a static electric field along the axis. The schematic shown in figure 10-1 illustrates how amplification is achieved. An electron striking the wall of the channel will liberate secondary electrons. These liberated secondaries will be accelerated down the channel by the electric field until they too collide with the channel wall, liberating still more secondaries. In this fashion, multiplication is accomplished, provided of course, that the effective secondary emission ratio of the surface of the wall is sufficiently large.

If the trajectories of all of the electrons were as simple as that shown in the schematic, the continuous channel would be a nearly perfect multiplier. Unfortunately, this is not the case. The secondary emission ratio and the trajectories of the individual electrons are statistical quantities and, hence, exhibit fluctuations. These fluctuations ultimately manifest themselves in the undesirable noise of the multiplier. In figure 10-1 we have listed five possible sources of noise in the continuous-channel multiplier. The first of these includes effects such as the variation of the secondary emission ratio, δ, due to the variation in the angle of incidence of the primary electron,

and the variation in δ due to imperfection in what might be called a "perfect surface" (i.e., pure homogeneous surface). This effect is present in conventional multipliers as well, and is expected to be small when compared with the remaining four on the list. The next two items depend on the state of the art of the continuous-channel multipler fabrication. In any individual channel these effects will not give rise to any significant fluctuation in the gain; however, the variation of these quantities does result in a fluctuation of the average gain of different channels and thus will cause fixed pattern noise. In any case, having recognized that these effects exist, we will now dismiss them, anticipating that these effects will be controllable by advancements in technology.

Items 4 and 5 (along with the small contribution from 1) constitute the real fundamental effects which place a lower limit on the noise. It is easy to understand why these last two items lead to a variation in δ. If, in a channel of cylindrical geometry, an electron is emitted nearly tangential to the channel wall, then the time of flight of this electron is considerably less than the time of flight of an electron emitted normal to the wall, with a small initial velocity (fig. 10-2). Since the distance traveled down the channel in a uniform field is proportional to the square of the time of flight,

CONTINUOUS CHANNEL MULTIPLIER

SOURCES OF NOISE IN CONTINUOUS CHANNEL MULTIPLIER

1. NORMALLY OBSERVED VARIATION OF THE SECONDARY EMISSION RATIO, δ.
2. VARIATION IN δ DUE TO THE VARIATIONS IN THE SURFACE CONSTANTS.
3. VARIATION IN δ DUE TO FIELD IRREGULARITIES.
4. VARIATION IN δ DUE TO VARIATION IN THE ANGLE OF EMISSION.
5. VARIATION IN δ DUE TO VARIATION IN EMISSION VELOCITY.

FIGURE 10-1

TYPICAL ELECTRON TRAJECTORIES IN CCM

SECONDARY EMISSION RATIO δ FOR MgO FILM

FIGURE 10-2

63

MULTIPLICATION CHAINS   INCIDENT ELECTRON

| | ELECTRON YIELDING | | SECONDARY | | ELECTRON ESCAPING |
| | NO SECONDARIES | | ELECTRON | | FROM CHANNEL |

━━━━━━━━━━━━━━ KEY ━━━━━━━━━━━━━━
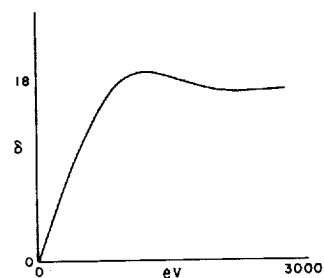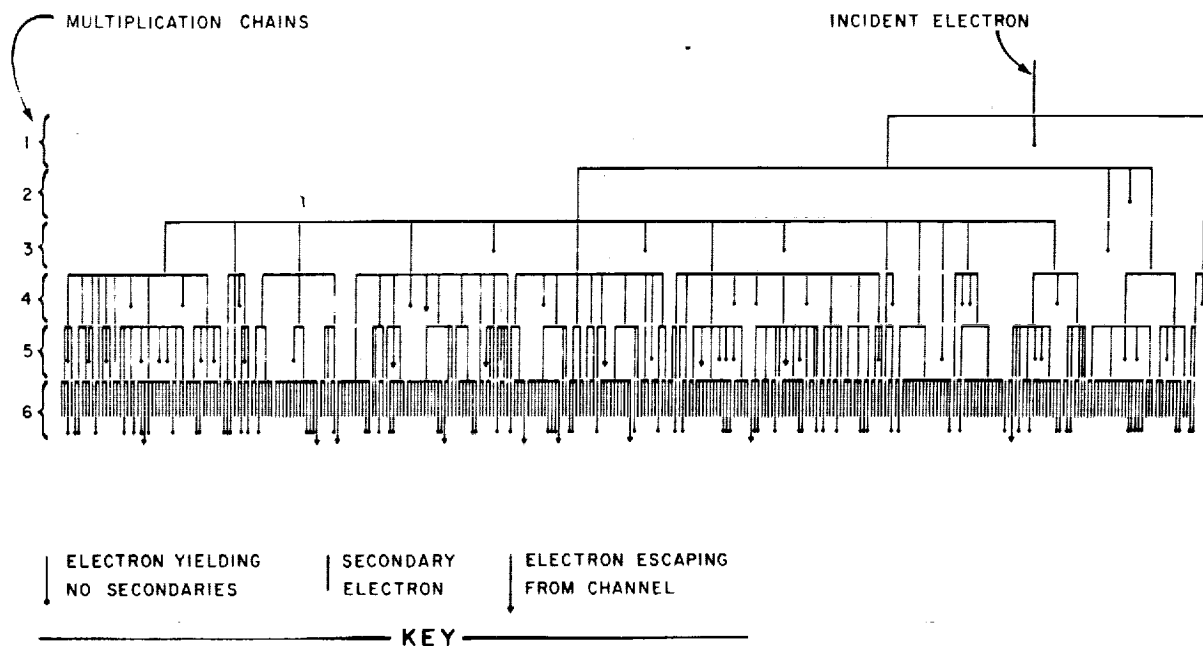
FIGURE 10-3.—Continuous-channel electron multiplication "tree."

and since the energy acquired by an electron is simply the field intensity multiplied by the distance the electron has traveled down the channel, it is obvious that the energy of the electron upon impact with the channel wall is proportional to square of the time of flight. Reference to a curve of the secondary emission ratio versus energy (fig. 10-2) shows that values of δ between zero and some maximum δ are possible. For the purposes of demonstration, a chain of events has been followed in a tube 200 radii in length (fig. 10-3). The only fluctuating quantity in this multiplication chain is the secondary emission velocity vector. This is, of course, just one of many possible chains, and perhaps it is not even "typical"—but it does serve to illustrate the statistical nature of the multiplication. It is quite striking that of the three secondaries liberated at the second step, only one has initiated any appreciable gain at step 6. The chart indicates that after six steps, most of the electrons are still in the channel. A more detailed inspection of the position of the electrons would reveal that those electrons in the sixth step which belong to the group giving a large gain are over halfway down the channel, while those electrons in the sixth step which are part of the small gain group are only about one-quarter of the way down the channel.

64

It is still possible for the electrons in the low-gain group to participate in a significant amount of multiplication, but the length of the channel available for this multiplication is only about three-fourths the length of the complete channel. All of this is quite qualitative; the purpose of it is only to emphasize the role items 4 and 5 play in contributing to the noise of the continuous-channel multiplier.

Figure 10-4 shows the choice of geometry for a more quantitative calculation of the noise. An
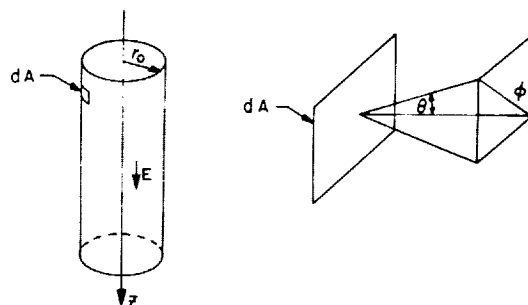
$$\frac{\Delta z}{r_0} = \frac{E r_0}{W} \frac{\cos^2 \theta}{(1 - \sin^2 \theta \cos^2 \phi)^2} + \frac{2 \cos \theta \sin \theta \cos \phi}{(1 - \sin^2 \theta \cos^2 \phi)}$$

$$df = A w^{\frac{1}{2}} e^{-aw} dw \frac{\cos \theta \sin \theta \, d\theta \, d\phi}{\pi}$$

FIGURE 10-4

electron, with initial energy ω, emitted in the direction described by the angles θ and ϕ will travel a normalized distance $\dfrac{\Delta z}{r_0}$, given by the expression in figure 10–4. Note the presence of the product Er_0 in the expression for $\dfrac{\Delta z}{r_0}$. That is, the radius of the channel may be scaled down, providing the field is increased accordingly without affecting the results. Now the fraction of electrons from the element dA emitted into the elements $d\omega$, $d\theta$, and $d\phi$ at ω, θ, and ϕ is, from theoretical and experimental considerations,[1] given by the second expression in figure 10–4. It would be desirable to analytically compute from these equations the fraction of electrons which arrive at the element

$d\left(\dfrac{\Delta z}{r_0}\right)$ at $\dfrac{\Delta z}{r_0}$, but this has not been possible. Instead, a numerical Monte Carlo calculation has been performed in which values of θ, ϕ, and ω were selected according to a cosine distribution of direction and a Maxwellian velocity distribution and the resulting $\dfrac{\Delta z}{r_0}$ calculated. Some results of these computations are shown in figure 10–5, for different values of Er_0. The area under any element of the curves gives directly the fraction of electrons which fall into that element. The fraction may also be interpreted as the probability that an electron falls into the element $d\left(\dfrac{\Delta z}{r_0}\right)$ at
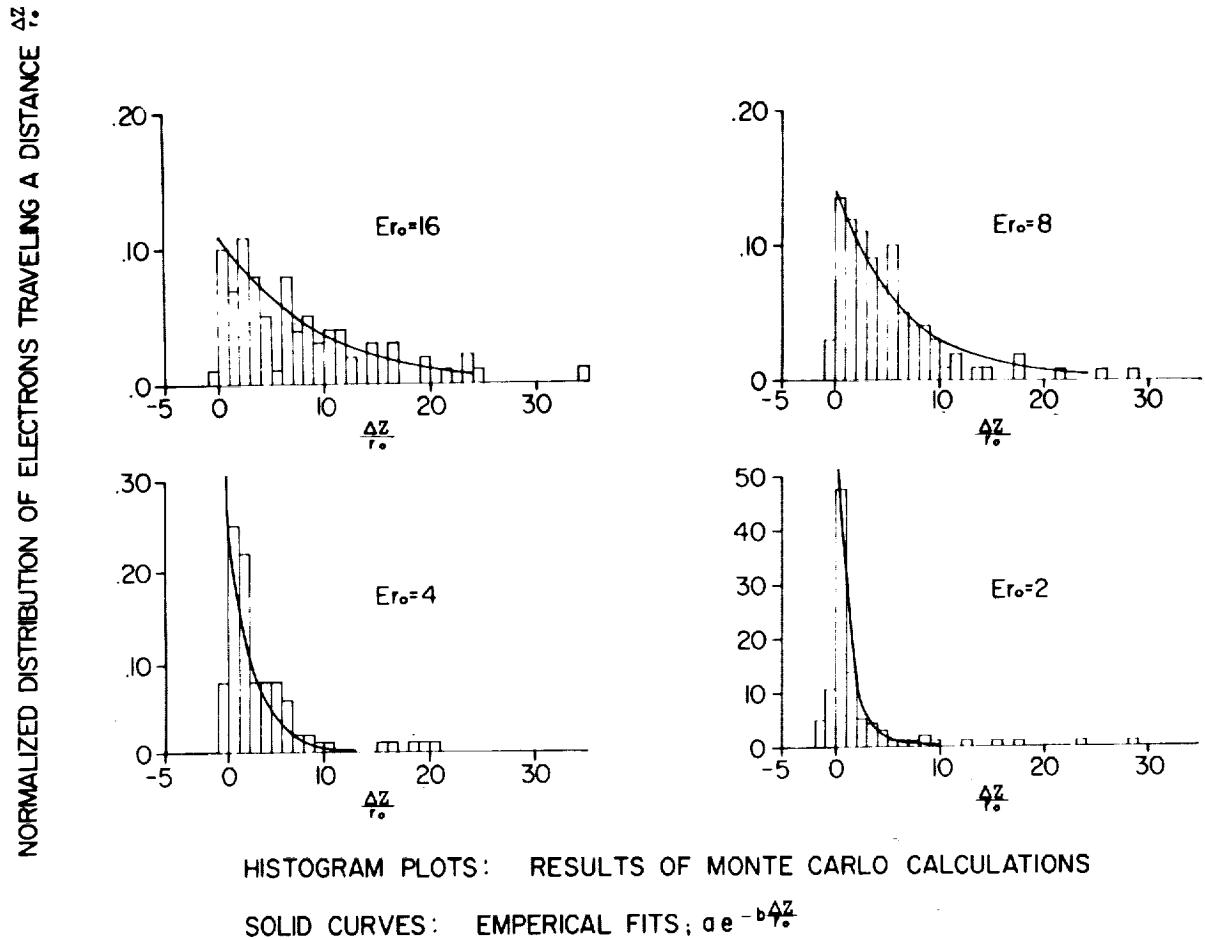

HISTOGRAM PLOTS: RESULTS OF MONTE CARLO CALCULATIONS

SOLID CURVES: EMPERICAL FITS; $a\,e^{-b\frac{\Delta z}{r_0}}$

FIGURE 10–5.—Distribution of electrons after one impact.

$\dfrac{\Delta z}{r_0}$. One may observe (fig. 10–5) that these curves are reasonably well approximated by the function

$$ae^{-b\frac{\Delta z}{r_0}} \text{ for } 0<\frac{\Delta z}{r_0}<.$$

This expression may not hold for very large values of Er_0, but these large values are uninteresting anyway, at least for channels of small diameter as used in image intensifiers.

Now the low-energy range of a secondary emission curve can be coarsely fit by a straight line from $\omega=0$ to some ω, say $\omega=\omega_0$ (fig. 10–6).

SECONDARY EMISSION
RATIO δ
FOR MgO FILM
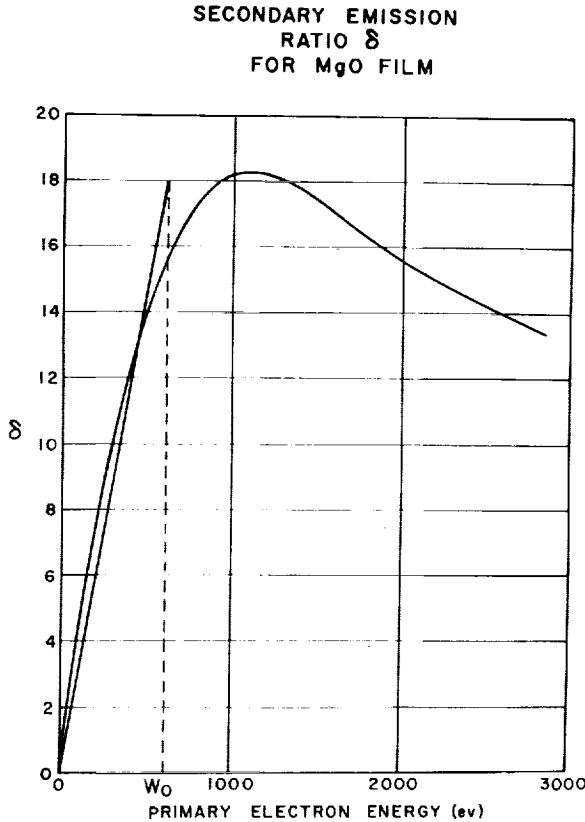
FIGURE 10–6

This approximation will be valid if no electron in the channel ever acquires an energy greater than ω_0. We can be assured of this if we consider only channels whose length, L, is

$$L\leq\frac{\omega_0}{Er_0} \qquad L \text{ is in units } r_0.$$

The particular curve shown in figure 10–6 is from the experiments of Whitten and Laponsky on MgO thin film,[2] and for this case ω_0 is around 600

66

ev. For most substances the value of ω_0 would be somewhat lower, around 400 ev. The limiting of the channel length may appear to be a rather stringent condition. Actually, for the lower values of Er_0, only a very few electrons will ever exceed ω_0 anyway. We may then extend the length of the tube beyond the critical length and neglect the small contribution from those electrons whose energies exceed ω_0. Obviously, the further one extrapolates the results beyond this limiting value of length, the greater the errors become.

Using this approximation to the secondary emission curve and the empirical probability distribution functions, one may compute analytic expressions for the mean gain, $\bar{G}$, and the variance, σ^2, for a channel of length L. The expression for the mean gain is shown in figure 10–7. C is the slope of the line approximating

$$\bar{G}=\frac{a}{b}e^{-bL}\ \text{COSH}\ \sqrt{aCEr_0}\ L$$

$$L \lessgtr \frac{W_0}{Er_0}$$

$$\Lambda = \frac{\left(\frac{S}{N}\right)_{\text{PERFECT}}}{\left(\frac{S}{N}\right)_{\text{IMPERFECT}}} = \sqrt{1+\frac{\sigma^2}{\bar{G}^2}}$$

FIGURE 10–7

the curve for the secondary emission ratio. One may also define a noise figure, Λ, to be the signal-to-noise ratio of a "perfect" channel mutiplier divided by the signal-to-noise ratio of the real channel mutiplier. The "perfect" channel multiplier is considered to have a nonfluctuating gain equal to the gain of the real multiplier. The expression for Λ is also shown in figure 10–7.

A curve of the mean gain as a function of the channel length for a few values of Er_0 and C is shown in figure 10–8. The value of $C=0.03$ (volt)$^{-1}$ is from the previous curve of Whitten and Laponsky, while the value $C=0.01$ (volt)$^{-1}$ is for a fictitious secondary emitter having a maximum
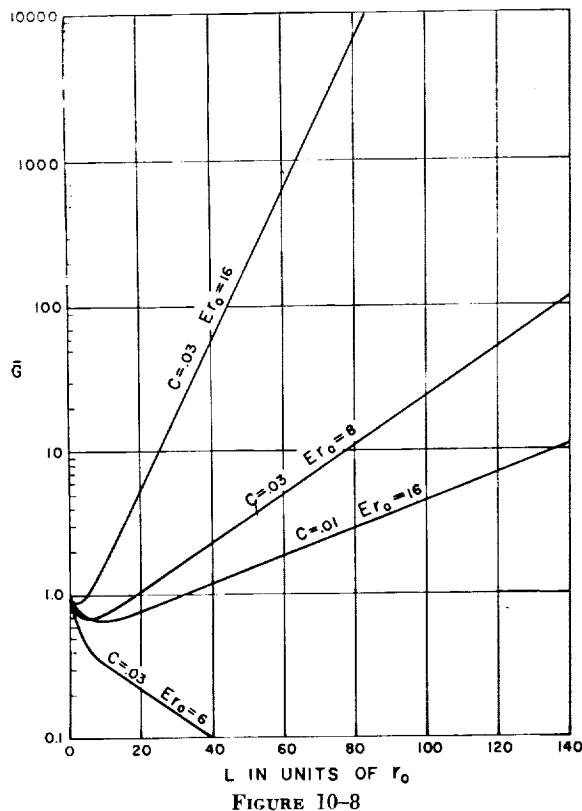
FIGURE 10-8

FIGURE 10-9

value of $\delta=4$ for a primary electron energy of 400 electron volts. Note that the channel multiplier has a gain less than one for any length when $Er_0=6$ and $C=0.03$. The gain for $Er_0=8$ and $Er_0=16$ become less than 1 as well if the slope C of the secondary emission ratio curve drops below 0.018 and 0.007, respectively. A comparison of the various curves indicates quite clearly that appreciable values of gain can be achieved only with combination of a large value of Er_0 and a large value of C. For channels of small radii this corresponds to large field strengths and a good secondary emitter.

Figure 10-9 exhibits the noise figure versus gain for the interesting values of Er_0. Again we see that a good noise figure is achieved only with a large value of Er_0 and a large value of C. (In obtaining these curves the calculations have been extended far beyond the limits of our approximations, so the curves at most indicate only the order of magnitude.) Also plotted on figure 10-9 is the theoretical noise figure for a well-focused dynode
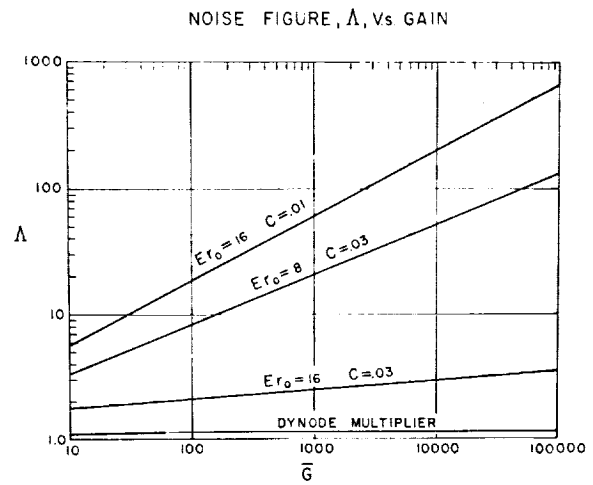
multiplier. This curve was obtained by taking the average secondary emission ratio to be 5 and varying the number of stages to achieve the appropriate gain. A comparison of the curves indicates clearly that the noise resulting from the variation of the secondary emission velocity vector is significantly large. Moreover, as the gain is increased (i.e., the channel lengthened), the noise figure continues to increase; this is in contrast to the ordinary dynode structure for which the noise figure approaches a constant value as the gain is increased.

In concluding then, we have seen that good performance of small channel multipliers requires large values of Er_0 and large values of C. As the channels are made smaller and smaller, the strain on the technology required for their fabrication will be greater and greater, for it will be necessary to form excellent secondary emitting surfaces in practically inaccessible areas and to support enormous field strengths across these areas.

Acknowledgments

67

Appendix

Calculation of Noise Figure A

Let $\zeta = \dfrac{Z}{r_0}$ and define

$$p(\zeta_i - \zeta_j)d\zeta_i \qquad -\infty \zeta_i < +\infty \qquad (1)$$

as the probability that an electron liberated at ζ_j arrives in the element $d\zeta_i$ at ζ_i. Also define

$$\pi(L - \zeta_j) = \int_L^\infty p(\zeta_i - \zeta_j)d\zeta_i; \qquad (2)$$

i.e., the probability that an electron liberated at ζ_j exceeds the coordinate $\zeta = L$. Define

$$\delta = \delta(\zeta_i - \zeta_j) \qquad \zeta_i - \zeta_j \geq 0$$
$$\delta = 0 \qquad \zeta_i - \zeta_j < 0 \qquad (3)$$

to be the S.E. ratio resulting from a primary electron liberated at ζ_j and impinging at ζ_i. (This last expression states that all primaries that travel a direction opposed to the field lead to zero secondary emission ratio. This is not precisely true, but as the energy of the primary in this instance is less than its initial energy, it is a good approximation.)

Now if n electrons are liberated at $\zeta = 0$, the mean number of them which exceed $\zeta = L$ without striking the channel wall is

$$N_0 = n\pi(L) \qquad (4)$$

The mean number of them which strike the channel wall at ζ_1 is

$$np(\zeta_1)d\zeta_1$$

The mean number of electrons liberated at ζ_1 is

$$np(\zeta_1)d\zeta_1\delta(\zeta_1)$$

The mean number of these which exceed L is

$$dN_1 = np(\zeta_1)d\zeta_1\delta(\zeta_1)\pi(L - \zeta_1) \qquad (5)$$

Summing dN_1 over all possible values of the impact position ζ_1, we obtain

$$N_1 = n\int_{-\infty}^L \delta(\zeta_1)p(\zeta_1)\pi(L - \zeta_1)d\zeta_1$$

$$= n\int_0^L \delta(\zeta_1)p(\zeta_1)\pi(L - \zeta_1)d\zeta_1 \qquad (6)$$

since from equation 3, $\delta(\zeta_1) \equiv 0$ for $\zeta_1 < 0$.

Now N_1 is the contribution, of the total mean number of electrons emerging from the channel, which arises from one-step processes.

The mean number of electrons liberated at ζ_1 which strikes at ζ_2 is

$$np(\zeta_1)d\zeta_1\delta(\zeta_1)p(\zeta_2 - \zeta_1)d\zeta_2$$

The mean number of electrons liberated at ζ_2 is

$$np(\zeta_1)d\zeta_1\delta(\zeta_1)p(\zeta_2 - \zeta_1)d\zeta_2\delta(\zeta_2 - \zeta_1)$$

The number of these which exceed L is

$$d^2N_2 = np(\zeta_1)d\zeta_1\delta(\zeta_1)p(\zeta_2 - \zeta_1)d\zeta_2\delta(\zeta_2 - \zeta_1)\pi(L - \zeta_2) \qquad (7)$$

Summing over all possible values of ζ_2, we obtain

$$dN_2 = Np(\zeta_1)d\zeta_1\delta(\zeta_1)\int_{-\infty}^L \delta(\zeta_2 - \zeta_1)p(\zeta_2 - \zeta_1)\pi(L - \zeta_2)d\zeta_2$$

$$dN_2 = Np(\zeta_1)d\zeta_1\delta(\zeta_1)\int_{\zeta_1}^L \delta(\zeta_2 - \zeta_1)p(\zeta_2 - \zeta_1)\pi(L - \zeta_2)d\zeta_2 \qquad (8)$$

Summing again over all ζ_1,

$$N_2 = n\int_{-\infty}^L \int_{\zeta_1}^L \delta(\zeta_1)\delta(\zeta_2 - \zeta_1)p(\zeta_1)p(\zeta_2 - \zeta_1)\pi(L - \zeta_2)d\zeta_1 \qquad (9)$$

N_2 is the contribution, of the total mean number of electrons emerging from the channel, which arises from two step processes.

In an analogous way the contribution from all those electrons resulting from a Kth step process is

$$N_k = n\int_0^L \int_{\zeta_1}^L \cdots \int_{\zeta_{k-1}}^L \delta(\zeta_1)\delta(\zeta_2 - \zeta_1)$$
$$\cdots \delta(\zeta_k - \zeta_{k-1})p(\zeta_1) \cdots p(\zeta_k - \zeta_{k-1})$$
$$\cdots \pi(L - \zeta_k)d\zeta_k \qquad d\zeta_{k-1} \cdots d\zeta_2 d\zeta_1 \qquad (10)$$

We may write the previous equation as

$$\frac{N_k}{n} = \bar{g}_k = \int g_k(\zeta_1 \ldots \zeta_k)dPg_k(\zeta_1 \ldots \zeta_k) \qquad (11)$$

where $\bar{g}_k$ is the gain for a K step process, and

$$g_k(\zeta_1 \ldots \zeta_k) = \delta(\zeta_1) \ldots \delta(\zeta_k - \zeta_{k-1})$$

and,

$$dPg_k(\zeta_1 \ldots \zeta_n) = p(\zeta_1) \ldots p(\zeta_k - \zeta_{k-1})\pi(L - \zeta_k)d\zeta_k \ldots d\zeta_1$$

is the probability of obtaining $g_k(\zeta_1 \ldots \zeta_k)$ which is identically equal to the probability that an electron impacts at K specified values of ζ before exceeding the channel. Obviously since $\overline{g}_k$ is the exception value of the "gain function" g_k, we must interpret the variance, $\overline{(g_k-\overline{g}_k)^2} = \sigma_k^2$, as

$$\sigma_k^2 = \left[\int\int g_k^2 dP g_k\right] - \overline{g}_k^2 \qquad (12)$$

Now since each of the k processes are statisically independent, the total mean gain $\overline{G}$ is

$$\overline{G} = \sum_{k=0}^{\infty} \overline{g}_k \qquad (13)$$

and the total variance is

$$\sigma^2 = \sum_{k=0}^{\infty} \sigma_k^2 \qquad (14)$$

Now if n electrons are introduced into the channel, we obtain a sample, y_n, consisting of n; values of the function G. We may write

$$y_n = {}^1G + {}^2G + {}^3G \ldots {}^nG \qquad (15)$$

where the superscripts indicate different value of the function G. If n were always constant, the mean value of the y_n's would be

$$\overline{y}_n = n\overline{G} \qquad (16)$$

and the variance, $\sigma_{y}^2{}_n$ of the y_n's would be

$$\sigma_{y}^2{}_n = n\sigma^2 \qquad (17)$$

In general, n (the input signal) is not constant, and we must consider the fluctuations in the size of the sample, y_n, as a result of the fluctuations in n. Let $P({}^1G)$ be the probability of obtaining a specific ${}^1G$. We have not formulated an expression for $P({}^1G)$, but we know that

$$\sum_{{}^1G} {}^1G P({}^1G) = \overline{G} \qquad (18)$$

and

$$\sum_{{}^1G} ({}^1G)^2 P({}^1G) = \overline{G^2} \qquad (19)$$

where the sums (or integrals) are taken over all possible values of ${}^1G$.

Let $P(n)$ be the probability of obtaining a sample of size n. The probability of obtaining a specific y_n is then

$$P(y_n) = P({}^1G)P({}^2G) \ldots P({}^nG)P(n) \qquad (20)$$

With this notation, the average value of the y_n's is

$$\overline{y}_n = \sum_n \sum_{{}^1G} \ldots \sum_{{}^nG} y_n P(y_n)$$

$$\overline{y}_n = \sum_n \sum_{{}^1G} \ldots \sum_{{}^nG} ({}^1G + {}^2G + {}^3G$$
$$\ldots {}^nG)P({}^1G) \ldots P({}^nG)P(n)$$

$$\overline{y}_n = \sum_n n\overline{G}P(n) = \overline{G}\sum_n nP(n) = \overline{n}\overline{G} \qquad (21)$$

and $\sum y_n^2$, the variance of the y_n's is

$$\sigma y_n^2 = \left[\sum_n \sum_{{}^1G} \ldots \sum_{{}^nG} ({}^1G + {}^2G\right.$$
$$\left. \ldots {}^nG)^2 P({}^1G)P({}^2G) \ldots P({}^nG)P(n)\right] - \overline{y}_n$$

$$\sigma y_n^2 = \left[\sum_n (n\overline{G^2} + n(n-1)\overline{G}^2)P(n)\right] - \overline{y}_n^2$$

$$\sigma y_n^2 = \overline{n}\overline{G^2} + (\overline{n^2} - \overline{n})\overline{G}^2 - \overline{n}^2\overline{G}^2 \qquad (22)$$

The case of most interest is when n is Poisson distributed; then

$$\overline{n^2} - \overline{n}^2 = \overline{n} \qquad (23)$$

and equation 22 becomes

$$\sigma_{y}^2{}_n = \overline{n}\overline{G^2} \qquad (24)$$

Now making use of the identity

$$\overline{G^2} - \overline{G}^2 - \sigma^2 \qquad (25)$$

equation 24 becomes

$$\sigma_{y}^2{}_n = \overline{n}(\sigma^2 + \overline{G}^2) \qquad (26)$$

Now the signal-to-noise ratio of this imperfect multiplier is given by

$$\frac{S}{N}_{\text{(Imperfect)}} = \frac{\overline{y}_n}{\sigma y_n} = \frac{\overline{n}\overline{G}}{\sqrt{\overline{n}(\Sigma^2 + \overline{G}^2)}} \qquad (27)$$

$$\frac{S}{N}_{\text{(Imperfect)}} = \frac{\overline{n}}{\sqrt{1 + \dfrac{\sigma^2}{\overline{G}^2}}} \qquad (28)$$

A perfect multiplier would have $\sigma^2 \equiv 0$; hence,

$$\frac{S}{N}_{\text{(perfect)}} = \overline{n} \qquad (29)$$

69

Defining a noise figure Λ as

$$\Lambda = \frac{\left(\dfrac{S}{N}\right)_{\text{perfect}}}{\left(\dfrac{S}{N}\right)_{\text{imperfect}}} \qquad (30)$$

we obtain

$$\Lambda = \sqrt{1 + \frac{\sigma^2}{\bar{G}^2}} \qquad (31)$$

with $\bar{G}$ and $\bar{\sigma}^2$ given by equations 13 and 14.
To evaluate $\bar{G}$ and σ^2, we assume

$$p(\zeta) = ae^{-b\zeta} \qquad 0 \leq \zeta < \infty$$

$$\delta(\zeta) = CEr_0\zeta \qquad 0 < \zeta \leq L \qquad (32)$$

Then

$$\pi(L) = \frac{a}{b} e^{-bL} p(\zeta_1) p(\zeta_2 - \zeta_1)$$

$$\dots p(\zeta_k - \zeta_{k-1}) \pi(L - \zeta_k) = a^k \left(\frac{a}{b}\right) e^{-bL} \qquad (33)$$

and

$$\bar{g}_k = a^k \frac{a}{b} e^{-bL} (CEr_0)^k \int_0^L \int_{\zeta_1}^L$$

$$\dots \int_{\zeta_{k-1}}^L \zeta_1(\zeta_2 - \zeta_1) \dots (\zeta_r - \zeta_{k-1}). \qquad (34)$$

$$d\zeta_k \dots d\zeta_1$$

$$\bar{g}_k = a/b e^{-bL} (aCEr_0)^k \frac{L^{2k}}{(2k)!} \qquad (35)$$

$$\bar{G} = \sum_{k=0} \bar{g}_k = a/b e^{-bL} \cosh \sqrt{aCEr_0} \, L \qquad (36)$$

In the same way

$$\sigma_k^2 = a_k \left(\frac{a}{b}\right) e^{-bL} (CEr_0)^{2k} \int_0^L \int_{\zeta_1}^L \dots \int_{\zeta_{k-1}}^L \zeta_1^2(\zeta_2 - \zeta_1)^2 \dots (\zeta_k - \zeta_{k-1})^2 d\zeta_k \dots d\zeta_1 - \left(\frac{a}{b}\right)^2 e^{-2bL} \frac{(aCEr_0)^{2k}L^{4k}}{[(2k)!]^2} \qquad (37)$$

$$\sigma_k^2 = \left(\frac{a}{b}\right) e^{-bL} a^k (CEr_0)^{2k} \frac{2^k L^{3k}}{(3k)!} - \left(\frac{a}{b}\right)^2 e^{-bL} \frac{(aCEr_0)^{2k}L^{4k}}{[(2k)!]^2} \qquad (38)$$

Now

$$\sum_{k=0}^{\infty} \frac{[(2a)^{1/3}(CEr_0)^{2/3}L]^{3k}}{(3k)!} = \tfrac{2}{3} e^{\frac{-(2a)^{1/3}(CEr_0)^{2/3}L}{2}} \cos \sqrt{3/2} \, (2a)^{1/3}(CEr_0)^{2/3}L + \tfrac{1}{3} e^{+(2a)^{1/3}(CEr_0)^{2/3}L} \qquad (39)$$

and

$$\sum_{k=0}^{\infty} \frac{(\sqrt{aCEr_0}L)^{4k}}{[(2k)!]^2} = \frac{J_0(2\sqrt{aCEr_0}L) + I_0(2\sqrt{aCEr_0}L)}{2} \qquad (40)$$

where J0 and I0 are the zero order Bessel function of first kind and modified function of the first kind. Finally we obtain

$$\sigma^2 = \left(\frac{a}{b}\right) e^{-bL} \left\{ \tfrac{2}{3} e^{\frac{-(2a)^{1/3}(CEr_0)^{2/3}L}{2}} \cos \sqrt{3/2}(2a)^{1/3}(CEr_0)^{2/3}L + \tfrac{1}{3} e(2a)^{1/3}(CEr_0)^{2/3}L \right\}$$

$$- \left(\frac{a}{b}\right) e^{-2bL} \frac{J0(2\sqrt{aCEr_0}L) + I0(2\sqrt{aCEr_0}L)}{2}$$

Discussion

I. LEVIN: What is the structure of the channel? Is it a tube of MgO or MgO evaporated on a metal surface?

J. M. GRANT: This paper is purely an analysis, and the fabrication of any particular structure is not considered. The calculations assume only hypothetical surfaces which are representative of an average and an excellent emitter, the surface was assumed to have the secondary emitting properties of MgO thin film.

W. C. WILEY: I pointed out that the measured noise figures obtained at Bendix are comparable with those obtained with discrete dynode multipliers and do not support the analysis given in the paper. Several reasons for this were given involving the validity of the original assumptions.

70

J. M. GRANT: I neglected to indicate that for each input electron striking the channel wall at its entrance ($z=0$), one secondary electron was assumed to be emitted. If this first impact is characterized by a secondary emission ratio different than one, the values of gain exhibited in this paper will be increased by that ratio and the noise figures decreased by square root of the ratio. However, I do not believe this fully accounts for the discrepancy between noise values you have measured and the predictions of this analysis. With regard to the validity of the assumption, I have confidence that they are completely justifiable. Probably the most significant effect which was neglected is the dependency of the secondary emission ratio on the angle of incidence of the primary electron; again, however, I feel that this could not account for the apparent difference between the analytical and measured results.

J. W. HICKS, JR.: Did your gain figures apply to number of electrons or energy?

J. M. GRANT: The gain figure is the ratio of the number of electrons emerging from the channel to the number entering the channel.

References

1. KOLLATH, R.: *Sekundärelektronen—Emission fister Kröper ber Bestralung mit Elektronen.* Handbuch der Physik Band XXI, 1956.

2. WHETTEN, N. REY, and LAPONSKY, A. B.: *Secondary Electron Emission from MgO Thin Films.* J. of Applied Phys., vol. 30, 1959, p. 432.

11. LIMITATIONS TO RESOLVING POWER IN ELECTRONIC IMAGING

A. E. Anderson and R. J. Schneeberger, *Research Laboratories, Westinghouse Electric Corp.*

Introduction

The performance of an electronic imaging system is limited by two system characteristics—the fidelity with which the image is reproduced and the noise present in the information-bearing channel. The ability of the eye to distinguish a pattern in a noisy signal has been previously investigated for cases in which the noise was assumed to result from the quantum nature of the signal.[1][2] More recently, a similar investigation was carried out for conventional television presentations, in which there is an additive noise independent of the signal strength, and the final image contrast, brightness, and magnification can be adjusted at will by the observer.

This paper deals with methods of specifying and measuring the fidelity of a reproduced image in terms of an appropriate amplitude response factor. Mention is made of the concept of noise equivalent pass band introduced earlier by Schade.[3] A selective amplifier for obtaining a direct measure of the sine wave response factor is described. Finally, a quantitative discussion of the manner in which system noise interferes with image resolution is presented. It is emphasized that throughout the discussion, only "white" noise is considered. Since other kinds of noise due to amplifier peaking characteristics and fixed pattern fluctuations frequently are present in certain types of systems, it is evident that future work should be directed towards the manner in which various non-gaussian fluctuations limit system performance.

Amplitude Response Considerations

Figure 11-1 shows the response of an imaging system to four different test objects. The line object (1) results in a symmetrically broadened image which is identified with the aperture flux distribution of the system. The response to a step function (2) is a gradual transition from dark to light. In (3) is shown the response to a square

wave input which results in a wave modified in shape, and reduced in amplitude. If the output is normalized so that the area under the curve is unchanged, the amplitude of the output wave relative to that of the input wave is defined as the square wave response factor, $r(N)$. In (4) is shown the response to a sine wave input, which is a wave reduced in amplitude but unmodified in shape. The sine wave response factor, $R(N)$, is defined as the ratio of the amplitude of the output sine wave to that of the input wave—the areas under the curves again being made equal. It is the property of maintaining the shape of the wave that permits the simple manipulation of cascaded systems when the sine wave response factor is used.

From early studies of resolution and detail contrast characteristics of photographic and television images, it has long been apparent that the sharpness of an image has no fixed relation to the limit of resolution of the system, but depends rather on the steepness and form of the intensity or luminance curve representing a unit function transition; i.e., a sharp edge. The differences in response characteristics indicate that a comparision of image definition by a single figure of merit requires the evaluation of a measure such as an equivalent re-
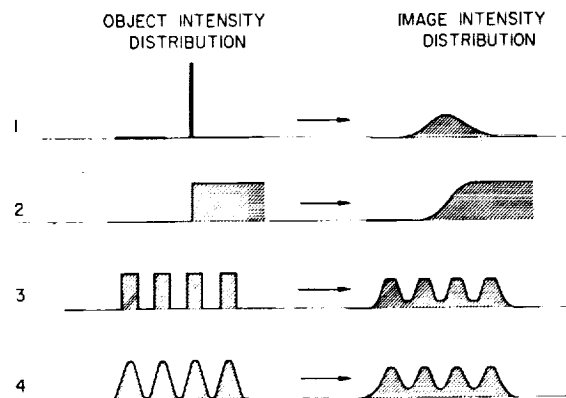

FIGURE 11-1.—Response of an imaging system to various object shapes.

sponse characteristic that can be specified by one significant number. It is important that this equivalent measure agree with a visual impression of sharpness. Schade[3] has introduced such an equivalent measure amd calls it an equivalent pass band of constant amplitude extending to the line number, N_e, as defined by

$$N_e = \int_0^\infty [R(N)]^2 dN,$$

where $R(N)$ is the sine wave response factor.

In entertainment and/or industrial television where a relatively few salient features of a picture convey the desired information, evaluation by the single figure of merit, N_e, is useful and valid. For applications concerned with surveillance, astronomy, or radiography, one is more concerned with the resolution limit of the picture than with its visual impression. For the latter applications, a response factor such as the sine wave response factor, $R(N)$, seems to be the more meaningful approach. A straightforward integration will, of course, yield N_e if desired.

Measurement of Sine Wave Response

Patterns which generate square wave forms are much simpler to construct accurately than those for sine wave, since a sine wave pattern needs a continuously varying intensity distribution. Such patterns are available for the visible wavelength region but would be very difficult to construct for the infrared or ultraviolet. Coltman[4] has shown that the difficulty of experimentally providing a sine wave test pattern can be avoided by measuring the response to a square wave (bar pattern) and calculating by a simple formula the corresponding sine wave response factor.

In this section, an alternate scheme is described whereby a selective amplifier is used to eliminate all harmonics above the fundamental, thereby obtaining a direct measure of the sine wave response from a square wave input. In addition to obviating the tedious calculations involved in converting from a square wave to a sine wave response, the use of a selective amplifier results in a reduction of noise in the oscilloscope display. Accurate measurements are then made possible at signal levels where the noise from a wide band amplifier would be comparable or greater in magnitude to the signal. This is especially important in view of very small values of signal-to-noise ratios at which the eye can extract useful

information from images. A selective amplifier has been built and used successfully in measuring the sine wave response of a far infrared pickup tube where the signal level at high line numbers is comparable in magnitude to that of the background fixed pattern noise.

The procedure for making sine wave response measurements on any signal generating tube with the selective amplifier is as follows:

(1) A square wave test pattern of the desired number of cycles is focused on the sensitive surface of the tube. For a given scanning velocity, the tube generates a signal whose frequency is proportional to the size of the test pattern at the distance used.

(2) The resulting output signal is amplified by a selective amplifier tuned to the fundamental frequency of this signal.

(3) The output of the selective amplifier is displayed on an oscilloscope screen arranged to display one line of the scan.

(4) The sine wave voltage output is measured from the amplitude of the oscilloscope display, calibrated by driving the amplifier and oscilloscope from a standard input.

The selective amplifier should have high Q for rejection of noise outside the frequency in use. In order that a small number of signal bars may be used to measure the equilibrium amplitude of the signal, the impedance must not be too high. The most important feature of the signal presented to the selective amplifier is that it has an abrupt beginning and ending as a single line is scanned. Hence, only a finite number of cycles is present. This places a limitation on the degree of selectivity which can be used in the amplifier, and Q values around 10 are used in the tunable amplifier. Consider the response of a single tuned circuit to a sine wave current of frequency, f, and peak amplitude, I_0, turned on at time, $t=0$.
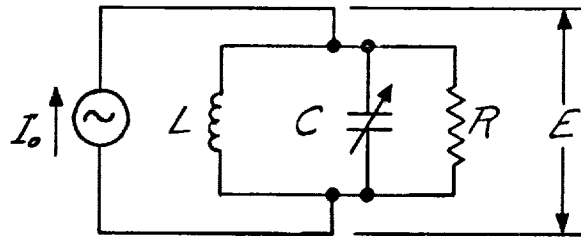
The well-known solution is

$$E = I_0 R (1 - e^{-\omega t/2Q}) e^{j\omega t},$$

74

where $Q=R/\omega L$ and $\omega=1/\sqrt{LC}=2\pi f (f=$ frequency in cycles/sec).

INPUT   RESPONSE
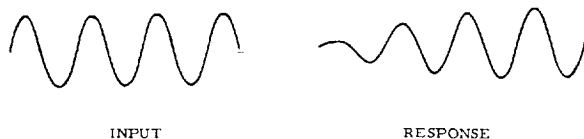
The response of several electronically isolated tuned circuits in cascade is considerably more complex, but it can be seen immediately from the above that for a given number of tuned circuits there is a definite upper bound for the permissible Q for each coil if the amplifier is to allow the signal to approach as much as 95 percent of its equilibrium value during the scanning of a single line. Since the "skirt" selectivity of an amplifier with a given bandwidth improves as the number of tuned circuits increases, a balance must be struck between simplicity and idealized characteristics in choosing the number of tuned circuits. In practice, there seems to be little to be gained by going beyond two tuned circuits, since this appears to provide more than adequate selectivity. The response to a step input of two tuned circuits in cascade is

$$E(t)=E_0\left[1-e^{t/\tau}-\frac{t}{\tau}\,e^{-t/\tau}\right],$$

where $\tau=2Q/\omega$.

Noise Limitations to Resolving Power

Coltman and Anderson have shown that it is possible to derive certain relationships between image detail and signal-to-noise ratio required without recourse to any experiment. They arrive at the following theorem which is not restricted to television-type displays, but, subject to certain postulates, applies to any display whatever: *The strength of white noise required to mask an image signal is directly proportional to the linear size of the image.*

For the case of a television display, it is assumed that the viewer can change at will the gain, background brightness, and viewing distance; it is apparent that only the signal-to-noise ratio is important in determining the threshold. We may thus restate the results: *The signal-to-white-noise ratio required for detection of an image is inversely proportional to the linear dimension of the image.*

A corollary of the above may also be inferred from the same argument: *The optimum viewing distance for detection of an image in white noise is directly proportional to the image size.*

Assume a television image of a vertical sine wave bar pattern, having enough lines showing in the picture so that the effect of the finite frame size may be ignored. The theorem proposed states that the threshold signal-to-noise ratio is inversely proportional to the linear dimension of the image, or proportional to the number of lines n per cm.

$$N_{threshold}=\text{const}\left(\frac{\text{screen signal}}{\text{screen noise}}\right)\text{lines/cm}.$$

(1)

In Eq. (1), the screen noise is measured by the brightness fluctuation on some small area of the screen. When this fluctuation is related to the noise impressed on the scanning beam of a kinescope, the following relation can be stated:

$$N_{\text{lines/picture}}=k\left(\frac{Ate_h e_v \Delta f}{R}\right)^{1/2}\frac{\text{signal}}{\text{noise}},$$

(2)

where A is an area on the picture which is small compared to the frame size, but large enough to contain several resolution elements. Frame time is denoted by t; $e_h\,e_v$ is the product of the horizontal and vertical sweep efficiencies; Δf is the system bandwidth; and R is the aspect ratio.

Now, if the noise in question arises, as is usually the case, from a white noise source located prior to the bandwidth-limiting circuits of the system, the noise current is itself proportional to $\sqrt{\Delta f}$. Eq. (2) in this case implies that the threshold value for signal recognition is independent of the system bandwidth. The requirement on the sample area, A, noted above and the use of an integrating time, t, larger than the frame time, is essentially equivalent to assuming that the eye—and not the system—sets the bandwidth.

To test the relationships stated above, an experimental investigation of the visibility of sine wave bar patterns was carried out using a television monitor displaying accurately measured sine wave signals and white noise. A block diagram of the equipment is shown in figure 11-2. Sine wave bar patterns of different number of lines per picture with different additive noise levels were displayed to a number of observers in a manner designed to obtain threshold values. The results of a series of runs are given in figure 11-3.

The amount of data taken was limited; and conditions of surround brightness, time interval
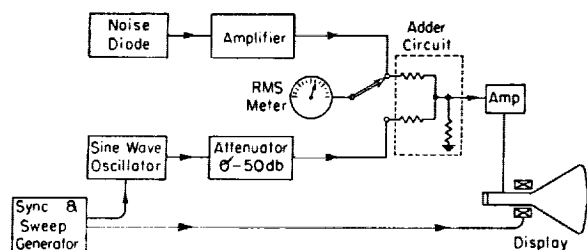
FIGURE 11-2.—Arrangement for displaying measured signals and noise—the synchronized sine wave oscillator produced a vertical sine wave bar pattern of variable intensity on the display, while a fixed measured white noise was superimposed.

between tests, etc., were not carefully controlled, so that the data presented here do not constitute a definitive study of this particular visual parameter. They suffice, however, to demonstrate the relationships derived above, to provide a numerical value of the constant, k, in (2), and to outline the area of validity of the theoretical treatment. It is of great interest to note the extremely small signal-to-noise ratios required, clearly showing the great extent to which integration takes place in the eye. From the position of this line and the 5.0-mc bandwidth used, we can evaluate the constant in (2) and write:

$$N_{\text{threshold}} = 615 \sqrt{\Delta f} \cdot \frac{\text{signal}}{\text{noise}},$$

where Δf is measured in megacycles per second, and N is line pairs per picture width.

The signal current in the information channel will, of course, be a function of many system parameters. In particular, as a result of finite scanning apertures, electron-optical aberrations, etc., the signal response will diminish for fine patterns. It is convenient to describe this effect by the sine wave response function which was discussed in the previous section.

Such a response curve of a typical image orthicon is plotted as the upper curve in figure 11-4. The intercept at a signal-to-noise ratio of 0.22 is arbitrarily chosen for an example. The value is maintained essentially unchanged for low line numbers, and is called here the coarse-pattern signal-to-noise ratio. At higher line numbers, the signal (and therefore the signal-to-noise ratio) diminishes as shown. Also plotted in figure 11-4 is the previously derived curve of figure 11-2 which establishes for each line number the threshold of signal-to-noise ratio. The abscissa of the

76
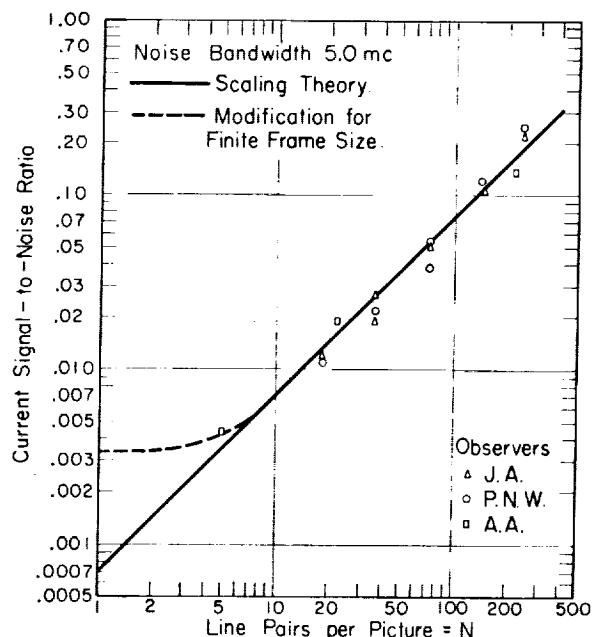
FIGURE 11-3.—Threshold signal-to-noise ratio as a function of number of cycles of the sine wave bar pattern displayed—the linear relationship extends over two decades, and departure is observed only for very small line numbers.

intersection of the two curves gives the resolution limit corresponding to the coarse-pattern signal-to-noise ratio chosen.

By making a series of such choices, the curve of figure 11-5 is derived, which gives the resolution limit as a function of the coarse-pattern signal-to-
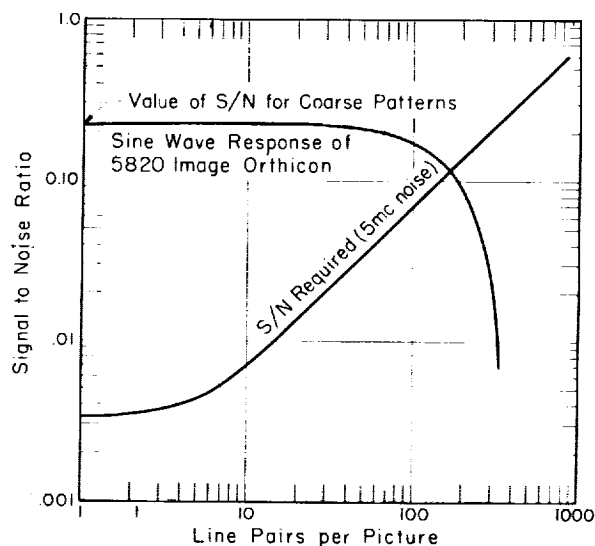
FIGURE 11-4.—Limiting resolution established by the intersection of curves representing available and required signal-to-noise ratio.
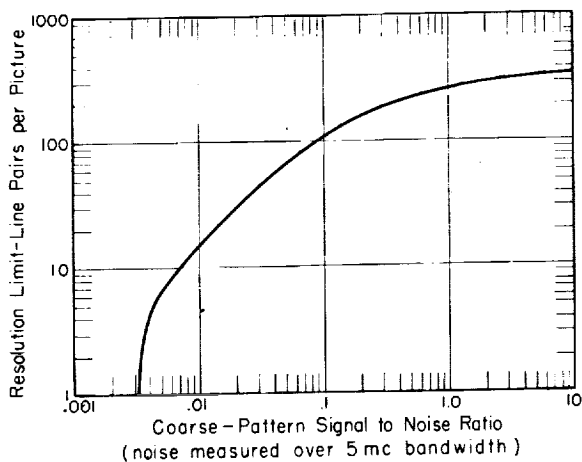
FIGURE 11–5.—Calculated resolution limit for a typical image orthicon as a function of the signal-to-noise ratio for large patterns.

noise ratio. The curve approximates over a decade a direct proportion between signal-to-noise ratio and resolution limit; it drops rapidly at the lower end due to the inability of the finite picture to display enough lines, while at the upper end it flattens out as the effects of finite local spots reduce the available signal.

It should be noted that these curves assume an electrical channel of flat response and wide bandwidth. The 5-mc band over which the noise is measured is used only to establish a numerical value for the signal-to-noise ratio. Both noise (assumed white) and signal may extend well beyond this limit.

For an image orthicon operated at low light levels, the noise is essentially fixed, so that the signal-to-noise scale can be replaced by a properly established scale of scene illumination. The conversion factor will be a function of the photosurface response, the optics used, and the object contrast, but the shape of the curve will remain fixed. Experimental confirmation is afforded by some data taken by Hannam [6] on two image orthicons employing different target materials, giving the observed resolution as a function of illumination. These data have been plotted in figure 11–6 with the illumination scale shifted for each tube to obtain the best fit to the theoretical curve. Considering the semisubjective nature of such measurements, the agreement is satisfactory.

This example serves to demonstrate the validity of the proposed method for determining the limiting resolution versus light level for any pickup tube whose performance is limited by white noise. In practice, it should be necessary only to measure

the signal-to-noise ratio at a high-enough light level where instrumentation is not a problem and to establish the limiting resolution at that light level. These data then can be combined with the sine wave response function to generate a curve like the example in figure 11–5, but with an absolute scale of illumination on the abscissa.

Nonwhite Noise

The effects of nonwhite noise on the resolution limit remain to be investigated. The following two areas are of immediate interest:

(1) Pickup tubes without return beam multiplication or pretarget intensifiers are limited in performance by amplifier noise. It is known that for the standard high-peaked amplifier where the noise is concentrated in the high frequency portion of the information channel, greater noise power outputs can be tolerated under this condition than under the condition of uniform frequency distribution.[7] Since the frequency distribution is essentially the same for all useful amplifiers of this type, a quantitive investigation should yield information which would be applicable to a large variety of situations.

(2) Fixed pattern noise due to nonuniformities in gain over the imaging area have a deleterious effect on the resolution limit, particularly under low contrast conditions. Grain structure in targets, intensifier layers, phosphors, etc., contribute to this effect. Since it is unlikely that the frequency distribution follows a fixed law as in (1) above, investigations would have to be limited to specific situations.

Conclusion

For imaging systems, whose output is viewed by the eye, and which are limited by white noise, the resolution limit can be predicted from a knowledge of only two parameters, the noise power per unit bandwidth, and the sine wave response of the system.

A selective amplifier can be used with signal-generating pickup tubes to obtain a direct measure of the sine wave response from a square wave input. In addition to obviating the tedious calculations involved in converting from a square wave to a sine wave response, the use of a selective amplifier results in a reduction of noise in the
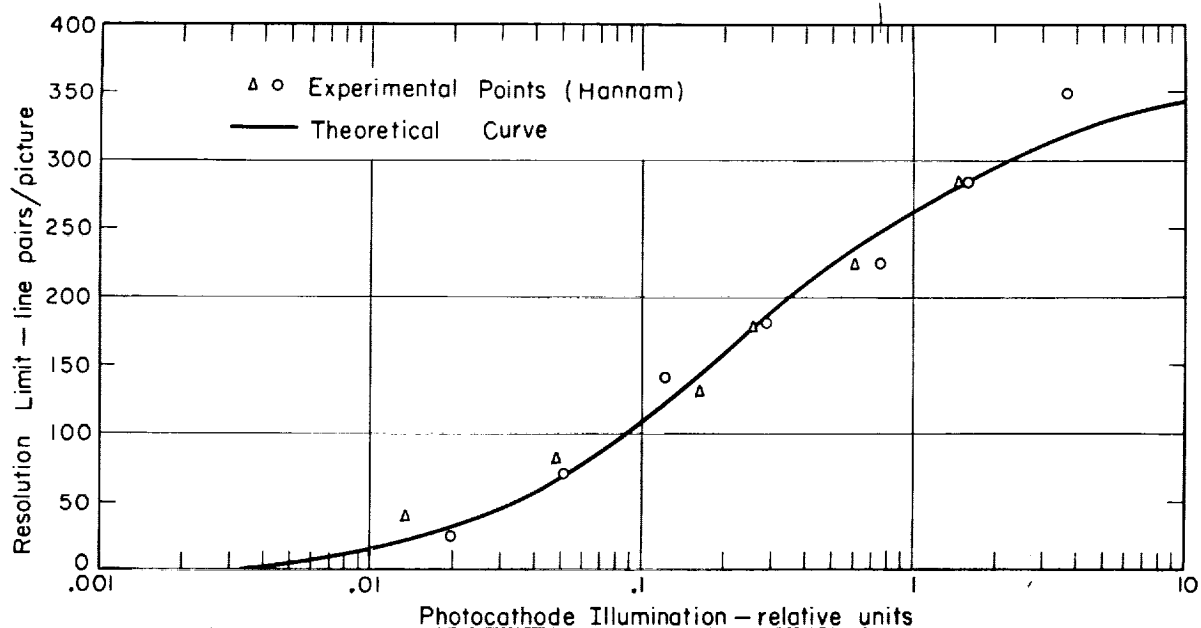
77

FIGURE 11-6.—Comparison of experimental and calculated resolution for two image orthicons.

oscilloscope display. Because the demands on signal-to-noise ratio increase linearly with the line number, and the sine wave response usually falls off with at least the square of the line number, the resolution limit varies only slowly with signal input.

Future work should utilize the methods described in this paper for quantitatively investiga-ting the effects of nonwhite noise on the resolution limit.

Acknowledgment

The authors wish to thank Messers. L. F. Mollenauer and R. O. McIntosh for contributing the section on "Measurement of Sine Wave Response."

Discussion

F. F. HALL, Jr.: Would you mention the brightness of the monitor screen?

R. J. SCHNEEBERGER: Each viewer was permitted to adjust the brightness of the monitor screen to suit himself.

J. JOHNSON: What was the size of the equivalent sampling aperture used in the signal-to-noise measurements? In the figure in which you show the intersection of a sine wave response function and a signal-to-noise function (fig. 11-4), how do you decide on the common scale in which to plot the two functions?

R. J. SCHNEEBERGER: In the measurements on the signal-to-noise ratio required to detect a given resolution, both signal and noise were artificially generated and the amplifier was flat with a rather sharp cutoff at 5 mc/sec. To establish a scale, it is necessary only to measure the signal-to-noise ratio at one convenient line number and at a high-enough light level where instrumentation is not a problem.

J. F. ROESLER: You mentioned using a photocathode of 100 microamps per lumen sensitivity. Was this a S-20 (trialkali) cathode and measured by a 2,780° K light source?

R. J. SCHNEEBERGER: The arguments presented are based on the current from the photocathode and are therefore independent of the particular type of photocathode.

References

1. ROSE, A.: J. Opt. Soc. Amer., vol. 38, 1948, pp. 196–208.
2. COLTMAN, J. W.: J. Opt. Soc. Amer., vol. 44, 1954, pp. 234–237.
3. SCHADE, O. H.: Natl. Bur. of Standards Circ. 526, 1954, pp. 231–258.
4. COLTMAN, J. W.: J. Opt. Soc. Amer., vol. 44, 1954, pp. 468–471.
5. COLTMAN, J. W., and ANDERSON, A. E.: Proc. IRE, vol. 48, 1960, pp. 859–865.
6. HANNAM, H. J.: Development of New Thin Film Targets for the Image Orthicon. Contract DA–44–009–ENG–3652.
7. THOMPSON ET AL.: RCA Rev., vol. 6, 1941, pp. 114–117.

12. LOW CONTRAST THRESHOLD IMAGING

G. A. Morton, *Conversion Devices Laboratory, Electron Tube Division, Radio Corp. of America*

Abstract

The threshold imaging of low contrast objects presents a somewhat different problem from that of high-contrast imaging. It is advantageous to use a television camera tube in order to take advantage of its contrast enhancement capabilities, and to use image intensification so that the limiting noise is due to the statistical fluctuations of photoelectrons rather than system noise. The limit of contrast sensitivity is then determined by the statistics of the intensification system and storage capacity of the camera tube. These limits are discussed and methods of increasing the effective storage capacity of the system are proposed.

Introduction

The treatment of threshold imaging is generally from the standpoint of high-contrast objects at very low light levels. The problem of observing low-contrast objects is of equal importance. While the general approach to the problem is similar to that of high-contrast objects, nevertheless, there are important differences and differences which affect the means used for making the observation.

When using an electronic intensifier to aid in viewing a high-contrast object at low light levels, the limiting of sensitivity is usually set by a background in the viewing device (in particular, a nonuniform background) and the practical upper limit to the integration time (i.e., storage time) permitted by the intensifier. For example, where it is a direct-view intensifier image tube, the integration of the eye, namely, 0.2 second, is the maximum allowed storage time. On the other hand, if the device is an intensifier orthicon, the storage time may be much longer, the limit being set by target leakage.

For low-contrast images, the average illumination is generally high enough so that the background of the device does not set the limit to the sensitivity. Instead, the limit is set by—

    1. The contrast resolution of the eye.

    2. The statistics of the gain mechanism of the intensifier.

    3. The storage capacity of the viewing device.

    4. The integration time.

The limit set by the contrast resolution of the eye can be easily surmounted by the use of a television camera tube rather than a direct-view image tube since with the former it is possible to enhance the contrast as much as necessary by suitably setting the background level and the gain system. For this reason, the following discussion assumes that some form of television camera tube will be used.

For reasons that will become apparent as the discussion proceeds, it is advantageous to use an intensifier. The statistics of this intensifier will be considered in detail.

The question of integration time and storage capacity will be reserved for a later section.

The Statistics of Intensifiers

Going back to the basic argument which has been so successfully used in discussing the limiting sensitivity for imaging, it is assumed that a perfect image sensor is one which is capable of counting the photons arriving on the sensing surface. A threshold sensitivity can then be calculated in terms of the statistical fluctuation of the incident photons and the number of excess photons there are in an illuminated area. This is shown in figure 12-1. In this figure, the equation for the limiting sensitivity in terms of image contrast is given. This leads to an expression for contrast limit in terms of resolution, illumination, and certainty coefficient k.

$$\frac{\Delta I}{I} > k \sqrt{\frac{4}{3} \frac{l^2}{A_c \gamma \kappa T}} \frac{1}{\sqrt{2I}} \tag{1}$$

where

    I = average (background) illumination
    γ = cathode quantum efficiency
    κ = photons/lumen
    A_c = cathode area
    l = TV lines

79

Interpreting this argument in terms of a practical sensing device, it must be first recognized that photons cannot be sensed and counted directly, but must be allowed to interact with matter to produce a chemical or an electrical event. When this event is the emission of a photoelectron, quantum efficiencies in the blue as high as 30 percent to 35 percent can be achieved so that if there were no further degradation of sensitivity, the threshold illumination would be less than a factor of 2 greater than that required for an ideal device.

One of the conditions which has to be fulfilled in order to avoid further degradation of sensitivity is that the limiting noise must be due to the statistical fluctuation of the photoelectrons from the scene being imaged with no increase from noise introduced by the system. An image orthicon does not achieve this maximum sensitivity because, over the working range of interest, the limiting noise is that due to the return electrons in the scanning beam rather than the shot noise of the photoelectrons. The camera tube can be modified so as to increase its sensitivity by interposing a two-dimensional current amplifier between the photocathode and the storage target. This amplifies both the image signal and the photoelectron shot noise. In order to insure that the photoelectron noise be greater than the beam noise, the gain of this amplifier should be of the order of 50. Where such an amplifier is used, it immediately raises the question of the effect of such an amplifier on the statistics of the amplified electrons. It is of interest to consider two cases; one where this amplifier employs secondary emission and includes several cascaded stages to achieve the required total gain, and an intensifier
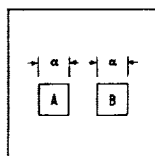
$N_A = n_A a^2 T$

$N_B = n_B a^2 T$

$N_A - N_B \gtrsim k \sqrt{N_A + N_B}$

WHERE n_A, n_B = NUMBER OF ELECTRONS/CM²/SEC.

IN TERMS OF ILLUMINATION:

$n_A = \gamma \kappa I_A$

$n_B = \gamma \kappa I_B$

ALSO $a^2 = \frac{4}{3} \rho^2$ WHERE I_A, I_B = LUMENS/FT²

γ = QUANTUM EFFICIENCY
κ = PHOTONS/LUMEN
C_A = CATHODE AREA
ρ = TV LINES (4:3 ASPECT RATIO)

HENCE $I_A - I_B \gtrsim k \sqrt{\frac{4\rho^2}{3C_A \gamma \kappa T}} \sqrt{I_A + I_B}$

FIGURE 12-1.

where the gain is obtained in a single stage as can be accomplished with an intensifier consisting of a phosphor-photocathode combination. Such an intensifier screen consists of a phosphor film optically coupled to a photocathode so that electrons striking the phosphor cause photoelectrons to be emitted from the corresponding point on the photocathode. With 25 KV between the cathode and intensifier, gains of 50 to 80 have been obtained.

Extensive measurements on secondary emission multipliers show that the pulse height distribution of single electrons from the photocathode is ex-
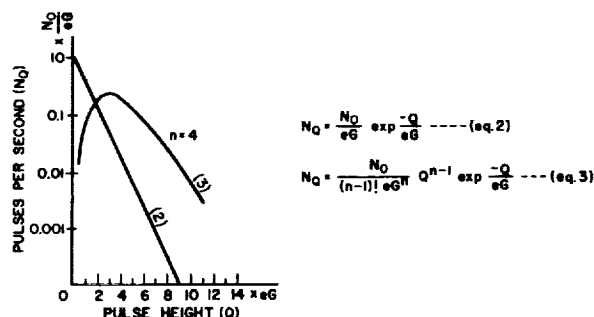
FIGURE 12-2.

ponential as illustrated in figure 12-2. The form of this distribution can be expressed by Eq. (2).

$$N_Q = \frac{N_0}{eG} \exp -\frac{Q}{eG} \tag{2}$$

where

N_Q = number of pulses/sec per unit pulse height with pulse height Q
N_0 = number of electrons/sec from cathode
G = gain of multiplier
Q = charge in pulse at multiplier output

If groups of exactly n electrons leave the photocathode, the pulse height distribution becomes that expressed by Eq. (3).

$$N_Q = \frac{N_0}{(n-1)!eG^n} Q^{n-1} e^{-Q/eG} \tag{3}$$

where n = number of electrons per group.

For illustration, the form of this distribution for exactly four electrons from the cathode is shown on the figure. It can be readily shown that with this distribution, groups of electrons with an average number of n electrons and random in origin, thus having a r.m.s. deviation of $\sqrt{n}$ about

this average, after multiplication will have a pulse height distribution with an r.m.s. deviation of $\sqrt{2n}$. The r.m.s. deviation is unaffected by the gain per stage over the range of gains giving an exponential pulse height distribution for single electrons (i.e., up to gains of 6 to 8 per stage or more). Therefore, an intensifier based on this form of amplification would require 40 percent more illumination than the ideal device.

On the other hand, an intensifier screen having a gain of 50 with a pulse height distribution which is essentially Gaussian introduces a negligible increase in the r.m.s. deviation of the electrons amplified. Thus there is a significant advantage in using a single high-gain amplifier stage between cathode and storage target for low-contrast threshold imaging.

Integration Time and Storage Capacity

The most important limit to low-contrast sensing is that imposed by the limited storage capacity of the image orthicon target. A normal image orthicon working in the full storage range (e.g., below the knee) has a maximum signal-to-noise ratio of about 30. This ratio can be increased somewhat by increasing the target capacity. However, this effect is technologically difficult to accomplish and the target capacity can only be increased slightly without introducing basic problems. In terms of contrast, two areas of brightness, B and $B+\Delta B$, would produce two areas on the target having charges equal to $Q=kBT$ and $Q+\Delta Q=k(B+\Delta B)T$ and a contrast

$$\left(\frac{\Delta B}{B}\right)_{min} = \left(\frac{\Delta Q}{Q}\right)_{min} = 1/30, \text{ or 3 percent.}$$

The value of the contrast cannot be reduced by increasing Q either through intensification or increased storage time since this would simply increase the surface potential of the target to a point where the operation was above the knee. Therefore, under conventional operation, the low-contrast sensitivity of an intensifier orthicon is set by the limited storage capacity.

The effective storage capacity of the system may, however, be greatly increased by the use of multiple storage. The steps required for multiple storage are indicated in figure 12–3. The intensifier orthicon is operated at a frame rate which is much higher than the permissible integration period. The black level is set so that the video signal contains the noise and noise plus signal only and the d.c. component of the stored signal
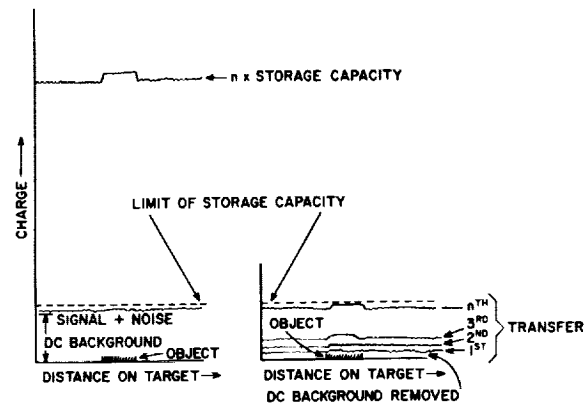
FIGURE 12–3.

is rejected. This video signal is then stored on a storage tube and accumulated for a time equal to the allowed integration time. During this second storage, the noise from successive frames increases by the square root of the number of the frame while the signal increases linearly. Thus, there is an enhancement of the contrast sensitivity. It should be emphasized that for maximum effectiveness, the noise which is stored on the storage tube must be that due to the shot noise of the electrons from the primary photocathode. For this reason, there must be an intensifier stage between the photocathode and the target. The double storage is a method of eliminating the d.c. component of the signal from a low contrast image and its environs. This component of charge does not contain useful information. Figure 12–4 shows a schematic circuit block diagram of a double storage system.

It is possible to accomplish the equivalent of double storage in a single device. Figure 12–5 shows one way in which this may be accomplished.

FIGURE 12–4.

81

Figure 12-5.

The intensifier element is similar to that described. Electrons from the primary cathode are amplified by the intensifier screen and then strike the storage target where they produce secondary emission a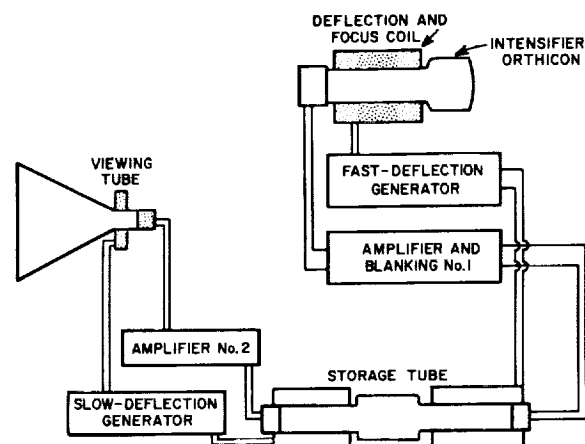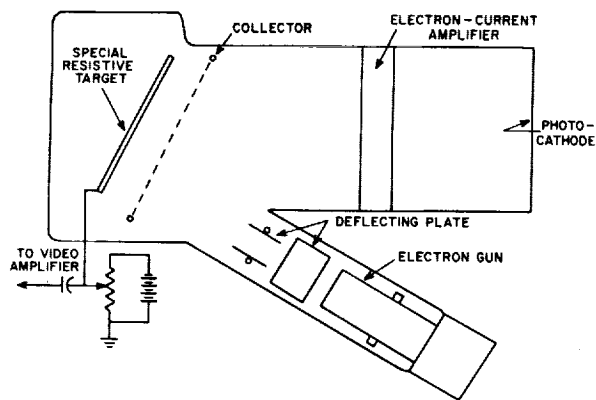s in the case of the normal image orthicon. The low-velocity scanning beam and the electron image fall on the same side of the target. The intensifier gain is assumed to be sufficient so that the charge stored on the target is great enough to make the use of a return beam secondary emission multiplier unnecessary. The signal is removed by the capacitative coupling between the signal plate at the back of the target and the element of the target surface. The target is made of a slightly conducting dielectric whose thickness is chosen to give high capacity per unit area between the front surface and the signal plate.

In operation, the beam holds the front face of the target at essentially cathode potential while the signal plate is made negative. The operation of this tube can be described as follows: the potential between the front surface of the target and the signal plate causes a constant current to flow. The target resistance and bias voltage is adjusted so that this current is approximately equal to the average current of the low-

contrast image and its background. The target resistance is made large enough so that the variations in potential over the surface due to the image cause a negligible change in the current flow through the target. This current flow represents a continuous drawing off of the d.c. component of the background.

In operation, during a frame time, the excess charge accumulated by the target is only that needed to accumulate the noise and signal from the scene under observation. For clarification, the following quantitative example is cited. Let us assume that the background illumination causes the release of 10^8 electrons/cm^2/sec from the primary cathode and that a storage time or frame rate of 1 per second is employed. Assuming 10^4 picture elements per cm^2, the rms deviation in the number of electrons per element per frame will be 100, or 1 percent of the photocurrent. If it is assumed that five times the rms deviation is sufficient charge to accommodate the statistical fluctuations, 95 percent of the photo current constitues the d.c. background. If, now, the intensifier element has a gain of 100, the current reaching the target will be 1.6×10^{-9} amps/cm^2. The voltage between the front of the target and the signal plate is adjusted so that the current flowing through the target equals $1.6 \times 10^{-9} \times 0.95$. The resistance of the target would be adjusted so that the voltage required to produce this current would be 100 volts or more. This is large compared to the signal voltage due to the stored image, which will be of the order of a few tenths volt. This means that the resistance through the target should be of the order of 1.6×10^{11} ohms/cm^2. This type of operation gives results equivalent to a normal target having 20 times the charge storage capacity. It must be made clear that a camera tube of this type has not yet been developed. However, the principle may be of value if the need arises for a camera tube for viewing very low-contrast images.

Discussion

M. R. Dachs: Don Cope, in discussion of the isocon, said that target noise is approximately the same magnitude as beam noise; therefore, will adding additional storage elements increase noise once again?

G. A. Morton: At the levels under discussion, the beam noise, if an intensifier stage is not used, is much larger than the target noise. An intensifier stage is used to bring the photocurrent shot noise up to a value above beam noise (the signal is, of course, also amplified by the same amount). Under these circumstances, the second storage does not cause a significant increase in noise.

H. DAY: What advantage does the use of a resistive target have over using a flood beam to provide the uniform charge: Also high capacitance target: In what way does the noise of the resistance current contribute to the noise in the stored signal? Dosen't this decrease the S/N gains made by integration?

G. A. MORTON: A flood or spray beam can be used to provide the uniform charge to compensate the d.c. background component. It presents problems of uniformity and avoidance of scattered electrons reaching the signal multiplier which, while nonfundamental, are technically difficult. The very high target capacity required to achieve significant improvement in the contrast places demands of high beam current and low beam impedance on the gun that cannot at present be realized. Background compensation with a resistive target adds noise to the stored signal, as does compensation with a spray beam to an even greater extent. However, this noise is below the shot noise of the primary photoemission when an intensifier is used and does not significantly lower the S/N ratio of the system.

G. SUITS: Can't the use of long persistent phosphors perform the same function as an electrostatic storage screen?

G. A. MORTON: The second integration can be performed with either a long persistence phosphor or photographic film. However, these means decrease the flexibility of the system inasmuch as they do not permit a second contrast enhancement by the gain and black-level adjustment which is possible when a storage tube is used for the second integration.

G. W. GOODRICH: A comparison was made between the expected performance of secondary-emission-based intensifiers and phosphor-photocathode intensifiers. The latter was said to be better because it has a stage gain of 50. Since the pulse height distribution of multipliers is experimentally found to be exponential, regardless of gain per stage, there is some question whether similar results will not be found in the pulse height distribution from phosphor-photocathode combinations. Are there any experimental results to substantiate the superiority of the phosphor-photocathode combinations?

G. A. MORTON: The statistical performance of a phosphor-photocathode combination was estimated from the behavior of a phosphor used for scintillation counting, which shows a gaussian pulse height distribution rather than the exponential distribution exhibited by secondary emission multipliers.

A. E. ANDERSON: The certainty coefficient K obtained for the threshold bar pattern detection at low-contrast images is 5 which is in good agreement with that estimated for isolated objects in your paper.

13. PERFORMANCE OF IMAGE ORTHICON TYPE INTENSIFIER TUBES

JAMES S. PARTON and JOHN C. MOODY, *Warfare Branch, USAERDL*

Introduction

During the past several years the Warfare Vision Branch of the U.S. Army Engineer Research and Development Laboratories has been evaluating various types of image orthicon tubes used as image intensifiers in low-light level, remote-viewing systems. This is a part of a research and development program to provide a nighttime remote-viewing capability for the U.S. Army. This paper is specifically concerned with the experimental evaluation of the intensifier image orthicon and the image orthicon tube types. Both of these tube types utilize multialkali (S–20) photocathode surfaces and a magnesium oxide target material. A wide target to mesh

spacing reduces capacitance between target and mesh and provides a greater signal voltage for a given amount of charge on the target at low-light levels.

The following tube factors were measured:

Intensifier electron gain.
Transfer characteristics.
Signal-to-noise ratio.
Aperture response (Ne).
Static limiting resolution.
Dynamic limiting resolution.
Rise and decay time response.

Experimental Setup

The test facility shown schematically in figure 13–1 was used to provide controlled and carefully

$$E = \frac{B \; T_L \; T_F}{4 f^2 (1 + m)^2}$$

$f = {}^1/_{No}$ OF LENS

m = MAGNIFICATION

T_L = LENS TRANSMISSION
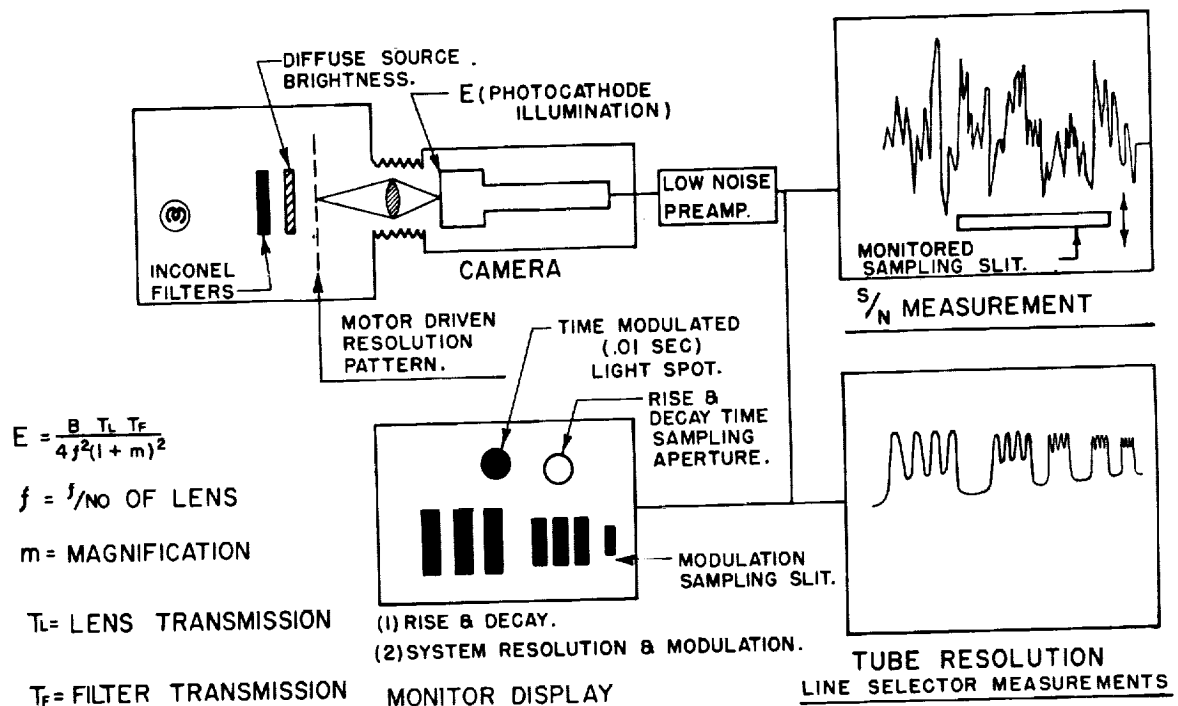
T_F = FILTER TRANSMISSION

FIGURE 13–1.—Experimental setup.

measured photocathode highlight illumination through the range of 10^{-1} to 10^{-8} foot-candles. This range of photocathode illumination is sufficient to simulate all nighttime scene brightness conditions. All of these measurements were made using light of 2,870° K color temperature. The tubes were evaluated using highlight photocathode illumination rather than scene highlight brightness. The television camera is a standard RCA TK-31A field camera system, modified by using a low noise video preamplifier. The preamplifier noise is equivalent to 3×10^{-9} amperes rms noise through the 18-kilohm load resistor. A conventional 525-line picture, 30 frames and 60 fields per second was used in taking the data. The bandpass of the video amplifier chain is 6 megacycles. The pickup tube was operated at temperatures equal to or slightly above ambient for the room.

Intensifier Electron Gain Measurements

Figure 13-2 shows the intensifier section gain as a function of accelerating voltage. Electron gain is defined as the current emitted from the second photocathode divided by the current emitted from the first photocathode. The second photocathode current was carefully measured by means of an electrometer inserted in series with the second photocathode. The primary photocathode current was calculated from a known light flux falling on the photocathode surface. The ratio was thus determined after the dark current was subtracted from the readings. A theoretical maximum gain of about 90 is possible in the intensifier section of these tubes. Gains of 60 have been achieved as is shown by the curve of figure 13-2.
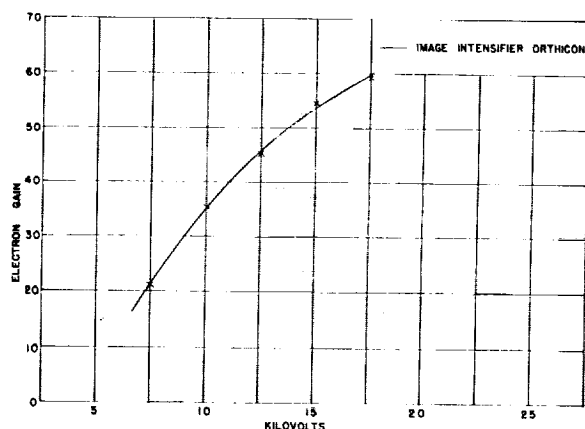

FIGURE 13-2.—Intensifier stage electron gain versus voltage.

Transfer Characteristics

The transfer characteristics for the two tube types are shown in figure 13-3. These measurements were taken using a line-selecting oscilloscope so as to see only one scan line of information in each frame time. A signal was taken directly from the output of the image orthicon tube and fed into a sensitive preamp of an oscilloscope. The voltage step generated by the oscilloscope was used to calculate the image orthicon output current on the basis of the load resistor used by the image orthicon camera.

The two types of tubes evaluated produce curves of similar slopes, neither possessing a definite knee. The curves are separated by a factor of about 10.

Signal-to-Noise Ratio Measurements

A Tektronic type 545 oscilloscope connected as a line-selecting oscilloscope was used to measure the signal-to-noise ratio. A black to white transition for a single line taken from the TV picture was displayed on the oscilloscope. The peak signal was taken as the black to white amplitude with the noise averaged out. The noise was measured in the black region since the noise content is greater here than in the white regions. A photomultiplier tube with a horizontal slit 1 centimeter in length and about 0.002 inch in width accepts focused light from the oscilloscope pattern as this slit is moved in the vertical direction. The maximum and the 0.6 amplitude points are noted on a meter measuring the photomultiplier tube output current. One-half the displacement of the 0.6 value was taken as the noise level. Figure 13-4 shows a unity signal to noise ratio for the intensifier orthicon at about 10^{-7} ft.-c. photocathode illumination and unity signal-to-noise ratio at 7×10^{-6} photocathode illumination for the high-gain target image orthicon.

Aperture Response

The aperture response was measured using a set of vertical bar patterns of various line numbers per inch. The amplitude response for each line number was recorded from an oscilloscope choosing as unity amplitude a low line number response. These values were squared and a curve plotted for aperture response.

The area included under this aperture response curve was taken as the value for the equivalent
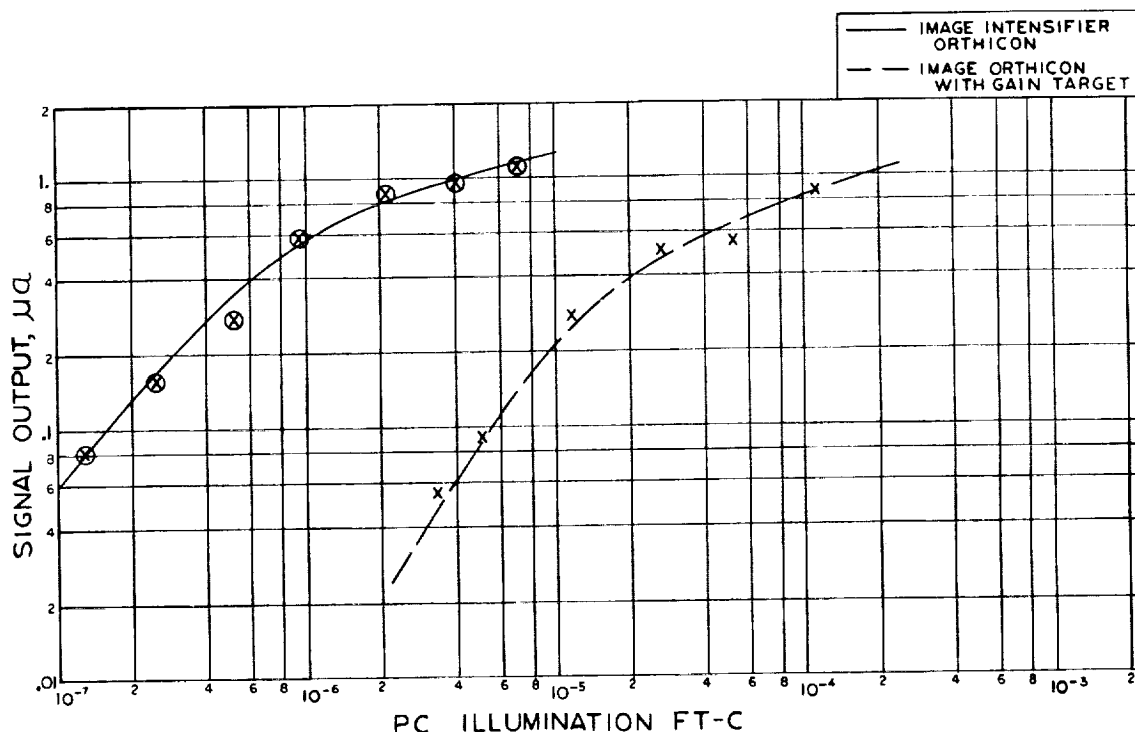
line number (Ne)[1] in TV lines for the system. For a standard (5820) type image orthicon, a (Ne) value of 230 is typical when the tube is operated near the knee of its characteristic curve. The values for the two types of tubes evaluated are shown in the table below for several levels of photocathode illumination.

Equivalent line Number Ne, TV lines, at each photocathode illumination in foot-candles

Tube	2×10^{-5}	2×10^{-6}	2×10^{-7}	2×10^{-8}
Image intensifier orthicon...............	......	135	125	73
Image orthicon with high-gain target.....	95	9C	......	......

Static Limiting Resolution

Static limiting resolution is taken as the highest TV line number that can be resolved while viewing the kinescope. This was done throughout the range of photocathode illumination levels under which the tubes are operated. Standard RETMA patterns and bar patterns were used for these measurements. These tubes possess very good sensitivity as shown in figure 13-5 at low light

levels. The intensifier image orthicon can resolve 200 TV lines at about 4×10^{-8} ft-c. photocathode illumination, while the image orthicon with the high-gain target can resolve 200 TV lines at about 4×10^{-7} ft-c. photocathode illumination. The intensifier image orthicon is about 10 times more sensitive than the image orthicon with the high-gain target for the same TV line number.

Dynamic Limiting Resolution

For measuring limiting dynamic resolution, a mechanism was used which moved bar patterns of varying line numbers per inch across the field of view of the TV camera in various periods of time. A human observer at the kinescope determined which line number he was able to resolve for these conditions. This TF line number was taken as the limiting resolution for the specified time; e.g., the time required for a point to traverse the photocathode in the horizontal dimension. In figure 13-6 it should be noted that the intensifier image orthicon is about 100 times more sensitive than the image orthicon with the high-gain target under conditions of a moving scene. It should also be pointed out that these tubes require from 10 to 100 times more light to resolve
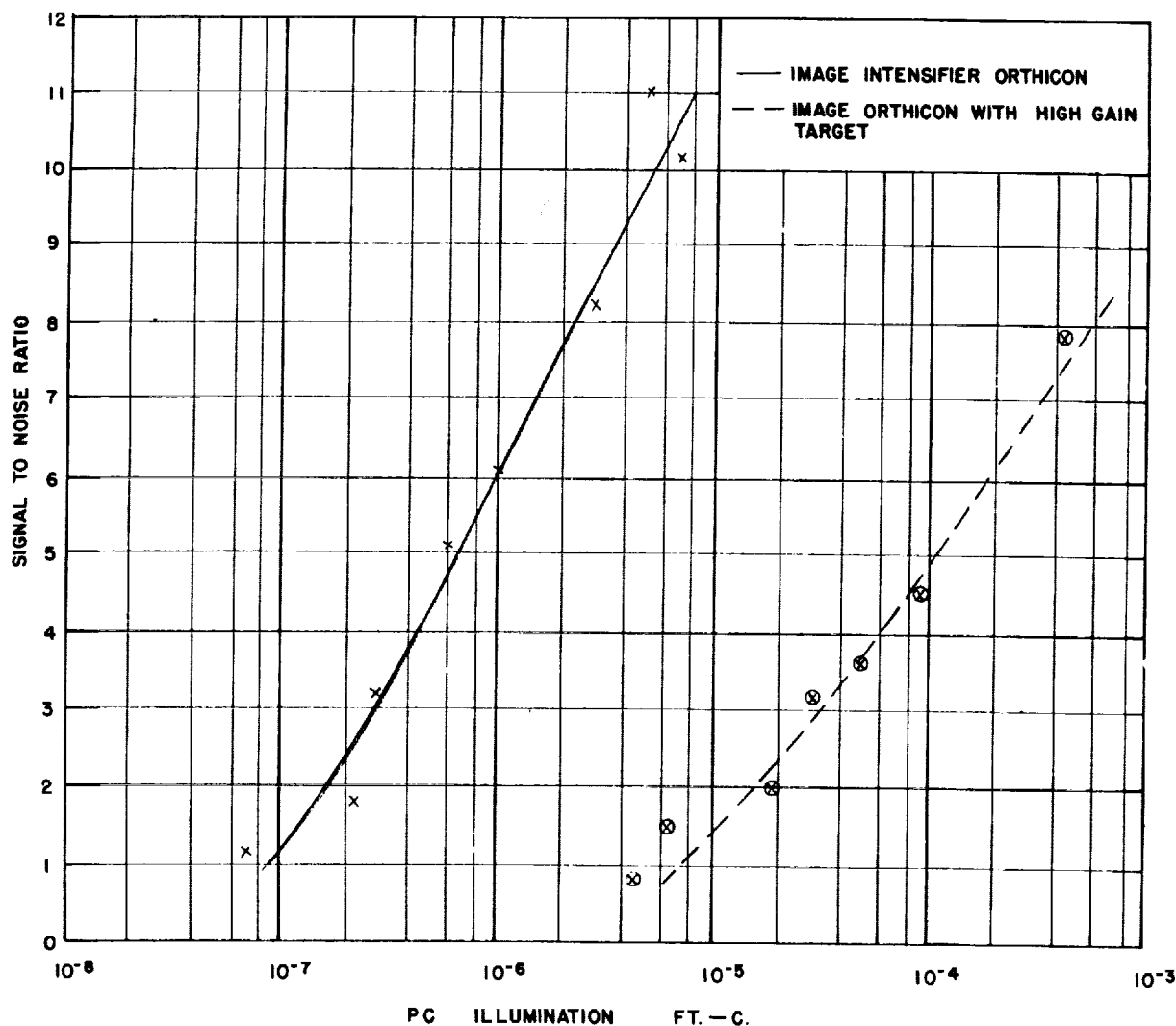
FIGURE 13–4.—Signal to noise versus PC illumination.

Rise and Decay Time Characteristics

the same TV line number as under static conditions.

Another approach to measuring dynamic limiting resolution is to measure the rise and decay of a spot of light falling on the photocathode, e.g. the system response to a step function input. Here the camera was focused on a spot of light ¼ inch in diameter. The television system was then adjusted for optimum operating conditions. A photomultiplier tube was presented this spot of light from a kinescope. The output from the photomultiplier tube was displayed on an oscilloscope and the time measured for this spot of

light to go from a zero level to its maximum amplitude when the light source was chopped by a camera mechanism equipped with focal plane shutter. The time required for the spot to disappear from the kinescope was also noted. This data appears in the table below. No attempt has been made to correlate this information to dynamic resolution. This approach seems the most logical method whereby dynamic resolution may be measured. Note from the table that if a rise, decay sum is taken for each tube type at their lower operating limit a difference of a factor of 100 appears in photocathode illumination. This is the same difference as appeared in the dynamic resolution curves.

88

Rise and decay characteristics for intensifier orthicon and high-gain target orthicon using ¼-inch spot size

Light level PC ft.-c.	Rise		Decay	
	Time I.I.O.	Secs I.O	Time I.I.O.	Secs I.O
1.1×10^{-4}	....	0.05	....	0.15
5.7×10^{-5}	....	.05	....	.25
1.4×10^{-5}	....	.15	....	.25
4.1×10^{-6}	0.1	....	0.15	....
6.9×10^{-6}	....	.15	....	.30
3.6×10^{-6}	....	.3	....	.40
5.1×10^{-7}	.1	....	.2	....
1.3×10^{-7}	.2	....	.2	....
6.3×10^{-8}	.2	....	.3	....

Comparison of Ideal and Available Performance of Pickup Devices

Ideal performance of any type of picture pickup device is performance limited only by the finite number of available light quanta. Fluctuations in the number of photons received from the scene being viewed constitute a fundamental noise limit to the information available from the scene. Rose [2] has derived a relationship for the ideal performance of any picture pickup device, using as a test object, a dark square on a lighter background. Here an attempt is made (see fig. 13-7) to compare the performance of the intensifier image orthicon with the ideal performance for a pickup device. Certain arbitrary
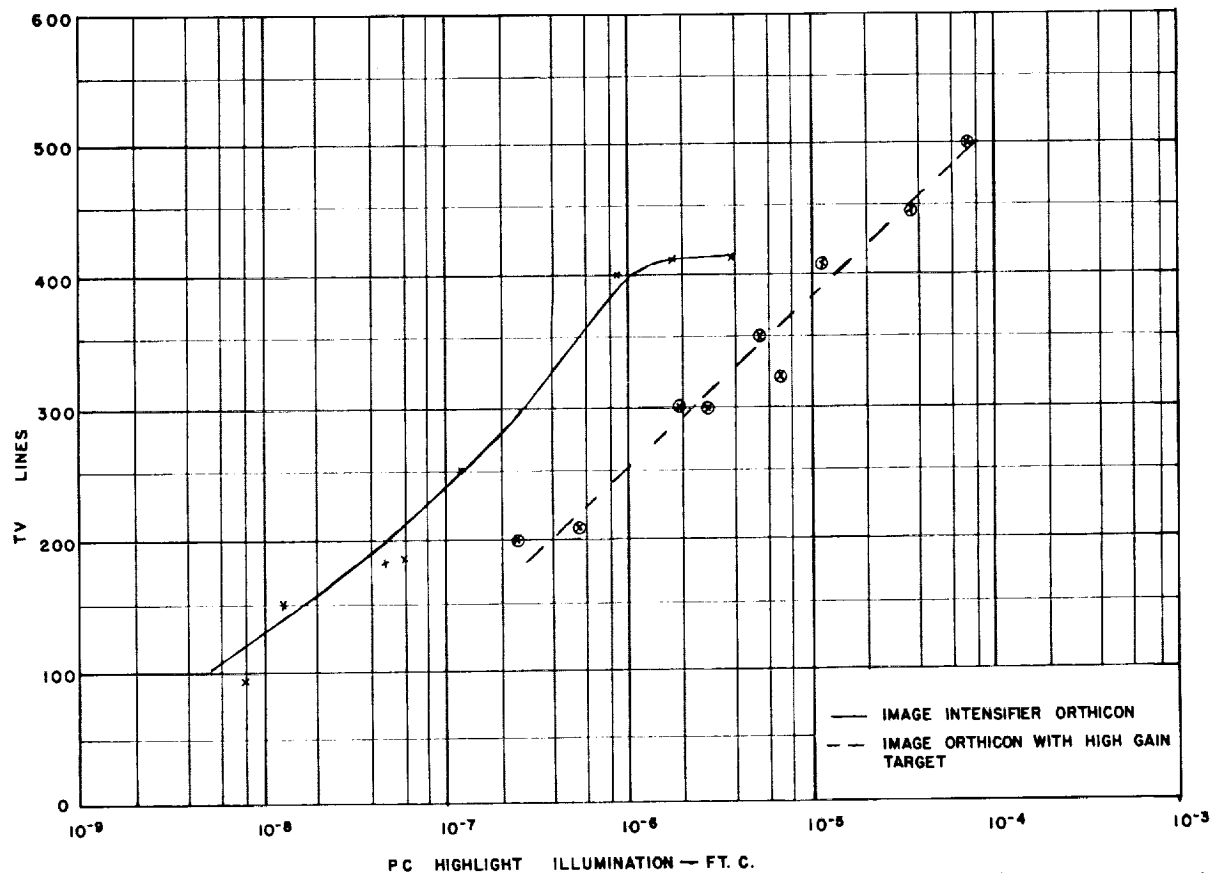
FIGURE 13-5.—Limiting resolution versus PC illumination.
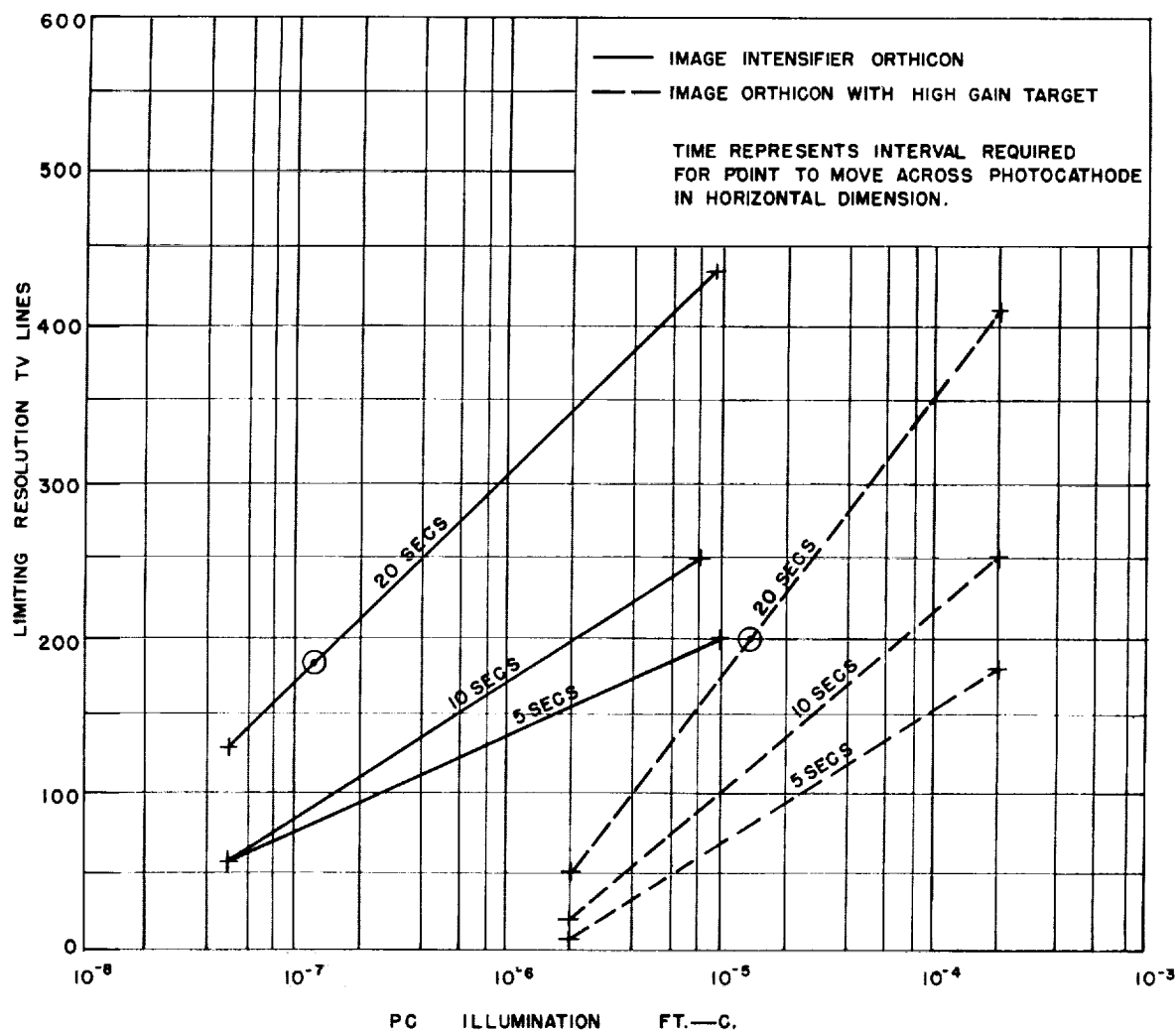
FIGURE 13-6.—Dynamic resolution versus photocathode illumination.

values must be selected for Rose's relationship. The two values most in question are threshold signal-to-noise ratio and integration time. The values used are shown below. This relationship was converted at this laboratory to a form more suitable for use with image orthicon tubes using geometrical optics and assuming a 4 by 3 picture aspect ratio.

$$E=\frac{4k^2eR^2}{3C^2StA}$$

E= photocathode illumination due to background illumination in ft.-c.

k= threshold signal to noise ratio=1.2.

e= electron charge, coulombs.

R= limiting resolution, the number of squares which can just be detected against the background which will fit in the picture height.

C= contrast.

A= primary photocathode picture area in square feet.

t= exposure time or integration time=$\frac{1}{5}$ sec.

S= primary photocathode sensitivity, amperes/lumen (white light)=150×10^{-6} A/lumen.

90

FIGURE 13–7.—Theoretical limiting resolution squares of various contrast.

Conclusion

In conclusion, it is pointed out that these pickup tubes are quite sensitive when looking at a static scene. The photon noise limitation is being approached at low light levels. However, for moving scenes these tubes suffer considerably. A small amount of motion of the scene seems to require that the light level be from 10 to 100 times greater for the same resolution as under static conditions. This condition is very serious in both tube types and mor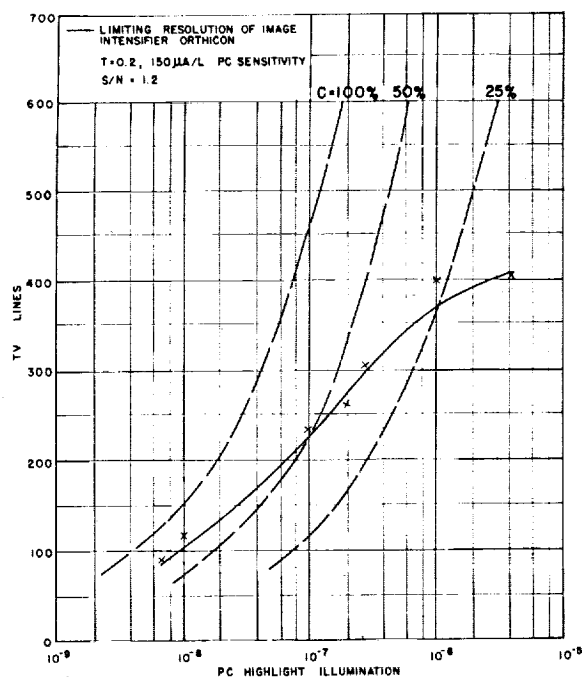e pronounced in the image orthicon with the high-gain target. Pickup tubes for low light level operation, with the ability to resolve moving scenes, are needed in order to provide the military with remote-viewing systems needed in many applications.

The authors would like to thank Mr. John Johnson and Mr. Myron W. Klein of the Warfare Vision Branch, U.S. Army Engineer Research and Development Laboratories, for their continued interest and many helpful suggestions and discussions.

Discussion

R. H. HARDIE: What is meant by 100 percent contrast?

J. S. PARTON: A 100-percent contrast, as referred to here, is for a ratio of the brightness in the white area to the brightness in the black area of 100 to 1. For all practical purposes this is considered to be 100 percent contrast.

J. WATERS: What is meant by your statement that a single-stage intensifier orthicon is almost cathode noise limited?

J. S. PARTON: If we look at the curves shown in figure 13–6, we see the theoretical curves for an ideal pickup tube plotted from work done by Rose.[2] If we superimpose a limiting resolution curve of the image intensifier orthicon tube, we find at a photocathode illumination level of 10^{-8} ft.-c. and a scene contrast of 100 percent, we are very near this theoretical limit.

C. D. SALZBERG: Can some of the degradation of limiting resolution with moving targets be attributed to the observer, or is it solely a deficiency in the tubes?

J. S. PARTON: If we look at the curves shown in figure 13–5, we see that the tines shown for a spot of light to move across the photocathode are quite long. In this experimental setup, a 10-inch monitor was used which gave the observer ample time to determine what line number he had resolved. The observer could repeat the test as often as was required to make a decision. The degradation of resolution is a loss in the pickup tube rather than an observer limitation.

F. B. MARSHALL: Did you say 10^{-8} foot-candles to the photocathode occurs for typical nighttime illumination?

J. S. PARTON: Typical nighttime illumination levels vary from 10^{-2} to 10^{-5} foot-candles on the ground. Due to the reflectance of the scene and lens transmission, the photocathode illumination is between the value of 10^{-7} and 10^{-8} foot-candles.

References

1. SCHADE, O. H.: New Systems of Measuring and Specifying Image Definition, Optical Image Evaluation. Natl. Bur. Standards Circ. 526, 1954, pp. 231–258.
2. ROSE, A.: Television Pickup Tubes and the Problems of Vision. Advances in Electronics, vol. 1, Academy Press, New York, 1948.

14. GAIN AND RESOLUTION OF FIBER OPTIC INTENSIFIER

Paul J. Dolon and Wilfrid F. Niklas, *The Rauland Corp., subsidiary of Zenith Radio Corp.*

Introduction

High-gain, photoelectronic image intensification is applied under conditions of low incident light levels whenever the integration time required by a sensor or recording instrument exceeds the limits of practicability. Examples of such situations are (aerial) night reconnaissance,[1] the recording of radioactive tracers in live body tissues,[2] special radiography in medical[3] or industrial applications,[4] track recording of high energy particles,[5] etc.

High-gain, photoelectronic image intensification may be achieved by several methods; some of these are listed below:

(a) Cascading single stages by coupling lens systems,

(b) Channel-type, secondary emission image intensifier,

(c) Image intensifier based upon the "multipactor" principle,

(d) Transmission secondary electron multiplication image intensifiers (TSEM tubes),

(e) Cascading of single stages, enclosed in one common envelope.

Cascading single stages by *coupling lens systems* is rather inefficient as the lens systems limit the obtainable gain quite severely. Channel-type image intensifiers[6] are capable of achieving high-gain values; suffer, however, from an inherently low resolution. Image intensifiers based upon the multipactor principle[7] appear to hold promise as far as obtainable resolution is concerned. However, the unavoidable low-duty cycle restricts the effective gain. TSEM tubes have been constructed showing high gain and resolution.[8][9] However, electrostatic focus, important for many applications, has not been realized for these devices. Resolution limitations with electrostatic focus might be anticipated due to chromatic aberrations.[10] Furthermore, the thin film dynodes appear to have a natural diameter limitation wherever a mesh support cannot be tolerated.

Cascaded single stages enclosed by a *common envelope* have been constructed with high gain and high resolution.[11][12] These tubes may differ both in the choice of the electron optical system and in the design of the coupling members. The electron optical system may be either a magnetic or electrostatic one. The magnification may be smaller, equal, or larger than unity.

An electrostatic system suffers generally from image plane curvature leading to defocusing in the peripheral image region if a flat viewing screen (or interstage coupler) is utilized, while a magnetic system requires accurate adjustment of the solenoid, which is heavy and bulky. As it will be discussed later, peripheral defocusing can be improved on by utilizing curved fiber couplers. It should be noted, however, that the paraxial resolution is quite similar for both electron optical systems.

It is felt that fiber-coupled double- (and multi-) stage image intensifiers will gain considerable importance in the future. Therefore, we shall consider in this paper the theoretical gain and resolution capabilities of such tubes. The luminous efficiency and resolution of single stages, fiber couplers, and finally of the composite tube will be computed.

It will be shown theoretically that the high image intensification obtainable with such a tube and contact photography permits the utilization of extremely low incident light levels. The effect of device and quantum noise, associated with such low input levels, will be described.

After these theoretical considerations, constructional details of a fiber-coupled, double-stage X-ray image intensifier will be discussed. Measured performance characteristics for this experimental tube will be listed.

The conclusion shall be reached that fiber-coupled, double-stage tubes represent a sensible and practical approach to high-gain image intensification.

93

Basic Design of a Fiber-Coupled, Double-Stage Image Intensifier

The tube design which forms the basis of the theoretical discussion shall be described now. The electron optical system (see fig. 14–1) is based in principle on the focusing action of concentric spherical cathode and anode surfaces.[13] The inner [anode] sphere is pierced, elongated into a cup, and terminated by the phosphor screen. The photoelectrons emitted from a circular segment of the cathode sphere are focused by the positive lens action of the two concentric spheres, pass through the [negative] lens formed by the anode aperture, and impinge upon the cathodoluminescent viewing screen. The cylindrical focusing electrode permits adjustment of the positive lens part by varying the focusing potential. The anode potential codetermines the gain, G, and magnification, M, of the stage.

Both the photocathode and the image plane of such an electrode configuration are curved concave as seen from the anode aperture. The field-flattening property of the biconcave fiber coupler can be utilized to alleviate the peripheral resolution losses resulting with a flat phosphor-screen or coupling member. For the same reason, the output fiber plate is planoconcave, its exposed flat side permitting contact photography if a permanent record is desired. As it will be shown later, the field-flattening properties of the inter-stage and output fiber coupler comprise indeed the main advantage of such a design.

The second photocathode and both phosphor surfaces are deposited on the fiber plate substrates. The photocathode sensitivities S, phosphor efficiencies P, and anode potentials V of the individual stages shall be distinguished by means of subscripts I and II in the text, where required. Both stages are assumed to have unity magnification.

Theoretical Discussion of Flux Gain

Flux Gain of a Single Stage

The luminous gain of a single stage [14] with $M=1$ (flux gain) is, to a first approximation, given by the product of the photocathode sensitivity S (amp/lumen), the anode potential V (volts), and the phosphor conversion efficiency P (lumen/watt). In general, P is a function of V and the current density,[15] but it shall here be assumed as a constant.

The luminous efficiency $S_L(\lambda) \equiv S_L$ of a photocathode depends on the maximum radiant sensitivity $S_w^{\max}$ and on the spectral distribution of the incident light $E(\lambda) \equiv E$ by the relation:*

$$S_L[\text{amp/lumen}] = S_w^{\max}[\text{amp/watt}] \times \frac{\int ES d\lambda}{680 \int EV d\lambda}$$

(1)

where

$S \equiv S(\lambda)$ . . . normalized radiant photocathode sensitivity.

$V \equiv V(\lambda)$ . . . standard visibility function.

The luminous flux gain of a single stage is given by:

$$G_L[\text{lumen/lumen}] = \frac{S_w^{\max} \int ES d\lambda}{680 \int EV d\lambda} \times V \times P \quad (2)$$

If the input light distribution falls beyond the visible range, $G_L = \infty$ as expected, since $\int EV d\lambda = 0$. Such cases are not considered here.

Efficiency of Fiber Couplers

The efficiency of fiber optics plates depends on four factors: [16] [17]

(a) numerical aperture (N.A.).

(b) end (Fresnel reflection) losses (R).

(c) internal losses (I.L.).

(d) packing efficiency (F.R.).

The numerical aperture of the fibers is given by:**

$$\text{N.A.} = n_0 \sin \alpha_i^n = \sqrt{n_c^2 - n_j^2} \quad (3)$$

where

$\alpha_i^n =$ maximum acceptance angle.

$n_c =$ index of refraction of core glass.

$n_j =$ index of refraction of cladding.

The angle α_i^n is measured in the medium of index n_0. Settled phosphors, as generally used in image intensifiers, have low optical contact with the substrate surface,[16] hence $n_0 = 1$ shall be assumed. The numerical aperture should be in general close to unity. This condition can be satisfied, e.g., with $n_j = 1.50$ and $n_c = 1.76$ or equivalent glass combinations.

---

*The derivation of this equation is contained in the appendix.

**The discussion of the numerical aperture and fiber efficiency is restricted to meridional rays only. A more comprehensive theory, taking also skew-rays into account, has been worked out by R. Potter. [18]
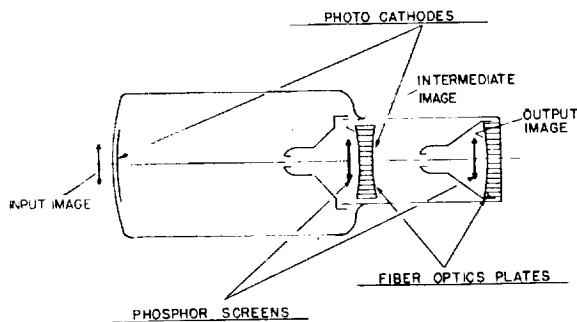
94

FIGURE 14-1.—Schematic cross section of the theoretically
discussed double stage tube.

A sufficiently good approximation for determining the end reflection losses R can be obtained from the angle independent Fresnel formula:

$$R=(n_c-n_0)^2/(n_c+n_0)^2 \qquad (4)$$

For phosphor to fiber and fiber to air surfaces, and assuming $n_c=1.76$, we obtain $R=7.5$ percent. This value may be reduced to 4.6 percent by means of a (very thin) glass layer of index 1.5. Hence, the $(1-R)$ factor for the output fiber coupler is $0.954^2=0.91$.

As the index of refraction of photosensitive surfaces of the SbCs-type [19] lies around 2, the Fresnel losses at the fiber-photocathode interface are about 0.5 percent and the $(1-R)$ factor for the interstage coupler is 0.95. It might be anticipated that multiple coatings will reduce end reflection losses even further.

The internal losses are due to absorption and the small but finite losses suffered in the numerous internal reflections due to deviations from the prescribed, cylindrical fiber cross-section and minute imperfections of the core-jacket interface. These losses depend on fiber diameter and length, absorption coefficient, the mean value of the loss per internal reflection and last but not least, on the angular distribution of the incident light. Explicit expressions (integral averages) are given in the literature.[17] Lacking reliable data for some of the variables, we are relying on experimental data of about 20 percent internal losses for ¼-inch long, small (5–10μ) diameter fibers.[20] This relatively high value is probably due to the small fiber diameters increasing the number of internal reflections. Since we are considering here relatively small diameter (1–1.5 inches) fiber plates, their average thickness can be kept below ¼ inch and their internal losses may be assumed as 15 percent (per plate).

The packing efficiency, F.R., of fiber plates did not receive much attention in the literature,

probably as it is high for the larger fibers generally used, until rather recently. For circular fibers in a closely packed hexagonal array, the packing efficiency is given by:

$$F.R.=0.906(d/D)^2 \qquad (5)$$

where
$d=$fiber core diameter
$D=$center-to-center spacing of fibers, and 0.906 is the ratio of the area of a circle to that of the circumscribed hexagon. For the small diameter fibers now technically feasible and required for about 100 lp/mm resolution, $D=6\mu$. The cladding thickness is about 0.5μ, hence, $d=5\mu$ and F.R.$=0.63$.

Thus, the efficiency τ for each of the two fiber couplers is given by—

	N.A.$\times$(1$-R$)$\times$(1$-$I.L.)$\times$F.R.			
τ(interstage)	1	0.95	0.85	0.63=0.51
τ(output)	1	.91	.85	.63= .49

or approximately 50 percent each.

It must be remembered that the fiber plates replace a glass window and a (mica) membrane, in addition to an optical output lens system. The efficiency τ_l of an f/1 lens at the magnification $m=1$ is:

$$\tau_l=\frac{0.8}{4(f/1)^2(m+1)^2}=0.05$$

Neglecting absorption, the end losses of the coupling membrane and the output window $(n=1.5)$ would be 6 percent and 8 percent. Thus, the combined efficiency of the elements replaced by the two fiber plates (with a combined efficiency of 0.25) is 0.043 or *about six times less than that of the two fiber plates.*

Gain of Fiber Coupled Image Intensifiers

Including the brightness gain $1/M^2$ due to the M^2 area demagnification, the overall gain of a fiber coupled double stage image intensifier is:

$$G_L=\left(\frac{s_w^{max}\int ESd\lambda}{680\int EVd\lambda}VP\right)_I\times\tau_{\text{i. st.}}$$

$$\times\left(\frac{S_w^{max}\int ESd\lambda}{680\int EVd\lambda}VP\right)_{II}\times\tau_{\text{out p.}}\times 1/M^2 \qquad (6)$$

It is obvious that the careful choice of photocathode which maximizes $s_w^{max}\int ESd\lambda$ for a given input E (in the case of the second stage, for the first phosphor screen emission) is very important.*

*See also the appendix.

95

The same considerations should govern the choice of the second-stage phosphor screen for matching with the spectral sensitivity of the ultimate sensor (e.g., photographic emulsion).

We have evaluated the "matching integrals" for two types of photocathodes (S–11 and S–20) and three types of light input. The input light distributions considered are P–11 and P–20 phosphor emission and the so-called "night light" (N.L.) as given by H. W. Babcock and J. J. Johnson.[21] The integrals (in Å units) are listed in table 14–I below:

TABLE 14–I

	P–11	P–20	N.L.
$\int EV d\lambda$	166	821	548
$\int ES_{11} d\lambda$	830	354	511
$\int ES_{20} d\lambda$	800	600	750

The luminous gain of the discussed tube was calculated from Eq. (6) for the 16 possible combinations of S–11 and S–20 photocathodes and P–11 and P–20 phosphor screens, for night light and P–20 light input. (The P–20 input is of interest because it corresponds roughly to the light emission of conventional X-ray fluorescent screens.) The following efficiencies obtained from JEDEC and RCA specifications were used:

$S_{wN}^{max} = 50$ m amp/watt $P_{11} = 36$ lumen/watt (aluminized)

$S_{w20}^{max} = 64$ m amp/watt $P_{20} = 62$ lumen/watt (aluminized)

The following table (14–II) lists the (luminous) gain values computed according to Eq. (6) with $V_1 = V_2 = 20$ KV, $M = 1$:

TABLE 14–II

Input light	II Stage / I Stage	S_{20}–P11	S_{20}–P20	S_{11}–P11	S_{11}–P20
N.L.	S_{20}–P11	5760	9800	4630	8000
P20	S_{20}–P11	3080	5200	2500	4250
N.L.	S_{20}–P20	1520	2600	680	1160
P20	S_{20}–P22	800	1400	360	640
N.L.	S_{11}–P11	3040	5200	2440	4200
P20	S_{11}–P11 .	2360	4000	1800	3260
N.L.	S_{11}–P20	800	1400	360	640
P20	S_{11}–P20	640	1080	280	480

Theoretical Discussion of Paraxial Device Resolution

Resolution Limitations in a Single Stage

The resolution limitations for a single stage are given by the inherent resolution of the electron optical system as well as the resolution capabilities of the cathodoluminescent viewing screen.

The resolution capabilities of an electrostatic system depend on both the choice of magnification and chromatic aberrations. It has been stated previously [10] that a minifying electrostatic system yields a lower resolution than a magnifying system or a system with unity magnification.

Furthermore, the chromatic aberrations depend on the chosen high voltage. In general, a high anode voltage reduces chromatic aberrations and thus increases the obtainable resolution.[13]

The possibility of a space charge blowup of the screen crossover of the elementary electron bundles has also been pointed out.[22] It is obvious that such an influence can only be expected in the final stage of an image intensifier at rather high output levels. Space charge influences will also decrease at increased voltages.

Electrostatic systems of the pseudo-symmetric type have been tested for resolution capabilities by applying electronography.[23][24] A resolution of 70–80 line-pairs per millimeter appears to be feasible.

The inherent resolution of a cathodoluminescent phosphor screen decreases with increasingly aggregate thickness (with increasing anode voltage), decreases with decreasing porosity (thus the advantage of cathodophoretic phosphor deposition) and might be impaired by the normally used

aluminum mirror. Thus, in general, elementary light optical effects, light scatter, and electron scatter determine the obtainable resolution limit. It should be noted that photoluminescence, due to "Bremsstrahlung" generated within the viewing screen by electron impact, appears to be important only if anode voltages in excess of 30 KV are utilized. It has been stated that settled cathodoluminescent phosphor screens may have a limiting resolution of 60 lp/mm[25][26] at high voltage values of approximately 20 KV. For the further discussion, we shall thus assume an electron optical resolution of 80 lp/mm and phosphor screen resolution of 60 lp/mm.

Resolution Capability of Fiber Couplers

The major factor influencing the obtainable fiber coupler resolution is the center-to-center spacing D. Since fibers are arranged in a closely packed array, the closest line separation is the height of the equilateral triangle with sides D, or $\sqrt{0.75}\ D$. Thus (with D in microns), the resolution is in (line pairs per mm) $578/D$. The requirement of 100 lp/mm resolution is satisfied with $D=6\mu$. As it will be shown later, this high-resolution value is required to avoid limiting the overall resolution by the coupler resolution.

It must be appreciated that the fiber spacing is a correct measure of the resolution only if the object-fiber distance is less or equal to D. The resolution of the fiber plate deteriorates rapidly if this condition is not fulfilled. Irregularities of the fiber array may lower the resolution locally.[27] Due to the high numerical aperture of the fiber couplers, only a very small fraction of the light escapes from one fiber into another, and only a small fraction of this amount reaches the output, hence crosstalk should not influence the resolution of the fiber plates appreciably.

Overall Resolution of Cascaded Resolution Transducers

The overall resolution of a device containing several resolution-limiting components can be estimated assuming each individual resolution value is given by a square wave response.

Assume the η resolution limiting components have resolution capabilities of η (lp/mm) and corresponding image elements $\alpha_i=\frac{1}{4}\eta^2$ (mm^2). Because of their random coupling (assuming the worst possible case), the upper limit of the effective image element area A is $A_{max}=\sum_1^n \alpha_i$. This corre-

sponds to a *lower limit for the effective resolution* (overall resolution) of $R_{min}=(\sum_1^n 1/\eta^2)^{1/2}$. With perfect coupling, A_{min} is given by the largest individual α_i and R_{max} by the corresponding lowest η value.

For the tube under consideration, the resolution-limiting components are the electron optics (its limiting resolution assumed as 80 lp/mm per stage), the settled phosphor screens (60 lp/mm each), and the two fiber couplers (100 lp/mm each). The resulting effective *minimum* resolution is 32 lp/mm. Without the fiber plates, the minimum resolution were 34 lp/mm (48 lp/mm per stage); hence the fiber couplers are not seriously impairing the obtainable resolution.

In the case of glass- or mica-couplers (with $n=1.5$), the phosphor emission (in a medium with $n_0=1$) propagates in a core of half angle 42° ($\sin^{-1} 1/1.5=42°$). Thus, spreading of a light spot through the coupler equals roughly twice the thickness of the membrane. The resolution of the (60 lp/mm) phosphor screen would be reduced to 28 lp/mm if a membrane thickness of 5μ is assumed. A simple output window would be used together with a lens system to couple to the ultimate sensor; hence its effect on the resolution is negligibly small. As the minimum resolution on the output phosphor screen is 23 lp/mm, and as the resolution of a coupling lens system is essentially better than that, 23 lp/mm is also the (minimum) resolution at the ultimate sensor.

The efficiency and (paraxial) resolution characteristics of four possible coupler combinations can now be compared:

TABLE 14-III

Interstage coupler	Output coupler	Coupler efficiency (per-cent)	Paraxial resolution (minimum) (lp/mm)
Mica sheet....	glass window and lens.	4	23
Fiber plate....	.....do.........	2	32
Mica sheet....	Fiber plate.....	45	23
Fiber plate....	.....do.........	25	31

It should be noted that the peripheral resolution may be expected to be about the same with fiber interstage coupler (due to its field flattening

properties), but will be essentially lower with the plano-parallel mica sheet.

Device and Quantum Noise Limitations

Device Noise

The vacuum photoelectronic image intensifier is a relatively low noise device. Sources of noise in the device are—

(a) Field emission from the photocathode or from other tube components;

(b) Ion bombardment induced secondary electron emmission from the photocathode;

(c) "Bremsstrahlung," giving cause to spurious fluorescence and photoelectron emission;

(d) Thermionic emission from the photocathode.

Spurious electrons created by any of these processes may either reach the phosphor screen and contribute directly to the noise level, or they may create luminescence from the glass of the tube envelope, thus causing spurious photoemission from the cathode. The first three sources of noise may be sufficiently reduced or fully eliminated by careful design and processing of the tube. The thermionic emission contributes under such circumstances 60 to 75 percent of the device noise.[3] It is about 80 to 100 electrons/cm² sec for an S-11 photosurface (10^{-17} A/cm²) and may be further suppressed by moderate (dry ice) cooling. However, 100 electrons/cm² sec thermionic emission or even total device noise of 170 electrons/ cm² sec may be essentially less than the minimum input signal as limited by quantum noise considerations.

Quantum Noise

An image intensifier with luminous flux gain of 10^4 is able to utilize 10^{-6}—10^{-7} ft.-c. sec. input exposure; e.g., for contact photography. At such low levels, the signal, as represented by the number N of photoelectrons (minimum number of information carrying quanta or particles anywhere in the device) emitted from one resolution element A_c of the photocathode during the exposure time t, may be rather low. Due to the random nature of photoemission, N contains a random error of $\sqrt{N}$, leading to a signal-to-noise ratio $\sqrt{N}$. At $N=k^2$ the signal is detectable above the noise with a probability expressed by the certainty coefficient k. $k=3$, e.g., corresponds to

*The effect of any kind of II-stage noise on the output is quite negligible as compared to that of I-stage noise.

80 percent detection probably,[28] $k=5$ to 90 percent, etc.

N may be calculated from the photocathode illumination L (given in ft-cs) and the quantum-efficiency of the photocathode S_Q (given in electrons/photons) by the equation:

$$N\,[\text{electron}] = L\,[\text{lumen/ft}^2] \times n/L \left[\frac{\text{photon/sec}}{\text{lumen}}\right]$$
$$\times S_Q\,[\text{electron/photon}] \times A_c\,[\text{ft}^2]$$
$$= t\,[\text{sec}] \tag{7}$$

The lumen-to-photon/sec conversion factor n/L and the photocathode quantum efficiency S_Q depend on the incident light distribution E by relations derived in the Appendix. Using these relations and expressing $A_c = \dfrac{1.076 \times 10^{-5}}{4 r_c^2}$ where r_c (lp/mm) is the resolution at the photocathode, we obtain:

$$N = 2.47 \times 10^{10} \frac{Lt S_w^{\text{max}} \int ES d\lambda}{r_c^2 \int EV d\lambda} \tag{8}$$

The minimum observable detail-contrast C is defined by the equation:

$$C = k/\sqrt{N} \tag{9}$$

Combining Eq. (8) and Eq. (9) and assuming $k=3$, we obtain:

$$C = 1.9 \times 10^{-5} \times \sqrt{\frac{\int EV d\lambda}{S_w^{\text{max}} \int ES d\lambda}} \times \frac{r_c}{\sqrt{Lt}} \tag{10}$$

Night light and S-11 photosurface yield:

$$C = 8.8 \times 10^{-5} r_c/\sqrt{Lt} \tag{10a}$$

Figure 14-2 shows C as function of the photocathode exposure Lt and parameter r_c for night light and S-11 and S-20 photosurfaces.

Design and Processing of a Two-Stage Fiber-Coupled X-Ray Image Intensifier

Electron Optical Design

Both stages of the fiber-coupled cascaded X-ray image intensifier utilize a pseudo-point symmetric electrostatic system. The first stage utilizes an aspherical cathode substrate (the photocathode is formed in the shape of an ellipsoid of rotation), a cylindrical focusing electrode, and a bullet-shaped anode (fig. 14-3 and fig. 14-4). The high voltage anode is electrically connected to the low voltage focusing electrode by a semicon-

DETAIL CONTRAST C AS
FUNCTION OF PHOTO
CATHODE EXPOSURE Lt
AND RESOLUTION r c
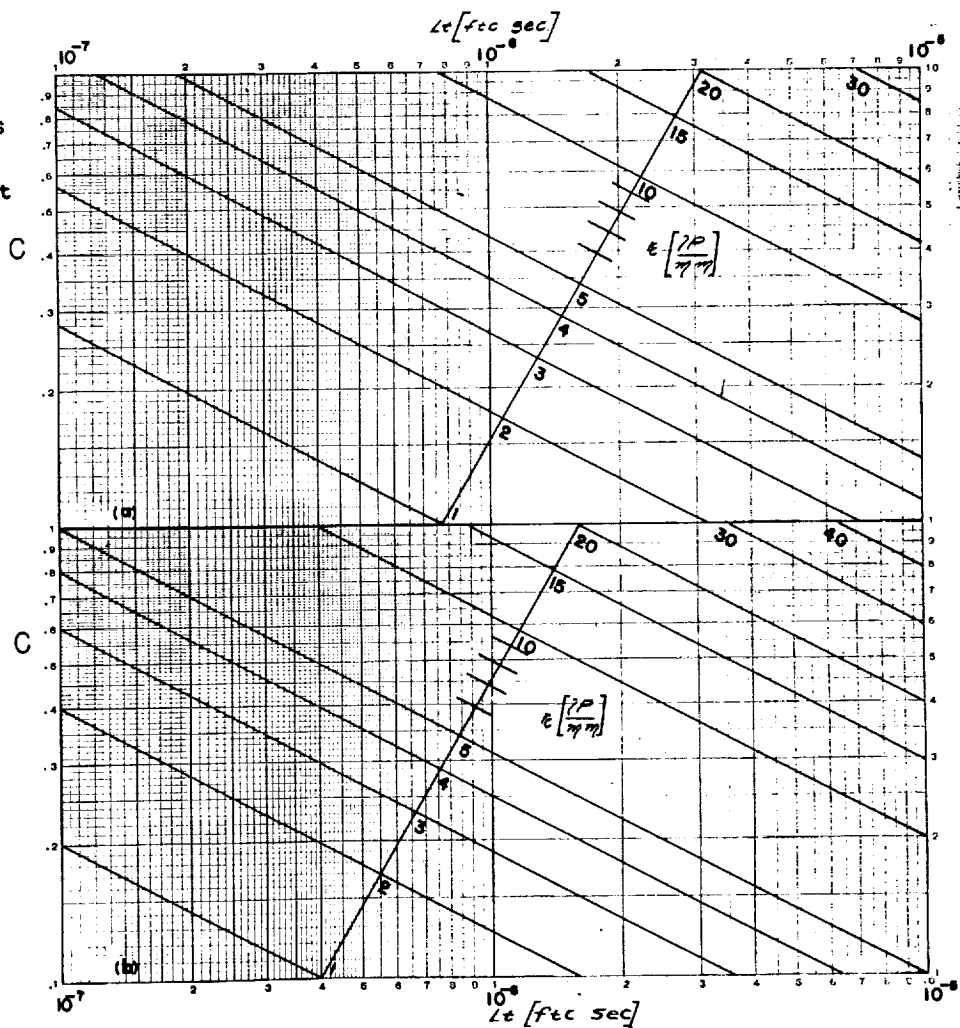NIGHT LIGHT INPUT

PHOTO SURFACE:
    S11 (a)
    S20 (b)

FIGURE 14-2.—Detail-contrast and resolution obtainable with S-11 and S-20 photosurfaces for night light.

ductive wall coating yielding a nonlinear axial potential gradient in the region of the anode aperture lens and reducing device noise appreciably.[30]

The second stage utilizes a flat cathode, a cylindrical focusing electrode, a bullet-shaped anode, and again a semiconductive wall coating between focusing electrode and anode. In addition, a spherical beam-former electrode at (second stage) cathode potential is applied as field flattening element. Both the first and the second stages minify to alleviate the resolution requirements on the first-stage phosphor screen.[31] The two stages are cascaded by a flat fiber coupler.

Fiber Coupler and Photocathode Processing

The photocathode of the first stage is deposited on top of an X-ray luminescent phosphor screen. The second-stage photocathode is deposited onto

a (flat) fiber coupler, carrying on the opposite side a settled phosphor screen (viewing screen of the first stage).

The fiber coupler efficiency was determined with 50 percent utilizing the light emission of P-20 phosphor.* Single cladding fibers of 22 microns diameter were utilized. The plate diameter was 1.25 inches, the thickness three-sixteenths of an inch. The index of refraction of the core was 1.793 and of the cladding 1.48, yielding a numerical aperture of 1.

S-11 photocathodes were used in both stages, applying external antimony evaporation. The primary cesiations of both photosurfaces were carried out in sequence utilizing simultaneous

*As the fiber-coupler used was designed for application to I.R.-light, the (measured) efficiency for P-20 light was rather low.
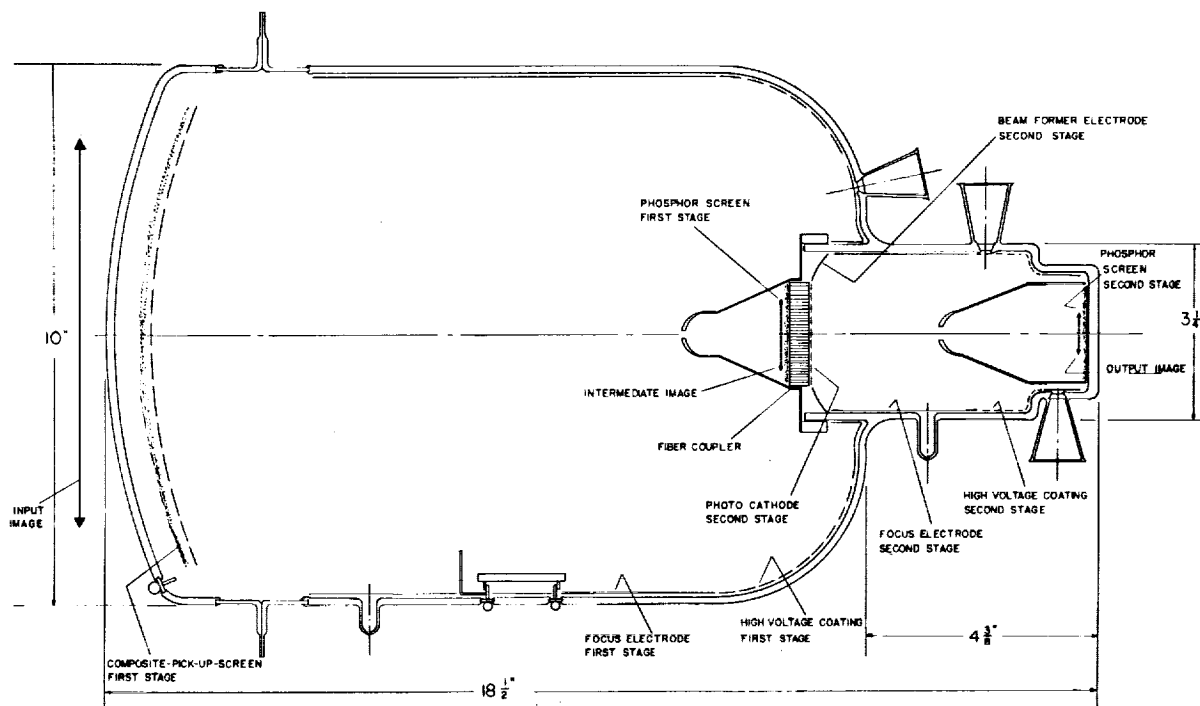
99

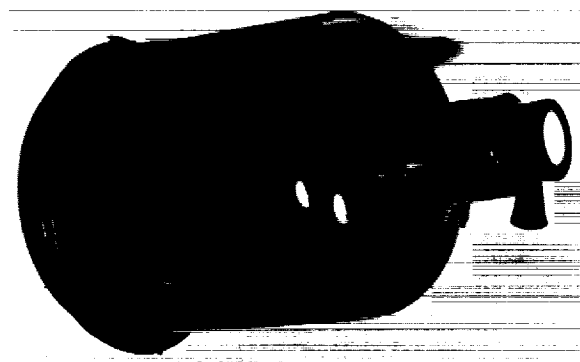FIGURE 14–3.—Design of fiber-coupled, two-stage, X-ray image intensifier.

FIGURE 14-4.—Photograph of fiber-coupled, two-stage, X-ray image intensifier.

monitoring. Both surfaces were overcesiated and oxidized simultaneously. The primary cesiations of the first stage cathode did not yield photosensitivity in the second stage due to a rather complete vacuum separation between the two stages. As both stages were pumped through independent tubulations, simultaneous oxidations could be carried out.

Performance of a Cascaded Fiber-Coupled X-Ray Image Intensifier

The experimental results obtained with the X-ray image intensifier discussed above and the measurement conditions are presented as follows:

TABLE 14–IV

$V_{total}=62$ KV...	Gain (rel. Patterson CB–2).	270,000.
$V_1=24$ KV......	Phosphor (viewing screens) efficiencies.	55 lumens/ watt.
$V_2=38$ KV......	Sensitivity first photo-cathode (S 11, P–20 light).	64 $\mu A/l$.
$M_{total}=1/17.....$		
$M_1=1/7.........$	Sensitivity second photocathode (S 11, P–20 light).[1]	13 $\mu A/l$.
$M_2=1/2.4......$		
Resolution (output) 10 lp/mm.	Pickup diameter......	22 cm.
Resolution (input) #30 mesh.	Interstage fiber coupler efficiency (P–20 light).	50 percent.

[1] Below average due to difficulties encountered during processing of this individual tube (overcesiation at tubulation tipoff).

The above data would result in a calculated gain figure of 330,000 for the two voltage settings, or approximately 20 percent above the measured gain. The discrepancy, besides the inherent error of the theory and the accumulated errors of the several measurements, is mostly caused by the fact that the second-stage phosphor efficiency, while comparable to that of the first-stage phosphor at equal watt inputs, was less than 55

100

lumens/watt at the high watt input rating of the second stage (phosphor saturation). The output resolution is essentially limited by the phosphor resolution of approximately 20 lp/mm (in both stages).

The quoted phosphor screen resolution is a rather low figure, but may be explained by the relatively high phosphor layer thickness, necessitated by the high voltage utilized.

For these computations, an electron-optical resolution of 60 lp/mm per stage has been assumed. It should be noted that the pickup screen-resolution of approximately 4 lp/mm (equivalent to approximately 70 lp/mm considering the overall magnification of 1/17) is of the same order of magnitude as the electron-optical resolution.

Conclusion

Modern image intensifiers are capable of achieving high-gain factors. The growing art of fiber optics offers the possibility of improved coupling between two or more of such tubes without excessive gain or resolution loss, such as potentially encountered with lens or membrane couplers.

The theoretical gain of double-stage image intensifiers, depending upon the performance of the individual stages and the efficiency of the coupler, is computed in detail. It is shown that double-stage cascade image intensifiers with night-light input and S–20 photocathodes should be capable of reaching flux gain values around 10,000 on a photographic emulsion if fiber optics is used for interstage and output couplers. Utilizing a fiber output coupler may increase the output coupling efficiency by a factor 10, as compared with a conventional lens system.

Resolution limits, as determined by the inherent phosphor-screen resolution, fiber diameter, etc., are described together with the consequences of random coupling of these resolution transducers. It is shown that a two-stage image intensifier with a fiber interstage coupler permits a theoretical overall resolution of 32 line-pairs per mm, while a 5 μ mica membrane should yield a resolution of only 23 line-pairs per mm. It is shown further that contact photography through an output fiber coupler yields a theoretical resolution of 23 line-pairs per mm for a mica membrane as interstage coupler, and 31 line-pairs per mm for a fiber plate as interstage coupler.

The design of a high-gain, double-stage X-ray image intensifier is outlined, utilizing minification in both stages and fiber coupling between the stages.

At an overall voltage of 62 KV and an overall magnification of 1/17, the double-stage fiber-coupled X-ray image intensifier yields a brightness gain of $2,7.10^5$ (as compared with a standard fluoroscopic screen), an output resolution of 10 line-pairs per mm, and an input resolution of a #30 mesh.

Pertinent expressions determining the contrast/detail reproducibility, as limited by quantum noise, are derived. It is shown that high-gain image intensifiers are essentially limited by quantum noise.

The conclusion appears permissible that fiber-coupled image intensifiers, each stage possibly being a self-contained vacuum vessel, might represent the ultimate approach to achieving high gain consistent with high reliability.

Appendix

The sensitivities of photocathodes are published in terms of the maximum radiant sensitivity S_w^{max} [amp/watt] and the normalized radiant sensitivity distribution S. Phosphor data are available in terms of luminous efficiency P_L [lumens/watt] and phosphor emission spectral distributions p (normalized). Conversions of watt-lumen-photon/sec quantities are based on the following equations:

$$L \text{ [lumen]} \Big/ \frac{680 \int EV d\lambda}{\int Ed\lambda} = W \text{ [watt]} = n \text{ [photons/sec]} \cdot hc \cdot \int Ed\lambda \Big/ \int E\lambda d\lambda \tag{A/1}$$

$$\text{Radiant photocathode sensitivity } S_w \text{ [amp/watt]} = S_w^{max} \frac{\int ESd\lambda}{\int Ed\lambda} \tag{A/2}$$

$$\text{Luminous photocathode sensitivity } S_L \text{ [amp/lumen]} = S_w^{max} \cdot \frac{\int ESd\lambda}{680 \int EV d\lambda} \tag{A/3}$$

$$\text{Photocathode quantum efficiency } S_q \text{ [electron/photon]} = S_w^{max} \cdot \frac{\int ESd\lambda}{\int E\lambda d\lambda} \cdot \frac{hc}{e} \tag{A/4}$$

101

Similarly: P_w [watt/watt]$=P_L \int pd\lambda / 680 \int pVd\lambda$ (A/5)

$$P_q \text{ [photon/watt]}=P_L \cdot \frac{1}{680hc} \cdot \int p\lambda d\lambda / \int pVd\lambda$$ (A/6)

The (radiant, luminous, photon) flux gain of a single stage image intensifier is given by:

Radiant: G_w [watt/watt]$=S_w^{max}\{ \int ESd\lambda / \int Ed\lambda \} \cdot V \cdot P_L \{ \int pd\lambda / 680 \int pVd\lambda \}$ (A/7)

Luminous: G_L [lumen/lumen]$=S_w^{max}\{ \int ESd\lambda / 680 \int EVd\lambda \} \cdot V \cdot P_L$ (A/8)

Photon: G_q [photon/photon]$=S_w^{max}\{ \int ESd\lambda / \int E\lambda d\lambda \} \cdot V \cdot \frac{P_L}{680} \int p\lambda d\lambda / \int pVd\lambda$ (A/9)

Note, that if $E=p$ (same input and output light distribution), we obtain:

$$G_w = G_L = G_{Lw} = \frac{S_w^{max}VP_L}{680} \cdot \frac{\int pSd\lambda}{\int pVd\lambda}$$ (A/10)

The product of $n/L.S_q = \{ S_w^{max}/680 \} \cdot \{ \int ESd\lambda / \int EVd\lambda \} \cdot \frac{1}{c}$ is used in calculating the photoelectron emission due to 1 ftc input illumination. Conversion of S or G values for light distribution E_1 to a light distribution E can be accomplished by the equations:

$$\frac{G_w(E)}{G_w(E_1)} = \frac{S_w(E)}{S_w(E_1)} = \frac{\int ESd\lambda}{\int E_1Sd\lambda} \cdot \frac{\int E_1d\lambda}{\int Ed\lambda}$$ (A/11)

$$\frac{G_L(E)}{G_L(E_1)} = \frac{S_L(E)}{S_L(E_1)} = \frac{\int ESd\lambda}{\int E_1Sd\lambda} \cdot \frac{\int E_1Vd\lambda}{\int EVd\lambda}$$ (A/12)

$$\frac{G_g(E)}{G_g(E_1)} = \frac{S_g(E)}{S_g(E_1)} = \frac{\int ESd\lambda}{\int E_1Sd\lambda} \cdot \frac{\int E_1\lambda d\lambda}{\int E\lambda d\lambda}$$ (A/13)

For a given input E, the relative response of two photosurfaces S_a and S_b and hence G_a and G_b (regardless whether they are luminous, radiant or quantum figures) is:

$$\frac{G(S_a)}{G(S_b)} = \frac{S_a}{S_b} = \frac{S_{w,a}^{max} \int ES_ad\lambda}{S_{w,b}^{max} \int ES_bd\lambda}$$ (A/14)

All integrals have to be evaluated between 0 and ∞. For incandescent light and other wide band distributions, the possible filter effect of the input window must be accounted for.

Acknowledgment

Discussion

R. G. STOUDENHEIMER: The gain of the two-stage intensifier should have been high enough to show very distinctly the scintilation of individual X-ray photons. Can you describe the appearance of these scintillations?

W. F. NIKLAS: Quantum noise is already visible in X-ray image intensifiers having a brightness gain of approximately 1,000 relative to Patterson CB-2. It should be noted here that an X-ray image intensifier is capable of reproducing every X-ray quantum absorbed in the X-ray pickup screen, as each X-ray quantum releases approximately 1,500 "visible light" photons from the pickup screen.

J. W. HICKS: Did you make any contrast measurements on calculations?

W. F. NIKLAS: Unfortunately, no detailed contrast measurements were carried out on the double-stage fiber-coupled X-ray image intensifier. However, the large area contrast, determined by shielding one-half of the input screen, appears to be quite comparable to the large area contrast of a single stage.

R. L. ZASTROW: A gain of 270.000 "relative to Patterson" was quoted. Could this definition of gain be clarified?

W. F. NIKLAS: The gain of X-ray image intensifiers is conventionally determined by comparing the brightness (in foot-lambert) obtained on the final output screen of an X-ray image intensifier with the brightness of a Patterson CB-2 fluoroscopic screen (in foot-lambert), both the X-ray image intensifier and the fluoroscopic screen excited by sortlike X-radiation.

N. S. KAPANY: For your experimental model, did you use a fiber optics and window in addition to the single coupler plate?

W. F. NIKLAS: Our experimental double stage X-ray image intensifier utilized a fiber interstage coupler and a clear output window.

References

1. BOWERS, A.: *Low Brightness Photography by Image Intensification.* Sec. Symp. Photo-El. Image Dev., London, 1961.
2. FUCKS, W., KNIPPING, H. W., LIESE, E., and BUDDE, W.: Z. Ntf., 11b, 1956, p. 142.
3. THOMAS, C. C.: *Cinefluorography.* Proc. 1st Ann. Symp. on Cinefluorography, 1958.
4. GREEN, D. T., and NIKLAS, W. F.: *An Image Intensifier Tube With High Gain for 1MeV Photons.* Mtg. Sec. Non-Destr. Testing, 1961.
5. JONES, L. W., and PERL, M. L.: *An Image Intensifier-Scintillator Device for Determination of Profiles and Images of Weak Beams of Ionizing Particles or Quanta.* Tec. Rep., Univ. of Mich., 1961.
6. BURNS, J., and NEUMANN, M. J.: Adv. El. and Phys., vol. XII, 1960, p. 97.
7. FOREMAN, P. H., and THUMWOOD, R. F.: *An Image Intensifier Tube Using the Multipactor Principle.* 2d Symp. Photo-El. Image Dev. London, 1961.
8. WILCOCK, W. L., and EMBERSON, D. L.: Nature, 185, 1960, p. 370.
9. WACHTEL, H. M., DOUGHTY, D. D., and ANDERSON, A. E.: *The Transmission Secondary Emission Image Intensifier.* Proc. Image Intensifier Symp., 1958.
10. BEURLE, R. L., and WREATHALL, W. M.: *Some Electron Optical Studies of Solenoid Focusing Systems.* 2d Symp. Photo-El. Image Dev., London, 1961.
11. STOUDENHEIMER, R. G.: Adv. El. and Phys., vol. XII, 1960, p. 41.
12. DAVIS, G. P.: *Experiences With Magnetically Focused Cascade Image Intensifiers.* 2d Symp. Photo-El. Image Dev., London, 1961.
13. SCHAGEN, P., BRUINING, H., and FRANCKEN, J. C.: Philips Res. Rep. 7/2, 1952, p. 119.
14. EBERHARD, E. H.: Priv. Comm, 1960.
15. LEVERENZ, H. W.: *An Introduction to Luminescence of Solids.* J. Wiley & Sons, Inc., 1950, p. 351.
16. KAPANY, N. S., and CAPELLARO, D. F.: J. Opt. Soc. Am., 51/5, 1961, p. 23.
17. HOPKINS, R. E., and POTTER, R. J.: *Cinefluorography.* Proc. 1st Ann. Symp. on Cinefluorography, 1958, p. 228.
18. POTTER, R. J.: *Transmission Properties of Optical Fibers.* Mtg. Opt. Soc. Am. Ottawa, 1959.
19. WALLIS, G.: Ann. D. Phys. 16/17, 1956, p. 401.
20. KARKOW, W.: Priv. Comm., 1961.
21. BABCOCK, H. W., and JOHNSON, J. J.: Astrophysics, vol. 94, 1941, p. 271.
22. McGEE, J. D., Priv. Comm., 1961.
23. HILTNER, W. A., and NIKLAS, W. F., *A Low Background Image Tube for Electronography.* Lect. 2nd. Symp., Photo-El. Image Dev., London, 1961.
24. LALLEMAND, A., DUCHESNE, M., and WLERICK, G.: Adv. El. and Phys., vol. XII, 1960, p. 5.
25. SCHAFFERNICHT, W.: Priv. Comm., 1958.
26. BUERLE, R. L.: Priv. Comm., 1960.
27. KARKOW, W.: Priv. Comm., 1961.
28. LUM, M. D., and GUDERLY, K. G.: *On the Evaluation of Strongly Enlarged Photographs.* (Quoted by R. K. H. Gebel, ARL–12, 1961.)
29. TOL, T., OOSTERKAMP, W. J., and PROPER, J.: Philips Res. Rep., 10/2, 1955, p. 141.
30. NIKLAS, W. F.: Am. J. Roentgen Rad. Ther. and Nuc. Med., 85/5, 1961, p. 323.
31. WOODHEAD, A. W., TAYLOR, D. G., and SCHAGEN, P.: *A Two-Stage Electrostatic Image Intensifier with Large Photocathode Area.* 2d Symp. Photo-El. Image Dev., London, 1961.

15. COMPARISON OF THE MERITS OF IMAGE CONVERTERS WITH MAGNETIC AND WITH PROXIMITY FOCUSING

G. PAPP, *Components and Instrumentation Laboratory, ITT Laboratories*

Introduction

In a recent paper [1] the resolution in a magnetically focused image tube was evaluated. It is interesting to compare its results with the resolution of the "proximity focusing," the imaging which exists in an image converter tube with closely spaced photocathode and phosphor.

It is interesting to see that while the error Δr is a second-order expression of the velocity ratio v_0/v_a (where v_0 is the initial velocity of the electron, v_a, its velocity at the phosphor) in the magnetic case, it is a first-order expression with proximity focusing.

If instead of velocities we use the energy expressions, i.e., the voltage equivalent of these velocities, the blurring in the magnetically focused image tube is proportional* to v_0/v_a and in the proximity focusing, to $\sqrt{v_0/v_a}$. Since V_0 is in the order of 1 volt, at $V_a = 10$ KV phosphor voltage the relative error, $\Delta r/L$, is by a factor of 100 smaller in the magnetic case than with proximity focusing.

Consequently, while proximity focusing is quite satisfactory in image converters with close spacing and high accelerating voltage for infrared or visible applications, the very same device is not satisfactory in the far ultraviolet, since V_0 is here one to two orders of magnitude larger.

Detailed Discussion of the Proximity and Magnetic Focusing

In an image converter in which a photocathode and phosphor are closely spaced parallel planes, the image point of a point, P, on the photocathode is the point P_1, where the electrons, leaving the cathode with zero initial radial velocity hit the phosphor. Electrons, with initial radial velocity v_{r0}, end up in the vicinity of the image point at a distance Δr from P_1. The average value of Δr gives the "accuracy of the focusing," the reciprocal of which will be proportional to the resolution: $R = 1/k\Delta r$ where k is a factor in the order of 1, the value of which is dependent upon the definition of resolution. In the present case k can be determined easily for any well-formulated resolution definition.

Since the closely spaced parallel plane arrangement produces a uniform homogeneous field between the cathode and the anode, the resolution is uniform along the whole image tube, except a peripheral section of width comparable to the cathode anode distance.

A potential difference V_a between the cathode and anode produces a homogeneous electric field of intensity

$$E = -\frac{V_a}{L} \qquad (1)$$

perpendicular to the cathode surface. In a polar coordinate system with origin at P and Z axis parallel to the field intensity, the electrons are accelerated only in the Z direction, according to equation

$$\ddot{z} = \frac{e}{m} \cdot \frac{V_a}{L} \qquad (2)$$

where $-\dfrac{e}{m}$ is the specific charge of the electron,

$-1.759 \cdot 10^{11}$ coul/kg, V_a is the potential of the anode in volts ($V_{cathode} = 0$), L is the cathode-anode distance, in meters.

The trajectory of an electron (see Fig. 15-1) is described consequently by the equations

$$r = v_{r0} t \qquad (3)$$

$$\varphi = \varphi_0 \qquad (3a)$$

$$z = v_{z0} t + \frac{1}{2} \frac{e}{m} \frac{V_a}{L} t^2 \qquad (3b)$$

---

*The proportionality factor is in both cases $2L$, twice the distance between cathode and phosphor, as shown below.

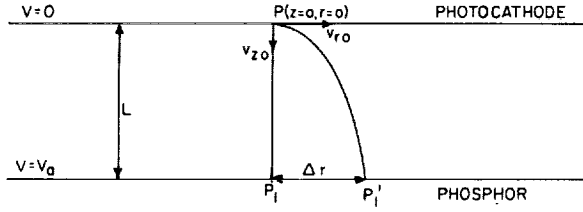where v_{ro} and v_{zo} are the initial radial and axial velocities, φ_o the initial polar angle.

FIGURE 15-1.—Electron trajectory in an image tube with proximity focusing.

For $z=L$, equation (3b) gives the time of flight

$$t=\frac{-v_{zo}+\sqrt{v_{zo}^2+2\frac{e}{m}V_a}}{\frac{e}{m}\frac{V_a}{L}}$$

$$=\frac{2L}{v_a}\cdot\frac{-v_{zo}+v_a\sqrt{1+(v_{zo}/v_a)^2}}{v_a} \qquad (4)$$

$$\cong\frac{2L}{v_a}\left(1-\frac{v_{zo}}{v_a}+\frac{1}{2}\left(\frac{v_{zo}}{v_a}\right)^2\right) \qquad (4a)$$

where v_a is the end velocity of an electron starting with $v_{zo}=0$,

$$v_a=\sqrt{2\frac{e}{m}V_a} \qquad (4b)$$

The error in focusing, Δr, is the r value of the point of impact, according to (3)

$$\Delta r=v_{ro}t\cong 2L\frac{v_{ro}}{v_a} \qquad (5)$$

In the case of the magnetic focusing, with homogeneous magnetic field

$$B_z=B \qquad (6)$$

the electrons move along helical path with uniform angular velocity [1]

$$\omega=eB/m \qquad (7)$$

and complete a full revolution in a time

$$T=2\pi/\omega=2\pi m/eB \qquad (7a)$$

Adjusting the anode voltage V_a and the magnetic field B so that

$$t_0=2L/v_a=nT \qquad (8)$$

where n, the order of the focusing, is an integer, the electrons with zero initial forward velocity complete n revolutions, and are sharply focused to P_1.

Electrons with arbitrary initial forward velocity v_{zo} have, according to (4a) a time of flight shorter by

$$\Delta t=t-t_0=-2\frac{L}{v_a}\cdot\frac{v_{zo}}{v_a} \qquad (8a)$$

and arrive to the phosphor at a distance

$$\Delta r=v_{ro}\cdot|\Delta t|=2L\frac{v_{zo}}{v_a}\cdot\frac{v_{ro}}{v_a} \qquad (9)$$

from the focal point P_1.

Discussion of the Results

According to Eq.s (5) and (9), Δr, the error of the imaging is a first order expression in v_{ro}/v_a in the proximity focusing, a second order expression in the magnetic case.

If we introduce the voltage equivalent of the initial radial velocity v_{ro}, according to the equation

$$\frac{1}{2}mv_{ro}^2=eV_{ro}$$

Eq.s (5) and (9) can be expressed as

$$\Delta r=2L\sqrt{\frac{V_{ro}}{V_a}} \qquad (5a)$$

and

$$\Delta r=2L\sqrt{\frac{V_{ro}}{V_a}}\cdot\sqrt{\frac{V_{zo}}{V_a}}. \qquad (9a)$$

(5a) is a very convenient expression for the error calculation. In a tube with photocathode to phosphor distance $L=1$ mm, at an accelerating voltage $V_a=10,000$ volts, the error is

$$\Delta r\cong 2\sqrt{\frac{0.1}{10^4}}\text{ mm}\cong\frac{1}{160}\text{ mm}$$

and the resolution around 160 line-pairs per mm, if we use the image converter in the near infrared region where V_o is in the order* of $\frac{1}{10}$ volt.

*According to the photoelectric equation $V_o\leq 0.25$ volt for a light in the near infrared with $\lambda=9,000$ Å and a photocathode of threshold value $\lambda_w=11,000$ Å. The corresponding relationship in an image converter designed for the far ultraviolet at $\lambda=1,000$ Å and $\lambda_w=3,000$ Å is $V_o\leq 8.3$ volts. These equations give only an upper limit for the initial energy V_o because a part of the available energy is lost inside the photocathode. Since this is relatively more significant in the infrared case, we may estimate that the average initial energy is 50 to 100 times larger in the ultraviolet case than in the infrared.

The same image converter in the far UV region, with V_o in the order of 5 volts, gives

$$\Delta r \sim \frac{1}{22} \text{ mm}$$

and a resolution of about $R \sim 22$ line pairs per mm.

The corresponding figures in the case of a magnetic tube with cathode-phosphor distance $L=1''=25$ mm are $\Delta r \sim \frac{1}{2}\ 10^{-3}$ and $\frac{1}{4}\ 10^{-1}$ mm, and $R \sim 2,000$ line-pairs per mm and 40 line pairs per mm.

Statistical Evaluation

Since the value of Δr (which we now will call r for shortness) is proportional to v_{ro}, the statistics of v_{ro}, gives at once around each image point P_1, the current distribution of the electrons, the brightness distribution of the phosphor, or the density distribution of a photographic plate.

If we approximate the velocity distribution of the initial electron velocities by a Maxwellian distribution, the v_{ro} distribution will be

$$f(v_{ro}) = A v_{ro} \cdot e^{-\left(\frac{v_{ro}}{w}\right)^2} \tag{10}$$

The current arriving onto the area of the ring between radii r and $r+dr$ will be

$$di = cf(v_{ro})\,dv_{ro} \tag{11}$$

and the current density

$$j(r) = \frac{di}{dA} = \frac{cf(v_{ro})dv_{ro}}{2\pi r\,dr} \tag{12}$$

where

$$r = 2\frac{L}{v_a}v_{ro} \tag{12a}$$

The brightness distribution around each image point will be

$$f(r) = A_1 \cdot e^{-\left(\frac{r}{\rho}\right)^2} \tag{13}$$

where

$$\rho = 2\frac{L}{v_a}w \tag{13a}$$

The mean value of r, the radius of confusion, is

$$\overline{\Delta r} = \frac{\int_0^\infty rf(r)dr}{\int_0^\infty f(r)dr} \tag{14}$$

or

$$\overline{\Delta r} = \frac{\rho}{\sqrt{\pi}} \tag{14a}$$

If two points P_1, P_2 are at a distance S from each other, along the line P_1P_2 the brightness distribution on the phosphor will be

$$b(x) = A_1\left(e^{-x^2} + e^{-(x-s)^2}\right), \tag{15}$$

where $x=r/\rho$ and $s=s/\rho$. r is counted from the point P_1. The curves, for different values of s are given on figure 15–2, drawn for the value $A_1=2/\sqrt{\pi}$. The position of point P_2 is marked by a small arrow on each curve.

From the figure it can be seen that for s-values <1.4 a maximum appears at $x=\frac{1}{2}\,s$; the two dots are not resolved.

For $s>1.4$ values a local minimum appears at $x=\frac{1}{2}\,s$, the two dots can be distinguished. The values of the maxima and minima as well as the percentage modulation of the brightness are given on Table 15–I.

TABLE 15–I

Brightness Distribution in the Case of 2 Closely Spaced Points				
s	$b(0)$	b_{max}	$b(\frac{1}{2}s)$	Percent modulation
0.0	2.256	same	same	
.2	2.212	2.234	same	
.4	2.089	2.168	same	
.6	1.915	2.062	same	
.8	1.723	1.922	same	
1.0	1.543	1.758	same	
1.2	1.395	1.574	same	
1.4	1.787	1.382	same	
1.6	1.215	1.243	1.190	4.25
1.8	1.172	1.179	1.004	14.8
2.	1.148	same	.830	28.7
2.2	1.137	same	.672	40.8
2.4	1.132	same	.534	52.8
2.6	1.129	same	.416	63.0
2.8	1.128	same	.318	71.8

If 20 percent brightness drop between the two points is defined as the criterion for the resolution of the two separate points, this can be achieved by a spacing:

$$\Delta = \frac{s}{\rho} = 1.9 \tag{16}$$

or

$$s = 1.9\rho = 1.9\sqrt{\pi} \cdot \overline{\Delta r} \tag{16a}$$

The resolution is consequently

$$R = \frac{1\text{mm}}{s} = \frac{1\text{mm}}{3.35\overline{\Delta r}} \tag{17}$$
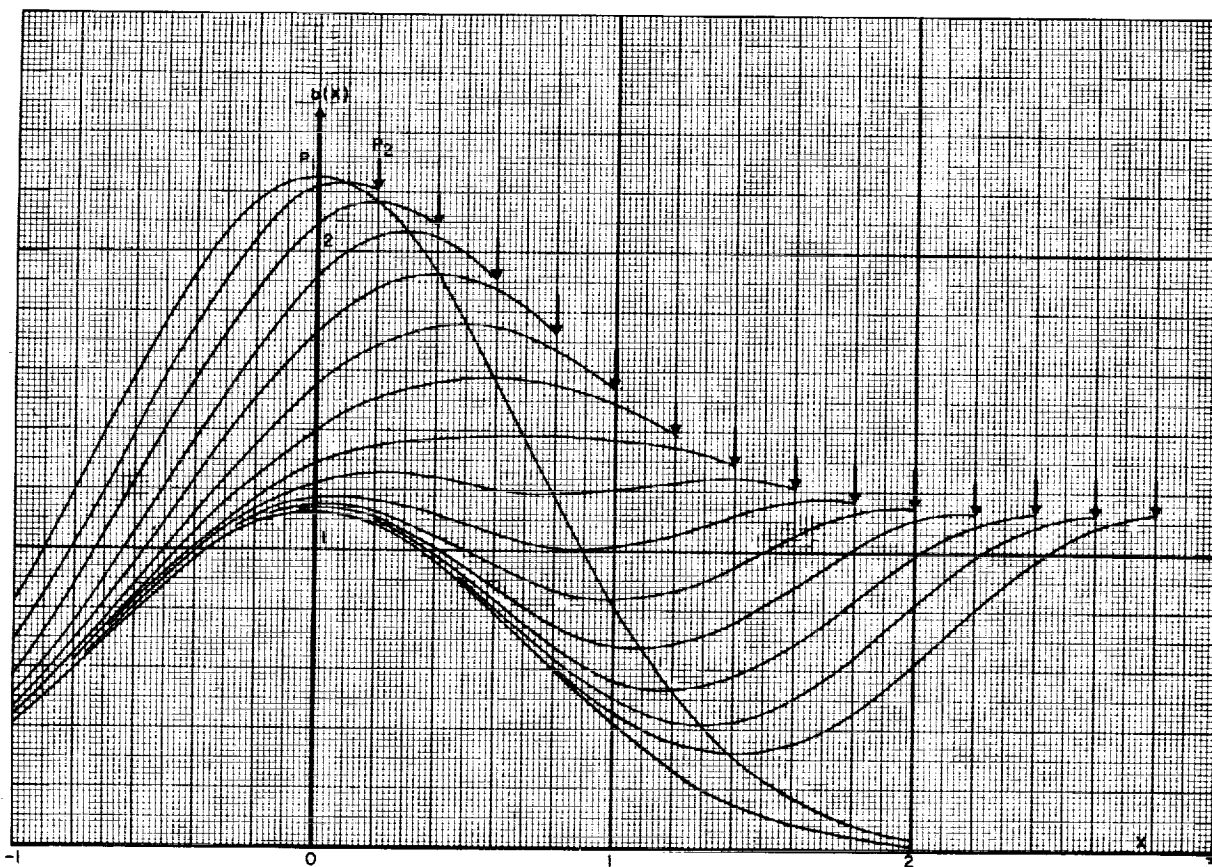
line pairs per millimeter.

FIGURE 15-2.—Brightness distribution in the case of two closely spaced points, P_1 and P_2.

The same is the result in the case of two parallel, infinitely thin, equally bright lines. This is evident at once if we write the initial velocity distribution in a rectangular coordinate system with x axis parallel to the two luminous lines.

Calculations for two infinitely thin lines of different intensity (but not Maxwellian density distribution) were made by Dichtburn.[2] Brightness evaluation for not infinitely thin lines is given, for example, in a paper by DeVore.[3] Calculations for many parallel lines are carried out in a Westinghouse report.[4] Though the brightness distribution around a luminous point in a magnetically focused image tube is not Maxwellian, the results are nevertheless similar.

Additional Comments

(A) The error formula (4) shows that in the case of proximity focusing good resolution can be achieved only with small cathode-anode spacing L. In the case of extended cathodes sensitive for infrared or visible light this requires some special technique, e.g., preforming the cathode and sealing it in vacuum, or using the

technique of reversing the cathode inside the tube after formation. For the far UV region, however, the case might be simpler since we can use cathodes which can be exposed to free air. Also, the higher work function in this case permits closer spacing. This does not compensate, however, for the loss of resolution due to the much higher v_0/v_a values.

(B) It has to be noted that the present paper discussed the electronic resolution only. Additional errors are introduced by the blurring of the optical imaging onto the photocathode, the blurring introduced in the phosphor layer, etc. Independent errors usually add quadratically

$$(\Delta r)^2 = (\Delta_1 r)^2 + (\Delta_2 r)^2 + (\Delta_3 r)^2 \qquad (18)$$

or in terms of resolutions

$$\frac{1}{R^2} = \frac{1}{R_1^2} + \frac{1}{R_2^2} + \frac{1}{R_3^2} \qquad (19)$$

(C) The deterioration of the resolution in the peripheral region in an image tube with proximity focusing is only gradual since the time of flight,

108

and with it the blurring increases only slightly toward the edges. In a magnetic tube the degradation of the resolution is more critical because the focusing condition, $t=nT$ is more and more violated. The curvature of the electric and magnetic fields introduces additional aberrations. Due to the great difference in the electric and magnetic field distribution in different tubes general formulas for the degradation of resolution cannot be given.

(D) A difference between the two methods is that while in the magnetic case focusing can be maintained at a well defined voltage V only, the electrostatic tube is "always in focus."

In the magnetic case a change ΔV_a in the accelerating voltage amounts to a change in the time of flight by

$$\Delta_1 t = -\frac{1}{2}\, t\, \frac{\Delta V_a}{V_a} \tag{20}$$

and results in a blurring

$$\Delta_1 r = v_{ro}|\Delta_1 t| = v_{ro}\, \frac{1}{2}\, \frac{L}{\bar{v}} \cdot \left|\frac{\Delta V_a}{V_a}\right| \tag{20a}$$

$$= L\, \sqrt{\frac{V_{ro}}{V_a}} \cdot \left|\frac{\Delta V_a}{V_a}\right|. \tag{20b}$$

(E) In the previous section we expressed the rule of the propagation of errors:

$$(\Delta r)^2 = (\Delta_1 r)^2 + (\Delta_2 r)^2 + \text{etc.} \tag{18}$$

We have to state however that it refers only to independent random variables. Thus, if $\Delta_1 r$ is the error (20a, b) due to incorrect focus voltage, while $\Delta_2 r$ is the electron-optical error (14) for exact focusing, Δr of equation (18) would represent the average error in a sufficiently large number of experiments, where ΔV varies randomly; or the resulting resolution of a long photographic exposure during which period the variation of ΔV is random and represent a sufficient number of sampling. In one singular experiment, however, where the misfocusing is constant, the square law for error addition definitely does not hold. The error has to be evaluated for different cases individually. If the time error in the focusing condition, $t=nT$, due to voltage misalignment is δ_1, and

that due to the initial velocity δ_2, the resulting error will be

$$\Delta = \delta_1 + \delta_2 \tag{21}$$

the focusing error

$$\Delta r = v_{ro} \cdot |\Delta| \tag{21a}$$

and the radius of confusion

$$\overline{\Delta r} = \overline{v_{ro}} \cdot \overline{|\Delta|} \tag{21b}$$

Since the value of δ_2 is always negative while δ_1 can be both positive and negative, the following different cases can be considered.

(1) $\delta_1 = 0$. Only the statistical error is present.

$$\Delta = \delta_2 \tag{22}$$

and the mean value of $|\Delta|$ will be*

$$\overline{|\Delta|} = \tfrac{1}{2}\Delta_2 \tag{22a}$$

(2) $\delta_1 < 0$.

$$\overline{|\Delta|} = |\delta_1| + \tfrac{1}{2}\Delta_2 \tag{22b}$$

the focusing error is the sum of the voltage and statistical errors.

(3) $\delta_1 > \Delta_2$.

$$\overline{|\Delta|} = |\delta_1| - \tfrac{1}{2}\Delta_2 \tag{22c}$$

the focusing error is the difference of the voltage error and statistical error.

(4) $\delta = \Delta_2$.

$$\overline{|\Delta|} = \tfrac{1}{2}\Delta_2 \tag{22d}$$

the error is the same as in the case (1).

(5) $0 \leqq \delta_1 \leqq \Delta_2$. The focusing error Δ takes both positive and negative signs. The statistical evaluation of $\overline{|\Delta|}$ leads to the result

$$\overline{|\Delta|} = \frac{\delta_1^2}{\Delta_2} - \delta_1 + \tfrac{1}{2}\Delta_2 \tag{22e}$$

$\overline{|\Delta|}$ has a value $\tfrac{1}{2}\,\Delta_2$ both at $\delta_1 = 0$ and $\delta_1 = \Delta_2$, as it was stated in (22) and (22d); but in between $\overline{|\Delta|}$ has a minimum

$$\overline{|\Delta|}_{\min} = \tfrac{1}{4}\Delta_2 \tag{23}$$

at

$$\delta_1 = \tfrac{1}{2}\Delta_2 \tag{23a}$$

as shown on figure 15–3.

*For the sake of simplicity we assume here a uniform distribution for δ_2 between the limits 0 and $-\Delta_2$.
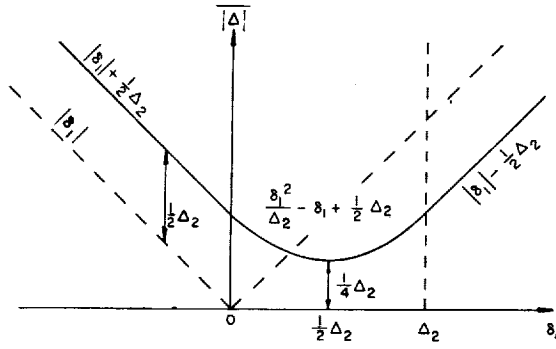
FIGURE 15-3.—Effective focusing error $\overline{|\Delta|}$.

The error Δr is only half as large here as at the "ideal" focusing, $\delta_1 = 0$. This effect was discussed, though, through a different approach in a previous paper.[1] The numerical result is different due to the different statistics assumed.

(F) The superposition of a systematic and a statistical error δ_1 and δ_2 always has to be considered along the lines followed in the previous section. The strange result obtained for $\overline{|\Delta|}$, that $\overline{|\Delta|}$ is the sum of the two errors in one case, the difference of them in another case, and an intermediate value in between, is intimately connected with the fact that we artificially defined the focus voltage as the one proper for the electrons with zero initial forward velocity. In experimental practice one always focuses a tube to the minimum blurring by focusing to the electrons with average initial forward velocity $\overline{v_{zo}}$, i.e., for $\delta_1 = \frac{1}{2}\Delta_2$. In this case a "systematic" misfocusing

$$\delta_1^* = \delta_1 - \frac{1}{2}\Delta_2 \qquad (24)$$

results in an error

$$\overline{|\Delta^*|} = \frac{1}{4}\frac{\delta_1^{*2}}{\Delta_2^*} + \Delta_2^* = \Delta_2^*\left(1 + \frac{1}{4}\left(\frac{\delta_1^*}{\Delta_2^*}\right)^2\right), \qquad \text{if } \delta_1^* \leq 2\Delta_2^*$$

$$\qquad\qquad (24a)$$

and

$$= |\delta_1^*|, \qquad \text{if } \delta_1^* \geq 2\Delta_2^* \qquad (24b)$$

where

$$\Delta_2^* = \frac{1}{4}\Delta_2 = \overline{|\Delta|}_{\text{min}} \qquad (24c)$$

These formulas can be derived from (22e), (22b) and (22c) by applying the transformations (24) and (24c).

Both (24a) and (24b) are similar to the result of the quadratic addition of errors

$$\Delta_q^* = \sqrt{\delta_1^{*2} + \Delta_2^{*2}} \qquad (25)$$

110

This can be seen by an expansion of (25)

$$\Delta_q^* \cong \Delta_2^*\left(1 + \frac{1}{2}\left(\frac{\delta_1^*}{\Delta_2^*}\right)^2\right), \qquad \text{if } \delta_1^* \ll \Delta_2^* \qquad (25a)$$

$$\cong |\delta_1^*| \cdot \left(1 + \frac{1}{2}\left(\frac{\Delta_2^*}{\delta_1^*}\right)^2\right), \qquad \text{if } \delta_1^* \gg \Delta_2^* \qquad (25b)$$

or by the direct comparison of the plots of $\overline{|\Delta^*|}$ and Δ_q^*, as shown in figure 15-4.
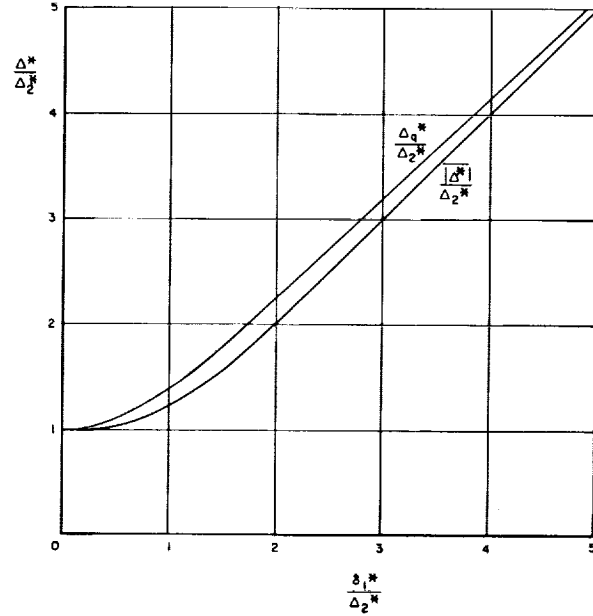
FIGURE 15-4.—Comparison of $\overline{|\Delta^*|}$ and Δ_q^*.

Summary

A magnetically focused image converter with parallel and homogeneous electrical and magnetic fields is compared to one with proximity focusing. Both methods give a 1:1 magnification and can be applied to large image areas. As long as the homogeneity of the fields is maintained, the resolution will be uniform in both cases over the whole face plate.

The accuracy of focusing in the two cases is given by equations (4) and (9). While the error is a first order expression of the ratio of the initial and end velocities in the proximity focusing, the error is a second order expression in the magnetic case. This shows the superiority of the magnetic focusing.

By taking account of the statistical distribution of initial velocities, the resolution obtainable with proximity focusing is calculated. Particular attention is drawn to the fact that, in an actual

experiment, the errors of different origin are not always independent of each other and therefore do not add quadratically. This is analyzed for the magnetic case.

References

1. PAPP, G.: *Limits of Resolution in Magnetically Focused Image Converter Tubes.* (To be pub. in IRE Trans. on Nuclear Science, April 1962.)
2. DICHTBURN: Light, p. 237.
3. DeVORE, H. B.: Proc. IRE, vol. 36, 1958, p. 335.
4. Priv. comm.

16. THE CHARACTERISTICS OF PHOTOCATHODES UNDER HIGH LIGHT LEVELS

MARSHALL P. WILDER and BERNARD R. LINDEN, *CBS Laboratories, a Division of Columbia Broadcasting System, Inc.*

Introduction

There has recently been an interest in the characteristics of photocathodes under very high light levels. It is common knowledge that emission of high photocurrent densities leads to a degradation of photocathode response. Some workers have even reported fatigue phenomena at emission current density levels as low as 1 $\mu a/cm^2$. Many manufacturers have determined empirically that 20 $\mu a/cm^2$ photocurrent density is a maximum level, above which irreversible degradation takes place.

CBS Laboratories is investigating cathode fatigue at high photocurrent density. The objectives are to achieve a better understanding of the phenomenon and to improve the ability of cathodes to withstand fatigue. Preliminary results show some interesting properties of fatigue phenomena. Most of the results refer to cesium antimony cathodes, although some data will be presented on other common types of photocathodes.

Experimental Results

Figure 16–1 is a photograph of the experimental apparatus used to take measurements on photocathode fatigue. A standard 35-mm slide projector, with a blue filter (Corning type 5113), illuminates the photocathode. The energy density onto the photocathode was 4.64 $\mu w/cm^2$.

Figure 16–2 shows the results of measurements on two Cs-Sb cathodes. One cathode was opaque deposited on a nickel substrate, and the other was semitransparent deposited on glass. The superiority of opaque cathodes over semitransparent ones suggested that the conductivity of the surface might be playing an important role. Accordingly, data were taken on semitransparent Cs-Sb cathodes deposited on a transparent conductive (TC) coating. This coating was formed in the usual way by spraying a solution of tin chloride onto the surface of a heated faceplate.

A comparison of the results from Cs-Sb on TC coatings with Cs-Sb on glass only is shown in figure 16–3. Tubes #0088Z and #0474Y had standard semitransparent Cs-Sb cathodes deposited on soda-lime glass (Corning #008). The sensitivities of these tubes dropped rapidly with time for the photocurrent density shown. The incident light was from a tungsten source filtered by a blue filter. Both cathodes level off at approximately 15 $\mu a/cm^2$ photocathode emission even though they started at different initial values of emission. Interestingly enough, the ratio of final to initial sensitivity is smaller for unfiltered tungsten light than for blue light. This indicates that the red sensitivity drops off faster than the blue sensitivity.

Tubes #0475Y and #0472Y in figure 16–1 were fabricated with semitransparent Cs-Sb cathodes deposited on a transparent conductive (TC) coating of tin oxide on soda-lime glass. Not only was it possible to draw considerably higher initial cathode currents, but these current levels remained relatively stable for approximately 10

FIGURE 16–1

Photocurrent (ua)

2000
1800
1600
1400
1200
1000
800
600
400
200

Photocurrent Density (ua/cm^2)

120
106
93.3
80
66.6
53.4
40
26.6
13.3

#0475Y (TC Coating)

#0472Y (TC Coating)

#0209Y (S4 Solid Ni Base)

#0088Z

#0474Y

0   1   10   100   1000
Hours
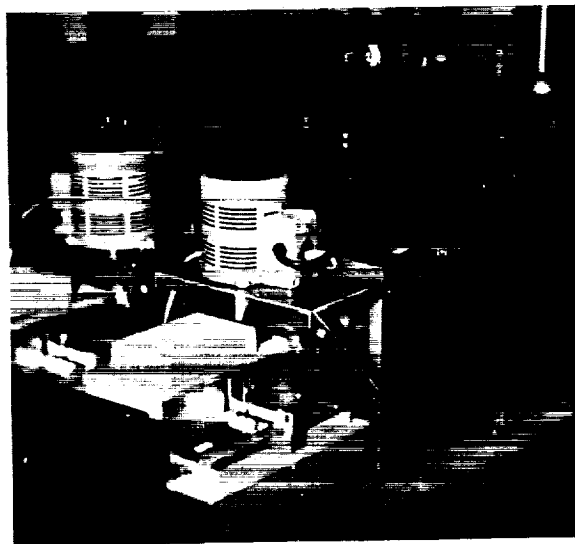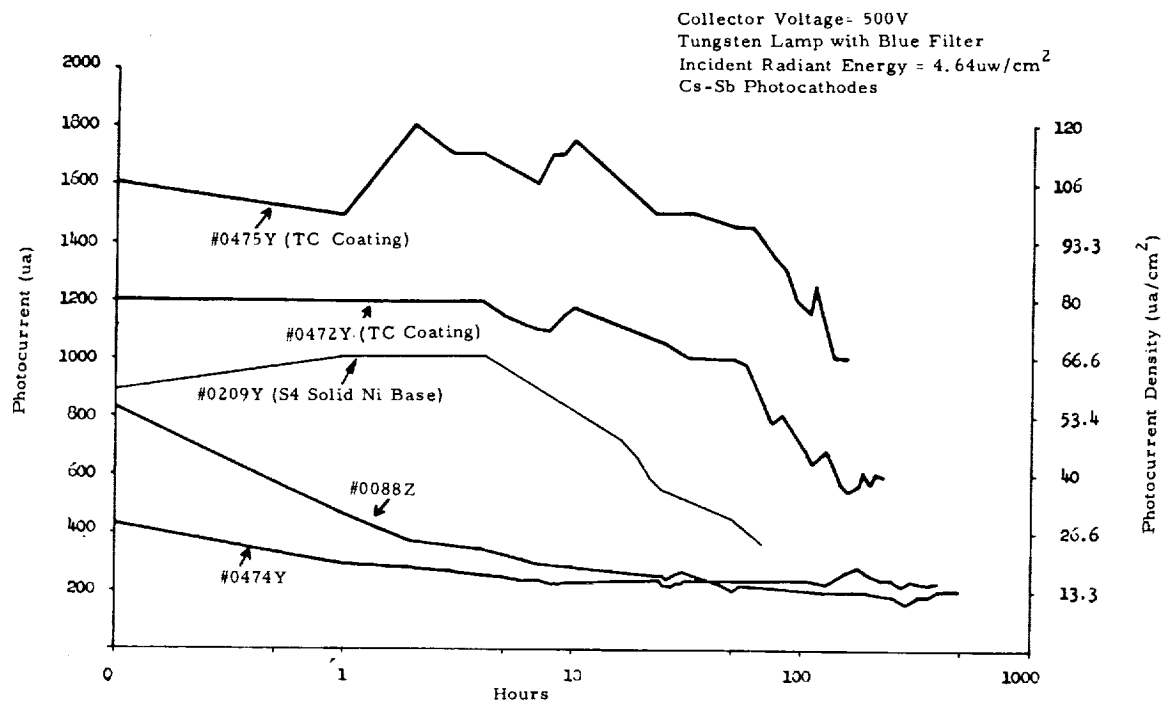
FIGURE 16-2

hours. They did not drop to 50 percent of initial sensitivity until after approximately 100 hours. Clearly an improvement in stability had been obtained with the addition of the TC coating.

In the next experiment we exposed a standard Cs-Sb cathode to the same light level as before with no voltage applied to the tube. No degradation of the cathode was observed over a period of

Photocurrent (μa)

2000
1800
1600
1400
1200
1000
800
600
400
200

Photocurrent Density (μa/cm^2)

120
106
93.3
80
66.6
53.4
40
26.6
13.3

#0475Y (TC Coating)

#0472Y (TC Coating)

#0088Z

#0474Y

0   1   10   100   1000
Hours

FIGURE 16-3

114

eleven hours of continuous illumination. When voltage was applied to the cathode, the sensitivity fell in the manner shown in the lower curves of figure 16-3. These data give credence to the assumption that the falloff is intimately associated with the photocurrent, rather than with heat fr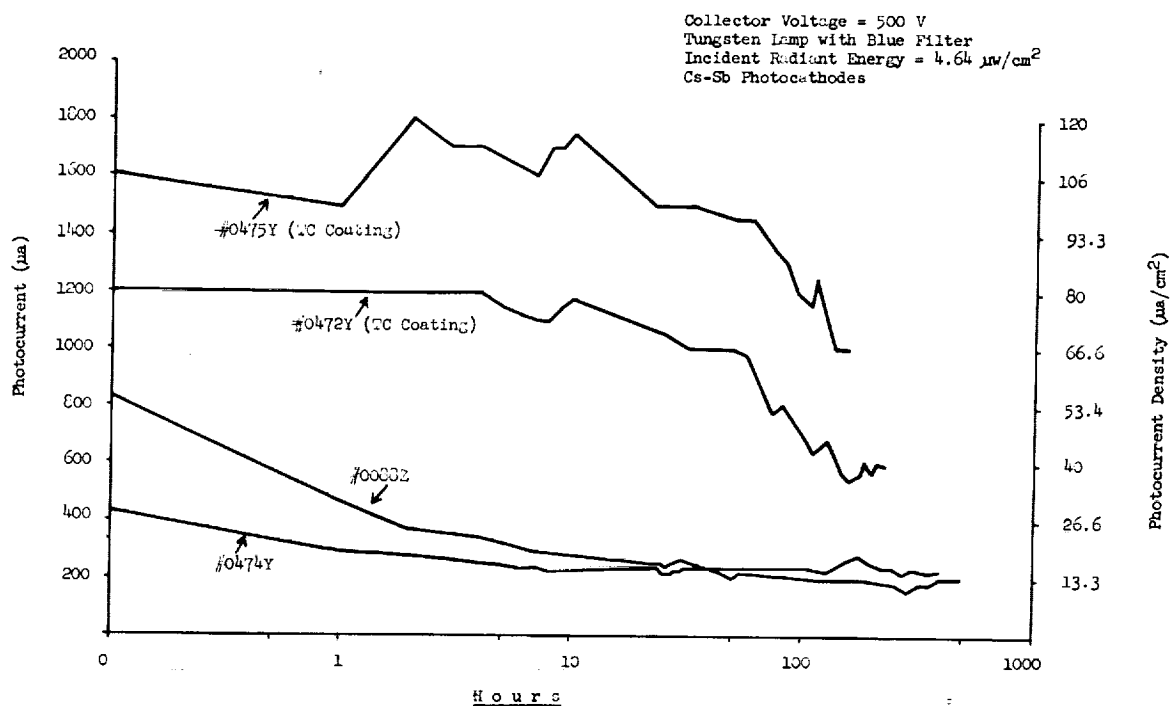om the incident light. A further check was made to note the effect of cooling the photocathode with an airstream from a blower while drawing current; the deterioration ccurred as before.

Visual examination in the illuminated area, after loss of sensitivity, showed a complete lack of the characteristic red wine color associated with a good Cs-Sb photocathode.

It appeared that the main cause of deterioration was a loss of cesium from the Cs-Sb film. To test this thesis, a Cs-Sb cathode with no TC coating was exposed to high light density from a mercury arc over a limited area. The current drawn indicated an initial value of 100 $\mu a/cm^2$. As usual, the sensitivity decreased. Since this tube contained a multiplier, it was possible to observe the area cathode sensitivity on a flying spot scanner. Figure 16-4a is a photograph taken from the monitor. The thin dark line shows loss of sensitivity due to light from the mercury arc focused on the cathode. The loss of sensivitity in the rectangle at the center was due to light from a tungsten lamp. By releasing more cesium in the tube and baking the tube for ½ hour at 150° C, it was possible to bring back some of the sensitivity (fig. 16-4b). By repeating this procedure all the original sensitivity was restored as shown in figure 16-4c. A visual examination subsequent to the above exhibited an almost complete fill-in of the former deficient area with the characteristic red wine color of Cs-Sb.

Since the initial tests were made on Cs-Sb deposited on lime glass, it was decided to test a Cs-Sb cathode deposited on fused silica. This would tend to show whether impurities from the glass substrate were contributing to the fatigue effects. Figure 16-5 shows the results. It is evident that no signicant improvement has been attained.

Figure 16-5 also shows data on semitransparent Ag,Cs-O and Ag-Bi-Cs-O photocathodes. The photocurrent levels are lower in these cases because the light level was kept constant for all tests and because of the lower sensitivity to blue light of these cathodes. Nevertheless, it is interesting to note that these cathodes appear to be relatively stable at these current levels. Until more data have been obtained, it is not possible to draw definite conclusions. It is of interest to note that the more stable cathodes are those which have relatively good conductivity or which are deposited on a conductive substrate.

Finally, data on semitransparent Na-K-Cs-Sb cathodes show fatigue characteristics which are no better than those of semitransparent Cs-Sb. It should also be mentioned that allowing the tubes to rest in the dark in no way caused the cathode to recover any sensitivity lost by exposure to intense illumination.

A recent publication by Keyoshi Miyaki [1] theorizes that temperature effects due to joule heating of the cathode due to lateral flow of photocurrent is cause of deterioration. This is consistent with the fact that the more conductive cathodes show less fatigue. If this were the case, one should expect a general deterioration of the cathode surrounding the illuminated area as well as in the area itself. This does not appear to be the case.
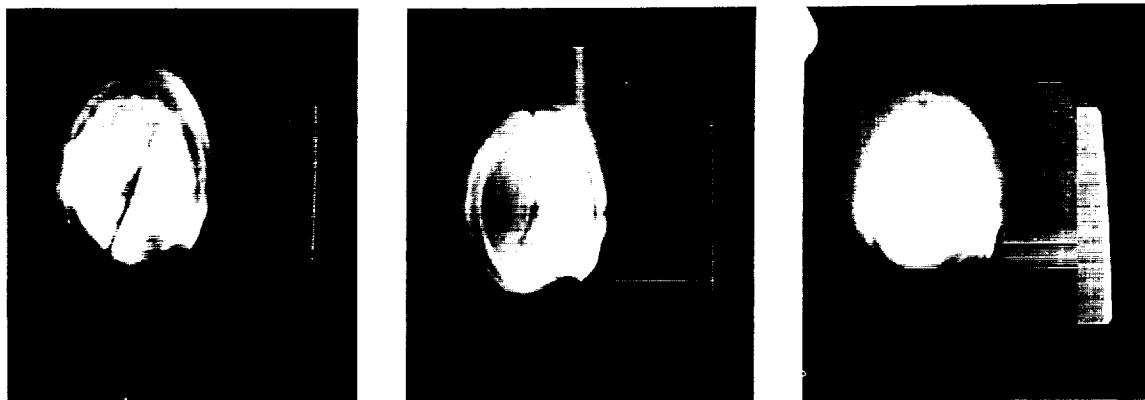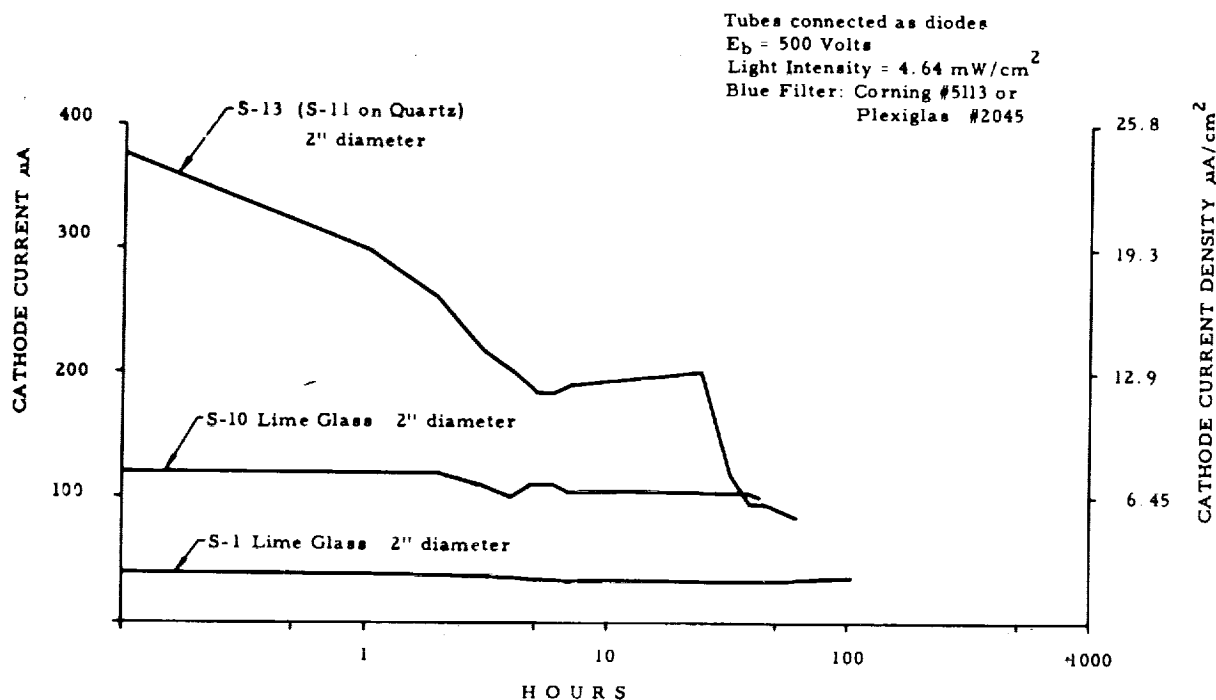

FIGURE 16-4

115

FIGURE 16-5

Whatever the cause may be, it is certain that cesium leaves the cathode and that this results in a permanent loss of sensitivity provided no more cesium is added. This is consistent with the fact that the red sensitivity drops faster than the blue sensitivity. Furthermore, the standard semi-transparent cathodes tend to approach a common sensitivity independent of the initial sensitivity as seen in figure 16-3. It is conjectured that this is the bare antimony layer with perhaps a small amount of cesium still attached to the lattice.

Ion Bombardment Effects

Positive ion bombardment is an important cause of cathode fatigue. One way of eliminating this effect is to run the tube at less than 30 volts. Since this is impossible in all but simple photodiodes, some other means must be found.

A review of the electron accelerating anode structure employed in most phototubes, image tubes, intensifiers, and electron multiplier tubes reveals the anode electrode structure to be a highly efficient ion focusing array. This structure gathers all the (+) ions resulting from emission current striking an atom or molecule of residual gas in the space between cathode and anode, and focuses them into a relatively small spot at the center of the photocathode. This abuse of the cathode reduces its efficiency to an extent which

is directly proportional to electron emission. To reduce, or possibly eliminate this destructive effect, the source of (+) ions should be reduced by a more complete exhaust, and by reducing to a minimum the amount of hardware and possible porous ceramic insulation in the tube. All procedures possible should be used to bake gas out of those elements necessary for tube construction before, during, and after exhaust and particularly during tube seasoning. Choice of materials with a low vapor pressure is paramount. Most essential is the removal of all excess Cs from the tube and any other undesirable metallic films which might break down under bombardment of emitted electrodes or electrical strain and give rise to gas. A collector anode design should be chosen which will defocus and spread out the remaining positive ions uniformly over the surface of the cathode. There are several ways to accomplish this.

Ring electrodes spaced along the axis of the tube can be used to defocus the ions if the potentials are correctly chosen. Figure 16-6 shows a sketch of this approach. An ion barrier grid made of fine-mesh screen parallel to and close to the cathode will collect electrons efficiently and greatly limit the volume of the tube in which (+) ions detrimental to the cathode can form. This approach has some merit but there are several
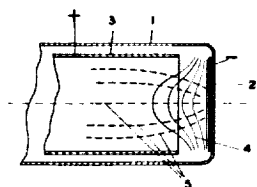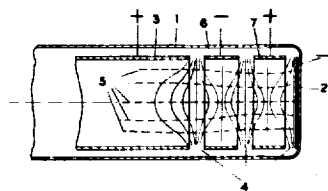
116

FIG. 1

FIG. 2

WALTER HEIMANN

FIGURE 16-6

When focus of the electrons is required, as in an image tube, this may be accomplished by an external magnetic field which will focus the electrons while only lightly affecting the ions because of the differences in their masses. This approach has the advantages of all the previous suggestions without their disadvantages. Photocathodes employing this design were built and a considerable improvement in life was noted. In this respect magnetically focused image tubes have an advantage over electrostatic tubes.

It is believed that the majority of the positive ions formed in conventional image intensifiers are the result of electrons striking free Cs atoms left over from conventional "in situ" processing. To avoid this difficulty and leave out the auxiliary electrodes such as shields, evaporators, alkali vapor sources and the like, the photocathode can be mounted on a suitable ring to be processed separately from the rest of the tube. There are a number of ways of doing this. One process which suggests itself is to form a cathode in a bell jar where it can be thoroughly tested before transfer to the final tube.

The advantages of this procedure are many. Thus, it is possible to place the Mn and Sb evap-

important drawbacks. In all cases except a photodiode, this screen's transmission will reduce the current to the phosphor screen or first dynode and degrade the tube's signal-to-noise ratio; also, in the case of image tubes, it will reduce resolution to one-half the space between adjacent wires in the mesh. Some improvement in this respect can be achieved by increasing the spacing between mesh and cathode which in turn increases (+) ion formation. Unfortunately, the high resolution required for modern image intensifiers and image tubes in general cannot be achieved by employing currently available fine-mesh screens.

Another approach which appears to have considerable merit suggests the use of a spiral wall coating of high-resistance conductive material arranged to axially accelerate the cathode electron emission toward the anode without focusing it while acting on (+) ions in an identical manner in the reverse direction (fig. 16-7). This accelerator has a further advantage in that no strong gradients are developed at any point during the flight of the electrons from cathode to anode.
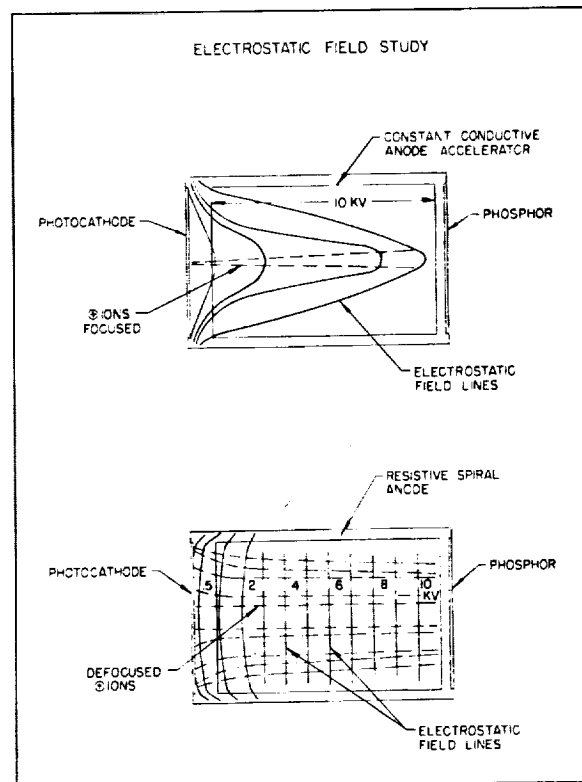

FIGURE 16-7

117

orators.at an ideal location to allow for efficient laydown of these important materials.

Above all, there will be no cesium or other alkali metals in the main body of the tube. It is expected that this will considerably reduce the ion bombardment effects resultant under high photocurrent densities.

In order to examine the cathode characteristics in a bell jar environment, a number of phototubes with various cathode surfaces were cracked open while reading their output. The change in sensitivity, as a function of time, was noted (fig. 16-8). As can be seen from the curves, all cathodes except one actually rose in sensitivity for the first 5 minutes and then returned to their original value 10 minutes later.

A possible explanation for this effect may be associated with the oxidation of excess Cs not needed for the amount of Mn and Sb present; or, possibly secondary electrons are added to the primaries as a result of emission when electrons strike gas atoms in the relatively poorer vacuum of the bell jar. Further tests will be undertaken

in a vacuum several orders of magnitude higher to determine which effect is dominant.

Techniques such as these in combination with recent improvements in vacuum technology will undoubtedly result in cathodes which have longer life under high emission current density.
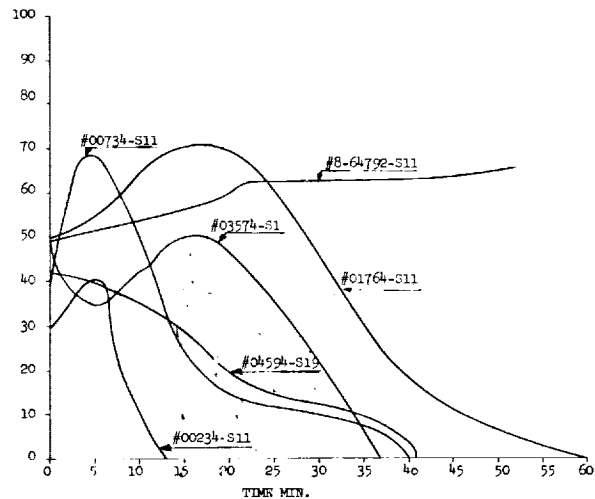

FIGURE 16-8

Discussion

H. SHABANOWITZ: Was stability of photocathode sensitivity increased at elevated temperatures? Were non-cesium-bearing photocathode examined?

B. R. LINDEN: No data were taken on cathodes at elevated temperatures. Some data were taken on bialkali photocathodes (Na-K-Sb). They showed approximately the same characteristic drop as Cs-Sb on glass. They also improved with a conductive coating.

A. H. SOMMER: Could you confirm or eliminate ion bombardment as the cause of fatigue by using a low anode voltage of, say, 5 volts so that ions are not formed? Have you any explanation for the absence of fatigue during the first 10 hours of life test?

B. R. LINDEN: The problem with using low voltage up to now is that the geometry of the tube would not allow current saturation at the light levels under consideration.

W. F. NIKLAS: Questioned the formation of ion spot at vacua better than 10^{-3} mm Hg.

B. R. LINDEN: Our experience definitely indicates ion spot formation at a vacuum better than 10^{-3} mm Hg. The light level was 10^4 foot-candles.

C. V. STANLEY: What was the pressure in the bell jar when the formed photocathodes were exposed to it?

B. R. LINDEN: The pressure reading on a Philips gage located close to the top of the oil diffusion pump was 10^{-6} mm Hg. The vacuum at the photocathode itself was probably not this good.

Reference

1. MIYAKI, KEYOSHI: Rev. Sci. Instr., vol. 32, 1961, pp. 929-933.

17. SPECIAL PHOSPHOR SCREENS FOR IMAGE TUBES*

D. A. CUSANO, *Research Laboratory, General Electric Co.*

Introduction

Simple or cascaded image converter tubes contain three important components: (1) the photoemissive surfaces, (2) the electron-optics and associated power supply, and (3) the phosphor screens. The majority of past development effort has been devoted to (1) and (2) and carried out under military sponsorship. Until fairly recently, phosphor technology has always been borrowed from the cathode ray tube and fluorescent lamp fields. Pace could easily be kept with the various electronic improvements and innovations in image tubes. This situation is no longer so. Attention should now be given to substantial modification or actual replacement of present fine-particle screens if resolution is not to remain limited by the phosphor. This is particularly important for multistage tubes. Attention should also be directed from ordinary cathodoluminescence to other luminescent effects such as cathodoelectroluminescence (CEL) [1-3] where, for example, the overall gain or storage capabilities of image tubes can be improved.

Over the past decade there has been a continuing interest in continuous layer phosphors made by vapor reaction. [4-5] Most of the effort has been directed to development of high-contrast, high-resolution transparent screens for special cathode ray tubes. The remaining effort has been largely devoted to the study of thin film electroluminescence and related electro-optical effects. This paper will deal largely with the results of a research contract (DA-44-009-ENG-4151) arranged to extend technology in vapor-reacted films specifically to the problem of phosphors for image tubes.

This contract was divided into two distinguishable portions from the standpoint of experiment: materials involved and phenomena. The first part was concerned with the improvement which

might be made in efficiency-resolution characteristics of image tubes by replacing present granular screens with vapor-reacted zinc sulfide or zinc oxide layers that are thin, but translucent or volume scattering. The general objective was to achieve much higher resolution than has been heretofore obtained, or is possible, with conventional powder screens and at the same time, to reach an efficiency as near as possible to that of the efficient P–20 viewing screen. The second half of the contract was devoted to studying vapor-reacted zinc sulfide layers which exhibit cathodoelectroluminescence (CEL) and thus show an enhancement of luminescence when voltage is applied during electron bombardment. In this case, improvement in efficiency-resolution was also sought. However, it was to come in this case from an increased electron to light conversion efficiency since electrons bombarding a CEL phosphor control its electroluminescence [1-3] rather than solely producing cathodoluminescence.

Previous Thin Film "Evaporation" Studies

With the exception of vapor reaction work, most of the effort to prepare continuous layers of phosphors has centered around evaporation in a bell jar. It has always been a great temptation to put a phosphor (no matter how complex it may be regarding impurity and chemical structure) into a suitable heater and vacuum vaporize it onto a substrate held at room temperature or slightly above. In the case of ZnF_2:Mn, such straightforward evaporation indeed produces a transparent deposit which has a chemical composition, optical characteristics, and a luminescent efficiency quite close to those of the original powder. [6] In general, however, one or more of the following things happens: (1) the activator center "breaks up" and is "lost" by selective and nonuniform evaporation of the phosphor impurities; (2) the host crystal dissociates upon heating and results in a deposit with a considerable departure from stoichiometry; (3) the condensate

119

deposits in an amorphous or different crystalline form from that of the original phosphor; and (4) the low substrate temperature prohibits the adequate diffusion of condensed impurities for the reconstruction of activator centers. These difficulties have entailed considerable departure from vacuum evaporation techniques and led to methods now termed one-step, two-step, modified two-step, etc., [7-8] such methods involving various modifications and heat treatments, both in and out of the bell jar, to restore the condensed deposit to that of the original phosphor or, in some cases an equally interesting one. (An example of the latter is that of reacting the condensed deposit with the substrate itself.) Activity in the various laboratories has mostly concerned the P-1, or Zn_2SiO_4:Mn, phosphor. The powder counterpart is a green, emitting material with a maximum efficiency for laboratory samples of about 35 lumens per watt at 15-kilovolt excitation.[9] Commercial screens come closer to 25 lumens per watt.

The Allen B. Du Mont Laboratories recently terminated a contract DA-44-009-ENG-3714, on the evaluation of "evaporated" deposits of the P-1 phosphor for image tubes. From the point of view of maximizing an efficiency-resolution product, it was hoped that control of the texture of the phosphor layer would allow sufficient scattering out of the emitted light with adequate preservation of resolution. However, the silicate deposits are fabricated by high-temperature reaction between deposited oxide components and between these and quartz or glass substrates. The task of controlling phosphor texture by this type of preparation has not been a simple one although some samples of undetermined resolution have been made which have a luminescent efficiency of about 7.4 lumens per watt.

Vapor-Reacted Sulfide and Oxide Phosphors

In many thin film phosphor applications, transparent scattering-free deposits have been desired, the cathodoluminescent efficiency not always being the foremost consideration. In the case of image tubes, however, it was recognized that improvement in resolution could only be significant in over-all performance if the efficiency of the deposited phosphor was not too far below that of the fine-grained P-20 phosphor (Zn, CdS:Ag,Cl). The P-20 powder phosphor has the highest known laboratory efficiency of about 80

lumens per watt [9] at 15 kilovolts, and good image tube samples run as high as 45 lumens per watt.

The vapor reaction method, [4-5] as contrasted to the various procedures mentioned above, has been employed with particular success in the preparation of transparent films of zinc-cadmium sulfides. Five-inch transparent P-11 screened tubes are already in production and being used for low noise, high resolution c.r. applications.* These polished nonscattering films offered very high resolution—up to 500 line-pairs per millimeter. However, in a truly nonscattering condition, the same phosphors are down an order of magnitude in luminous efficiency from present P-20 screens—a large part of this poor performance due to internal light trapping. No change or net loss in efficiency-resolution would be had by using these screens in image tubes. In addition, it would be quite difficult to make use of very high resolution with the conventional optics used in many applications. For these reasons, the present work involved, alternatively, the approach of making the brightest screens possible, making use of and often increasing the light scattering or translucent nature of the films rather than polishing them to a smooth finish. (The high refractive index of zinc sulfide is not a disadvantage for scattering films as it is for transparent, nonscattering deposits.) A useful resolution goal of about three times that of P-20 screens (i.e., ~120 line-pairs per millimeter) was sought.

Figure 17-1 depicts schematically the arrangement used in preparing the phosphors studied on this contract. In essence, the vapor reaction method [4-5] is chemically similar to one which is frequently used for growing single crystals. The growth occurs on a hot ($>$400° C) surface from reaction between the vapors or gases which contain the elemental constituents of the phosphor as well as the impurities to be incorporated therein.**

The preparations investigated included zinc sulfide and oxide samples with emission bands in the blue, green, and yellow region of the spectrum.

*General Electric Co., Cathode Ray Tube Department, Syracuse, N.Y.

**Insofar as there is considerable evidence that II-VI compounds dissociate at high vaporation temperatures, the "hot wall bell jar evaporation" method for forming II-VI phosphor films[10] may also involve reaction of dissociated constituents. If HCl is added during evaporation, then the salts of the elemental constituents could similarly be involved in reaction.
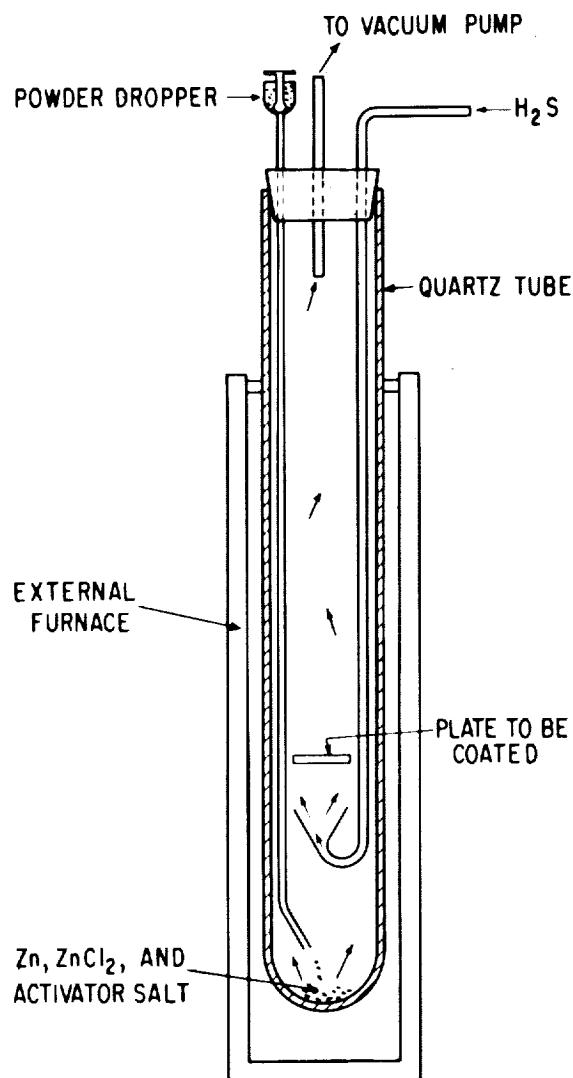
FIGURE 17-1.—Vapor reaction coating arrangement for ZnS phosphor layers.

The main activator examined was copper. It was incorporated by utilizing either a predeposit or postdeposit of copper (sometimes both), the latter requiring an additional heating cycle beyond that of the sulfide deposition itself. All the other activators and the coactivator chlorine were incorporated from the vapor, the most usual way.[4-5] About 40 or more films were made, only a few alike in the conditions of preparation.

The coating thickness was taken to two or three microns to make full use of 10- to 25-kilovolt electron bombardment. A few samples were made thin to determine particularly the effect on resolution. Many samples were prepared on thin precoats of various evaporated materials to nucleate growth in different ways. Various glass substrates were examined to explore their effect on luminescence efficiency and deposit texture. For the most part, coating temperature was held about as high as the particular glass could take. There was very little evidence that luminescent efficiency did not decrease with temperature reduction.

Resolution Measurements

Resolution was measured by optical means, since many zinc sulfide and oxide phosphors luminesce to ultraviolet as well as cathode ray excitation. In essence, this optical measurement provided a simple and rapid means of determining a value of resolution corresponding to a lower limit of what is expected for excitation by cathode rays. (In the near ultraviolet (3,650 Å), zinc sulfide has a high index of refraction, about 2.7.[11] Therefore, lateral scattering of ultraviolet at the phosphor surface would, if anything, give poorer apparent resolution than that obtainable under electron excitation.)

The optical equipment is shown in figure 17-2. A 3,650 Å image of a resolution chart transparency was projected onto the scattering phosphor sample to be examined, usually on the film side. A Corning 5,840 filter was used in front of the SP4 mercury lamp to further reduce the intensity of the weak 4046Å line in this lamp, beyond that already accomplished by the dark glass envelope. A good quality lens was employed which had adequate transmission to ultraviolet. Brightness was no problem. The resolution pattern, in luminescent light, was viewed with a microscope through the glass side, as it would be in actual image tube use. To avoid any possibility of observing blue radiation from the ultraviolet lamp, a Wratten 8 (K2) filter was employed as shown, between the observer and the microscope.

Resolution measurements were obtained for more than two dozen samples as grown. Values for many sulfide layers reached 84 line-pairs per millimeter, twice as high as P-20 values. Thinner samples gave more than 96 line-pairs per millimeter, while several samples gave low values of 56 to 63 line-pairs per millimeter. Very high values of 140 to 154 were obtained with a ZnO:Zn screen, indicating, for one thing, that the resolution capability of the measuring system was at least that good.

Unpolished vapor-reacted sulfide phosphors as grown scatter only at the air-phosphor surface. Some of the light which reaches the observer
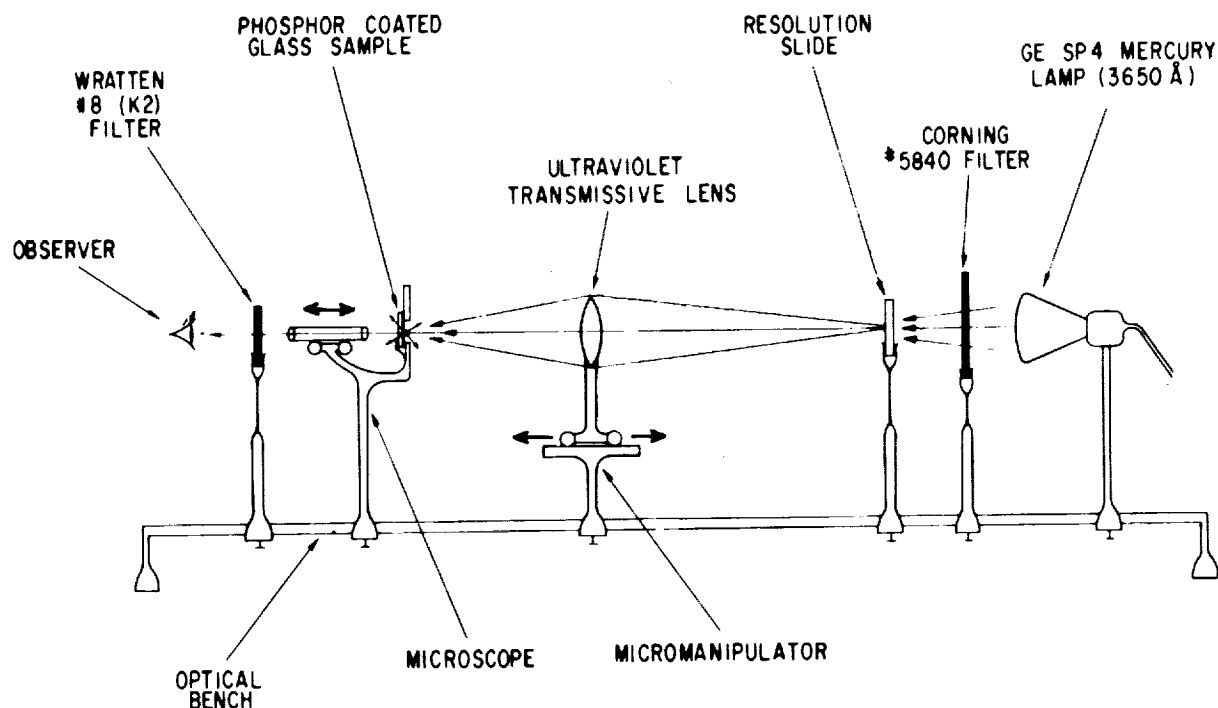
FIGURE 17-2.—Arrangement for measuring optical resolution of phosphors.

involves long paths through the transparent interior, with the result that the spot size is considerably enlarged. This appeared to be the reason for the low resolution of some samples. The ZnO:Zn screen, which had by far the best resolution, contained an appreciable volume-scattering nature. This was evidenced by the fact that it could not be polished to transparency as could most sulfide layers.

Two techniques were studied to make sulfide layers possess volume as well as surface scattering character. The first, already mentioned, involved precoating the glass substrates with a thin layer of material which nucleates the subsequent sulfide growths so that these deposits consist of disoriented, microcrystallite structure. The second, and more successful, was that of etching the deposits with acid just long enough to cause selective attack at grain boundaries and along microcrystallite surfaces. The air-phosphor interfaces so produced were effective light scattering sites. Resolution before and after etching is shown for several samples in Table 17–I. In two instances, the resolution improved considerable, rising to about 115 line pairs per millimeter, or nearly three times that of standard P–20 screens. In four other cases, the improvement was not as large.

TABLE 17-I

Sample No.	Phosphor	Resolution (line pairs/mm)	
		Before HCl etch	After HCl etch
S–485	ZnS:Cu,Cl	63(70)	77
S–487	ZnS:Cu,Cl	70(77)	77
S–492	ZnS:Cu,Cl	70(70)	115
S–500	ZnS:As,Cl	70(63)	115
S–501	ZnS:As,Cl	70(70)	77
S–502	ZnS:Cu,Cl	84(77)	77

( ) Measurements made by a second observer.

Efficiency Measurements

In order to maintain proper screen potential and approximately double the light reaching the observer, nearly all image tube phosphor screens were backed by a thin reflecting metallic coating, usually of aluminum. The aluminum, if deposited directly on these rough surfaces, is gray in appearance and poor in reflection when viewed through the phosphor. This depended in degree on the particular scattering nature of each sample. To avoid this difficulty, aluminum was first evaporated to 0.1 micron on a self-supporting lacquer film, the free surface of this then pressed

122

onto the phosphor, and the lacquer film burned off subsequently in an air bake.

Some two dozen phosphor samples were examined under electron bombardment in a demountable cathode ray tube. The spectral distributions were found to be relatively independent of bombarding voltage and were obtained at 15 kilovolts and $0.1\mu a/cm^2$. The spectra are plotted in figures 17–3 and 17–4. From the area under the product of visibility curve and these spectral distributions, the lumen equivalents, or lumens per output watt, were calculated for each sample. The results obtained are listed in the

fourth column, of table 17–II. The suffix E and U in the sample label indicates respectively whether the sample had or had not been etched in HCl solution.

Cathodoluminescent brightness was measured with a SEI exposure meter for two values of current density, 0.01 and $1\mu a/cm^2$, and three bombarding voltages, 10, 15, and 20 kv. The aluminum backing maintained the phosphor at anode potential during bombardment. The maximum brightness values obtained, whether at 10, 15, or 20 kv, were converted directly to *lumens per watt* efficiencies via the formula below:

$$\text{(Efficiency in lum/w)} = \frac{\text{(Brightness in ft-L)} \ (1.07 \times 10^{-3} \ \text{lum/cm}^2\text{-ft.l})}{\text{(Beam potential in volts)} \ \text{(Beam current density in amp/cm}^2)} \tag{1}$$

and are tabulated in table 17–III, fourth column. In general, higher efficiencies were found for higher voltage operation.

The lumens per watt efficiencies, in turn, were

converted to *energy* efficiencies using the lumen equivalents of table 17–II, fourth column, in the expression below:

$$\text{(Energy efficiency)} = \frac{\text{(Efficiency in lum/w)}}{\text{(Lumen equivalent in lum/w)}} \tag{2}$$

These results are plotted in table 17–III, again for 10, 15, or 20 kv, whichever value was highest. These energy efficiencies are an indication of phosphor performance quite independent of emission color.
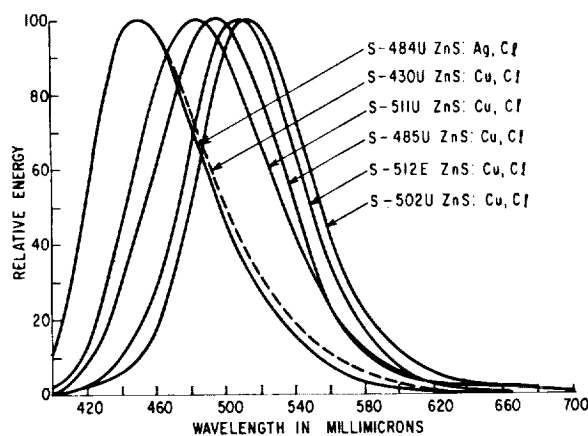
to be compared to values of about 45 for the present P–20 image tube powder screens, and values from 20 to 25 for the older P–1 powder screens. Several films, those shown and others, exhibit energy efficiencies from 3 to 5 percent. For comparison, the energy efficiency of P–20 and P–11 screens is about 10 percent and that for P–1 powder screens between 4 and 5½ percent.

As regards resolution, the values obtained optically are quite high, especially for the etched samples which offered 115 line-pairs per milli-

FIGURE 17–3.—Spectral distributions of ZnS:Ag,Cl and several ZnS:Cu,Cl vapor-reacted phosphors under cathode ray excitation.

Conclusions Concerning Translucent Vapor-Reacted Phosphor Films

As can be seen from table 17–III, the lumen-per-watt efficiencies of two or three vapor-reacted films have reached values of 13 to 17. These are
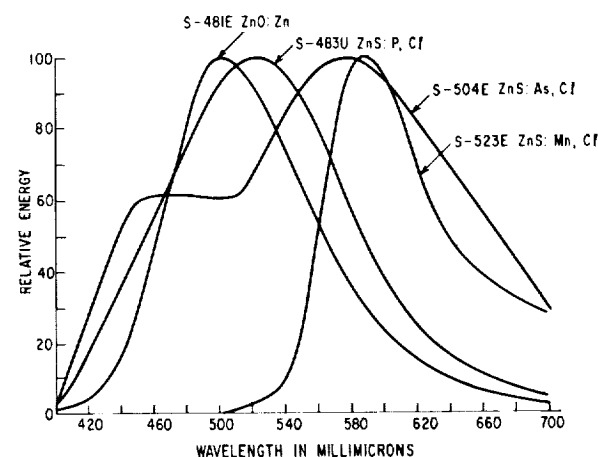

FIGURE 17–4.—Spectral distributions of ZnS:P,Cl, ZnS: As,Cl, ZnS:Mn,Cl, and ZnO:Zn vapor-reacted phosphors under cathode ray excitation.

TABLE 17-II

Sample	Phosphor	Substrate	Lumen equivalent (in lumens/watt)	Peak wavelength (Å)
S–430 U	ZnS:Cu, Cl	Lime glass	150	4,540
S–511 U	ZnS:Cu,Cl	Pyrex	272	4,850
S–485 U	ZnS:Cu,Cl	Lime glass	295	5,050
S–512 E	ZnS:Cu,Cl (etched in HCl)	Pyrex	368	5,100
S–502 U	ZnS:Cu,Cl	Lime glass	425	5,130
S–504 E	ZnS:As,Cl (etched in HCl)	Pyrex	309	5,750+4,550
S–481 E	ZnO:Zn (etched in HCl)	Pyrex	358	5,000
S–483 E	ZnS:P,Cl (etched in HCl)	Pyrex	354	5,220
S–523 E	ZnS:Mn,Cl (etched in HCl)	Pyrex	276	5,900
P–20 [1]	Zn,CdS:Ag,Cl	(Powder phosphor)	515	5,500
P–20 [2]	Zn,CdS:Ag,Cl	(Powder phosphor)	500	5,500
P–1 [2]	Zn₂SiO₄:Mn	(Powder phosphor)	475	5,250

[1] This report.
[2] Data from Bril and Klasens.

TABLE 17-III

Sample	Phosphor	Peak wavelength (Å)	Maximum lumens per watt efficiency	Maximum energy efficiency (in percent)
S–430 U	ZnS:Cu,Cl	4,540	4.5 (4.8)	3.0 (3.2)
S–511 U	ZnS:Cu,Cl	4,850	13.4 (10.7)	4.9 (3.9)
S–485 U	ZnS:Cu, Cl	5,050	11.4 (11.8)	3.9 (4.0)
S–512 E	ZnS:Cu,Cl	5,100	13.5 (14.3)	3.6 (3.9)
S–502 U	ZnS:Cu,Cl	5,130	8.6 (8.6)	2.0 (2.0)
S–504 E	ZnS:As,Cl	5,750+4,550	10.7 (3.6)	3.5 (1.2)
S–481 E	ZnO:Zn	5,000	4.3 (2.7)	1.2 (.8)
S–483 E	ZnS:P,Cl	5,202	10.7 (17.1)	3.0 (4.8)
S–523 E	ZnS:Mn,Cl	5,900	5.7 (2.1)	2.1 (.7)

x0.01 μa/cm².
(x) 1 μa/cm².

meter. The present P–20 screens give about 40 line-pairs per millimeter. Since there is no reason why the best efficiency and best resolution found to date could not be produced in a single specimen, the performance of films is found for the first time to be competitive with the P–20 screens on the basis of a simple efficiency-resolution product. As viewing screens, these green ZnS:Cu,Cl or ZnS:P,Cl samples should be more attractive than P–20 fine-grained screens, if the optics involved dictate that resolution should be somewhat more important than efficiency. Blue-green emitting films of ZnS:Cu,Cl used with either S–11 or multialkali photocathodes, offer slightly better efficiency-resolution products than powder P–11 powder screens. Hence they may find use in cascaded tubes. For such cascaded tubes, where one may desire a single phosphor to be used at both the intermediate and viewing stages, the blue-green emitting films of ZnS:Cu,Cl would be best suited.

In short, many of the scattering vapor-reacted deposits investigated here have exhibited cathodoluminescent efficiencies considerably higher than any made to date by other film methods. Some of these deposits of high resolution and general quality will find use in special cathode ray tubes in addition to image tubes. Since there is no

124

theoretical reason why such translucent or scattering sulfides should not some day be just as efficient as their powdered phosphor counterparts, further development efforts should lead to translucent thin film screens with the presently achieved resolution of 120 line-pairs per millimeter and an energy efficiency nearer to 10 percent.

Introductory Comments on CEL Intensifying Screens

In addition to being the most efficient phosphors under cathode ray excitation, granular zinc sulfides represent the best electroluminescent material known to date. Furthermore, related materials such as cadmium sulfides and selenides are very sensitive photoconductors to the visible and infrared. For some time, it has been hoped that a series combination of a photoconducting and electroluminescent layer (PC+EL) would offer a solid-state amplifying screen[12-14] that would perform as well as, and eventually replace, vacuum image converter tubes. However, the characteristics sorely needing improvement before this replacement can be seriously considered are the slowness of response, the insensitivity to very low radiation levels, and the inherently poor resolution (~ 2 lines/mm).[12]

Single-layer PEL screens[1-3] have also been considered as possibilities for image tube replacement. The important advantage over the two-layer intensifiers is that of much higher resolution. The PEL phenomenon is observed with vapor-reacted layers of ZnS:Mn,Cl, ZnS:Mn,X,Cl and ZnS:X,Cl where X is either P, or As, or Sb. These phosphors are grown on TiO_2 coated glass, the transparent TiO_2 film being one electrode and a metallic layer applied on top of the phosphor the other. (See fig. 17-5.) When an image of radiation in the near ultraviolet or blue region of the visible falls upon the screen and a d.c. voltage (usually less than 100 volts) is impressed across the phosphor as shown, this type of solid-state amplifier emits an image in the yellow region of spectrum whose intensity is more than 10 times that in the incident beam. This intensification is accomplished[15] via a control exerted by the input radiation on the ability of the phosphor to electroluminesce; i.e., to derive electrical energy from the voltage source and convert it into visible light.

Although better in resolution than a (PC+EL) screen, the PEL intensifier still does not compete with conventional image tubes at very low light levels. However, there was yet to be explored
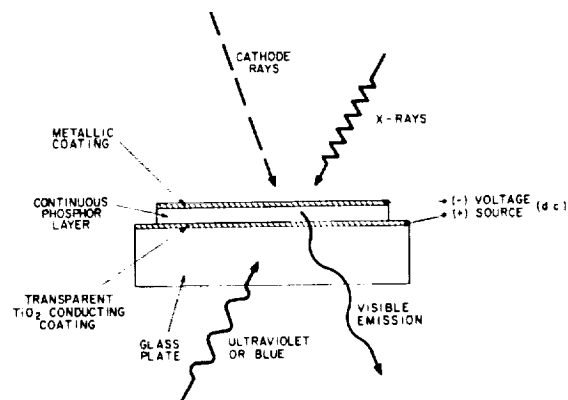
FIGURE 17–5.—Arrangement for observing PEL and CEL effects.

the related solid-state phenomenon of cathodo-electroluminescence (CEL),[1-3] i.e., the control of electroluminescence in these screens exerted directly by incident electrons rather than photons (see also fig. 17-5). The remainder of this paper has to do with this CEL effect, not as a phenomenon competing with electronic image conversion, but rather for its possibilities of improving overall performance of these image tubes as a replacement for present viewing screens. Since the phosphors were to be no more than about 5 microns thick, and could be polished if desired, no serious resolution problem was anticipated. Furthermore, the screens appeared to function best in a region of cathode ray intensity from 0.25 to 250 μ watt/cm^2, very much in the realm of present image tube operation. Since the CEL layer would not be required to detect an image at low levels at which it arrives at the photocathode, the obstacle of sensitivity at very low intensities would be circumvented.

Effort on CEL was devoted primarily to efficiency-resolution improvement, but related things such as memory or image retention were given some attention.

CEL Sample Preparation

Pyrex disks were coated with transparent TiO_2 to a thickness of about 0.3 micron. These coatings were formed by the usual technique of reacting $TiCl_4$ vapor with H_2O vapor while the samples are held at approximately 250° C. Subsequent deposition of zinc sulfide phosphors leads to chemical reduction of the coatings such that they become semiconducting and can serve as transparent electrodes.[4 5]

Various phosphor modifications were prepared on these TiO_2-coated bases. The activator

manganese is a necessary impurity [15][16] and was included in preparation of all samples. However, since other activators such as phosphorus, arsenic, and antimony can produce PEL[17] or influence PEL characteristics of manganese phosphors,[15][16] they were also examined.

The coactivator chlorine seems to be a second important impurity for CEL phosphors. It is considerably more effective than other halides. Properties like resistivity and photosensitivity do not depend to first order on manganese, but they do on this coactivator. Chlorine content was intentionally varied for some of the preparations. A few samples were prepared with group IIIB coactivatior such as Ga and In, alone and in conjunction with chlorine.

Other variations made for the purpose of influencing CEL properties involved thickness of samples, surface nature (unpolished or polished), and final electrode identity. The electrode materials were all directly evaporated metals about 0.1 micron thick—namely, aluminum, indium, gold, copper, and silver. Aluminum and gold electrodes behaved similarly and reasonably well for all screens, with aluminum preferred in general.

Experimental Results and CEL Behavior

The following comparison is typical of that made between a CEL screen and an aluminized P–20 granular phosphor. Both phosphors were bombarded side by side in a demountable cathode ray tube with a raster of appropriate size. The CEL screen was a polished, nonscattering ZnS: Mn,As,Cl phosphor with a top electrode of 0.1-micron aluminum, nearly the same thickness as that on the P–20 viewing screen. With no voltage applied to the CEL screen, its light output was considerably lower than that of the P–20. However, with a d.c. voltage of 85, the brightness under 15 kilovolts became considerably higher than that of the P–20, particularly at the low current densities. A plot of steady state brightness versus current density for each screen is shown in figure 17–6. The plot for the P–20 is essentially linear, indicating a constant efficiency of 45 lumens per watt. (This corresponds to an energy efficiency of about 10 percent.) The numbers adjacent to the CEL curve give the brightness ratios of CEL to P–20 phosphors at various current densities. At about 4×10^{-5} microamperes per square centimeter, the energy efficiency of the CEL screen is about 200 percent. In essence, this means that via cathode ray
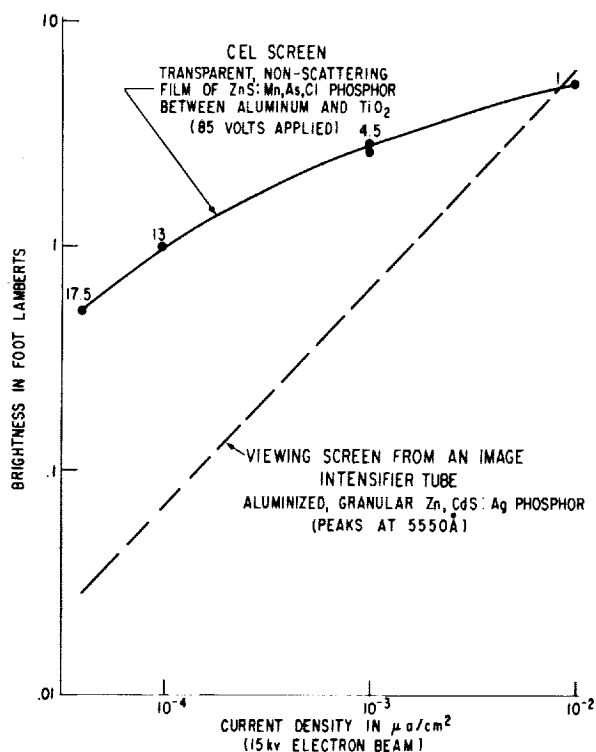
Figure 17–6.—Brightness versus current density for a CEL screen and a P–20 viewing screen from an image converter tube. Brightness ratios of CEL to P–20 noted along solid line.

control of d.c. electroluminescence it is possible to produce twice as much energy in visible emission than is present in the cathode ray beam itself.

Another manner of presenting steady state data is shown for a second sample in figure 17–7. Here, the CEL brightness is plotted against that of the P–20 screen under the same excitation. The dotted straight line is one of equal brightness. Data are shown for several voltages. A fair appreciation of the CEL mechanism can be obtained by subtracting the cathodoluminescent (no field) light output from the CEL output. The results are plotted as dotted lines on the same figures. These curves now show saturation with increasing P–20 brightness; in other words, increasing current density. The saturation value increases with bombarding voltage, but eventually saturates too. Briefly, for each bombarding voltage, there is a certain value of d.c. electro-luminescence which can be "turned on" in any fraction, or in full, by proper choice of incident electron density. Also, there is a maximum amount that can be "turned on" regardless of the

126

100
50
30

BRIGHTNESS OF CEL SCREEN IN FOOT LAMBERTS
ZnS: Mn, As, Cl, 35 VOLTS APPLIED

25 kv
20 kv
15 kv

10
RISE TIMES IN
SECONDS
5

10 kv
3

1
CATHODOLUMINESCENT
EMISSION
.5

.3
5
4½

.1
10
7
3
LINE OF EQUAL
BRIGHTNESS

.05

.03
.01   .03 .05   .1   .3 .5   1   3   5   10   30 50 100   300 500

BRIGHTNESS OF P-20 POWDER SCREEN IN FOOT LAMBERTS
(APPROX. LINEAR WITH CURRENT DENSITY)

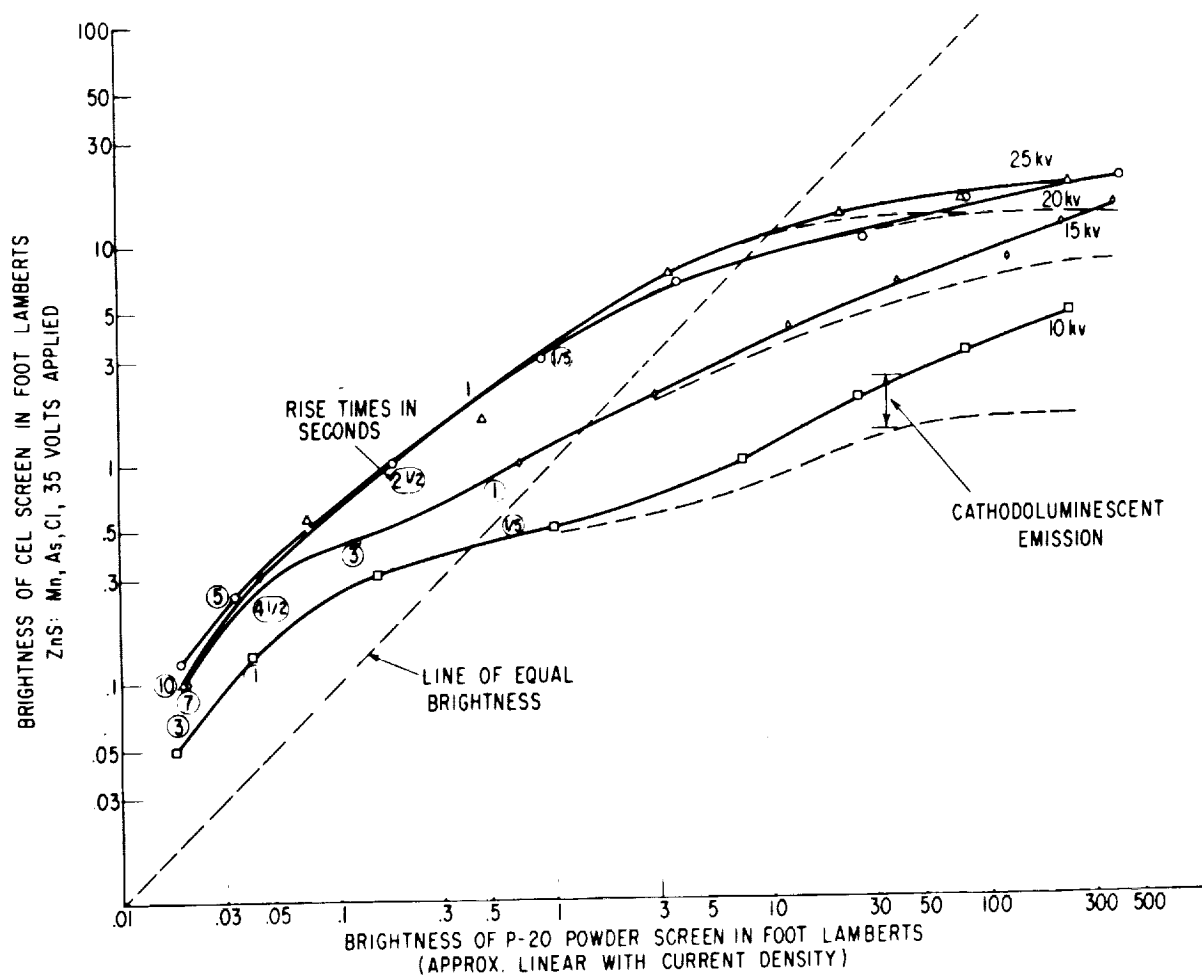FIGURE 17-7.—CEL screen versus P-20 screen brightness for several beam voltages. Encircled numbers give CEL rise times under operating conditions given by nearest section of solid curves.

value of bombarding voltage. The latter is about 13 foot-lamberts for the sample of figure 17-7 but can be as high as 50 foot-lamberts in other cases. Such values, for only 40 volts applied, are consistent with maximum d.c. EL which can be obtained by special surface treatment of these same zinc sulfide samples.[15][16]

The buildup and decay of light output in CEL is not exponential with time. However, a rough idea of the time it takes for the light output to increase to about two-thirds of its steady-state value following the switching on of a cathode ray beam of a given current density and voltage is given in figure 17-7. The "time constants," in seconds, are shown as encircled numerals and pertain to that particular section of the solid line curve they are closest to. As can be seen, the buildup time decreases with increasing current density, and also seems to increase with bombarding voltage.

The decay times, for some phosphor preparation, are shorter than the buildup times at high intensity, but approach them at low intensity. For other screens, however, the decay times are appreciably longer than the rise times. For these samples, pulsed d.c. operation ($f \sim 100$ cycles per second or less) was able to help by shortening decay times considerably, but this had little or no effect on buildup times. In still other samples currently under study, attempts were made to actually increase decay times for image storage tube possibilities.

A CEL sample, electroded with a semitransparent gold film ($75 \sim$A), was examined in the optical resolution equipment described earlier in this report. Without applied voltage, the resolution of this sample was observed to be about 65 line-pairs per millimeter. With a voltage applied, the resolution was easily seen (the brightness increased) to stay the same. There was no

127

apparent field spreading of the light. Although this measurement was actually one of PEL, the CEL resolution is bound to be the same or possibly better.

Conclusions Concerning CEL Intensifying Screens

It has been shown that CEL screens consisting of vapor-reacted zinc sulfide films subjected to electric fields exhibit greater light output than P-20 image tube screens under identical electron bombardment. The bombardment range is from 10^{-5} to 10^{-2} $\mu a/cm^2$ and 5 to 25 kv, well in the operating range of the final stages of image converter tubes. In the current density region between 10^{-5} and 10^{-4} $\mu a/cm^2$, the ratio of CEL to P-20 brightness can be greater than 10. The resolution of the CEL phosphors, measured optically, is about 65 line-pairs per mm, or 40 percent better than that of P-20. Hence, the efficiency-resolution product of image tubes can be increased markedly by employing CEL screens in place of P-20 screens for the viewing phosphor.

A disadvantage of CEL screens for some image tube applications is the slowness of response, particularly in the lower current density region where the efficiency-resolution improvement is greatest. It is shown in the appendix to this paper that it is not likely that rise times can be improved greatly since the present zinc sulfide layers are exhibiting nearly maximum performance as cathodoconductors. Hope for further improvement lies in (1) lower resistivity CEL samples, (2) lower resistivity cathodoconductor plus electroluminescent thin film screens, or (3) considerably improved electroluminescent efficiency during CEL. Nevertheless, it is strongly believed that the true worth of the CEL screens as they now stand can only be evaluated in actual image tube operation (demountable or otherwise). It is urged that this be carried out in the near future.

Summary

Two means of improving the performance of luminescent elements used in image tubes are discussed. Translucent vapor-reacted zinc sulfide layers have been produced with resolutions, measured optically, of up to 115 line-pairs per millimeter. At the same time, such layers have exhibited cathodoluminescent efficiencies from 13 to 17 lumens per watt. Although the efficiency-resolution product turns out to be the same as for P-20 powder screens, these films should be

useful where resolution is more important than efficiency, such as, for example, in multistage image tubes.

Vapor-reacted zinc sulfide layers which exhibit enhancement of luminescence under applied voltage and during electron bombardment offer up to an order of magnitude of improvement in efficiency resolution. These CEL (i.e., cathodo-electroluminescent) screens are brighter than P-20 screens in the range from below 10^{-5} to 10^{-2} microamperes per square centimeter—by more than 10 times at the lower end of this range. A disadvantage of CEL screens for some image tube applications are the long response times when compared to those for P-20 or other simple cathodoluminescent phosphors. The long decay times of CEL screens need not be a similar disadvantage.

Acknowledgments

Appendix

It is obvious, for some image tube applications, that the CEL screen response times will be a disadvantage which more than offsets the improvement in efficiency-resolution that would be achieved by using a CEL screen. That this situation cannot be markedly improved by making small order refinements in zinc sulfide preparations is evident from an appreciation of the CEL mechanism. The analysis is by no means precise, but does place a reasonable limit on what can be obtained with the present approach and materials.

In CEL, incident electrons control the number of free electrons in the phosphor, and these in turn produce radiant energy in the form of visible light by accelerating in the direction of the field and giving up part of their energy in exciting

luminescent centers. By considering the CEL mechanism as composed of two parts, the first effect becomes one of cathodoconduction and the second, one of d.c. electroluminescence. The first is the time-dependent, radiation-sensitive process. Similarly, the PEL mechanism could be thought of as photoconductive and d.c. electroluminescent part, here photoconduction being the rate-determining process depending on the incident ultraviolet or visible intensity.

For the photoconductive process, the Rose-Redington [18] [19] theoretical analysis has led to a maximum performance equation

$$\frac{\text{(Gain in electrons/incident photon)}}{\text{(Response time in sec.)}} \leq \frac{1}{\text{(Res. in ohms) (Cap. in farads)}} \quad (3)$$

Measured under irradiation

which determines the maximum gain and shortest time constant for a given condition of operation in terms of the measurable quantities of resistance and capacitance during operation. We can extend this to apply to cathodoconduction under 25-kilovolt electron bombardment by writing

$$\frac{\text{(Gain in electrons/incident electron) } (5 \times 10^{-4})}{\text{(Response time in sec.)}} \leq \frac{1}{\text{(Res. in ohms) (Cap. in farads)}} \quad (4)$$

Measured during bombardment

The numerical factor of 5×10^{-4} above takes into account the fact that it takes about 12.5 ev to form each electron hole pair from the incident 25-kilovolt electrons. (This value is estimated from the 20-percent cathodoluminescent efficiency of zinc sulfide phosphors.)

A CEL screen, with 40 volts applied and a cell area of 1 cm^2, exhibited a steady-state cathodo-current of 1.5 ma under 25 kilovolt and $10^{-4} \mu a/cm^2$ electron bombardment. The cathodoconductive electron gain is thus 1.5×10^7 and the resistance 2.7×10^4 ohms. (These figures incidentally, represent a cathodoconductive electrical power gain of $\sim 2.5 \times 10^4$.) The capacitance, although not measured during bombardment as it rigorously should be, is estimated from other measurements to be in the neighborhood of 4×10^{-9} farads. Substitution of these values in Eq. (4) above gives:

$$(\text{Response time in sec.}) > 0.75 \text{ sec.}$$

The response time measured experimentally for this sample under the excitation conditions above is about 2 seconds.

Within the accuracy of this approximate analysis, then, the CEL screens are exhibiting maximum cathodoconductive performance.

Discussion

J. F. Roesler: Would you elaborate on the construction of vapor reacted phosphors? Can you give a reference?

D. A. Cusano: Several references on vapor reaction and vapor-reacted phosphors are given in this paper (see refs. 2 and 11). Most detail is given in my doctoral dissertation, available from University Microfilms, Inc., Ann Arbor, Mich., in Xerox copy or microfilm.

W. F. Niklas: What is the resolution of cathodoelectroluminescent phosphor screens?

D. A. Cusano: As described in this paper, a resolution of 65 line-pairs per millimeter was obtained optically for ~ 5 micron cathodoelectroluminescent phosphors (while voltage was applied). This measurement was made with 3,650 Å ultraviolet. However, it is expected that resolution under electron bombardment will be the same or possibly better.

R. G. Stoudenheimer: The light output of the cathodoelectroluminescent phosphor did not appear to approach zero at very low bombarding currents. Does this indicate a residual background brightness at zero bombarding current? If so, what is the level of this residual brightness?

D. A. Cusano: A residual background brightness does occur for CEL samples at zero bombarding current, and it can vary from one sample to another in area uniformity and magnitude. Unlike two-layer EL—PC structures, the phosphor in single-layer intensifiers is always under field stress, regardless of the level of irradiation. For the samples of figures 17-6 and 17-7, the background levels are 0.01 foot-lambert or less.

Reference

1. CUSANO, D. A.: Phys. Rev., vol. 98, 1955, p. 546.
2. CUSANO, D. A.: IRE Trans. of Nucl. Sci., No. 4, 1956, p. 102.
3. CUSANO, D. A.: Proc. of Image Intensifier Symp., October 1958.
4. STUDER, F. J., and CUSANO, D. A.: J. Opt. Soc. Amer., vol. 45, 1955, p. 493.
5. CUSANO, D. A., and STUDER, F. J.: *Enlarged Abstracts of Electronics Div.*, No. 65, Electrochem. Soc. Mtg., May 1955.
6. WILLIAMS, F. E.: J. Opt. Soc. Amer., vol. 37, 1947, p. 302.
7. FELDMAN, C., and O'HARA, M.: J. Opt. Soc. Amer., vol. 47, 1957, p. 300.
8. KOLLER, L. R.: Abs. 29, Electrochem. Soc. Mtg., May 1957.
9. BRIL, A., and KLASENS, H. A.: Philips Res. Rep., vol. 7, 1952, p. 401.
10. KOLLER, L. R., and COGHILL, H. D.: J. Electrochem. Soc., vol. 107, 1960, p. 973.
11. PIPER, W. W., MARPLE, D. T. F., and JOHNSON, P. D.: Phys. Rev., vol. 110, 1958, p. 323.
12. KAZAN, B., and NICOLL, F. H.: Proc. IRE, vol. 43, 1955, p. 1888.
13. DIEMER, G., KLASENS, H. A., and VON SANTEN, J. G.: Philips Res. Rep., vol. 10, 1955, p. 401.
14. WHITE, W. C.: U.S. Pat. No. 2,650,310, August 1953.
15. CUSANO, D. A.: Doctoral Dissertation, Rensselaer Polytechnic Institute, January 1959 (Listed in Dissertation Abstracts XX, No. 2, 1959).
16. CUSANO, D. A.: Int. Conf. on Luminescence Proc., October 1961.
17. CUSANO, D. A.: Phys. Rev., vol. 106, 1957, p. 504.
18. ROSE, A.: Helv. Phys. Acta, vol. 30, 1957, p. 242.
19. REDINGTON, R. W.: J. Appl. Phys., vol. 29, 1958, p. 189.

18. TRANSMISSION SECONDARY EMISSION FROM LOW DENSITY DEPOSITS OF INSULATORS

G. W. GOETZE, *Research Laboratories, Westinghouse Electric Corp.*

Introduction

The principle of transmission type-secondary electron multiplication has been applied successfully for current amplification in several direct-viewing image amplifiers.[1][2] Up to the present time, the secondary electron yield from insulating films deposited on a thin, electron permeable metal foil has been limited to a maximum of about 6 to 8 secondaries per primary electron incident on the front surface.

It is evident that for many reasons, it is desirable to increase this ratio. Since the total gain of such an image amplifier is proportional to the mean dynode yield to the nth power, where n is the number of dynodes, at least 4 to 5 dynodes are required in order to obtain an electron gain in excess of 1,000 required for the photographic recording of single photoelectron events using typical refractive optics. The total number of stages, however, determines the resolution which can finally be obtained, so that the ultimate resolving power is improved if fewer stages result in the same overall gain.

The contrast degradation of such image amplifiers is, among other factors, determined by the ratio of penetrating primaries to true secondaries. The penetrating primaries are not focused from stage to stage, and cause a general background at the tube output. This effect can seriously limit the detectability of a weak image against a high image background. Therefore, an increase in the ratio of secondaries to penetrating primaries will improve the contrast performance. In addition, it can be assumed that dynodes with high yields will have a more favorable statistic of amplification. A third reason for dynodes with higher secondary yield is the fact that the overall tube voltage can be held much lower for the same overall gain.

The standard films, consisting typically of a compact layer of alkali halide—such as potassium chloride—about 500 Å thick, are prepared by vacuum evaporation onto a conductive backing. The conductive backing of 200-300 Å Al is carried either by a coarse metal mesh or by an edge-supported film of aluminum oxide of about the same thickness.

Significant charging of the secondary emitting insulator surface has not been observed. It has, however, long been recognized that much greater yields can be obtained when internal electric fields exist in the secondary emitting layer that enhances the emission process. For example, very high yields have been observed in reflection by Jacobs and coworkers[3] from porous magnesium oxide layers if the surface was charged up positively to give electric fields of the order of 10^6 V/cm across the layer. These authors reported secondary emission ratios as high as 10,000 to 1, but they also stated that the mechanism causing these high gains is fundamentally different from the standard emission phenomenon. They explain this mechanism of field dependent secondary emission as a process similar to that of a Townsend avalanche, where a true secondary electron is accelerated sufficiently within the porous layer by the electric field so that additional multiplication can take place. This effect was never investigated for transmission secondary emission. It appeared also doubtful that this type of emission could be used for imaging purposes since it is well known that the secondary emission from such layers responds slowly and is very noisy due to the involved mechanism of multiplication.

However, the very good agreement between experimental evidence given by Jacobs and his hypothesis of a Townsend avalanche in the porous layer, which can be thought to be a gas of rather large molecules under very high pressure, suggested the possibility that there might also exist the effect which may be compared to the mode of operation of an ionization chamber. In this case,

131

one would have to change conditions, that is, the applied field and the particle density, so that the internal field within the porous layer enhances the escape probability of the secondaries, but does not lead to additional ionization and breakdown. In order to investigate this possibility, transmission-type dynodes were made with low density deposits of various insulators such as KCl, MgO, and BaF_2.

Certain Basic Properties of Dynodes With Low Density Deposits

These dynodes consist of a thin film of Al of about 300 Å thickness which is supported by a coarse Ni mesh, having 20 holes per linear inch and a wire diameter of 0.5 mil. The mesh is mounted on a stainless-steel ring with an inner diameter of 1 inch. The secondary emitter is evaporated from a tantalum dimple which is placed 2 inches from the substrate in an argon atmosphere at a pressure of 2 mm of Hg. The presence of the inert gas during evaporation results in a very porous layer of the emitter on the substrate. The density of this layer is one-to-two orders of magnitude below that for vacuum evaporation. It varies with the pressure of the inert gas. It is also a function of the distance between crucible and substrate, the substrate temperature, and depends on rate of evaporation. Figure 18-1
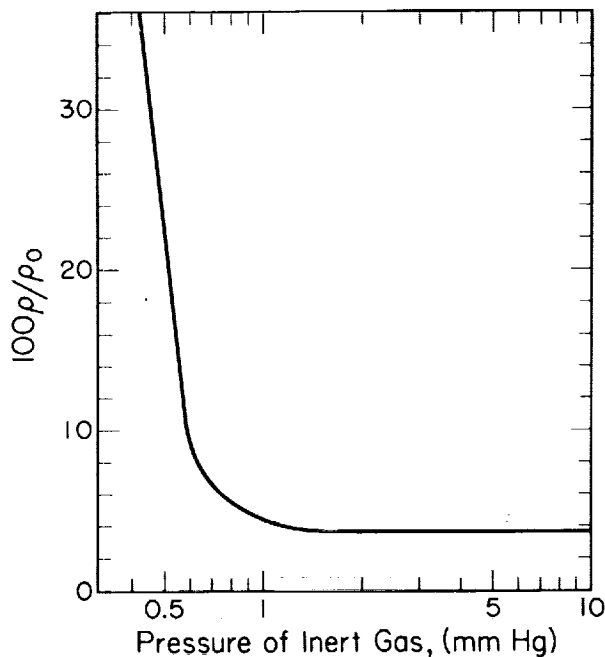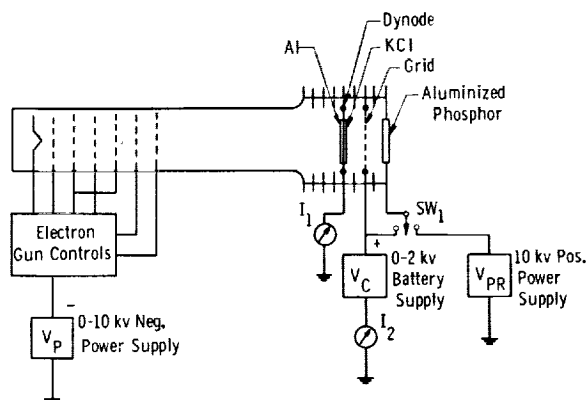

FIGURE 18-2.—Demountable system for dynode testing.

shows a plot of density versus pressure for a given set of conditions.

The dynodes are inspected by optical and direct weighing techniques. It was found that the best layers possess a density of 1 to 5 percent of the bulk material. Typical thicknesses range from 10 to 40 μ, which is equivalent to 100 to 400 $\mu g/cm^2$. These dynodes are pretested in a demountable electrode arrangement shown schematically in figure 18-2.

An electron gun supplies the primary electrons which form a raster of about 1 cm^2 on the dynode to be tested. Typical beam currents are 10^{-8} to 10^{-9} amp. The energy of the primary electrons can be adjusted between zero and 10 kv by a variable power supply connected between the cathode of the gun and ground. The conductive backing of the dynode is connected over a vacuum tube electrometer to ground. A positive voltage, V_C, which can be varied between zero and 2 kv is connected over a second vacuum tube electrometer to a fine grid. This grid is placed about 6 mm apart from the emitting surface of the dynode—this distance may be changed without affecting the results. In normal operation, the aluminized phosphor is connected to this grid and the secondary current, I_2, is collected by these electrodes and indicated by the second meter. The difference, I_2-I_1, in the reading of both meters indicates the primary current. The phosphor can also be connected to a post-accelerating voltage, V_{PR}, in order to display and center the raster, and to check if any localized emission takes place which will show up as bright spots superimposed on the raster.

Early tests indicated that although high yields could be obtained, it proved difficult to prevent localized emission centers and instabilities. The
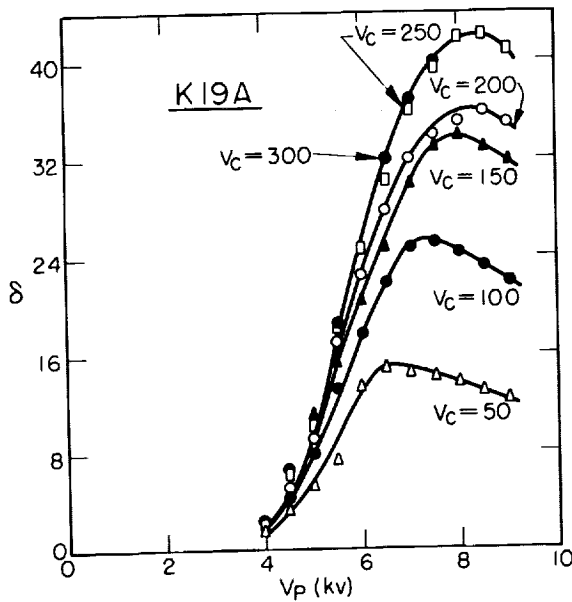

FIGURE 18-1.—Relative density as function of inert gas pressure.

FIGURE 18-3.—Secondary yield of low density KCl layer as function of primary electron energy for different collecting voltages.

FIGURE 18-4.—Secondary yield as function of collecting potential for different primary electron energies.

KCl-low-density layers could be formed, however, in such a manner as to give uniform yields without instabilities, provided that the grid potential, V_C, was not allowed to exceed a certain critical value. Typical results obtained for the stationary secondary yield as a function of primary voltage for various grid voltage settings are shown in figure 18-3 for the case of a KCl target 12 μ thick. It is seen that as the grid voltage is raised and, thereby the internal electric field is increased, the yield reaches much larger values than can be obtained in the absence of such a field. As the collecting voltage is further increased, a saturation effect becomes noticeable so that no further significant increase in yield takes place. This dependency of the yield on collecting potential may be even more clearly seen in figure 18-4, where the yield is plotted as a function of collecting voltage for a fixed primary energy. Initially, δ increases quite rapidly with V_C until it approaches a limiting rate and may eventually level off to a plateau. Still further increase of V_C leads to a rapid rise as indicated for the 5 kv curve, which is found to be associated with high instability and visible localized discharges that may become self-maintaining.

Figure 18-4 is seen to be very suggestive of the characteristic current-voltage curve for a gas discharge with its initial rise followed by a plateau and finally another steep rise in current.

The situation believed to exist in these films is stated below. As a result of secondary electrons
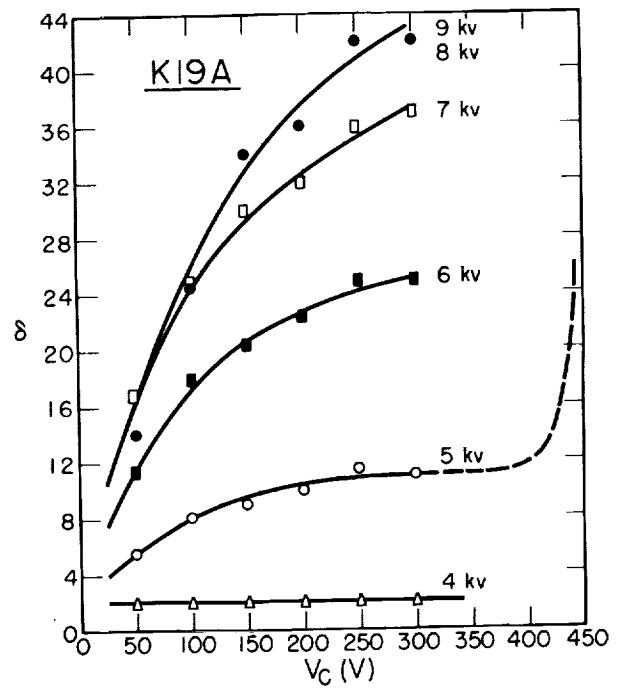
escaping, the positive charge density will be greatest near the exit surface, giving rise to an internal field directed so as to superimpose a drift velocity of the secondaries toward the surface.

The maximum potential which the exit surface can assume with respect to the conductive backing is that of the collecting electrode. Under this condition, the electric field across the low density layer becomes V_C/d, where d is the thickness of the layer. It was found that local breakdown takes place whenever a field strength of about 5×10^5 V/cm is exceeded, which means a collecting voltage in excess of 500 V for a layer 10 μ thick.

A finite time, t, is required to charge the exit surface up to the collecting electrode potential, V_C, and therefore to obtain a stationary secondary yield. During this time, a steady increase in yield from initially rather low values is observed.

The following equation, representing the relation between charge and voltage of a parallel plate condenser, has been found to be in very good agreement with experimental observations:

$$t = \frac{D \cdot V_C \cdot 10^{-13} \cdot A \text{ sec}}{d(\bar{\delta}-1) J_P \cdot V \text{ cm}}$$

where $\bar{\delta}$ is the average yield during time t, and J_P is the beam current density. D is the dielectric constant which was assumed to be unity, since

133

more than 95 percent of the volume occupied by the low density deposit is vacuum, and d is the thickness of the layer. It is found that it takes many hours at typical current densities encountered in imaging of 10^{-12} amp/cm² or less, before the saturation in secondary current is reached and a stationary high yield is obtained. Alternatively, it is possible to charge these dynodes almost instantaneously by flooding with correspondingly higher current densities. Once equilibrium is established, the surface charge does not deteriorate for many hours due to the very high resistivity of such layers and the response time is extremely short. It should be mentioned in this connection that pattern storage is possible in these films whenever they are not uniformly charged to saturation. These memory properties are presently being investigated at our laboratories.

From the experiments described, it appears that internal electric fields in porous deposits of insulators allow one to extract a large fraction of all the secondary electrons formed by the primary ionization mechanism. It is therefore apparent that, in addition to true secondary emission without field enhancement and the phenomenon of secondary electron induced internal multiplication processes, the effect of secondary emission with field enhanced escape probability also exists.

Application of Low Density Deposits in Image Amplifiers

After these encouraging initial results, several image amplifier tubes were constructed to test the imaging characteristics of such films. They consist of a cesium antimonide photo surface, a single high-gain dynode, a potential control grid, and a blue P11-type phosphor. The useful area
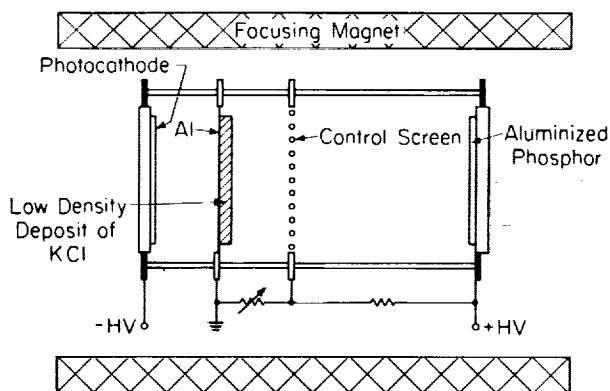

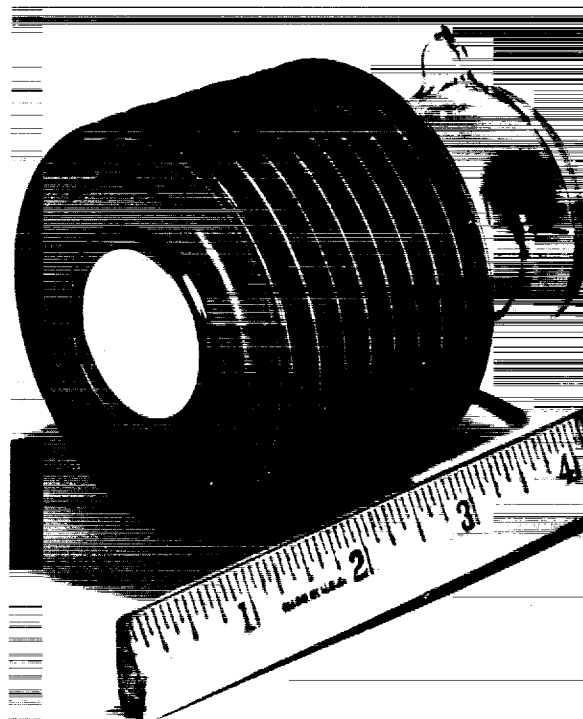FIGURE 18–5.—Cross section of image amplifier with high-gain dynode.

FIGURE 18–6.—Photograph of image amplifier.

is 1 inch and focusing is accomplished by an axial magnetic field. A cross section of such a tube is shown in figure 18–5. Figure 18–6 shows a photograph of a sealed-off tube. In testing these tubes, it was found that the electron gain of the dynode was, in general, slightly higher after processing of the photocathode. Most of the tubes so far built could be operated with stable electron gains in excess of 50. The electron gain as a function of primary energy in one of these tubes with a particularly heavy dynode (40 μ) is shown in figure 18–7. At the point where an electron gain of 100 was measured, "scintillations" in the illuminated areas became visible, indicating localized discharges across the low density layer.

The photon gain of these tubes is in the order of 1,000 to 2,000. A photograph of a test pattern taken with such a tube is shown in figure 18–8. The two meshes superimposed on the pattern are the dynode support and the potential control screen. The distance between two wires of this mesh is 1.25 mm. The photographed resolution is, therefore, found to be 15 lines/mm. More recent experiments have shown that resolution in excess of 24 lines/mm can be obtained with such tubes. The contrast degradation was found to be substantially less than that observed in
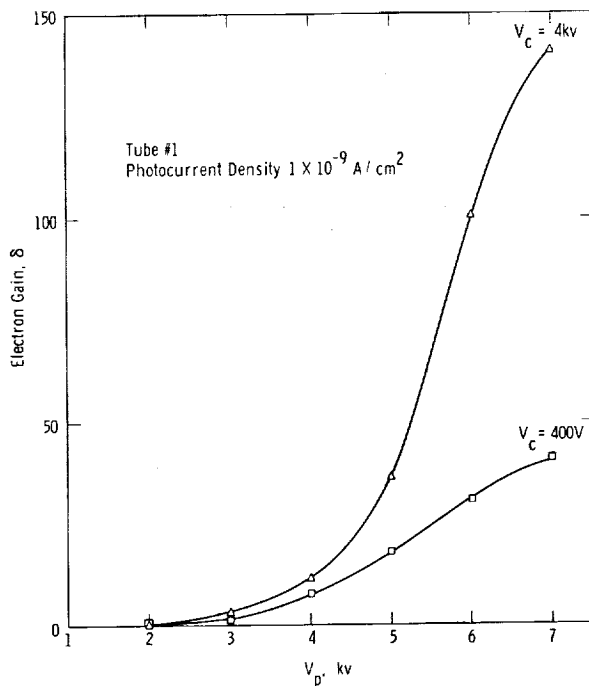
FIGURE 18–7.—Electron gain as function of primary voltage for a sealed-off tube.

FIGURE 18–8.—Test pattern as reproduced by two-stage image amplifier tube.

tubes at comparable gains using conventional dynodes.

The phenomenon, field-enhanced transmission-type secondary electron emission from low density deposits of suitable insulators, will need further investigations before the physical principles involved may be regarded as completely understood. It has been demonstrated, however, that this
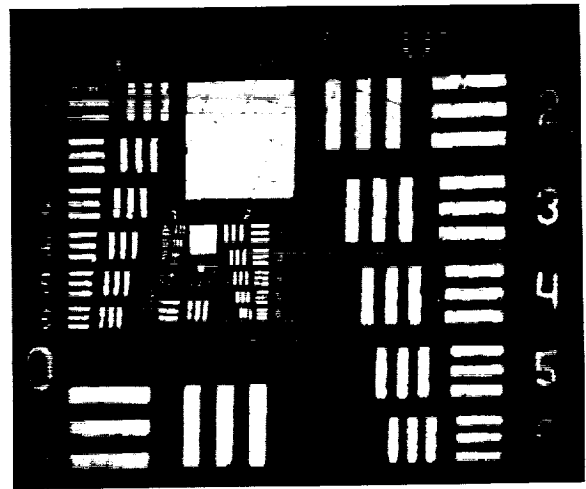
effect can be employed usefully in practical devices.

Discussion

G. A. MORTON: Once the film surface has been charged, what is the speed of response of the layer to changes in current density?

G. W. GOETZE: We have measured it to be faster than 10^{-7} sec.

M. H. ZINN: Have you measured the velocity distribution of the secondary electrons? Based on MgO results, you may have more electrons over 50 volts (defined previously as transmitted primaries) than are actually transmitted through target.

G. W. GOETZE: No; we have not yet measured the velocity distribution of the secondary electrons from these layers.

W. T. POWERS: Can one integrate an image on the dynode and then read it by flashing a light into the tube?

G. W. GOETZE: Yes; one can. We have, for example, integrated a low light level image on an initially uncharged target for about 30 minutes. The signal could then be displayed by uniform illumination of the photocathode.

W. F. NIKLAS: In London, you reported longer delays. Now you mention 10^{-7} sec. Would you elaborate on this?

G. W. GOETZE: One has to distinguish between the response time due to an instantaneous signal which is very fast ($<10^{-7}$ sec), and the time required to charge the exist surface of the dynode up to a

135

certain potential which is a function of the primary current density, and can therefore be very long for low current densities.

D. A. CUSANO: Since one is achieving here a major fraction of the high secondary emission yield due to field-assisted transport of electrons from the interior and incident sides of a TSE target, should not one examine other materials than alkali-halide targets, putting more attention on good transport properties rather than low field or "no field" conventional secondary emission characteristics?

G. W. GOETZE: This should be very interesting indeed, and we are planning to do so.

References

1. WACHTEL, M. M., DOUGHTY, D. D., GOETZE, G. W., ANDERSON, A. E., and STERNGLASS, E. J.: Rev. Sci. Instr., vol. 31, No. 5, 1960, p. 576.
2. WILCOCK, W. L., EMBERSON, D. L., and WEEKLEY, B: Proc. of 7th Scintillation Counter Symp., Nos. 2, 3, 1960, p. 126.
3. JACOBS, J. FREELY, and BRAND, F. A.: Phys. Rev., vol. 88, 1952. p. 492.

19. FIELD-INDUCED PHOTOEMISSION*

R. E. SIMON and W. E. SPICER, *Conversion Devices Laboratory, Electronic Tube Division, Radio Corp. of America*

Field-induced photoemission is an effect in which electrons are excited from a solid into vacuum in response to incident radiation. Unlike conventional photoemission in which all of the escape energy comes from the radiation, in field-induced photoemission part of the energy which an electron must have to escape from the solid is provided by an electric field. This effect opens up the possibility of relatively long wavelength infrared photoemission and also of developing a photoemitter sensitive through the visible and the near infrared. Field-induced photoemission was first observed during the course of work supported by the U.S. Army Signal Research and Development Laboratory. Work on this effect has subsequently been supported by ERDL.

In conventional photoemission, a photon must excite an electron from its equilibrium energy state in the solid to the vacuum potential. Since, in photoemitters of high quantum yield, the electrons are excited from the valence band, the minimum energy which a photon must have in order to cause the ejection of an electron is the energy band gap of the semiconductor, E_g, plus the electron affinity, χ, as shown in figure 19-1(a). In field-induced photoemission, the photon excites an electron only across the band gap and a localized internal electric field accelerates the electron to sufficient kinetic energy to allow it to escape over the surface barrier. In the emitter shown in figure 19-1(b), the localized electric field is provided by a reverse biased $p-n$ junction. Alternatively, it may be provided by means of a surface barrier layer or a thin insulating layer across which a potential is applied.

It is convenient to divide field-induced photoemission into three steps: (1) excitation of carriers by light and diffusion to the high field region; (2) acceleration to high energy in the high field region; (3) motion of carriers to the surface and emission. The excitation of carriers can be described in terms of the optical absorption constant. It is well known that the mechanism of absorption of photons in the vicinity of the band gap in semiconductors is usually through the production of electron-hole pairs. Goucher[1] has shown that one electron-hole pair is produced per absorbed photon to an accuracy of 10 to 15 percent in the wavelength region from 1 μ to 1.7 μ. The diffusion of electrons to the high field region can be described in terms of the diffusion length for minority carriers.[2] It should be noted that the excitation and diffusion of carriers in field-induced photoemitters is similar to that in $p-n$ junction photoconductors.

The acceleration of electrons to high energy in the high field region of the $p-n$ junction is the decisive aspect of this device. The energy which an electron in the conduction band of a semiconductor can gain from an electric field is limited by the strength of interaction of the electron with the semiconductor lattice atoms and with the other electrons in the solid. At low electric fields, the principal interaction between an electron and the lattice occurs through excitation and absorption of acoustical phonons. However, as the electric field is increased, many of the electrons gain enough energy to excite optical phonons ($\sim$0.03 ev in germanium).[3] Since in each interaction a relatively large amount of energy is transferred to the lattice, interaction of an electron with optical phonons is an important energy loss mechanism. The mean free path of an energetic electron between interactions with optical phonons has been estimated to be about 200 Å.[4] At higher fields, the electrons have enough energy to excite a valence band electron into the conduction band leaving a hole in the valence band. The thresh-

137
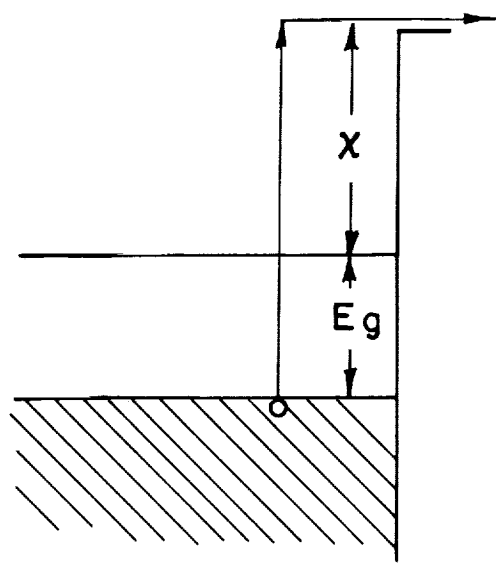
(a)
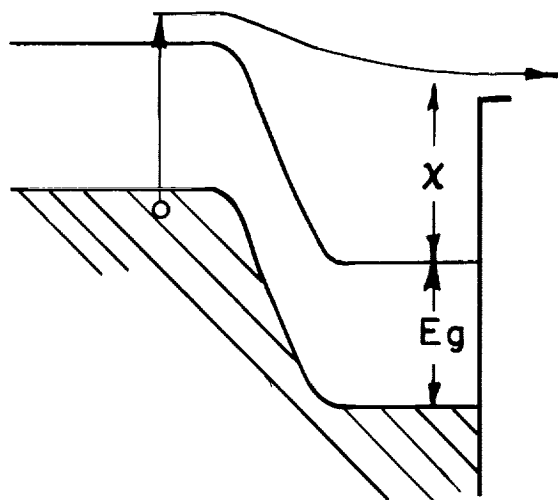
(b)

FIGURE 19–1.—Schematic band diagrams of (a) a conventional photoemitter, (b) a p–n junction field-induced photoemitter.

old for this pair production interaction, E_{pp}, has been found to be about two to four times the band gap energy. When an electron has sufficient energy to produce pairs, this interaction occurs with high probability (with a mean free path of 15 Å).[4] It is believed that because of this inter-

action, the number of electrons with energy above the threshold for pair production is relatively small. Thus, this energy is effectively the upper limit of the electron energy distribution. In addition to these interactions, intervalley scattering must be considered when a material with a many-valleyed band structure, such as germanium, is considered.[5] While the mechanisms outlined above are well recognized, an adequate theoretical treatment of these in the high field region of a p–n junction has not been made.

The third step in the emission process is the transport of energetic carriers to the surface and emission. Figure 19–2 shows schematically the
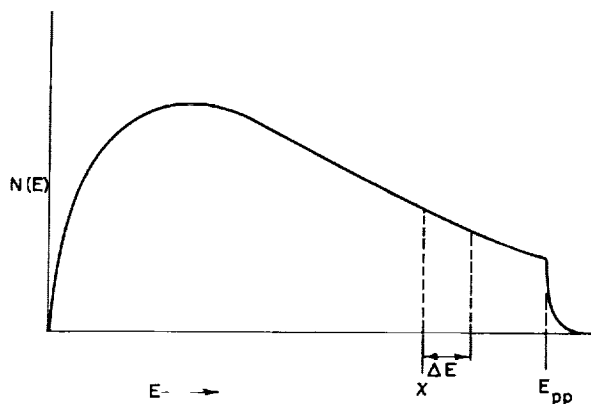
FIGURE 19–2.—Schematic energy distribution of electrons after passing through the high field region of a reverse biased p–n junction.

electron energy distribution at the end of the high field region. The distribution is, for the purpose of discussion, arbitrarily chosen to resemble a Maxwell Boltzmann distribution at low energies, but is cut off sharply at the threshold energy for pair production for reasons described above. For the purposes of illustration, let us neglect the statistical nature of the energy loss processes and assume that each electron with energy greater than χ loses energy ΔE in moving from the high field region to the surface. The energy lost in traveling to the surface is proportional to the distance the electrons must travel. The electrons which can be emitted are those with energy greater than $\chi + \Delta E$. It is evident than that in order to obtain appreciable field induced photoemission, the electron affinity must be low and the high field region must be close to the surface.

From the discussion given above, it can be seen that the materials from which a field-induced photoemitter can be made should have the following properties: In the region where electrons

are excited, the material must absorb radiation in the wavelength region of interest and the absorption length must be smaller than, or comparable to, the diffusion length. In the high field region and between the high field region and the surface, the material must have a high threshold for pair production, and the interaction between the energetic electrons and the lattice must not be strong. The surface of the emitter must have a low electron affinity. Finally, it must be technologically possible to fabricate the device from these materials.

Several examples indicate how difficult it is to satisfy all of these conditions with a single material. Some ionic crystals such as CsI[6] have extremely low electron affinities, but electrons interact strongly with the polar optical phonons in these materials, and it is probably not possible to accelerate electrons to high enough energy without breakdown occurring.[7] Materials with strong absorption in the infrared are expected to have low threshold energies for pair production. Silicon and germanium, which satisfy most of the other requirements, have high electron affinities (~ 4 ev).

Most of our work has been done on silicon and germanium using a cesium surface treatment to reduce the electron affinity. We have found that the adsorption of approximately 3×10^{14} cesium atoms on the surface of silicon crystals which have been etched and then heated to about $800°$ C in vacuum produces a reduction of the photothreshold, E_T, from 4.8 ev to 1.4 ev. A similar reduction is found in the photo-threshold of germanium. From the photo-threshold measurements, it is not possible to derive a value for the electron affinity since it is not known whether the electrons originate in the valence or conduction band of the semiconductor. If they originate in the conduction band, the electron affinity is equal to E_T. If they originate in the valence band, the electron affinity is $E_T - E_g$ or 0.3 ev for silicon.

Field-induced photoemission was first observed from silicon[8] as shown in figure 19-3. The schematic diagram of the experimental tube in the inset of the figure shows the geometry of the crystal. The silicon crystal contained a grown $p-n$ junction which was perpendicular to the emitting surface. After treating the crystal with cesium, the photoelectric yield curve with no voltage applied was obtained. With a reverse bias of 9 volts applied across the $p-n$ junction, the photoelectric threshold was moved from 1.4 ev to 1.1 ev,
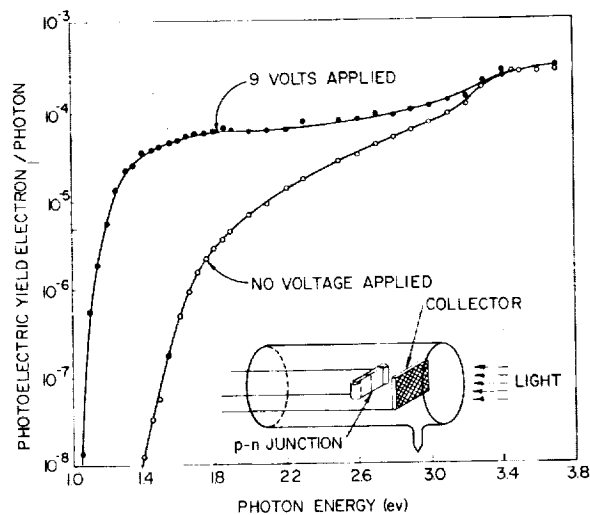
FIGURE 19-3.—Spectral response of conventional photoemission (no voltage applied) and field-induced photoemission from a cesium treated silicon $p-n$ junction. Inset shows schematic diagram of the experimental tube.

the band gap energy of silicon. By imaging the source of the field induced photoemission on a phosphor screen, it was shown that the emission came from the region where the $p-n$ junction intersects the emitting surface. The photoemission with no internal field applied came from the entire surface. The quantum yield shown in figure 19-3 is not absolute since the light beam was larger than the emitting area. In order to determine the quantum efficiency in the most sensitive region of the field-induced photoemitter, an apparatus was constructed with which a small spot of light could be made to traverse the surface of crystal, and field-induced photoemission was measured as a function of position along the crystal. The results of these measurements are shown in figure 19-4. When the width of this beam and the shape of this curve are taken into account, a lower limit for field-induced photoemission is found to be 10^{-3} electrons per incident photon. This is a lower limit because the emitting region may be smaller than the light spot and the tails on the sides are probably caused by diffusion of electrons to the junction. Thus the emission takes place from a region less than a few tenths of a millimeter wide along the crystal. It should be emphasized that this value for the quantum efficiency is a lower limit for this sample. It is not the maximum quantum efficiency, since
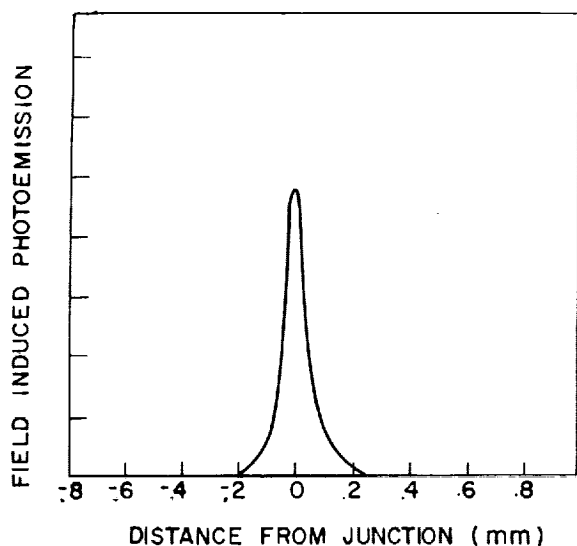
139

FIGURE 19-4.—Field-induced photoemission current as a function of distance between a scanning light spot and the junction.

there is no reason to believe this geometry and cesium treatment are optimum.

Measurements using a sample of similar geometry have been made using a germanium p-n junction.[9] In these measurements, the results shown in figure 19-5 were obtained. Again, it can be seen that with no field applied across the crystal, a photoelectric threshold of 1.4 ev is observed. However, when reverse bias is applied
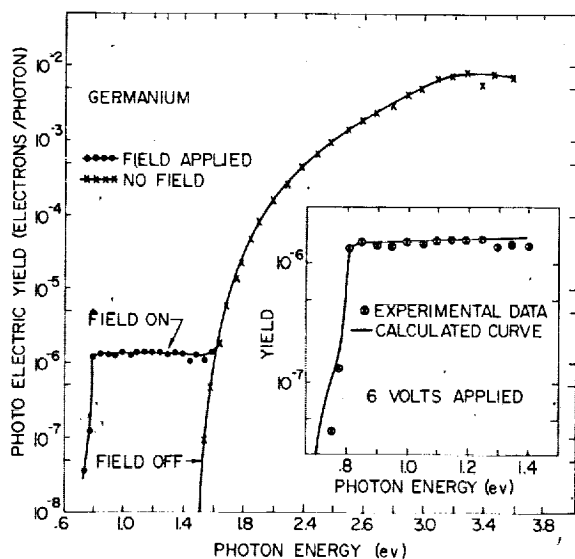

FIGURE 19-5.—Spectral response of conventional (no field) and field induced photoemission from cesium-treated germanium p-n junction. Inset shows fit between experimental results and the calculated curve.

140

across the crystal, the photoelectric threshold is extended to 0.7 ev or about 1.7 μ. The very flat shoulder due to field-induced photoemission can be explained simply in terms of the spectral dependence of the optical absorption of germanium. If a simplified geometry is assumed, the following expression for the spectral dependence of field induced photoemission can be derived.[8]

$$Y = C \frac{\alpha(h\nu)}{\alpha(h\nu) + 1/L}$$

α is the absorption constant for a photon with energy $(h\nu)$, L is the diffusion length, and C is a constant proportional to the probability that an electron reaching the junction is emitted. The inset in figure 19-5 shows the fit between the calculated and experimental curves. A similar fit can be obtained with the field-induced photoemission from silicon where the spectral response does not rise as sharply as from germanium. As in silicon, the emission has been shown to come from a small region where the junction intersects the emitting surface and values for the photoelectric yield of field-induced photoemission shown in figure 19-5 are too low by a factor of at least 30.

The voltage dependence and the dark current for the germanium p-n junction is shown in figure 19-6. The magnitude of the field-induced photoemission current is arbitrary since it depends upon the light intensity. The dark current or hot electron emission is due to thermally excited electrons on the p side of the junction which diffuse to the junction and to thermal excitation in the junction. This can probably be greatly reduced by using junctions with improved reverse characteristics or by cooling the crystal. The point where the voltage dependence of field-induced photoemission deviates from the hot electron emission is probably where pair production begins.

It is obvious that if field-induced photoemission is to be used in a practical device, an emitter of such a geometry that emission can be obtained over a large area must be developed. Much of our recent effort has been directed toward fabricating such devices by producing p-n junctions parallel to the emitting surface by diffusion. Since the depth of the n-type skin must be made extremely thin—on the order of 200 Å—new technology must be developed. However, no insuperable difficulties appear to be present.
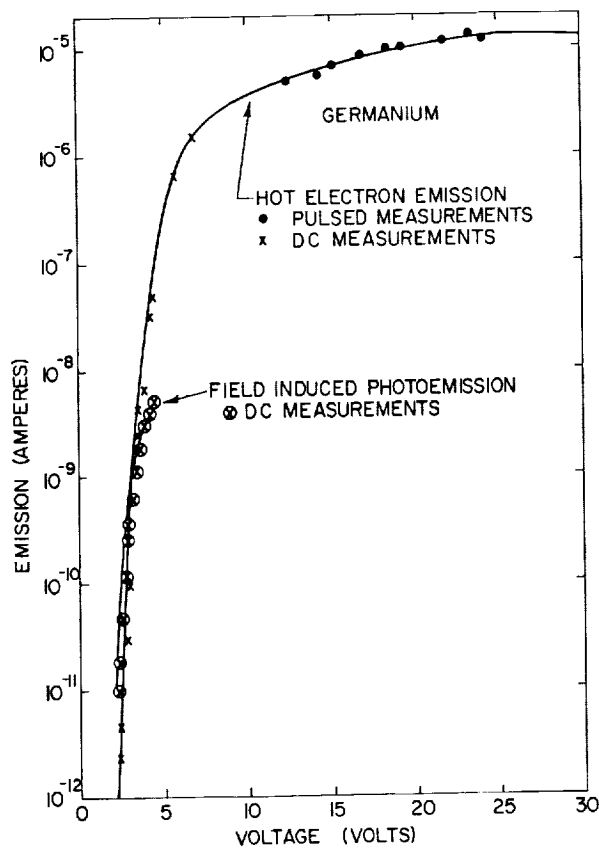
Figure 19-6.—Dark current (not electron emission) and field-induced photoemission as a function of voltage at room temperature.

Figure 19-7.—Possible configurations for field-induced photoemitters.

It should be emphasized that the systems described above are only a few special cases of the principle of field-induced photoemission. Many other materials and combinations of materials are useful in devices in which radiation is used to excite carriers and an electric field is used to emit them. Several examples are shown in figure 19-7. Figure 19-7(a) shows an emitter in which the inversion layer at the semiconductor produced by adsorbing sesium on the surface is used to provide a high field region. Figure 19-7(b) shows a p-n junction between different materials where long wavelength radiation is used to excite electrons in the narrow band gap material, but the acceleration to high energy takes place in a wide band gap material where the threshold for pair production is large. In figure 19-7(c), a device analogous to a phototransistor is shown where radiation absorbed in the p-type material is used to

control the flow of electrons to the high field region. The number of electrons controlled per photon can be as high as 100.[10] In figure 19-7(d), a metal-insulator-metal sandwich is shown in which radiation excites electrons over the barrier into the conduction band of the insulator where the high field accelerates it to energies where it can pass through the metal into vacuum. Many other configurations are possible.

The greatest potential of field-induced photoemission is in detection of infrared radiation. This effect may make possible image orthicons and image intensifiers sensitive to infrared. It can make possible infrared multipliers of high sensitivity. It is believed that the dark current can be reduced by cooling. Assume that the noise in the dark current can be reduced by cooling to 10 counts per sec. Then a field-induced photoemitter with a quantum yield of 10 percent will have a noise equivalent power (NEP) of 4×10^{-18} watts for radiation of 5 microns.

In evaluating the potential of field-induced photoemission, one must keep in mind the many unsuccessful attempts to extend the range of conventional photoemission into the infrared. Field-induced photoemission is a new and promising approach to this problem.

141

Discussion

M. P. WILDER: What was the collector potential?

R. E. SIMON: 67.5 v was used as the collector voltage.

G. SUITS: Why do you wish to avoid the condition of pair production while the vacuum tube intensifier designers work hard to get all the "pairs of secondaries" they can get?

E. E. SIMON: In a semiconductor where both electrons and holes can produce pairs, an effect can occur which is analogous to the Townsend discharge in gases and makes the multiplication unstable. Therefore, when a field-induced photoemitter is biased in the multiplication range, the emission current tends to be no longer proportional to the incident radiation.

W. F. NIKLAS: Would it be possible to allow pair production to accelerate the electrons thus produced again, possibly in a manner similar to the electron emission from Al_2O_3?

R. E. SIMON: This would be possible if only the electrons or only the holes produced pairs so that the regenerative mechanism mentioned in the answer to the previous question was not operative.

G. A. MORTON: Would you expect the directions of the "hot" photoelectrons to be randomized in the short distance of the surface junction? If they are not random, will not the quantum efficiency be higher?

R. E. SIMON: The exact form of the electron velocity destribution is not known, but the scattering by phonons is isotropic. If the mean free path is greater than, or comparable to, the distance between the junction and the surface, the distribution will be directed toward the direction of the electric field. If the electric field is perpendicular to the surface, then increased quantum yield would be expected.

References

1. GOUCHER, R. S.: Phys. Rev., vol. 78, 1950, p. 816.
2. SHOCKLEY, W.: Bell Syst. Tech. J., vol. 28, 1949, p. 435.
3. BROCKHOUSE, B. N.: J. Phys. Chem. Solids, vol. 8, 1959, p. 400.
4. WOLFF, P.: Phys. Rev., vol. 95, 1954, p. 1415.
5. HERRING, C.: B.S.T.J., vol. 34, 1955, p. 237.
6. TAFT, E. A., PHILIPP, H. R.: J. Phys. Chem. Solids, vol. 3, 1957, p. 1.
7. FROLICH, H., and MOTT, N. F.: Proc. Roy. Soc., vol. 171, 1939, p. 496.
8. SIMON, R. E., and SPICER, W. E.: Phys. Rev., vol. 119, 1960, p. 621.
9. SIMON, R. E., and SPICER, W. E.: J. App. Phys., vol. 31, 1960, p. 1505.
10. SHIVE, J. N.: J. Opt. Soc. Amer., vol 43, 1953, p. 239.

20. FIBER OPTICS COUPLING FOR MULTISTAGE IMAGE INTENSIFIERS

N. S. KAPANY, *Optics Technology, Inc.*

I. Introduction

During recent years image intensifiers have been developed in which photoelectrons emitted from a photocathode are accelerated to form an intensified image on a phosphor screen. It is natural that a number of attempts have been made to obtain high image intensification by cascading these image tubes. Table 20–I includes typical parameters of some of the present multistage image intensifiers. Successful fabrication of small-size image intensifiers with high resolution and high photometric gains would obviously give rise to a variety of novel applications. The problem of coupling several intensifier tubes together is of major importance both from resolution and light collection efficiency stand-points. Three approaches to solve the coupling problem are possible: (1) a fast lens system; (2) thin transparent membranes; and (3) high resolution and high numerical aperture fused fiber optics.

The method of using a fast lens or mirror system to focus an image of the cathode of the preceding tube to the anode of the next is obvious. However, the requirements on the optical system are severe. It is required to work at low aperture ratio so that it can collect a large fraction of the photons emitted by the phosphor which emits as a Lambertian source. Furthermore, the resolution requirements are high for large field angles and low aperture ratio. As an example, an f/1 lens working at unit magnification collects only about 9° of the light emitted by the phosphor in the forward hemisphere. This contains only 2 percent of the total energy with additional losses within the lens system. Thus, a lens system is considered to be highly wasteful and bulky for the purpose of cascading interstages. With the developments of high-resolution electron-optical systems, an even more severe demand is placed on the lens designer because of the requirements of high resolution over wide field as well as high numerical aperture.

The second approach to this problem consists of using a thin membrane of the order of 5 to 50 microns thick, with the phosphor deposited on one side and the photocathode on the other side. This system is capable of higher photometric efficiency than a lens system. However, it is not only fragile but, as will be shown in section II, also introduces loss in resolution. It will be shown that the resolution of this system is governed by the thickness of the transparent membrane, the spot size on the phosphor, and the angular emission characteristics of the phosphor. Experimental measurements on the emission characteristics of the transparent and settled phosphors, as well as the loss in resolution caused by a 50-micron-thick membrane, are made and will be described in section II.

By far the most efficient method of interstage coupling is considered to be the use of fused fiber optics.[1,2,3] With the availability of fused plates of 5-micron or smaller fibers and $N.A. \geq 1$, it has become possible to collect most of the light emitted by the phosphor and conduct it to the photocathode at the other end. An image resolution of 100 lines/mm and higher is quite feasible with fiber optics. A practical advantage offered by fiber optics lies in the fact that each stage can be constructed, processed, and tested separately, and only stages with high performance need to be cascaded. This would reduce the rejection rate inherent in the existing method of processing multistage image intensifiers.

However, a great deal of confusion and misunderstanding exists regarding optimum requirements of various parameters of fiber optics coupling plates. Various important characteristics of fused plates for coupling may be classified as follows:

(a) *The fiber numerical aperture* $N.A. = (N_1^2 - N_2^2)^{1/2}$.—This is governed by the refractive index of the fiber core (N_1) and the coating material (N_2).

143

Table 20–I.—Typical parameters of some of the present multistage image intensifiers

Type		Cascade intensifier — External coupling (3-stage)	Cascade intensifier — Internal coupling (3-stage)	Transmission secondary emission (6-stage)	Channeled image intensifier (5-stage)	Image converter diodes (3-stage) — Present (single-stage)	Image converter diodes (3-stage) — Under development
Electron gain	Per stage		5	6–8	2–3		
	Overall		2,000	1,500			
Photon gain	Per stage	10^2	50	10^2		10	30.
	Overall	10^5	10^5	7.2×10^4			10^3.
First cathode diameter, cm		5–10	5	2.5	5	3	10.
Cathode type		$SbCs_3$	$SbCs_3$	$SbCs_3$	$SbCs_3$	$SbCs_3$	$SbCs_3$ I–VI group and multialkali.
Cathode sensitivity, microamps/lumen		15	15	10	10	30	50.
Screen phosphor	Type	P11, P20 or P15.	P11	P11	P11, P20	P11	P11 and transparent.
	Diameter, cm	5	5	1	2.5	3	10.
Dynode				Al-KCl, Al_2O_3-Al-KCl	Ag-Mg, Be-Cu		
Dynode diameter, cm				1	2.5 (50 mesh screen).		
Overall voltage, kv		12–18	10–20	35	2	12	25–50.
Coupling		Lenses or filaments. (Fused plates of fibers under experimental study).	Glass bulb.				Fiber fused coupling plates.
Limiting resolution, l.p./mm		15–20	8–15	15	13	10	50–100.
Operation		Linear acceleration.	Linear acceleration.	Magnetic focusing.	Linear acceleration.	Without electro-optics.	Without electro-optics.

This term governs the acceptance angle and therefore the light-gathering power of the fiber. When fibers of N A. less than one are used to transport light from a phosphor, a certain fraction of energy refracts out of the fiber and contributes to the degradation of contrast in the image.

(b) *Interstitial absorbing coating.*—A second coating to each fiber, if it is highly absorbing in thicknesses of the order of a few wavelengths, is useful for eliminating the energy refracting out of fibers of N.A.<1, as well as eliminating the energy incident in the interstitial regions within the fibers.

(c) *Resolution.*—For perfectly insulated fibers the limit to the resolution is set by the fiber di-

ameter. It is possible to fabricate fiber fused plates with fiber diameter as small as 1 to 2 microns and $N.A. \geq 1$.[4] However, it should be realized that cascading of fused fiber plates will give rise to some loss in resolution. For example, if two plates, each capable of resolving R lines/mm, are cascaded, then the resolving power is reduced to approximately $\frac{R}{\sqrt{2}}$ lines/mm.

(d) *Vacuum-tightness.*—This is obviously essential for fused plates at the input and output ends of the image intensifier. Even if an image intensifier is so constructed that all stages are in the same envelope, it is considered desirable that

the coupling plates be vacuum-tight to avoid any degassing and photocathode poisoning.

(e) *Photocathode poisoning.*—Lead glasses, impurities, and degassing can cause deterioration of the photocathode. Therefore, it is essential that high N.A. fibers of nonlead glasses be used.

(f) *Sealing.*—In order to seal the fused plates to the envelope, it is obviously required that the coefficient of thermal expansions of the fused plate and the envelope be matched. Attempts to form graded seals, have met with limited success.

These criteria are particularly relevant to the applications of fused fiber optics plates for coupling interstages and end windows (for image input or contact photography at the image output end). However, it should be stated that other forms of fiber optics assemblies present a considerable potential when used in conjunction with image intensifiers. For example, fiber assemblies of scintillating fibers serve as X-ray image converter screens and for high-energy particle tracking. On the other hand, the fiber optics distortion corrector and field flatteners can simplify the design and enhance the performance of these electron optical systems. Furthermore, assemblies of fibrous configurations of photoconductive materials seem to have considerable value in solid-state image intensifiers from resolution as well as light gain standpoints.

This paper will describe a number of experiments designed to evaluate the properties of fiber optics coupling plates. Section III deals with photometric efficiency, resolution, interstitial absorbing, and photographic problems. A diode-type image intensifier has been chosen for some preliminary experiments, although the results are relevant to other types of image intensifiers. The preliminary performance data of a three-stage diode using fiber optics coupling will be described in section IV.

II. Image Transfer Using Thin Membranes[*]

When a thin transparent membrane is used to transfer an image from a phosphor deposited on one side to a photosensitive material such as a photocathode or a photographic emulsion on the other, certain losses in resolution and contrast occur. This is primarily due to the spread of the luminescence radiation across the thickness of the membrane. The loss in resolution is a function of (a) the spot size on the phosphor; (b) the angular flux distribution of the flux emitted by the phosphor which will be shown later is dependent on the degree of optical contact between the phosphor and the substrate; (c) the thickness of the membrane; and (d) the degree of optical contact between the membrane and the photosensitive material.

Figure 20-1 shows the two planes (x-y and x'-y') corresponding to the two sides of the membrane. The intensity distribution $I(x)$ in the spot on the phosphor screen in the x-y plane is known to be close to a symmetrical Gaussian curve [5] and can be represented by the term $e^{\frac{-r^2}{2}}$. If $F(\theta)$ is the angular flux distribution of the energy emitted at any point in the phosphor and t is the membrane thickness, then $I(x')$ flux distribution at any point on the other end of the membrane is given by:

$$I(x')=\frac{I_0}{t^2}\int_0^{\phi=2\pi}\int_0^{r=\infty} F(\phi)\ \exp\left(\frac{-r^2}{2}\right)\ \cos^2\theta\cdot r\cdot dr d\phi$$

where

$$\cos\theta=\frac{t}{(t^2+x^2+r^2-2rx'\ \cos\phi)^{\frac{1}{2}}}$$

$I(x')$ gives a close representation of the intensity distribution at the photosensitive surface if it is in optical contact with the membrane. If the photosensitive surface is not in optical contact, then the refraction effects at the interface would have to
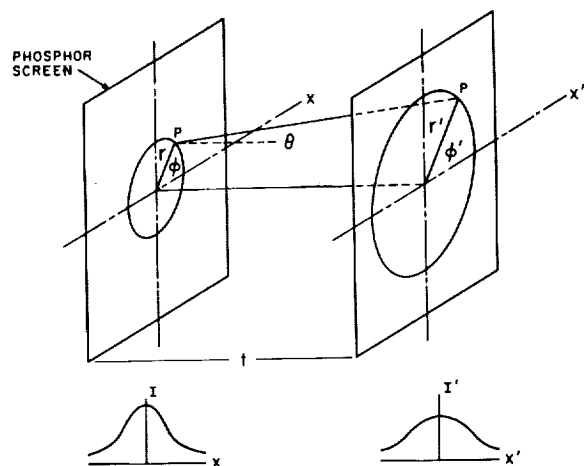

FIGURE 20-1.—Geometry for calculation of intensity distribution in the point spread function of contact printing through a thin glass window.

145

be taken into account. This term therefore defines the point spread function of the overall system. If one wishes to express the performance in terms of spatial frequency response,[6] then Fourier transform of $I(x')$ would be required; i.e., the spatial frequency response would be given by:

$$F(\omega) = \int_+^- \int_\infty^\infty I(x',y') \cdot \exp\ (2\pi i \omega x') dx' dy'$$

where $F(\omega)$ is the response for the spatial frequency ω. The cutoff point of this curve would give the resolving power of the system (refer fig. 20-4(b)). However, a critical parameter in the determination of the influence of the thin membrane on image quality is the polar emission curve $F(\theta)$ of the phosphor and this will now be discussed.

Phosphor Emission

All phosphors emit as Lambertian sources; however, the refraction at the substrate modifies the angular flux distribution. Of course, the refractive indices of the phosphor and substrate and their degree of optical contact are some of the essential parameters. The newly developed transparent phosphors can be assumed to be in complete optical contact with the substrate. On the other hand, settled phosphors, with large particle sizes, have varying degrees of optical contact with the substrate. It is relatively simple to calculate the angular flux distribution in the substrate when the

phosphor can be assumed to have either complete optical contact or no optical contact. Figure 20-2(b) shows the expected theoretical curves for the two extreme cases and it should be noted that when the optical contact is zero, then the emission curve is peaked in the forward direction due to Fresnel reflection.

Figure 20-2(a) shows the experimental arrangement used for measuring the angular flux distribution of energy from settled phosphor and transparent phosphor. The refraction effects at the other end of the substrate are eliminated by cementing a semicircular glass plate of the same refractive index as the substrate. A small region of the phosphor is excited by incident electrons. A photomultiplier was mounted on a goniometer and the signal at varying angles to the normal recorded.

Figure 20-2(b) shows the experimental data on a transparent phosphor (P5 type) and a settled phosphor (P11 type). Both curves fall in between the two theoretical curves for no optical contact and complete optical contact conditions. The mechanisms contributing to this difference are particle size and shape, depth of electron penetration, scattering within the phosphor and degree of optical contact with the substrate. However, from these experimental results it can be stated to a first approximation the transparent phosphor is essentially in complete optical contact and for the settled phosphor optical contact is small. The
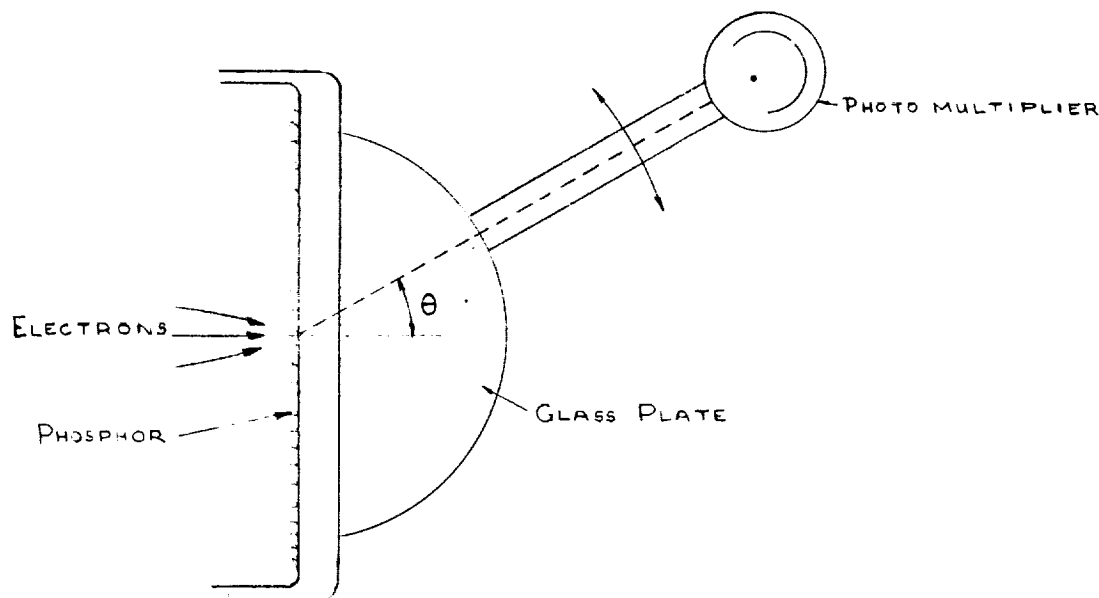
FIGURE 20-2(a).—Diagram of the optical setup used for measurement of angular flux distribution of energy from phosphor in the substrate.

146
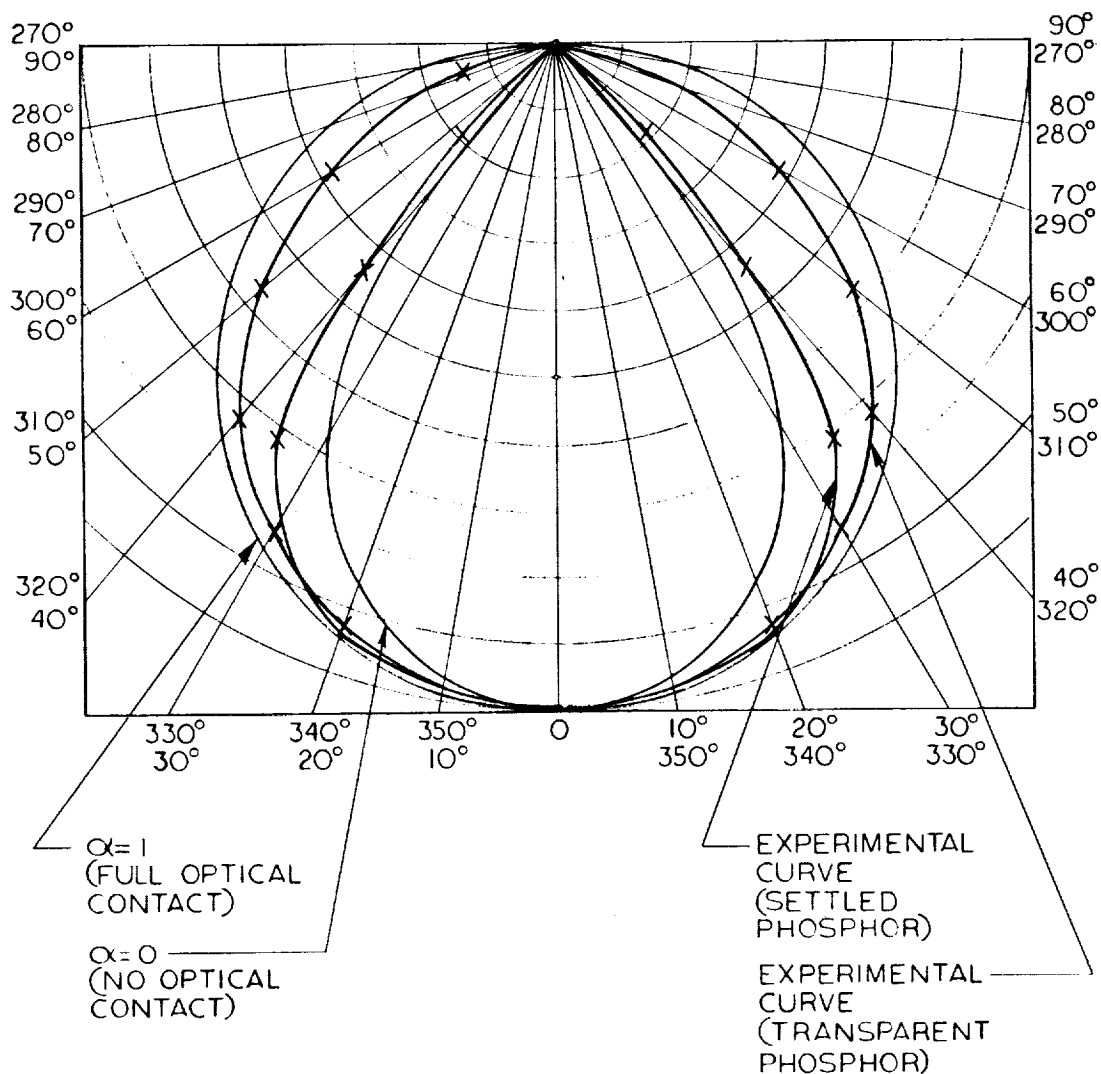
Figure 20-2(b).—Theoretical and experimental curves of polar energy distribution of transparent and settled phosphors

significance of the results in figure 20-2(a) to the spread function $I(x')$ is obvious and, as will be shown later in this paper, they also play a role in other areas; e.g., in determining fiber efficiency.

Resolution measurements

Detailed measurements of the loss in resolution on contact printing through a 50-micron glass membrane have been made. The image of various test objects was formed on the phosphor deposited at one end of the membrane and a comparison of the image on the phosphor was made with the image produced on a film placed in intimate contact with the other side of the membrane. Figure 20-3 shows the loss in resolution in the image of the great nebula in Andromeda on a phosphor (center photo taken with a lens) and the further deterioration on the image quality

on contact printing through the membrane (bottom). It is to be seen that the final image not only suffers from degradation in contrast but that there is a distinct loss of detail as compared to the incident image on the phosphor.

Figure 20-4(a) shows microdensitometer traces of a slit, slit images on the phosphor (taken with a lens), and the phosphor image printed through the 50-micron-thick membrane. The 0.002-inch-wide slit test object is degraded to an approximately Gaussian intensity distribution image on the phosphor with 0.008-inch half peak width and a total width of approximately 0.016 inch. The contact printing through the membrane has further degraded the image to an intensity distribution with half peak width of 0.125 inch and total width of approximately 0.025 inch.

147
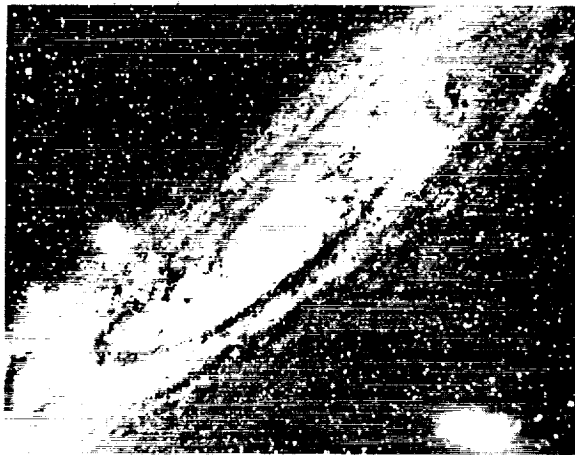
Great nebula in Andromeda.

Picture on the phosphor.

Contact print through a 50 μ glass window.

FIGURE 20-3.—Illustrating loss in resolution on contact printing through a thin window.
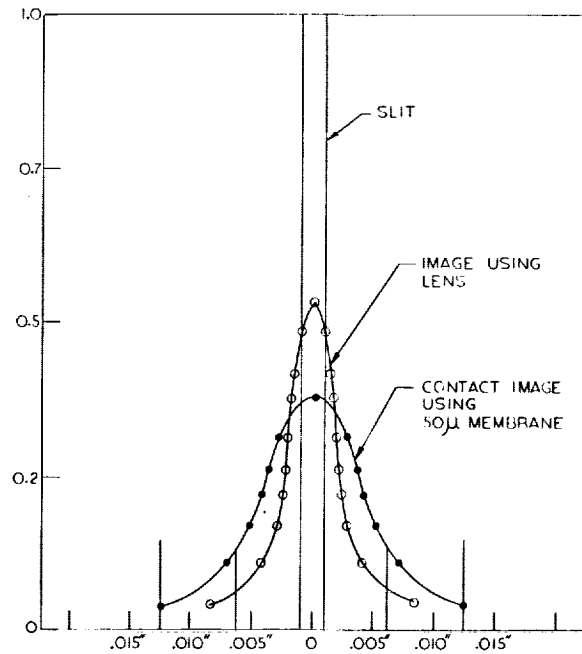
FIGURE 20-4(a).—Microdensitometer curves of the spread in image of a slit caused by the phosphor and contact image using a 50-micron membrane.

In order to obtain a more quantitative measure of loss in resolution on contact printing through a membrane, a variable frequency sine wave test object [7] was used and the spatial frequency response of the system was measured. Figure 20-4(b) shows the reduced data for spatial
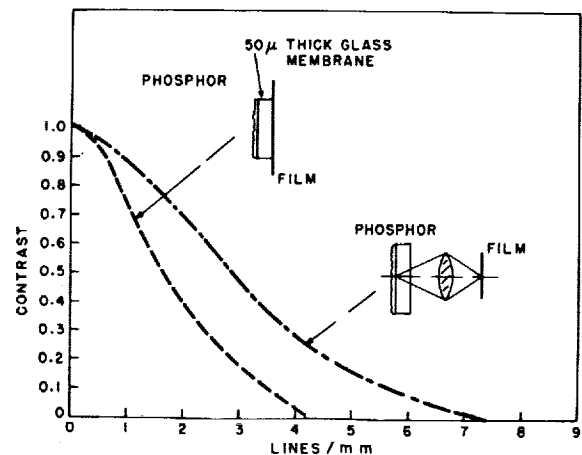
FIGURE 20-4(b).—The spatial frequency response of a periodic image on the phosphor and through a 50-micron glass membrane.

frequency response in the image on the phosphor as taken with a high-quality lens and also the response in the image using contact printing. Contrast in the image of the sinusoidal test objects

148

is plotted as a function of cycles per millimeter. The contrast is defined as follows:

$$C = \frac{I_{max} - I_{min}}{I_{max} + I_{min}}$$

where I_{max} is the intensity of the maxima and I_{min} the intensity of the minima for a given line spacing in the image of the test object. Figure 20-4(b) shows the degradation in contrast and loss in resolution from 7.5 lines/mm on the phosphor to nearly 4 lines/mm on contact printing through the membrane. This gives a quantitative measure of loss in image resolution caused by using a thin membrane between the phosphor and the photosensitive surface. It should be stated that the data in figure 20-4(b) could be derived analytically from the line spread function in figure 20-4(a) by calculating its Fourier transform.

III. Fiber Optics Coupling Plates

The basic theory of light conduction along small diameter fibers has been treated extensively in the literature,[1-4] and it is demonstrated that for high-quality fibers of diameter greater than a few microns the photometric efficiency is governed primarily by the fiber numerical aperture. With reference to figure 20-2(b), it is clear that when fibers are employed to transport an image from a transparent phosphor, then the acceptance angle in the fiber is required to be at least 75° (half angle). On the other hand, for settled phosphor this half angle in the fiber can be as small as 50°. However, it should be remembered that these angles are within the fiber, and when refraction effects at the entrance end of the fiber are taken into account, this corresponds to fiber N.A. ≥ 1. Thus it is clear that for maximum efficiency the fiber coupling plate should be composed of fibers of N.A. ≥ 1 and of highly transparent core and coating materials. Under these conditions nearly all the flux captured by the fibers is transported to the photosensitive surface.

Resolution Loss on Coupling

Since individual fibers in a plate integrate the flux incident on them the smallest detail in the transmitted image is governed by the fiber size. The pieces of information transmitted by an array of fibers can therefore be calculated simply by geometrical considerations. The sampling theory states that if a unidirectional spatial illuminance object function contains no frequencies higher than R lines/mm, the function is completely specified by giving its ordinates at a series of points $(\frac{1}{2}R)$ mm apart. Since each fiber in an array corresponds to a sampling aperture, the sampling interval for a single row of fibers is approximately equal to the fiber diameter D. For a close packed array the sampling interval depends somewhat upon object orientation and the fiber packing arrangement. Therefore, $R = \frac{1}{2D}$ is the highest resolution attainable with a fiber array. On the other hand, the influence of object orientation on image quality is of particular interest near the limiting resolution and it varies from $R = \frac{1}{2D}$ in a few discrete orientations to $R = \frac{1}{3D}$ in general.

Further considerations of sampling theory indicate that when an image is transmitted through cascaded fiber plates, the resolution is degraded. This is primarily due to a lack of perfect alinement in corresponding fibers in the cascaded fused plates which is almost impossible to achieve in practice. Even though the fiber diameter can be maintained constant in a number of plates, it does not seem possible to obtain perfect registration of the centers of all fibers in a number of plates. The registration is considered difficult even when almost identical plates from the same boule are used. The equivalent sampling aperture for two cascaded plates can be imagined as an aperture of diameter D (corresponding to fibers in the first plate) sampled in a random fashion by another aperture of diameter D (corresponding to fibers in the second plate). It can be shown on statistical considerations that the equivalent sampling aperture diameter for two fused plates, each of diameter D, is approximately equal to $\sqrt{2}D$. A number of theoretical approaches have been made in order to estimate the loss in information caused by cascading optical elements. An empirical expression that has been commonly used relates the resolving power of two cascaded optical systems R^* with the resolving powers R_1 and R_2 of the two systems as follows:

$$\left(\frac{1}{R^*}\right)^2 = \left(\frac{1}{R_1}\right)^2 + \left(\frac{1}{R_2}\right)^2$$

Thus the resolving power of two plates consisting of equal diameter fibers would be reduced to $R^* = \dfrac{R_1}{\sqrt{2}}$. Further extensions of these considerations show that the resolving power of n cascaded plates, all of fiber diameter D, is approximately given by:

$$R^* \sim \frac{R_1}{\sqrt{n}} \sim \frac{1}{3\sqrt{n}D}$$

Experimental measurements of loss in resolution caused by cascading a number of plates have been made. Three fused fiber plates of 2-inch diameter and consisting of 5-micron fibers of N.A.$=0.95$ were used. The circular cross section of fibers was maintained during the fusion process. Figure 20-5 shows a macroscopic image of a test
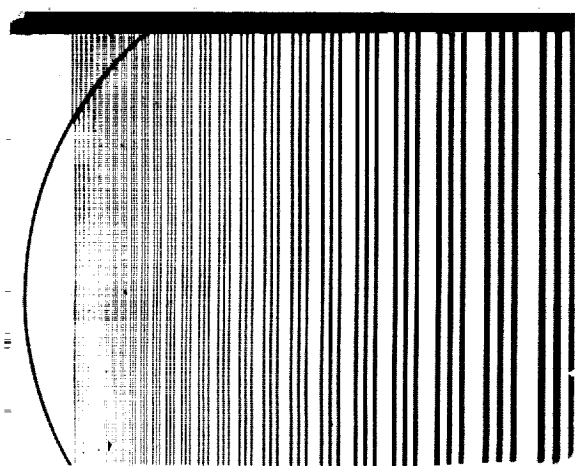

FIGURE 20-5.—Illustrating the imaging properties of a 2-inch-diameter fused plate of 5-micron fibers with N.A.$\simeq 1$. This plate has yielded resolution of 100 lines/mm.

object transmitted through the fused plates. Individual fibers cannot be seen in the picture because of the film graininess. A test object was imaged on one end of a fused plate and the resolution in the transmitted image was measured. Then the second fused plate was cascaded with the first plate and the change in resolution was observed. Finally, a third fused plate was cascaded and the resolution of the three stages was measured. Figure 20-6(a) shows the photomicrographs of a line test object, the images through one stage, two stages, and three stages of the 5-micron-diameter fiber fused plates. The resolution measurements were 100 lines/mm for single

stage, 60 to 70 lines/mm for two stages, and approximately 30 to 40 lines/mm for the three stages of the fiber fused plates.

A more quantitative determination of the loss in resolution was made by using a sine wave test object and measuring the spatial frequency response of single stage, double stage, and triple stage of the 5-micron-diameter fused plates. The reduced data are plotted in figure 20-6(b) and it is seen that not only the limiting resolution goes down in accordance with visual observations, but also a substantial degradation in contrast transfer occurs.

These experiments have indicated the effect on resolution of cascaded fiber fused plates. It is obvious that even using 5-micron fibers, a resolving power in excess of most existing multistage image intensifiers is achievable. A factor of two or higher resolving power can be obtained using smaller diameter fibers. The essential condition in the use of fiber coupling plates is that the equivalent sampling aperture of the cascaded plates be a factor of two or more smaller than the spot size on the phosphor. It is clear from the results on fused plates used in this experiment that better performance is achievable using fiber optics coupling plates than either with a lens system or a thin membrane. At present it seems that considerable advances in electron optics, photocathodes, and phosphors would be required to utilize the ultimate resolution capabilities of fiber optics.

Interstitial Opaque Coatings

A second coating of a highly absorbing material is considered to be of value since it serves to absorb the energy refracting out of the fibers (when the fiber N.A. is low) and also the energy incident at the regions in between the fibers. A number of experiments on image transfer from a Lambertian image plane (phosphor) have indicated that loss in resolution and contrast occurs without the use of this absorbing coating, although this effect is not too serious when fibers of N.A. ≥ 1 are used in conjunction with a settled phosphor. This is primarily due to the lack of optical contact between the phosphor and the fibers resulting in most of the energy striking the fiber wall at angles greater than critical. Further studies on the imaging characteristics and light efficiency of various types of fibers under different sets of conditions are now in progress and will be reported elsewhere.
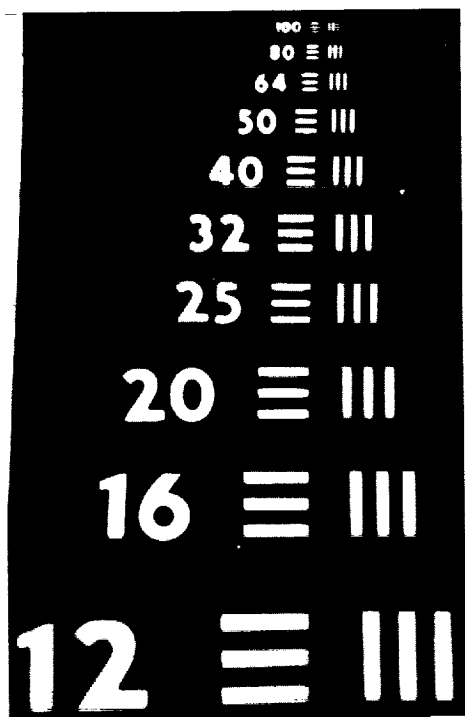
Resolution chart.
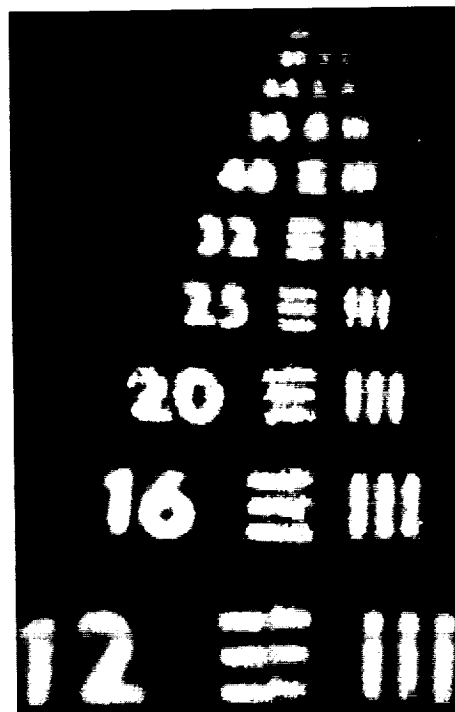
One fiber plate image.
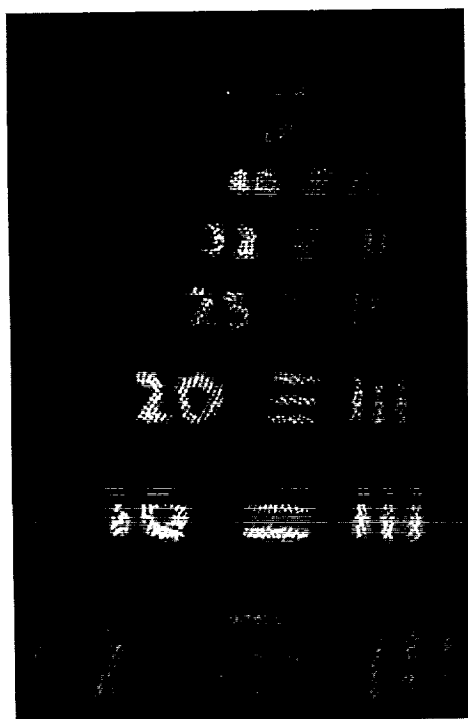
Two fiber plate image.
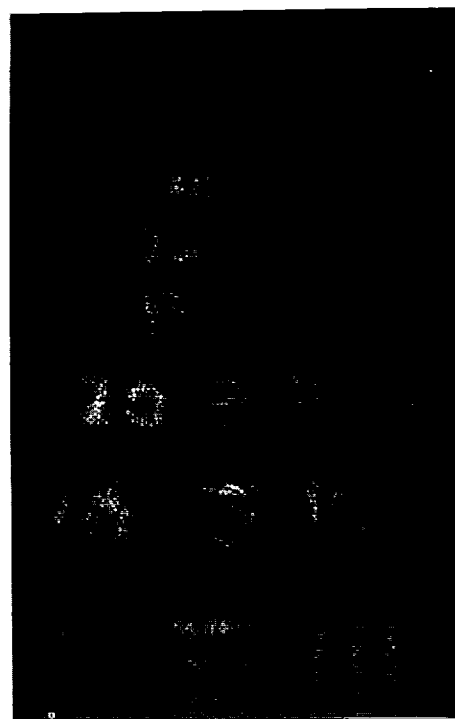
Three fiber plate image.

FIGURE 20–6(a).—Illustrating the loss in resolution on coupling a number of fiber plates using 5-micron diameter fibers of N.A.≃1.
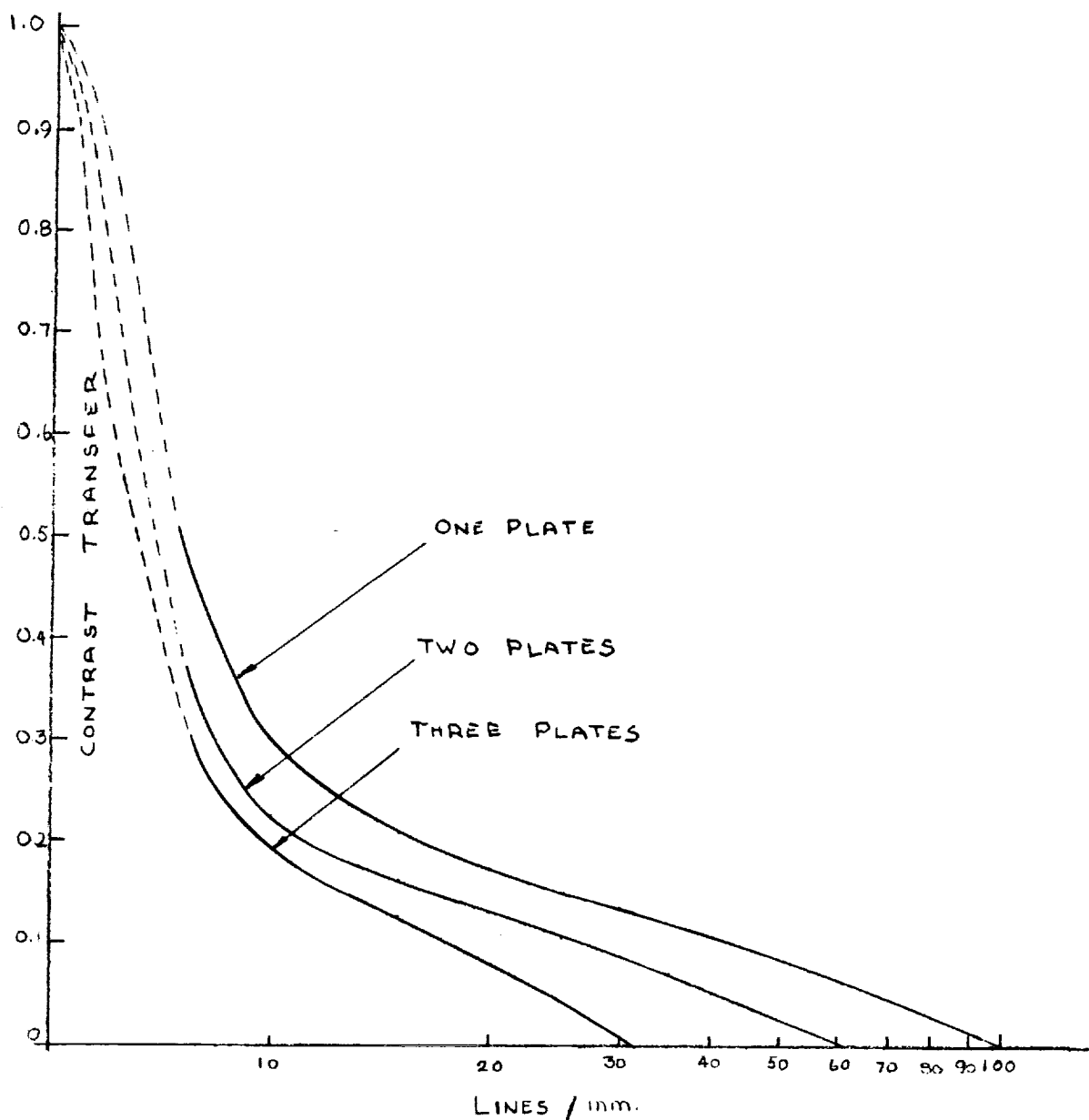
FIGURE 20–6(b).—The spatial frequency response under the conditions described in figure 20–6(a).

Photocathode Poisoning

It is obvious that for fused fiber plates to be used successfully in coupling interstages, they must be subject to photocathode deposition. Fibers made of glasses with high lead content, impurities and improper sealing tend to poison the photocathodes. Unfortunately, most high refractive index glasses to be used with high N.A. fibers suffer from these drawbacks and little success has been achieved using lead glasses. A number of other approaches have been made to overcome this problem, but the results to date

are far from optimum. One method consists of fusing a thin glass membrane of another glass at the exit face of the fiber fused plates and then depositing the photocathode on it. Although this serves to isolate the photocathode from the high index fibers, it suffers from loss in resolution as discussed in section II. Yet another method, at present in experimental stages, consists of vacuum depositing a very thin coating of SiO or tin oxide on the fused plate.

As discussed in section II, it has become possible to fabricate high N.A. fibers of non-lead-

152

content glasses. Fiber fused plates of these glasses have been used successfully in a three-stage diode without affecting the photocathode performance.

Photographic Recording

The photographic recording of the output image of a multistage image intensifier using fiber optics requires careful attention. It is obviously desirable to use a final fiber fused plate window for contact photography. This requires the fusion of the plates to the envelope and therefore imposes restrictions on the thermal properties of the fused plates. On the other hand, the camera design requirements are different. For optimum performance it is required that the film be placed in intimate contact with the fused plate. Because of the large angle of divergence of light emerging from the fibers, the tolerance for spacing between the fibers and film is stringent. This tolerance can be relaxed at the expense of photometric efficiency by using low N.A. fibers for the end window. In order to avoid film damage and scratching, the film advance motion has to be performed after retracting the film from the fused plate. Furthermore, a reflex viewing system is desirable.

The development of a camera capable of bringing the film in intimate contact with the fibers during photography, film retraction motion coupled with the film advance mechanism and a built-in reflex viewing system is at present in progress. Its design details and performance criteria will be reported elsewhere.

IV. Image Intensifier Studies

Because of the simplicity of construction and small physical size, the diode-type image intensifier was chosen as a means of demonstrating the interstage coupling capability of fiber optics fused plates. It seems appropriate to briefly consider the manner of construction of such units and the method of introducing the fiber plates. The fabrication of a single-stage unit will be described and the techniques then extended to multistage units.

Figure 20-7(a) shows a multistage image intensifier but it is representative of the construction of a single-stage unit. The tube was constructed in two sections which are assembled after preliminary surface preparation is completed. A standard P11 phosphor is deposited on the window at the back section and has an aluminized coating of 3 to 4 kv equivalent thickness. Initial steps of photocathode preparation are performed on the window in the front section of the tube. A conventional cesium antimony photocathode surface is used, the antimony coating being applied before the tube is assembled. Since the completed photocathode surface cannot be exposed to air, the reaction of the cesium with the antimony cannot be performed until after the tube has been evacuated. Due to the short length of the tube, it is not possible to use all-glass construction. This is because the heat required to join the two sections would damage the prepared cathode and anode surfaces. As a result, kovar to glass seals are used in both sections so that the seal is made between two pieces of kovar. Heli-arc welding of the two sections results in minimum heating of the structure. The reentrant design of the tube permits increased spacing between the kovar end plates to minimize external high voltage breakdown. Spacing between the cathode and anode surfaces is maintained at approximately 4 mm; the overall length of the tube, excluding sealoffs, is approximately 1 inch. The useful photocathode surface is approximately 1.25 inches in diameter. Gains of the order of 10 are possible with voltages from 10 to 12 kv. Resolution is dependent on accelerating voltage and is typically approximately 10 lines/mm in a single-stage unit.

In multistage units the length of the tubes is increased to accommodate the additional fiber fused plate elements in the common volume. The fiber optics plates are approximately $\frac{1}{16}$-inch thick and consist of 5-micron fibers of N.A.=1. The plates are supported on annular metal disks which are in turn supported by wire feedthroughs in the sidewall of the tube. The cathode and anode surfaces are prepared as previously described and the surfaces are electrically connected in a given plate.

The construction shown lends itself to two-stage operation in that optimum spacing can be maintained between the wire feedthroughs and the kovar end plates. However, as can be seen in figure 20-7(a), the spacing between the electrodes supporting the fiber plates is small in a three-stage unit. Staggering the position of the electrodes helps to minimize voltage breakdown. Since a common volume contains all of the photocathode,

153

FUSED FIBER PLATE

GLASS

P II PHOSPHOR

CS₂ Sb PHOTOCATHODE

KOVAR

20 MEG

40 MEG   40 MEG   40 MEG

HIGH VOLTAGE
POWER SUPPLY
0-15 KV
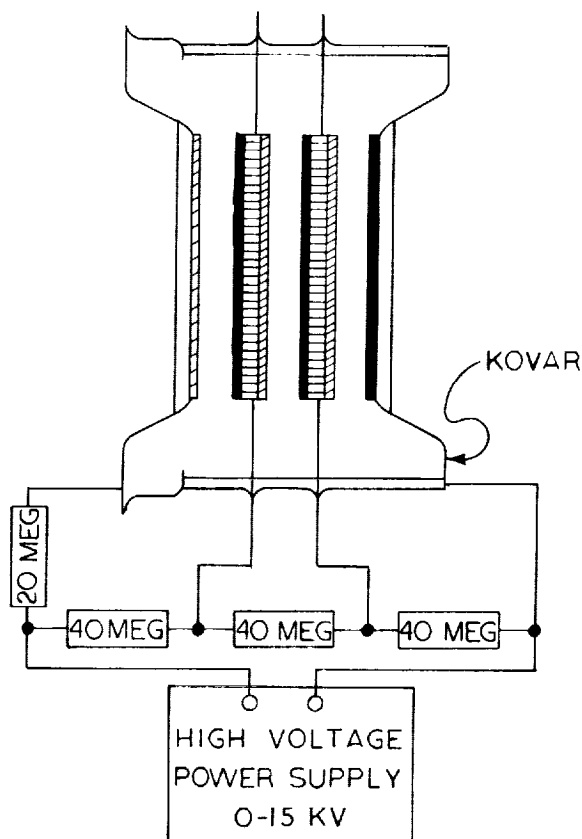
FIGURE 20-7(a).—Diagram of a three-stage diode type image intensifier using two fused fiber plates of 5-micron fibers of N.A.≅1.

a single side-arm containing cesium is used to react all of the surfaces. By illuminating one of the surfaces, the photoelectric current can be measured to indicate the progress of the reaction. Photographs of one- and three-stage units are shown in figure 20-7(b).

To determine the resolution capabilities of the intensifiers, a standard bar chart was imaged on the input photocathode, resolution being measured at the output anode surface. There is a 1:1 correspondence between the input and output images. Resolution is approximately 10 lines/mm for the single-stage unit and 5 lines/mm for the three-stage unit. There is no measurable variation in resolution over the entire field. Photographs of the input and output images are shown

Single-stage unit.
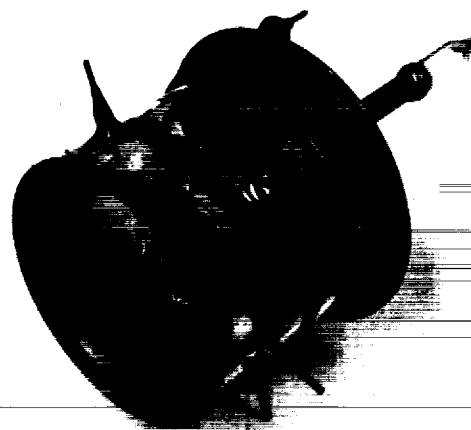
Three-stage unit.

FIGURE 20-7(b).—Photographs of the experimental models.

in figure 20-8. In addition to the bar chart test object, reproduction of a Kodachrome slide is illustrated. Loss of contrast is evident in the output of the three-stage tube. This is due in part to the fact that the stages were operated

154
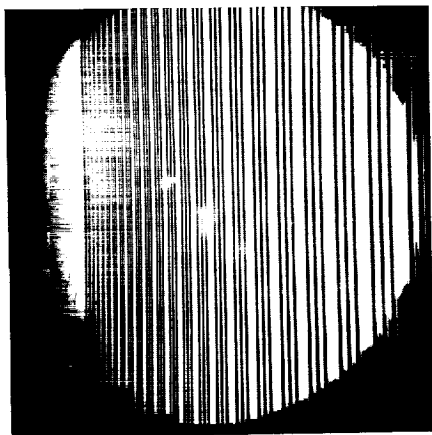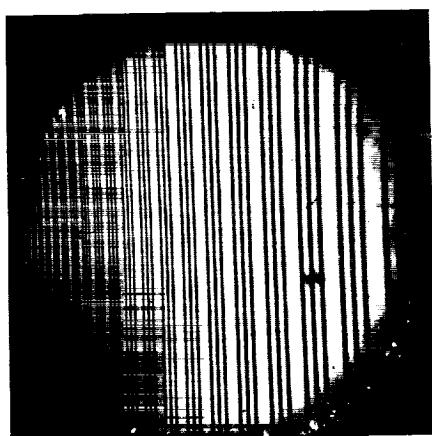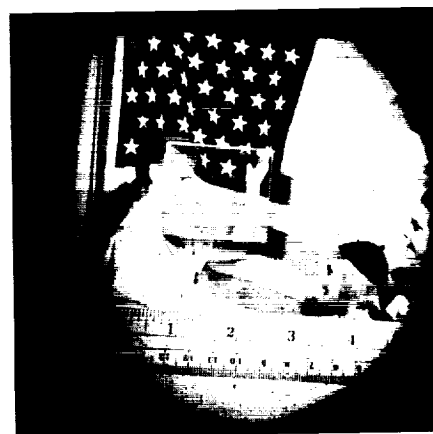
Test objects.

Image through
single stage.
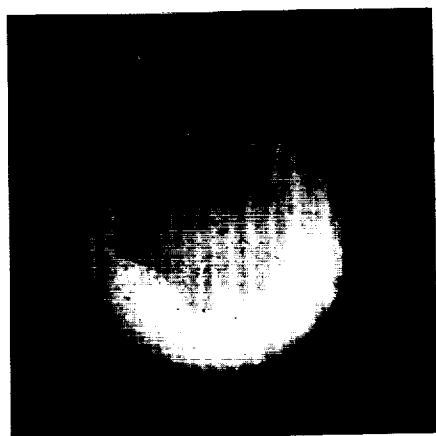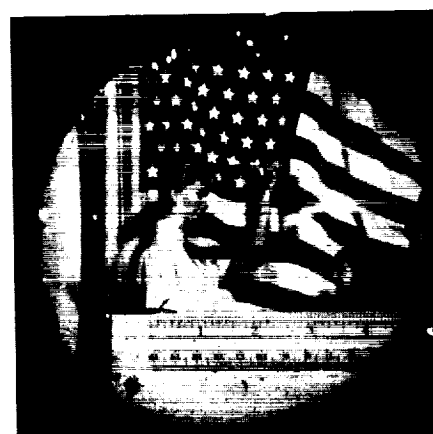
Image through
three stage.

FIGURE 20–8.—Photographs of test objects and images through the three-stage image intensifier illustrated in figure 20–7(b).

appreciably below optimum voltage in order to minimize voltage breakdown. The active area of the three-stage unit is only ¾-inch diameter which accounts for the difference in image size. The distortion apparent in the three-stage pictures is due to a defect in the first anode surface, a small portion of the aluminum film having peeled off. Whereas detailed measurements on the performance of this intensifier are not available at present, it is shown that high-resolution fused plates capable of fusion to the envelope and photocathode deposition can be built for incorporation into different types of multistage image intensifiers.

A precise evaluation of the influence of any single component on the information transfer characteristics and photometric gains of a multistage image intensifier is considered to be a very sophisticated problem. It requires an understanding of the individual and cumulative influences of a number of parameters on the performance of the device. More obvious of these parameters are (a) the angular distribution and wavelength of incident and output radiation; (b) electron optical aberrations—varying over the field; (c) phosphor point spread function; (d) the interstage coupling elements characteristics; (e) spectral and angular emission characteristics of the photocathode and phosphor; (f) the film parameters; and (g) psychophysiological effects of the observer viewing the output image. This paper has dealt primarily with the influence and properties of various methods available for interstage coupling and the gains possible with fiber optics. Further work on image evaluation of multistage image intensifiers taking due account of the above-mentioned parameters needs yet to be undertaken.

Conclusions

A detailed analysis of various methods available for coupling multistage image intensifiers shows the advantages offered by fiber optics. Fused plates of high N.A. have been fabricated and are capable of yielding image resolution of 100 lines/mm and higher. It is shown that the effective resolution of a number of coupled plates n, each with resolving power R, is approximately given by $\frac{R}{\sqrt{n}}$. This factor should be taken into account at the design stage. The problems of sealing, vacuum tightness, cathode poisoning, and contact photography of the output image have been treated in detail. The preliminary experiments on a three-stage diode intensifier have demonstrated the gains available using fiber optics coupling. Further developments along these lines are expected to yield high-quality multistage image intensifiers with high resolution and light gains.

Acknowledgments

Discussion

B. LIPPEL: Referring to your slides showing two or more fiber plates in contact, can this be done nicely when the plates are manufactured with identical fiber spacing? I am thinking of moiré effects. Should the average spacings be deliberately made different?

N. S. KAPANY: In a number of different experiments that we have conducted with cascaded fiber fused plates, we have not had any severe problems with moiré effects. In principle, such moiré patterns may exist regardless of the fiber spacing in the two plates, so long as the fiber diameters as well as their spacing in the individual plates are highly uniform. Therefore, I do not see much advantage to be gained by deliberately making the average spacing between the fibers in the two plates different.

J. J. VAN DER SANDE: Efficiencies of 30 to 35 percent for optical coupling image tubes are now possible, which is eight times higher than the value shown by Dr. Kapany in one of his slides.

N. S. KAPANY: In my paper I compared the efficiency of fused fiber optics coupling plates with that of an f/1 lens system working at 1:1 conjugate position. It would seem to me that the efficiencies of 30 to 35 percent being quoted are somewhat optimistic. Furthermore, it should be stated that for coupling of images from large tubes—say 5 inches in diameter—a very severe demand is placed on the lens design because of the requirement of low f-ratio as well as wide field angle. In view of the higher order aberrations, as they behave in such optical systems, it is obvious that a very severe compromise has to be made between the photometric efficiency, field angle, and resolving power. With the recent

developments in high resolution electron optics for large tubes up to 5 inches or more in diameter, it would seem to me that expecting 30 to 35 percent coupling efficiency with spot sizes as small as 5 to 10 microns using lens systems is perhaps stretching the imagination somewhat.

G. PAPP: Mr. Kapany indicated that the cascading of two or three fiber plates reduces the resolution by a factor of $\sqrt{2}$ or $\sqrt{3}$. As I tried to explain in my paper (No. 15), the quadratice addition of errors is valid, only in the case of independent, random variables. This cannot be claimed in the cascading of two fiber plates. It would be true if the two plates would wobble or rotate compared to each other. In the case of stationary plates, there is a systematic error introduced at every point. The errors themselves, rather than the squares, add, resulting in the decreasing of resolution by a factor of 2 or 3, rather than by $\sqrt{2}$ or $\sqrt{3}$.

References

1. KAPANY, N. S.: *Fiber Optics.* Concepts of Classical Optics by Strong, John (Appendix N). W. H. Freeman & Co., San Francisco, pp. 553–579, 1958.
2. KAPANY, N. S.: *Electro-Optical Systems Using Fibre Optics.* Optica Acta, vol. 7, 1960, pp. 201–217.
3. KAPANY, N. S., and CAPELLARO, D. F.: *Fiber Optics.* VII. Image Transfer From Lambertian Emitters, J. Opt. Soc. Am., vol. 51, 1961, pp. 23–31.
4. KAPANY, N. S., and BURKE, J. J.: *Fiber Optics.* IX. Waveguide Effects, J. Opt. Soc. Am., vol. 51, 1961, pp. 1067–1078.
5. WHITE, L. E.: *Measuring Spot Size of High Resolution Cathode Ray Tubes.* Electronic Equip. Eng., Aug. 1959.
6. SCHADE, O. H.: R.C.A. Rev., vol. 9, pp. 5, 245, 490, and 653.
7. KAPANY, N. S.: *Optical Image Assessment.* Nature, vol. 188, December 1960, pp. 1083–1986.

21. UNCONVENTIONAL FIBER OPTICS

WALTER P. SIEGMUND, *American Optical Co.*

Introduction

Fiber optics, in the form of vacuum-tight tube faces for use in image intensifiers, has been described in several papers of this symposium as well as in the previous symposium held in 1958.[1] It is the purpose of this paper to discuss certain aspects of this type of fiber optics as well as to describe a number of examples of other configurations and applications, which have been termed unconventional, although this term is necessarily relative in such a rapidly changing field. The presentation is divided into three parts covering unusual materials, configurations, and applications which are intended to illustrate some of the diversification which this field has undergone during the past few years.

Unconventional Fiber Optics Materials

Conventional optical fibers consist of a flint glass core and a crown glass coating. The choice of these materials is based on the requirement that the index of refraction of the core be higher than that of the coating as well as certain thermal compatibility requirements. Ordinary crown and flint glasses can be selected which fulfill these requirements, and several such combinations have been extensively used in optical fibers. To meet new requirements, however, such as improved transmission in the infrared and ultraviolet region of the spectrum, it has been necessary to investigate other materials.

To extend the transmission into the infrared beyond the limit of about 2–2.5 μ for flint glass, fibers have been developed based on arsenic trisulfide glass. In particular, fibers have been prepared having a core of stochiometric $As_2 S_3$ ($n_{1\mu} = 2.47$) and a coating of a modified arsenic sulfide glass having a lower refractive index ($n_{1\mu} = 2.416$). This combination of refractive indices provides a nominal numerical aperture (i.e., the sine of the half angle of the acceptance cone) of 0.5 which corresponds to a relative aperture of f/1. Typical fibers have a diameter of 60 microns, including a

coating thickness of 4 microns. Short lengths of these fibers (7 mm) have measureable transmission out to 12 microns wavelength, while longer lengths (18 inches) transmit out to 7 microns. Figure 21-1 shows the relative transmittance as a function of wavelength for three different fiber lengths.

The actual transmittance measured at a specific wavelength (2.44 μ) using a narrow passband filter was found to be approximately 65 percent for a 6-inch length, not including end losses. By overcoating similar fibers with an organic lacquer ($n_{1\mu} = 1.5$), it was found possible to increase the transmittance at 2.44 μ to 80 percent for a 6-inch length. This increase is believed to be due to successful trapping of light by the lacquer-glass interface, which is otherwise scattered beyond the acceptance angle of the glass coating-glass core interface and lost.

Although image intensifiers do not yet work out in the infrared as far as arsenic trisulfide, it
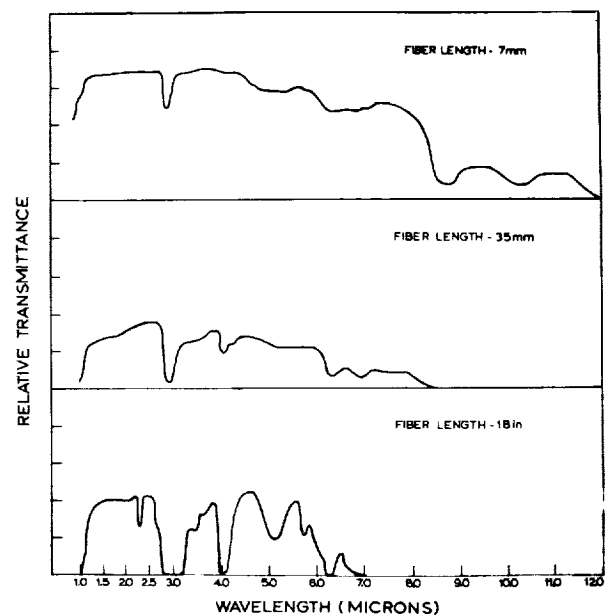
FIGURE 21-1.—Relative transmittance of coated arsenic sulfide glass fibers.

159

may offer encouragement to know that fiber optics for this spectral region have already proven feasible.

The gains made in extending the transmission of fiber optics into the ultraviolet have been less dramatic. Although, in principle, quartz fibers could transmit well into the U.V., their low refractive index makes it practically impossible to provide a suitable coating to protect them from contamination and subsequent loss in transmittance. For this reason quartz is also completely unsuitable for fiber optics tube faces in which a large numerical aperture, hence a large difference in refractive index, is essential. Since conventional high-index flint glasses tend to absorb strongly even in short path lengths in the violet or very near ultraviolet spectrum, a search was made for glasses which could provide both high numerical aperture and somewhat better U.V. transmittance. It was found that the lanthanum
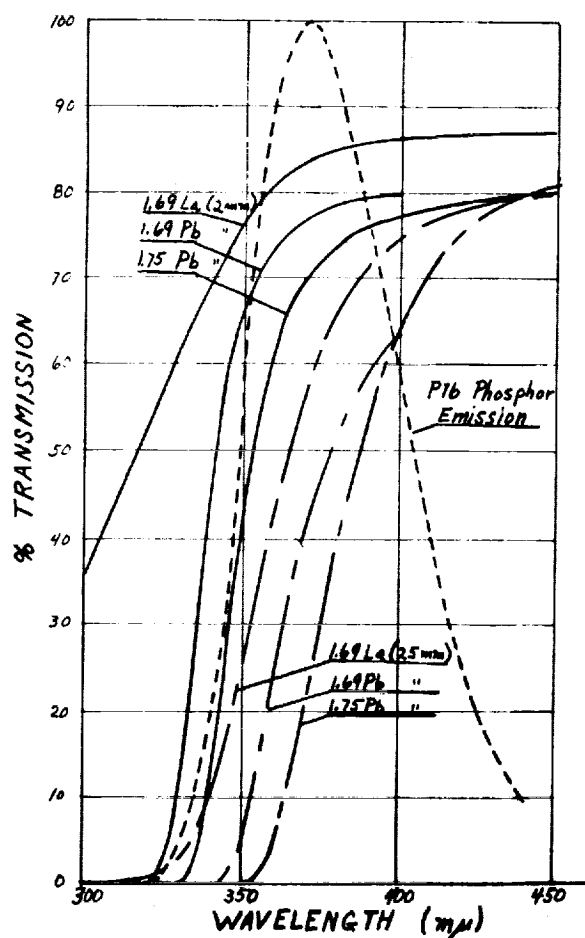
FIGURE 21-2.—Transmission of high index fiber optics core glasses for two different thicknesses (2 mm. and 25 mm.). In the near UV.

160

crown glasses provide these properties. The transmittance of one example of this type of glass is shown in figure 21-2 along with curves for two common flint glasses. Also shown is the emission curve for type P-16 phosphor to indicate the significance of the improved U.V. transmittance of the lanthanum glass for a thickness of around 25 mm or so.

Another advantage of some of the high-index lanthanum glasses is that they do not contain lead which can interact at high temperatures with photocathode materials, causing both the glass and the cathode to deteriorate. Although barrier coatings have been developed to prevent this interaction with lead-containing fiber optics, a better solution is to eliminate the lead altogether.

Nonbrowning glass is another unconventional material which has recently been applied to fiber optics. In applications where large doses of nuclear radiation are likely to be encountered, ordinary optical glasses may darken or even become opaque depending on the dose, the shielding, and the glass composition. Nonbrowning glasses designed to minimize this darkening often contain cerium which unfortunately is itself a glass colorant. For short fiber lengths (tube face applications) the intrinsic coloration might not be objectionable; however, for lengths of the order of 2 feet or more (flexible borescope applications), it can be fatal. For example, fibers drawn from a nonbrowning glass of intermediate refractive index (Schott type F-2-RS, $n=1.62$) were found to be practically opaque over a length of 24 inches, while a 2-mm-thick tube face made from the same fibers showed only a trace of coloration. Although other types of nonbrowning glasses are available, the prospects for long fibers do not appear favorable.

Unconventional Fiber Optics Configurations

With the possible exception of the fiber optics tube face, the flexible borescope or "fiberscope" is the most common form of fiber optics in use today. A variety of industrial and medical applications have already been found for these devices. The principles and basic properties of fiberscopes have been extensively described in literature.[2-6] They are of interest in connection with image intensifiers as a means of coupling optical components to image tubes or one image tube to another where conditions demand a flexible path and relatively high light transmission. Although the fiberscope as a device has become fairly familiar,

at least to workers in the field of optics, examples of instruments having unusual dimensions might appropriately be included within the scope of this paper.

An example of a fiberscope of unusual length is shown in figure 21-3. This instrument is approx-
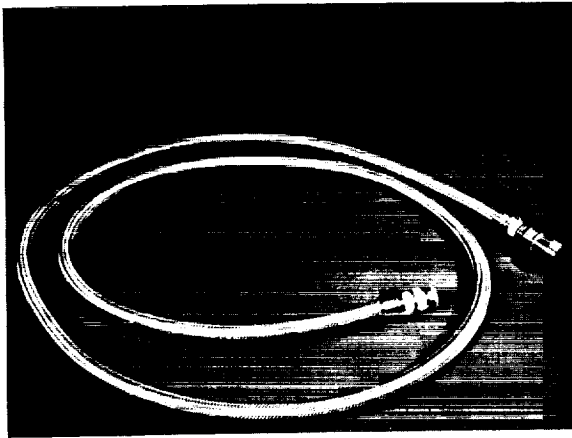
FIGURE 21-3.—Industrial-type fiberscope, 150 inches long and 1 inch in diameter.

imately 150 inches long and 1 inch in diameter. It contains in the neighborhood of 800,000 fibers, each 10 microns in diameter. The cross section of the fiber bundle itself is 8 mm by 10 mm, i.e., about the same as a 16-mm cine frame, and standard 16 mm camera objectives are used with the instrument. A number of these fiberscopes are in use as inspection devices.

By way of contrast, the instrument shown in figure 21-4 is an example of a small-diameter type fiberscope developed primarily for medical use. This particular instrument actually contains two fiber bundles, one to carry light from an external lamp (not shown) down to the distal end and the other to bring the image back to the eyepiece. A small lens at the distal end casts an image of the object onto the entrance end of the image-carrying bundle. This bundle consists of approximately 40,000 fibers, each 7.5 microns in diameter. The illuminating bundle consists of a relatively few larger sized fibers since resolution is not a consideration in this case. This bundle is made up in two sections which are joined at the Y-shaped junction just below the eyepiece. The particular application for which this instrument was built is intracardiac visualization; however, a number of other diagnostic applications have been suggested for such instruments.

The image-carrying fiber bundles of both the above examples are made up of "multifibers" which consist of a number of precisely arranged individual coated filaments fused together to make a larger building block which can be systematically assembled to produce the desired cross section. A photomicrograph of this type of multifiber is shown in figure 21-5. In this example the large squares containing 36 smaller filaments in a 6 by 6 array are each 36 microns on a side and each filament is about 6 microns across. The corners of the multifibers are slightly rounded in the drawing process, but otherwise they can be stacked together with relatively little waste area between fibers.

Another kind of multifiber is illustrated in figure 21-6. In this case a great many more elementary filaments have been fused together to form a rigid fiber optics "image conduit". The example shown contains exactly 73,441 filaments, each 12 microns across, assembled in a hexagonal

FIGURE 21-4.—Medical-type fiberscope, 36 inches long and ⅛ inch in diameter.
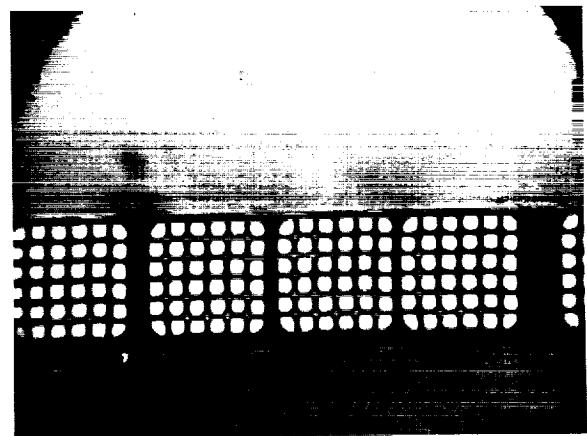
FIGURE 21-5.—Photomicrograph of "multifibers" used in flexible fiberscopes.

161
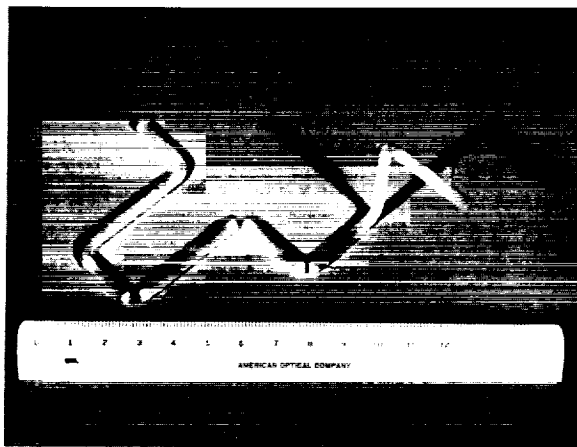
FIGURE 21-6.—Rigid "image conduit" consisting of over 73,000 fibers.

FIGURE 21-8.—Oblique view of same plate.

array, and is capable of transmitting a fairly detailed image. This material can also be bent, as shown by simply heating it over a flame and will retain its image-transmitting properties.

Unconventional Fiber Optics Applications

The use of fiber optics for direct recording from cathode ray tubes is well known; however, fiber optics can also be used to advantage in visual CRT displays. Through the use of a special fiber optics tube face consisting of double-coated fibers in which the outer coating is made of a light-absorbing glass, it is possible to substantially increase the contrast of the CRT screen image under high ambient light conditions. The principle of the double-coated fibers is illustrated in figures 21-7 and 21-8 which show two views of a demonstration tube face at different obliquities.

When viewed head-on (fig. 21-7) the double-coated fibers, which are arrayed in the pattern of the letters "WS," transmit almost as well as the surrounding fibers. When viewed obliquely (fig. 21-8) beyond the acceptance angle of the fibers, the double-coated fibers appear dark because light rays penetrating the fiber walls (i.e., those outside the critical angle for total reflection) are absorbed by the outer coating. In the surrounding fibers this stray light is transmitted and hence these fibers appear as bright as they did head-on.

In a similar manner a CRT tube face made up of these double-coated fibers prevents the ambient light incident upon the tube face beyond the acceptance angle of the fibers from reaching the diffusely reflecting phosphor screen. By making the acceptance angle as small as permissible, the total ambient light reaching the screen can be substantially reduced.

Figure 21-9(a) shows an experimental CRT incorporating such a tube face. The dark circular

FIGURE 21-7.—Head-on view of fiber optics face plate containing both single- and double-coated (absorbing type) fibers.
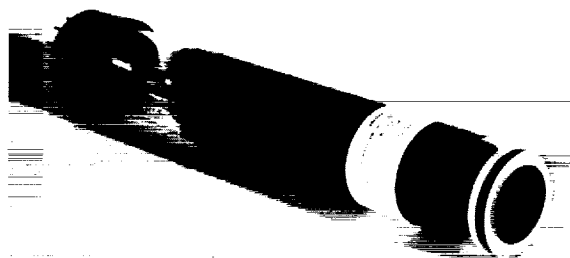
FIGURE 21-9(a).—Experimental CRT containing double-coated (absorbing) fibers.

162

FIGURE 21-9(b).—Trace on CRT showing high degree of contrast obtainable in the presence of strong side-lighting.

area of the faceplate contains the fused bundle of double-coated fibers. Figure 21-9(b) shows this tube installed in a cathode-ray oscillograph. It can be seem that the trace on the CRT screen has excellent contrast despite strong sidelighting which was provided by desk lamps on either side of the scope just outside the fiber acceptance angle. It might be noted that a further advantage of such a faceplate is the absence of parallax between the screen image and the face of the tube, thereby permitting more accurate measurements to be made on the image.

Encoding and decoding of optical images was one of the first applications suggested for fiber optics.[4] Any fiber bundle in which the fiber ends at one end of the bundle are randomly disposed relative to the other end of the bundle, can be used to encode and subsequently decode an image. Of greater practical significance, it is also possible to produce a matched pair of fiber coders employing random scrambling. On the other hand, producing a larger number of matched coders with a high order of scrambling becomes a far more formidable problem.

To meet the requirements for a large number of identical units but having a comparatively simple form of code (for use in signature verification in banks), a form of fiber optics coder was developed consisting of a number of layers of fibers which are systematically laid up at various predetermined angles to one another. An image encoded with such a bundle, therefore, consists of a corresponding number of rows of dots shifted laterally by known amounts. An example of coded image of a portion of a standard Air Force resolution chart is shown in figure 21-10(a).
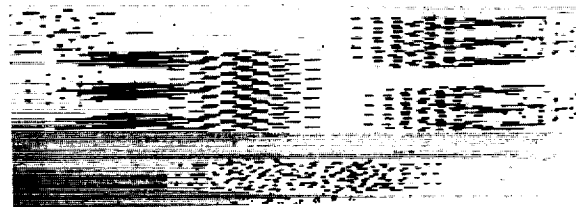
(a) Encoded image (reversed in printing).

(b) Partially decoded image.

(c) Completely decoded image.

FIGURE 21-10.—Encoded and decoded images obtained with fiber optics coder.

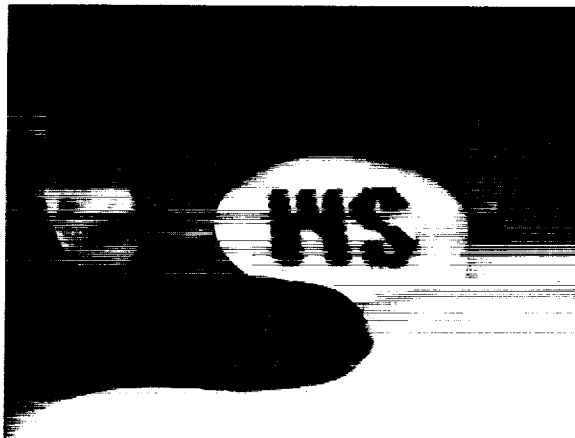Incomplete decoding resulting from a residual rotation error in positioning the decoder over the coded message is shown in figure 21-10(b). Complete decoded is shown in figure 21-10(c). As many as 30 or more identical coders have been made using this approach.

Tapered fiber optics bundles lend themselves to some unusual applications. One example is an image forming device based on the so-called "compound eye" characteristic of certain insects such as the housefly. The fibers of the tapered bundle correspond to the individual channels or "ommatidia" of the compound eye. By designing the fibers to accept only a relatively small cone of light and then arranging them so that there is little or no overlapping among the acceptance cones of neighboring fibers, it is possible to obtain a crude image forming device without the use of lenses.

A small tapered fiber bundle which has this property is shown in figure 21-11. When the flared end of the bundle is pointed at a coarse target, an image can be seen at the small end. This is illustrated in figure 21-12. The large vertical bars comprise the target, placed about

163

FIGURE 21-11.—Tapered fiber bundle analogy of insect "compound eye."
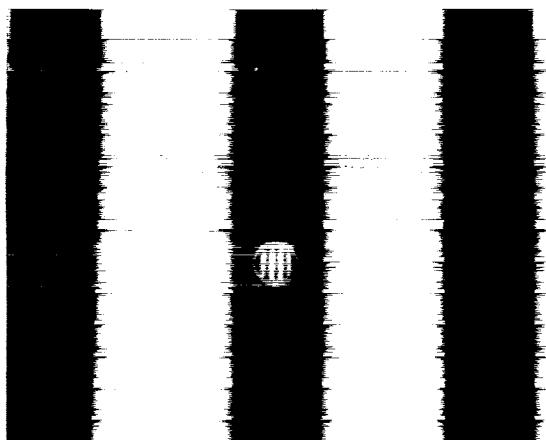
FIGURE 21-12.—Image produced by fiber bundle shown in figure 21-11.

FIGURE 21-13.—Distortion produced by non-uniformly-tapered fiber bundle.

18 inches in front of the tapered bundle. The image formed by the bundle can be seen within the circle; i.e., the small end of the bundle.

Image distortion compensation is another unusual application for fiber optics made possible through the use of tapered fiber bundles. Since ordinary image distortion (the "pincushion" or "barrel" distortion characteristic of simple lenses) is a nonlinear variation in image magnification, it can be compensated by a fiber optics bundle in which the fibers are distributed uniformly at one end of the bundle and displaced in a nonuniform manner at the other end to correspond to the nonlinear variation in image magnification. It has been found possible to prepare nonuniformly tapered fused fiber bundles having this property.

An example of such a bundle placed over a square grid pattern is shown in figure 21-13. This bundle is actually in the form of a flat plate

about ⅜ inch thick and 1¼ inches in diameter; however, the fibers themselves are tapered and displaced within the bundle giving rise to the "barrel" distortion shown. When the plate is inverted, the opposite "pincushion" distortion results.

Tapered fiber bundles also can be used to advantage in fiber optics field flatteners when either the numerical aperture or the field of view of the lens system (or both) is large. In a tapered fiber field flattener the axis of the individual fiber can be arranged to coincide with the principal ray incident upon it so that the maximum-sized cone of light will be accepted by the fiber. This avoids losing light rays from the lens which otherwise would fall outside the acceptance cone of the fibers.

For the case of a refractive lens system, the image field is usually inward curving and an expanding tapered bundle is used. An example of a small tapered field flattener of this type is shown in figure 21-14 alongside a common pin. The concave entrance face of the bundle is 2 mm in diameter and the fiber diameter is 2 microns. The flat exit face is 5 mm in diameter and the taper angle is about 60°.

For the case of a mirror optical system, the image field is generally backward curving and a condensing-type tapered bundle is used. This has the additional advantage that light is concentrated by the tapered bundle which results in higher illumination at the output of the bundle than at the input. The numerical aperture or "optical speed" of the system is thus actually increased by means of such a tapered fiber optics "image condenser."

164

FIGURE 21-14.—Small field flattener incorporating a tapered fiber bundle.

FIGURE 21-16.—Experimental camera based on the optical system shown in figure 21-15.

FIGURE 21-15.—Optical system incorporating a tapered fiber bundle as an "image condenser."

This application has been demonstrated in a special optical system designed as part of an Air Force study on ultra-high-speed photographic objectives. The optical system is shown schematically in figure 21-15. The optical system was designed with a nominal relative aperture of f/0.58 which combined with transmission losses produced a T-stop rating of T-0.7.

The camera built to house the system is shown in figure 21-16. It is designed to be taken apart (fig. 21-17) to permit loading a single film for each exposure. The film is held against the fiber bundle by means of a backing plate and thumb screw.

An example of a photograph made with this camera is shown in figure 21-18. The source of light was moonlight (¾ full) and there was a light cover of snow on the ground. The exposure time was 1 second at full aperture on Eastman Tri-X film with ordinary processing. Although originally conceived and demonstrated as a photographic objective lens, this type of optical system could be adapted for use with an image intensifier where its high relative aperture would be

FIGURE 21-17.—Rear half of camera showing fiber bundle and film support clamp.

FIGURE 21-18.—Photograph made by moonlight using experimental camera.

165

particularly valuable as one approaches quantum noise limitations.

References

1. POTTER, R. J., and HOPKINS, R. E.: *Fiber Optics and Its Application to Image Intensifier Systems.* Image Intensifier Symp., October 1958.
2. BAIRD, J. L.: Brit. Pat. No. 20,969/27, 1927.
3. LAMM, H.: Z. fur Inst. K., vol. 50, 1930, p. 579.
4. VAN HEEL, A. C. S.: Nature, vol. 173, 1954, p. 39 (letter).
5. HOPKINS, H. H. and KAPANY, N. S.: Nature, vol. 173, 1954, p. 39 (letter).
6. HOPKINS, H. H., and KAPANY, N. S.: Optica Acta, vol. 1, 1955, p. 164.

22. APPLICATIONS OF IMAGE ORTHICONS IN SOLAR AND STELLAR ASTRONOMY

WILLIAM C. LIVINGSTON, *Kitt Peak National Observatory*

Introduction

When considering the merits of different image tubes for astronomical problems, it is worth while to differentiate between transducers which employ the photographic emulsion and those which do not. Certainly as far as resolution is concerned, the technique of electronography developed by Lallemand in France, and represented at this symposium by Walker, and Hiltner and Niklas, is without equal. Electronography circumvents most of the objectionable features of the unaided photographic plate such as low efficiency and reciprocity failure. There remains the matter of the saturation of the emulsion before desired accuracy is achieved and certain other practical difficulties in the recording of transitory phenomena at high light levels. When these effects introduce limitations, a signal-generating, charge-integrating tube, such as the image orthicon, complements the electronography process. In this paper we shall describe three astronomical observations, two solar and one stellar, which could only have been obtained with an image orthicon.

The Image Orthicon as an Aid to Increased Precision

The detection and measurement of weak lines in the spectrum of the solar photosphere is a difficult problem. Photographic photometry has a limited accuracy of about 1 percent because of unpredictable variations in sensitivity over the emulsion surface. Another photometric tool, the scanning photocell, shows a constant sensitivity, but because it explores the spectrum point by point, it is susceptible to errors caused by atmospheric transparency fluctuations and intrinsic changes in the spectrum. The image orthicon combines the panoramic property of the emulsion with the capacity for calibration of the photocell. For observations of the sun the image orthicon

camera was mounted on the head of the spectrograph of the 150-foot tower telescpoe of the Mount Wilson Observatory (fig. 22–1). This spectrograph is of the Littrow type and the grating used gave a dispersion of about 11 mm per angstrom. The orthicon was positioned so that spectrum dispersion was in the direction of the vertical scan of the tube. By adjusting the amplitude of the horizontal scan so that the reading beam just covered the width of the spectrum, and by reducing the bandwidth of the video amplifier so as to just resolve an element in wavelength, the scanning beam became fan shaped, and was analogous to the analyzing slit of a microphotometer. The oscillogram of the orthicon current output is a direct intensity record of the spectrum. In figure 22–2 a tracing of the raw orthicon output is compared with a record of the same spectral region as published in *The Photometric Altas of the Solar Spectrum* by Minnaert et al.

The signal/noise ratio of the raw output of the orthicon is insufficient for the study of weak lines. However, because of the signal-generating feature of the tube, this signal may be readily integrated
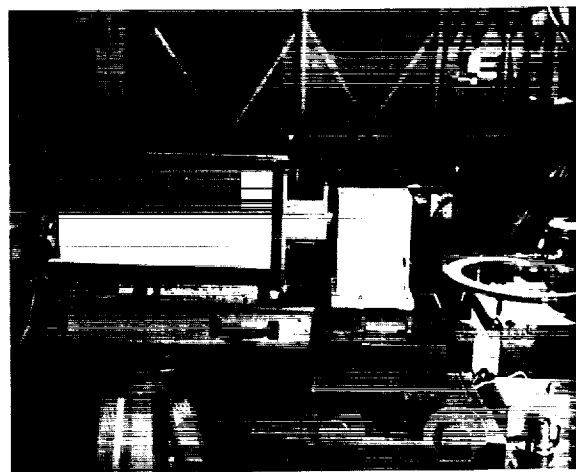
FIGURE 22–1.—Image orthicon camera mounted on spectrograph of 150-foot tower telescope, Mount Wilson, Calif. Solar image is visible at right.

167
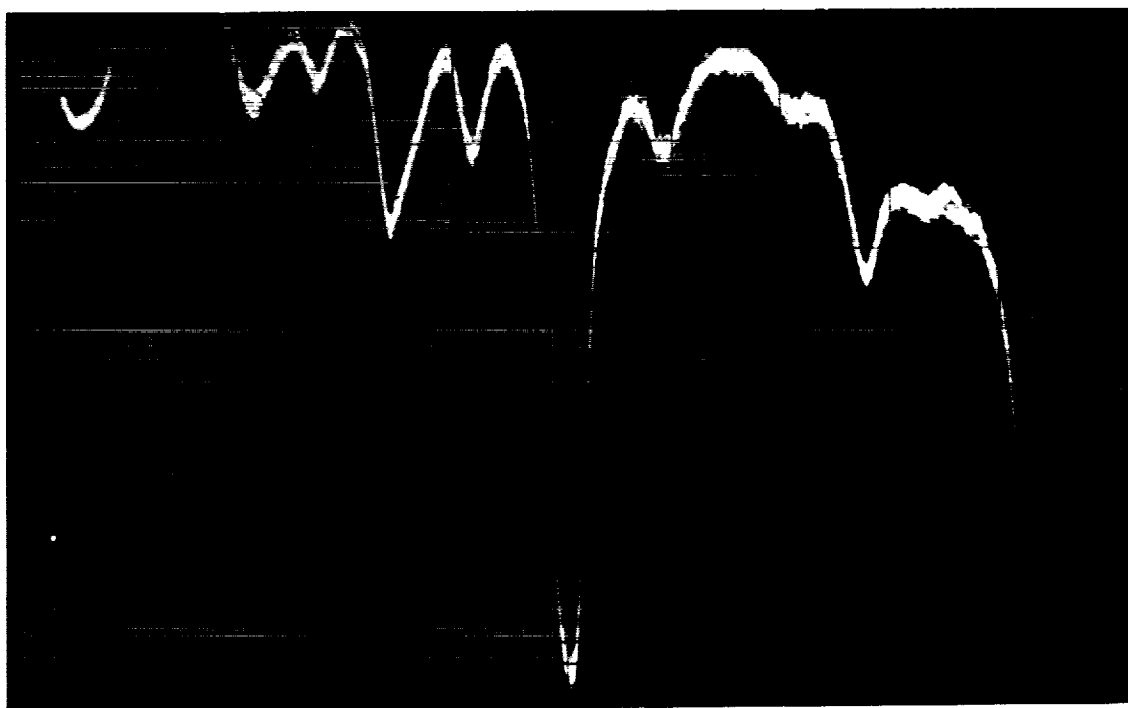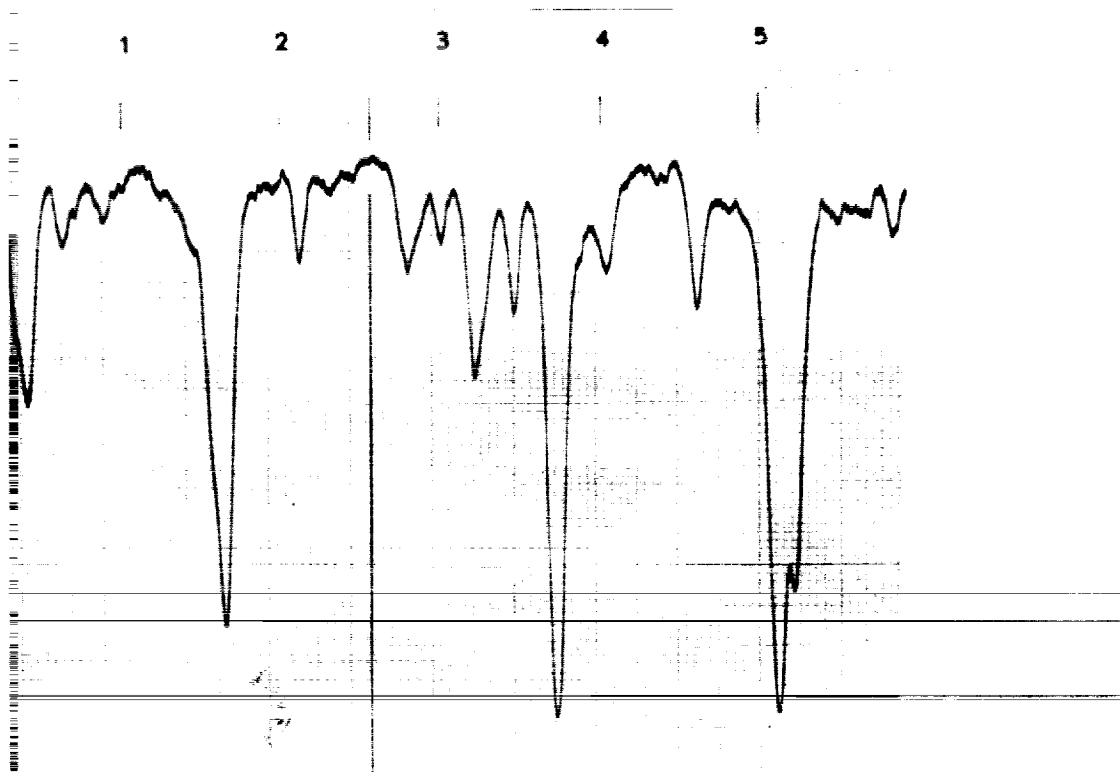
FIGURE 22–2.—Comparison of a tracing from the Minnaert "Atlas" with a direct intensity record made with the orthicon.

168
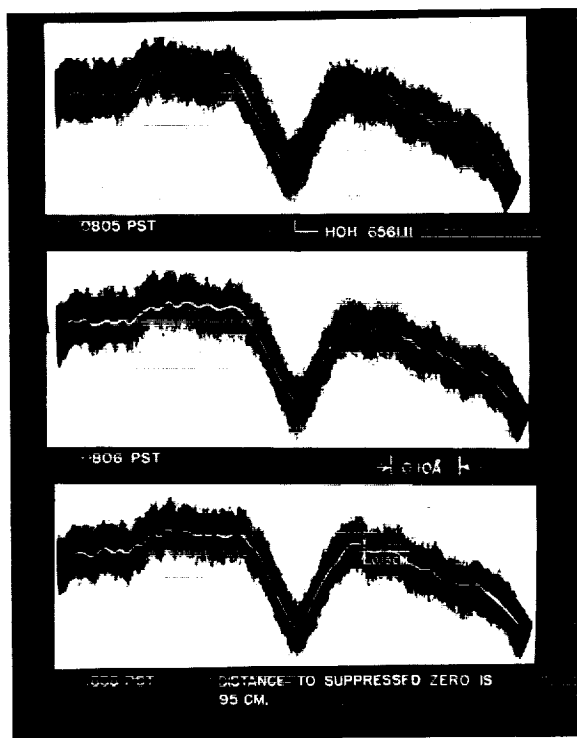
FIGURE 22-3.—Measurement of a weak line in the wing of Hα.

at high speed, externally, in order to increase the signal/noise. The integration may be done on the phosphor of the recording cathode-ray tube. After a sufficient number of scans, the peak-to-peak noise forms an envelope which closely defines the true mean.

This technique of phosphor integration is illustrated in figure 22-3. Three consecutive sets of observations, each of 150 scans, have been obtained of a region in the wing of Hα. The weak feature immediately to the right of the water vapor line has an equivalent width of about 0.3 mA. If this quantity is considered to be at the limit of detection, a precision of 0.1 percent (of the continuum) is achieved.

For more than a few hundred scans, the method of phosphor integration becomes quite inefficient. To obtain higher accuracy the scans must be integrated numerically with a digital computer. Kitt Peak National Observatory is, at present, preparing to use such a technique which promises an observational precision of 0.01 percent.

Spectrum of a Sunspot

The nature and cause of a sunspot remains as one of the unknowns of the solar surface. Little work has been done on the spectrum of the spot because the observations require the best of seeing and there is always an uncertainty as to how much the light from the photosphere has diluted the much weaker spot spectrum.

To observe the spot spectrum the entrance slit to the spectrograph is diaphragmed to about 1 millimeter, and the spot image is held over this opening during the exposure. Figure 22-4 is a record of 150 scans made in a total of 10 seconds. During this exposure the usual disturbances due to seeing occurred and produced the observed envelope of scans. Since the photosphere is much brighter than the spot, scans displaying high intensity can be considered spurious. Obviously, an integration of these scans would produce a mean spectrum of the photosphere and sunspot. However, the lower edge of the scan envelope represents a spot spectrum of high purity.

Observations of Stars Against a Bright Background

The storage capacity of the photographic emulsion depends on the number of grains in each picture element. As a result of exposure to light, the developed grains may overlap, reducing the number which can contribute to the blackening, and the emulsion saturates.

A charge-integrating tube, such as the image orthicon, is also subject to saturation but for a different reason. In the orthicon the photocharges can add together within an element until the resulting potential rise reduces the ability of the element to collect more charge. Saturation is said to occur when the potential of the target membrane equals the potential of the collecting
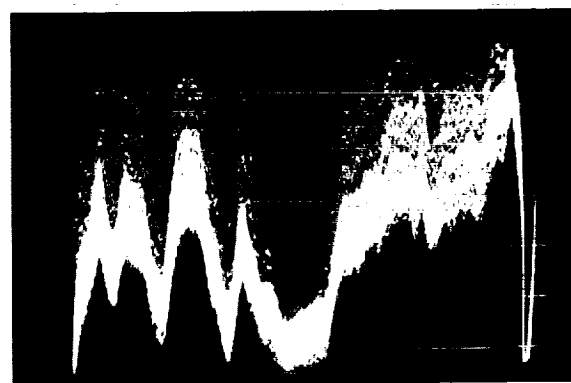
FIGURE 22-4.—Attempt to record the spectrum of a small sunspot (centered on Hβ).

169
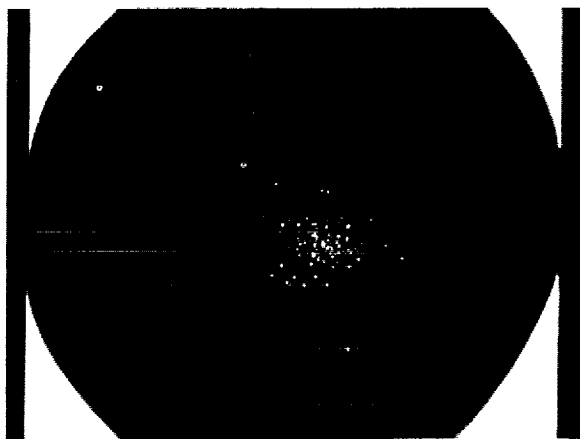
(a) $V_T = -3$, volts.
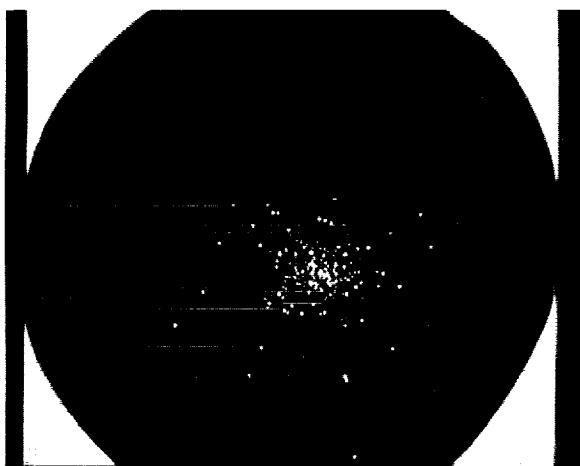
(b) $V_T = -2$ volts.
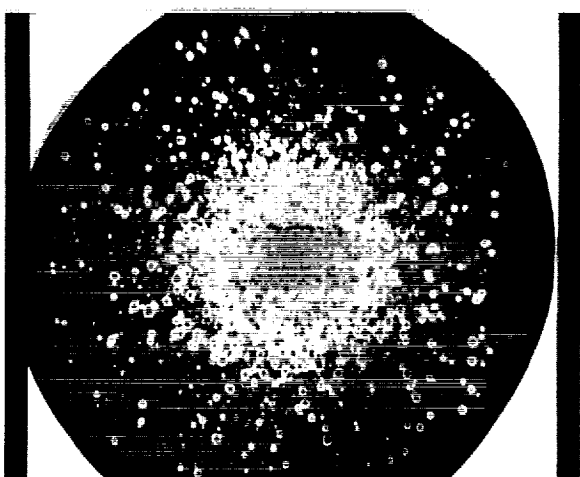
(c) $V_T = +2$ volts.

FIGURE 22-5.—A single exposure on Globular Cluster M3 with following readouts at different target mesh voltages.

mesh. However, so far as the image section is concerned, there is no reason why the target mesh voltage should not be advanced during exposure so as to keep ahead of the rise in target potential. If this is done, the resulting "swing" in target potential due to photocharges may amount to 10 volts, or more, instead of the usual 2 volts. The information capacity of the tube has been proportionately increased.

In order to read the charge patterns developed in the image section, special care must be exercised. The beam will, in fact, not land on the target if the target is more than about 2 volts positive with respect to the beam. Apparently, increased reflectivity, or secondary emission, reduces the ability of the beam to land and be modulated by the target. Also resolution suffers because the local strong fields easily deflect the slow-moving electrons of the reading beam. These difficulties are avoided by varying the potential of the target mesh in such a way that the beam "sees" a constant potential field at all times. During the scan, every picture element receives the same quantity of charge from the beam. The video signal is simply the voltage variations of the target mesh.

A verification of the above principles may be found in the following astronomical observations.

A particular image orthicon (GE 7802) is noted to have a "target cutoff voltage" of -1 volt. With the tube in the dark, the target is scanned repeatedly until it accepts no electrons at a mesh voltage of $+4$ volts. The orthicon is then exposed for 17 seconds to an image of the Globular Cluster M3 at the Cassegrain focus of the Kitt Peak 36-inch reflector. The target is then reduced to -3 volts and readout (fig. 22-5(a)). The threshold images of this exposure must have caused a potential rise of 5 volts on the membrane. Only the brightest stars show up against the background of the nucleus. A second read at -2 volts (fig. 22-5(b)) shows many fainter stars and there is a reversal of the images of the previously recorded bright stars. In a final read at $+2$ volts the beam is unable to land except in the outer regions of the cluster image where stars to fainter than 19th magnitude are recorded. Thus, in a single exposure, stars in the nucleus were recorded as well as faint peripheral images, and the wide latitude of response of the image section is demonstrated.

Conclusions

The signal-generating property of the orthicon is especially useful for solar observations. It permits the direct intensity recording of spectra, clarifies the effects of "seeing" on spectral purity near image discontinuities, and facilitates the coupling of external storage to the tube. With external storage the signal can be effectively integrated to obtain a photometric accuracy of 0.1 percent.

The charge-integrating property of the orthicon is important for stellar work. A wide latitude of response for the tube has been demonstrated. Wide latitude implies that the tube should be useful for the detection of faint stars against a bright sky background.

Appendix

Description of the Camera

An image orthicon camera especially designed for astronomical applications was employed in obtaining the reported observations. Mechanical features include provision for cooling the tube to dry ice temperatures and an optical head which is a permanent part of the camera. The head includes a projector with test patterns for the alinement and calibration of the tube while on the telescope. Electrical features include direct-coupled scanning, gating, and amplifier circuits.

The solar observations were made with a bandwidth of about 5kc. Repetition rate was 15 exposures per second. The tube used for the solar work was an RCA 6474.

Stellar observations were made with the GE 7802. This tube has an MgO target, a target-to-target mesh spacing of 10 mils, and a field mesh which is located on the scanned side of the target. A raster of 2,000 lines and an equivalent television bandwidth of 80 Mc was employed. Sequential scanning prevented a loss of resolution due to the "crosstalk" between the scan fields and the image section.

Figure 22-6(a) shows the excellent uniformity of the 7802. The overall response of the tube is seen to be uniform within ±1 percent. Figure 22-6(b) shows that the beam modulation attained at optimum exposure is 65 percent.

The field mesh permits good resolution out to the very corners of the image. The standard RETMA test chart is completely resolved (fig. 22-7). To further test the resolution capability of the tube, we refer to a kinescope enlargement of a National Bureau of Standard chart (fig. 22-8). The number "4.5" corresponds to a resolution of 30 line-pairs per millimeter (or 1,500 TV lines) at the target. The crossed diagonal lines are due to the target mesh. This mesh confuses and thus limits the resolution. If one can ignore the mesh, a cutoff resolution of about 45 line-pairs is estimated.

EDGE OF TARGET
BEAM OFF
MAX. LIGHT ±1%
DARK (ZERO) ±1%
AREA USED

UNIFORMITY
(A DOUBLE EXPOSURE)

FIGURE 22-6(a).—Vertical video waveform showing uniformity of response of a particular orthicon.

i_B
i_S
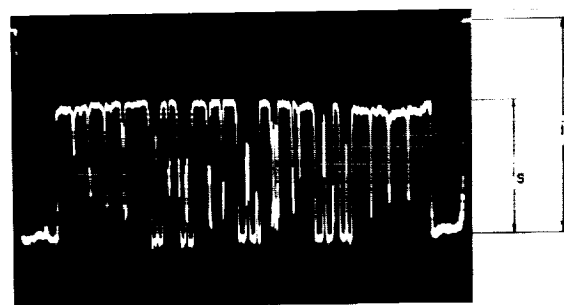
BEAM MODULATION - M

$$M = \frac{i_S}{i_B} \sim .65$$

FIGURE 22-6(b) Beam modulation.

171
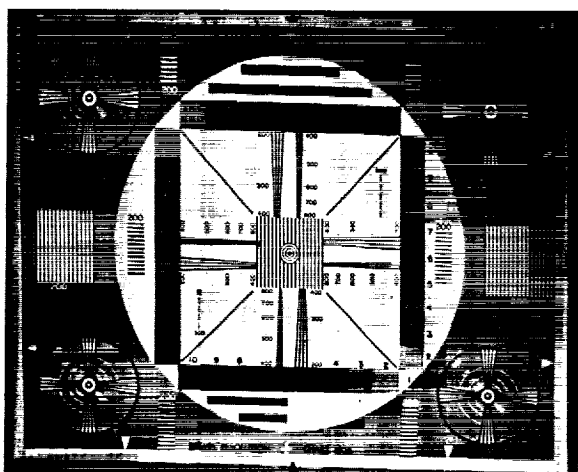
FIGURE 22-7.—Televised RETMA resolution test chart.
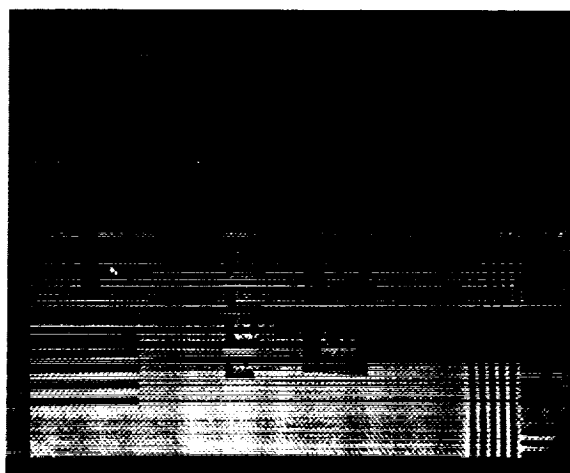
FIGURE 22-8.—Kinescope enlargement showing target mesh pattern, 2,000 scan lines, 80-Mc bandwidth.

Discussion

A. B. DOTY: In your paper, reference was made to 2,000 TV lines and 80 megacycles. Could you expand on this a little—for example, at what field rate did you achieve 2,000 lines?

W. C. LIVINGSTON: The line rate was 7.875 kc and the frame rate was 3.75 cps. These rates yield noninterlaced raster of 2,100 scan lines neglecting blanking and retrace time. The 80 Mc was referred to as an "equivalent television bandwidth." The high frequency cutoff point (—3db) of the video amplifier display channel was 10 Mc. If we assume that the standard television channel requires 8 Mc to transmit a single frame in $^1/_{30}$ second, then this same channel would have to be increased $(10 \div 8) \times (30 \div 3.75)$ = 10 times, or to 80 Mc to carry the equivalent information.

F. B. MARSHALL: Concerning the slide sequence in which we saw finally 20th-magnitude stars [figs. 22-5 (a), (b), and (c)], what is the other lower magnitude limit? What is the latitude of a single exposure, expressed in magnitudes?

W. C. LIVINGSTON: The brightest stars in the cluster are about 11 magnitude. However, the crowding of the stars in the nucleus may produce stellar images which are effectively much brighter. This complicated the measurement and was ignored. The latitude with "target feedback" has not been determined exactly, but is estimated at more than 7 magnitudes. The normal latitude of the orthicon is not much more than 2 magnitudes.

W. T. POWERS: Do you experience any difficulty with transit time in the scanning section, when running the system with target feedback?

W. C. LIVINGSTON: The target feedback scheme uses a slow scan readout of about 1-kc line rate. For full resolution, the dwell time on a picture element is about 10^{-6} seconds which is long compared with the amplifier rise time, about 10^{-7} seconds, which is in turn long compared to the electron transit time which is about $6(10^{-9})$ seconds. Transit time might be a limiting factor at standard television scan rates.

M. R. DACHS: What is the angular star size on photo plate and output of image orthicon? What would star size be with 1-microsecond exposure?

W. C. LIVINGSTON: The tests described were made at the Cassegrain focus where the scale is 17.5 seconds of arc per mm. A 1½ second of arc image, which is considered good, is crossed by 6 TV scan lines. I don't know what the image shape and size of a 1-microsecond exposure would be. I can guess that it would not have been much below a second of arc due to an imperfect mirror figure.

J. A. HYNEK: How long does it take for sky background to limit the length of an exposure?

W. C. LIVINGSTON: With a particular 5294 orthicon, a dark sky, and no filter, the background was reached in 4 seconds. A tube such as the 7802, which has a relatively high capacitance target, takes much longer to reach the sky limit.

23. THE IMAGE ORTHICON

G. G. BARTON, JR., FAST *Observatory, Northwestern University*

This paper will be presented in two parts. The first part will consider the image orthicon as an electronic device, with a suggestion toward future developments as seen from a consumer's vantage point. The second part will deal with present astronomical observations and techniques, performed at Northwestern University, FAST Observatory. As we are dealing with the astronomical side of the image orthicon, most of the reported values will be stated in stellar magnitudes. To convert these values to a sensible system, take 2.5 to the power noted as stellar magnitude, or the antilog of the product of $0.4 \times$ stellar magnitude.

I have been, under the mentorship of Dr. J. A. Hynek and the sponsorship of the Smithsonian Institution, Northwestern University, and George C. Marshall Space Flight Center, actively engaged with the application of television to astronomy for the past 3 years. During this period I have learned much about the strengths, weaknesses, and other factors affecting its application to astronomy and related fields.

This image tube is a sensitive photoelectric device with the capability of resolving, in two dimensions, points in the area defined by the accompanying optical system. As with the photocell, the image tube was thought incapable of internal integration of information until Dr. Goetze's paper. Integration or storage of information with this device is most readily accomplished with photographic film, but as the output coupling is difficult, either the resolution, speed, or ease of operation is affected and the maximum capabilities of the tube degraded. Finally, the absolute speed of an image tube system is a direct function of the speed of the recording film.

The image tube led to the development of the image scanning tube, known in its various forms as the iconoscope, vidicon, Ebicon, and image orthicon. The image orthicon, as the previously mentioned tube, utilizes the photoelectric currents from the photocathode to produce useful information. Unlike the photocell and image tube, the image orthicon can internally integrate the incoming information over a reasonable period of time and present it then on command. The output of the image conversion tube is in the form of an electrical signal and can thus be recorded or displayed by a number of devices singly or simultaneously.

The image orthicon is not a perfect device, but during our investigations and experiments we have possibly determined the next step in the evolutionary path which will perhaps overcome the present difficulties and deficiencies.

Though many readers are sophisticates of image orthicon technology, I should like to briefly review the electrical operation of this tube. The image orthicon is in reality two tubes in one envelope: the image tube and the orthicon, or scanning and readout tube. The image section operates on the same principles as the image tube, with the exception that the photoelectrons from the semitransparent photocathode are accelerated toward the target by 600 volts instead of 10 to 50 kv. As the electrons impinge on the target, they generate approximately 6 to 10 secondary electrons which are removed by the target grid. The target is fabricated mainly from very thin glass sheets or ultrathin MgO films. After the secondary electrons are ejected from the target, the target then has a pattern of positive charges remaining on it in the same geometrical pattern as the optical pattern falling on the photocathode. To extract the information, the orthicon section now scans the target with a low-current, low-velocity, finely focused beam of electrons. These electrons are normally totally reflected from the blank target, return to the output dynode system, and are amplified in number by secondary emmission from the dynodes.

Reflection at the target is caused by charging the insulating target to a negative potential by the collection of scanning electrons. When sufficient scanning electrons have been collected

by the target to produce a negative potential equal to the energy of the highest velocity electrons in the scanning beam, the beam thereafter will be almost totally reflected.

When an image is projected on the photocathode, the resulting positive charge image on the target will accept electrons from the scanning beam. The scanning beam will then be diminished by an amount proportional to the charge or image at some particular position and time. The return beam is then amplified by the dynode system and appears as a signal across the load resistor.

Very shortly after the installation of the telescope and television system at Organ Pass Satellite Tracking Station in 1958, we came to the following conclusions as a result of our astronomical observations:

(a) When the system is operating at normal frame rates, a small amount of general diffuse light falling on the photocathode in addition to the optical image can improve the image orthicon sensitivity by approximately ¾ stellar magnitudes or a factor of 2.

(b) Photographic integration of the kinescope output can produce up to ¾ magnitude increase in information by improvement of signal to noise ratio.

(c) Electronic integration, that is target or beam pulsing techniques, can produce up to 5 stellar magnitudes or 100 ×, increase in recorded information. It was also noted that beam pulsing was the superior method. The image orthicon tube produces a linear integration curve with little reciprocity failure when strongly cooled. At −40 C, integration time was limited by sky fog and ambient light before tube effects became noticeable.

(d). MgO target image orthicons are by far superior to image orthicon tubes with glass targets when using integration techniques, and in the main are more sensitive by a factor of 2 stellar magnitudes or 6.25 ×. As electron conduction is the main mode of charge transfer in the MgO target, burn-in and other deleterious effects noted with glass targets are not evident.

After a suitable period, during which we completed investigations and modifications of the RCA commercial television camera chain, we were invited to Palomar Observatory, through the offices of Dr. William Baum, to run a series of observations with their 20-inch Cassegrain telescope. The results of these tests, reduced by

J. Kimmel of Palomar, showed the system's speed, on the first approximation, to be 550 × that of 103AO film. If the quantum efficiency of this film is taken as one-tenth of 1 percent, then the image orthicon tube should demonstrate a photoelectric efficiency of 55 percent. Though I consider the image orthicon tube the greatest invention since the discovery of the wheel, I am aware that the age of miracles has passed. Dr. Baum suggested that this ultrahigh speed may be due to a memory effect in the tube. To test this hypothesis, the system was moved back to Organ Pass, N. Mex., and a series of experiments performed there, using a light source approximating a star field with known differences in brightness. Within a few hours, the memory was detected. Investigating further we found the memory was due to the incapacity of the scanning system to remove all the information from the target.

During the experiments, we also allowed extraneous light to fall on the photocathode to simulate skylight. When this light, as in the case mentioned a few minutes ago, falls on the photocathode, greater sensitivity was noted. The sensitivity increased by a factor 2.5 magnitude or 10, at which point the system saturated and the output signal deteriorated due to noise.

Subsequent tests lead us to the conclusion that the speed of the system was less than 550 × 103AO and thus can be considered one of those fortuitous errors that open new vistas. If we now equate these various factors, we can obtain a reasonably good idea as to the subtleties of image orthicon tube operation. We noted an increase in sensitivity of 10 when the photocathode was illuminated by the proper intensity of extraneous light. This leads us to a conclusion that only 10 percent of the information stored on the target during normal operation is removed at low light levels. Under these conditions we may expect the following mechanism to occur. Let us assume that 100 units of information per image is placed on the target and one integration period later the beam sweeps off one-tenth of that information. During the second integration period an additional 100 units of information is collected and added to the 90 units remaining from integration period 1. When the target is now swept or scanned, 10 percent of this information is removed, or in effect 19 percent of the information arriving in one integration period. This mechanism operates until equilibrium is attained where the target is

174

storing 10 × the information arriving in one integration period, and the beam is sweeping 10 percent of this or 100 percent of the information arriving in one integration period. This is, of course, a simplification and to more exactly determine the complete mechanism of memory and equilibrium, one would have to carry out a detailed analysis knowing all parameters effecting beam modulation.

These experiments led ultimately to hypersensitization techniques which are briefly outlined as follows. We know the electron scanning beam is modulated by a positive charge appearing on the target and only 10 percent of the electron in the beam interact with the target. It is also known that when the photocathode is illuminated by extraneous light, that the interaction percentage can be increased by a factor of 9, under optimum conditions. This is due to an increased general positive charge generated on the target by the extraneous light. The physical basis of this hypersensitivity is, the target is normally negatively charged to approximately −4 to −5 volts by the electrons in the scanning beam. As the scanning beam is thermionically generated, the energies of the electrons emitted fall on a Maxwellian curve. Therefore the insulating target will assume a charge as great as the highest energy electrons impinging on it. The scanning beam, to see the positive image, must penetrate this negative barrier which repels all but the most energetic electrons. Returning the bulk, that is 90 percent as noise.

To overcome this barrier, hypersensitization utilized just previous to readout, an additional positive bias on the target mesh to lower the barrier and a positive bias on grid 5 to increase the beam velocity. When this technique is used, the number of electrons capable of penetrating the barrier potential can be increased for a factor of 9.

Unfortunately hypersensitization is a one-shot effect and the target must be discharged and relaxed for a short time before the next integration period. These past few paragraphs have outlined our philosophy on the next proposed evolutionary stage of image orthicon development. We propose that the utilization of a monokinetic or monochromatic scanning beam will overcome the major difficulties now facing the image orthicon in astronomical or other scientific applications. The application of a monochromatic scanning beam to the image orthicon tube should produce the following results for reasons to be shortly set forth. (a). One should expect a scanning efficiency increase of a factor of 9. (b). Dynamic range or gray scale should be also increased by a factor of 9. (c). Resolution should be increased by a factor of 4. The first two statements are based on experimental results obtained through hypersensitization studies.

We noted a few moments ago that hypersensitization can increase the electron barrier penetration by a factor of 9. It is quite possible that a monochromatic beam can produce the same results in a continuous fashion. If the velocity spread in the scanning beam is reduced from 4 or 5 volts to one-tenth of a volt, the negative barrier existing on the target is reduced accordingly. When a positive charge appears on the target, it will no longer be buried in the 4- or 5-volt negative potential, but will only have to overcome a one-tenth of a volt barrier. With a monochromatic beam the positive image charge should remain the same as in the present tube, but will be enhanced in relation to the much smaller barrier. As the beam scans across the positive image, all electrons in the beam will have a chance to see the charge and complete neutralization can be expected. Under these conditions the beam current can be set to be completely absorbed by the brightest image and reduced proportionately by the fainter images. We may therefore expect such a tube to demonstrate beam modulation in excess of 90 percent as against the present 10 percent modulation.

The dynamic range of the present tube is, according to our past observations, approximately 2.5 stellar magnitudes wide. When an image exceeds this range it will expand in size until discharge equilibrium is attained. We claim that a monochromatic beam will expand the dynamic range by an additional 2.5 magnitudes, as the present images below threshold are not seen due to the present 1 to 9 signal-to-noise ratio. If the modulation is increased by 9, the signal-to-noise ratio will be increased by the same factor. The present upper limit of the dynamic range should remain reasonably constant while the lower limit is extended to images 2.5 magnitudes fainter.

The resolution increase factor of 4 has been intuitively determined, as the monochromatic beam should be capable of much finer and more delicate focus at the target. There should be a decrease in longitudinal chromatic aberration of the electron beam that effects beam transit time back to the dynodes and one should expect less

175

Image Orthicon   Monochromatic Electron Gun
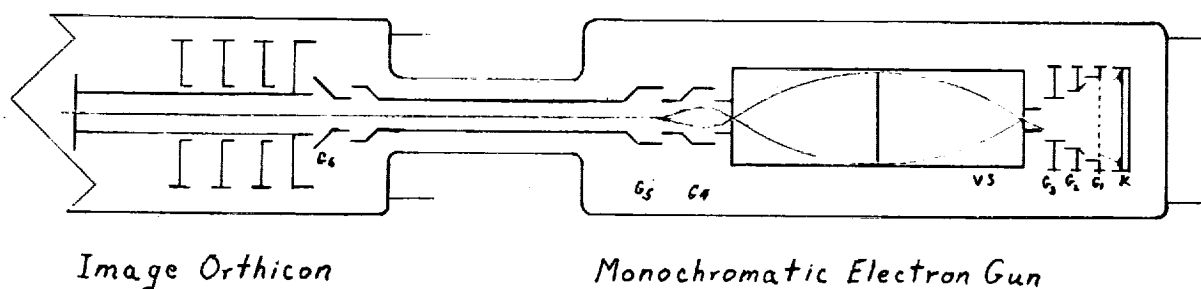
FIGURE 23-1

random scattering at the target. There are opponents to this theory, and their criticism and philosophies are to be as readily honored or rejected as mine.

Before launching into a description of a monochromatic gun for use with the image orthicon, I desire to impress upon you that we do not claim any originality as to the use of such a device, but claim only the efficacy of such a device and a probable first step in the construction of a workable gun.

I shall now outline an approximate design and structure of such a gun. As you will note on viewing the drawing of this gun, it is not an integral part of the image orthicon proper. (See fig. 23-1.) It has been placed behind the tube for several reasons. The first reason is to obviate the necessity of reengineering the image orthicon. Those of you concerned with the manufacture of these tubes can readily appreciate the engineering difficulties arising from even minor modifications. As the present cathode and exhaust port are in line, it is immediately apparent that a straight-line construction would be the simplest. A magnetic velocity selector type of monochromator requires an axial field of approximately 10 Gauss at these velocities. This field, though small, would interfere with the present focusing field and perhaps degrade performance of the image

orthicon if the gun were incorporated in the present tube envelope. Finally, with the separation of the two components shown, a split-tube socket can be used to connect into the present orthicon base connections. The gun operates on the following principles: The cathode K on the right is in the form of an annulus of $\frac{1}{2}$-inch radius, which generates a conical shell of electrons which are in turn controlled by grid 1 (G). As the cathode and velocity selector both operate at or near ground potential, the shape, separation, and potential of grids 1, 2, and 3 have to be carefully determined to focus the electron beam at the entrance aperture of the velocity selector. The velocity selector (vs) has an entrance and exit aperture on its axis and an annular aperture in its center. The radius of curvature of the chosen electron velocity is adjusted by the axial magnitude field so it will be equal to $\frac{1}{2}$ the radius of the annulus. After the electrons have passed through the annulus, they are magnetically refocused on the exit aperture and allowed to drift into the field between the velocity selector and G-4. G-4, G-5, and G-6 are used to focus, collimate, and finally decelerate the electron beam as it passed into the original cathode housing. With an arrangement such as this, no light from the cathode can fall on the target and the dynodes may be cooled without cooling the cathode.

Discussion

R. H. HARDIE: I would like to hear whether any of our industrial colleagues consider the monochromatic beam feasible, and whether work on such is in progress or being planned.

G. G. BARTON, Jr.: A representative of Westinghouse answered that such a gun has been attempted, but with little success, due to the low beam current generated by the device.

J. WATER: Can hypersensitization, by exposure to weak diffused light, be used at normal target scan ratios?

G. G. BARTON, Jr.: Hypersensitization can be effected by low light level illumination of the photocathode by secondary sources at any chosen integration interval. This method of hypersensitization has the disadvantage of having to balance the illumination due to the primary source with that being

generated by the secondary source in order to obtain the optimum gain. It is suggested that should you wish to record or view low level illumination for periods up to several seconds, Grid 5 should be modulated with a positive going sawtooth wave with a period of several seconds. This method will produce much cleaner readout and higher gain with little effect on beam signal-to-noise ratio. The disadvantage of this method is the necessity of discharging the target after each sawtooth reaches maximum possible potential.

W. F. NIKLAS: Dr. Livingston reported a resolution value of 45 lines/mm. You mentioned a desired improvement by a factor of 4. Do you desire an ultimate resolution of 180 lines/mm.?

G. G. BARTON, Jr.: As we have been dealing with low level illumination, I have based my thinking on a factor of 10 line-pairs/mm. It was most gratifying to hear that Dr. Livingston was able to obtain the value of 45 line-pairs/mm without going to special devices. It has been my experience, when working with threshold images, that any improvement of resolution, when using standard I.O. tubes, causes a decrease in sensitivity. This is, of course, the story connected with all light sensing systems, but it is my contention that the incorporation of the monochromatic gun will allow us to reach approximately 40 line-pairs/mm without compromising speed.

24. NUCLEAR TRACK PHOTOGRAPHY*

G. T. Reynolds, D. B. Scarl, R. A. Swanson,** J. R. Waters, and R. A. Zdanis, Palmer Physical Laboratory, Princeton University

Recent applications of image intensifier systems, to problems involving the photography of ionizing particles in scintillation chambers, have served to emphasize the improvements necessary in the image intensifier before this technique can become a reliable source of important contributions to nuclear physics. Although impressive and confident claims are often presented by industrial laboratories engaged in producing image intensifiers relating to cathode efficiency, background noise, overall gain, resolution, distortion, etc., experience of users proves that very seldom indeed are all of these accomplishments available simultaneously in a given tube of useful dimensions.

Even so it has been possible, at considerable expense, for several nuclear physics groups to set up scintillation chamber, image intensifier systems capable of photographing minimum ionizing tracks. Such a system, employed by the Princeton University group, is shown in figure 24-1. The filament scintillator was butted directly against the end window of the first image tube. This tube was a two-stage RCA electrostatic focusing type C 70050, end window thickness 0.025 inch and gain approximately 3,000, for an overall voltage of 25 Kev. The first tube was coupled by a pair of f/1.9 lenses to an RCA two-stage intensifier orthicon. The final track presentation was made on the screen of a kinescope, photographed conventionally. The decision to use presentation by means of a closed television system technique was based on several factors. In the first place, the video amplifier of the system should provide a gain factor of the order of 50 to 100 before noise begins to limit. Presentation on the kinescope provides a valuable ease of viewing and noting immediately the effect of

changes in the system without the need of photography or viewing in a lighttight environment. Furthermore, the output of the orthicon is suitable for data storage or processing devices without the need of an intermediate photography stage. An end view of the filament chamber is shown in figure 24-2. These filaments which were supplied by Pilot Chemical Co., are 0.029 inch +0.001 inch in diameter and are individually suspended in a nylon net to prevent serious contact between filaments. The chamber was 2 inches in diameter and 3 inches long. Some examples of tracks obtained with this system are shown in figure 24-3. The overall gain of the system, exclusive of the effective gain of the video amplifier, was estimated to be $9 \times 10^4 \pm 35$ percent.

The system described above was assembled in order to investigate the capture of μ^- mesons in carbon according to the following reaction:

$$\mu^- + C^{12} \rightarrow B^{12} + \nu \qquad (1)$$
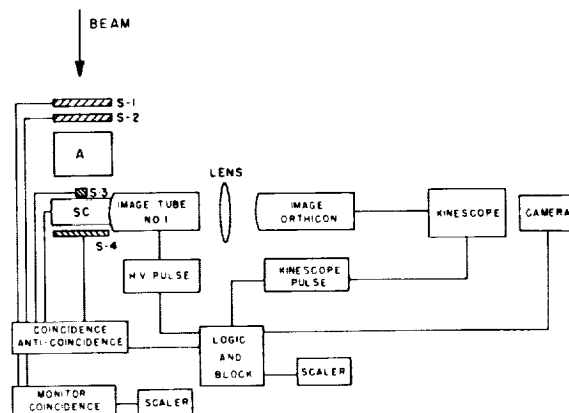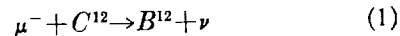
Figure 24-1.—Schematic of intensifier system used to photograph cosmic ray μ mesons.

179
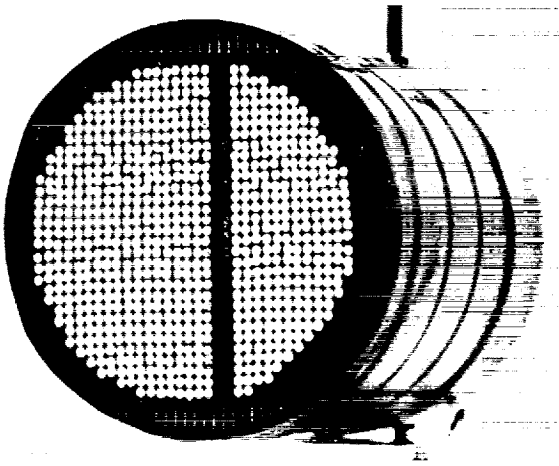
FIGURE 24-2.—Filament scintillation chamber used in the system of Figure 1.

The B^{12} decays with a mean life of approximately 30 milliseconds according to the reaction:

$$B^{12} \rightarrow C^{12} + e + \bar{\nu} \qquad (2)$$
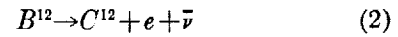
There are two points of interest in this study. First, a measure of the branching ratio of μ decay to μ capture to the ground state of B^{12} (reaction (1)) affords a comparison between the μ-nucleon coupling constant and the β-decay coupling constant. Previous efforts to measure this have led to conflicting results.[1-6] Secondly, the helicity of the neutrino can be measured as follows: When the μ^- mesons arise from π^- meson decay in flight according to

$$\pi^- \rightarrow \mu^- + \bar{\nu} \qquad (3)$$

conservation of angular momentum requires a specific relationship between the helicity (relation
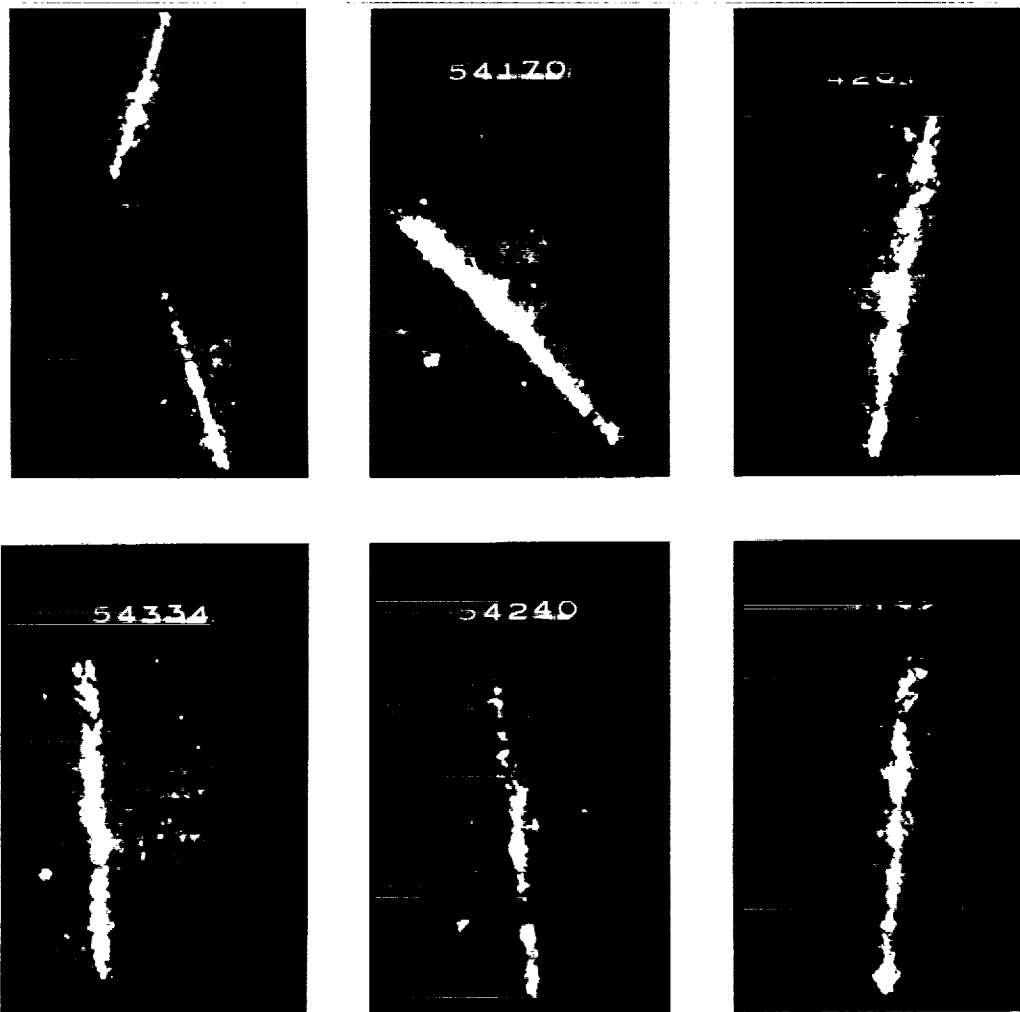
FIGURE 24-3.—Examples of minimum ionizing cosmic ray μ mesons.

180
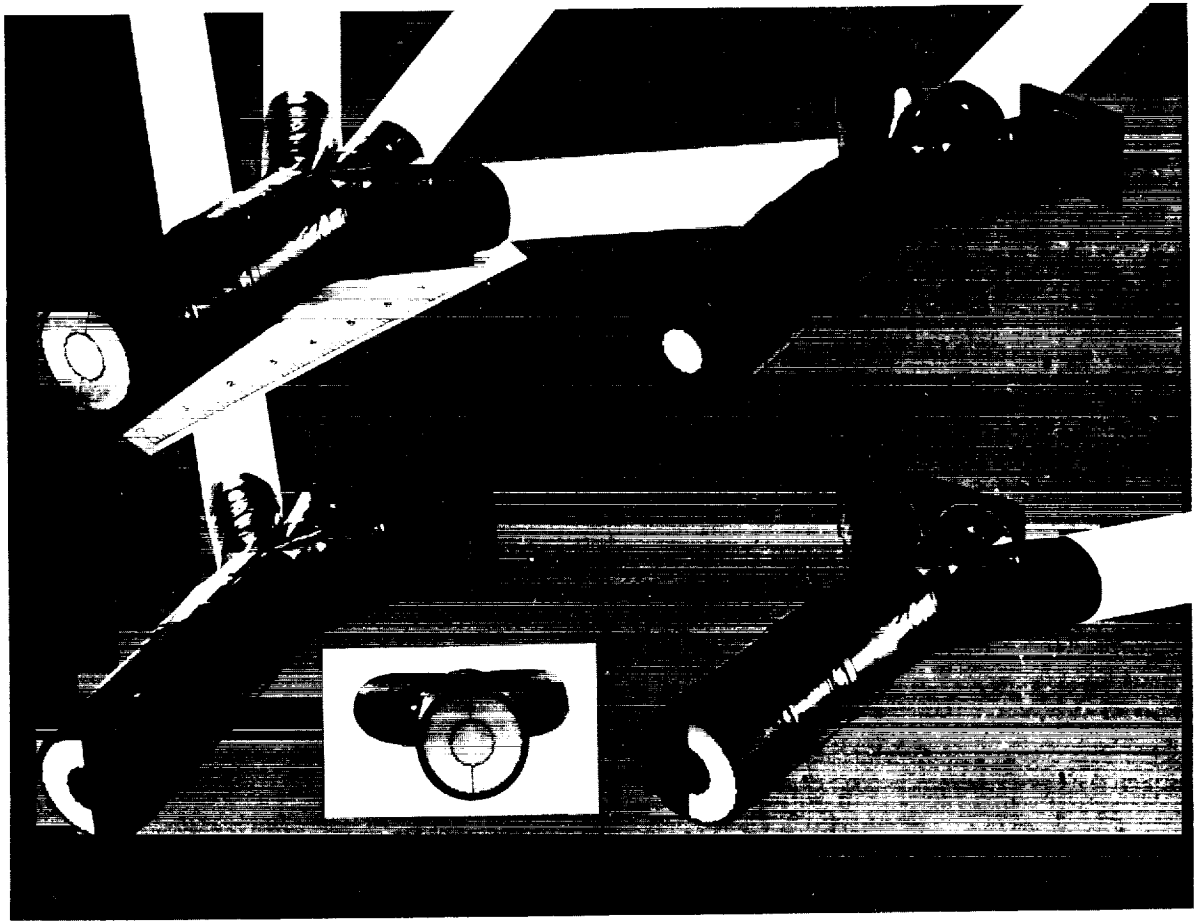
FIGURE 24-4.—Filament chamber used in the $\mu-$ capture experiment.

between linear momentum and spin) of the μ^- and that of the $\bar{\nu}$. The μ^- capture, according to reaction (1), results in the polarization of the B^{12} in a specific sense depending on the helicity of the μ^-. This sense can be determined by observing the asymmetry of the subsequent β-decay of B^{12}.[7 8] To detect this asymmetry it is necessary to prevent depolarization of the B^{12} prior to its decay. Previous attempts to detect the B^{12} polarization[9-11] have led to inconclusive results, possibly due to depolarization as a result of collisions with atomic magnetic fields. We estimate these fields to be the order of several thousands of gauss, and so provided an external field of 25,000 gauss in the region of the B^{12} formation and decay to attempt to "lock in" the B^{12} spin.

The first phase of the μ^- capture experiment (branching ratio) has been performed. The second phase (helicity) has not been run as yet, but the performance of the system with the magnetic field has been observed and it will be described.

The C^{12} is provided in the plastic scintillator. The chamber used in the experiment is shown in figure 24-4. It is divided into three sections, optically insulated. The separate sections are viewed at one end by separate photomultipliers by means of the light pipes shown, and the chamber as a whole is viewed at the other end by the image intensifier system. Due to an accident, the image tube used to obtain the tracks shown in figure 24-3 was not available for the experiment. An RCA three-stage tube (C 73491) was used in conjunction with a single-stage intensifier orthicon (C 74036) and the system operated as follows. When the scintillation counter telescope, including the three counters that constitute the chamber, indicated a μ^- had stopped in the center section of the chamber, the counter system determined whether or not the μ^- decayed in a gate of 10 μseconds. (The mean life for μ decay is $\sim$ 2 μsec.) If the μ did not decay, the image of the chamber was shifted by magnetic deflecting coils at the output phosphor of the intensifier tube. The image was

181
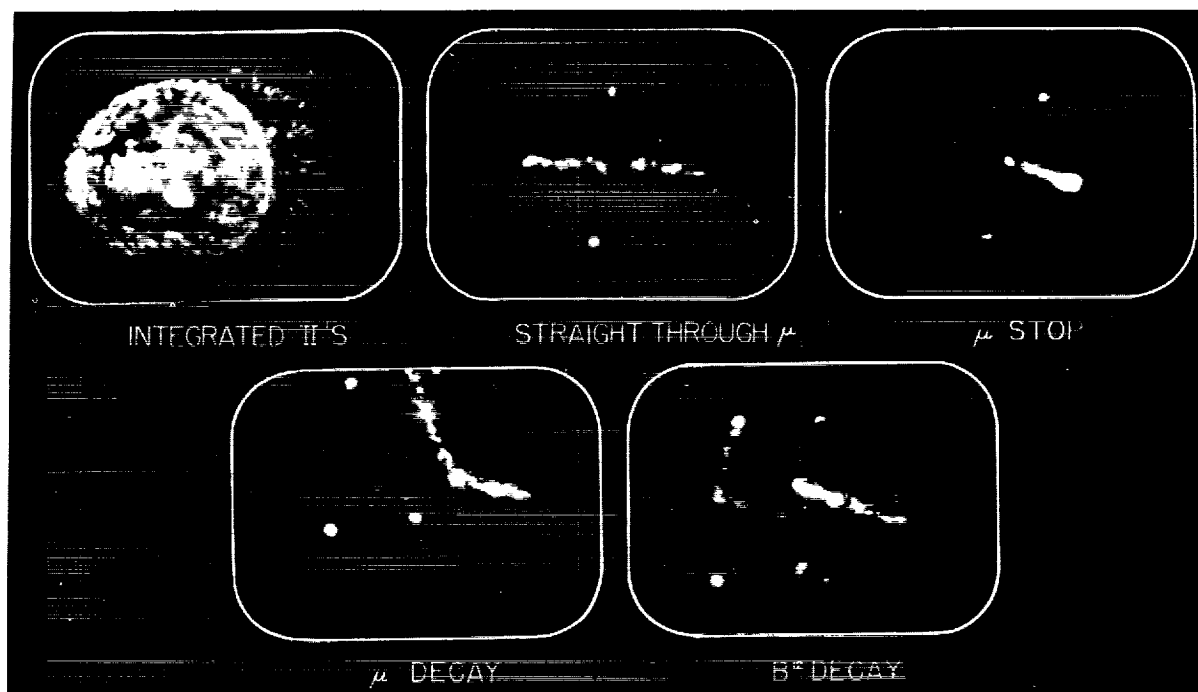
FIGURE 24-5.—Examples of π, μ, μ stop, μ decay, and B^{12} decay tracks obtained in the $\mu-$ experiment.

held in the deflected position for an interval 3 to 60 milliseconds following the μ stopping. If in this interval, the counter system indicated a B^{12} decay (the electron of reaction (2) has an upper energy limit of $\sim$ 13 Mev), then the orthicon target was scanned and the entire event presented on the kinescope screen for photographing. In order to determine that the decay electron seen in the displaced image did in fact originate from
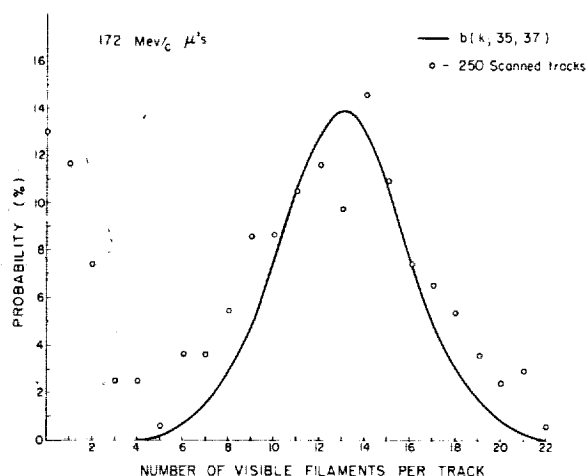
FIGURE 24-6.—Distribution of the number of filaments observed per track for straight through μ's.

the end of the stopping μ^- track, two filaments of the chamber were lighted continuously with small bulbs attached to long thin glass light pipes to serve as fiducial marks. Since the decay in the displaced image was known to occur in an interval of 3 to 60 milliseconds after the μ stop, no confusion resulted from μ decays. Since the fiducial marks serve to define the region of the decay track and the end of the μ track, background tracks are not a problem. Typical results are shown in figure 24-5. The data are currently being analyzed, but remarks can be made on the performance of the system. The estimated overall gain of the system is $5 \times 10^4 \pm 35$ percent exclusive of the gain of the video amplifier stage. Cosmic ray tracks appeared "good" in preliminary runs, but the tracks obtained in the μ capture run were poor. A detailed analysis of 250 straight through μ tracks was made in order to determine the nature of the difficulty and the results are shown in figure 24-6. These particles traversed, on the average, 35 filaments. In each case the number of filaments appearing as spots of light was counted. If a filament is considered either "off" or "on," and if the filaments are independent, then with p as the probability of an individual filament being lit, and $q=1-p$, the probability

182

of seeing k filaments lit when n are traversed is given by the binomial distribution

$$b(k; n, p) = \frac{n!}{(n-k)!k!} p^k q^{n-k}$$

The circles in figure 24–6 are the observed distribution and the solid line corresponds to $p=0.37$. Thus we conclude that with the system used, the probability of seeing a filament through which a particle has passed is only 0.37.

If now we assume that the emission of electrons from the photocathode is Poisson, and that the system is capable of viewing a single electron emitted from the cathode, then from the results above the probability of seeing no electron is

$$0.63 = P(O) = \frac{\lambda^0}{O!} e^{-\lambda}$$

from which the average number of photoelectrons per filament is $\lambda=0.54$. If one uses the usually accepted figures for the efficiency of the plastic scintillator, the attenuation in the filament, and the measured efficiency of the cathode, then the average number of electrons per filament is expected to be 3, in marked disagreement with the number obtained for λ above. This makes it necessary to conclude that some combination of the following possibilities is operating:

  a. The efficiency of the scintillator material is not as high as previous measurements indicate.

  b. The attenuation of the filament scintillators is worse than previous measurements indicate.

  c. The first cathode efficiency is low when operated in the fringe magnetic fields encountered.

  d. The system (including film) results in only a fraction of the single electrons being photographed.

  e. The system in fact requires the order of 3 or 4 electrons per filament in order to record.

Subsequent checks on the system indicate that the last of these possibilities is the most reasonable. Evidently the system yielding the tracks of figure 24–3 was in itself marginal, so that the slightly inferior system used in replacement (with overall gain, exclusive of video amplifier, $\sim 5 \times 10^4$) was not capable of giving really good tracks on a statistical basis. This serves to emphasize the difficulty and expense encountered in achieving an adequate intensifier system to perform useful nuclear physics.

In preparation for using the chamber in the 25,000 gauss field described above, studies were made coupling a glass light pipe array to the filament chamber. In spite of initial optimism on the part of the commercial laboratories, it proved impossible to purchase a satisfactory lightpipe. Therefore we fabricated one in our laboratory in the form of a bundle of individual glass fibers whose diameters matched those of the scintillator filaments. Each scintillator filament was coupled to a glass fiber with a short, thin-walled aluminum sleeve. The fibers were 18 inches long, inner core index 1.6, clad (for mechanical protection) in glass of index 1.4. Measurements showed that 70 percent of the light from the scintillator gets into the glass, of which 55 percent is transmitted 18 inches. Thus, approximately 65 percent of the light is lost by the coupling. Cosmic ray tracks photographed with this arrangement are shown in figure 24–7.

There are other experiments that have characteristics extremely well suited to the scintillation chamber, but in view of the expense and marginal performance of image tubes available in the United States, we are planning to perform them by means of spark chambers. We have, however, an RCA C 70035 tube with an 8-inch cathode and 0.040-inch-thick end window which was originally intended for these experiments. This tube has been incorporated in a device that has performed very well as a beam detector for high-energy external accelerator beams of π mesons and protons. A filament scintillation chamber 5 inches in diameter and $1\frac{1}{4}$ inches long was mounted on the face of the image tube. In one-half of the chamber the filaments were close packed (not separated by nylon threads as were those in the chambers described above), and in the other half the filaments were placed individually in loose-fitting thin-walled (0.0015 inch) aluminum tubing and then stacked. The large cathode tube output demagnifies by a factor of 6. This tube was lens coupled to the single-stage intensifier orthicon C 74036 and the system placed in the beam of 735 Mev/c π mesons and protons at the Brookhaven Laboratory Cosmotron. The image tubes were mounted in $\frac{1}{4}$-inch wall soft iron pipes and no difficulty was experienced with magnetic fringe fields. The advantage of such a system in beam detection, compared to methods used to date, consists in the good space resolution (about
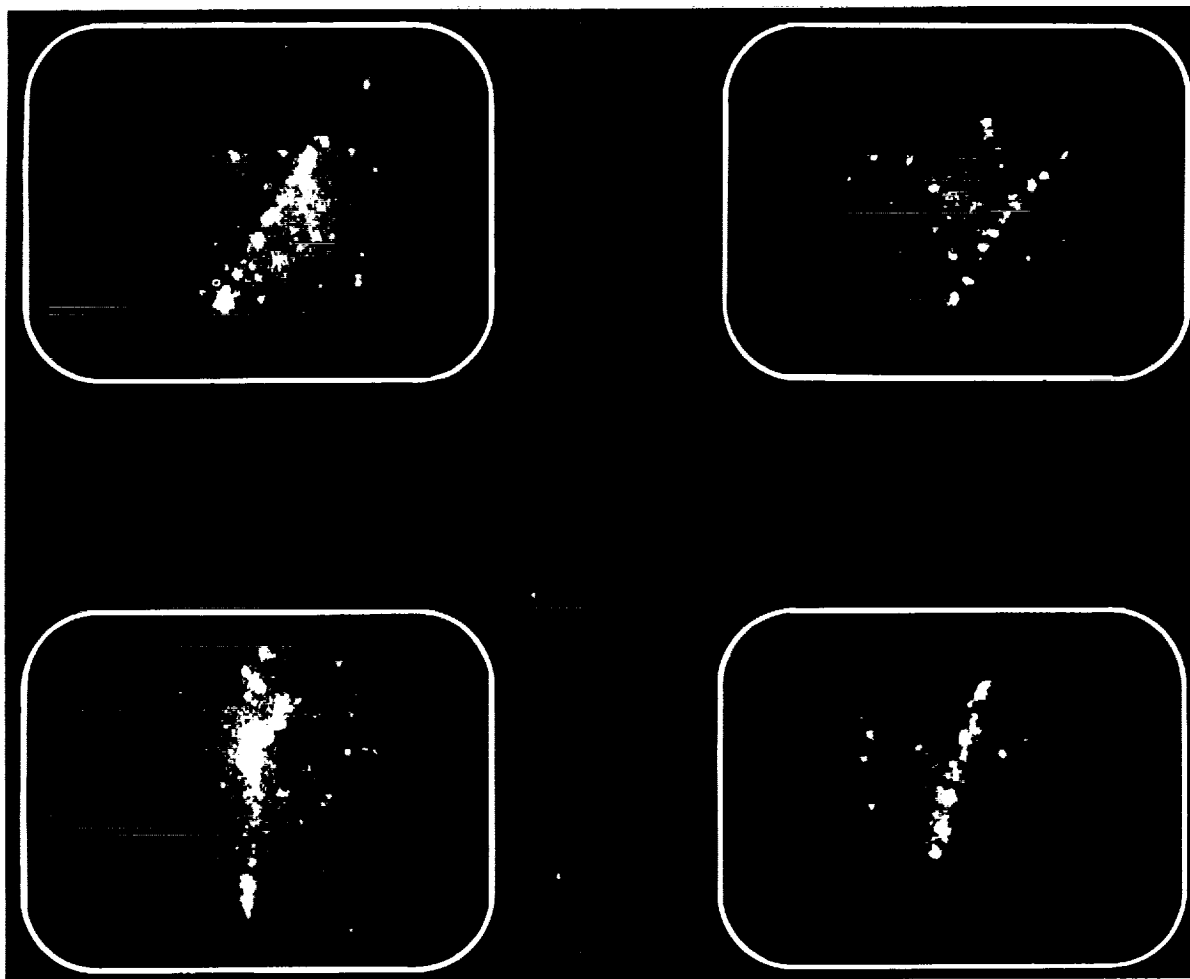
FIGURE 24-7.—Tracks obtained with the chamber coupled to the first cathode by means of an 18-inch glass light pipe.

1 mm); the ability to see each particle in a weak beam (each particle, going along the length of the filament, gives approximatey 30 times the light given by a minimum ionizing particle at right angles to the axis of the chamber); and in the fact that the TV system allows remote and continuous viewing. This latter feature makes it possible to view continuously the effects of various changes in the magnets used to focus the beam. Some results of this application are shown in figures 24-8 through 24-11. In figures 24-8 and 24-9 a weak π beam is shown. Figures 24-10 and 24-11 show the effect on beam profile of changing the current in one of the quadrupole pairs used in focusing. It is clear that there is light leakage from one filament to another in the close packed half of the chamber (right-hand half in the view). It is not clear that the filaments in the aluminum tubing pipe light as effectively

as the nylon-suspended filaments used in the μ^- capture work. This point is being checked in a later run, which will be reported elsewhere.

The following remarks indicate the important features of an image intensifier system that would prove very useful in nuclear physics work. They are based on the recent successes achieved in British laboratories in constucting high-performance transmission secondary electron tubes (TSEM). This tube was first provided, in a practical operating sense, by Wilcock at Imperial College, London, and is now available from a British manufacturer at a reasonable price. In itself it is capable of providing sufficient gain for the photography of single electrons, and has good noise characteristics. Its main limitation is in the relatively small area cathode, a feature that is being improved. It is relatively easily gated. Thus, a system for a typical nuclear physics

184
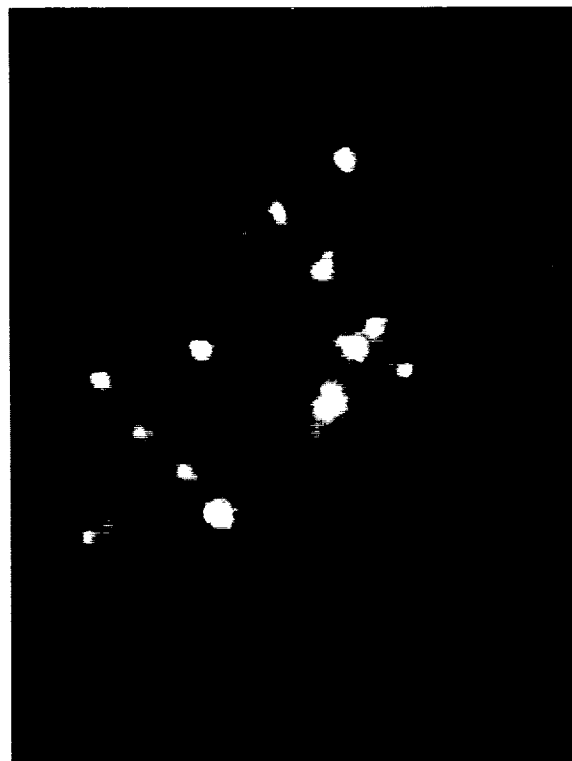
FIGURES 24-8, 24-9.—Profile of a low intensity π beam.
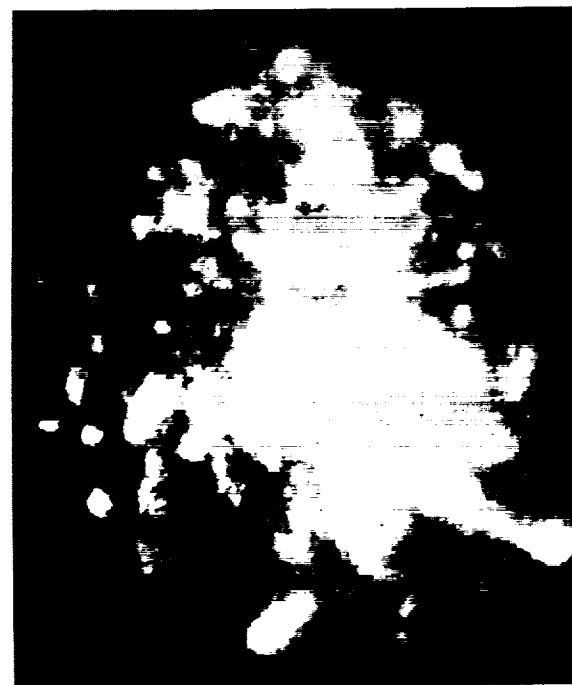
FIGURES 24-10, 24-11.—Effect of quadrupole focusing on π, p beam profile.

185

application could be constructed using this as a second tube, lens coupled to a high resolution conventional sensitive orthicon, such as is available in the GE–GL 7967. The first tube of the system should have a large area cathode of quantum efficiency at least 15 percent, preferably mounted on a fiber optics window (for which there has as yet been no practical success achieved). The output of this first stage should be demagnified to the order of 1 inch or so. With such an arrangement the TSEM could be gated to provide the short time resolution required. The phosphor of the first stage should have a short decay, ~ 1 μsec, and not show the long-life components that hamper the phosphors so far provided. In view of the light loss encountered in lens coupling, a better arrangement is obviously to have the first tube consist of two stages in the same envelope, with the second stage provided with a low voltage gating grid.

An important consideration is first-stage noise. Although some claims have been made for low noise, practical experience shows that this is often a limiting effect. It is important that, at the operating voltage required to give the advertised gains, the noise meet the following considerations. If the cathode noise emission is N electrons per cm^2 per second, and if the magnification factor is one-eighth, say, then at the output stage there are 64 N electrons per cm^2 per sec. If the sensitive gating time is 30 milliseconds (i.e. a TV frame interval), then there appear on the photograph $64 \times 3 \times 10^{-2} \times N$ light spots per cm^2. If the number that can be tolerated is, say, two spots per cm^2, then N must be ~ 1, which is clearly difficult to achieve. If a previous gating stage is gated for 1 millisecond, then N can be 30. If the gating is for 10 microseconds, then N can be several thousand. A relation between N and a more conventional noise designation can be made as follows. Suppose a tube with 1:1 magnification is operating at 10 Kev, with an output phosphor of 5 percent efficiency. Then N electrons per cm^2 per sec from the cathode will result in

$$N \times 10^4 \times 5 \times 10^{-2} \times 1.6 \times 10^{-19} = 8 \ N \times 10^{-17}$$
$$watts/cm^2$$

Thus, if the noise figure is 10^{-12} watts/cm^2, the N implied is $\sim 10^4/cm^2/sec$.

Discussion

A. B. DOTY: You mentioned an 8-inch tube. Can you identify this tube by number and manufacture?

G. T. REYNOLDS: The 8-inch diameter image intensifier tube referred to in the paper was manufactured by RCA, Lancaster, Pa. The tube designation is C70035.

References

1. GODFREY, T. N. K.: Phys. Rev., vol. 92, 1953, p. 512.
2. LOVE, W., MARDER, S., NADELHAFT, I., SIEGEL, R., and TAYLOR, A. E.: Bul. Am. Phys. Soc., vol. 4, 1959, p. 81.
3. FETKOVICH, G., FIELDS, T. H., and McILWAIN, R. L.: Bul. Am. Phys. Soc., vol. 4, 1959, p. 81.
4. ARGO, H. V., HARRISON, F. B., KRUSE, H. W., and McGUIRE, A. D.: Phys. Rev., vol. 114, 1959, p. 626.
5. FLAMAND, G., and FORD, K. W.: Phys. Rev., vol. 116, 1959, p. 1591.
6. MAIER, E. J., BLOCH, B. L., EDELSTEIN, R. M., and SIEGEL, R. T.: Phys. Rev. Letters, vol. 6, 1961, p. 417.
7. WU, C. S., AMBLER, E., HAYWARD, R. W., HOPPES, D. D., and HUDSON, R. P.: Phys. Rev., vol. 105, 1957, 1413.
8. JACKSON, J. D., TREIMAN, S. B., and WYLD. H. W., JR.: Phys. Rev., vol. 107, 1957, p. 327.
9. LOVE, W. A., MARDER, S., NADELHAFT, I., SIEGEL, R., and TAYLOR, A. E.: Phys. Rev. Letters, vol. 2, 1959, p. 107.
10. LOVE, W. A., MARDER, S., NADELHAFT, I., and SIEGEL, R. T.: Phys. Rev. Letters, vol. 4, 1960, p. 382.
11. BLOCH, B. L., Rep. NYO 9280, Carnegie Institute of Technology, November 1960.

25. A REPORT ON THE IMAGE ORTHICON USING SLOW READOUT

J. H. DeWitt, *Dyer Observatory, Vanderbilt University*

Prior to the development of the magnesium oxide target for the image orthicon by Wargo, Hannam, and Day, our work was directed toward the use of glass target tubes in planetary photography. Two developments have made it possible to look at the image orthicon as a contender in the field of amplification of light at very low levels. The magnesium oxide target, which has a thickness of approximately ten-millionths of an inch, has the property, when cooled to a reasonably low temperature, of storing an electronic image over a period of tens of minutes without appreciable deterioration. The second development is the practical manufacture and utilization of the trialkali photocathode in the image orthicon tube. This photocathode shows a sensitivity improvement of about 3.5 to 1 at 4,300 AU over the regular S-10 photocathode. It also has a remarkable sensitivity in the red region above 6,000 AU.

Under a National Science Foundation grant, our work has been directed toward the development of practical equipment which could be used day by day in an observatory, and which would not require the services of personnel other than the astronomer and an electronics technician. It is felt that this objective in a large measure has been achieved. Although it has proved that the use of the slow scan technique does not improve directly signal-to-beam noise ratio, a number of important results ensue from the use of slow readout which indicate that such a system is the correct one to use in astronomical applications. Some of the advantages of slow readout are as follows:

(1) Circuits have been designed using degenerative beam control which automatically compensate certain deleterious effects in the image orthicon and which permit an improvement in signal-to-noise ratio of approximately 2-1. These methods would be difficult of application to a fast readout system.

(2) The band width (100 kc) employed renders magnetic data storage much easier of accomplishment than with fast readout.

(3) The beam current required to discharge a given spot on the target is reduced in a ratio of 100-1 or more.

(4) The kinescope reproducing the picture in the slow scan system operates at low beam current which improves definition.

(5) Photography of the kinescope is simplified. Most pictures are taken at f/8 with tri-X plates.

(6) With slow readout, the camera and kinescope deflection coils are connected directly in series so that once the picture dimensions are established, there is little change in aspect or linearity with tube deterioration.

There are advantages offered by a signal-producing tube system which merit its consideration for use in many astronomical problems. The equipment which has been developed utilizes a camera which weighs a total of 40 pounds, including the cooling unit. When it is attached to the output of the telescope, information can be fed by cable to the operating and control equipment in a lighted and heated room. The entire electronic equipment can be put together, using parts and tubes which are available from manufacturers today.

Two scanning techniques are utilized. Under fast scan conditions the system becomes a regular closed-circuit television system, having approximately 500 lines at 30 noninterlaced pictures per second. This fast system is very useful in alining the telescope on star fields or other objects which are to be studied. The sensitivity under these conditions is such that with a 24-inch reflector (f/16) an object such as the Ring Nebula in Lyra can just be seen. When sources of weak light are to be studied, the equipment is changed to the slow scan condition. In this condition

scanning is at the rate of 120 lines per second. The picture can be read out at a vertical rate of one sweep in 4 seconds. A pushbutton permits a second readout to be displaced by one-half line which makes it possible to record pictures having 960 lines.

The magnesium oxide target image orthicon has been found to have in effect two modes of response to incident light. This can be explained most easily by assuming that a certain time is required for the target to become conductive, after which time electrons from the reading beam find their way through the target quite easily and emerge as secondaries on the mesh side. It appears that a rigorous theory of this phenomenon is not forthcoming at the present time, for it has to do with conduction through a crystalline structure which in itself forms a very thin film. If the following assumptions (which may or may not be rigorously correct) are made, then the effects which are observed are explained. It is assumed that when primary electrons first strike the target, the secondaries which are emitted come from the crystal lattice on the side of the target from which the primary electrons arrived. In time, a conducting path through the target is developed. Before this conducting path reaches the opposite side of the target, no information can be extracted even though the reading beam is allowed to scan continuously. Once the conducting path gets through to the back side of the target, then its positive charge attracts electrons from the reading beam which go through the target quite easily and emerge as secondaries on the front side. Under these conditions, the tube is quite a number of times more sensitive than it is under condition of charge buildup.

When an image is stored in the target it is possible to read-out part of the charge at regular intervals as long as the charge is being replenished from the front side. If the light image is turned off, it is possible to read-out most of the stored charge in one scan if the mesh voltage is increased just before the beam is turned on. It appears that the manner in which to use the tube, to achieve best results, is first to allow the target to become charged in order that the desired information will appear on the back side (the side toward the reading beam). After this condition is reached, the beam should be turned on at intervals which are spaced, so that the information being read out on each scan, just balances the information being fed in by primary electrons

from the photocathode. Under these conditions, advantage may be taken of the integrating properties of the photographic plate used to store the information. For example, if four readouts are made on one picture, the lens stop on the camera is adjusted so that the density of the picture will be the same as it would have been with one readout. But the signal-to-noise ratio will be improved by the square root of 4. Practical tests indicate that this law is obeyed quite well in our equipment. In any case, it is essential that the target be allowed to charge up between scans to the most desirable level, otherwise multiple scans will not produce the best signal-to-noise ratio.

The Z–5396 image orthicon has a target mesh spacing of 0.08 inch. The useful range of the tube is determined on the low end by beam noise, and on the upper end by the degree to which the beam can discharge the target. Bright stars produce larger images than faint ones as is the case with direct photography. Objects of very high light level in the field of view cause redistribution of secondary electrons which reduces the sensitivity of areas nearby.

One of the difficulties encountered with the trialkali photocathode was that its sensitivity in the red end of the spectrum caused it to pick up light from the thermionic cathode and its heater. This limited seriously the storage time which could be utilized in the tube. The manufacturer has now incorporated a light shield in the new tubes which reduces this effect approximately 4 to 1. Even though the shield has been helpful, the tube is still limited in storage time to approximately 1 minute if it is operated at the rated heater voltage of 6.3. In the slow readout system, the required beam current is so low that it is possible to operate the heater at 2.5 volts. This makes it possible to expose the photocathode over a long period of time without encountering any fogging effects from the thermionic cathode.

Before the testing of the equipment at the telescope, it was tested in the laboratory utilizing an artificial star pattern and standard TV resolution patterns of varying sizes having 100 percent contrast. A light box with imaging lens is employed in which the test pattern may be placed. Neutral density and color filters may be inserted in the light path. The artificial star pattern consists of radial lines of artificial stars behind which are neutral density filters of varying degrees of absorption. There are 12 steps of 0.5

magnitude each. Artificial star sizes have been adjusted so that the images which are produced at the photocathode of the tube or photographic plate under test are equivalent to images having a diameter of 1 second of arc at the output of the 24-inch F-16 telescope. In making conparisons with photographic plates, photographs are taken first with the plate substituted for the image orthicon. Curves have been prepared showing minimum detectable density versus time for type 103 aO and type 103 aU plates. With these plates, Wratten type 47 and 29 filter are used respectively. Measurements of the same plates, with test patterns, indicate that they have resolutions of the order of 40 line-pairs per millimeter, at a density of 0.36 which corresponds to the density of a minimum detectable star image of 1-inch equivalent diameter. Tests with the Z-5396 image orthicon show that there is no detectable reciprocity failure in the tube. The measured gain in blue light, when compared with a 1-minute exposure on new photographic plates (out of a recently received shipment), is 112 and in red light on the same basis is 114. Owing to reciprocity failure in plates, it is obvious that the gain must be specified at a certain exposure time; otherwise it is meaningless. With a good batch of 103 aO plates it appears that reciprocity failure between 1 minute and 600 minutes is 1.5 magnitudes, and with 103 aU plates reciprocity failure between 1 and 600 minutes is approximately 2.2 magnitudes. The image orthicon gains must be adjusted for this reciprocity failure if the comparison is made on a 600-minute basis.

This may be summarized as follows:

	Plate exposure time 103 aO), 1 minute	600 minutes
Blue light (#47 filter): Fast gain on basis of minimum detectable artificial star image.................	112	450

	Plate exposure time (103 aU), 1 minute	600 minutes
Red light (#29 filter): Fast gain on basis of minimum detectable artificial star image.................	114	900

NOTE.—Fast gain only is quoted for the reason that slow gain, corresponding to the time it takes for target to reach an equilibrium or fully conductive state, depends to some extent on its previous condition. In any case, the time required to reach this condition is only 2 or 3 minutes at maximum, when the light level corresponds to that requiring a 600-minute (10 hours) exposure for photographic plates.

Tests made with television-type resolution patterns show that the image orthicon system, at present, has a resolution of between 10 and 15 line-pairs/mm over most of the 40-mm diameter photocathode. No great effort has been made as yet to improve this figure although some improvement is possible. Theoretically the tube is limited to about 23 LP/mm by the collector mesh. In case the equipment is used for the study of spectra, where resolution is limited only by the apparatus, and not by the atmosphere, the measured gain of the image orthicon over the photographic plate should be divided by the square of the resolution ratio of the two devices.

Assuming 40 LP/mm for the plate at the lower exposure limit, and 10 LP/mm for the tube, then all gains using test patterns should be divided by 16.

Measured gains using test patterns without correction for relative resolution are as follows:

	103 aO plate, 1 minute	600 minutes
Blue light (#47 filter): Gain=	225	900

	103 aU plate, 1 minute	600 minutes
Red light (#29 filter): Gain=	228	1800

Light amplifiers appear to have their most useful application under conditions where the photographic plate is not now limited by the light of the night sky. This is true in the case of high-dispersion spectrographs and large focal length telescopes. In the case of spectrographs, it should be possible to obtain spectra of rapidly changing objects, such as variable stars, which cannot be obtained at the present time.

In the case of long-focus telescopes, a point is reached at which no correction need be made in light amplifier gain because of poor resolution. The atmosphere itself limits stellar images on plates to a diameter of about 1 second of arc, according to a number of authorities. This means that the resolution of the atmosphere would be the equivalent of 10 LP/mm in a telescope having a focal length of 75 feet. Long focal lengths and high F ratios are needed if we are to take advantage of the light amplifier; otherwise, it will be limited by night sky light.

In July of this year, the equipment was taken to the Lowell Observatory for tests on the Morgan 24-inch reflector and DTM spectrograph, at the invitation of Drs. Hall and Ford. The DTM spectrograph is arranged so that plates can be taken directly at its output, using any one of three camera lenses. Electronic devices can be tested at an alternate output using the same

lenses. Comparisons were made of spectra taken with plates using the 7-inch lens and with the image orthicon Z-5396 tube using the 12-inch lens. In the attached group of spectra there is a comparison of the star Beta Ophiuchi. (See fig. 25-1.) In addition, there are a number of spectra of stars of different types which were made with the 12-inch lens at the output of the DTM spectrograph. The bottom spectrum in this group indicates that 7.83 magnitude is reached in 10 minutes' exposure time. The dispersion is 25 A/MM at the photocathode.
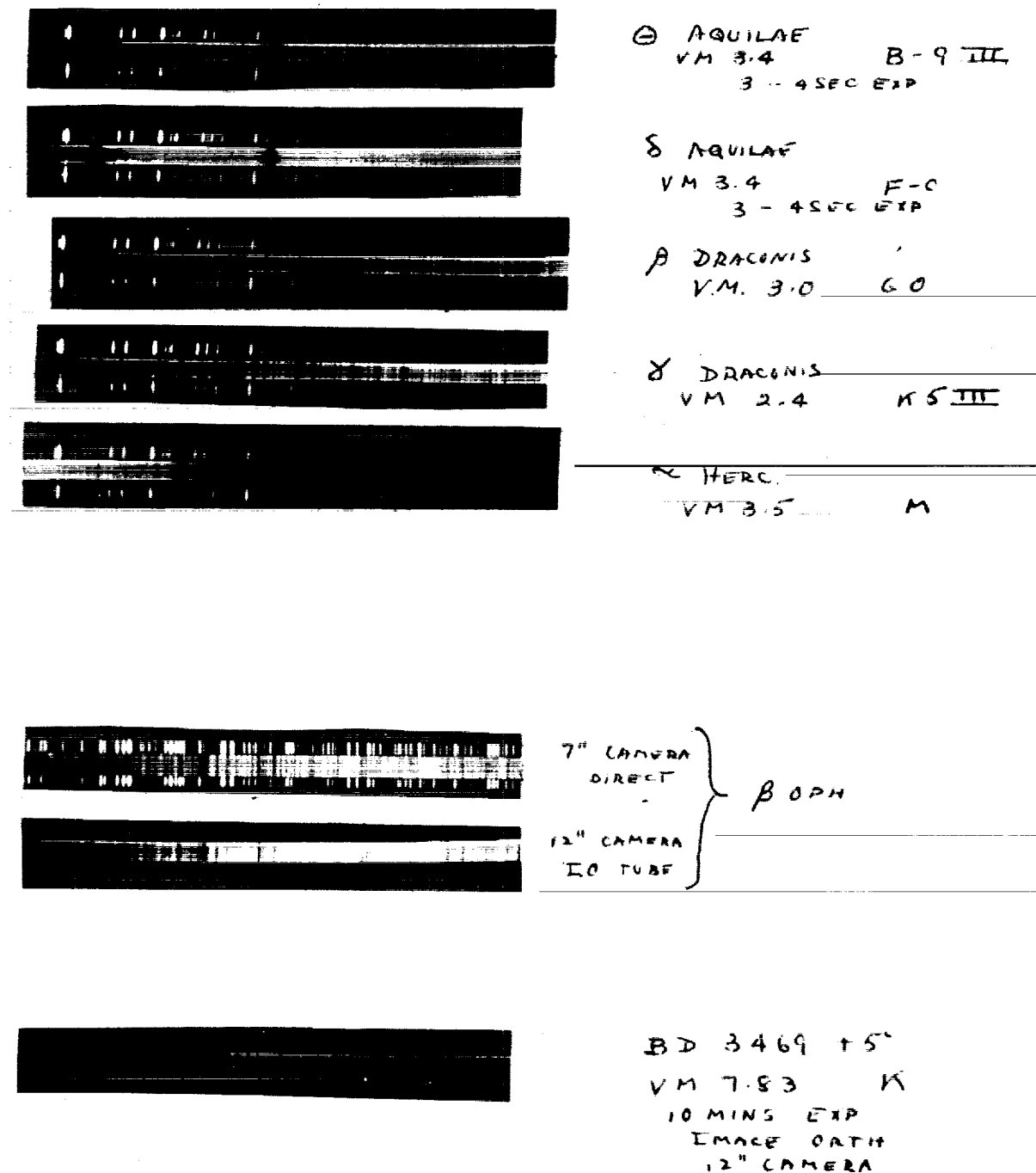
FIGURE 25-1.—Test of Dyer Observatory image orthicon light amplifier at Lowell Observatory. 12-inch camera DTM spectrograph on Morgan 24-inch reflector Z-5396 tube. S-20 surface.

In the course of our work at Lowell, it was found that the speed of the image orthicon was such as to make it difficult to use classical widening techniques. Accordingly, an electronic widener was added to the camera which permits widening at a rate of 120 sweeps per second. To achieve this, deflection coils were added around the image section of the tube. A 120-cycle sawtooth wave is applied to the coil, which is approximately oriented to widen the spectrum on the orthicon target at right angles to the direction of spread. A second deflection coil fixed at an angle of 90° permits fine adjustment of the direction of widening. The degree of widening is controlled through the 120-cycle sawtooth wave current in the deflection coils.

Photographs made directly at the output of the F-16 Cassegrain focus of the 24-inch reflector indicate that stars in the outer regions of the globular cluster M-13 of 19th magnitude can be reached in 100 seconds, exposure time. Other photographs which were made using multiple readouts of 4 seconds' storage are shown in the attached reproductions. Also attached is a photograph of M-57 (Ring Nebula in Lyra). This photograph represents five 4-second integrations interlaced with five additional 4-second integrations. (See fig. 25-2.) The 15th-magnitude star in the center of the nebula is easily reached in 4 seconds. The additional readouts serve to smooth the general appearance of the picture.

Work is underway on a magnetic tape storage device, to use with our equipment, which employs ¼-inch tape in standard cartridges. These tapes are operated at 40 inches per second and will record the entire bandwidth of 100 kc per second during a period of 4 or 8 seconds. By recording the readout of the orthicon, it is possible later to display the data on an oscilloscope or a kinescope. This will give considerably more flexibility in adjustment of the apparatus for optimum conditions for photography.

At the present it appears that the most useful type of tube for use in the equipment would be one similar to the GE Z-5396, which utilizes the S-20 trialkali photocathode, but which also would incorporate a field mesh. It is hoped that

FIGURE 25-2

developmental tubes of this type will be available shortly. Our experience seems to indicate that tubes having a trialkali photocathode have better target storage characteristics, than ones utilizing photocathodes having a high cesium content such as the S-10. Cesium condensed on the target increases lateral leakage, which causes poor definition in images stored over a long period of time. The field mesh has the property of reducing beam bending in the readout process, causing the tube to produce a considerably better picture in areas of abrupt transition from black to white. It also has the property of reducing greatly spurious images which result from focusing of the first dynode of the tube.

We feel that a considerable advantage has been gained in this research through the use of tubes and other components which are common to the television industry. Our equipment has now reached a state where it should soon be useful on a routine basis in a working observatory.

Discussion

E. LEVINTHAL: Could you explain again signal-to-noise improvements of displaced second sweep?

J. H. DEWITT: The image orthicon has the property of reading ahead of itself on vertical sweep. In an interlaced system, the first sweep reads out practically all of the information stored on the target. Since it is being read out at a greater rate, there are more charges picked up per second by the beam, hence a better signal-to-noise ratio. In our system, the target is read out at the higher rate. A second image is placed on it and it is again read out at the same rate with the lines displaced so as to create a 960-line picture with good signal-to-noise ratio.

192

26. THE APPLICATION OF THE LALLEMAND ELECTRONIC CAMERA TO STELLAR SPECTROSCOPY*

MERLE F. WALKER, *Lick Observatory, University of California*

A Lallemand electronic camera was installed at the Lick Observatory in the fall of 1959 by Prof. A. Lallemand and Dr. M. Duchesne.[1] The camera was mounted at the focus of the 20-inch Schmidt camera of the coudé spectrograph of the 120-inch reflector, and has been used regularly since its installation for the observation of stellar spectra. The details of this installation, together with a complete description of the electronic camera, has been given elsewhere.[1] Thus, it is necessary here only to review briefly the operating characteristics of the system.

The electronic camera is a "direct electronographic" system, in which a photocathode, an electrostatic lens system, and a photographic plate are introduced into a single evacuated chamber. There are no intermediary films, phosphors, or electronic systems between the photocathode and the final receptor to degrade and distort the information provided by the photoelectric surface. Consequently, the Lallemand electronic camera has the following characteristics:

1. *Speed.*—Each photoelectron produces a track consisting of about 10 grains of silver and having a length of about 10 μ in the Ilford G5 plates used to record the electronic image. Thus, the speed of the system depends only upon the quantum efficiency of the photoelectric surface. The gain in speed of the electronic camera over a Kodak 103 aO plate, at a wavelength of 4,000 Å, is shown in figures 26-1 and 26-2. For these tests, the camera was mounted at the focus of the coudé spectrograph and the comparison spectrum source was used as a standard lamp. Exposures were made both with the camera and on Kodak 103 aO plates, using three different neutral filters in the light path, and for each filter, adjusting the exposures to give the same threshold images with the camera and with the 103 aO plate. Figure

26-1 shows the three sets of spectra obtained. In each set, the uppermost spectrum was recorded with the electronic camera and Ilford G5 plates; the lower with Kodak 103 aO. The exposure times are: (1) Topmost set: electronic camera, 10 minutes; Kodak 103 aO, 7 hours 2 minutes. (2) Middle set: electronic camera, 1 minute; Kodak 103 aO, 25 minutes. (3) Bottom set: electronic camera, 2 seconds; Kodak 103 aO, 15 seconds. The exposure times of each of the three plate pairs, adjusted for differences in the plate limits, differences in the sensitivities of the photocathodes used, and for the additional light-loss caused by the mounting bracket of the electronic camera,[1] are plotted in figure 26-2 in terms of the gain in speed of the electronic camera over the 103 aO plate as a function of the exposure time with the camera. The figure shows, as one would expect, that the speed gain varies with the exposure time, owing to the reciprocity failure of the photographic plate. The curve in figure 26-2 represents the variation which one would expect assuming the correctness of the usual rule that the exposure time with a 103 aO plate must be increased by a factor of 3 to increase the plate limit one magnitude. These speed gains refer to photocathodes of average sensitivity, about 40 μA/lumen; with the very best cathodes, the speed is nearly twice that indicated in the figure. In assessing these speed gains, it must be kept in mind that the ultraviolet sensitivities of the cathodes used in the electronic camera are low, owing to the absorption of the conducting coating applied to the glass cathode mountings.[1]

2. *Resolution.*—The resolving power of the electrostatic lens system is very high. In practice, the axial resolution is limited not by the lens system, but by the length of the electron tracks in the nuclear plates. As mentioned earlier, Ilford G5 plates (which are the most sensitive to elec-

3886   **4144**   **4383**
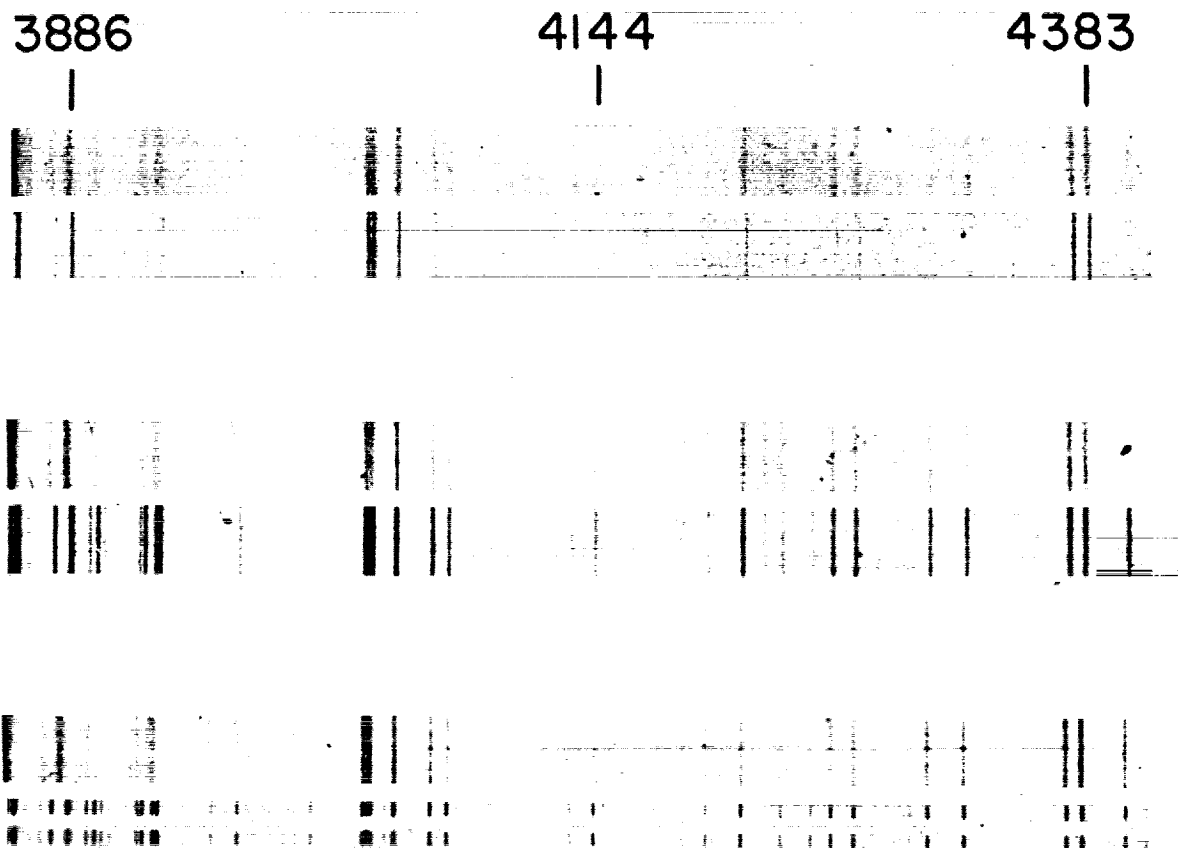
FIGURE 26-1.—Comparison of the speed of the electronic camera with Kodak 103 aO plates. The upper spectrogram in each of the three sets was made with the electronic camera and Ilford G5 plates; the lower was obtained with Kodak 103 aO. Exposure times: *Upper set:* electronic camera, 10 minutes; Kodak 103 aO, 7 hours 2 minutes. *Middle set:* electronic camera, 1 minute; Kodak 103 aO, 25 minutes. *Lower set:* electronic camera, 2 seconds, Kodak 103 aO 15 seconds.

trons) have electron track lengths about 10 μ in length and the resolving power is considerably better than that of Kodak 103 aO, even allowing for the reduction of 0.75 between the cathode and the plate occasioned by the electron optical system.[1] Ilford C2 plates have a lower sensitivity to electrons—by a factor of about 4—but they have a resolving power comparable to that of Kodak Microfile film.[2] The diameter of the photocathode of the electronic camera is 18 mm, and the high electronic resolution is preserved over more than two-thirds of this diameter.[1] In actual use at the focus of the coudé spectrograph the field of good definition is only about 10 mm in diameter, presumably owing to incorrect design of the curvature of the first surface of the glass lens on which the cathode is deposited, and which is used to bend the focal plane of the Schmidt camera to the radius of the photocathode required

by the electron optics. Also, some difficulty is experienced in placing the electronic camera accurately in the focal plane of the spectrograph camera,[1] and the resolution of the plates obtained during some runs at the telescope suffers for this reason. The focus of the electronic plates reproduced in figure 26-1 is soft owing to incorrect optical focusing of the camera.

3. *Discrimination.*—Owing to the high quantum efficiency of the photoelectric surface and to the fine grain of the nuclear plates, the electronic camera should be able to discriminate fainter sources against a bright background than is possible using ordinary photographic plates.

4. *Linearity.*—Experiments at the Paris and Meudon Observatories[2][3] have shown that when Ilford G5 or C2 plates are exposed to electrons rather than light, the blackening of a surface element of the plate is proportional to the number

194
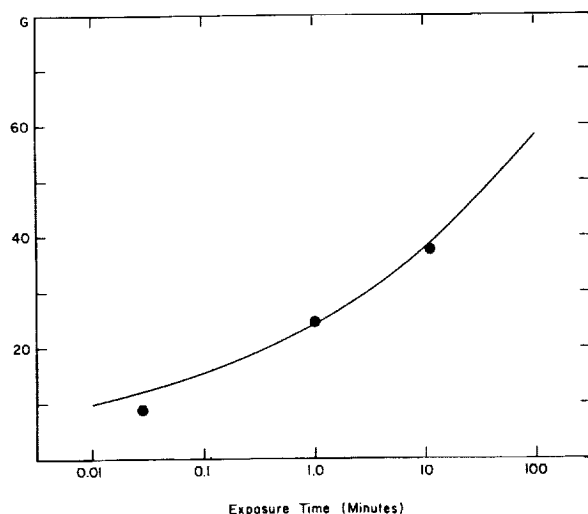
FIGURE 26–2.—Comparison of the speed of the electronic camera with Kodak 103 aO plates at 4,000 Å. The points represent the data in figure 26–1 corrected as indicated in the text and expressed in terms of the gain in speed of the electronic camera over the 103 aO plate as a function of the exposure time with the camera. The curve represents the variation in speed-gain, with exposure time calculated on the assumption that the exposure time of the plate must be increased by a factor of three for each one-magnitude increase in the plate limit.

of incident electrons, and hence to the intensity of the incident light. This linearity of response is maintained up to a photographic density of 3.[3] The effect of this linear response is to make the electronic plates look rather "washed out" compared to ordinary photographs. This is shown in figure 26–1. In the figure, it will be seen that the intensities of the faintest lines are about equal on the electronic plates and on Kodak 103 aO, but that the strongest lines appear much stronger on the 103 aO plates.

5. *Signal-to-noise ratio.*—During 1960, several improvements were made at the Lick Observatory in the operation of the electronic camera. These included:

(1) Semiautomatic refilling of the liquid air dewars on the camera, to avoid the necessity of terminating the exposure after 45 minutes in order to add liquid air.

(2) Use of a titanium-ion pump, which improves the vacuum inside the camera from a few times 10^{-6} mm Hg to about 3×10^{-9} mm Hg and completely eliminates the "ionic spot"—a dark spot on the electron-optical axis of the nuclear plates caused by the ionization of residual vapor in the camera.

(3) Vacuum storage of the nuclear plates before use.

(4) Extreme precautions in the cleaning and preparation of the tube to insure having the interior parts as clean as possible.

(5) Elimination of corona discharges around the camera during its operation.

As a result of these improvements, it is now possible to preserve a single photocathode for 2 successive nights of observation and to expose each plate up to 4 or, under the very best conditions, as much as 6 hours before the parasitic blackening of the plate becomes excessive. Using the electronic camera at the focus of the 20-inch camera of the coudé spectrograph of the 120-inch reflector, and with a dispersion of 48 A/mm on the photocathode, or 65 A/mm on the nuclear plate, it is possible to obtain an unwidened spectrum of a star of $m_{pg}=16$ in about 3 hours, with a good cathode and good seeing. That this limit is not fainter results from the fact that the 48 A/mm dispersion is considerably outside the range for which the spectrograph was designed and represents a compromise between efficient operation of the spectrograph and the securing of a reasonable length of spectrum on the photo cathode of the electronic camera. Consequently, a good part of the speed of the camera is utilized in overcoming the low efficiency of the optical system.

During the last 2 years, electronic observations of a number of objects of different type have been obtained with the 120-inch coudé spectrograph mostly at the above-mentioned dispersion of 48 A/mm. These include nuclei of extragalactic nebulae, old novae, stars in globular clusters, and gravitationally contracting stars in extremely young clusters. Accounts of some of the scientific results obtained have been published elsewhere.[1][4-8] Of these programs, only two will be described here. One is to illustrate the use of the electronic camera in two of the three types of spectroscopic observations for which an image intensifier is particularly valuable. The other is high time resolution spectroscopy, and observation of the spectra of faint stars, for which the exposure times would be excessively long using conventional photography. The third type of observation for which the electronic camera would be particularly advantageous is the spectrophotometric study of line profiles, for which the fine grain of the nuclear plates and the linear response of the system will provide higher accuracy than

195

can be obtained from ordinary photographic plates; so far, high-dispersion observations of the type needed for such problems have not been attempted.

The application of the electronic camera to high time-resolution spectroscopy is illustrated by observations of the explosive variable AE Aqr. AE Aqr is a spectroscopic binary having a period of 0.70 day and consisting of a small, hot star and a relatively cool, late-type companion of spectral typed dK0.[9] The system exhibits intrinsic variations in light, characterized by occasional novalike explosions having amplitudes of three magnitudes in blue light and by rapid, complex explosions of about one-half magnitude in blue light, lasting from one to several hours.[9] Between the latter outbursts, the star remains fairly constant at minimum light, about $m_{pg}=12.5$. In order to understand the nature of the processes occurring in this system, it is desirable to obtain observations of the spectroscopic changes associated with the rapid variations in light. To resolve these changes, it is necessary to be able to photograph the spectrum in an interval of not more than about 15 minutes. However, the system is so faint that it would be difficult to obtain widened spectra with a dispersion of 48 A/mm in this time even with the 200-inch Palomar reflector. Thus, the results discussed below represent data which probably could not have been obtained by any other means.

Observations of AE Aqr have been obtained on 3 nights in 1960 and one night in 1961. The observations in 1960 were made with cathodes having sensitivities only about half, or even less, of the average sensitivity to which the speed gains in figure 26-2 refer. Even so, it was possible to obtain spectra of AE Aqr in 20 to 30 minutes, at minimum light and 12 to 15 minutes, during an explosion. In 1961, a better cathode was available and the exposures were about 12 minutes at minimum light and 7 minutes at maximum. With the very best cathodes, these 1961 exposures could be made still shorter by nearly another factor of 2. During the observations, the star was monitored photoelectrically by other observers at the Crossley reflector, and the measures were immediately reported to the 120 inch as a guide to when to expose the plates, in order to obtain spectra at minimum light and at different times during the explosions. Figures 26-3 and 26-4 show the results obtained on August 14, 1960 (UT). Figure 26-3 shows the light curve of AE

Aqr in ultraviolet light obtained (in this instance by Dr. A. E. Whitford) with the Crossley reflector and indicates the times at which the spectroscopic observations, shown in figure 26-4, were obtained.

Preliminary examination of the material so far obtained shows that the activity of the system is very complex. In general, a new "event" begins before the preceding one has ended. Thus, it is difficult to isolate the spectroscopic changes associated with a single explosion. The most clear-cut example of these changes so far obtained is shown in figures 26-3 and 26-4. Figure 26-3 shows that plate ECL-83 was taken during a fairly undisturbed minimum, while ECL-84 was taken during a single, rapid maximum. Comparison of these spectra show that during this explosion the emission lines of hydrogen and Ca II became stronger and broadened asymmetrically toward the violet, while the absorption spectrum of the late-type component became filled in by continuous emission. Other series of observations show that the broadening of the emission lines is not always toward the violet. Sometimes the lines broaden toward the red, and sometimes they broaden symmetrically. This result shows that the explosions arise in localized areas within the binary system. The analysis of many such observations, together with a knowledge of the phase in the spectroscopic orbit at the times of observation, may eventually make it possible to learn something not only of the nature of the explosive process, but also in what parts of the system the outbursts most frequently originate. That they are not confined to one specific area is already shown by the fact that at the same spectroscopic phase, explosions producing emission lines broadened both to the red and to the violet have been observed.

An example of the application of the Lallemand electronic camera to the spectroscopic investigation of very faint stars is the observations which have been made of faint, gravitationally contracting stars in the Orion Nebula and NGC 2264 having ultraviolet excesses. The existence of these ultraviolet excess stars was first discovered photographically by Haro,[10] and independently by Walker[11] from photoelectric observations. The nature of the ultraviolet excess is not understood. It has been shown that the excess cannot be explained in terms of Balmer emission, if the emitting region is optically thin.[10] However, the excess could be due to Balmer emission if the Balmer lines originate in an optically thick layer

196
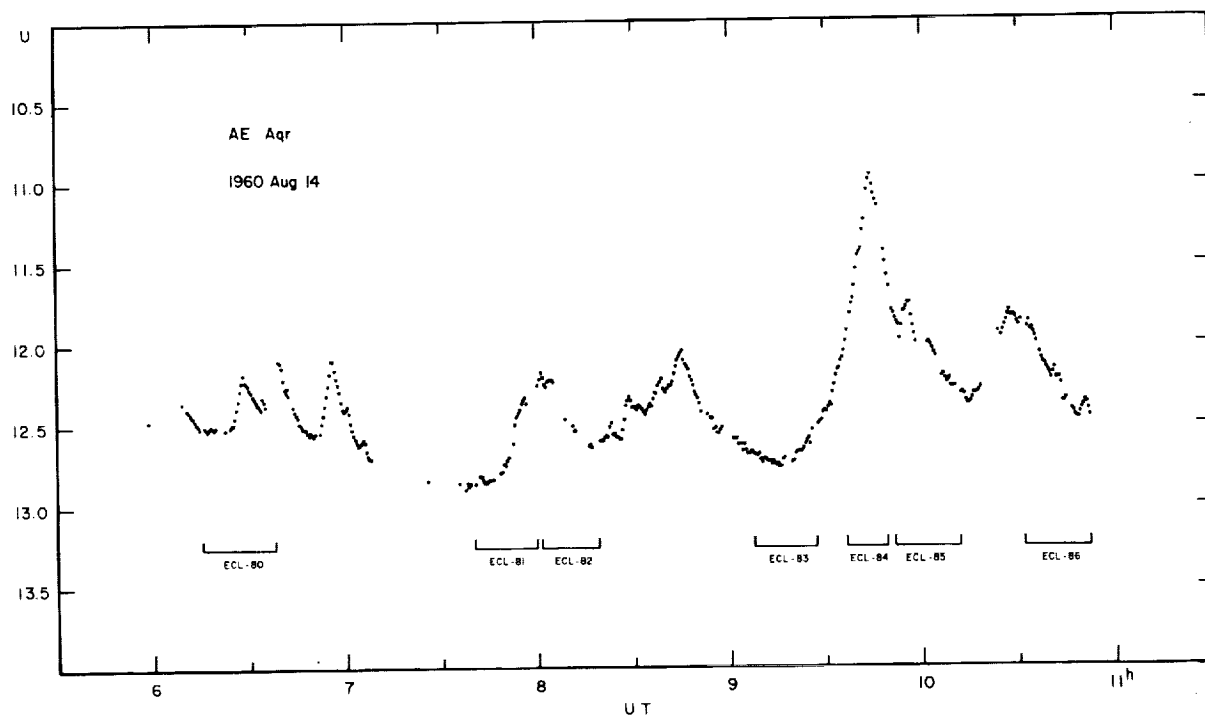
FIGURE 26-3.—Photoelectric light curve of AE Aqr in ultraviolet light. This light curve was obtained by Dr. A. E. Whitford on August 14, 1960 (UT), with the Crossley reflector, simultaneously with the spectra shown in figure 26-4.
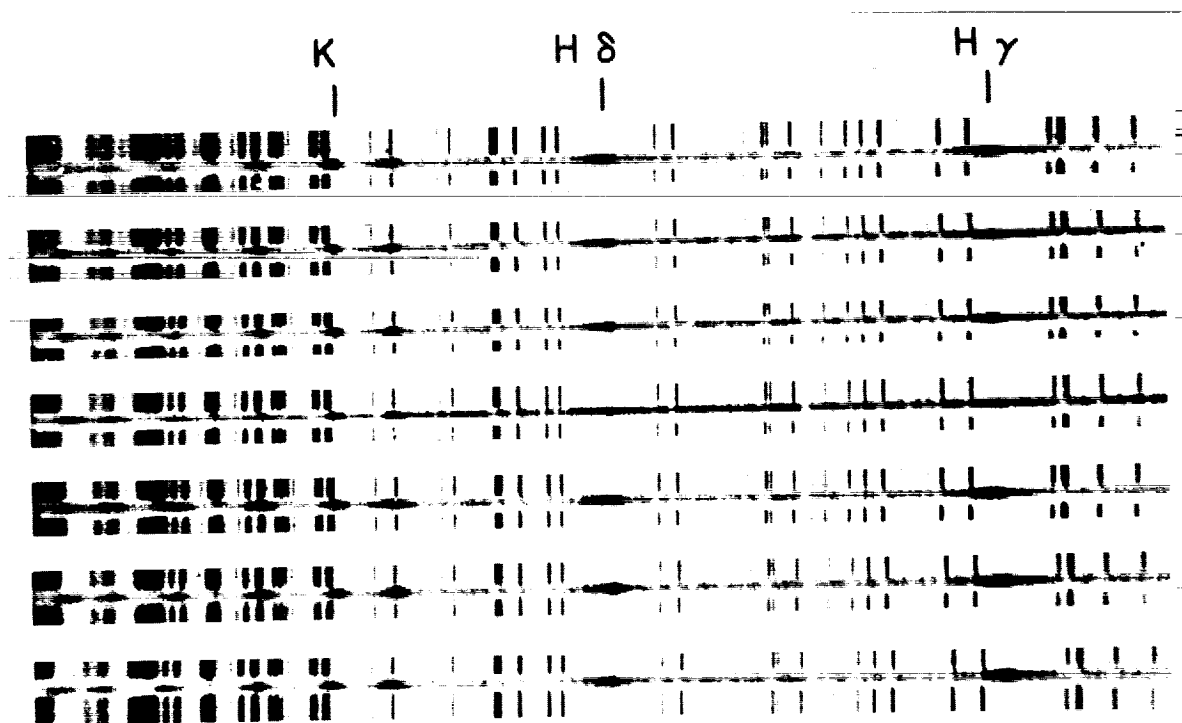
FIGURE 26-4.—High time-resolution spectra of AE Aqr, taken with the electronic camera and the 120-inch reflector on August 14, 1960 (UT). The plate numbers are, from top to bottom, ECL-80 through ECL-86. The times at which the plates were taken are marked on the light curve in figure 26-3.

197

and if the lines actually run together 100 Å longward of the Balmer limit, due to the low resolving power of the spectrograph used in the earlier investigations (430 A/mm at Hγ).[12] Observations of ultraviolet excess stars using a higher dispersion are clearly desirable in order to determine whether the excess results from Balmer emission or from some new and unknown emission process.[13][14]

Spectra of the four stars having ultraviolet excesses so far observed are reproduced in figure 26–5, and data concerning these spectra are given in the following table:

TABLE 26–I

Star	Date (UT) 1960	mag_{pg}	UV excess (mag)	Exposure h m
VY Ori (upper).	Nov. 24	≥16	Large...	2 08
VY Ori (lower).	Dec. 23	15	...do....	2 10
YY Ori (upper).	Nov. 24	14.3	0.8.....	1 35
YY Ori (lower).	Dec. 23	14.3	0.8.....	1 00
MO Mon.....	Dec. 24	14.8	1.0.....	2 00
IP Mon......	Dec. 24	14.5	0.3.....	1 33

In general, it will be seen from figure 26–5 that the spectra are similar to those of other T Tau stars, showing bright lines of hydrogen, Ca II, and in some cases Fe I, Ti II, and He I. In three of the stars—VY Ori, MO Mon, and YY Ori—the underlying late-type absorption spectrum is either partly or totally obliterated by a blue continuum. The ultraviolet excesses of VY Ori, MO Mon, and YY Ori are easily seen in figure 26–5. The excess is particularly outstanding in the uppermost spectrum of VY Ori, taken when the star was at minimum light, $m_{pg} \geq 16$. On this plate, the continuous spectrum shortward of $H\ \delta$ is below the plate limit, and only the emission features are visible until the onset of the ultraviolet excess at about 3,800 Å.

The most remarkable feature of the spectra is the presence of redward-displaced hydrogen absorption lines in YY Ori and MO Mon. While no absorption features are seen in VY Ori, it is probable that redward absorption exists since in this star as in YY Ori and MO Mon, the lower members of the Balmer emission lines are shifted to the violet by amounts ranging from −100 to −170 km/sec at Hδ and which decrease with
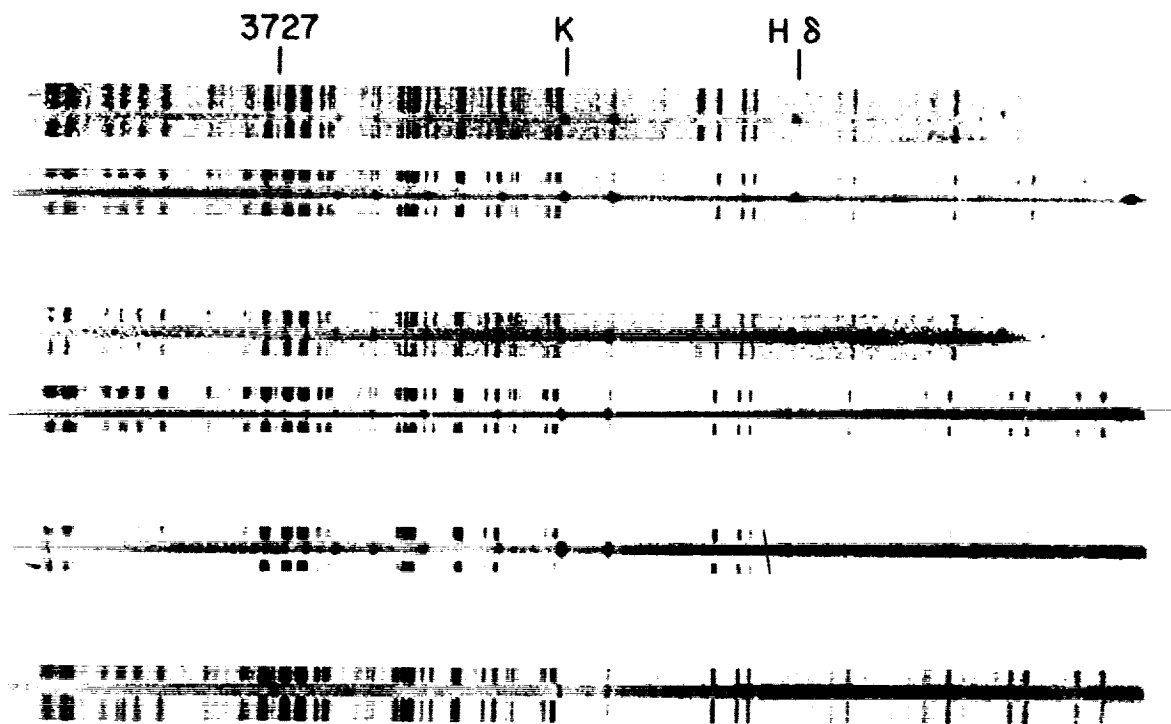

FIGURE 26–5.—Spectra of faint, gravitationally contracting stars in the Orion Nebula and NGC 2264 having ultraviolet excesses. From top to bottom the stars are: VY Ori (two plates), YY Ori (two plates), MO Mon, and IP Mon. Data concerning these spectra are given in the text.

198

increasing quantum number, becoming constant and approximately equal to the cluster or absorption line velocity at about H 10 or H 12. There is no evidence of redward-displaced absorption lines in IP Mon. However, this is not surprising as the star has a very small ultraviolet excess and displays an essentially normal late-type absorption spectrum, with only Ca II H and K emission cores.

The velocities of the redward-displaced absorption features range from +150 to +200 km/sec and do not vary with the quantum number of the line. There seems little doubt that these features originate in a layer of material overlying both the late-type stellar continuum and the higher layers in which the blue continuum and the emission features are formed, and that the material in this outer layer is falling onto the surface of the star. Even though the number of stars observed is small, the fact that evidence of infall is found in each star having a large ultraviolet excess would suggest that in these stars, unlike the majority of T Tau stars, infall of material dominates over ejection of matter by the stars. However, more observations are needed, for the phenomena occurring around these objects are very complex, as is shown by a plate of YY Ori taken 24 hours after the lower plate of this star shown in figure 26–5. This plate shows that the redward-displaced absorptions have faded out (but are probably still present, as the hydrogen emission lines have the same displacement to the violet) and a new absorption feature has appeared with a velocity of —108 km/sec, indicating that a new, expanding layer has formed.

The nature of the ultraviolet excess is still not clear. Spectrophotometric tracings show that in every case the excess begins at about 3,800 Å. thus, the excess cannot be caused by the confluence of the Balmer emission lines themselves, since these are resolved to H 17 or H 18. However, since it is clear that self-absorption plays a large role in these objects, it is perhaps possible that the excess could be caused by the extreme wings of emission lines whose central intensities are cut down by self-absorption. Further increases in dispersion will not help in the solution of this problem. We are already limited by the intrinsic widths of the emission lines themselves. In order to determine the nature of the ultraviolet excess, observations of the intensity distribution shortward of the Balmer limit or the Paschen limit, will be required, or perhaps the discovery of stars having a large excess but little or no hydrogen emission. Whatever the nature of the ultraviolet excess, it is interesting to speculate whether it could be produced in some way by the infall of material onto these stars.

Acknowledgments

References

1. LALLEMAND, A., DUCHESNE, M., and WALKER M. F.: Pub. A.S.P., vol. 72, 1960, p. 268.
2. LALLEMAND, A., DUCHESNE, M., WLÉRICK, G., AUGARDE, R., and DUPRÉ, F. M.: Ann. d'Ap., vol. 23, 1960, p. 328.
3. VERNIER, P.: Bull. Astr., vol. 22, 1959, p. 83.
4. WALKER, M. F., LALLEMAND, A., and DUCHESNE, M.: Comptes Rendus, vol. 250, 1960, p. 975.
5. LALLEMAND, A., DUCHESNE, M., and WALKER, M. F.: Pub. A.S.P., vol. 72, 1960, p. 76.
6. WALKER, M. F.: Ap. J., vol. 133, 1961, p. 438.
7. WALKER, M. F.: Ap. J., vol. 133, 1961, p. 1081.
8. WALKER, M. F.: Comptes Rendux, vol. 253, 1961, p. 383.
9. JOY, A. H.: Ap. J., vol. 120, 1954, p. 377.
10. HARO, G., and HERBIG, G. H.: Bol. Obs. Tonantzintla y Tacubaya, No. 12, 1955, p. 33.
11. WALKER, M. F.: Ap. J., Suppl., vol. 2, No. 23, 1956.
12. BÖHM, K. H.: Z. fur A., vol. 43, 1957, p. 245.
13. AMBARTSUMIAN, V. A.: Communications, Burakan Obs. No. 13, 1954.
14. AMBARTSUMIAN, V. A.: The Non-Stable Stars. Symp. at Burakan, pp. 9 and 70, 1957.

27. IMAGE INTENSIFIERS FOR SOLAR PHOTOMETRY

Edwin W. Dennison, *Sacramento Peak Observatory, Air Force Cambridge Research Laboratories*

To date the standard method of making solar photometric observations has been by the means of photographic materials. The one exception to this practice is the use of photomultiplier tubes for measurements in the solar spectrum. Both of these techniques have their limitations: (*a*) The photographic emulsions are limited by low effective quantum efficiency, cumbersome reduction techniques, and poor uniformity; (*b*) the photomultiplier technique permits the measurement of only a single area at any one instant of time. Thus, for example, measurements made over a large field are generally more efficient with photographic techniques because of the simultaneous acquisition of information at all points in the field.

At the Sacramento Peak Observatory we chose the image orthicon tube for our initial experiments with image intensifiers for several reasons. First, all the photoelectronic and electronic processes within the tube are essentially of a linear nature. Secondly, although the signal integration takes place over the entire field, the readout signal is derived by sweeping the image in a point-by-point manner. This latter fact makes signal manipulation such as information storage or conversion to isophotes a more practical possibility.[1]

Our efforts have been made with the goal of attempting to determine the intrinsic limitations of the image orthicon tube. Initially, our comparisons have been between the orthicon and high-speed photographic materials. Ultimately, of course, we must compare the orthicon performance with the intrinsic limitations imposed by the statistical fluctuations of the photon image.

Our results to date indicate the following general conclusions:

(*a*) At approximately the same resolution and photometric accuracy the orthicon shows a very substantial speed gain, approximately 500. This would appear to be too large a factor and more testing will be necessary to more quantitatively establish the resolution in photometric differences. Undoubtedly, when proper compensation is made for the differences in resolution and photometric accuracy, the gain factor will be substantially reduced.

(*b*) We have not as yet been able to improve photometric accuracy by increasing exposure time. That is, we are apparently limited by the target storage capacity. Clearly it should be possible to improve photometric accuracy by averaging the output presentation over a series of separate target scans.

(*c*) Because of the character of the beam noise, the image orthicon appears to show a limited dynamic range. That is, we are unable to make photometric measurements of images in which there is a large range of intensities over the field.

(*d*) The image orthicon is very satisfactory for use with an isophote contour generator.

(*e*) The image orthicon system is most convenient to use and adjust once the initial period of circuit development is completed.

Our experiments have been made with a GE type Z5294 image orthicon and our entire television system was constructed for us under a contract with the Eberline Instrument Corp. of Santa Fe, N. Mex.

Accepting the fact that much additional work is required to perfect and adjust the electronic circuits associated with the image orthicon, we definitely feel that this is a useful approach to the problem of improving solar photometric measurements. The orthicon's outstanding advantage, namely, reduced exposure time, offsets the existing disadvantages of lower photometric accuracy and limited dynamic range. The primary limitation in image resolution on the solar surface arises from the terrestrial atmospheric turbulence which disturbs the relatively long exposure times, generally from 1 second to 1
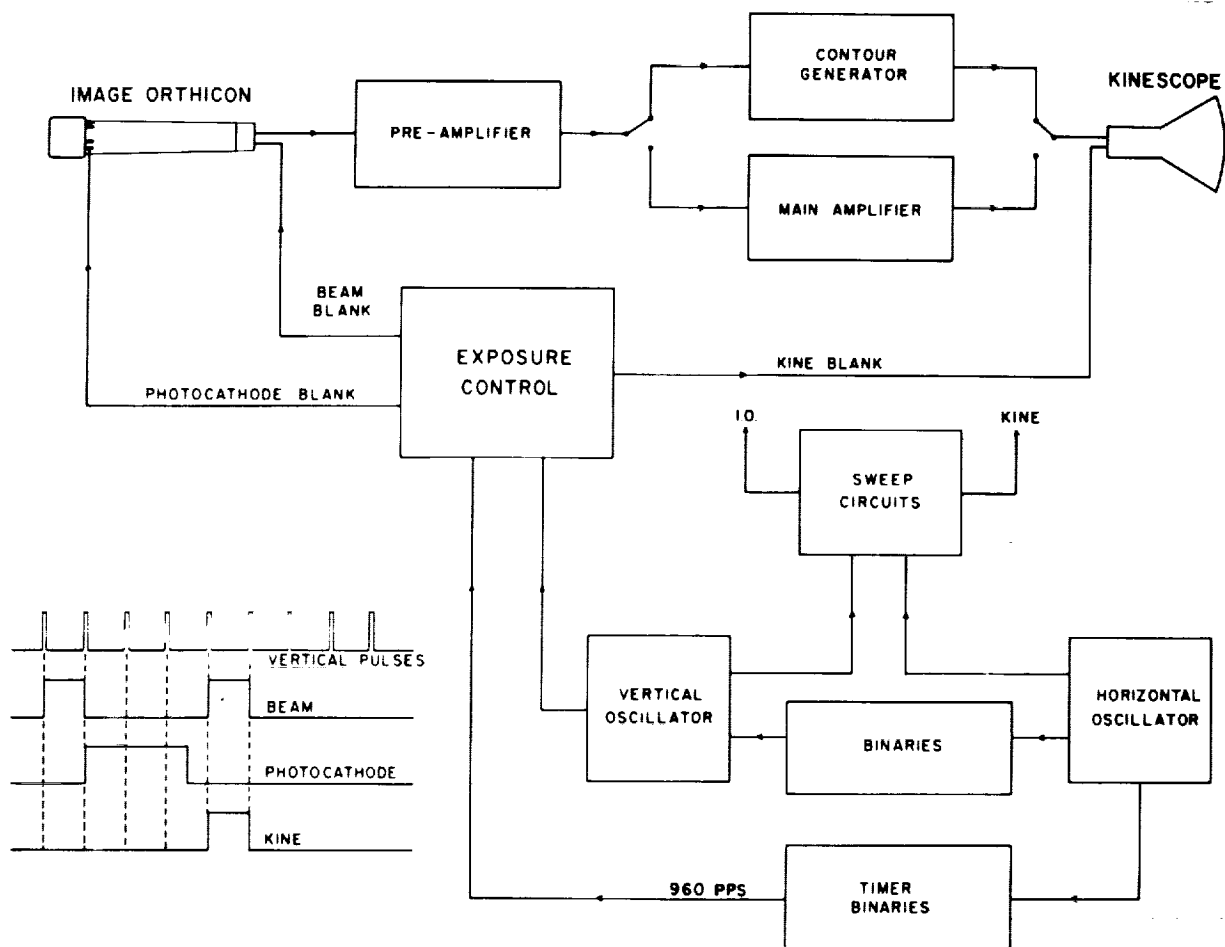
FIGURE 27–1.—Basic operational diagram of the field photometer using an image orthicon as a signal generating light intensifier.   Lower left-hand insert shows exposure control patterns used for exposures larger or shorter than standard frame time of 1/30 sec.
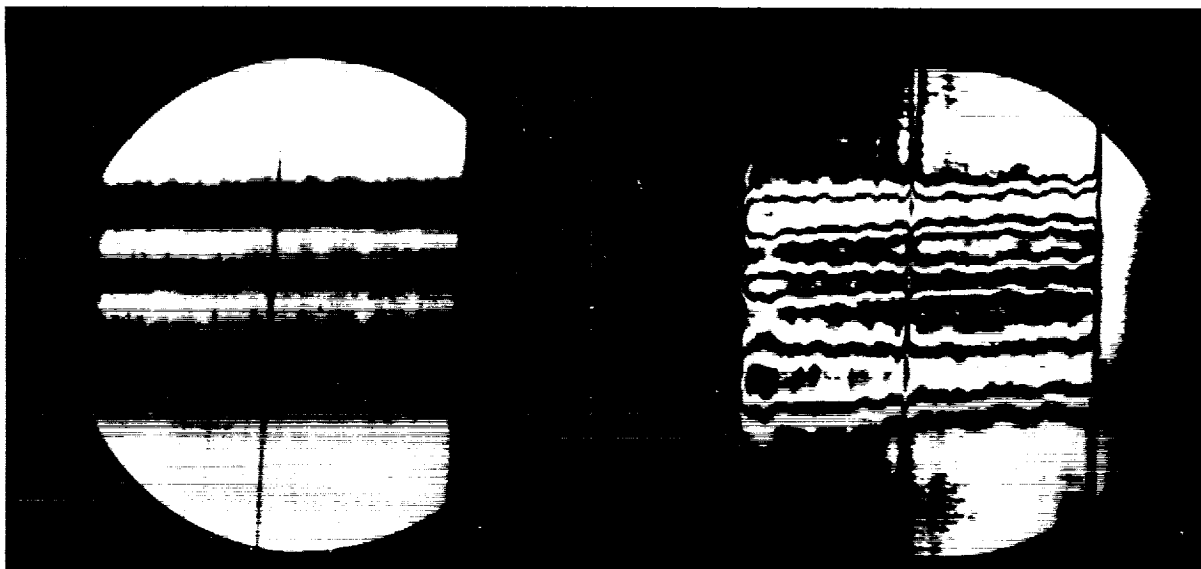
FIGURE 27–2.—Halftone and contour pictures showing Doppler structure on the solar surface.   The vertical line is a hair across the spectrograph slit.   Fifteen-millisecond exposure.
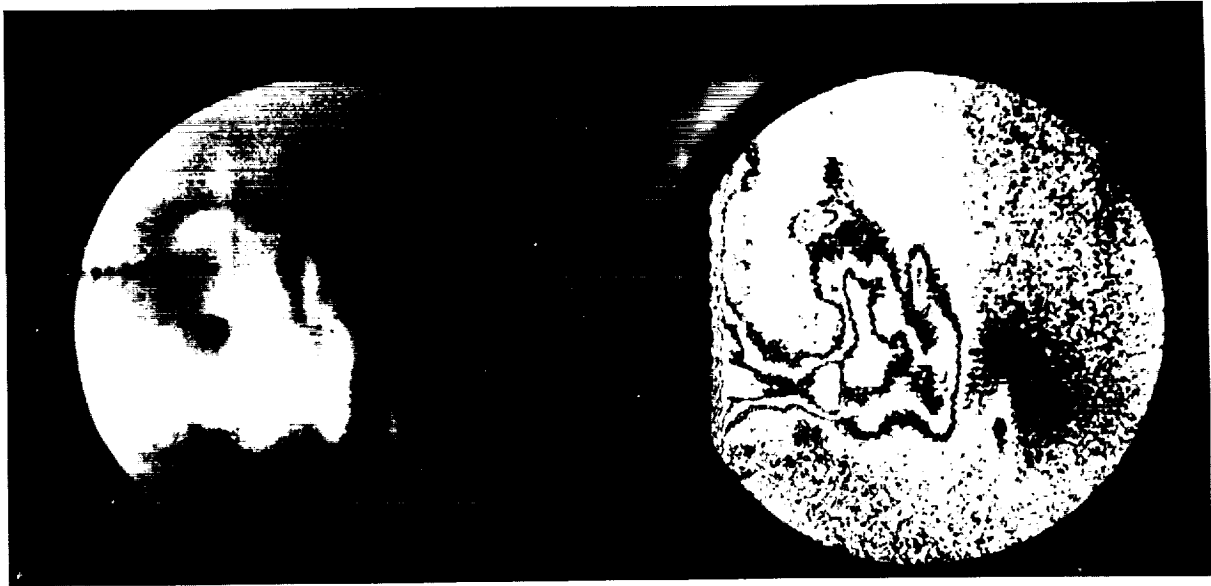
Figure 27-3.—Halftone and contour picture made with the spectrograph slit placed across a solar prominence. One-tenth second exposure.

minute, required by high-speed photographic materials. It has been our experience, and also that of others working in the field, that under conditions of excellent seeing the resolution on the sun improves as the exposure time is decreased to approximately one-twentieth or one-fiftieth of a second. Clearly, the image orthicon allows us to make observations with our high-dispersion spectrograph at very short exposure time with an improvement in resolution resulting from essentially stopping the atmospheric-induced image motion. These techniques are only prac-

tical when applied to low-contrast images such as weak to moderate intensity solar lines, the solar corona, the solar chromosphere over a limited range of heights, etc.

There exist, of course, other areas of solar photometry for which the limitations imposed by the image orthicon are serious and other types of image intensifiers will be required. Experiments will be conducted using non-signal-generating image intensifiers and other forms of signal-generating image intensifiers as they become available.

Reference

1. DENNISON, E. W.: *Advances in Electronics and Electron Physics.* Vol. XII, 1960, p. 307.

28. ASTRONOMICAL APPLICATIONS OF IMAGE INTENSIFIERS

W. G. FORD, JR., and M. A. TUVE, *Department of Terrestrial Magnetism, Carnegie Institute of Washington*

Cascade and Mica-Window Tubes in Astronomical Applications

The Carnegie Image Tube Committee was formed in 1954 to investigate possible methods of image intensification for astronomical applications. At that time it was not clear which of several proposed methods would yield the most useful results. Professor Lallemand had already demonstrated with considerable success the potentialities of his electronographic technique for both faint star photography and for spectroscopy. But because of the operational difficulties involved in the use of the Lallemand device, systems better suited for routine use were sought.

Just after the last ERDL Image Intensifier Symposium, in the fall of 1958, we obtained our first cascaded tubes from RCA and were able to demonstrate to our satisfaction their potential usefulness in astronomical applications. After a series of tests on the 40-inch reflector at the U.S. Naval Observatory's Flagstaff Station, we reported [1,2] that the main shortcomings of the electrostatically focused cascaded tubes were: (1) poor phosphor screens, (2) small area of good definition, and (3) insufficient gain. Phosphor screens improved markedly and the later electrostatically focused tubes could be operated at higher voltages, with acceptably low background, so that the gain was adequate for many of our purposes. It was apparent that magnetically focused tubes would provide good resolution over areas 40 mm in diameter and larger. The development of these tubes is described by R. G. Stoudenheimer in this symposium (Paper No. 6).

Single-stage converters with phosphor screens deposited on thin end windows [3-6] are an attractive alternative to cascaded tubes, or imaging electron multipliers, for some problems. With these tubes photographic film is pressed into optical contact with the thin window in order to provide efficient transfer of the optical image from the phosphor screen to the photographic emulsion. In spite of the thickness of the mica window being as little as 8 microns, these tubes have proved to be remarkably reliable and convenient. They have been particularly useful to Russian astronomers in infrared spectroscopy.[7-9] In this country, L. W. Fredrick at Lowell Observatory has made a survey of stellar spectra in the 0.9- to 1.2-micron region [10] with electrostatic mica-window tubes made for the Carnegie Image Tube Committee by ITT Laboratories. These electrostatic tubes have had small areas of good definition, but magnetically focused tubes show promise for spectroscopic work of good definition over 40 mm.

The preliminary samples of both the magnetic cascaded tubes and the magnetic mica-window tubes which we have evaluated thus far have been beset with such technological difficulties as field emission, low photocathode sensitivity, ion spots, etc. Continued development work should soon eliminate these temporary difficulties. We believe that when this is done, these image tubes will provide a method of utilizing the high quantum efficiency of photocathodes in routine astronomical observations. Then, astronomers will have an alternative for many applications to the more difficult techniques of Lallemand and the complex image orthicon circuits of DeWitt and Livingston described elsewhere in this symposium.

Short-Exposure Applications

Earthbound astronomers must work with images which change constantly, due to the movement of turbulent air cells of varying optical density. By making sufficiently short exposures, we can minimize the effect of poor seeing.

Consider the problem of measuring the separation of close double stars. Visual observers found long ago that sharp, well-defined images are seen more frequently with telescopes of small aperture than with larger telescopes. For this reason, telescopes of moderate size are frequently "stopped down" to increase the probability of catching sharp images. At the same time, however, the

205

images are making rapid, random excursions from a mean position. Short exposures are required, therefore, in order to have a chance at recording relatively stationary images. Clearly, a compromise must be made between small aperture and short-exposure time.

An image intensifier permits shorter exposure times to be used effectively in this application. The usual procedure has been to use a negative lens to enlarge the image on the photocathode, so that the size of the image is determined almost entirely by the seeing. Since exposures are of only a few milliseconds' duration, spurious emission is rarely a problem.

G. Wlérick, J. Rösch, and M. F. Dupré have obtained excellent photographs of both double stars and planets with a Lallemand tube attached to the 60-cm F/30 refractor at Pic du Midi. Many exposures are made on a single plate and the sharpest images selected for measurement.

The Carnegie committee has explored the use of cascaded intensifiers in this application. We attached a small, electrostatically focused two-stage tube, made by RCA, to the Lowell Observatory 24-inch refractor. A negative lens gave a scale at the photocathode of 3 seconds of arc/mm, and a movie camera with a fast relay lens was used to photograph the phosphor screen. For a resolution of 13 lp/mm, this gives us a potential resolving power for the detector of 0.25 second of arc, assuming that the telescope optics are that good. The gain of the best of our RCA two-stage tubes was sufficient for millisecond exposures on double star pairs down to around 8th magnitude.
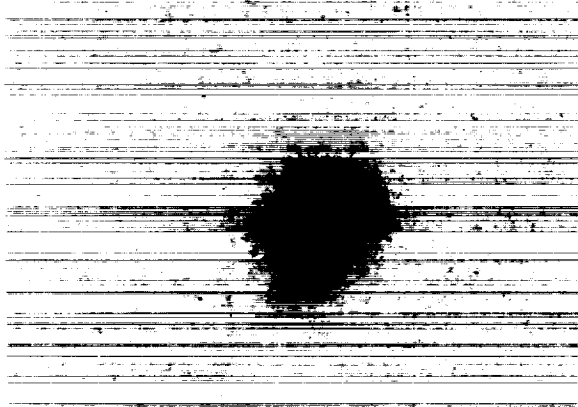
FIGURE 28-1.—Microphotograph of an image of the visual binary 51 Aquilae obtained by L. W. Fredrick with an RCA electrostatic cascade tube. The separation of the two stars was measured on a series of similar photographs and found to be 0.46±0.05 second of arc.

206

This work has been pursued by Dr. Fredrick, at Lowell, with considerable success. Figure 28-1 shows a microphotograph made of one of Dr. Fredrick's images.

This same technique can be applied to planetary photography. The extremely low contrast of planetary detail makes the problem more difficult. We tried photographing Mars with this equipment during the 1958 opposition, but the phosphor graininess in the tubes available then, completely masked any low-contrast detail.

DeWitt's ingenious image tranquilizer [11] has provided another method of reducing the effects of transverse image motion. Perhaps a similar compensation system can be applied to other intensifier tubes.

Faint Object Photography

In order to see exactly how an image intensifier can be used in photographing weak astronomical objects, consider the process of photographing, with a conventional plate, a faint star. Because of the light of the night sky, this is a contrast-limited problem. Dr. Morton has dealt with the statistics of low-contrast imaging in an elegant manner elsewhere in this symposium (Paper No. 12), so it is only necessary here to indicate how these considerations apply to telescopic work.

Modern photographic plates are sufficiently sensitive so that with telescopes of small f-ratio they are fogged to appreciable density with only moderately long exposures. With an f/3.5 instrument, for example, a 30-minute exposure on a moonless night typically yields a background density due to the sky of around 0.6. A weak image must stand above this general background by an appreciable amount if it is to be detected.

The image of a faint star will just be recognized if the number of blackened grains due to the star in the image, S, is equal to

$$k[(B+S)+B]^{1/2},$$

where k is the coefficient of recognition and B is the number of background grains in an element of equal area. Since for faint stars S is small compared with B

$$S_0 \approx [2B]^{1/2}.$$

An expression for the magnitude of a threshold image can be derived using the notation and method of Baum in his classic paper on the detection of faint images against the sky background:[12][13]

n = Average number of eligible unscattered photons per second received per unit area at the surface of the earth from a faint star.

N = Average number of eligible photons per second received per unit area at the surface of the earth from unit solid angle of sky background.

t = Effective integration time.

q = Average quantum efficiency of the system.

D = Aperture of the telescope.

F = Focal length of telescope.

α = Angular diameter of the star image.

m = Magnitude of the star within the wavelength band of the system.

M = Magnitude per unit solid angle of sky background.

The number of blackened grains in the star image is

$$S = (\pi/4)nD^2 qt$$

and in a background element, $B = (\pi/4)ND^2\alpha^2 qt (1+R)$, where R is the ratio of the background contributed by the detector to the sky background.

The magnitude of a threshold star,

$$m_0 = M - 2.5 \log (n_0/N).$$

From the expressions above for S and B, we obtain

$$(n_0/N) = \alpha^2(1+R)S_0/B$$
$$= \sqrt{2k}\alpha^2(1+R)/B^{1/2}$$

Of course, there is a limit to the number of blackened grains in an image element. If E is the maximum number of statistically independent grains per unit area, then B saturates at a value equal to $\alpha^2 F^2 E$ and

$$(n_0/N) = \sqrt{2k}\alpha(1+R)/FE^{1/2}$$

This indicates that the longer the focal length of the telescope and the finer the grain of the plate, the fainter the stars which can be photographed. The limiting magnitude does not depend directly on either the quantum efficiency of the detector or the integration time. High quantum efficiency is necessary to make exposure times feasible, but it is the storage capacity of the system that determines how faint we can go.

With the Lallemand tube and the barrier-film variations of it, the limiting magnitude is made fainter by the use of very fine-grain, electron-sensitive plates. Each photoelectron makes a blackened grain; or in the finer emulsions, a track. Thus, the quantum efficiency as we have defined it (the number of independent registered events per photon) remains high if the photocathode has a high quantum efficiency in the more conventional sense.

Increasing the limiting magnitude of a telescope, by using an image intensifier such as a cascade tube, to permit exposures on finer grained, and hence slower plates, depends on the uniformity of the phosphor screen. (See fig. 28-2.) But the sensitivity of available photographic materials falls off so rapidly, for only slight improvements in photographic granularity, that this is not a particularly promising approach.

Another way is to use the efficiency of an image tube system to improve the limiting magnitude which can be reached with a telescope of given aperture and to increase the effective focal length of the instrument. This is not a difficult optical requirement. At Flagstaff, Lowell Observatory has a 24-inch Cassegrain reflector with three interchangeable secondary mirrors. These give focal ratios of f/16, f/32, and f/104.

We have made test exposures on this telescope with each of the secondary mirrors in connection with our program for evaluating image tube performance. The most successful exposures, thus far, have been made with the preliminary samples of magnetically focused cascade tubes from RCA and ITT. The ion spots and field emission in the first sample tubes have restricted their usefulness, but nevertheless, these test exposures have indicated that this method is quite promising.[14]

Spectroscopy

The most extensive application of image intensifiers by astronomers probably will be in spectroscopic problems. The specifications which must be met by intensifiers used successfully in these problems are more severe than those for any other application. For example, resolution is more important here than in faint object photography since the width of the image is just the projected spectrograph slit width, rather than the much larger seeing-limited diameter of a stellar image. In general, the real or information gain of an intensifying system over an unaided photographic plate is the product of the gain in exposure time and the square of the ratio of the resolution of the system to the resolution of the plate.
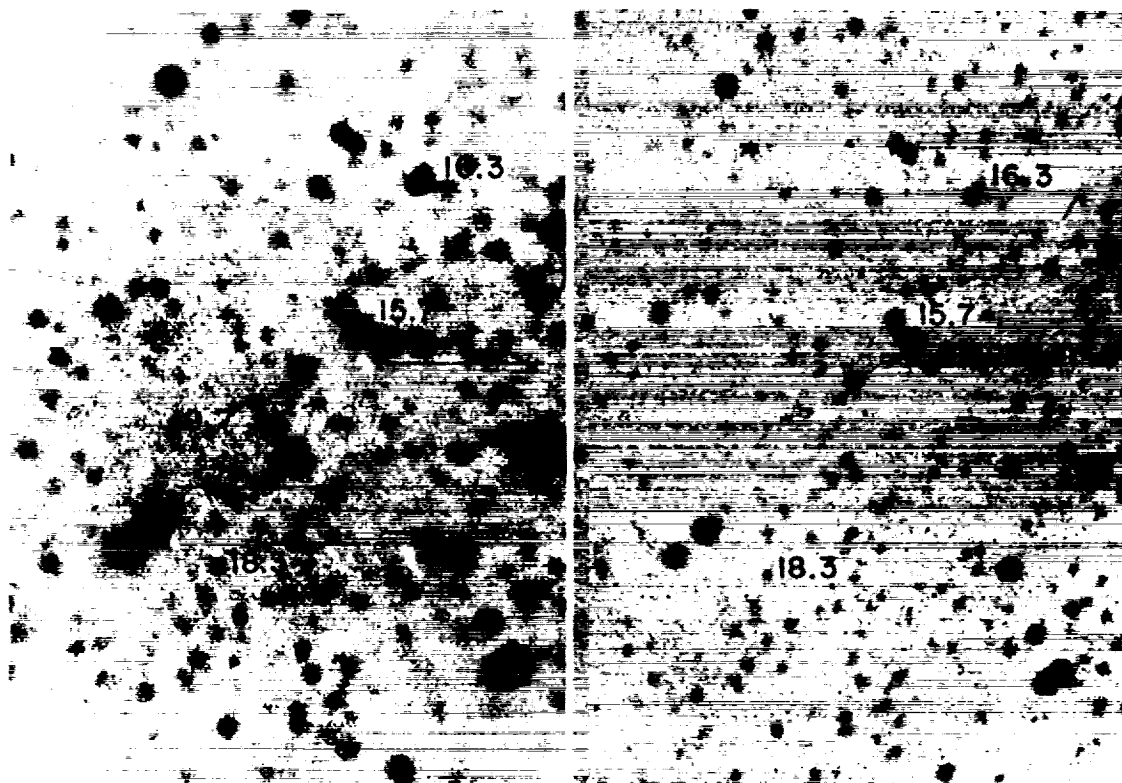
5 min. exposure with coscoded tube
on $\overline{\text{IV}}$ - G

20 min. exposure directly
on IIa - D

FIGURE 28-2.—Comparative exposures obtained on the U.S. Naval Observatory 40-inch reflector. The 5-minute exposure was made on a slow, fine-grain emulsion (type IV-G) with the aid of an RCA electrostatic cascade tube with a P20 phosphor screen. The 20-minute exposure is directly on a moderately fast photographic plate (type IIa-D) having approximately the same spectral response as the multialkali photocathode.

One application of image intensifiers in astronomical spectroscopy is in photographing spectra of time-varying phenomena. Here the speed of the image tube system can be used to obtain spectra of events whose actual duration may be less than the exposure required for an unaided plate. Walker has used the Lallemand tube to record the spectra of the irregular variable AE Aquarii during an outburst.[15]

The gain provided by an intensifying system can also be used to obtain spectra of fainter objects than can be obtained directly in the same exposure time. Or, alternatively, the gain can be used to detect weaker features in the spectrum by increasing the information storage capacity of the system; for example, with slow, fine-grained plates.

A final application of image intensifiers is in providing better detectors in regions of the spectrum where conventional plates are relatively inefficient. In particular, intensifiers with S1 photocathodes will provide great increases in sensitivity over existing photographic plates.

Summary

The major emphasis of the Carnegie Image Tube Committee during the past year or so has been on the promotion of the industrial development of magnetically focused image intensifiers.

Work during previous years has demonstrated the feasibility and usefulness of two general types of image-intensifying devices. One type involves pressing photographic film into optical contact

208

with a thin mica window in order to provide efficient transfer of an optical image from a phosphor screen to the photographic emulsion. The second general type of device relies on some method of internal electron multiplication to produce an image on a phosphor screen that is sufficiently bright to be photographed with conventional lenses. To date, for us the most successful has been the cascaded tube having an internal phosphor screen and a second photocathode in optical contact with it.

Photographic emulsions, as used in astronomy, require about 1,000 quanta of incident light per developable grain of silver halide, whereas a good photoelectric cathode will emit one primary photoelectron for every 7 to 10 incident quanta. Thus an ideal gain in sensitivity of perhaps 100 over that of the regular photographic procedures may be possible. In actual practice, and over an extended wavelength range, this potential gain factor is perhaps more like 40 or 50.

In addition to studies aimed at achieving the maximum useful gain with sealed-off tubes, the committee has sought to develop image tubes at industrial laboratories which would give good gains over photographic procedure and yet be simple to use, relatively permanent in calibration, and generally available to all astronomers. Prototype image tubes became available for testing this year from industrial suppliers under support of a National Science Foundation grant. This grant was made after the earlier Carnegie efforts and tests were carried out, in order to underwrite the rather large industrial costs for prototype development. These tubes promise to be highly useful in many fields of astronomical research. Using special fine-grained phosphors of high resolving power, and with magnetic focusing using permanent magnets, three types of image tubes can now be manufactured each of which provides a practical gain of a factor of 10 or more over photography. Spectroscopic researches, and new work on double stars have been strikingly successful with the prototype tubes, and it is hoped that initial manufacture of these tubes in modest numbers can be arranged during the coming year.

Acknowledgment

Discussion

W. F. NIKLAS: Could you please comment on the mica-window tube utilizing electronography?

W. K. FORD: We have not worked with an electronographic mica-window tube. The recent work of McGee and Wheeler, described in the London symposium in September 1961, indeed looks very promising.

J. WATERS: Have you evaluated the magnetically focused tube made by Twelfth Century Electronics in England, and if so with what results?

W. K. FORD: No. We have, however, evaluated both Wilcock's imaging electron multiplier and TSEMs developed and made at the Westinghouse Research Laboratories. These tubes will be competitive, for our purposes, with the cascade tubes when they are available in larger sizes and with slightly improved resolution. Of course, the spurious background, due to penetrating secondary electrons, must be kept low.

References

1. TUVE, M. A., FORD, W. K., JR., HALL, F. S., and BAUM, W. A.: Pub. Astr. Soc. of the Pacific, vol. 70, 1958, p. 592.
2. Report of Committee on Image Tubes for Telescopes. Carnegie Institute of Washington Year Book 58, 1959, p. 309.
3. KRASOVSKY, V. I.: Doklady Akad. Nauk., vol. 66, 1949, p. 53.
4. KRASOVSKY, V. I.: Bul. Cri. Astrop. Obs., vol. 5, 1950, p. 100.
5. ZACHAROV, B., and DOWDEN, S.: Symp. on Photoelectric Imaging Devices, London. September 1958.
6. VOLKOV, I. V., ESIPOV, V. F., and SHCHEGLOV, P. V.: Doklady Akad. Nauk., vol. 129, 1959.
7. LUKASHENJA, V. T., and KRASSOVSKY, V. I.: C.R. Acad. Sci., U.S.S.R., vol. 79, No. 2, 1951.
8. LUKASHENJA, V. T., and KRASSOVSKY, V. I.: C.R. Acad. Sci., U.S.S.R., vol. 80, No. 3, 1951.
9. LUKASHENJA, V. T., and KRASSOVSKY, V. I.: C.R. Acad. Sci., U.S.S.R., vol. 81, No. 5.
10. FREDERICK, LAURENCE, W.: Lowell Obs. Bull., No. 114, 1961.

11. DeWitt, J. H., Hardy, R. H., and Seyfert, C. K.: Sky and Telescope, vol. 17, 1957, p. 8.

12. Baum, W. A.: Trans. Int. Astr. Union, vol. IX, 1957, p. 681.

13. Baum, W. A.: *The Detection and Measurement of Faint Astronomical Sources.* Star and Stellar Systems, vol. II, Univ. of Chicago Press, 1962.

14. Report of Committee on Image Tubes for Telescopes. Carnegie Institute of Washington Year Book 60, 1961, p. 339.

15. Sky and Telescope, vol. 22, 1961, p. 255.

29. EXPERIMENTS WITH THE BENDIX CONTINUOUS-CHANNEL MULTIPLIER

G. W. Goodrich and W. C. Wiley, *Research Laboratories Division, The Bendix Corp.*

Introduction

Because of the interest being expressed in continuous-channel multipliers, we would like to discuss the results of some of the experimental work done in this area at Bendix Research Laboratories. At the same time, we would like to acknowledge the interest and support of the Astrophysics Branch of the National Aeronautics and Space Administration which made many of these measurements possible. Since the time available for presentation is rather limited, it will only be possible to present a summary of the most important results.
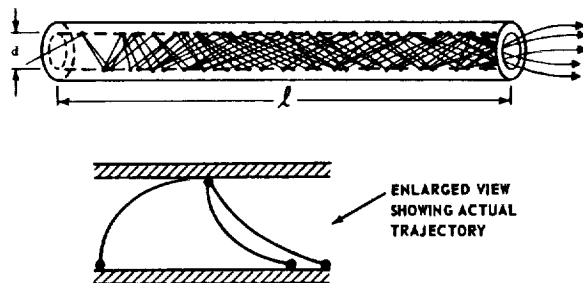

FIGURE 29-1.—Principle of channel multiplier.

As shown in figure 29-1, a continuous-channel multiplier consists of a long thin tube, the inside surface of which contains a high-resistance coating. When a potential difference on the order of 1,000 to 2,000 volts is applied between the metalized ends, a uniform electric field is established within the channel. A secondary electron within the channel will, in general, be created with a transverse velocity equivalent to about 1 electron volt of energy. This transverse velocity will carry it across the tube while the electric field accelerates it down the tube. By proper proportioning of diameter and field strength, a sufficient amount of energy is imparted to the typical electron so that it will, on the average, generate more than one secondary upon collision with the opposite wall.

Thus, a cascading action is instigated which can produce electron gain which exceeds 10^6. Arrays of such multipliers appear to be useful for image intensifiers. Among intensifiers which operate on the multipactor principle, continuous-channel multiplier intensifiers appear likely to offer advantages in ease of fabrication, minimization of electric field gradients, and freedom from cross-talk. Among other intensifiers as a whole, continuous-channel multiplier intensifiers appear to offer advantages in size, weight, operating voltage, and simplicity of operation.

Experimental Results

An accurate analysis of operating characteristics of continuous-channel multiplier presents formidable problems because these characteristics depend upon the statistical distribution of emission energies, emission angles, and upon secondary emission ratios, as both a function of energy and angle of incidence. Many of these properties are presently not known. In addition, exact analytically derived relationships are too complex to provide much design insight. For this reason, we have turned to empirical methods to establish the characteristics. However, one useful result from trajectory analysis, which is virtually self-evident anyway, is that the device can be scaled in such a fashion that similar gain characteristics are maintained, if both length and diameter are changed in proportion. The potential applied between the ends is held unchanged.

Gain measurements as a function of applied voltage and length-to-diameter ratio have been made on tubes ranging from 0.004 inch to 0.04 inch. Figure 29-2, which happens to be for a 0.022-inch I.D. channel, is representative of such measurements. As can be seen, gains up to about 10^6 are obtained. Feedback commonly occurs when the gain exceeds about 10^6 for tubes smaller than 0.022 inch. A somewhat lower limit applies
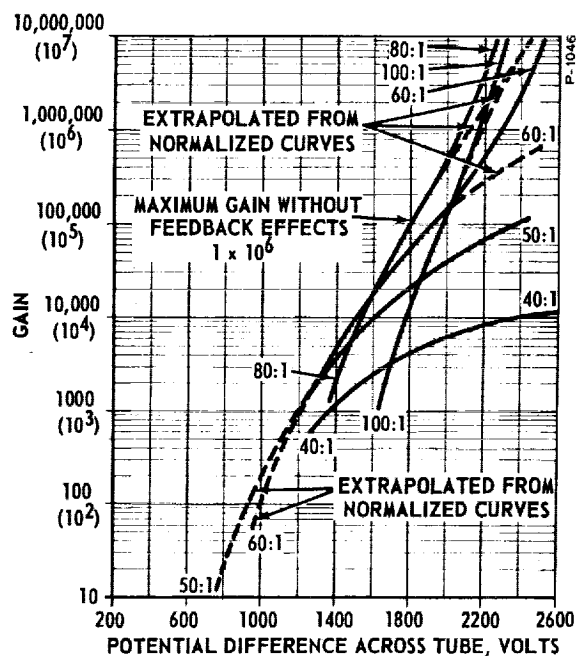
211

FIGURE 29-2.—Gain characteristics of 0.022-inch tubes.

FIGURE 29-3.—Noise factor.

to larger channel diameters. The region of about 10^3 to 10^5 electron gain is of greatest interest in image intensification and feedback is not in evidence here. Thus, gain appears adequate.

Because of the statistical distribution of impact energies, there is particular reason for investigation of noise addition to signals. Measurements of RMS noise, added to a signal by a continuous-channel multiplier, have been made as follows. A known input current was initiated in a channel by a Sr[90] beta source. The output current was directed into an electrometer circuit with a known RC time constant. A regular sequence of readings was taken from the electrometer at intervals separated by a large number of time constants. The fractional RMS noise was then computed from these readings and divided by the fractional RMS noise expected in the input current from shot noise considerations. The results are shown in figure 29-3. The X-axis represents normalized potential gradient; i.e., the number of volts increase in potential in a distance along the long axis of the tube equal to one diameter. The Y-axis represents noise factor; i.e., the fractional RMS noise in the output divided by the fractional RMS shot noise in the input current.

Plotted on the same figure, for comparison, is the noise factor to be expected purely on the basis of Poisson emission statistics such as would
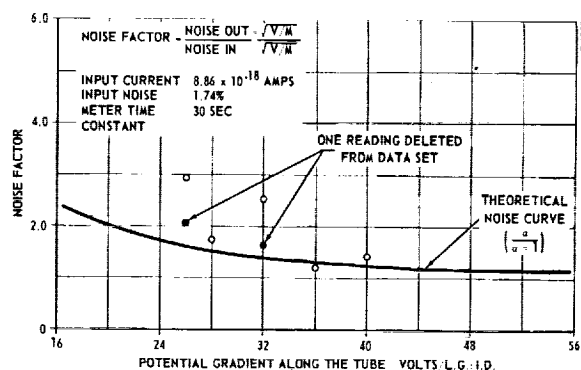
be predicted in a discrete multiplier with the same gain per stage as the average gain per impact in the channel. The reliability of the data points increases substantially from left to right. This is because the gain, and therefore the output current, is 20 times higher for the extreme right point than the extreme left and the electrometer was relatively much less subject to capacitive coupling with objects moving in the room and to meter reading errors. Both spurious effects will produce fictitiously high noise factors. In this sense, the measurements to the left constitute an upper bound more than a determination. In any event, if one takes the noise factor of about 1.4 which is found around 36 to 40 volts, diameter as typical, it is interesting to note that it is the same distribution as could be expected from an exponentially decreasing pulse height distribution. This distribution has been experimentally found for a number of multiplier devices such as TSFE intensifiers and conventional photomultipliers, although it is not predicted by Poisson statistics. It can further be shown, that if the first impact of a photoelectron going into a continuous-channel multiplier is made to produce a plurality of secondaries, the contribution to noise of the continuous-channel multiplier is reduced. For example, if six initial secondaries are produced, the continuous-channel multiplier contribution to the overall noise factor, (based on the 1.4 noise factor obtained above), will be only 0.08. There appears to be no obstacle to realizing some such arrangement in practice. While no serious noise problems have been indicated by this work, it should be recognized that the number of such measurements is not great, and more work would be useful in this area.

212

Discussion

J. M. GRANT: What is the maximum value of the secondary emission ratio of the channel surface, and at what primary energy does this occur?

G. W. GOODRICH: In our work, measurements of the performance of secondary emitting surfaces have always been made in terms of overall continuous-channel multiplier performance. Therefore, this number is not available. Since many quantities are interconnected in a complex fashion, we believe this procedure is easier, and gives more realistic information than separate measurements of secondary emission ratio as a function of energy and angle of impact, etc. In extrapolating measurements made on various emitters, I believe more realistic results would be obtained if the value for C, in your work, were determined at the average energy of impact (around 100 electron-volts for $Er_0 = 16$ volts) rather than an arbitrary determination at the primary energy corresponding to the maximum secondary emission ratio. This will give values of C from 0.03 to 0.05 for commonly used secondary emitters.

G. PAPP: What is the inside coating of these multipliers, and how do you maintain uniform field distribution along the channels?

G. W. GOODRICH: The channels are comprised of a semiconducting metallic oxide coating on a glass substrate. Uniformity of the field is maintained by providing uniform surface resistivity in the semiconducting material. Since the fabrication of the surfaces requires a certain amount of art and the area is of a general proprietary nature, more specific details cannot be given at this time.

W. F. NIKLAS: Did I understand you correctly in that you have knowledge of the velocity distribution of the TSE electrons?

G. W. GOODRICH: The secondary electrons in the continuous-channel multiplier are normal secondaries rather than transmission secondary electrons (TSE), so we do not have information about the velocity distribution of TSE electrons.

30. EXTREME ULTRAVIOLET DETECTION WITH THE BENDIX SINGLE-CHANNEL PHOTOMULTIPLIER *

D. W. Angel, H. W. Cooper, W. R. Hunter, and R. Tousey, *U.S. Naval Research Laboratory*

The continuous-channel photomultiplier developed by the Bendix Research Corp., and described in the previous paper by G. W. Goodrich and W. C. Wiley, promises to be useful as a detector of extreme ultraviolet radiation. Its tiny size, combined with high sensitivity, makes it unique among photocells. In this paper, there are presented the first results of a study of the response of a few channel photomultipliers to extreme ultraviolet radiation. Ordinarily, to scan an image photoelectrically, a small movable aperture is placed in the image plane, and a phototube with large enough cathode to cover the entire image is situated behind the scanning aperture. The channel photomultiplier, however, is so small that it serves also as the aperture.

Figure 30-1 is a diagram of the channel multiplier and the basic circuit, and figure 30-2 is a photograph of an actual channel, with leads attached. A beam of nearly parallel extreme ultraviolet radiation was allowed to enter one end of the channel, at a small angle to the axis. As will be shown later, the optimum angle was found to be 15° to 20°. Photoelectrons ejected from the semiconducting internal surface were accelerated down the channel by the high voltage, with multiplication taking place at each collision on the wall. The emergent electrons were collected by a small plate, maintained at about 67 v positive, and the current was measured by a suitable amplifier and recorder.

The particular channels studied were four in number, of 0.215-mm internal diameter, and length to bore ratio of approximately 50. One channel of 0.41-mm bore was also tested.

The extreme ultraviolet radiation was produced by a 1-meter grating vacuum monochromator. Figure 30-3 shows at the upper right the chamber, attached to the exit slit, into which the fixture holding the channel is introduced hori-
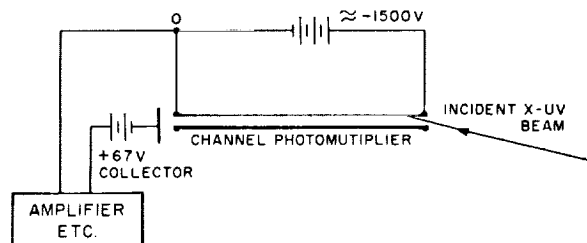
FIGURE 30-1
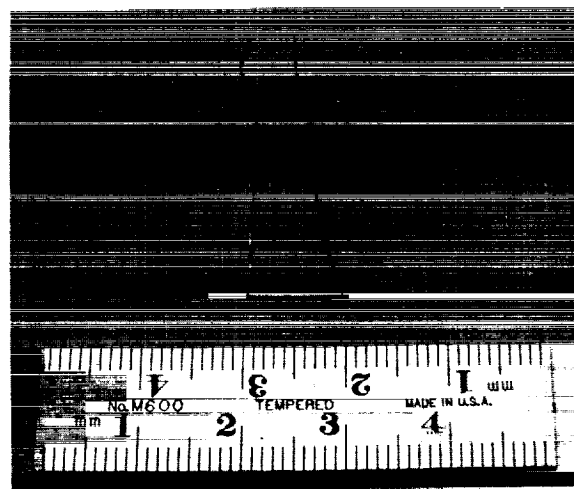
FIGURE 30-2

zontally. The vertical fixture at the top of the chamber was provided for monitoring the beam. A fluorescence sensitized 1-P21 photomultiplier monitor was used during all the measurements, and for determining the beam intensity at each wavelength, relative to Lyman-alpha, 1,216 Å. For making an absolute determination of the energy at Lyman alpha, the 1-P21 was removed and an ionization chamber with LiF window introduced in its place.

The fixture holding the channel photomultiplier is shown removed in figure 30-4. The channel may be seen in place, held to a Kel-F
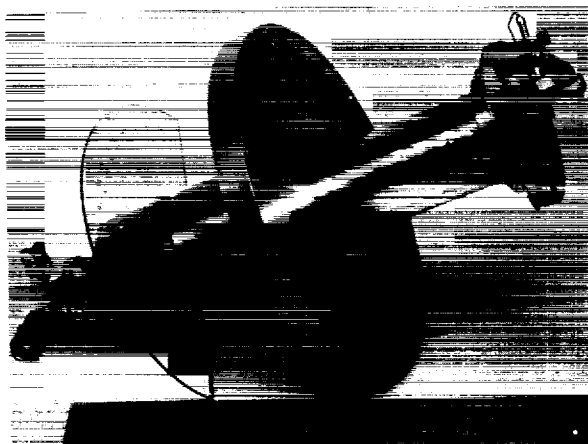
FIGURE 30-3

FIGURE 30-4

support, on the end of a shaft. This fixture permitted rotating the channel through measured angles with respect to the light beam around an axis passing through the end where the light was incident.

The chamber containing the multiplier was evacuated by a separate 2-inch diffusion pump, with liquid nitrogen trap, shown at the center of figure 30-3, so as to pump away rapidly the small amount of gas coming through the exit slit. The vacuum was maintained at 10^{-6} mm Hg or

better during all measurements, a value sufficient to remove all possibility of gas ionization effects. In some of the first tests, with a poorer vacuum, difficulties were encountered from contamination of the multiplier, probably with decomposition products of backstreaming oil from the pump. The result was an overshoot whenever the photomultiplier was exposed to radiation; the current rose quickly, then dropped in a few seconds to a steady value of the order of half the initial value. This phenomenon was not observed with proper evacuation.

Measurements of spectral response were made for one channel, set at 15° to the beam, and operated at 1,500 volts. The data are presented in figure 30-5, together with values of photoelectric
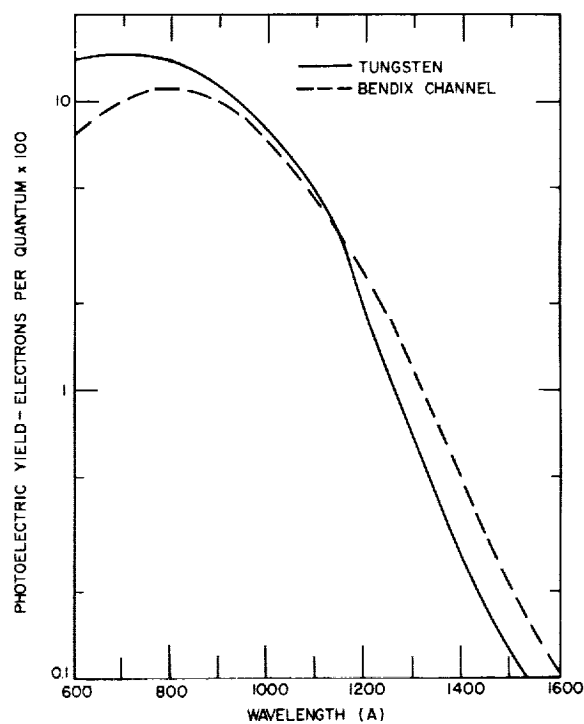
FIGURE 30-5

yield for untreated tungsten, obtained by Hinteregger and Watanabe [1] ($\lambda > 1,000$ Å) and Walker, Wainfan, and Weissler [2] ($\lambda < 1,000$ Å). Because the gain of the channel photomultiplier was not known, only relative values of photoelectric yield were obtained. As plotted, they were adjusted to agree with the values of tungsten between 1,000 and 1,100 Å. The spectral response of the channel multiplier was quite similar to that of tungsten, although the photo-emitting surface on the inside of the channel was not tungsten, but was an oxide of some other metal. Like phototubes with

tungsten cathodes, however, the channel photo-multiplier is blind to visible, and near ultraviolet radiation, and to most of the Schumann region.

To test the stability and reliability of the channel photomultipliers, a number of runs of output versus applied voltage were made at 1,216 Å and 584 Å. Results for one channel are presented in figure 30–6. Data on three other
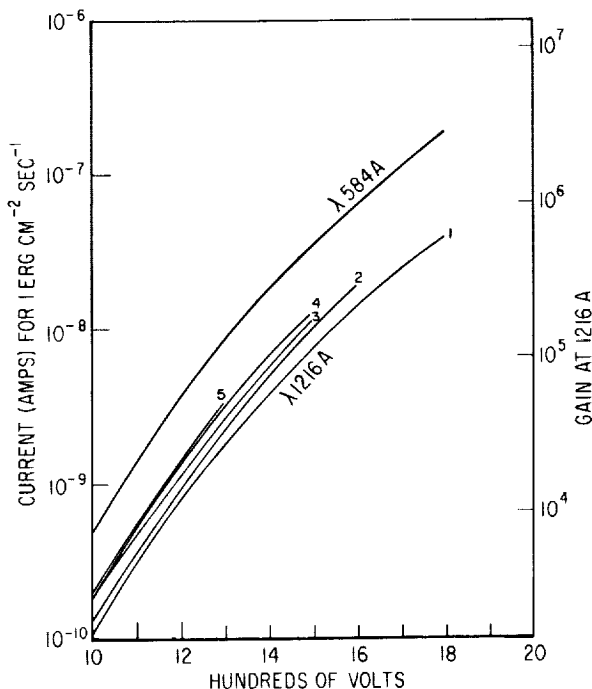
FIGURE 30–6

channels were similar. The channels were irradiated at 15° to the axis. The ordinate is the current output in amperes, for an irradiance value of 1 erg cm^{-2} sec^{-1}. To obtain the actual measured currents, it is necessary to multiply by the irradiance. This value was 0.4 erg cm^{-2} sec^{-1} for λ1,216 Å, and 0.009 erg cm^{-2} sec^{-1} for λ584 Å. Thus the actual current output ranged from 4×10^{-11} to 10^{-8} amperes at λ1,216 Å, and from 10^{-11} to 10^{-9} at λ584 Å.

The several curves for λ1,216 Å refer to different runs on the same channel. These were made over a period of 4 days, as follows: Run No. 1 at λ1,216 Å was made on the first day. After staying overnight in a 1-mm Hg vacuum, a run was made at λ584 Å; this was followed by a ½-hour exposure to air and then run No. 2 at λ1,216 Å. Run No. 3 was made 2 hours after the second run. The multiplier was then left over-

night in a 1-mm vacuum, next placed on the diffusion pump for 4 hours without the liquid nitrogen. Then the trap was filled and run No. 4 was made. After this, the multiplier was removed and placed in a desiccator overnight, and run No. 5 was made on the fourth day.

It can be seen that the sensitivity of the multiplier increased with use by nearly a factor of 2, but appeared to steady down after several runs. The other tubes tested showed a nearly identical increase with use, but showed somewhat lower sensitivity values; in one case about one-half as great as for the first tube.

The channel photomultipliers showed fatigue when overloaded, either by excessive voltage, or by too much radiation. This was manifested by a gradually declining output current. After a short rest period, however, recovery appeared to be complete or nearly so. The several runs indicate by their terminal points the voltage at which fatigue was first observed. When new, the tubes appeared to withstand without fatigue a higher voltage than after use. Current values were of the order of 10^{-8} amps at these upper limits, but 10^{-9} amps is probably a safer limit for this size multiplier.

It was possible to calculate the gain at λ1,216 Å by assuming that the values of photoelectric yield determined by reference to tungsten (fig. 30–5) are correct. These calculated values of gain at λ1,216 Å, that is, electrons output per photo-electron, are shown by the scale at the right of figure 30–6. Useful gains between 10^4 and 10^5 were attained.

The channel photomultipliers, as used in this study, were operated far above the region of single photon counting. For example, a current output of 10^{-9} amp, with gain of 10^4, means 6×10^5 photo-electrons per second. As a result, the statistical noise in the output was negligible. Noise was sometimes encountered, but this was produced in the light source. By proper operation of the discharge tube and monochromator, the output current could be made nearly noise free.

The current value with no light was usually of the order of 10^{-12} amp, which was negligible compared to the current being measured. This was mainly a leakage current, and was reduced by cleaning with acetone to less than 10^{-13} amp. It is probable that the true dark current was very small, and that with more refined cleaning procedures, the leakage current could be reduced still further.

The response against angle of incidence was studied in detail for only the first photomultiplier received, of bore 0.41 mm. The result is shown in figure 30–7. The maximum response occurred
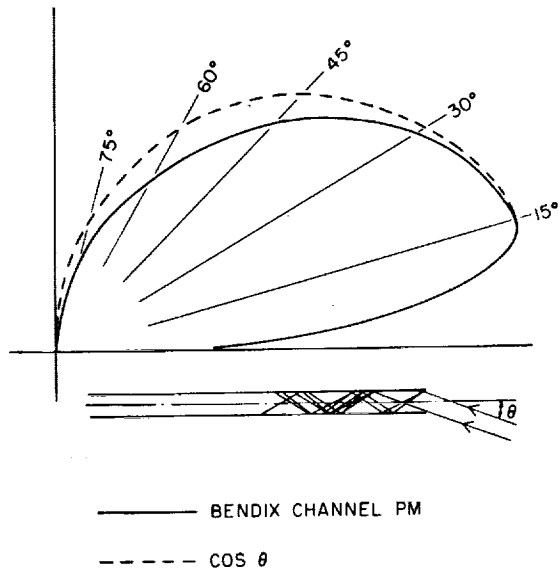

Figure 30–7

with radiation incident at about 15° to the axis. For other photomultipliers the maximum ranged to angles as great as 20°. On axis, the response was reduced to 30 percent, presumably because some of the radiation passed all the way through the channel without striking the wall. Since most of the portion intercepted by the wall was incident far down the channel, the photoelectrons received less amplification. The on-axis value is not of significance, since it must be strongly dependent on the degree to which the radiation is parallel.

At angles greater than 15° the response followed approximately a cosine curve as would be expected, since this is the function describing the projected area of the end of the channel. Actually, the response fell below the cosine curve. This might be expected, since some photoelectrons produced very close to the end of the channel may be ejected outward and not captured by the field inside the channel. As the angle of incidence approaches 90°, the beam becomes confined to the very end; at lesser angles, because of the greater angle of incidence and the increased reflectance value, the beam penetrates well down the capillary and all the photoelectrons are captured. Another possible explanation is that the

photoelectric yield is reduced, near normal incidence, as is known to be the case for potassium.

The application for which the channel photomultiplier is being considered is the monitoring of the sun's disk in the light of the Lyman-alpha line of hydrogen. This portion of the project is under the direction of J. D. Purcell, C. R. Detwiler, and R. Tousey. The measurements are to be made from the solar-pointed portion of the NASA S–17 orbiting solar observatory.

Figure, 30–8 is a schematic of the instrument.
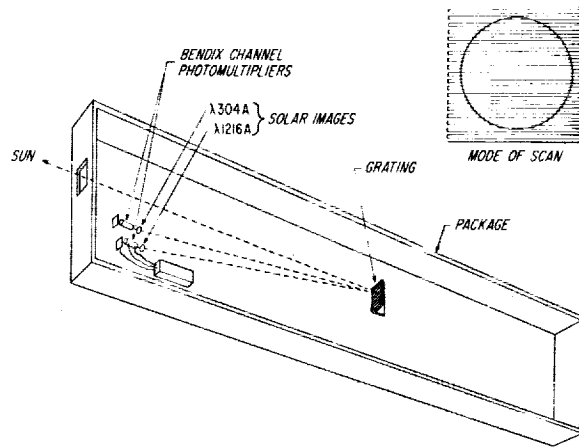
Figure 30–8

The sun's radiation is incident on a diffraction grating which forms nearly stigmatic images of the sun in the various monochromatic line emissions. For the wavelength diffracted normally to the grating, the image is completely stigmatic. It is planned to employ a 1-meter radius grating, producing an image of the sun 4.6 mm in diameter. One channel photomultiplier will be placed at the center of the sun's Lyman-alpha λ1,216 Å image. A channel of 0.15-mm bore will be used; this will intercept an area of the sun 1° of arc in diameter, thus providing a picture by turning the entire instrument in a raster type of motion, as indicated by the insert in figure 30–8. The motion will be through 40° of arc in one direction, then stepped down through 1° and scanned back again, and so forth until a 40- by 40-foot area centered on the sun has been covered.

The use of the channel photomultiplier in this instrument has two great advantages. First, its near complete lack of response to the intense visible and near ultraviolet solar radiation serves automatically to reject the strong stray light included in the spectrum produced by the single

218

grating. Second, its simplicity and extremely small size and weight adapt it perfectly to this satellite scanning application.

It is also planned to use one or more additional channel photomultiplier detectors to monitor the sun in other wavelengths. For example, a channel will be placed in the image produced by the 304 Å line of ionized helium. The third order image, 912 Å, will probably be employed, since it falls near the grating blaze. It will be essential, however, to eliminate the intense scattered light from Lyman-alpha, $\lambda 1,216$ Å, to which the channel is sensitive. This can be accomplished by introduction of a thin film of aluminum into the beam, at a position a few mm in front of the channel. Aluminum is opaque at all wavelengths greater than 850 Å and

transmits well at 304 Å. Photoelectrons ejected from the aluminum can be prevented from entering the channel by keeping the aluminum at a potential a few volts positive relative to the end of the channel.

Acknowledgments

References

1. HINTEREGGER, H. E., and WATANABE, K.: J. Opt. Soc. Amer., vol. 43, 1953, p. 604.
2. WALKER, W. C., WAINFAN, N., and WEISSLER, G. L.: J. Appl. Phys., vol. 24, 1953, p. 1318.

31. MEDICAL APPLICATIONS OF IMAGE INTENSIFICATION

EUGENE C. KLATTE, *Indiana University School of Medicine*

During the last 2 years image intensification has gained wide clinical acceptance in the field of radiology. The image amplifier is an important adjunct to fluoroscopy. With intensification of the fluoroscopic image one to several thousand times, dark adaption has become unnecessary. Fluoroscopic resolution has become markedly improved and diagnostic acumen thereby increased. The disadvantage of present-day amplifiers is their bulk. Palpation of the abdomen—particularly in the upright position—is more difficult and the constant movement of the increased weight of the image tube is tiring. Remote-control fluoroscopic units have been developed [1] [2] but they are quite costly and have not been generally accepted. In spite of the disadvantage, the increased clarity of the fluoroscopic image and the lowering of radiation dose to the patient are so advantageous that most radiologists plan to replace their conventional fluoroscopic units as soon as it becomes economically feasible.

The main debt of the field of radiology to image intensification is that it is now possible to obtain sufficient light from the fluoroscopic screen to be able to perform cineradiographic procedures with little more radiation dose than that necessary for conventional fluoroscopy. For some time cineradiography has been considered a useful experimental tool. It has now been established as an important part of the armamentarium of the radiologist in the study of dynamic function.

There are three basic types of screen intensification systems being used in medical cineradiography today. The first system employs the electrostatic triode image converter. Fluoroscopic viewing is by means of a mirror optical periscope and the cine recording are taken directly from the output phosphor of the image tube.*

The second system employs an extremely sensitive image orthicon connected by means of

mirror optics to a conventional fluoroscopic screen.† The intensified image is viewed on a television monitor and the image may be recorded by means of a kinescope or a video tape system.

In the third system the fluoroscopic image is focused by means of mirror optics on the input screen of a light amplification tube.†† The intensified image can be filmed off the output phosphor, or viewed through a periscope or television system.

There may be various combinations of the above methods. The most common is the combination of an electrostatic triode image converter and an image orthicon. This combination is capable of amplifying the fluoroscopic image over 50,000 times.

The high-contrast resolution of currently available amplification systems is 30 to 50 line-pairs per inch. This is less than one-half that obtained with conventional radiographs and is currently the main limiting factor of cineradiography. There is a noticeable improvement in the apparent resolution of cineradiographs when viewed in motion, due to the superimposition of several images during the latent period of the eye. A common factor which decreases image resolution is the direct result of manufacturing improvements of amplification systems, lens systems, and film emulsion. Due to increased speed of these systems, cineradiographs may be obtained at such low radiation doses that a marked deterioration of image quality has resulted. Many radiologists do not realize that a certain number of information-bearing photons must be absorbed by the input phosphor of the image tube in order to form a clear confluent image which can then be amplified and recorded. [3] With very low radiation levels, the statistical fluctuation of the number of photon per given area may cause a marked decrease in low contrast resolution.

*Manufactured by General Electric, Keleket, Philips, Picker, Westinghouse.

†Manufactured by Marconi.
††Manufactured by Old Delft.

It has been our experience that with image amplification systems of beyond 2,000 gain, it is frequently necessary to decrease the speed of the lens system in order to obtain good diagnostic clinical studies.

The radiation dose of any particular cineradiographic examination is dependent upon a number of factors: the quality of the X-ray beam, whether the unit is synchronized, the image amplification factor, the speed of the lens system, the filming speed and the type of film used for recording. With present-day units, it is now possible to perform cineradiographic examination of the heart in an adult patient at 30 frames per second for from 0.1 to 10 r per minute.

Clinical Applications

Cineradiography has long been recognized as a useful research tool; however, only in the last few years has it been established as an important clinical tool. Cineradiography is now recognized as the best radiographic method of studying dynamic function.

In the study of the pathological anatomy and physiology of congential heart disease, the cineradiographic method is ideal.[4-6] A general advantage of the cineradiographic method is that the filming unit is an integral part of the cardiac catheterization unit so that the patient does not need to be moved to another area for filming. Also one can observe the image during the filming sequence; the diagnosis can usually be made and the necessity of future angiographic sequences with different injection sites or different projections can be made immediately. At Indiana University Medical Center, we study all patients with congenital heart disease with selective cinecardiography at the completion of cardiac catheterization. This philosophy was adopted for the following reasons. In many cases, inadequate catheter exploration occurs. It frequently is impossible to pass the catheter into the outflow vessels or left heart. Confusing catheter findings may be present due to the streaming effect of blood. The cineradiographic method is also more accurate than oxygen determinations in diagnosing small left to right shunts. By visualizing the anatomy of the abnormality, the surgeon is frequently better able to plan in advance the best surgical approach. This method also supplements the catheterization findings so that a more secure preoperative diagnosis is possible. At

our institution, over 2,000 children with congenital heart disease have been satisfactorily studied by this method.

The value of selective left heart cinecardioangiographic techniques in acquired heart disease is now firmly established.[7] It is the most accurate method of evaluating insufficiency lesions of the aortic and mitral valves.[8] It also gives valuable information as to the pathological anatomy of a valve and is helpful in determining whether a valvuloplasty or valvular replacement may be necessary.

In the study of coronary artery disease, selective cineangiographic techniques have been of considerable value in accurately outlining the extent and location of atheromatous changes. These studies can be correlated with electrocardiography to better evaluate this indirect method. With the beginning of surgical correction, the necessity of exact information in determining the course of these individuals has become extremely important.

The urinary tract is another organ system in which cineradiography has proven to be a valuable method of study.[9] The beauty of the method is that the dynamics of these motile visiers may be demonstrated with a gonadal dose of less than 200 milliroentgens. The principle utilization of this technique at our institution has been in the study of bladder and urethral abnormalities in children. Over 400 children have now been studied. The diagnoses of bladder neck contracture, urethral stenosis, posterior urethral valves, neurogenic dysfunction of the bladder, and ureteral reflux can now be reliably made. The study of the dynamics of the upper urinary tract is important in differentiating normal calycine and ureteral contraction from deformity or stricture.[10] The importance and reliability of this method of examination cannot be overemphasized. Of children referred with symptoms of urinary tract disease, less than 30 percent are normal. Many have conditions such as bladder neck contracture, the correction of which may be lifesaving.

In order to adequately study the gastrointestinal tract, the functional dynamics must be closely examined. This is routinely attempted at fluoroscopy but rapidly occurring events cannot be appreciated. Also during such examinations, the radiologist must maneuver the patient and manipulate the X-ray machine while he is attempting to arrive at diagnostic conclusions.[11]

By obtaining a permanent record on cine film, these distractions are eliminated and later he may more carefully analyze and interpret the results. Also during conventional fluoroscopy, it is usually possible to study in detail only one section of the fluoroscopic image at one time. The action must therefore be viewed repeatedly through a number of cycles with additional dose to the patient and operator. In contrast to this, if a filmed record is obtained, the radiologist may analytically study the film record on multiple viewings, focusing his attention first on one area and then another until the full amount of information is appreciated. The film is also a permanent portion of the patient's record so that the dynamic appearance of various lesions can be longitudinally studied and compared. The cine method admirably records the abnormal dynamics of neurological disorders of the pharynx and esophagus, vascular lesions of the esophagus, and abnormalities of the esophagogastric junction. The rapid filming rate makes the difficult differentiation of an H-type tracheoesophageal from aspiration comparatively easy. By carefully noting the dynamics of the contracting stomach, extremely early cancers may be demonstrated before other radiographic signs are present.

In corrective orthopedics, the recording of motion is an invaluable aid. The stability of a spinal fusion, the detection of ligamentous and disk damage in whiplash injuries of the neck, the effect of various maneuvers on the hip of a child with suspected dysplasia, and cinepneumoarthrography in the study of joint motion are only a few of the practical applications in this field.

There are several other fields in which cineradiography has been proven to have practical application. In corrective speech therapy, it is possible to analyze the defective movements of the tongue and palatine structures;[12] in orthodontia, the study of malocclusion and temporomandibular action can be more decisively evaluated. The

dynamics of the uterus in habitual abortion may be more easily appreciated when hysterosalpingograms are studied in motion. With image amplification devices of sufficient size and with improvement of image resolution, cineradiography may add to the thoroughness of cerebral angiography by the recording of all vascular phases.

Future

The principal limitation of image intensification in radiology is the limited resolution and field size. If image tubes could be developed with resolution comparable to conventional radiographs, the entire filming method would be revolutionized. Radiographs could be obtained at a fraction of the radiation dose currently utilized. Miniaturization would then become feasible with a tremendous saving of film and storage facilities.

Summary

1. Image intensification has dramatically improved radiological methods.

2. With intensification of the fluoroscopic image, dark adaptation has become markedly improved and diagnostic acumen thereby increased.

3. Cineradiography offers the simplest method of rapidly recording the dynamic motions of any anatomical area for analytic study.

4. The most useful clinical applications currently established for cineradiography are selective cardioangiography, voiding cystourethrography, dynamic derangements of the gastrointestinal tract, and joint studies in corrective orthopedics.

5. The limiting factors of present amplification systems are field size and resolution. Upon the solution of these problems, the entire filming method of radiology would be revolutionized and radiographs could be obtained at a fraction of present radiation dose.

Discussion

I. LEVIN: Image intensifiers have also been used to study microanimals (chiggers, etc.) and insects at night in their habitats in the tropics.

References

1. JUTRAS, A.: *Teleroentgen Diagnosis by Means of Video Tape Recording.* Amer. J. of Roentgenology, vol. 82, 1960, pp. 1099–1102.
2. DUCKETT, G.: *Daylight Telefluoroscopy.* Amer. J. of Roentgenology, vol. 84, 1960, p. 566.
3. CAMPBELL, J., KLATTE, E. C., AND SHALKOWSKI, R. A.: *Factors Influencing Image Quality in Cineroentgenography.* Amer. J. of Roentgenology vol. 83, 1960, pp. 345–353.

4. KLATTE, E. C., CAMPBELL, J. A., AND LURIE, P. R.: *Technical Factors in Selective Cinecardioangiography*. Radiology, vol. 73, 1959, pp. 539-546.

5. CAMPBELL, J. A., AND KLATTE, E. C.: *Current Status of Cinefluorography in Cardiac Diagnosis*. Progress in Cardio-vascular Disease, vol. 2, 1959, pp. 20-35.

6. SONES, J. M., JR.: *Cinecardioangiography*. Pediat. Clin. North Amer., vol. 5, 1958, pp. 945-979.

7. JUDSON, W. E., KLATTE, E. C,. AND RAUSCH, N. H.: *Cinecardioangiography in the Diagnosis of Acquired Heart Disease*. Circulation, vol. 22, 1960, p. 768.

8. JONTZ, J. G., KLATTE, E. C., AND KING, H.: *The Quantitation of Acute Experimental Mitral Insufficiency With Left Heart Cinecardioangiography and Pressure Studies*. Surgical Forum, vol. 10, 1960, pp. 466-469.

9. GARRETT, R. A., AND KLATTE, E. C.: *Cineurography*. J. of Urology, vol. 83, 1960, pp. 498-500.

10. GREENWOOD, F. G.: *Cineradiography in Urinary Tuberculosis*. Brit. J. of Radiology, vol. 30, 1957, pp. 493-496.

11. POTSAID, M. S.: *Kineradiography*. New England J. of Med, vol. 264, 1961, pp. 178-184 and 232-237.

12. KIRKPATRICK, J. A., AND OLMSTED, R. W.: *Cinefluorographic Study of Pharyngeal Function Related to Speech*. Radiology, vol. 73, 1959, pp. 557-559.

224

32. DESIGN AND PERFORMANCE OF AN IMAGE INTENSIFIER FOR ASTRONOMICAL APPLICATION*

W. A. HILTNER, *Yerkes Observatory, University of Chicago*, and W. F. NIKLAS, *The Rauland Corp.*, a *Subsidiary of Zenith Radio Corp.*

Introduction

The interest in image intensification for astronomical application is based upon the difference in quantum efficiency of the photocathode and the photographic emulsion. If we assume that a photocathode of the S–11 type is utilized (maximum quantum efficiency approximately 15 percent), and if we assume that the quantum efficiency of the photographic plate is approximately 0.1 percent, a gain of 150 may result. If an S–20 photocathode is used (maximum quantum efficiency approximately 20 percent, or if the light level incident upon the photographic emulsion is very low so that the reciprocity law is not valid, higher gain values can be achieved. These considerations are only applicable when the quantum sink of the system, i.e., that stage where the average quantum number incident upon a single information element per time unit is a minimum, is located in the photocathode and nowhere else.

Increasing the quantum efficiency of the primary sensor is, however, only then equivalent to a true information gain if the resolution capability of the image-intensifying system is at least equivalent to the resolution capability of the photographic emulsion.

Image intensifiers of several types have been used in astronomical applications. High-gain multistage tubes, either cascaded, or of the TSEM type, have been used previously.[1][2] Highly sensitive TV pickup tubes, such as intensifier image orthicons,[3] and image orthicons with magnesium oxide targets,[4] have been applied in closed-circuit television chains to solar and lunar photography as well as to spectroscopy.[5]

The most successful system, however, is possibly the combination of electronography and image intensification. Lallemand,[6] Walker,[7] and others have developed image tube electronography to such a maturity that it appears now possible to carry out practical astronomical work.

The image tube described in this paper differs from the Lallemand tube inasmuch as the photographic emulsion is separated from the vacuum space of the image tube by a thin aluminum oxide membrane. Hiltner and coworkers have described this system previously.[8][9] It is shown in figure 32–1, which is self-explanatory.

Advances in tube technology have now permitted the building of high-resolution, low-background electrostatic image intensifiers which, applied to electronography, enable astronomers to use this system for routine observations.

This paper describes the requirements for an image tube for electronography in astronomical applications, and discusses specifically the necessary high-resolution and the low-background level.

After this introductory discussion, the design and performance of the image tube for electronography shall be described in detail, with particular emphasis upon the means utilized for achieving extremely low noise levels.

The experimental results obtained with this tube will be discussed and an image tube system will be described, which is in use at Yerkes Observatory, Williamsbay, Wis. Finally, some electronographs obtained with the system will be shown as examples for actual performance.

Design of Image Tube for Electronography

Requirements

The discussion of requirements in this section does not claim completeness, and pertains merely to specifications formulated at the onset of developing an image tube for electronography.

Electron transparent Al_2O_3
window 0.0001mm thick.
Prevents photocathode decay
by emulsion outgassing.

Photocathode

Photographic
Emulsion

Doors through which
emulsions are inserted
and retracted.

Light

Path of photoelectrons

Electron lens
20,000 volts

Vacuum in this
chamber at all
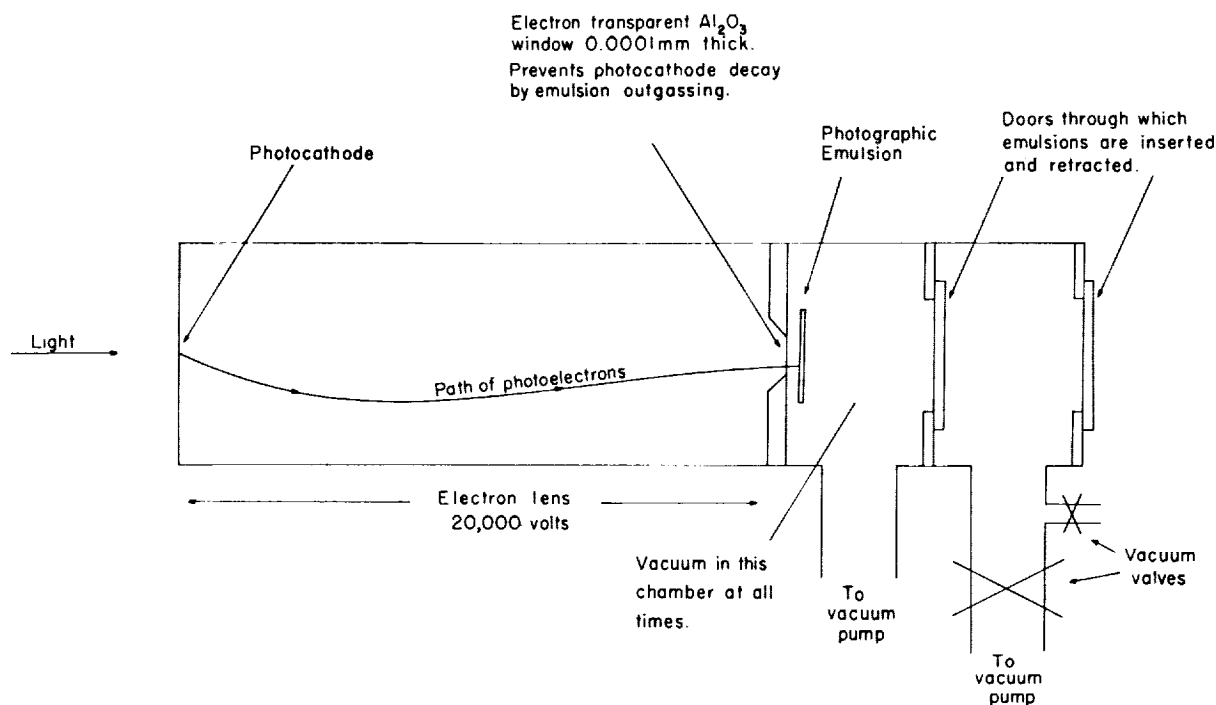times.

To
vacuum
pump

Vacuum
valves

To
vacuum
pump

FIGURE 32-1

An image tube of this type appears to be useful if the diameter of the input photocathode is approximately 1 inch. As a rather high resolution is required on the output of this device, unity magnification is preferably selected (output resolution equals input resolution). A central resolution of at least 40 line-pairs/mm is desirable, together with only a slightly lower peripheral resolution.

The quantum yield of the photocathode should be high to obtain proper gain values. The spectral response of the cathode should obviously lie in the visible band. Both these requirements indicate that an S–20 or an S–11 photocathode should be chosen.

The long exposure time, necessary to record faint images projected onto the photocathode, postulate a very low background of the image tube. Thus, precautions have to be taken to minimize all causes for spurious emission from the photocathode.

Discussion of the Requirements

The high *resolution* required opens up the question of electrostatic versus magnetic focusing. An image converter with a magnetic focusing system may consist of a flat photocathode and a flat anode with a homogeneous electrostatic field

between these two electrodes.[10] A homogeneous magnetic field is superimposed parallel to the electrostatic field. The homogeneous electrostatic field is generally approximated by impressing a linear potential increase between cathode and anode onto the cylindrical tube wall by means of conductive rings (carrying potentials increasing in discreet steps) or by means of a conductive spiral.

An electrostatic triode system, generally used as a focusing structure in image intensifiers, may consist of a spherical cathode, a cylindrical focus electrode, and a spherical, pierced anode.[11] It has been shown that the image plane curvature of a magnetic system is, in principle, smaller than the image plane curvature of an electrostatic system, resulting in improved peripheral resolution.[12] However, the image plane curvature of the latter system can be reduced appreciably by adjusting the strength of the negative aperture lens formed by the pierced spherical anode, as well as by utilizing a focus electrode of a diameter which is large compared with the effective photocathode diameter. Thus, a satisfactory image plane curvature may be obtained with an electrostatic system.

The *resolution limitations* of such an image intensifier are mainly of an electron optical nature.

226

Neglecting space charge effects in the elementary beams and chromatic aberrations [13] (due to variations in exit velocity of the photoelectrons), the paraxial resolution appears to be limited in both systems by astigmatism mainly caused by either beam deflection due to magnetic stray fields, or due to asymmetric radial components of the electrostatic field.* In the case of the magnetic system, maintaining strictest parallelity between the superimposed magnetic and electrostatic fields is required to avoid astigmatic distortion. Furthermore, fringe fields on both sides of the focusing magnet ought to be minimized. For the electrostatic system, proper mechanical alinement of the components is a necessary condition. Comparing the probability of astigmatic distortions, it appears that an electrostatic system, if properly designed and executed, can be quite competitive in paraxial resolution to a magnetic system.

The decision whether a magnetic or an electrostatic system should be used is ultimately dependent upon the background (noise) performance of these two structures.

Factors contributing to *spurious emission from the photocathode* (background) in image intensifiers have been discussed to some extent by Essig.[14] It might nevertheless be worth while to elaborate on this point.

The thermionic emission of photocathodes is doubtlessly one of the major factors contributing to background. While it is known [15] that the thermionic emission of a trialkali photocathode at room temperature is somewhat lower than the thermionic emission of a conventional antimony-cesium cathode, cooling of both surfaces to at least dry ice temperature might be required to reduce the thermionic emission to an acceptable level.

Residual gases in image intensifiers can be ionized by electron impact. The positive ions are accelerated toward the photocathode, giving cause to secondary electron emission. The secondary electrons are accelerated toward the output of the tube, contributing to parasitic blackening of the photographic emulsion mainly in the center of the image (ion spot).

Field emission between tube components appears to be the most important contribution to the background. The probability of field emission increases with both the number of tube components acting as possible sources of field emission,

---

*It is assumed here that the magnetic system does not suffer from S-band distortion.

and the magnitude of the potential gradient between those components.

An electrostatic system, as described above, features essentially only one potential gap, namely, the gap between the (low potential) focus electrode and the (high potential) anode.

One will recall that this gap consists normally on an uncoated glass surface. During processing of the photocathode, alkali metal vapors may be adsorbed on the glass surface, leading to relatively high local potential gradients causing field emission. Photoelectrons are released from the cathode due to fluorescence resulting from field emission.

We shall describe later on how field emission was eliminated quite successfully. Indeed, the elimination of this shortcoming leads to an electrostatic system, possibly superior in background performance to a magnetic system, as the "high voltage coating" used in the electrostatic system between focus electrode and anode, cannot be applied readily with equal success to a magnetic system.

Description of Image Tube for Electronography

The electrostatic image intensifier for electronography is shown in the photograph of figure 32-2 and schematically in figure 32-3. Visible light radiation impinges from the left onto the curved Sb-Cs(0) (S-11) photocathode (1), giving cause to electron emission. The electrons are accelerated and focused by the electrostatic field formed by the cylindrical focus electrode (2) and the spherical pierced anode (3). An electron image of the light distribution on the photocathode is formed on the photographic emulsion (4) separated from the vacuum space enclosing the photocathode by the aluminum oxide foil (5).
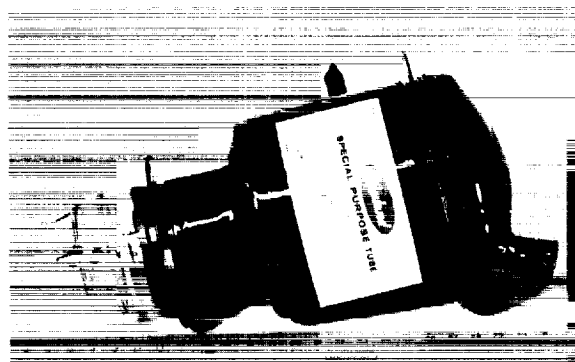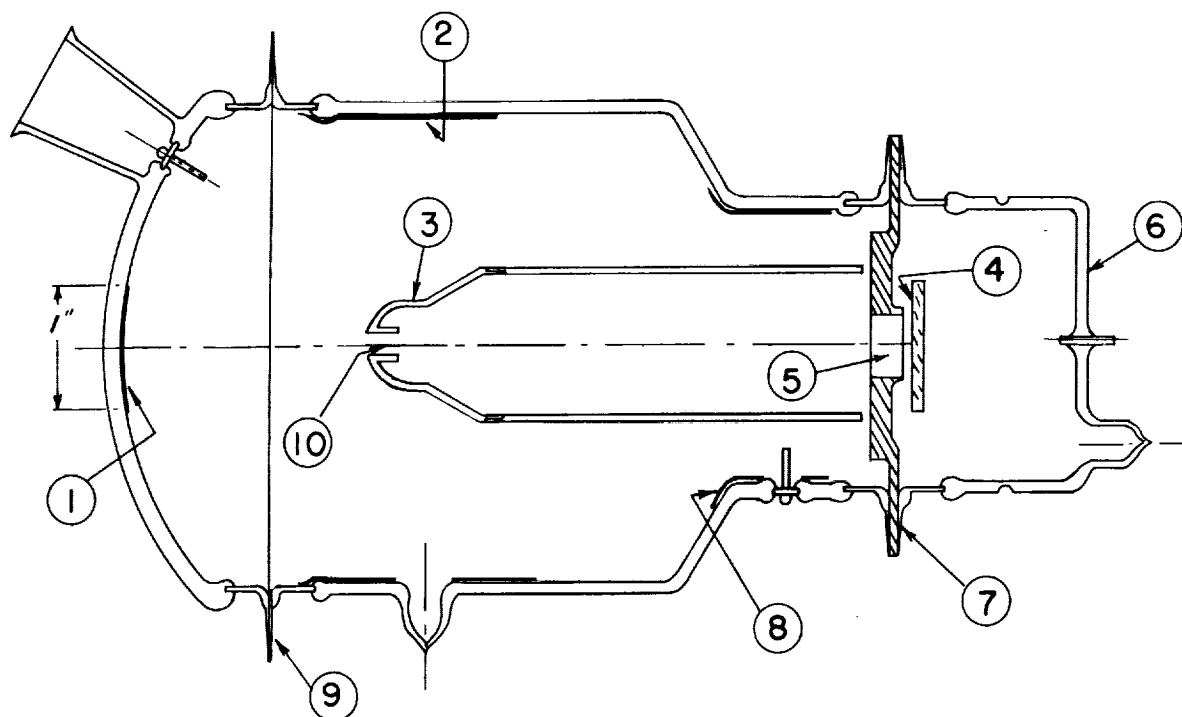

FIGURE 32-2

227

1. PHOTOCATHODE
2. CYLINDRICAL FOCUS ELECTRODE
3. ANODE
4. PHOTOGRAPHIC EMULSION (inserted after tube is placed in operation)
5. ALUMINUM OXIDE FOIL
6. REMOVABLE SECTION (to permint insertion of emulsions)
7. KOVAR FLANGES (heliarc welded)
8. HIGH VOLTAGE SECTION OF TUBE
9. KOVAR FLANGES (heliarc welded)
10. ANODE APERATURE LENS

FIGURE 32-3

One will appreciate that the section (6) of the tube is cracked off, after the tube has been inserted into a "demountable" vacuum system, achieving a vacuum-tight seal along the metal flanges (7). The disposable glass section is removed through an air lock.

The main advantage of the present tube for electronography is the low noise background, obtained by reducing field emission between tube components almost entirely. This has been done by applying a semiconductive wall coating between the focus electrode (2) and the high voltage section (8) of the intensifier. This coating consists essentially of chromium oxide applied by means of a proper binder. It should be noted that the chromium oxide is not the active component of the coating. The binder, if properly prepared and treated, consists of an amorphous inorganic oxide having the property of gettering

a predetermined amount of cesium vapors during processing of the photocathode. The cesium adheres quite strongly to the binder, requiring temperatures in excess of 400° C for removal.

The thus completed wall coating, consisting of chromium oxide—binder—cesium, yields a controlled conductivity between the focus electrode and the high voltage section of the tube, equalizing local potential gradients in such a manner that the probability of field emission is reduced appreciably.

The photosurface is produced by evaporating antimony onto the substrate in demountable vacuum system and subsequently transferring the evaporated antimony layer in room air to the tube envelope, completing the tube by applying a "cold" seal (heli-arc welding along the flanges (9)). Thereafter, the tube is baked and the photocathode activated.

The external antimony evaporation has the advantage of assuring an even photocathode and restricting the photoemissive surface, thus reducing spurious electron emission from photosensitive layers deposited on tube elements other than the cathode.

The anode aperture lens (10) has been designed to increase the image distance, resulting in a decreased image plane curvature.

The photocathode is substantially smaller than the tube envelope of approximately 3-inch diameter. The "filling factor" of the electron-optical system is quite small, resulting in utilization of the central part of the (curved) image plane only. Thus, no substantial differences between central and peripheral resolution should be expected.

Care has been taken to effect proper mechanical alinement of the tube parts for reduction of astigmatic distortion. The Kovar flanges are demagnetized before using the image tube and magnetic shielding is applied. The Al_2O_3 film, separating the emulsion from the photocathode, is made by anodizing commercial aluminum foil and subsequently removing the remaining metallic aluminum. The film, 1,000–1,500 Å thick, is then transferred from the provisional holder to the final mount, a Kovar disk with an aperture. Vacuum-tight sealing of the film to the rim of the aperture is achieved by aerosol.

Mass-spectroscopic tests have indicated* that no helium leakage is detectable, even if the pressure differential between both sides of the film is as high as 500 microns of Hg. No difficulties have been encountered in evacuating or baking tubes with such films.

Since the film cannot withstand atmospheric pressure, a glass cap is fabricated over the foil as mentioned previously. This glass cap is removed after the tube is installed on the vacuum lock and the lock evacuated. This then permits access to the electron focus with photographic emulsions for exposure as desired. Also, the cap contains a flat disk to protect the foil when the cap is broken off. This disk, only a few millimeters from the foil, is painted with a phosphor. The phosphor permits preliminary evaluation of the tube in advance of attachment to the vacuum system.

*The authors are obliged to Mr. L. Gray of the Rauland Corp. for planning and execution of these tests.

System for Image Tube Electronography

The system, as indicated in the introduction, requires a kinetic vacuum in order that emulsions may be inserted and retracted without damage to the photocathode. In the laboratory, small oil diffusion pumps have been used, requiring a liquid nitrogen trap. Ion pumps could possibly be applied, although they do require a rather strong magnetic field and produce disturbing electromagnetic radiation. However, to make the system completely mobile, as is necessary at the focus end of a telescope, we have found it convenient to introduce cryogenic pumps. Figure, 32–4 shows a schematic drawing of the telescopic model. Two dewars, one for either side of the vacuum lock, contain liquid hydrogen shielded by liquid nitrogen. This shielding, of course, greatly reduces the loss of the hydrogen. With one charge of a mixture of ortho and para hydrogen, the dewars will maintain a vacuum of approximately 2×10^{-7} mm of Hg for 4 days. The hydrogen dewars may be recharged, before the earlier charge is exhausted. Therefore, the vacuum may be maintained indefinitely.

We emphasize that no part of the image tube itself is ordinarily cooled. The hydrogen and nitrogen are used only for evacuating the two chambers, one on either side of the air lock.

Figure 32–5 is a photograph of the image tube, plate-changing mechanism, and cryogenic system attached to the 40-inch refractor of the Yerkes Observatory and figure 32–6 is a closeup.

Results

The resolution of the image tube has been tested with settled and evaporated phosphor screens as well as with electronography. Unfortunately, the settled phosphor screens used had been intended for image tubes with 35-kv anode voltage; thus, the phosphor thickness exceeded by far the value required for the 20-kv anode voltage used with the image tubes for electronography. The resolution, determined with those screens, was nevertheless 20 lp/mm, which is in good agreement with the theoretically expected resolution capability of the phosphor layer.

Next, evaporated phosphor screens, designed for optimum performance at 15 kv, were utilized in this 20-kv tube. Resolution values of 40 lp/mm were observed.
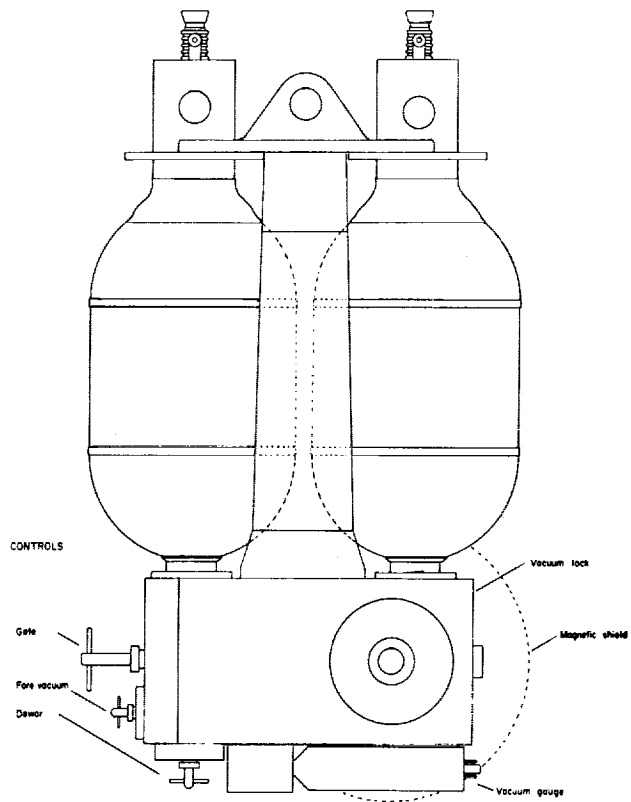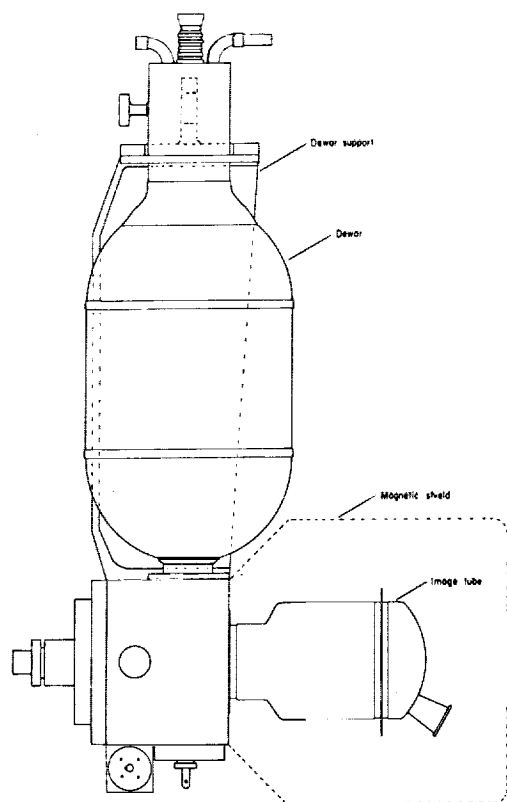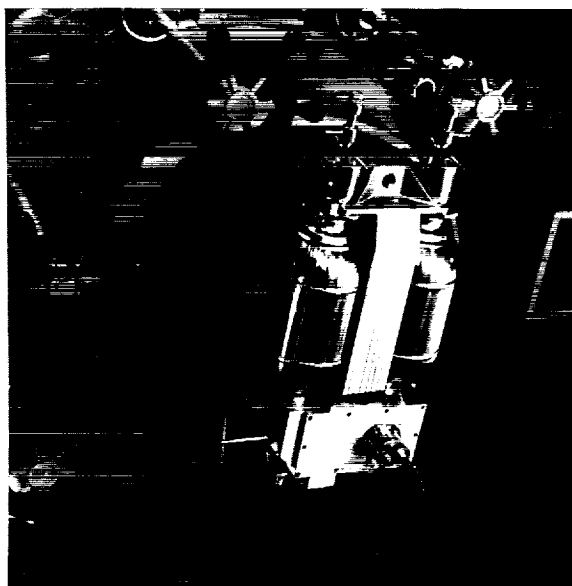
FIGURE 32-4

FIGURE 32-5

FIGURE 32-6

It should be noted here that proper focusing of the image tube is judged by visual observing of a phosphor screen—be it settled or evaporated phosphor—and that the resolution thus obtained

is predominantly limited by the inherently restricted resolution capabilities of these cathode luminescent screens. This means that it is quite difficult to decide when proper focus has been achieved for electronography. Using the focus adjustment, as obtained with an evaporated phosphor screen, and replacing the phosphor by Ilford G-5 emulsion, with an inherent resolution capability of approximately 70–80 lp/mm, resulted in resolution values of 55–60 lp/mm over the entire field of view. These results may not yet represent the ultimate resolution capability of this system.

While earlier tubes displayed slight astigmatic distortions, disturbing to some extent at resolution values above 45 lp/mm, recent image tubes showed no distortion at 55–60 lp/mm. No indication has been found as yet that the electron scatter occurring in the Al_2O_3 film is a serious factor in limiting the obtainable resolution.

The background has been tested by replacing the emulsion with a settled screen (P–20 phosphor) and observing the phosphor with a refrigerated RCA 1P21 photomultiplier followed by a scaler. Cooling the photocathode to dry ice temperature permitted, at least in first approximation, to differ between thermionic background and tube noise. It was found that 75 percent of the background of these tubes at room temperature or approximately 80 electrons/cm²sec is due to thermionic emissions.

Next, the background was evaluated by electronography with the photocathode at room temperature as well as cooled by dry ice. With the photocathode at ambient temperature, exposures of 2 hours are required for the background density to exceed 0.10. If the photocathode is refrigerated, exposure times in excess of 10 hours appears to be reasonable.

It should be noted that image tubes of the type described here display in general a markedly higher background when the anode is grounded and the photocathode is at (high) negative potential. The image tube for electronography is operated in just this manner. Thus, the background values, quoted above, refer to this mode of operation.

The level of the background can also be illustrated by a comparison with the sky background at the focus of the f/19 Yerkes 40-inch refractor. The sky background is 160 times greater than the tube background with the photocathode at ambient temperature and at negative potential.

The gain capability of the image tube may be demonstrated by comparing exposure times necessary to obtain a density of 0.2 for photography of the sky background with and without image tube. In using classical photography, several tens of hours were required to detect the sky background as observed with an f/19 telescope. Direct photography of the sky background with the image tube gave a density of 0.2 in 15 minutes.

The photocathode sensitivities (S–11 characteristic) to 2,870° K incident light were determined with a standard light source and were ordinarily in the range of 20–35 uA/L. Experiments are in progress to improve upon this performance parameter.

The stability of the photocathode is closely connected with the vacuum tightness of the Al_2O_3 film. Individual tubes have been operated as long as 2 weeks on the cryogenic system, with the vacuum lock cycled over 200 times, without any damage to photocathode or Al_2O_3 film.

In contrast, removal of the film with a photographic plate in place* resulted in severe deterioration of the photocathode sensitivity after a few hours.

Conclusion

In summary, it is our judgment that we have an operational system capable of—

    1. High resolution (similar to that of classical photography).

    2. Long exposures with little background.

    3. Working at the shot noise of the photocathode current.

    4. Operating over long periods of time.

    5. Easy setup and operating on a routine basis.

It is recognized, however, that future astronomical results obtained with the image tube for electronography represent the ultimate acceptance test for a system of this sort.

Acknowledgment

*The emulsion was not outgassed previous to insertion into the vacuum system.

ment of the entire system by designing and assembling the plate changing mechanism. We are grateful to the National Science Foundation for providing several pieces of capital equipment.

Discussion

H. DAY: The spacing from the Al_2O_3 film to the photographic emulsion is 20 microns and you resolve a 1-micron spot. How do you explain the scattering of only 1 part in 20—an apparent contradiction to generally accepted scattering laws? One loses about 2.5 kv in a 1,000 Al_2O_3 film. This represents scattering and should contribute to loss of contrast. Does it?

W. F. NIKLAS: The spacing between the aluminum oxide film and the photographic emulsion is approximately 20 microns. In fact, the photographic emulsion touches the mounting ring of the aluminum oxide film and thus touches the aluminum oxide film itself, at least along its perimeter. It might be assumed that there is a pressure gradient between the vacuum space enclosing the photographic emulsion and the vacuum space enclosing the photocathode in such a manner that a slight bowing of the aluminum oxide film results toward the vacuum space enclosing the photocathode. This is the reason why we assume the above-quoted spacing. The measured electronographic resolution of the image tube is 55–60 line-pairs per mm. This means that a spot of approximately 8 microns can be resolved. Thus, the amount of scattering encountered is only approximately 1 part in 2.5.

References

1. BAUM, W. A.: Adv. El. and Phys., vol. XII, 1960, p. 1.
2. WILCOCK, W. L., and BAUM, W. A.: *Some Astronomical Tests of an Imaging Photomultiplier.* 2d Symp. Photo-El. Image Dev., London, 1961.
3. GEBEL, R. K. H.: *Light Amplification and its Usefulness in Astronomical Observation.* WADC Tech. Note. 59–290, 1960.
4. DeWITT, J. H.: *Report on the Image Orthicon Using Slow Readout.* 2d Symp. Photo-El. Image Dev., London, 1961.
5. SPALDING, JOHN, DUGAN, JOHN F., and HEMENWAY, CURTIS L.: *Experiments with High-Sensitivity Image Orthicons.* Lect. 108, Mtg. Amer. Astr. Soc., 1961.
6. LALLEMAND, A., DUCHESNE, M., and WLERICK, G.: Adv. El. and Phys., vol. XII, 1960, p. 5.
7. WALKER, M. F.: *Recent Astronomical Observations Obtained With the Lallemand Electronic Camera.* 2d Symp. Photo-El. Image Dev., London, 1961.
8. HILTNER, W. A.: Conf. Photoelectric Photometry, 1953
9. HILTNER, W. A., and PESCH, P.: Adv. El. and Phys., vol XII, 1960, p. 17.
10. DAVIS, G. P.: *Experiments With Magnetically Focused Cascade Image Intensifiers.* 2d Symp. Photo-El. Image Dev., London, 1961.
11. SCHAGEN, P., BRUINING, H., and FRANCHEN, J. C.: Philips Res. Rep., vol. 7, No. 2, 1952, p. 119.
12. BAKER, H., and PAPP, G.: Image Intensifier Symp., 1958.
13. BEURLE, R. L., and WREATHALL, W. M.: *Some Electron Optical Studies of Solenoid Focusing Systems.* 2d Symp. Photo-El. Image Dev., London, 1961.
14. ESSIG, S. F.: Adv. El. and Phys., vol. XII, 1960, p. 73.
15. SOMMER, A. H.: IRE-NS, vol. 3, 1956, p. 8.

232

33. ON A SATELLITE SURVEILLANCE CAMERA USING COMPOUND OPTICS AND IMAGE ORTHICON PHOTOSENSORS (FACET EYE CAMERA)

W. F. WOEHL, *Air Force Missile Development Center, Holloman Air Force Base*

The use of photoelectric-electronic image intensification in the surveillance of orbiting and suborbital objects presents design problems of a special kind, different from the requirements connected with the application as an aid to photo-visual and photographic instrumentation; e.g., in astronomy, nuclear track photography, or medical problem areas. The surveillance instrument is a metric tool; the information which it is required to provide are, briefly stated, highly accurate position-time data on moving point targets, in real time, and over an extended portion of the diurnal cycle. This requirement involves:

a. High angular resolution and accuracy.

b. Long focal length optics.

c. A large field, giving high acquisition probability.

d. High photometric sensitivity, to be able to record also fast-moving point targets.

e. Daytime recording capabilities.

f. Accurate outer orientation and inner calibration data.

g. Image coordinate counting and readout in real time, acceptable to computer input registers.

h. Accurate time correlation system.

i. Target discrimination and identification devices based on stored reference data.

j. Data links to supplementing systems, and efficient data reduction programing.

The desired minimum accuracies are an angular position accuracy of ± 10 seconds of arc, and location of the significant event points in the time scale to 0.1 millisecond. The requirement for daytime recording capability decides for a long focal length telescopic optics, in order to have a narrow cone of acceptance for the quanta originating from the sky background and accumulating on the single sensor element. Size of the resolution element in the photosensor, together with the focal length of the imaging system, determine the available angular resolution of the system.

The solution which was attempted is the combination of compound telescopic optics (optical facets) with image orthicon camera tubes as photosensors, electronic image enhancement, and digital image coordinate counting and readout in real time. Because of the use of optical facets as imaging components, the name "Facet Eye Camera" has been coined for this system. In the following paragraphs, a brief outline is given of the design and performance of this system.

The compound optical system consists of 25 refractor telescopes, with 75-inch focal length and 5-inch clear aperture. In combination with the available usable sensor area of the image orthicon tubes of 1.1 by 1.1 inch, each telescope covers a field of 52 by 52 minutes of arc in the object space. As shown in figure 33–1, the telescopes are effectively arranged as a three-row fan assembly, with angular spacings between the telescopes and rows of 47 minutes of arc. The total field covered by the fan in this way is $7°$ by $2.5°$. This fairly wide field is associated with the rather long focal length of 75 inches, yet only paraxial rays are being used, with consequently low values for the Seidel aberrations. This is thought to be a novel optical concept.

The 25 telescopes form optical images of adjacent segments of the object space on the photosurfaces of a related number of image orthicon tubes, as figure 33–2 illustrates. The camera bodies contain the preamplifiers for the video signals, sweep circuits, sweep failure protection circuits, blanking amplifiers and rectifiers, and power circuitry. The video signal is fed through coaxial cables into the camera control station where the signal complex is treated for improvement of its information content, such as increase in contrast, signal-to-noise ratio, and background suppression. The improved images are finally
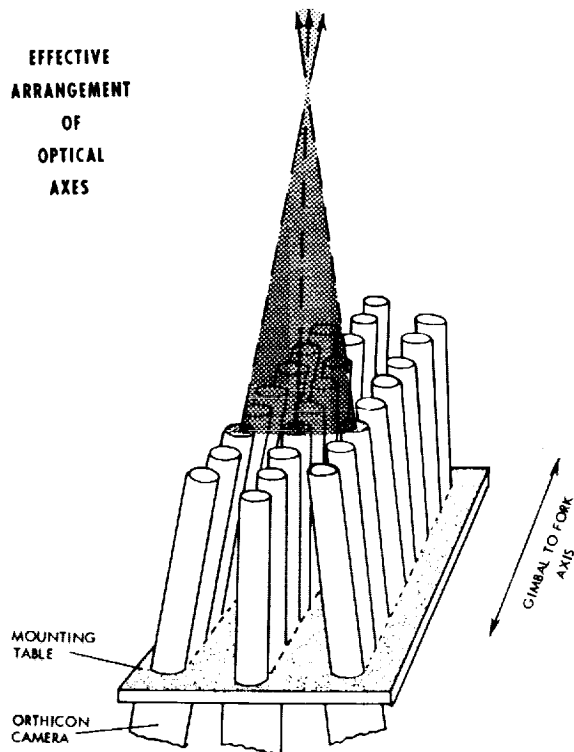
MOUNTING
TABLE

ORTHICON
CAMERA

GIMBAL TO FORK AXIS

FIGURE 33–1.

presented for visual inspection and photographic recording on the screens of 25 monitor-oscilloscope tubes which can be seen in figure 33–3. This photo shows the main part of the control station.

Physically the 25 telescope-camera units are arranged as a 5 by 5 assembly, seated on a four-axes mount, which provides the combined capabilities of an alt-azimuth and an equatorial mount. Figures 33–4 and 33–5 show the assembly. The arc-shaped fork moves in steel rollers on top of the base plate; if the gimbal-to-fork axis is being pointed to Polaris, we have an equatorial mount, the gimbal rotation then represents the siderial movement required. All four movements are motor driven, the gimbal rotation and the plate rotation having variable speed Graham drives with remote speed changers attached.

The whole mount-camera assembly is housed in a 24-foot astrodome not shown here; a 10-foot-wide shutter opens from zero to 135° elevation across the zenith and allows full use of the telescope fan assembly. The dome drive is synchronized with the mount movement, as usual. As pointed out, the new camera is supposed to be a highly accurate metric tool. A number of provi-

sions have been made in order to achieve this objective.

To calibrate the outer orientation of the camera, that means, the true angular position of the optical axes, the star background is being photographed as coordinate reference system, as is done in the case of ballistic camera work. Thus, no high precision dials or encoders are required, being replaced by shaft angle position transmitters on the mount, and synchro receivers at the control station. The main mode of operation is as a preset transit fan.

Special care has been taken to avoid functional errors like nonlinearities, image rotation, field distortions within the electronic image transfer process which would cause final position errors, and to provide means to measure residual errors.

The most important circuit component which has been incorporated to this end is a central timer generator synchronizing all drive pulses, the blanking, the shading controls, the keyed clamps and the linearity control pattern. The functional flow chart in figure 33–6 illustrates the principle more fully. The flow of the image information can be easily seen; the bandpass filter can reduce the bandwidth from 2.6 Mc to 1.6 and 1.0 Mc. Black and white clipping is applied, and composite shading (saw tooth and parabolic shading for horizontal and vertical sweep.) is generated and supplied to the preamplifiers in the orthicon cameras. Clamping and shading are line synchronized by the timer generator. The random code generator, shown in the figure, supplies code pulses to the photocathode of the image orthicon tube, which break the flow of photoelectrons from the photosurface to the target plate. In this way, breaks in the event trace are introduced which are recorded together with WWV time pulses or pulses from a local high stability frequency standard in a separate time recorder. The time breaks can be effected also by an external source or manually operated.

The timer generator is really the center command device of the system, which synchronizes all command pulses needed for the simultaneous operation of the 25 camera chains. Figure 33–7 shows the detailed functional diagram for the timer generator.

The basic oscillator operates at 80.64 kc; this frequency is divided in several phantastron counter steps down to 60 cps. The 60 cps output synchronizes a blocking oscillator which drives
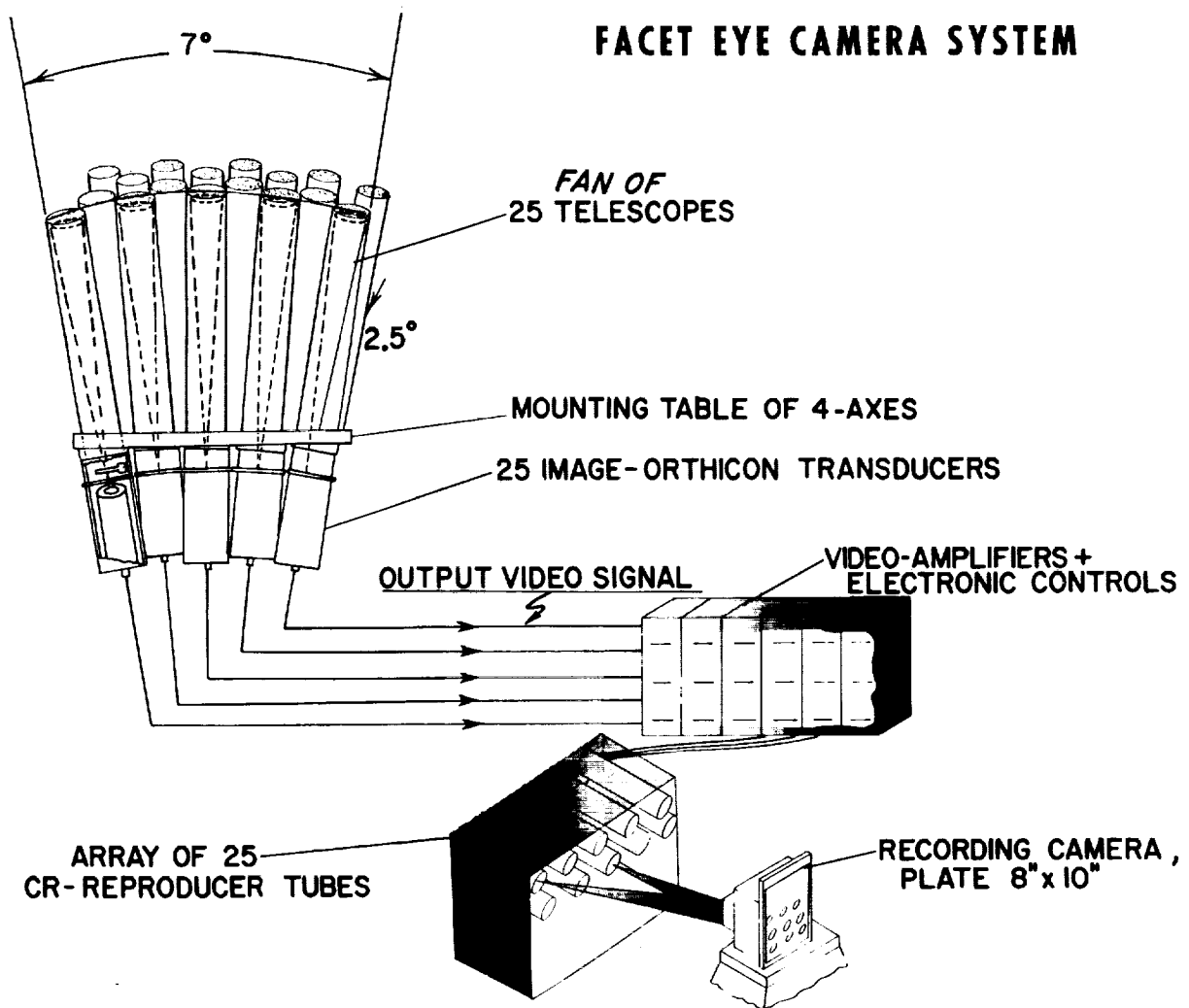
FACET EYE CAMERA SYSTEM

Labels in figure:
- 7°
- FAN OF 25 TELESCOPES
- 2.5°
- MOUNTING TABLE OF 4-AXES
- 25 IMAGE-ORTHICON TRANSDUCERS
- OUTPUT VIDEO SIGNAL
- VIDEO-AMPLIFIERS + ELECTRONIC CONTROLS
- ARRAY OF 25 CR-REPRODUCER TUBES
- RECORDING CAMERA, PLATE 8"x 10"

FIGURE 33–2.

a phase comparator. This detector compares the phase of the blocking oscillator with the 60-cps powerline; the error signal is used to drive an automatic frequency control circuit. This component sets the frequency of the 80.64-kc oscillator to an integral multiple of the power line frequency.

The derived timing signals are 10.080 cps for the horizontal sweep, 15 cps for the vertical sweep—the frame rate of the system is 15 frames per second, 672 lines noninterlaced operation—composite blanking, and 80.64 kc and 120 cps for a composite linearity blanking pattern which produces a cross-hatch pattern consisting of dark bars.

The most significant component incorporated to check linearity and detect functional disorders in the electronic system is the reticle line projector, shown in figure 33–8. It consists of four plastic

light guides which carry accurately machined cylindrical lenses at the end facing the image orthicon photo surface. The system of projected light lines together with the cross-hatch pattern is to be seen in figure 33–9. This device serves at the same time for the calibration of the angular relationship between the component fields, correlating field elements in different camera chains. This is an important procedure.

The critical effect which the setting of the three main controls of the orthicon camera, target voltage, beam current, and gain has on the sensitivity and quality of the image transfer process, requires an aid for optimum setting of the camera controls, specifically for daytime work. The device developed for this purpose is a collimated target simulator, shown in figure 33–10. It superimposes an artificial star of the desired luminous
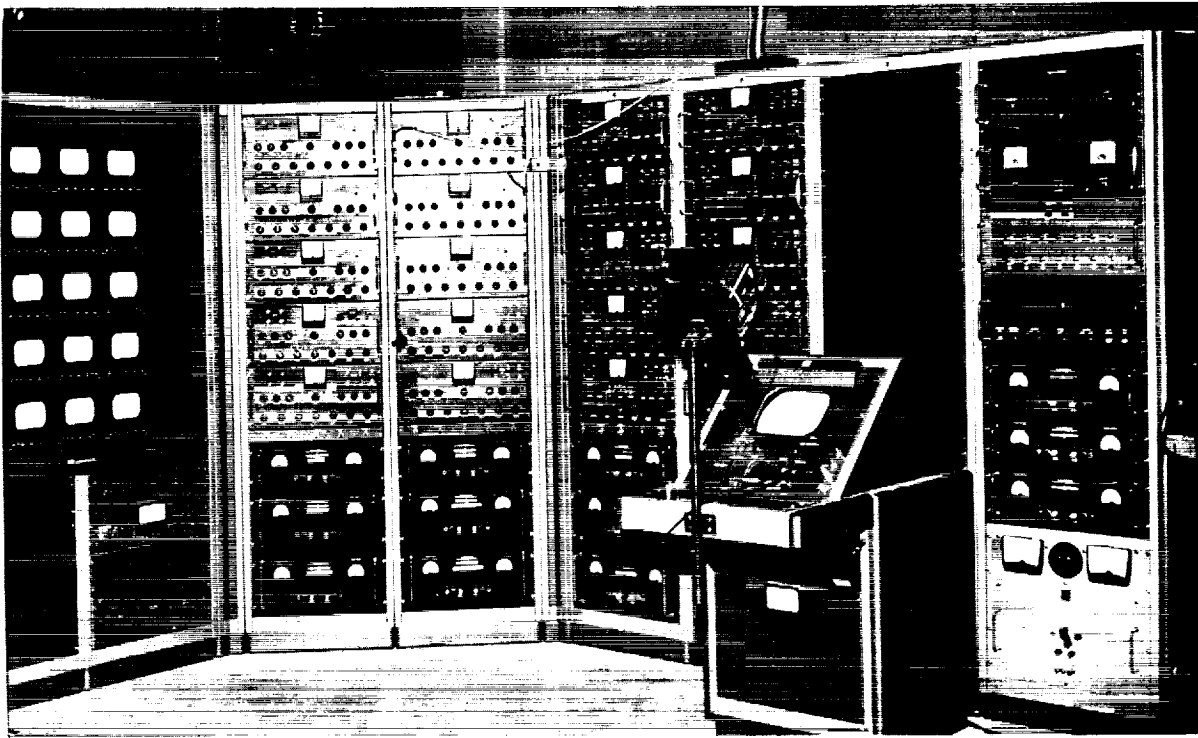
235

636674 O—62——16
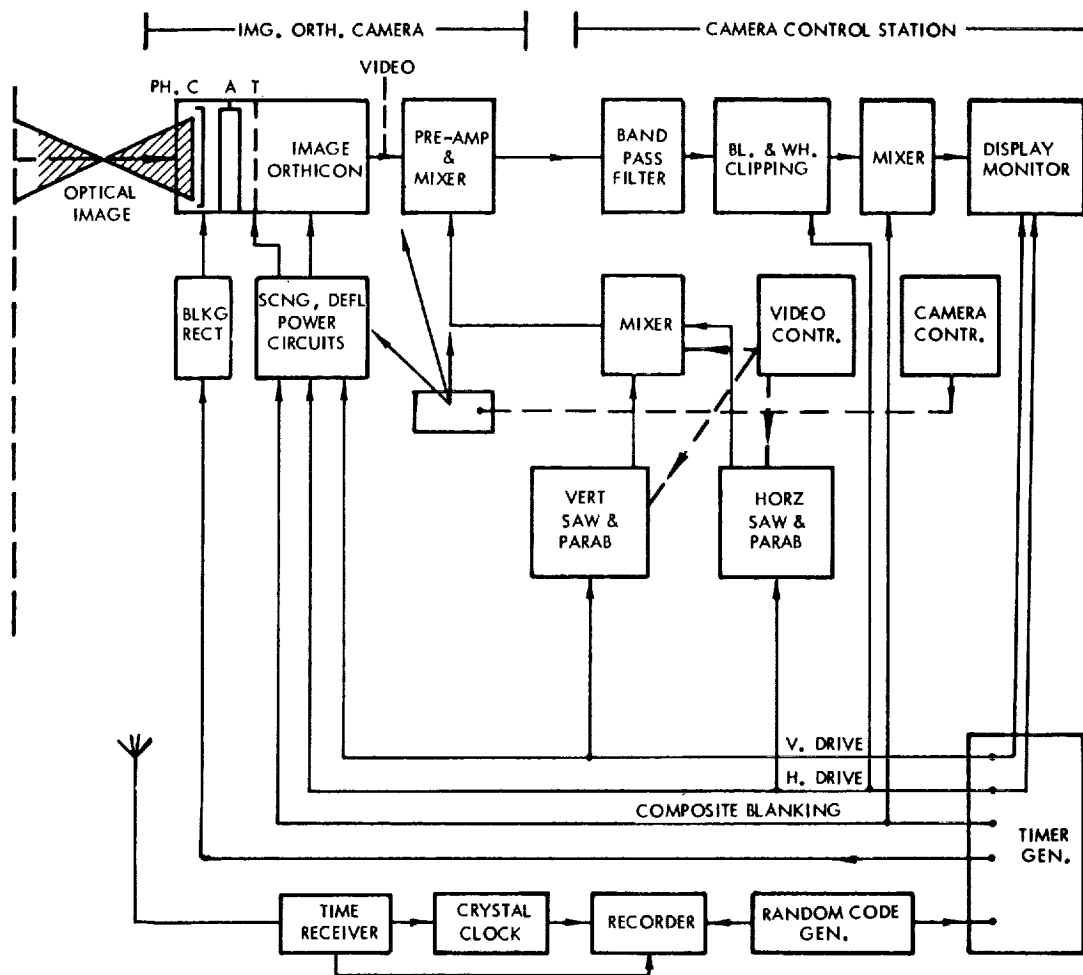
Figure 33-3.

Figure 33-4.

Figure 33-5.

236

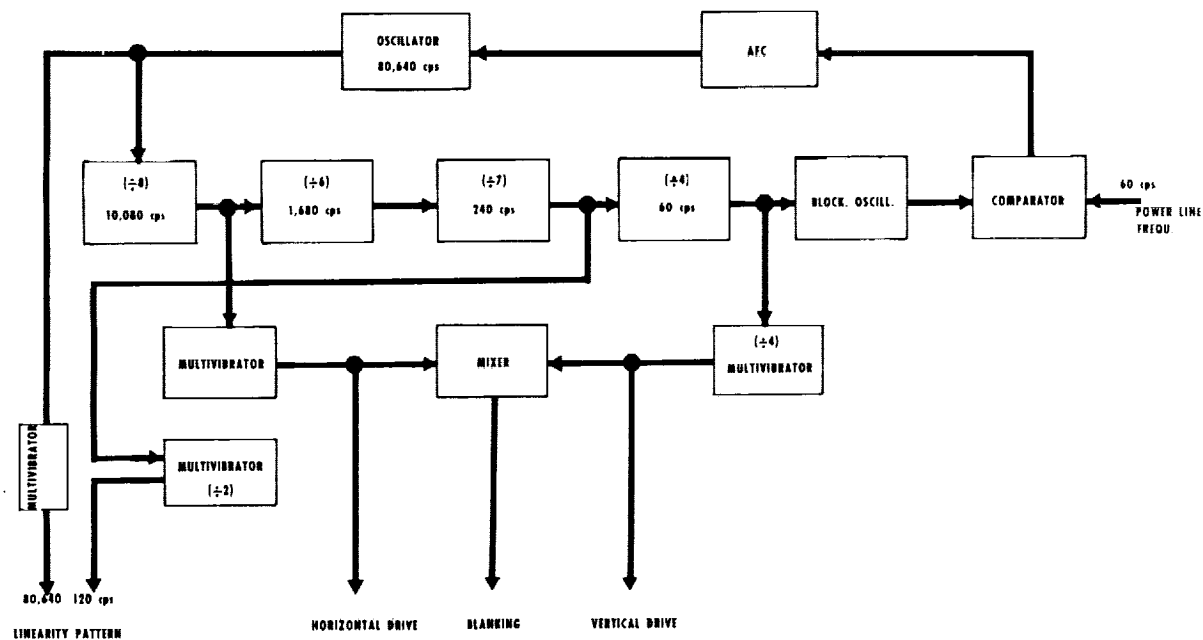## FACET EYE CAMERA SYSTEM (ONE CHAIN)

FIGURE 33-6.

intensity upon a portion of the natural sky background which is brought in by means of a beam splitter. At the same time this collimator which will be mounted on a precision sliding stage, in front of the telescope array, will be used for calibrating the angular spacing of the optical axes of the telescope-camera fan.

One of the main design objectives of the new camera is the extracting of position-time information in real time and in digital form. The process of scanning the charge replica of the optical image with an electron beam and generating video signals for the significant target points, which takes place in the image orthicon sensor tubes, provides the basic mechanism for measuring or

counting the coordinates of an image point. This phase is in the developmental stage; target point discrimination, centroiding, liminal contrast levels, economical use of storage registers, and logic circuitry are being studied at present.

Integrated for the full number of 25 camera chains, and laid out for several target points within each component field, this associated electronic equipment will be a fairly complex system.

The useful measure of the photometric sensitivity of a system tracking space objects is obviously the liminal recordable stellar magnitude of a target. This threshold depends of course upon the distance and velocity of the object, as these quantities determine, together with the focal
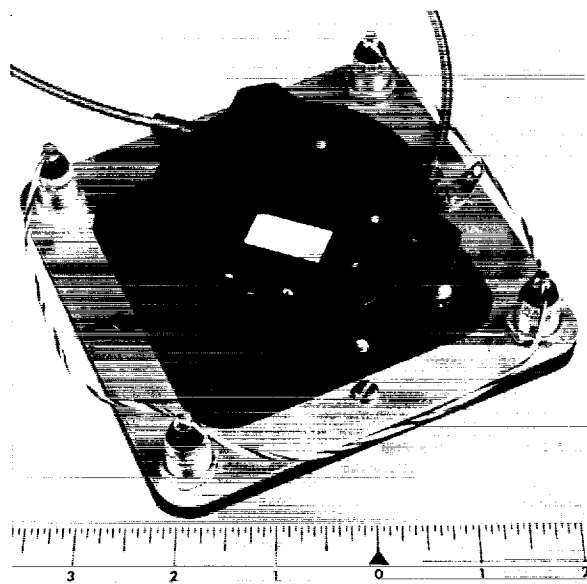
237

MASTER TIMER

FIGURE 33-7.

FIGURE 33-8.
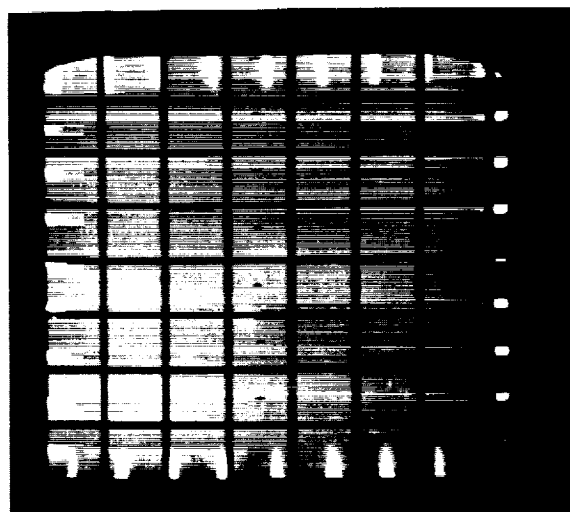

FIGURE 33-9.

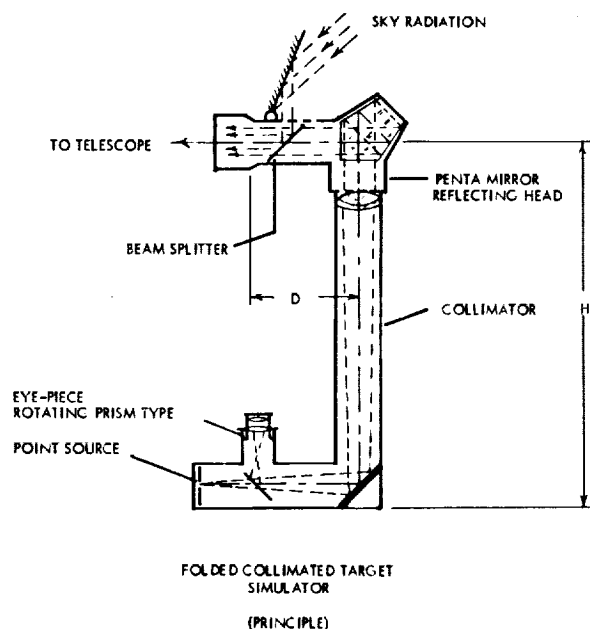FOLDED COLLIMATED TARGET
SIMULATOR

(PRINCIPLE)

FIGURE 33-10.

length of the optical system, the time the image dwells on a single sensor element, and light quanta are being accumulated on it.

The facet eye camera system is designed to record objects down to +3d magnitude in daytime, and +12th to +14th stellar magnitude objects at night. Image contrast of approximately ±10 percent, with respect to the background, can be sensed and utilized in the system, mainly by virtue of the effective background suppression possible in the circuitry. The gain in contrast discrimination and in absolute photometric sensi-

tivity are the two main quantities representing the special effectiveness of an optical-electronic sensor system.

A comparison of the effectiveness must be based upon the quantum efficiencies of the sensors and the specific transfer characteristics of the system. Thus, to compare the eye with the 'unaided photographic camera and the image intensifying system for the case of moving point targets, size of sensor resolution element, image velocity and optical system have to be included in the computation. This has been done for this special case in table 33–I. The average number of quanta per second and unit area of accepting aperture required for reliable detection of a target has been chosen to be the representative effectiveness figure. For easier comparison, the relative sensativities, the human eye equaled to unity, have been computed in the last row. As can be seen, a gain in effectiveness by a factor of approximately 125 has been obtained by the use of the image orthicon sensors. This is equivalent to a gain by 5.3 stellar magnitudes. One notes also how powerful the intensifier image orthicon or a similar advanced sensor can be. It must be pointed out again that the listed figures are computed for realistic tracking conditions, and are in fair agreement with observed data. Different assumptions, for instance, ideal conditions for the beam modulation process at the orthicon target plate, a monochromatic electron beam, and so on, are bound to give different performance figures, as have been published elsewhere.

TABLE 33–I.—*Effectiveness rating for moving point targets*

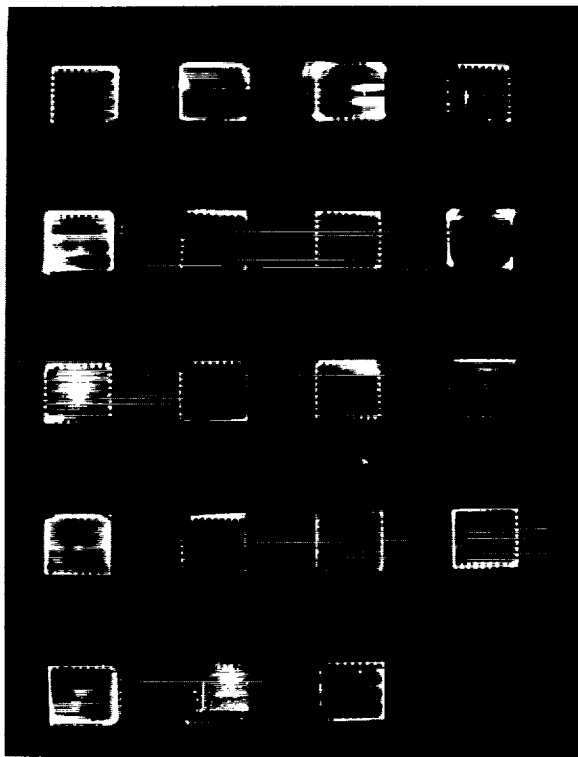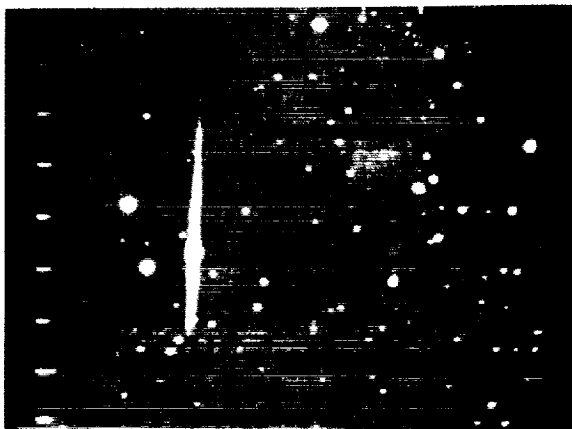| Sensor combination Quantity compared	Human eye	Photo emuls. w/7 inch f/2.5 lens $T=0.8$	Photo emuls. w/75 inch f/15 telescope $T=0.95$	GE image orthicon GL 7967 w/7 inch f/2.5 lens $T=0.8$	GE image orthicon GL 7967 w/75 inch f/15 telescope $T=0.95$	2-stage int. image orthicon C 73477 w/75 inch f/15 telescope $T=0.95$
Average size of resolution element (microns)	3	20	20	80	80	100
Quanta required for target detection	150	25,000	21,053	800	674	84.
Average velocity of image (mm/sec)	0.11	1.0	10.7	1.0	10.7	10.7
Accepting aperture (mm)	5	71.1	127	71.1	127	127
Average required quanta per sec, sq mm accepting area	280	314.8	888.7	2.5	7.1	0.7
Relative sensitivity	1	0.89	0.32	112	39.4	400

FIGURE 33-11.

FIGURE 33-13.

FIGURE 33-12.

Tracking satellites and planets constitutes a task very suitable for establishing working parameters for the camera and improving the different system's components. Though the present experimental facet eye camera system is still in the diagnostic phase and not yet perfect, the results obtained so far under the very restricted working conditions during this phase are very promising,
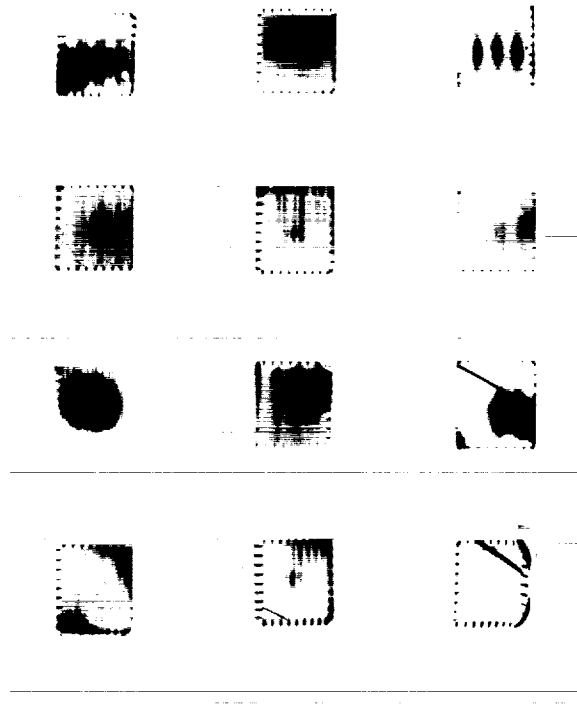
though not much effort could be spent to optimize the performance.

The following small selection of recordings may give an impression of the kind of information the system can provide at this stage. Figure 33-11 shows the array of display monitor screens, in which Satellite 1961 Xi 1-Discoverer XXV can be seen as a white trace crossing three component fields of the fan. Figure 33-12 shows the same satellite in a camera field of 8 by 8 degrees, associated with an optics of 7-inch focal length, incorporated as an aid to acquisition. Figure 33-13 shows again part of the monitor array with Satellite 1960 Iota 1-Echo 1 crossing. Figure 33-14 is a recording of Satellite 1961 Epsilon 1-Discoverer XX, passing at a distance of 640 miles. Figure 33-15 shows the trace of Satellite 1960 Nu 2, the carrier rocket of Courier 1B, at 830 miles slant range. Figure 33-16 is a photo of the moon taken during the eclipse of March 2, 1961. It shows the great possibilities provided by contrast enhancement and selected filtering. A Kodak Wratten filter No. 88A had been used. Figure 33-17 is a daytime photo of planet Jupiter taken in the afternoon. Figure 33-18 shows planets Jupiter and Saturn in early morning light shortly after
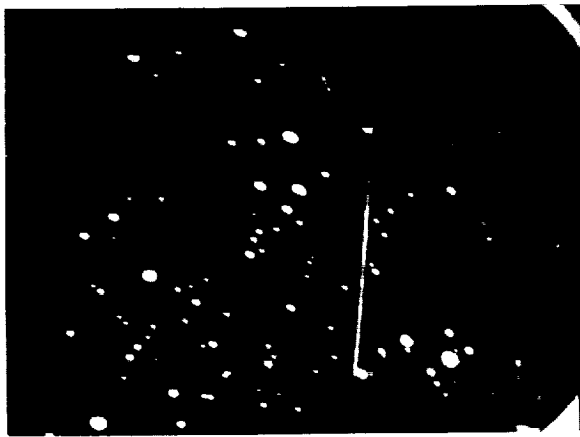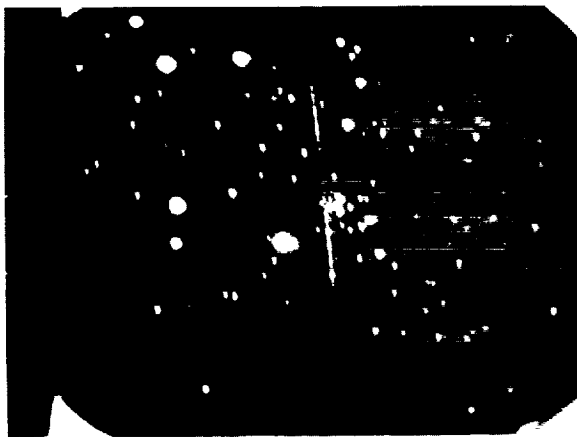
240

FIGURE 33–14.

FIGURE 33–15.

FIGURE 33–16.

sunrise. Saturn had a stellar magnitude of +0.8 at this time. Figure 33–19 shows planet Jupiter with 550 foot-lamberts daylight sky background.

It may be good to stop at this point and look ahead, visualizing future tasks. As mentioned before, a study for the real-time digital coordinate counting has been initiated and will provide an experimental model of a single camera readout comprising storage registers for coordinate data storage. The future development must build up the readout capability for all 25 camera chains and a sufficient number of target points, seeking the most economical way of achieving this. More advanced sensor tubes, improved optical systems, and automatic target detection and discrimination devices must be incorporated.

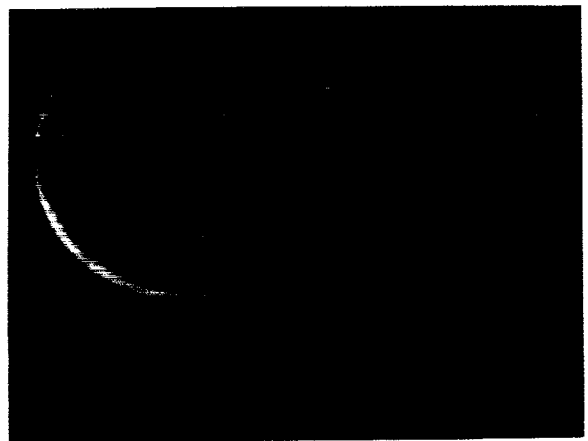Data links to electro ic computers and synchronous operation with electronic tracking systems are required. To obtain quantitative space position and time information, several camera systems have to be combined giving long base line synchronized triangulation data. Finally, the reduction process of the data contained in the composite image has to be optimized. Target identification with the help of stored reference data, and optimum computer programing are two more problems which have to be solved.
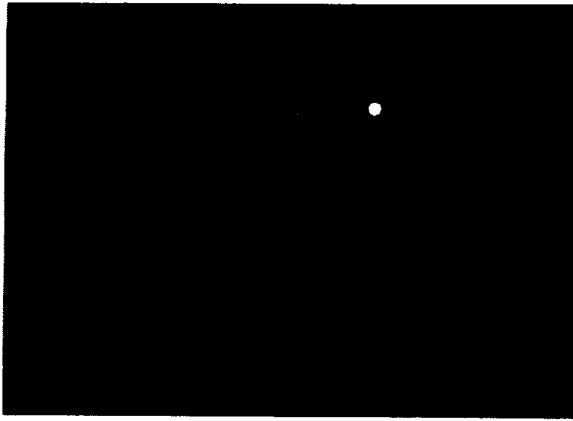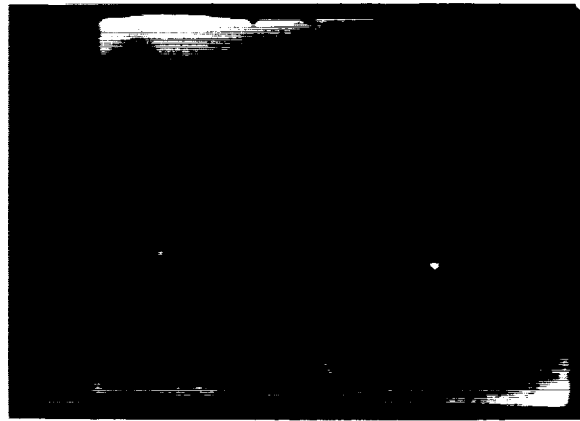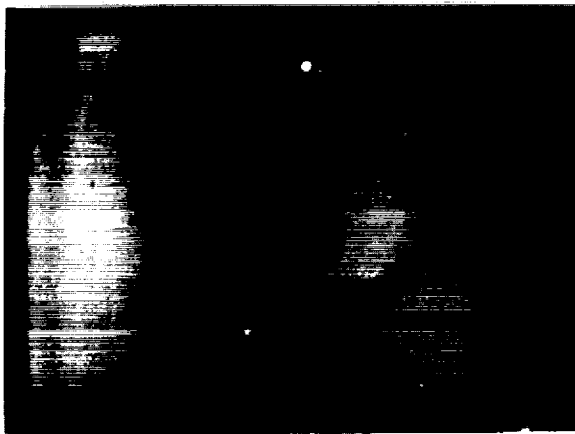
241

FIGURE 33-17.

FIGURE 33-19.

FIGURE 33-18.

In concluding, it is felt that the mating of the special compound optical imaging system with photophysical light amplification and electronic image enhancement, and extracting of the image coordinates in digital form and in real time, which are the main features of the facet eye camera, are fundamental assets for an efficient surveillance camera system. It is hoped that budgetary conditions will permit us to bring the system from the present intermediate step to its full planned capabilities possible with the technological knowledge and accomplishments which are at our disposal today.

Acknowledgments

A word of acknowledgment is due to the three main contractors who contributed to the development, manufacture, and integration of the hardware: ITT Federal Laboratories, Fort Wayne, Ind., who built the electronic system; Joseph Nunn & Associates, South Pasadena, Calif., who designed and built the mount; E. C. Larr-Optics, Altadena, Calif., who made the telescopes and associate optical equipment.

It is a very special pleasure to acknowledge the interest in this development of Mr. R. K. Gebel of the Aeronautical Research Laboratory, Air Force Office of Aerospace Research, who generously made available his wide knowledge and experience in the field of light amplification techniques.

Discussion

M. DACHS: What is the limiting equivalent star magnitude you expect to find in daylight and night with your camera?

W. E. WOEHL: We expect to find, at daytime, moving targets of third equivalent star magnitude, and at nighttime, of 12th to 14th stellar magnitude. This corresponds to the detection of a target of 1 square meter reflecting area with 50 percent reflectivity at 100 statute miles at daytime, and at 7,500 statute miles at nighttime. For a stationary target these figures would be 200 statute miles during the day and 30,000 statutes miles at night.

LIST OF CONFEREES

Aikens, R.
  Dearborn Observatory
  Northwestern University
  Evanston, Ill.
Anderson, A. E.
  Westinghouse Electric Corp.
  Research Laboratories
  Pittsburgh, Pa.
Anderson, P. C.
  Electrical Department, USAERDL
  Fort Belvoir, Va.
Appier, R. L.
  NASA-Goddard Space Flight Center
  Greenbelt, Md.
Assadourian, A.
  NASA-Langley Research Center
  Langley Air Force Base, Va.
Baker, H.
  ITT Federal Laboratories
  Fort Wayne, Ind.
Bargo, C.
  Boeing Co.
  Wichita, Kans.
Barton, G. B.
  Northwestern University
  Evanston, Ill.
Bastian, E.
  Chicago Aerial Industries
  Barrington, Ill.
Battisfore, A. E.
  U.S. Navy Hydrographic Office
  Washington, D.C.
Belknap, D.
  Ordnance Corps
  Washington, D.C.
Berler, S.
  Ordnance Technical Intelligence Agency
  U.S. Army
  Arlington, Va.
Best, G. H.
  Los Alamos Scientific Laboratory
  Los Alamos, N. Mex.
Bingley, F. J.
  Philco Corp.
  Philadelphia, Pa.
Bizzoco, F. F.
  Corps of Engineers
  U.S. Army
  Washington, D.C.

Blair, L.
  Office of the Chief Signal Officer
  U.S. Army
  Washington, D.C.
Boge, W. E.
  GIMRADA
  Fort Belvoir, Va.
Bolte, P. L.
  U.S. Army Armor Board
  Fort Knox, Ky.
Bonds, W. M.
  Varo, Inc.
  Arlington, Va.
Bouquet, F.
  Lockheed of California
  San Fernando, Calif.
Bradford, A. P.
  Electrical Department, USAERDL
  Fort Belvoir, Va.
Broderick, J. C.
  Westinghouse Electric Corp.
  Baltimore, Md.
Buddenhagen, T. F.
  Bell Aerosystems Co.
  Buffalo, N.Y.
Bunor, J.
  Warfare Vision Branch, USAERDL
  Fort Belvoir, Va.
Butterwick, G. N.
  Radio Corp. of America
  Electron Tube Division
  Lancaster, Pa.
Campeti, F.
  University of Rochester
  School of Medicine
  Rochester, N.Y.
Cashell, C. F.
  Electrical Department., USAERDL
  Fort Belvior, Va.
Causse, J. P.
  Electro-Mechanics Research, Inc.
  Washington, D.C.
Cawain, M.
  Dumont Laboratories
  Clifton, N.J.
Chandler, N. M.
  Texas Instruments, Inc.
  Washington, D.C.

Chase, M.
University of Michigan
School of Medicine
Ann Arbor, Mich.
Chasnov, B.
Electrical Department, USAERDL
Fort Belvoir, Va.
Chater, M.
General Electric Co.
Cathode Ray Tube Department
Syracuse, N.Y.
Cherrick, I. L.
NASA-Headquarters
Washington, D.C.
Clark, R.
U.S. Naval Photographic Interpretation Center
Washington, D.C.
Cleaver, O. P.
Electrical Department, USAERDL
Fort Belvoir, Va.
Clemente, J. A.
Pacific Missile Range
Point Mugu, Calif.
Colangelo, R. D.
Electrical Department, USAERDL
Fort Belvoir, Va.
Coleman, C. G.
U.S. Naval Photographic Interpretation Center
Washington, D.C.
Coombs, W. F.
Bausch & Lomb, Inc.
Electronics Department
Rochester, N.Y.
Cope, A. D.
Radio Corp. of America
Astro-Electronic Products Division
Princeton, N.J.
Cox, J. T.
Electrical Department, USAERDL
Fort Belvoir, Va.
Crost, M. E.
Signal Research and Divisions Labs.
U.S. Army
Fort Monmouth, N.J.
Cusano, D. A.
General Electric Co.
Research Laboratories
Schenectady, N.Y.
Dachs, M.
Farrand Optical Co.
New York, N.Y.
Daly, P. J.
Electrical Department, USAERDL
Fort Belvoir, Va.
Darne, F. R.
Bureau of Ships
U.S. Navy
Washington, D.C.

Day, H.
General Electric Co.
Research Laboratory
Schenectady, N.Y.
Dennison, E. W.
Sacramento Peak Observatory
Sunspot, N. Mex.
Deshields, S.
NASA-Headquarters
Washington, D.C.
DeWitt, J. H., Jr.
WSM-TV, Channel 4
Nashville, Tenn.
Dinhobel, F.
Goodyear Aircraft
Akron, Ohio
Dobras, A.
Warfare Vision Branch, USAERDL
Fort Belvoir, Va.
Dolon, P. J.
The Rauland Corp.
Chicago, Ill.
Dorrell, R. E.
Diamond Ordnance Laboratory
National Bureau of Standards
Washington, D.C.
Doty, A.
Aerospace Medical Laboratory
Wright-Patterson Air Force Base, Ohio
Doughty, D. D.
Westinghouse Electric Corp.
Research Laboratories
Pittsburgh, Pa.
Doverspike, G. E.
Department of Agriculture
Forest Service
Washington, D.C.
Dudley, R. E.
GIMRADA
Fort Belvoir, Va.
Dunkelman, L.
NASA-Goddard Space Flight Center
Greenbelt, Md.
Dyer, E. R.
National Academy of Sciences
Washington, D.C.
Eberhardt, E.
ITT Federal Laboratories
Components and Instrumentation Laboratory
Fort Wayne, Ind.
Engstrom, R. W.
Radio Corp. of America
Electron Tube Division
Lancaster, Pa.
Epstein, D. W.
Radio Corp. of America
Electron Tube Division
Lancaster, Pa.

Erickson, K. E.
U.S. Air Force
Wright-Patterson Air Force Base, Ohio

Esten, R. D.
GIMRADA
Fort Belvoir, Va.

Ethell, L.
NASA-Headquarters
Washington, D.C.

Fegely, W. D.
Westinghouse Electric Corp.
Baltimore, Md.

Feller, L. M.
Applied Physics Division, USAERDL
Fort Monmouth, N.J.

Fisher, J. F.
Philco Corp.
Philadelphia, Pa.

Flacco, A.
Radio Corp. of America
Camden, N.J.

Fleck, H. G.
Electro-Mechanical Research, Inc.
Washington, D.C.

Flory, L. E.
Radio Corp. of America
David Sarnoff Research Center
Princeton, N.J.

Ford, W. K., Jr.
Carnegie Institute of Washington
Washington, D.C.

Foshee, L.
U.S. Army Signal Intelligence Agency
Arlington, Va.

Fox, R. K.
Office of the Chief Signal Officer
U.S. Army
Washington, D.C.

Francis, G. W.
Radio Corp. of America
Electron Tube Division
Lancaster, Pa.

Freeman, C. F.
Electrical Department, USAERDL
Fort Belvoir, Va.

Frey, W. M.
Ballistic Research Laboratories
Aberdeen Proving Ground, Md.

Gauthier, R. V.
Electro-Mechanical Research, Inc.
Washington, D.C.

George, D. E.
General Telephone and Electronics Labs.
Bayside, Long Island, N.Y.

German, D.
Boeing Co.
Wichita, Kans.

Gill, J. R.
NASA-Headquarters
Washington, D.C.

Goetze, G. W.
Westinghouse Electric Corp.
Research Laboratories
Pittsburgh, Pa.

Goodrich, G. W.
The Bendix Corp.
Research Laboratories
Southfield, Mich.

Gramm, C. F.
Eastman Kodak Co.
Apparatus and Optical Division
Rochester, N.Y.

Grant, J. M.
ITT Federal Laboratories
San Fernando, Calif.

Graves, C. D.
Space Technology Laboratories, Inc.
Los Angeles, Calif.

Gray, N.
U.S. Army Combat Surveillance Agency
Arlington, Va.

Greilich, A. L.
Lawrence Radiation Laboratory
University of California
Livermore, Calif.

Groo, R.
Westinghouse Electric Corp.
Electronic Tube Division
Elmira, N.Y.

Haines, J.
General Electric Co.
Missile and Space Vehicle Department
Philadelphia, Pa.

Halbrook, J. W.
GIMRADA
Fort Belvoir, Va.

Hall, F. F., Jr.
ITT Federal Laboratories
San Fernando, Calif.

Hall, J. A.
Westinghouse Electric Corp.
Electronic Tube Division
Elmira, N.Y.

Hall, M. S.
National Cash Register Co.
Dayton, Ohio

Hall, W. C.
Corps of Engineers
U.S. Army
Washington, D.C.

Hallam, K. L.
NASA-Goddard Space Flight Center
Greenbelt, Md.

Hannam, H. J.
General Electric Co.
Cathode Ray Tube Division
Syracuse, N.Y.

Hannay, V. H. S.
British Liaison Office
USAERDL
Fort Belvoir, Va.

Hardie, R. H.
Dyer Observatory
Vanderbilt University
Nashville, Tenn.

Hass, G. H.
Electrical Department, USAERDL
Fort Belvoir, Va.

Heller, R. C.
Department of Agriculture
Forest Service
Washington, D.C.

Hembree, R. V.
NASA-Marshall Space Flight Center
Huntsville, Ala.

Hennes, J. P.
NASA-Goddard Space Flight Center
Greenbelt, Md.

Henriksen, S. W.
Corps of Engineers
U.S. Army
Washington, D.C.

Hickox, G. H.
USAERDL
Fort Belvoir, Va.

Hicks, J. W.
Mosaic Fabrications, Inc.
Southbridge, Mass.

Hickson, R. G.
GIMRADA
Fort Belvoir, Va.

Hildebrand, A. R.
Corning Glass Works
Corning, N.Y.

Hindman, E. R.
Electrical Department, USAERDL
Fort Belvoir, Va.

Hoffman, K. L.
Bureau of Naval Weapons
U.S. Navy
Washington, D.C.

Hoffman, R. E.
Radio Corp. of America
Electron Tube Division
Lancaster, Pa.

Holbach, R.
Admiral Corp.
Chicago, Ill.

Horner, J. P. M.
National Research & Development Corp.
Washington, D.C.

Hovland, C. A.
Boeing Airplane Co.
Aerospace Division
Seattle, Wash.

Howard, E. L.
Bureau of Naval Weapons
U.S. Navy
Washington, D.C.

Howe, P.
U.S. Air Force
Wright-Patterson Air Force Base, Ohio

Howlett, F. W.
U.S. Navy Hydrographic Office
Washington, D.C.

Huler, R. C.
Agricultural Research Center
Beltsville, Md.

Humiston, H. A.
Westinghouse Electric Corp.
Baltimore, Md.

Humphrey, R. G.
Ordnance Corps
Washington, D.C.

Hunt, O. H.
Bureau of Ships
U.S. Navy
Washington, D.C.

Hunter, W. R.
Naval Research Laboratory
Washington, D.C.

Huston, P. D.
Admiral Corp.
Chicago, Ill.

Hynek, J. A.
Dearborn Observatory
Northwestern University
Evanston, Ill.

Inany, F.
Lawrence Radiation Laboratory
University of California
Livermore, Calif.

Ingman, J. F.
U.S. Army Transportation Board
Fort Eustis, Va.

Izard, C. B.
National Security Agency
Fort Meade, Md.

Jarvis, W.
Electrical Department, USAERDL
Fort Belvoir, Va.

Johnson, A. B.
Bell Aerosystems Co.
Electronics Systems Section
Buffalo, N.Y.

Johnson, C. A.
Electrical Department, USAERDL
Fort Belvoir, Va.

Johnson, H. G.
Electrical Department, USAERDL
Fort Belvoir, Va.

Johnson, J.
Electrical Department, USAERDL
Fort Belvoir, Va.

Johnston, R.
Atomic Energy Commission
Washington, D.C.

Jones, D. T.
Office of Transportation
U.S. Army
Washington, D.C.

Kalibjian, R.
Lawrence Radiation Laboratory
University of California
Livermore, Calif.

Kapany, N. S.
Optics Technology, Inc.
Belmont, Calif.

Karkow, W.
Chicago Aerial Industries
Barrington, Ill.

Keene, L. F.
NASA-Marshall Space Flight Center
Huntsville, Ala.

Kelley, D. F.
Applied Physics Division, USAERDL
Fort Monmouth, N.J.

Kelly, T. R.
General Electric Co.
Missile and Space Vehicle Department
Philadelphia, Pa.

Kerr, J.
U.S. Continental Army Command
Fort Monroe, Va.

Kerkering, J. H.
Electrical Department, USAERDL
Fort Belvoir, Va.

Kessler, I.
Electrical Department, USAERDL
Fort Belvoir, Va.

Klatte, C. E.
Indiana University
School of Medicine
Indianapolis, Ind.

Klein, M. W.
Warfare Vision Branch, USAERDL
Fort Belvoir, Va.

Knight, K.
Minneapolis-Honeywell
Washington, D. C.

Koda, J.
Hughes Aircraft Co.
Vacuum Tube Products Division
Oceanside, Calif.

Koffman, L. A.
Corps of Engineers
U.S. Army
Washington, D.C.

Kong, E.
Nortronics
Hawthorne, Calif.

Kupperian, J. E.
NASA-Goddard Space Flight Center
Greenbelt, Md.

Laslett, L. J.
Atomic Energy Commission
Washington, D.C.

Lawrence, L. L.
U.S. Continental Army Command
Fort Monroe, Va.

Lempert, J.
Westinghouse Electric Corp.
Research Laboratories
Pittsburgh, Pa.

Levin, I.
Walter Reed Army Medical Center
Washington, D.C.

Leventhal, E.
Stanford University
School of Medicine
Palo Alto, Calif.

Liebson, W.
Electrical Department, USAERDL
Fort Belvoir, Va.

Lindemann, H. B.
Westinghouse Electric Corp.
Baltimore, Md.

Linden, B. R.
CBS Laboratories
Stanford, Conn.

Linn, H. E.
Corps of Engineers
U.S. Army
Fort Belvoir, Va.

Lippel, B.
Applied Physics Division, USAERDL
Fort Monmouth, N.J.

Livingston, W. C.
Kitt Peak National Observatory
Tucson, Ariz.

Luman, R. M.
U.S. Army Intelligence Board
Fort Holabird
Baltimore, Md.

Lunde, B.
NASA-Goddard Space Flight Center
Greenbelt, Md.

Lundquist, C. A.
NASA-Marshall Space Flight Center
Huntsville, Ala.

Lynds, C. R.
National Radio Astronomy Observatory
Green Bank, W. Va.

Maerz, R. H.
U.S. Army Combat Surveillance Agency
Arlington, Va.

Mangold, R.
Carnegie Institute of Technology
Pittsburgh, Pa.

Mansfield, W. O.
Westinghouse Electric Corp.
Electronic Tube Division
Elmira, N.Y.

Manzo, E.
General Precision, Inc.
Pleasantville, N.Y.

Marchesano, J.
Automation Laboratory, Inc.
Westburgen, Long Island, N.Y.

Margozzi, A.
NASA-Ames Research Center
Moffett Field, Calif.

Markham, K.
Air Force Flight Test Center
Edwards Air Force Base, Calif.

Marschka, F. D.
Radio Corp. of America
Electron Tube Division
Lancaster, Pa.

Marshall, F. B.
Westinghouse Electric Corp.
Baltimore, Md.

Martin, F.
Radio Corp. of America
Camden, N.J.

Marton, L.
National Bureau of Standards
Washington, D.C.

Matson, C.
Chicago Aerial Industries
Barrington, Ill.

Matte, H.
Dumont Laboratories
Clifton, N.J.

McCurdy, G.
Westinghouse Electric Corp.
Electronic Tube Division
Elmira, N.Y.

Meredith, E.
Warfare Vision Branch, USAERDL
Fort Belvoir, Va.

Messmer, J.
Advanced Research and Applications Division
California Division
Burbank, Calif.

Mestwerdt, H. M.
Air Force Systems Command
Wright-Patterson Air Force Base, Ohio

Millia, C. P.
U.S. Army Armor School
Fort Knox, Ky.

Mitchell, J. L.
NASA-Headquarters
Washington, D.C.

Moody, J.
Warfare Vision Branch, USAERDL
Fort Belvoir, Va.

Moor, J. C.
Radio Corp. of America
Electron Tube Division
Lancaster, Pa.

Morton, G. A.
Radio Corp. of America
David Sarnoff Research Center
Princeton, N.Y.

Mulders, G.
National Science Foundation
Washington, D.C.

Nail, N.
Eastman Kodak Co.
Research Laboratories
Rochester, N.Y.

Nekut, A. G.
Radio Corp. of America
Electron Tube Division
Lancaster, Pa.

Nelson, L. T., Jr.
Office of the Commandant
Fort Sill, Okla.

Nelson, R. E.
Radio Corp. of America
Lancaster, Pa.

Nelson, W. H.
Air Force Systems Command
Wright-Patterson Air Force Base, Ohio

Neupert, W. M.
NASA-Headquarters
Washington, D.C.

Nicoll, F. H.
Radio Corp. of America
David Sarnoff Research Center
Princeton, N.J.

Niklas, W. F.
The Rauland Corp.
Chicago, Ill.

Noel, D. E.
National Security Agency
Fort Meade, Md.

Nolan, P.
Farrand Optical
New York, N.Y.

Norris, R. N.
Westinghouse Electric Corp.
Baltimore, Md.

Ogland, J. W.
Westinghouse Electric Corp.
Baltimore, Md.

O'Neal, Patrick
Sylvania Electric Co.
Argus Division
Washington, D.C.

Orlando, C.
   Signal Research and Development Laboratory
   U.S. Army
   Fort Monmouth, N.J.
Ott, E. J.
   NASA-Headquarters
   Washington, D.C.
Papp, G.
   ITT Federal Laboratories
   Components and Instrumentation Laboratory
   Fort Wayne, Ind.
Parfitt, R. H.
   General Electric Co.
   Military Department
   Syracuse, N.Y.
Parrish, W. F.
   Westinghouse Electric Corp.
   Baltimore, Md.
Parton, J.
   Warfare Vision Branch, USAERDL
   Fort Belvoir, Va.
Pashler, P. E.
   General Electric Co.
   Research Laboratories
   Schenectady, N.Y.
Patteson, A. W.
   Electrical Department, USAERDL
   Fort Belvoir, Va.
Perl, M. L.
   Randall Laboratory of Physics
   University of Michigan
   Ann Arbor, Mich.
Pourciau, L. L.
   General Precision, Inc.
   Pleasantville, N.Y.
Powers, R. W.
   Aeronautical Chart and Information Center
   U.S. Navy
   Washington, D.C.
Powers, W.
   Dearborn Observatory
   Northwestern University
   Evanston, Ill.
Prince, M. D.
   Lockheed Georgia Co.
   Marietta, Ga.
Purdue, J.
   White Sands Missile Range
   White Sands, N. Mex.
Read, S., Jr.
   Frankford Arsenal
   Philadelphia, Pa.
Redfern, G.
   Aerojet-USAERDL
   Fort Belvoir, Va.
Rennilson, J. J.
   Jet Propulsion Laboratory
   Pasadena, Calif.

Replogie, F.
   Perkin & Elmer
   Norwalk, Conn.
Reynolds, G. T.
   Elementary Particles Laboratory
   Princeton University
   Princeton, N.J.
Richards, R. J.
   Aeronautical Chart and Information Center
   U.S. Air Force
   Washington, D.C.
Roach, J.
   U.S. Army Transportation Group
   Fort Eustis, Va.
Robinson, H. H.
   Dynamics Corp. of America
   Washington, D.C.
Rock, W.
   F.M.A., Inc.
   Washington, D.C.
Roesler, J. F.
   The Rauland Corp.
   Chicago, Ill.
Rogers, A. W.
   Office of the Chief Signal Officer
   U.S. Army
   Washington, D.C.
Roman, N. G.
   NASA-Headquarters
   Washington, D.C.
Rome, M.
   Machlett Laboratories, Inc.
   Springdale, Conn.
Rotnem, J.
   NASA-Lewis Research Center
   Cleveland, Ohio
Ruhge, J. M.
   Michelson Laboratory
   U.S. Naval Ordnance Tests Station
   China Lake, Calif.
Sadler, L. E.
   Corps of Engineers
   U.S. Army
   Washington, D.C.
Salzberg, C. D.
   Eastman Kodak Co.
   Apparatus and Optical Division
   Rochester, N.Y.
Sarna, D. S.
   Ordnance Tank Automotive Command
   Detroit, Mich.
Scheps, B. B.
   GIMRADA
   Fort Belvoir, Va.
Schneebaum, M. I.
   NASA-Goddard Space Flight Center
   Greenbelt, Md.

Schneeberger, R. J.
   Westinghouse Electric Corp.
   Research Laboratories
   Pittsburgh, Pa.
Seaton, S. L.
   U.S. Army Continental Command
   Fort Monroe, Va.
Segal, S.
   Electrical Department, USAERDL
   Fort Belvoir, Va.
Severiens, J. C.
   Atomic Energy Commission
   Washington, D.C.
Shabanowitz, H.
   Westinghouse Electric Corp.
   Electronic Tube Division
   Elmira, N.Y.
Shaffer, R. A.
   Westinghouse Electric Corp.
   Electronic Tube Division
   Elmira, N.Y.
Shaltis, W. J.
   Signal Office
   U.S. Army
   Washington, D.C.
Sheehan, E.
   Electrical Department, USAERDL
   Fort Belvoir, Va.
Sheldon, J. L.
   Corning Glass Works
   Electrical Products Division
   Corning, N.Y.
Shenker, M.
   Farrand Optical
   New York, N.Y.
Shepard, J. R.
   GIMRADA
   Fort Belvoir, Va.
Siedband, M. P.
   Westinghouse Electric Corp.
   Baltimore, Md.
Siegmund, W.
   American Optical Co.
   Southbridge, Mass.
Simon, R. E.
   Radio Corp. of America
   David Sarnoff Research Center
   Princeton, N.J.
Skorinko, G.
   Westinghouse Electric Corp.
   Research Laboratories
   Pittsburgh, Pa.
Slater, P. N.
   Armour Research Foundation
   Chicago, Ill.
Smith, R. A.
   U.S. Army Continental Command
   Fort Monroe, Va.

Smithgall, H.
   Sylvania Electric Co.
   Seneca Falls, N.Y.
Snell, P. A.
   CBS Laboratories
   Stanford, Conn.
Sommer, A. H.
   Radio Corp. of America
   Conversion Devices Laboratory
   Princeton, N.J.
Spilker, C. J.
   Office of the Chief of Engineers
   U.S. Army
   Washington, D.C.
Stanley, C. V.
   ITT Federal Laboratories
   San Fernando, Calif.
Stiles, G. J.
   Ballistic Research Laboratories
   Aberdeen Proving Ground, Md.
St. John, M. R.
   Air Force Systems Command
   Wright-Patterson Air Force Base, Ohio
Stoudenheimer, R. G.
   Radio Corp. of America
   Electron Tube Division
   Lancaster, Pa.
Stow, R. L.
   Westinghouse Electric Corp.
   Baltimore, Md.
Stowe, G. R.
   Electrical Department, USAERDL
   Fort Belvoir, Va.
Straub, H. W.
   Ordnance Corps
   Washington, D.C.
Streiffert, J.
   Eastman Kodak Co.
   Research Laboratories
   Rochester, N.Y.
Sturm, R. E.
   Dynamics Corp. of America
   Pikesville, Md.
Suits, G.
   U.S. Army Liaison Group
   University of Michigan
   Ann Arbor, Mich.
Sullivan, D.
   Naval Ordnance Laboratory
   Corona, Calif.
Swanson, N.
   Electron Physics Section
   National Bureau of Standards
   Washington, D.C.
Szegho, C. S.
   The Rauland Corp.
   Chicago, Ill.

Talley, R. E.
  U.S. Army Engineer School
  Fort Belvoir, Va.
Tasis, E.
  Pan American World Airways, Inc.
  Data Acquisition Systems
  Patrick Air Force Base, Fla.
Taylor, W. B.
  GIMRADA
  Fort Belvoir, Va.
Thomas, C., Jr.
  Electric Department USAERDL
  Fort Belvoir, Va.
Thomas, L. P.
  NASA-Flight Research Center
  Edwards Air Force Base, Calif.
Thomas, N. C.
  U.S. Army Transportation Research Command
  Fort Eustis, Va.
Thompson, J.
  Nichelson Laboratory
  Naval Ordnance Test Station
  China Lake, Calif.
Thompson, R. R.
  Bendix Research Laboratory
  Detroit, Mich.
Tiedeken, T. W.
  GIMRADA
  Fort Belvoir, Va.
Tousey, R.
  Naval Research Laboratory
  Washington, D.C.
Tuve, M.
  Carnegie Institute of Washington
  Washington, D.C.
Tyson, E.
  Air Force Systems Command
  Wright-Patterson Air Force Base, Ohio
Uhler, R. R.
  Electrical Department, USAERDL
  Fort Belvoir, Va.
Updegraff, J. W.
  Electrical Department, USAERDL
  Fort Belvoir, Va.
Van Atta, W. H.
  GIMRADA
  Fort Belvoir, Va.
Van Denbrock, J.
  Sylvania Electric Co.
  Argus Division
  Washington, D.C.
Van der Grijp, D. H. G. Van Bergen
  Corps of Engineers
  U.S. Army
  Washington, D.C.
Van der Sande, J. J.
  Old Delft Optical Co., Inc.
  Hicksville, Long Island, N.Y.

Van Deusen, W. B.
  U.S. Navy
  Washington, D.C.
Van Keuren, V.
  U.S. Naval Photographic Interpretation Center
  Washington, D.C.
Vass, E. R., Jr.
  Electrical Department, USAERDL
  Fort Belvoir, Va.
Veith, F. S.
  Radio Corp. of America
  Electron Tube Division
  Lancaster, Pa.
Walker, B. F.
  Bendix Corp.
  Baltimore, Md.
Wargo, P.
  General Electric Co.
  Cathode Ray Tube Department
  Syracuse, N.Y.
Water, J.
  Palmer Physical Lavoratory
  Princeton University
  Princeton, N.J.
Watson, R. B.
  U.S. Army Research Office
  Washington, D.C.
Watts, H. V.
  Armour Research Foundation
  Chicago, Ill.
Way, F.
  Bureau of Ships
  U.S. Navy
  Washington, D.C.
Webb, A.
  U.S. Army Combat Surveillance Agency
  Arlington, Va.
Weinberg, S.
  University of Rochester
  School of Medicine
  Rochester, N.Y.
Weischedel, R. C.
  General Electric Co.
  Syracuse, N.Y.
Whitehouse, W.
  University of Michigan
  School of Medicine
  Ann Arbor, Mich.
Wilder, M. P.
  CBS Laboratories
  Stanford, Conn.
Wiley, W. C.
  The Bendix Corp.
  Research Laboratories
  Southfield, Mich.
Wilson, L. N.
  Armour Research Foundation
  Chicago, Ill.

Wilson, N. G.
   Los Alamos Scientific Laboratory
   Los Alamos, N.Mex.

Wiseman, R. S.
   Warfare Vision Branch, USAERDL
   Fort Belvoir, Va.

Woehl, W. E.
   Air Force Missile Development Center
   Holloran Air Force Base
   Alamogordo, N. Mex.

Wolff, C. L.
   NASA-Goddard Space Flight Center
   Greenbelt, Md.

Woodbury, R. G.
   American Optical Co.
   Silver Spring, Md.

Woodson, W. H.
   Bureau of Naval Weapons
   U.S. Navy
   Washington, D.C.

Yanagisawa, S. T.
   Machlett Laboratories, Inc.
   Stanford, Conn.

Yeats, J. J.
   U.S. Army Armor Board
   Fort Knox, Ky.

Zastrow, R. L.
   Bendix Research Laboratory
   Southfield, Mich.

Zinn, M. H.
   USAERDL
   Fort Monmouth, N.J.